Imperial College
London

Improving Accuracy in Robotic Assisted Orthopaedic Surgery

by

Ferdinando Rodriguez y Baena

Submitted for the degree of Doctor of Philosophy
of the University of London and for
the Diploma of Imperial College

London, February 2004

BRL. LONDON. UNIV.

Abstract

In recent years, medical robotics and computer assisted surgery (CAS) have become the new standard of excellence in many surgical fields, including neurosurgery, minimally invasive heart surgery and general orthopaedics. However, the current state of the art in robotic assistance has yet to reach a stable condition, as researchers across the field are still struggling to meet the constraints associated with the surgical environment. The work described in this thesis focuses on two main areas: the development of novel solutions to improve the accuracy of robotic assisted surgical orthopaedic procedures, and the design of a robotic system as a concept demonstrator for minimal access Unicompartmental Knee Arthroplasty (UKA). The study builds upon the original implementation of an active-constraint robot (ACROBOT) for Total Knee Arthroplasty (TKA), described in [Jakopec, 2001].

Early research focuses on the activities which led to the first clinical application of the ACROBOT System, for a number of TKA procedures. An analysis of these early results, which have been published [Jakopec et al., 2001], highlighted the need to tackle accuracy related issues, such as stiffness, bone motion (clamping and motion detection), access and registration (robustness, accuracy, time). These activities, and related results, are presented.

The latter aspect, registration, is one of the main topics of this thesis, which has involved the development of an anatomical registration technique based on a point-touching scheme, suitable for both open surgery and minimal access knee surgery. Extensive validation through simulation and plastic bone trials has demonstrated that both the algorithm implementation and the robust point acquisition protocol are appropriate for fast and accurate registration of the tibia and femur in both TKA and UKA.

The ACROBOT System has been adapted to demonstrate the suitability of a hands-on robot for minimal access knee surgery. Hardware and software modifications are described, while early assessment of the system can be found in [Cobb et al., 2003; Jakopec et al., 2003a]. This thesis also describes the derivation and validation process of a novel hybrid registration algorithm, known as the Bounded ICP algorithm, suitable for minimal access registration of the femur. A discussion of the results and their implications has led to suggestions for future work.

Acknowledgements

Let me start with a few words of gratitude to all those who helped to make this thesis possible. First of all, I would like to thank my supervisor, Prof. Brian Davies, for his help and support and for having believed in me from the very beginning. I have learned a great deal during these three years and for this I am most grateful.

I am thankful to the Acrobot Company Ltd., in particular to Mr. Justin Cobb, for having given me the opportunity to be a part of such an exciting and challenging project. There have been difficult times, but it was all worth it. It was an honour for me to be able to contribute with my work to the technical success of such a unique system.

A huge thank you to the MIM team, for their help and support throughout my research. If it wasn't for every single one of them, Ed, Sam, Joao, Alex and Paula, it would have probably taken me twice as long to finish.

In particular, I thank my two mentors and two of the brightest people I have ever met: Matjaz and Simon. Having the privilege of seeing them in action has been an inspiration and it is something that I will treasure wherever I go. I hope that some of their genius and wisdom rubbed off on me!

Adrian I have to thank because, for one, he read and corrected my thesis. No amount of money could buy one such a favour, so thank you Ade! And thanks for being there for me whenever I needed help... forever in your debt!

I also thank Johann for his invaluable contribution to my project, and for being a friend. Without his clinical input and critical mind, we would have been lost on a number of occasions. Keep working your magic!

Above all, I thank my family. Everything I am, and everything I have achieved, I owe to them. Their vision and guidance are the reason I got where I am, and their unconditional love and support give me the strength to wake up every day and reach for the sky.

Contents

Abstract 1

Acknowledgements 2

Contents 3

List of Figures 8

List of Tables 16

List of Abbreviations 20

Glossary of Terms 22

1 Introduction 25

1.1 Introduction 25

1.2 Conventional Knee Replacement Surgery 27

1.2.1 Total Knee Arthroplasty 29

1.2.2 Unicompartmental Knee Arthroplasty 29

1.3 The ACROBOT System 32

1.4 Aims and Objectives 37

1.5 Outline of the Thesis 38

2 Literature Survey 39

2.1 Robotic Manipulators 39

2.2 Robots in Medicine 40

2.2.1 Robotic Assisted Orthopaedic Surgery 46

2.2.1.1 The CASPAR System 46

2.2.1.2 The ROBODOC System 47

2.2.1.3 The Rizzoli System 48

2.2.1.4 The Arthrobot System 48

2.2.1.5 The CRIGOS System 49

2.2.1.6 The MARS System 50

2.2.2 Robots for Minimally Invasive Surgery 50
2.2.2.1 The da Vinci System 51
2.2.2.2 The Zeus System 52
2.2.2.3 The Minerva System 53
2.2.2.4 The EndoBot System 54
2.2.2.5 The AESOP System 54
2.2.2.6 The Probot System 55
2.3 CAS Systems in Orthopaedics 56
2.4 Registration 59
2.4.1 Registration Methods 60
2.4.1.1 Dimensionality 60
2.4.1.2 Nature of Registration Basis 61
2.4.1.3 Nature and Domain of Transformations 61
2.4.1.4 Interaction 62
2.4.1.5 Optimisation Procedure 62
2.4.1.6 Modalities Involved 63
2.4.1.7 Subject and Object 65
2.4.2 Summary 66
2.5 Robotic Calibration 67
2.6 Robot Kinematics 69
2.6.1 Forward Kinematics 69
2.6.2 Inverse Kinematics 71
2.7 Conclusion 71

3 ACROBOT - A Hands-On Robotic System for TKA 73
3.1 Introduction 73
3.2 Gross Positioning System Integration 73
3.2.1 Modelling the VM Robot 76
3.2.2 Workspace Analysis 79
3.2.3 Calibration 82
3.2.3.1 Method 84
3.2.3.2 Results 85
3.3 Anatomical Registration for TKA 86
3.3.1 Planning and Execution Issues for Registration 87
3.3.2 The Iterative Closest Point Algorithm 89
3.3.3 Registration in the OR 92
3.3.4 Block Registration 93
3.3.5 Results 96
3.4 Discussion 97

3.5 Conclusion 98

4 Achieving Accuracy in the OR - The ACROBOT II **99**

4.1 Introduction 99
4.2 Robot Redesign 100
4.2.1 Gross Positioning System 100
4.2.2 Active Constraint Head 103
4.2.3 ACROBOT II System Overview 105
4.3 System Calibration 107
4.3.1 Gross Positioning System Accuracy Assessment 107
4.3.2 System Kinematics 114
4.3.3 Enhanced Calibration Method 116
4.3.4 Cutter Probe Calibration 118
4.3.5 Results 120
4.4 Clamping System Redesign 122
4.4.1 Bone Immobilisation 122
4.4.2 Bone Motion Monitoring 122
4.5 Conclusion 126

5 Registration Algorithm Optimisation **127**

5.1 Introduction 127
5.2 Objectives 128
5.3 Algorithm Optimisation 129
5.3.1 Closest Point Estimation and Monotonic Convergence 129
5.3.2 Accelerated Search 132
5.3.3 Global Minimum Identification 136
5.3.4 Defining a Robust Point Acquisition Protocol 138
5.3.5 Intra-Operative Guidance 142
5.3.6 Assessing Registration Accuracy in the OR 144
5.3.6.1 Defining Point-set Robustness Indicators 145
5.4 Empirical Validation 147
5.4.1 Error Representation 147
5.4.2 Simulation 149
5.4.2.1 Simulation Software 150
5.4.2.2 Modelling Initial Registration Inaccuracy 151
5.4.2.3 Adding Random Noise 152
5.4.2.4 Generating Random Point-Sets 154
5.4.2.5 Tests and Results 154
5.4.3 Registration With a Plastic Phantom 180

5.4.3.1 Experimental Setup 183
5.4.3.2 Defining a Reference Registration Transform 183
5.4.3.3 Tests and Results 185
5.5 Discussion 187
5.6 Conclusion 188

6 Active Constraints and Minimally Invasive Surgery 190
6.1 Introduction 190
6.2 Adapting the ACROBOT II System for MIS 191
6.2.1 Clamp Redesign 192
6.2.2 Soft Tissue Management 194
6.2.3 Intra-Operative Protocol for Minimal Access UKA 197
6.3 Anatomical Registration and MIS 208
6.3.1 A Point Acquisition Protocol for UKA 209
6.3.2 Intra-Operative Guidance 211
6.3.3 Protocol Validation 213
6.3.3.1 Simulation Tests and Results 214
6.3.3.2 Plastic Phantom Tests and Results 229
6.4 Discussion 231
6.5 Conclusion 232

7 Anatomical Registration for Minimal Access Surgery 234
7.1 Introduction 234
7.2 Minimal Access Femoral Registration 236
7.2.1 Assumptions 236
7.2.2 Locating the Hip Centre 238
7.2.3 The Bounded ICP Algorithm 238
7.2.4 Global Minimum Identification 245
7.3 Implementation 247
7.3.1 Pre-Operative Planning 247
7.3.2 Pelvis Fixation 247
7.3.3 Hip Centre Estimation 248
7.3.4 Clamping and Initial Registration 251
7.3.5 Distal Femur Point Collection 252
7.3.6 Assessing Registration Accuracy in the OR 252
7.4 Empirical Validation 253
7.4.1 Simulation 254
7.4.1.1 Simulation Software 254
7.4.1.2 Tests and Results 256

7.4.2 Registration with a Plastic Phantom 268
7.4.2.1 Experimental Setup 269
7.4.2.2 Tests and Results 270
7.5 Discussion 273
7.6 Early Clinical Results 274
7.7 Conclusion 275

8 Conclusion **277**
8.1 Overview 277
8.2 Summary 280
8.3 Future Work 280
8.3.1 Improvements to Hardware 281
8.3.2 Improvements to the Enhanced ICP Algorithm 281
8.3.3 Improvements to the Bounded ICP Algorithm 282
8.4 Conclusion 283

Bibliography **284**

Appendix A Distance-Based Hole Locating Algorithm **299**

Appendix B ICP Patient Simulation Results - TKA **305**

Appendix C Fiducial Screws Vs. Reference Point-Set **312**

Appendix D ICP Patient Simulation Results - UKA **315**

Appendix E Bounded ICP Proof **322**

Appendix F Bounded ICP Patient Simulation Results - UKA **325**

Appendix G Bounded ICP Extended Experimental Results **331**

Appendix H Author's Reference Articles **337**

List of Figures

1.1 Knee joint anatomy. 27
1.2 Anterior/posterior and medial/lateral leg alignment. 28
1.3 Kinemax total knee replacement implant [Stryker Inc., 2002]. 30
1.4 Incision length and procedure invasiveness for (a) Conventional TKA and (b) Conventional UKA. 31
1.5 Oxford unicompartmental knee implant [Biomet Inc., 2002]. 32
1.6 Preoperative planning for a TKA procedure with the ACROBOT System. 33
1.7 Original Active Constraint (AC) Head. 34
1.8 The active-constraint principle. 35
1.9 2.5D constraint boundary. 36

2.1 The Grey Arm passive robotic system [Lerner, 1999]. 42
2.2 The Paky system [Cadeddu et al., 1997]. 43
2.3 The Neuromate System Zamorano et al., 2000]. 43
2.4 The Steady-Hand robot [Kumar et al., 2000]. 45
2.5 The PADyC system [Schneider and Troccaz, 2001]. 45
2.6 The CASPAR System [Meister et al., 1998]. 47
2.7 The ROBODOC System [Taylor et al., 1994]. 48
2.8 Various stages of THA with the Arthrobot system [Chung et al., 2003]. a) The femur is exposed. b) The femoral head is removed, and the frame is attached to the femur, once the hole is made using a manual starter. c) A reamer shaped gauge is inserted into the femur. d) The frame is manoeuvred into place against the reamer-shaped gauge and locked into position. e) The gauge is removed and the robot installed on the frame to machine the cavity in the femur. f) The hole is completed, and the system is removed. g) The Arthrobot system prototype. 49
2.9 The CRIGOS system [Brandt et al., 1999]. 50
2.10 The MARS system [Shoham et al., 2003]. 51
2.11 The da Vinci system [Broeders and Ruurda, 2001]. 52

2.12 The Zeus system [Nio et al., 2002]. 53
2.13 The Minerva system [Flury et al., 1992]. 54
2.14 Docking station with two EndoBot manipulators (a), with a close-up of the arch joint (b), and the assembly for the roll and translational motion (c) [Kang and Wen, 2001]. 55
2.15 The AESOP system [Miller, 1988]. 56
2.16 The Probot system [Mei et al., 1996]. 57
2.17 The Galileo Nav and CAS Galileo system [PI Precision Ltd., 2002]. . 59
2.18 DH convention for affixing frames to links [Craig, 1989] 70

3.1 Preliminary ACROBOT System concept demonstrator (a), and original clamping system (b) used for early plastic bone and cadaver trials [Jakopec, 2001]. 74
3.2 ACROBOT System with the Armstrong VM gross positioner (in green) 75
3.3 Kinematic model for the ACROBOT System, comprising both the VM robot and AC Head. 77
3.4 ACROBOT head origin positions for the five femoral cuts. 79
3.5 Placement constraints for the knee joint origin w.r.t. the VM robot base co-ordinate system for an orientation of 0° (a), and 15° (b) from the vertical axis. 81
3.6 Calibration parameters for the ACROBOT System. 83
3.7 Calibration plate, and relative parameters. 85
3.8 ICP Registration flow diagram. 90
3.9 Snapshot of the intra-operative software display of the tibia during registration. The red circles represent the position of the points touched with respect to the 3D model, based on the current registration transform. 92
3.10 ACROBOT System accuracy loop. 94
3.11 Block touching technique. 95

4.1 Kinematic configuration of the new gross positioning system. 101
4.2 Gross positioning system placement with respect to the patient. . . . 102
4.3 The Active Constraint Head II. 104
4.4 New gross positioning system. 105
4.5 New active constraint head. 106
4.6 The ACROBOT II System, gross positioner and active constraint head. 106
4.7 ACROBOT II System schematic overview. 108
4.8 FARO Arm mechanical digitiser [FARO Technologies Inc., FL, USA]. 109
4.9 Least square fit of 3D data obtained from the mechanical digitiser as Z and Y are moved in a grid across their entire range of motion. . . . 110

4.10 Additional optical encoder mounted at the base of R. 114
4.11 Schematic kinematic model of the six DOF integrated ACROBOT II System. 115
4.12 Mechanical digitiser-cutter socket interlock. 116
4.13 Schematic illustration of the calibration parameters for the ACROBOT II System. 117
4.14 ACROBOT II calibration setup. 119
4.15 Calibration block used to calibrate the axial offset of the tool. 119
4.16 Error distribution for the four calibration parameter subsets after successful calibration. 121
4.17 New TKA clamping system. 123
4.18 Typical clamping system intra-operative setup. 123
4.19 Point based registration using ACROBOT II clamping system. 124
4.20 Intra-operative screen snapshot of the clamp re-registration procedure during point collection (a), and after the final computation (b). . . . 126

5.1 Closest point estimation for a triangular mesh. 129
5.2 Special mesh configurations complicating the closest point search. . . 130
5.3 u-v co-ordinates used to describe a triangle in 3D space. 131
5.4 Generating the triangle list describing all triangles to be checked for any given vertex. 132
5.5 Optimised k-d tree example based on [Friedman et al., 1977]. 135
5.6 Registration regions for the femur (a) and tibia (b) suitable for TKA. 138
5.7 Registration accuracy for typical hand-picked robust point-sets for the femur (a), and tibia (b), with no noise (I), and 2mm random noise added (II). 140
5.8 Improved GUI for the ACROBOT II System. 142
5.9 Intra-operative display during the region based point acquisition process. 143
5.10 Colour-coded display of a representative point-set showing probable point-touching accuracy of under 0.5mm for the femur (a) and tibia (b). 146
5.11 Co-ordinate systems attached to both the femur and tibia, used to provide a clinical interpretation of the registration error. 148
5.12 Simulation program screen-shot. 151
5.13 The shifted surface (a) is represented in grey against the original surface (yellow). The corresponding registered surface (b) for a pre-defined point set is also shown. All green points lie within 0.1mm of the mapped surface. 152

5.14 Axis/angle notation described in terms of three angles, α, β, and θ. . 153
5.15 Registration outcome for a 35 points point-set, expressed in terms of final rotational error for the entire range (a), and rotation and translation for the range where the global minimum has been consistently identified (b). 158
5.16 Registration outcome for a 15 points point-set, expressed in terms of final rotational error for the entire range (a), and rotational and translational error for the range where the global minimum has been consistently identified (b). 159
5.17 Relationship between RMS error and final rotational alignment for different local minima. 160
5.18 Ideal point distribution for both femur (a) and tibia (b), for 15 (I) and 35 (II) points per set. 161
5.19 Normal distribution plot for a 15 (a) and 50 (b) points point-set with 1mm random noise. 163
5.20 Registration accuracy for the enhanced ICP algorithm in terms of varus/valgus, anterior/posterior, axial, and translational components for different point-set sizes (10, 15, 20, 25, 30, 35, 40, 50, 75, 100) and maximum noise values (0, 0.5, 1, 1.5, 2), for the femur. 169
5.21 Registration accuracy for the enhanced ICP algorithm in terms of varus/valgus, anterior/posterior, axial, and translational components for different point-set sizes (10, 15, 20, 25, 30, 35, 40, 50, 75, 100) and maximum noise values (0, 0.5, 1, 1.5, 2), for the tibia. 170
5.22 Registration accuracy for the enhanced ICP algorithm, in terms of varus/valgus, anterior/posterior, axial, and translational components, executed without minima suppression for different point-set sizes and maximum noise values, for the femur. 176
5.23 Registration accuracy for the enhanced ICP algorithm, in terms of varus/valgus, anterior/posterior, axial, and translational components, executed without minima suppression for different point-set sizes and maximum noise values, for the tibia. 177
5.24 Average RMS error values obtained for different point-set sizes and maximum noise values for the femur. 178
5.25 Maximum RMS error values obtained for different point-set sizes and maximum noise values for the femur. 179
5.26 Experimental setup adopted for plastic bone trials with the ACROBOT II System for robotic assisted TKA. 184
5.27 Examples of reference point-sets for the femur (a) and tibia (b) with typical colour-code distributions and RMS error values. 185

5.28 Accuracy of registration outcome for 10 registration procedures using the enhanced ICP algorithm for both the femur (a) and tibia (b). . . 186

6.1 Early concept design of an active-constraint robotic system for Unicompartmental Knee Arthroplasty. 191
6.2 Layout of the main UKA skin incision and additional stab-wounds, required for the clamping system, over the knee joint. 192
6.3 Prototype clamp design. 193
6.4 Early concept designs for the UKA clamps insertion pins. 193
6.5 Technical drawing for the insertion pins of the UKA clamping system. 194
6.6 UKA bone clamp. 195
6.7 Tissue retaining tube: concept design. 196
6.8 Tissue retaining tube: final design. 196
6.9 Retaining tube, interchangeable handle, and unicompartmental knee prosthesis. 198
6.10 Graphical illustration of the cuts required to place both tibial and femoral components of the Oxford unicompartmental knee implant [Biomet Inc., 2002]. 199
6.11 Cutter inserts, used during UKA with the ACROBOT II System, shapes and dimensions. 200
6.12 UKA with the ACROBOT II System intra-operative clamping setup. 202
6.13 Intra-operative setup of the tissue retaining tube, during early testing on a conventional UKA procedure. 202
6.14 Relationship between hole depth and placement accuracy. 204
6.15 Typical registration scenario for UKA of the medial condyle. 204
6.16 Using the GPS at an angle to gain a range of motion in the missing degree of freedom, towards and away from the table. 206
6.17 ACROBOT II System intra-operative visual feedback during cutting of the femur (a) and tibia (b). 206
6.18 Typical registration scenario for UKA of the medial condyle. 207
6.19 Registration regions for the femur (a) and tibia (b) suitable for UKA. 209
6.20 Approximate size and location of the two additional femoral and tibial stab-wounds, needed for registration. 210
6.21 Relationship between the shape of the tibial tuberosity and rotational alignment, described using a snapshot of Acrobot's proprietary planning software. 212
6.22 Colour-coded display of the tibia and femur, used to ensure appropriate point collection through the main incision, as well as the tibial and femoral stab-wounds. 213

6.23 Ideal point distribution for both femur (a) and tibia (b), for 15 (I) and 35 (II) points per set. 215
6.24 Registration accuracy for the enhanced ICP algorithm in terms of varus/valgus, anterior/posterior, axial, and translational components for different point-set sizes and maximum noise values, for the femur. 221
6.25 Registration accuracy for the enhanced ICP algorithm in terms of varus/valgus, anterior/posterior, axial, and translational components for different point-set sizes and maximum noise values, for the tibia. . 222
6.26 Registration accuracy for the enhanced ICP algorithm, in terms of varus/valgus, anterior/posterior, axial, and translational components, executed for different point-set sizes and maximum noise values, without points assembled through the stab-wound, for the femur. 227
6.27 Registration accuracy for the enhanced ICP algorithm, in terms of varus/valgus; anterior/posterior, axial, and translational components, executed for different point-set sizes and maximum noise values, without points assembled through the stab-wound, for the tibia. 228
6.28 Accuracy of registration outcome for 10 registration procedures using the enhanced ICP algorithm for both the femur (a) and tibia (b). . . 230
6.29 Early clinical trials of robotic assisted UKA with the ACROBOT II System. 232

7.1 Accessible surfaces on the femur during conventional UKA. 236
7.2 Leg alignment in terms of knee and hip centres. 237
7.3 Effect of hip centre estimate error on the overall alignment of the leg. 238
7.4 "Physical model" for the Bounded ICP convergence theorem. 239
7.5 Phase I of convergence. 242
7.6 Phase II of convergence. 244
7.7 Distant local minimum affecting the Bounded ICP algorithm. 246
7.8 Pre-operative hip centre estimation. 248
7.9 Intra-operative pelvis fixation by means of auxiliary bed clamps, tightened against the patient's left (a) and right (b) sides. 249
7.10 Cutter insert used to generate a set of measurements for the distal femur location during hip centre estimation. 249
7.11 Intra-operative GUI for the hip centre estimation process. 250
7.12 Surgeon carefully moving the leg in a grid during *in vitro* testing. . . 251
7.13 Typical femoral point-set for the Bounded ICP algorithm. 253
7.14 Updated simulation software screen-shot. 255
7.15 Examples of stepping, nudging, pulling, and axially rotating of the current registration estimate. 255

7.16 Monotonic convergence for the Bounded ICP algorithm. 257
7.17 Set of 3D vectors describing possible hip centre estimate errors. . . . 258
7.18 Final error distribution for the Varus/Valgus (a), and Anterior/Posterior (b), components of the registration transform for different hip centre estimate errors. 260
7.19 Estimated versus actual registration accuracy, in terms of Varus/Valgus (a), and anterior/Posterior (b) components. 262
7.20 Error distribution in terms of anterior/posterior, varus/valgus, axial, and translational alignment for different initial error states and $1.5mm$ maximum noise. 263
7.21 Distribution of the axial rotational errors for different initial states. . 264
7.22 Relationship between RMS error and final rotational alignment for different local minima. 265
7.23 Error distribution in terms of anterior/posterior, varus/valgus, axial, and translational alignment for different initial error states and $0.8mm$ maximum noise. 266
7.24 Registration accuracy for the Bounded ICP algorithm in terms of varus/valgus, anterior/posterior, axial, and translational components for different point-set sizes and maximum noise values. 267
7.25 Plastic pelvis securely fixed to the operating table by means of custom designed bone clamps. 269
7.26 "Ball-and-socket" setup of the pelvis and femoral head. 270
7.27 Experimental layout for the hip centre estimation (a) and point collection process (b) during plastic bone testing of the Bounded ICP algorithm. 271
7.28 Screen-shot of the intra-operative GUI illustrating the distribution of 10 consecutive hip centre estimates. The picture shows both axial (a) and lateral (b) views. 271
7.29 Post-operative femoral implant alignment for UKA clinical trial carried out with the ACROBOT II System. 275

B.1 Registration accuracy for the enhanced ICP algorithm in terms of varus/valgus, anterior/posterior, axial, and translational components for different point-set sizes and maximum noise values, for the femur. 306
B.2 Registration accuracy for the enhanced ICP algorithm in terms of varus/valgus, anterior/posterior, axial, and translational components for different point-set sizes and maximum noise values, for the tibia. . 307
C.1 Lateral (a) and sagittal (b) views of a plastic phantom bone with fiducial marker screws. 313

C.2 Screen-shot of Acrobot's proprietary pre-operative software for fiducial screw identification. 313
D.1 Registration accuracy for the enhanced ICP algorithm in terms of varus/valgus, anterior/posterior, axial, and translational components for different point-set sizes and maximum noise values, for the femur. 316
D.2 Registration accuracy for the enhanced ICP algorithm in terms of varus/valgus, anterior/posterior, axial, and translational components for different point-set sizes and maximum noise values, for the tibia. . 317
F.1 Registration accuracy for the Bounded ICP algorithm in terms of varus/valgus, anterior/posterior, axial, and translational components for different point-set sizes and maximum noise values. 326

List of Tables

2.1 Robot classification table. 41
2.2 Table illustrating the nine classification criteria and relative areas of interest. 66

3.1 DH parameters for the 6 DOF VM robot, and 3 DOF AC Head. . . . 78
3.2 Upper and lower limits for all six joints of the GPS. 80
3.3 Final set of calibration parameters for the ACROBOT System. 85

4.1 Difference between derived (from the circle equation) and measured (encoder) joint angles for R. 112
4.2 Third axis backlash test. 113
4.3 DH parameters for the six DOF integrated ACROBOT II System. . . 115
4.4 Calibration parameters for the ACROBOT II System. 117
4.5 Individual contribution of each calibration parameter subset to the final accuracy of the ACROBOT II System. 120

5.1 Table used to define the closest point on a triangle for any point in 3D space. 131
5.2 Regions of interest for the femoral surface accessible during TKA. . . 139
5.3 Regions of interest for the tibial surface accessible during TKA. . . . 139
5.4 Execution speed for the enhanced ICP algorithm implementation with and without minima suppression (MS) for different size surface models. 156
5.5 Relationship between point-set size and registration robustness, expressed in terms of overall rotational and translational accuracy, for a set of robust point-sets describing a distal femur. 164
5.5 (cont'd) Relationship between point-set size and registration robustness, expressed in terms of overall rotational and translational accuracy, for a set of robust point-sets describing a distal femur. 165
5.6 Relationship between point-set size and registration robustness, expressed in terms of overall rotational and translational accuracy, for a set of robust point-sets describing a proximal tibia. 166

5.6 (cont'd) Relationship between point-set size and registration robustness, expressed in terms of overall rotational and translational accuracy, for a set of robust point-sets describing a proximal tibia. 167
5.7 Relationship between point-set size and registration robustness, expressed in terms of overall rotational and translational accuracy, for a set of robust point-sets describing a distal femur. 172
5.7 (cont'd) Relationship between point-set size and registration robustness, expressed in terms of overall rotational and translational accuracy, for a set of robust point-sets describing a distal femur. 173
5.8 Relationship between point-set size and registration robustness, expressed in terms of overall rotational and translational accuracy, for a set of robust point-sets describing a proximal tibia. 174
5.8 (cont'd) Relationship between point-set size and registration robustness, expressed in terms of overall rotational and translational accuracy, for a set of robust point-sets describing a proximal tibia. 175
5.9 Relationship between point-set size and registration robustness, expressed in terms of overall rotational and translational accuracy, for the set of best randomly generated point-sets describing a proximal tibia. 181
5.9 (cont'd) Relationship between point-set size and registration robustness, expressed in terms of overall rotational and translational accuracy, for the set of best randomly generated point-sets describing a proximal tibia. 182
5.10 Typical computation time requirements for point-set robustness assessment, obtained on a PC workstation running Windows® XP Professional, with a 1.8GHz Intel Pentium® 4 processor. 183

6.1 UKA cuts, and relative cutter inserts. 197
6.2 Regions of interest for the femoral surface accessible during UKA. . . 210
6.3 Regions of interest for the tibial surface accessible during UKA. . . . 211
6.4 Relationship between point-set size and registration robustness, expressed in terms of overall rotational and translational accuracy, for a set of robust point-sets describing a distal femur. 216
6.4 (cont'd) Relationship between point-set size and registration robustness, expressed in terms of overall rotational and translational accuracy, for a set of robust point-sets describing a distal femur. 217
6.5 Relationship between point-set size and registration robustness, expressed in terms of overall rotational and translational accuracy, for a set of robust point-sets describing a proximal tibia. 218

6.5 (cont'd) Relationship between point-set size and registration robustness, expressed in terms of overall rotational and translational accuracy, for a set of robust point-sets describing a proximal tibia. 219
6.6 Relationship between point-set size and registration robustness, expressed in terms of overall rotational and translational accuracy, for a set of robust point-sets describing a distal femur. 223
6.6 (cont'd) Relationship between point-set size and registration robustness, expressed in terms of overall rotational and translational accuracy, for a set of robust point-sets describing a distal femur. 224
6.7 Relationship between point-set size and registration robustness, expressed in terms of overall rotational and translational accuracy, for a set of robust point-sets describing a proximal tibia. 225
6.7 (cont'd) Relationship between point-set size and registration robustness, expressed in terms of overall rotational and translational accuracy, for a set of robust point-sets describing a proximal tibia. 226

7.1 Accuracy and precision of the hip estimation procedure developed for the ACROBOT II System for ten consecutive hip centre estimates. . 272
7.2 Accuracy of registration outcome for 10 registration procedures using the Bounded ICP algorithm. 273

B.1 Relationship between point-set size and registration robustness, expressed in terms of overall rotational and translational accuracy, for a set of robust point-sets describing a distal femur. 308
B.1 (cont'd) Relationship between point-set size and registration robustness, expressed in terms of overall rotational and translational accuracy, for a set of robust point-sets describing a distal femur. 309
B.2 Relationship between point-set size and registration robustness, expressed in terms of overall rotational and translational accuracy, for a set of robust point-sets describing a proximal tibia. 310
B.2 (cont'd) Relationship between point-set size and registration robustness, expressed in terms of overall rotational and translational accuracy, for a set of robust point-sets describing a proximal tibia. 311
C.1 Error difference between a fiducial-based registration transform and one obtained with a reference point-set. Values are expressed in component form for both the femur (a), and tibia (b). 314
D.1 Relationship between point-set size and registration robustness, expressed in terms of overall rotational and translational accuracy, for a set of robust point-sets describing a distal femur. 318

D.1 (cont'd) Relationship between point-set size and registration robustness, expressed in terms of overall rotational and translational accuracy, for a set of robust point-sets describing a distal femur. 319
D.2 Relationship between point-set size and registration robustness, expressed in terms of overall rotational and translational accuracy, for a set of robust point-sets describing a proximal tibia. 320
D.2 (cont'd) Relationship between point-set size and registration robustness, expressed in terms of overall rotational and translational accuracy, for a set of robust point-sets describing a proximal tibia. 321
F.1 Relationship between point-set size and registration robustness, expressed in component for using the $\{BONE\}$ co-ordinate system, for $0.5mm$ maximum random noise. 327
F.2 Relationship between point-set size and registration robustness, expressed in component for using the $\{BONE\}$ co-ordinate system, for $1.0mm$ maximum random noise. 328
F.3 Relationship between point-set size and registration robustness, expressed in component for using the $\{BONE\}$ co-ordinate system, for $1.5mm$ maximum random noise. 329
F.4 Relationship between point-set size and registration robustness, expressed in component for using the $\{BONE\}$ co-ordinate system, for $2.0mm$ maximum random noise. 330
G.1 Extended experiemental results for plastic femurs 1 and 2. 332
G.2 Extended experiemental results for plastic femurs 3 and 4. 333
G.3 Extended experiemental results for plastic femurs 5 and 6. 334
G.4 Extended experiemental results for plastic femurs 7 and 8. 335
G.5 Extended experiemental results for plastic femurs 9 and 10. 336

List of Abbreviations

A/P Rot	Anterior/Posterior Rotation about the anatomical axis of the bone
A/P Trans	Anterior/Posterior Translation
AC	Active Constraints
AC Head	Active Constraint Head
ACL	Anterior Cruciate Ligament
ACROBOT	Active-constraint robot, used to describe the original ACROBOT System prototype (six DOF anthropomorphic gross positioner plus three DOF aluminium active constraint head)
ACROBOT II	Redesigned ACROBOT System (three DOF "prismatic-prismatic-revolute" (P-P-R) gross positioner plus three DOF plus redesigned active constraint head)
Acrobot	The Acrobot Company Ltd. (London, UK)
Axial Rot	Axial Rotation about the anatomical axis of the bone
CAD	Computer Aided Design
CAM	Computer Aided Manufacturing
CAS	Computer Assisted Surgery
CMM	Co-ordinate Measuring Machine
CNC	Computer Numerical Control
CT	Computed Tomography
DOF	Degrees Of Freedom
D-H	Denavit Hartenberg (parameters)
FK	Forward Kinematics

GPS	Gross Positioning System
GUI	Graphical User Interface
HIFU	High Intensity Focused Ultrasound
ICP	Iterative Closest Point (approximation)
IGS	Image Guided Surgery
IK	Inverse Kinematics
M/L Trans	Medial/Lateral Translation
MHRA	Medicines and Healthcare products Regulatory Agency
MIS	Minimally Invasive Surgery
MRI	Magnetic Resonance Imaging
NC	Numerical Control
OR	Operating Room
P/D Trans	Proximal/Distal Translation
PCL	Posterior Cruciate Ligament
RAS	Robotic Assisted Surgery
RMS	Root Mean Square
THA	Total Hip Arthroplasty
TKA	Total Knee Arthroplasty
TURP	TransUrethral Resection of Prostate
UKA	Unicompartmental Knee Arthroplasty
V/V Rot	Varus/Valgus Rotation about the anatomical axis of the bone

Glossary of Terms

Acetabulum	The hollow, cup-like portion of the pelvis into which the head of the thigh bone (femur) fits.[1]
Anatomical axis	Refers to the angle subtended between the shaft of the femur and the shaft of the tibia in the coronal plane.
Anterior	Toward the front or in front of.
Artefact	Something artificial, a distortion that does not reflect normal anatomy or pathology, not usually found in the body e.g. in radiology, the appearance on an X-ray of a surgical metal clip that obscures the clear view of an anatomical structure.
Arthroplasty	The surgical repair of a joint.
Biomechanics	The study of the body in terms of its mechanical structure and properties. Locomotion of the body is one of the more important things to which the mechanical laws are applied for study.
Calibration	Process used to compensate for geometrical errors of a robotic system by identifying a more accurate geometrical relationship between the joint encoder readings and the actual position of the end-effector.
Cholecystectomy	A term that describes the surgical removal of the gallbladder.
Condyle	A rounded articular surface at the extremity of a bone.
Coronal	Vertical plane from head to foot and parallel to the shoulders.
Cruciate	One the most commonly injured ligaments which stabilises the knee joint.
Distal	Furthest to the attached end of a limb, opposed to proximal.

[1] All medical definitions are taken from the on-line database "Medic8® Family Health Guide," *http://www.medic8.com.*

Epicondyles	A bony projection on the inner side of the distal end of the humerus; the internal condyle.
Haptics	The science concerned with the tactile sense.
Intercondylar fossa	The deep fossa between the femoral condyles in which the cruciate ligaments are attached.
Laparoscopy	A surgical procedure in which a tiny scope is inserted into the abdomen through a small incision.
Lateral	Denoting a position farther from the median plane or mid-line of the body or of a structure.
Mechanical axis	Refers to the angle drawn between a line intersecting the centre of rotation of the femoral head to the centre of the knee and a line drawn from the centre of the knee to the centre of the ankle.
Medial	The side of the body or body part that is nearer to the middle or centre (median) of the body. Medial is also used to refer to the compartment of the knee that is closest to the other knee. The opposite of medial is lateral.
Modality	A method of treatment. In registration it defines the means by which a registration object is acquired.
Mono-modal	Registration technique where both images to be registered have been generated using the same technology.
Multi-modal	Registration of two images that have been generated utilising different modalities.
Osteophyte	A bony outgrowth or protuberance.
Patella	Knee cap.
Patellofemoral	The middle compartment of the knee joint.
Posterior	Situated in back of or in the back part of or affecting the back or dorsal surface of the body.
Prismatic	Joint producing linear motion.
Prostatectomy	The surgical removal of the prostate gland.
Proximal	Nearest to the attached end of a limb, opposed to distal.

Registration	Determination of a one-to-one mapping between the coordinates in one space with those in another, such that the points in the two spaces that correspond to the same anatomical point are matched to each other.
Revolute	Joint producing rotary motion.
Sagittal	Plane that bisects the body into a right and left half
Spinous	process Spinous process of a vertebra, the dorsal process of the neural arch of a vertebra.
Tibial	tuberosity An oval elevation on the anterior surface of the tibia about 3 cm distal to the articular surface, giving attachment at its distal part to the patellar ligament.
Thoracoscopic	Surgery done using one or more endoscopic instruments.
Transcutaneous	Entering through the dermis or skin.
Transosseous	Entering into or through bone tissue.
Unicompartmental	Referred to surgery to a single compartment of the knee.
Valgus	Outward, away from the mid-line, opposite of varus.
Varus	Inward, toward the mid-line, opposite of valgus.

Chapter 1

Introduction

1.1 Introduction

Recent advancements in both medical and computer technology have given life to a new era in the field of applied medicine. Discoveries in the fast growing areas of medical imaging, biomedical material science, and medical robotics have succeeded in defining a new standard for the accuracy, repeatability, and flexibility of a surgical procedure. By providing the surgeon with a set of new "tools," these technological advancements have the potential to revolutionise the way in which surgery is planned and carried out in the operating theatre.

The single most noticeable technological advancement blends state of the art imaging equipment with advanced data processing and tracking technology, providing an unparallelled degree of detail and flexibility during both planning and intervention. Computer Assisted Surgery (CAS), also known as Image Guided Surgery (IGS), is the name given to the technology in which preoperative slice data such as that acquired by Magnetic Resonance (MRI), or Computed Tomographic (CT or CAT scans) images are used to plan and guide surgical procedures. CAS has already been used for many applications, including neurosurgery, spine surgery, general orthopaedics, ENT (ear, nose and throat) surgery, and many more. CAS has become an invaluable tool during the planning of complex procedures by providing the surgeon with a complete three-dimensional model of patient-specific anatomy. This allows careful planning of the procedure, either pre-operatively or in the operating theatre just before surgery, to be performed with a high degree of accuracy. In addition, by communicating imaging data to the surgical field, CAS applications allow the surgeon to reproduce the plan precisely, with a higher degree of repeatability than conventional surgery.

As a result, normally invasive procedures can be made less invasive, thereby reducing patient recovery time, and previously inoperable cases can be carried out

successfully. In addition, a clear record of the procedure is available to the surgeon at all times, as tool positioning, surgery duration, and any other execution-related performance variable, are continuously monitored by the system.

However CAS does not stop the surgeon failing to follow the plan accurately. By providing audio/visual (usually) feed-back in the operating theatre, CAS systems enable the surgeon to check how the procedure is going, and what the next step in the plan is. However, it is entirely up to the surgeon to adequately follow the plan, and the final accuracy of the procedure is directly related to his or her ability to perform the operation correctly. This may be difficult to achieve if tissue or cutting forces disturb the described location of the tool during the procedure.

This drawback represents the major advantage of another innovative technology that has recently appeared in the medical field, Robotic Assisted Surgery (RAS). By blending the surgeon's expertise and judgement in the operating theatre with the accuracy and repeatability of a robotic system, the surgical outcome of any operation can be predicted and achieved with unparallelled reliability. A CAS system is used for the planning phase and for intra-operative visual feed-back, while the robotic system is used to accurately carry out the procedure according to plan.

One of the major shortcomings of this technology is the unwillingness of many surgeons to place most of the responsibility for the surgical outcome onto the robotic system alone. Many robotic systems presently available on the market, such as ROBODOC [Taylor et al., 1994] and CASPAR [Grueneis et al., 1999], are categorised as active robots (Section 2.2) in which all intra-operative staff are left observing the procedure without any real interaction with the machine. Once the robotic system is started, the surgeon is in charge of ensuring the procedure is accurately carried out by the robot according to his or her plan. However many of the decisions concerned with the procedure may be embedded in the robot controller (i.e., outside the control, or even the knowledge, of the surgeon), and, since ultimately the surgeon-patient relationship represents a critical aspect of any surgical procedure, a more interactive process may be preferred.

The concept of an active-constraint robot for orthopaedic surgery first appeared in the literature in 1994 [Ho et al., 1994], and blends the advantages of both CAS and RAS, without the drawbacks of a fully automated robot. The ACROBOT System, developed at Imperial College London, was originally proposed as an active-constraint robot for total knee replacement surgery (Section 1.2.1), which has, over the past ten years, developed into an advanced prototype suitable for clinical use. ACROBOT, which in the year 2000 became the lead product of the Acrobot Company Ltd., provides a "hands-on" approach to surgery, by means of a back-drivable robot. The procedure is carried out by the surgeon, while the robotic system prevents any wrong-doing by constraining the motion to a predefined region. The

ACROBOT System, which is explored in greater detail in Section 1.3, optimises both the outcome and "feel" of the operation by creating a synergy between the surgeon and the machine.

The author's research, which is sponsored by The Acrobot Company Ltd., started prior to the first clinical application of the ACROBOT System for a number of Total Knee Arthroplasty (TKA) procedures. It focuses on improving the accuracy of the system with regard to two specific operations, namely Total Knee Arthroplasty (TKA) and Unicompartmental Knee Arthroplasty (UKA). The following paragraphs provide a brief introduction to the research presented in the thesis. General knee anatomy and mechanics, alongside a brief description of the conventional technique for both TKA and UKA, are presented in Section 1.2. Section 1.3 provides an overview of the ACROBOT System and active-constraint concept, while the aim and research outline for this study can be found in Section 1.4 and Section 1.5 respectively.

1.2 Conventional Knee Replacement Surgery

In order to understand any form of knee disease and the resulting need for surgical intervention, a general overview of its anatomy and mechanics is necessary. As illustrated in Figure 1.1, the knee is a hinge joint composed of three compartments. The bony anatomy is made up of the femur, tibia, and fibula, while the compartments of the knee are medial, lateral, and patellofemoral.

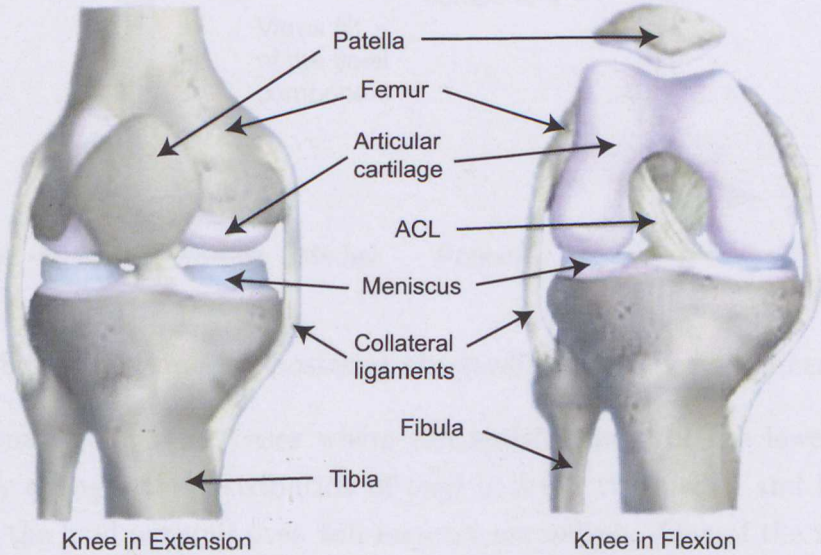


Figure 1.1: Knee joint anatomy.

Overall alignment of the knee can be described in terms of the anatomic and

mechanical axes. As illustrated in Figure 1.2, the anatomic axis refers to the angle subtended between the shaft of the femur and the shaft of the tibia in the coronal plane. In a healthy individual without knee symptoms, the average angle of the anatomic axis is 5° to 7° of *valgus*. The mechanical axis refers to the angle drawn between a line intersecting the centre of rotation of the femoral head to the centre of the knee and a line drawn from the centre of the knee to the centre of the ankle. In an ideal setting, these lines would be co-linear, yielding a mechanical axis of 0°. However, many knees actually fall in 1° and 2° of mechanical *varus* ("bow-legged"). Because of this relationship, when the knee is loaded, such as in a single-leg stance, 55 to 60% of the load is borne by the *medial* compartment, while the remaining load is distributed on the *lateral* side [Gray and Carter, 1992].

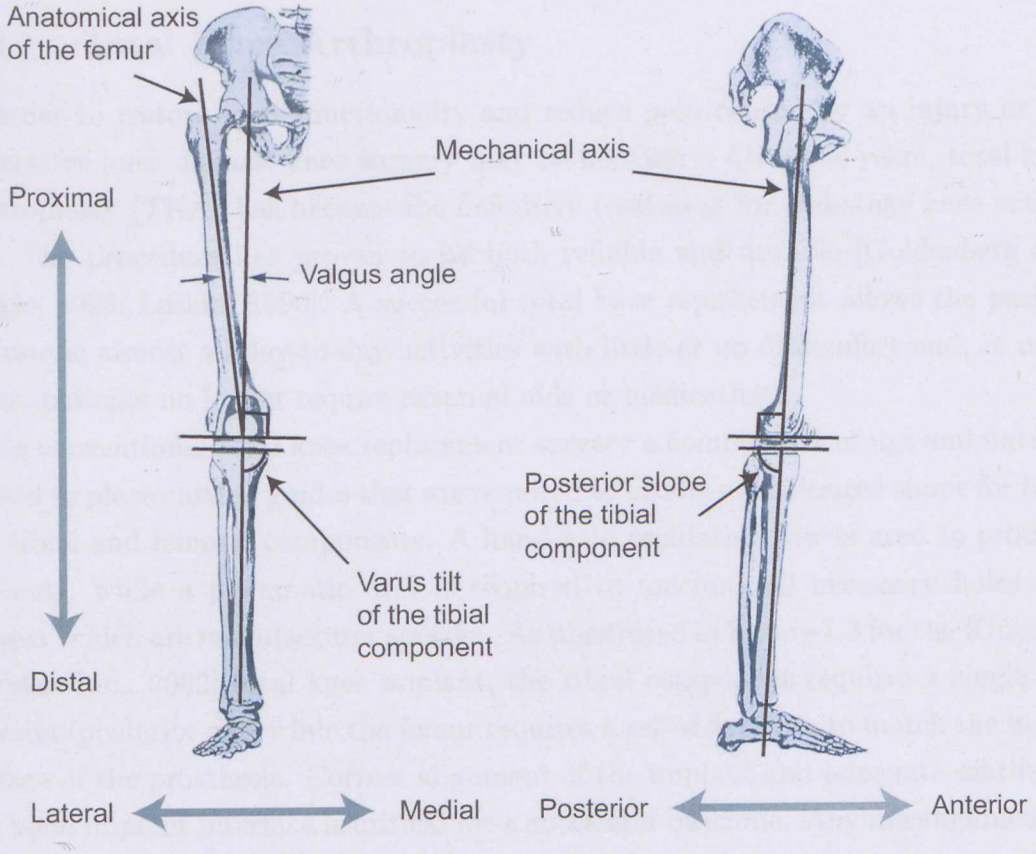


Figure 1.2: Anterior/posterior and medial/lateral leg alignment.

Unfortunately, in some cases where the malalignment of the lower extremity significantly changes the distribution of load between the medial and lateral compartments, the load per unit area will increase excessively. One of the most important properties of articular cartilage (Figure 1.1) is the ability to withstand impact loading. However, the capacity of the cartilage to withstand the elevated contact stresses is influenced by the load the cartilage bears (i.e. body weight) and load distribution. With progressive malalignment, more load is shifted to a single com-

partment, and the load per unit area is increased to the point at which it exceeds the remodelling capacity of the articular cartilage, leading to its degeneration. Once the protective layer of articular cartilage has been lost, direct contact of bone on bone produces pain and intra-articular debris, with progressively detrimental effects on patient mobility.

Arthroplasty is generally the treatment of choice for advanced knee osteoarthritis, however there are conditions that would preclude this treatment option, such as inadequate bone stock, osteoporosis, or neuromuscular conditions [Gray and Carter, 1992]. The following sub-sections provide a brief description of the conventional technique behind two of the most common surgical procedures carried out in these circumstances: total knee arthroplasty, and unicompartmental knee arthroplasty.

1.2.1 Total Knee Arthroplasty

In order to restore joint functionality and reduce pain caused by an injury or degenerative knee disease, knee surgery may be necessary. Over the years, total knee arthroplasty (TKA) has become the definitive treatment for end-stage knee arthritis. The procedure has proven to be both reliable and durable [Goldenberg and Figgie, 1998; Laskin, 1990]. A successful total knee replacement allows the patient to resume almost all day-to-day activities with little or no discomfort and, in most cases, patients no longer require external aids or medications.

In conventional total knee replacement surgery a complex set of jigs and fixtures is used to place cutting guides that are required to produce the desired shape for both the tibial and femoral components. A hand-held oscillating saw is used to produce the cuts, while a pneumatic drill is required to machine all necessary holes and flanges, which are manufacturer specific. As illustrated in Figure 1.3 for the Kinemax [Stryker Inc., 2002] total knee implant, the tibial component requires a single flat anterior/posterior cut, while the femur requires a set of five cuts to match the inside surface of the prosthesis. Correct alignment of the implant and adequate mating of the bone-implant interface is critical for a successful outcome. Any misalignment in the redefined mechanical axis or inaccurate bone cuts may cause premature implant loosening, resulting in pain, swelling and the need for revision surgery [Ahlberg and Lunden, 1981]. Various post-operative assessment tools, such as imaging devices (e.g. x-ray, CT) and CAS systems, and methodologies [Hewitt and Shakespeare, 2001] are available to the surgeon for placement accuracy estimation.

1.2.2 Unicompartmental Knee Arthroplasty

As described in Section 1.2, even a small deviation from the ideal mechanical axis of 0° may lead to excessive weight being sustained by a single compartment. In turn,



Figure 1.3: Kinemax total knee replacement implant [Stryker Inc., 2002].

uneven wear of the femoral/tibial interface will result in progressive malalignment of the knee joint, a condition known as unicompartmental degenerative knee disease. If left uncured, prolonged wear will eventually affect other compartments and surrounding ligaments, forcing the patient to evaluate the prospects of TKA.

However, especially on younger patients, who usually have higher expectations, unicompartmental knee arthroplasty (UKA) may prove to be a more suitable option. In UKA only one of the three compartments is replaced, therefore preservation of bone stock is a key feature. In addition, retention of the anterior cruciate, posterior cruciate, and normal patellofemoral joint maintains a closer semblance to normal knee kinematics, resulting in increased mobility compared to TKA [Feikes et al., 2000]. Finally, in the event of the deterioration of the unresurfaced compartment, conversion to a total knee implant is comparatively easy relative to revision surgery for a failed TKA.

Although originally similar to TKA, the surgical protocol for a less invasive operation has successfully been developed for UKA with promising results [Price et al., 2001]. As illustrated in Figure 1.4, in UKA the tibial and femoral components can be inserted through an 8cm incision, which is considerably smaller than the 15cm to 20cm cut required in TKA. As a result, rehabilitation is generally faster than that from TKA, and, as such, less traumatic to the patient.

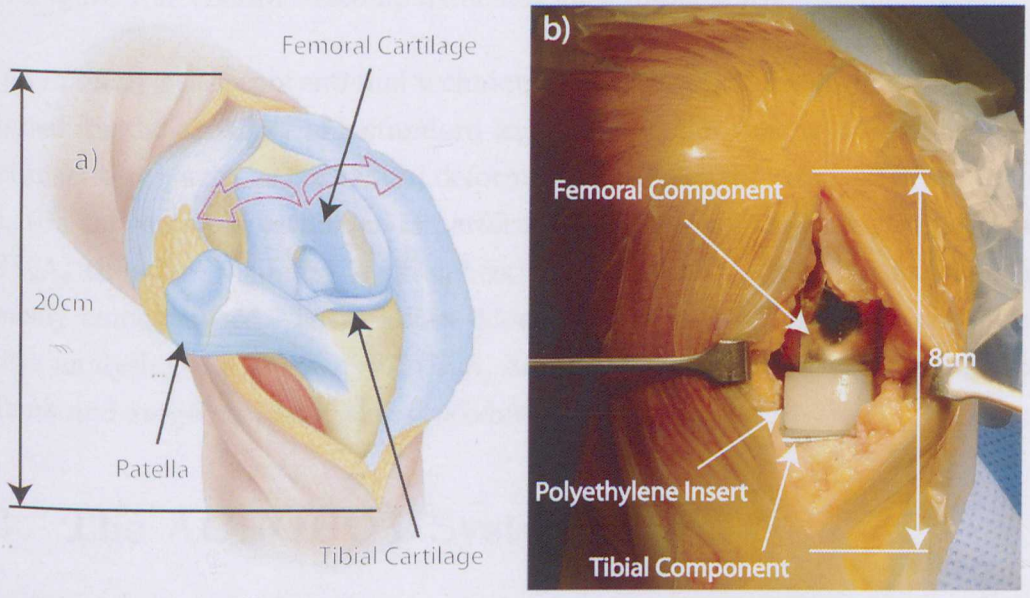


Figure 1.4: Incision length and procedure invasiveness for (a) Conventional TKA and (b) Conventional UKA.

Precise instructions for accurate unicompartmental component insertion are available from each implant manufacturer. However, accurate cut placement is extremely hard to achieve using conventional techniques. As for TKA surgery, a complex set

of jigs and fixtures is used to define the centre of the knee, and the centre of the ankle, which are required to place the cutting guides used to redefine the mechanical axis of the leg. The shape and number of cuts for each component is manufacturer specific, however the insertion process and the issues associated with it are similar. Figure 1.5 illustrates the shape of both femoral and tibial components of the Oxford [Biomet Inc., 2002] unicompartmental knee implant.

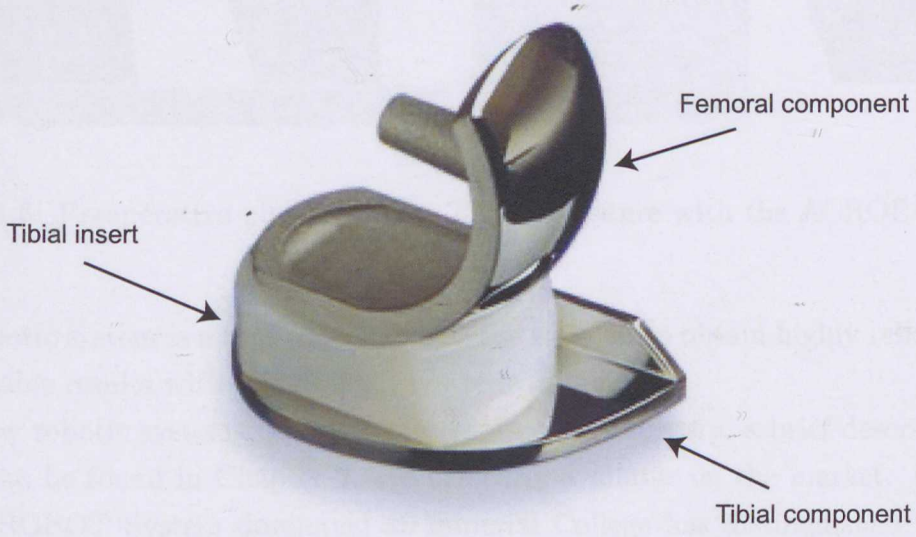


Figure 1.5: Oxford unicompartmental knee implant [Biomet Inc., 2002].

As in many other conventional techniques, the tooling and equipment for UKA is designed for the anatomy of a standard leg, and does not take into account patient-specific features, such as congenital deformities or abnormal localised wear. In addition, the conventional technique is performed through a smaller incision compared to TKA, therefore visibility is often restricted, and cut placement accuracy may be easily compromised. These issues, alongside the lack of long-term comparative studies analysing the longevity of UKA, have contributed to the scepticism of both patients and surgeons about this procedure.

1.3 The ACROBOT System

One of the advantages of a robotic system over conventional CAS systems is the ability to optimise surgical outcome by reducing the effects of human error and fatigue in the operating theatre. The increased accuracy and repeatability of a robot allows the surgeon to concentrate on the technically challenging and physically demanding aspects of the surgery, without worrying about the loss of performance resulting from inaccurate equipment placement, and from sub-optimal human performance.

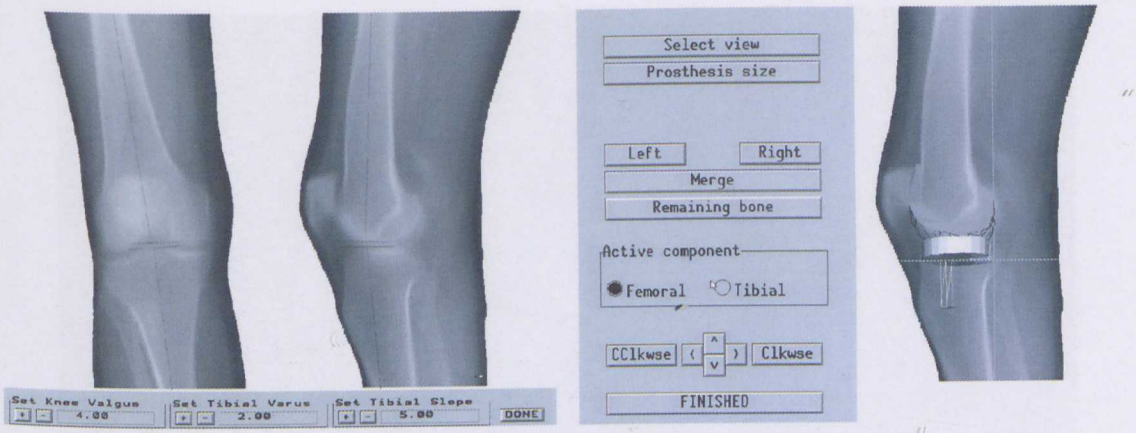


Figure 1.6: Preoperative planning for a TKA procedure with the ACROBOT System.

Any robotic system is a tool which enables the surgeon to obtain highly reliable and quantifiable results with a high degree of repeatability.

A few robotic systems for total knee replacement surgery, a brief description of which can be found in Chapter 2, are presently available on the market. However the ACROBOT System developed at Imperial College has distinguished itself by providing a hands-on approach to the procedure, which has proved successful in the medical world [Davies et al., 1997; Delp et al., 1998; Harris et al., 1997b; Ho et al., 1995c; Jakopec et al., 2001]. ACROBOT can be categorised as a semi-active system, and, as such, has been designed to constrain the surgeon's movements to a predefined region. Therefore the surgeon remains in charge of the operation by retaining full control of the system at all times. Since it was custom built for the specific task of TKA, the device is characterised by a small working envelope and minimal power requirements. In turn, these features, alongside the semi-active nature of the system, render the ACROBOT System inherently safe in the operating theatre, even though it is located in close proximity to both the patient and staff.

The planning stage of the ACROBOT System is much more thorough than the planning for conventional TKA, which simply involves placing prosthesis templates over x-ray images. First, a computed tomographic (CT) scan of the patient's leg is taken. The interactive planning software, developed at Imperial College, is then used to process CT images and plan the procedure: 3D models of the knee bones are built and the bone axes are determined. The surgeon then interactively decides on the prosthesis type, size and placement, as illustrated in Figure 1.6. The software provides a number of different 3D views of the leg and the implant, to help the surgeon plan the procedure. Once the prosthesis model is in the correct position over the bone model, the planning software generates the constraint boundaries, which are then transferred to the intra-operative robotic system.

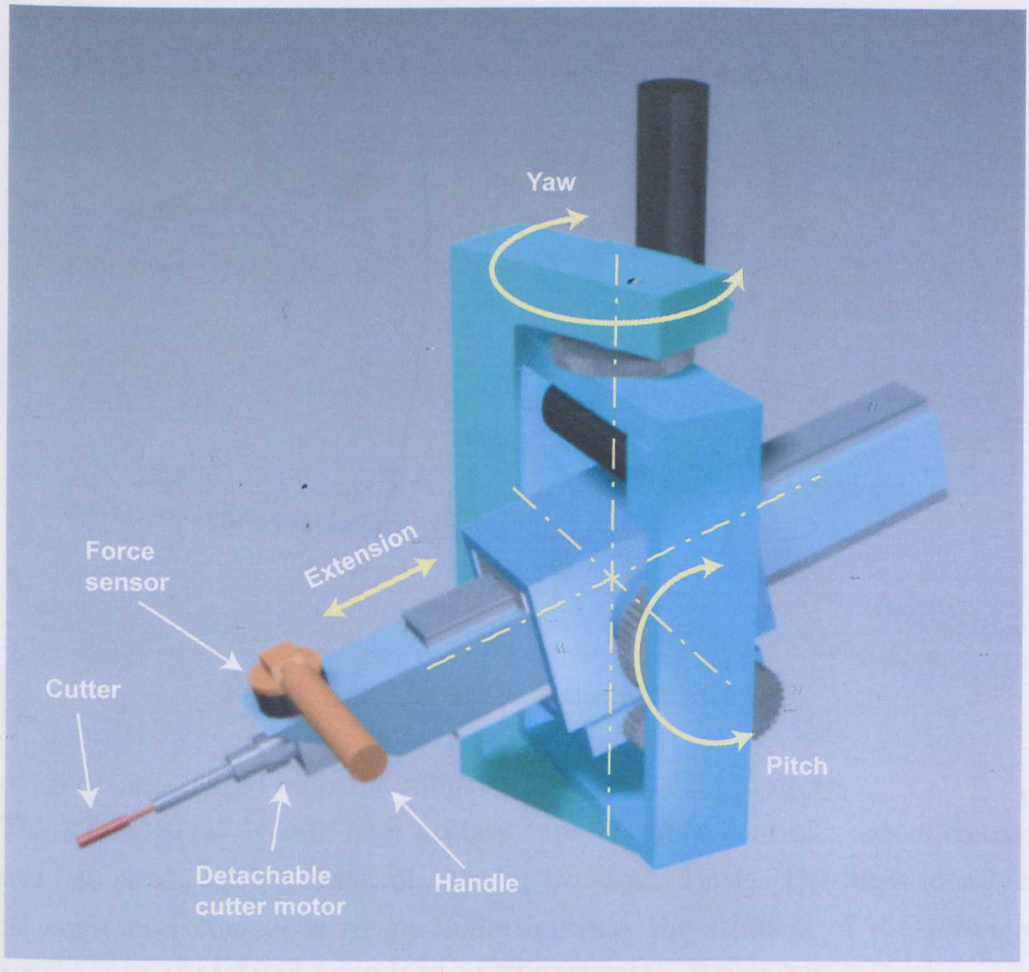


Figure 1.7: Original Active Constraint (AC) Head.

Intra-operatively, a small, low-powered, special-purpose active constraint head (AC Head) is mounted on a gross positioner to form the ACROBOT System. The AC Head is a spherical manipulator with three orthogonal axes of motion: Yaw, Pitch and Extension (Figure 1.7). It has a relatively small reach ($\approx 30cm$) and range of angles ($\pm 30^o$), which ensures accurate operation with low-powered motors. Consequently, the robot is relatively safe, because potential damage is limited in terms of force and is constrained to a small region. The mechanical impedance of the axes is low and similar for all axes, allowing the robot to be moved by the surgeon with uniform low force. The surgeon moves the robot by pushing the handle near the tip of the robot. The handle incorporates a 6-axes force sensor, which measures the guiding forces and torques. This force/torque information is used in active constraint control of the robot. A high-speed orthopaedic cutter motor is mounted near the tip of the ACROBOT System. Different rotary cutters and tools can be repeatably mounted into the motor. For sterility reasons, the cutter motor is placed in a special mount, which allows the motor to be removed and autoclaved before

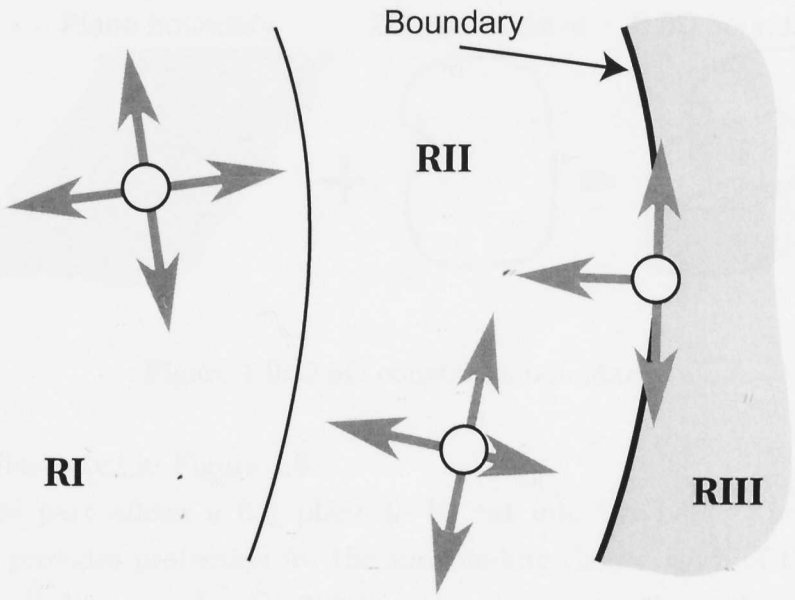


Figure 1.8: The active-constraint principle.

the surgery, and placed onto the robot at the start of the surgery.

The ACROBOT System uses a novel type of robot control - active constraint control [Ho et al., 1995b; Ho et al., 1995a; Ho et al., 1994]. The basic idea behind active constraint control is to gradually increase the stiffness of the robot as it approaches the predefined boundary, as illustrated in Figure 1.8.

In other words, when the servo system is back-driven by the surgeon, the robot is free to move inside the safe region (RI), due to low mechanical impedance of the robot. As a result, the surgeon can feel the cutting forces generated at the tip of the robot. At the boundary of the safe region, the robot becomes very stiff, thus preventing further motion over the boundary (RIII). In addition, the portion of the guiding force normal to the boundary is directly compensated, which substantially reduces the over-boundary error (this error is inevitable due to the limited motor power). To avoid instabilities at the boundary, the stiffness increases gradually over a small region close to the boundary (RII). Furthermore, only the stiffness in the direction toward the boundary is adjusted, to allow motion along or away from the boundary with a very low guiding force. This is achieved by a two level control. The inner loop ($2ms$) is a joint position/velocity control loop with friction, gravity and guiding force compensation. The outer, slower loop (approx. $10-15ms$, depending on the complexity of the boundary) is the boundary controller, which is executed in Cartesian space and adjusts the parameters of the inner loop, according to the robot's position and the surgeon's guiding force. Because of the nature of the prosthesis used, which requires a number of flat planes to be cut, the constraint boundary is defined as a "2.5D" boundary, formed from a plane and a closed 2D

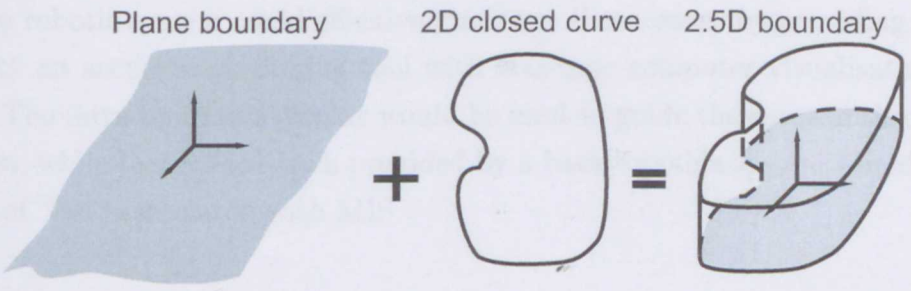


Figure 1.9: 2.5D constraint boundary.

outline, as illustrated in Figure 1.9.

The plane part allows a flat plane to be cut into the bone, whereas the 2D outline part provides protection for the surrounding tissue. Each of the two parts can be controlled separately. Considering the plane part, the stiffness is adjusted according to the distance to the plane. For the 2D outline, the nearest point on the outline is found (when projected onto the plane). The stiffness of the robot is then adjusted independently in normal and tangential directions to the outline at this nearest point. These stiffnesses, each of which is computed along three orthogonal axes, are then combined before being passed to the inner loop.

The technology developed for the ACROBOT System may prove to be the optimal solution behind robotic assisted UKA. By providing preoperative planning capabilities and accurate and repeatable component placement intra-operatively, a robotic system for UKA would allow the current technical barriers preventing more widespread use of this procedure to be overcome. By developing a suitable device, the benefits of UKA over TKA (described in Section 1.2.2), alongside those of robotic assistance over conventional surgery, could considerably increase demand for this type of procedure.

In addition, as UKA is a less invasive operation than TKA, it lends itself to a minimally invasive approach. Thanks to recent advancements in medical technology, Minimally Invasive Surgery (MIS) is a new kind of surgery which has become increasingly common in recent years. In comparison to conventional open surgery, MIS offers several advantages for the patient. As the incision is smaller, MIS causes less pain and less strain to the organism. In turn, this results in faster recovery, less risk of infection, less scarring, and the economic gains that result from a shorter illness time.

However, several limitations in the current technology have slowed down the widespread adoption of a minimally invasive approach. MIS results in restricted vision in the operating theatre, difficult handling of the instruments, heavily restricted mobility, and difficult hand-eye coordination with little or no tactile perception. A

hands-on robotic system could effectively address these issues by providing the surgeon with an accurate machining tool with real-time computer visualisation capabilities. The intra-operative display would be used to guide the surgeon through the operation, while tactile feed-back provided by a back-drivable system would replace the loss of "feel" associated with MIS.

1.4 Aims and Objectives

The aim of this study is:

> *To improve the accuracy of robotic surgery, and specifically of the ACROBOT System, as demonstrated by two orthopaedic operations, namely Total Knee Arthroplasty (TKA) and Unicompartmental Knee Arthroplasty (UKA).*

Research presented herein has resulted in the following objectives list:

- To redesign the hardware of both the robot and the clamping system, to improve the performance of the ACROBOT System in TKA, and to enable its use for minimal access UKA.
- To develop an anatomical registration method based on a point-touching protocol, to be used with a back-drivable robot for application to a range of orthopaedic procedures.
- To implement and validate robust anatomical point-touching strategies, including an intra-operative protocol, suitable for both open, and minimal access registration. These are to be demonstrated for both TKA and UKA to ensure alignment of the knee within $\pm 2^o$ and $\pm 2mm$.

The research presented in this thesis describes novel aspects of robotic design and calibration, with an emphasis on accuracy and safety. A patented bone motion monitoring technique is discussed, which also allows quick and accurate re-registration. Research on the topic of registration has resulted in the development of robust point touching strategies, which have been validated through simulation and plastic bone trials for both open and minimally invasive knee surgery. In particular, this thesis presents the full derivation and validation of a novel registration algorithm suitable for minimal access surgery, coined the Bounded ICP algorithm, which has been shown to substantially outperform the anatomical based method.

Although the author was involved in the ACROBOT System's clinical assessment for a number of TKA and UKA procedures, an analysis of the clinical data obtained

lies outside the scope of this thesis. TKA clinical results of the complete system can be found in [Jakopec et al., 2001; Jakopec et al., 2002a; Jakopec et al., 2003b; Jakopec et al., 2003c], two of which have been included in Appendix H for reference. The preliminary evaluation of an early Ethics Committee approved UKA study has recently been presented [Rodriguez y Baena et al., 2003; Jakopec et al., 2003a; Cobb et al., 2003].

1.5 Outline of the Thesis

The remainder of this thesis is organised in the following way. Chapter 2 provides a brief review of the techniques and technologies associated with this project, alongside a survey of currently available systems for knee surgery and minimally invasive surgery (MIS). Chapter 3 describes early research on gross positioning and registration, which led to the first clinical application of the ACROBOT System for a number of TKA procedures. Chapter 4 focuses on the hardware redesign of both the robot, and clamping system, carried out to address a number of issues raised during clinical use, which resulted in the ACROBOT II System. This chapter also describes the implementation of a novel bone motion monitoring technique, which has been patented.

Chapter 5 centres upon the development and validation process, through simulation and *in vitro* experimentation, of an anatomical registration technique based on the well known Iterative Closest Point (ICP) algorithm [Besl and McKay, 1992]. The technique and experimental results of a robust point acquisition protocol, suitable for open access knee surgery, are also presented.

Chapter 6 focuses on the adaptation process, which enabled the ACROBOT II System to be used as a concept demonstrator for hands-on robotic assisted UKA. Modifications to both the clamping system and the intra-operative protocol are described, and a registration protocol suitable for minimal access registration of the knee, including validation results through simulation and plastic bone trials, is presented.

Chapter 7 focuses on the derivation, implementation, and integration of a novel registration algorithm, the Bounded ICP algorithm, suitable for minimal access registration of the femur. The performance of the Bounded ICP algorithm, validated through simulation and in vitro experimentation, has shown a substantial improvement, in terms of accuracy and robustness, compared to the registration method and intra-operative protocol described in Chapter 6.

Chapter 8 provides a conclusion to the study, and outlines a numbers of remaining research issues, which have been identified as areas for future work.

Chapter 2

Literature Survey

This chapter provides a brief overview, with relevant references, of the main topics associated with the research presented in this thesis. Section 2.1 presents an introduction to robotic manipulators. Section 2.2 describes the application of robots in the medical field, with a focus on orthopaedics (Section 2.2.1), and minimally invasive surgery (Section 2.2.2). Section 2.3 presents an overview of computer aided surgical systems, while Section 2.4 describes the techniques and technologies associated with registration, which has been a topic of particular interest in this study. Finally, a brief outline of available calibration procedures for robotic systems has been presented in Section 2.5.

2.1 Robotic Manipulators

In the past thirty years, robots have become increasingly popular in most fields of research and manufacturing. Due to their high level of automation and broad scope of applicability, robots have become one of the most efficient and versatile tools for material handling. Some form of robotic interface can be found in automated assembly lines, used in most forms of mass production, and in research teams, which focus on different forms of trajectory planning, fuzzy logic and feed-back control.

The most common form of manipulator, however, is the industrial robot. Its origins date back to the early 1960s, almost a decade before the first CAD/CAM (Computer Aided Design / Manufacturing) systems appeared on the market in the 1970s, in an era where automation was starting to play a key role in the manufacturing environment. In the 1830s, the English inventor Charles Babbage [Wolovich, 1987] devised his analytical engine, the forerunner of the modern digital computer, which was to become the brains of today's industrial robots. Forty years later, Herman Hollerith perfected the first automatic calculator, a device which actually implemented Babbage's ideas. It was only after the development of control technol-

ogy in 1950s and 1960s, however, that human control of machines was replaced by numerical or computer control. Conventional lathes, for example, were replaced by Numerical Control (NC) and later Computer Numerical Control lathes, also known as CNC machines. In this progressively technological environment, robots came to represent the future; innovation and large investments were made to develop new analytical ways and better controlling structures to optimise their use. Robots, or programmable manipulators, are designed to move work pieces or tools along a specified path. They consist of a controller, a manipulator and end effectors. Sensing devices, or sensors, are used to enhance the robots performance and allow for feedback control to be implemented. They can be powered hydraulically, pneumatically or electrically. Robot applications, as mentioned earlier, can be found in virtually all branches of industry, particularly in automotive, electrical, electronic and mechanical engineering sectors.

Conventionally, robots' major application areas are materials handling, processing operations (for example spray painting), assembly and inspection. The reason behind their success lies in their ability to repeat their performance to a very high level of accuracy i.e. with greater consistency and repeatability. In other words, robots can be used to replace human labour in repetitive and monotonous tasks, with both a decrease in operating costs and an increase in quality of output.

More recently, however, technological advancements in design, assembly, and control have considerably broadened robots' area of applicability. The high degree of accuracy, precision, and repeatability of robotic systems have proved a valuable asset in other more demanding disciplines, such as "service robotics," an area which also includes the field of applied medicine. The following sections provide a brief overview of such devices, with a focus on robotic systems for orthopaedic surgery, since this is the main concern of this thesis.

2.2 Robots in Medicine

As described in Section 1.1, the application of robotic systems in medicine has proved extremely successful, and has revolutionised the way in which many types of main stream surgery are carried out. Due to their unparallelled level of accuracy and repeatability, robots have succeeded in defining a new standard for the success rate, quality of outcome, and learning expectations associated with their application [Pransky, 2001].

By providing the surgeon with a highly sophisticated tool for careful planning and precise execution, robotic systems have broadened the scope of surgical intervention, providing a means for treatment of previously inoperable conditions. In the past

ten years, research centres around the world have developed robotic systems for many types of medical applications, tailoring any specific implementation to the task for which it was developed. Neurosurgery, orthopaedics, heart surgery, and many other disciplines have already benefited from this technology, which has been constantly reviewed over the years as a witness to its success [Joskowicz and Taylor, 2001; Howe and Matsuoka, 1999; Davies, 2000; Cleary and Nguyen, 2001; Marescaux et al., 2002; Taylor and Stoianovici, 2003; Dario et al., 2003; Cepolina and Michelini, 2003; Davies, 2003].

Robotic systems can be categorised in many different ways, depending on the observer's standpoint. Table 2.1 provides a brief description of the main types of classifications that can be found in the literature.

Classification	*Description*	*Examples*
Field of Application	The medical field in which the robotic system is used	Orthopaedic systems, systems for neurosurgery, systems for heart surgery
Surgery Constraints	Type of access the surgery requires	Endoscopy (no incision required), minimally invasive surgery (e.g. laparoscopy), open surgery
Nature of the Surgery	The type of organ the surgery is carried out on	Hard tissue (i.e. skeletal system), soft tissue (e.g. prostate)
Nature of the System	The functional nature of the robotic system	Actively used (e.g. direct surgical tool) and passively used (e.g. holding devices)
Type of Robot	The physical nature of the robotic system	Passive robots and active robots

Table 2.1: Robot classification table.

The broadest and possibly most encompassing classification of robotic systems in medicine is listed under the heading "*Nature of the System*" in Table 2.1. Using this classification, robotic systems are categorised according to their functional nature i.e. according to the role they play in their field of application. Robots in medicine can play either an *active* role, such as direct surgical tools, or a *passive* role, such as holding devices. Due to the terminology used, this classification is sometimes confused with another well known classification in the robotic field, listed under the heading "*Type of* Robot" in Table 2.1. Robots are categorised as *active* if they are powered (e.g. electrically, pneumatically, etc.), and *passive* otherwise. Passive robots have joints and links, and may have encoders and digital lines, but do not have motors. Therefore, it is important to note that, in the following description, robotic systems are categorised according to their functional nature, not according to

their physical nature. For simplicity, systems used actively are referred to as *active systems*, and, similarly, systems used passively are referred to as *passive systems*. However, where appropriate, the distinction between passive systems (functional nature) and passive robots (physical nature) has been made.

The use of passive systems is usually limited to holding surgical instruments, and can be used as an additional aid to the surgeon or to replace more conventional equipment. Therefore, such systems are usually stiff and reliable, and are designed to be used for more than one application. Most passive systems, such as the Faro Arm [FARO Technologies Inc., FL, USA], which is a a co-ordinate measuring back-drivable manipulator, also used for ROBODOC's registration process [Middelstadt et al., 1998], and the Grey Arm [Lerner, 1999] illustrated in Figure 2.1, are not powered in any way (i.e. are passive robots), therefore their use in the operating theatre is inherently safe.

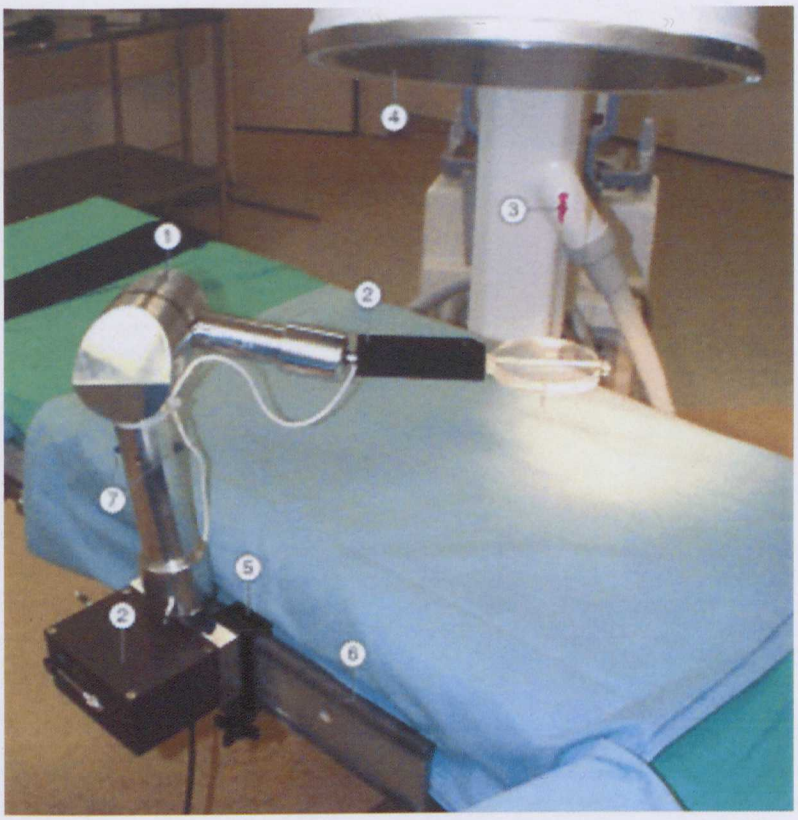


Figure 2.1: The Grey Arm passive robotic system [Lerner, 1999].

Some systems, however, while motorised (i.e. active robots) are still used passively. For instance, EndoAssist [Armstrong Healthcare Ltd., 2002] and the Paky system [Cadeddu et al., 1997] (Figure 2.2), automatically move to a predefined position, which may coincide with a probe's entrance trajectory, before locking and powering off. Passive systems are used as an additional aid to the surgeon dur-

ing handling of heavy equipment, or as an alternative to manual jigs and fixtures, such as Neuromate [Zamorano et al., 2000], which replaces the stereotactic frame in conventional neurosurgery (Figure 2.3). Since the motion of the robot is mutually exclusive to any contact with the patient, such systems do not raise any additional safety issues.

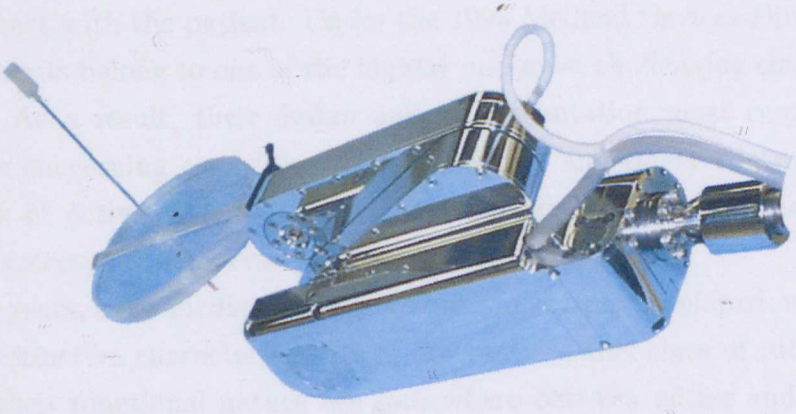


Figure 2.2: The Paky system [Cadeddu et al., 1997].

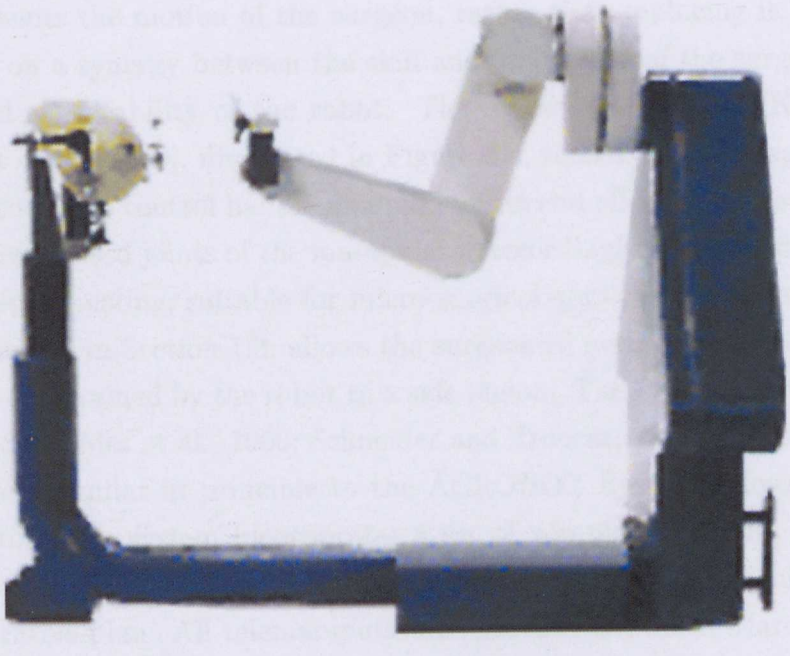


Figure 2.3: The Neuromate System Zamorano et al., 2000].

Fully active systems are on the opposite end of this classification. Such robots take an active role during surgery, directly affecting the procedure outcome. Systems such as Caspar (Section 2.2.1.1) and ROBODOC (Section 2.2.1.2) actually carry out the procedure according to a pre-operative plan. The surgeon becomes a supervisor of the procedure, which is autonomously completed by the robot, and monitored by

the intra-operative staff. The accuracy and reliability of active systems have proved to be a major asset to the surgeon, enabling even complex procedures to be carried out with ease. However, active systems present a number of complications, which have considerably slowed down their widespread adoption in the operating theatre. Firstly, active systems raise the greatest safety concerns, as they are fully powered on while in contact with the patient. Under the 1993 Medical Devices Directive [EEC, 1993] such robots belong to one of the highest and most challenging class of medical equipment. As a result, their design and implementation must comply to tight requirements concerning electric emissions, sterility, and safety control structures. The benefits of active systems over conventional techniques are clear, but their commercial success in the operating theatre is still in doubt.

In recent years, a few medical robotic systems have been developed, which present novel and distinctive characteristics that differentiate this class of robots from all others. As their functional nature lies somewhere between active and passive systems, such devices will be referred to as *semi-active* systems. Technically, semi-active systems are active robots, since they are usually powered on at all times. However, even though they are powered-on while in contact with the patient, their use usually complements the motion of the surgeon, rather than replacing it. Semi-active systems rely on a synergy between the skill and judgement of the surgeon, and the accuracy and repeatability of the robot. The Steady-Hand robot [Kumar et al., 2000; Kumar et al., 1999], illustrated in Figure 2.4, senses the force applied by the surgeon via the force control handle mounted on its end effector, and activates each of the seven motorised joints of the manipulator accordingly. This results in smooth motion and force scaling, suitable for micro-surgical applications. The ACROBOT System, described in Section 1.3, allows the surgeon to perform the operation "free-hand", while constrained by the robot to a safe region. The PADyC system [Troccaz et al., 1993; Schneider et al., 2000; Schneider and Troccaz, 2001], illustrated in Figure 2.5, is very similar in principle to the ACROBOT System. However, instead of using motors, the system incorporates a set of complex clutching mechanisms, known as *freewheels*, which are used to constraint the motion of each joint according to a pre-operative plan. All telemanipulators [Eadie et al., 2003; Marescaux et al., 2002; Rockall and Darzi, 2003], such as the master/slave da Vinci system (Section 2.2.2.1), belong to this category.

Finally, some medical robotic systems, while in contact with the patient, are not used for surgery at all. Under this category, some are used for diagnostics, such as the Hippocrate system [Pierrot et al., 1999; Degoulange et al., 1998], which aids the surgeon during ultrasound (US) 3D data reconstruction of arteries. The robot applies and holds an ultrasound probe on the patient with a specified force, and scans the path of an artery in order to construct its 3D model in software using

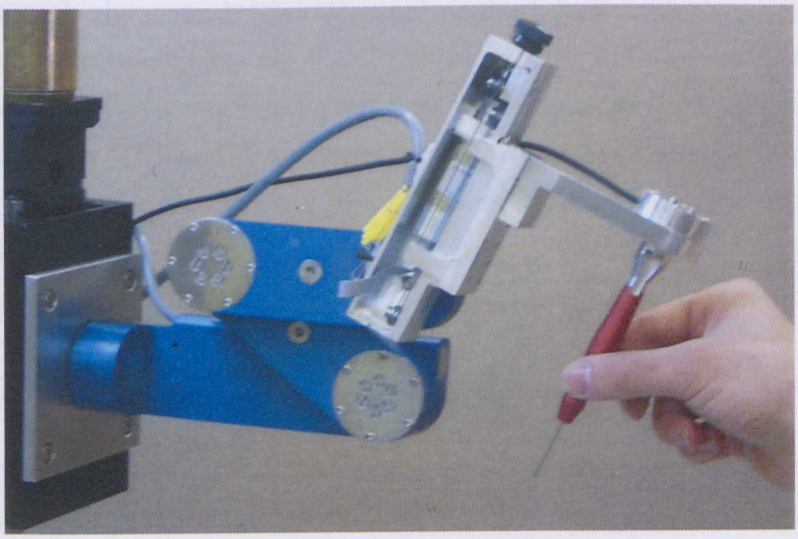


Figure 2.4: The Steady-Hand robot [Kumar et al., 2000].



Figure 2.5: The PADyC system [Schneider and Troccaz, 2001].

US data. Others are used for non-invasive treatment, such as UltraBot [Chauhan, 1999; Pather, 2001], which has been developed at Imperial College London for high intensity focused ultrasound (HIFU) treatment of liver tumours. Similarly, the AcuBot system [Stoianovici et al., 2003] can be used in radiological interventions to manipulate a needle or other slender surgical instrument in the confined space of an imager (such as an MRI or CT scanner) without inducing image artefacts.

The following sections provide a more detailed review of specific aspects of medical robotics, with a focus on Orthopaedics Surgery (Section 2.2.1) and minimally invasive surgery (Section 2.2.2).

2.2.1 Robotic Assisted Orthopaedic Surgery

Orthopaedic surgery deals with malfunctions associated with the skeletal system. As such, this type of surgery provides the perfect framework for robotic assistance, since all bones tend to maintain their original shape at all times, and can be locked into position if necessary. As opposed to soft tissue, which moves and deforms under load, hard tissue, such as bone, can be considered as a fixed object during surgery. Once registered (Section 2.4), locking and tracking mechanisms are used to ensure there is no undetected relative motion between the robot and the bone. By this means, computationally expensive real-time tracking and resulting control software updates, that are necessary in soft tissue surgery, can be avoided.

As a result, the use of robots in surgery has blossomed in the orthopaedics field. Hip, knee, and spine surgery have already benefited from this technology, but others, such as wrist surgery, pelvis reductions, bone tumour resections, are soon to follow. The following subsections provide a brief description of some of the more successful systems in this field.

2.2.1.1 The CASPAR System

The CASPAR (Computer Assisted Surgical Planning And Robotics) system, originally manufactured in Germany by Orto Maquet and illustrated in Figure 2.6, was subsequently acquired by URS AmBH, which ceased to trade in January 2003. CASPAR is a modified clean room robot, rendered safe for operating theatre conditions. The system manufacturers have developed advanced cutting algorithms, which take into account robot trajectories and cutting forces to optimise bone preparation [Meister et al., 1998]. CASPAR is an active system which was originally developed for Total Hip Arthroplasty (THA) [Grueneis et al., 1999]. More recently, however, the system has been used to perform a number of Total Knee Arthroplasty (TKA) procedures, with preliminary results reported in [Siebert et al., 2002]. The CASPAR system has also been used for Anterior Cruciate Ligament (ACL) reconstruction

using a fiducial based invasive registration method [Petermann et al., 2000]. Results of a two year study on ACL reconstruction between 2000 and 2002, have shown a good success rate, but increased operating time coupled with the drawback of an additional operation, required to insert the fiducial pins pre-operatively [Perrier, 2003].

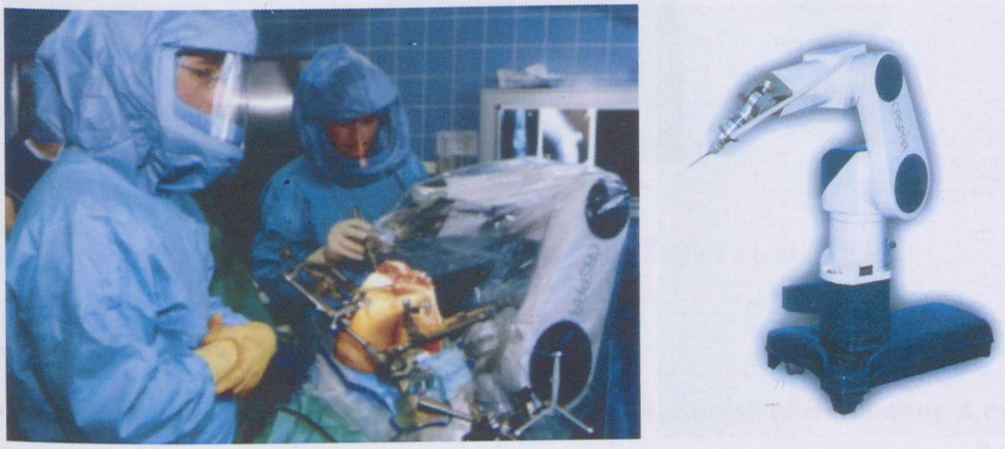


Figure 2.6: The CASPAR System [Meister et al., 1998].

2.2.1.2 The ROBODOC System

The ROBODOC Surgical Assistant System [Taylor et al., 1994; Birke et al., 2000], developed and marketed by Integrated Surgical Systems Inc. is a commercially available robotic system for THA. Based on a modified Scara type robot, the system presents a number of safety mechanisms, including redundant motion control, and a dedicated safety processor. As it has been on the market for over ten years, the system has undergone a number of clinical studies [Boerner et al., 1998], which have resulted in considerable improvements to both the system and surgical protocol.

Surgery is planned on the ORTHODOC planning system, which uses processed computer tomographic (CT) image slices [Webb, 1988] to produce a customised procedure outline for each patient, which is then automatically carried out by the intra-operative system. Originally, fiducial markers were used for registration, but recently an anatomical registration procedure, carried out with the aid of an external digitiser, has been developed [Cohan, 2001]. The ROBODOC system is illustrated in Figure 2.7. A set of Food and Drug Administration (FDA) approved trials, which was expected to have finished by the Autumn of 2002, is currently suspended, as the robot manufacturers are working to overcome legal complications.



Figure 2.7: The ROBODOC System [Taylor et al., 1994].

2.2.1.3 The Rizzoli System

The *Istituti Ortopedici Rizzoli* in Bologna are in the process of developing a custom built robotic system for robotic assisted total knee replacement surgery [Malvisi et al., 2001]. The system is composed of a pre-operative planning software, and an intra-operative robot, with custom built clamping devices, which are required to fix the robot and patient leg with respect to the operating table.

The robot is a custom designed five-degrees of freedom manipulator, mounted on a trolley with a steel plate. The surgery is performed in a semi-automatic mode, where the robot moves to a predefined position and orientation, and the surgeon then mills the bone away, with motion restricted to a single plane by a slider. A milling tool is used to machine the required flat surfaces for TKA, instead of a conventional oscillating saw. The next generation planned for the system will have an option for automatic bone resection, without surgeon interaction.

2.2.1.4 The Arthrobot System

In the mechanical engineering department at the Korea Advanced Institute of Science and Technology (KAIST), a novel robotic system for total hip arthroplasty is being developed [Kwon et al., 2001]. Even though the system is currently at an early stage, with a first prototype recently being completed and initial *in vitro* experiments being carried out, both the robot mechanics and registration technique present novel attributes. The robot, illustrated in Figure 2.8, is a master/slave system capable of autonomous motion, as well as direct surgeon interaction. The system, which has been designed for femur cavity machining, is mounted on a custom built fixture, also used for registration purposes.

The distal portion of the femoral cavity is machined in the conventional way, using a manual reaming process, which centres the distal end of the cavity relative

to the cortical bone. Then, a reamer shaped registration gauge is inserted in the prepared cavity, aligning the front of the gauge with the direction of the femoral neck, which defines the orientation of the final implant. The base of the custom-built three-degrees of freedom parallel manipulator is then attached to the registration gauge and the remaining machining is carried out using an *admittance display mode* control scheme [Kwon et al., 2001]. The process does not require CT data or pre-operative fiducial markers (Section 2.4.1.2). An overview of the system as a whole has recently been published [Chung et al., 2003].

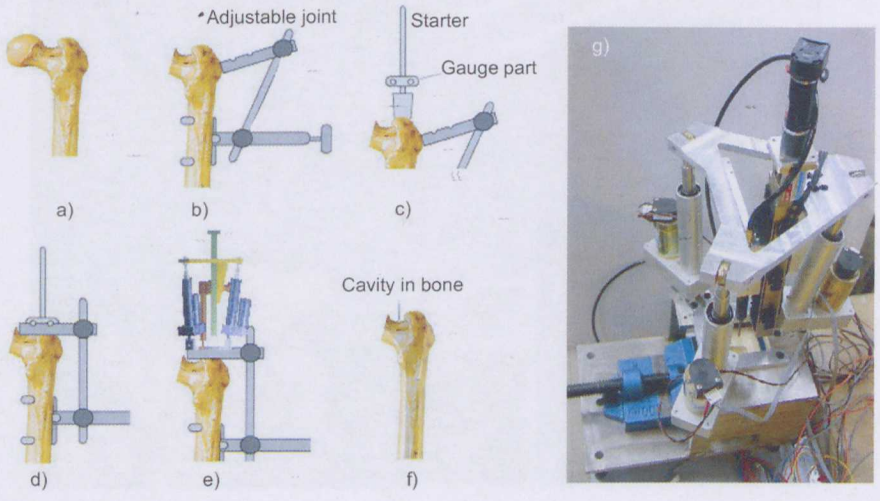


Figure 2.8: Various stages of THA with the Arthrobot system [Chung et al., 2003]. a) The femur is exposed. b) The femoral head is removed, and the frame is attached to the femur, once the hole is made using a manual starter. c) A reamer shaped gauge is inserted into the femur. d) The frame is manoeuvred into place against the reamer-shaped gauge and locked into position. e) The gauge is removed and the robot installed on the frame to machine the cavity in the femur. f) The hole is completed, and the system is removed. g) The Arthrobot system prototype.

2.2.1.5 The CRIGOS System

CRIGOS (Compact Robot for Image-Guided Orthopaedic Surgery) is a compact surgical robotic system used in orthopaedic surgery, being developed at Helmholtz Institute in Aachen [Brandt et al., 1999]. The system is built around a modified Stewart Platform, a compact parallel manipulator with a small working envelope, and a high level of stiffness and accuracy. The CRIGOS system aims to provide semiautomatic image guided positioning of linear tool guides for a number of applications, such as punction of cystic cavities, drilling for ACL-reconstruction, and the fixation of pedicle screws.

BIBL. LONDON UNIV.

A technique for calibrating X-ray images intra-operatively has also been developed to work in conjunction with the robotic system for intramedullary nails fixation in Total Hip Arthroplasty (THA). The CRIGOS system, an early prototype of which is illustrated in Figure 2.9, has successfully completed an initial set of *in vitro* experiments for the specific task of THA, with a more sophisticated robot currently being developed for plastic bone and cadaver trials.

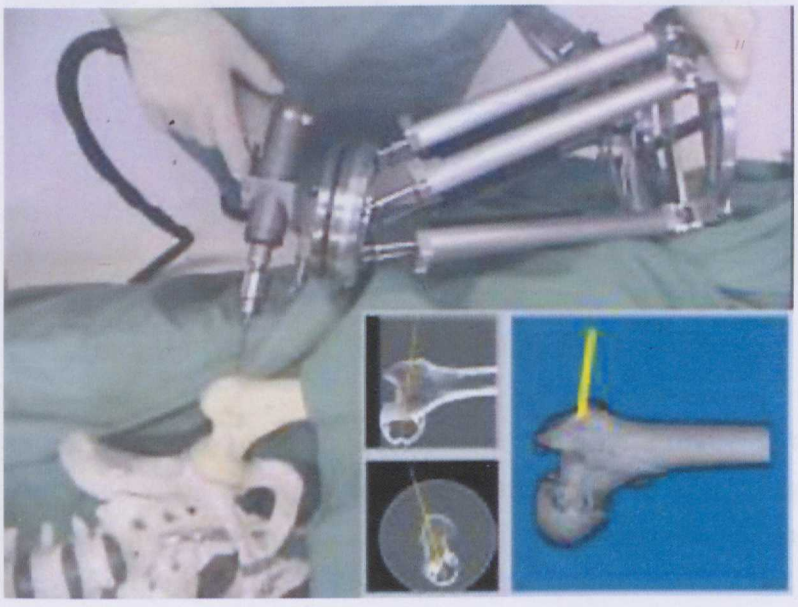


Figure 2.9: The CRIGOS system [Brandt et al., 1999].

2.2.1.6 The MARS System

A MiniAture Robot for Surgical procedures (MARS) system is currently been developed at the *Technion Israel Institute of Technology*. The system, illustrated in Figure 2.10, is being designed for surgical tool guidance during spinal pedicle screw placement, and for drill guiding for distal locking screws in intramedullary nailing. Like the Arthrobot system (Section 2.2.1.4), the MARS system mounts directly onto the spinous process, therefore avoiding the need to rigidly fix the patient to the operating table. MARS is currently undergoing preliminary *in vitro* trials [Shoham et al., 2003], with promising results.

2.2.2 Robots for Minimally Invasive Surgery

As described in Section 6.2, minimally invasive surgery (MIS) offers several advantages over conventional open surgery, and is quickly becoming the new standard for many operations. Advancements in the field of medical robotics and computer aided surgery (CAS) have opened new frontiers in the application of a minimally invasive

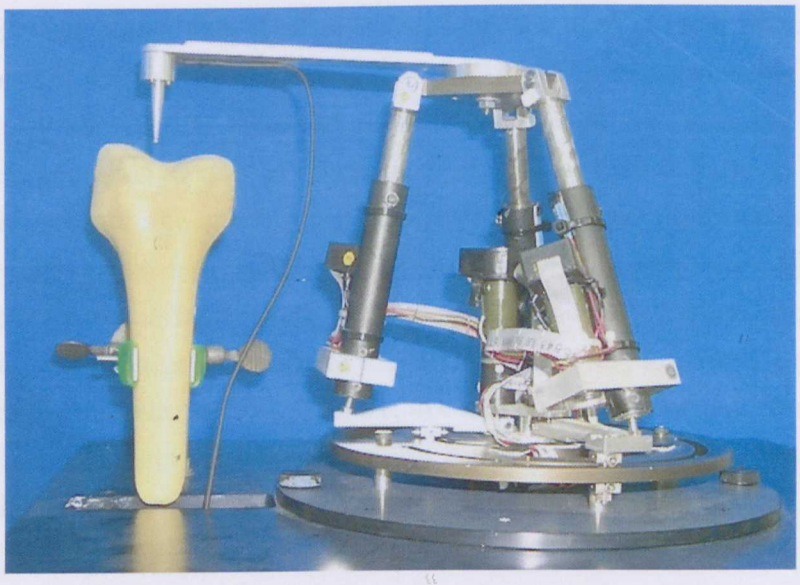


Figure 2.10: The MARS system [Shoham et al., 2003].

approach to surgery. The accuracy and reliability of robots, in conjunction with the advantages associated with image guided and computer integrated surgery (Section 2.3), have proved to be the right combination of technology and human expertise required to apply this approach to many surgical disciplines, including heart surgery, urology, and orthopaedics [Nakamura, 2000].

Restricted vision in the operating theatre, difficult handling of the instruments, heavily restricted mobility, and difficult hand-eye coordination with little or no tactile perception, which are usually associated with an MIS approach, can be successfully tackled with robotic assistance [Dario et al., 2003; Moran, 2003]. As a result, over the past ten years, research centres around the world have generated a number of robotic systems for MIS, some of which are now commercially available, while others are still in the development stage. The following sections briefly illustrate several of the more successful ones.

2.2.2.1 The da Vinci System

da Vinci is a telemanipulator manufactured by Intuitive Surgical Inc., used primarily in minimally invasive heart surgery [Broeders and Ruurda, 2001; Chitwood et al., 2000]. The system is composed of a master console and two slave manipulators. The surgeon is seated at the console, and operates the two slave arms via two master controls situated under the stereoscopic display used to view the operating field in three dimensions. The image is captured by a camera, mounted above the patient, which can be remotely operated by the surgeon sitting at the console. Since the surgeon can visually observe tissue motion intra-operatively, and move the master

to compensate the slave, this type of "open-loop" control is ideal for use with soft tissue, where tool actions continually move the target in unpredictable ways.

As currently the system does not include force feedback from the slave to the master, the surgeon has to rely on visual feed-back alone during surgery. This limitation, which represents one of the main disadvantages of telemanipulators in general, has considerably slowed down widespread adoption of this technology. The da Vinci system has shown to be inadequate when dealing with soft tissues in constant motion, like the beating heart [Jacobs et al., 2003]. However, attempts at providing a "stabilised platform" relative to the heart, are being made to help address this problem. The robot manufacturers have recently initiated a partnership with a group at Imperial College London, in an attempt to provide the da Vinci system with haptics capabilities [Borelli et al., 2004]. The da Vinci system, illustrated in Figure 2.11, has recently completed a number of clinical studies, proving the success of this technology when applied to minimally invasive cholecystectomy [Kim et al., 2002; Gutt et al., 2002], thoracoscopic surgery [Melfi et al., 2002], and radical prostatectomy [Intuitive Surgical Inc., 2002; Menon and Tewari, 2003].



Figure 2.11: The da Vinci system [Broeders and Ruurda, 2001].

2.2.2.2 The Zeus System

The Zeus system (Figure 2.12), originally manufactured by Computer Motion Inc., is in many ways similar to the da Vinci system, and was bought out by Intuitive Surgical Inc. in 2003. The surgeon sits at the master console and carries out the procedure by remotely controlling the slave manipulators, which are mounted next

to the patient. The system also provides force and motion scaling, which have successfully been used in minimally invasive heart and abdominal surgery [Detter et al., 2001; Uranus et al., 2002; Nio et al., 2002]. A number of comparative studies, which focus on the two most successful commercially available telemanipulator systems, da Vinci and Zeus, have been published [Sung and Gill, 2001; Dakin and Gagner, 2003]. Details of hardware and software modifications, which were carried out on the Zeus system to enable its use over large distances, can be found in [Butner and Ghodoussi, 2003].



Figure 2.12: The Zeus system [Nio et al., 2002].

2.2.2.3 The Minerva System

Minerva was a special purpose active robot for neurosurgery, developed at the University of Lausanne [Flury et al., 1992; Glauser et al., 1993]. As illustrated in Figure 2.13, the system is used in conjunction with a dedicated CT scanner for intra-operative imaging. CT data is used to register the patient, and to guide the end effector to a target entry point at the desired position and orientation. The robot then actively inserts a probe and removes tissue from a predefined area of the brain, while the motion is tracked by the system via periodically updated CT images displayed on the intra-operative console. A preliminary study including initial results can be found in [Glauser et al., 1995]. The need for dedication of a CT scanner to the robotic procedure made this an unusual and costly configuration, which has led to its abandonment.

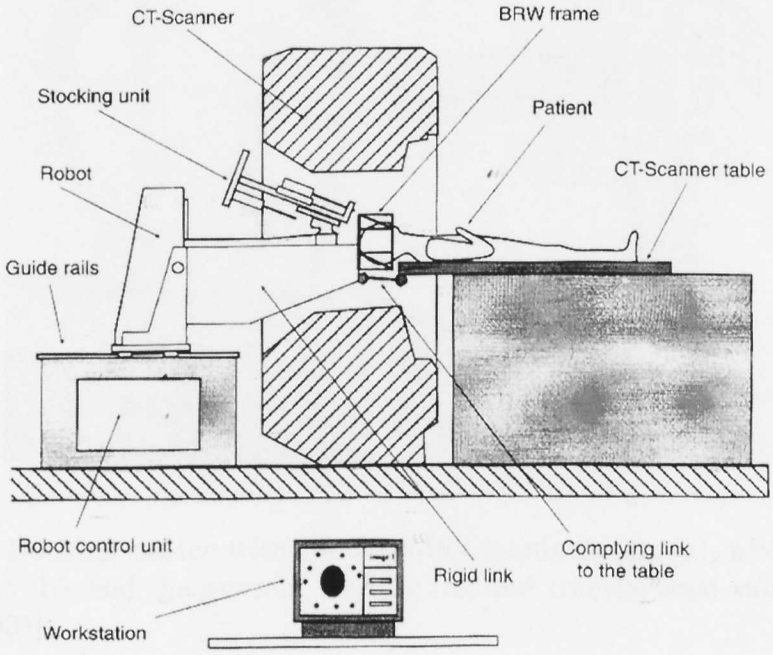


Figure 2.13: The Minerva system [Flury et al., 1992].

2.2.2.4 The EndoBot System

EndoBot is a system for robotic assisted endoscopy, developed in the Center for Automation Technologies, at the Rensselaer Polytechnic Institute, USA [Kang and Wen, 2001]. EndoBot can be used as a stand-alone minimally invasive tool or in pairs, for complex procedures such as stitching and knot tying. The robotic system consists of a four degrees of freedom (DOF) custom built manipulator, with a spherical wrist and a prismatic joint for the in/out motion. As illustrated in Figure 2.14, the system includes a docking station that offers interchangeable end tools for two EndoBot manipulators, and programmable collaboration with the surgeon. It can operate in manual mode, for training and to program desired motions that can then be carried out automatically; under shared control, for computer aided motion e.g. manual motion of one degree of freedom only; finally, it can run in autonomous mode, where it can actively perform operations under the surgeon's supervision. The system is at an early development stage, therefore many of the safety, and clinical issues have not been addressed yet.

2.2.2.5 The AESOP System

AESOP (Automated Endoscopic System for Optimal Positioning) is a commercially available system manufactured by Computer Motion Inc. [Miller, 1988]. Like the EndoAssist system described in Section 2.2, AESOP, illustrated in Figure 2.15, is

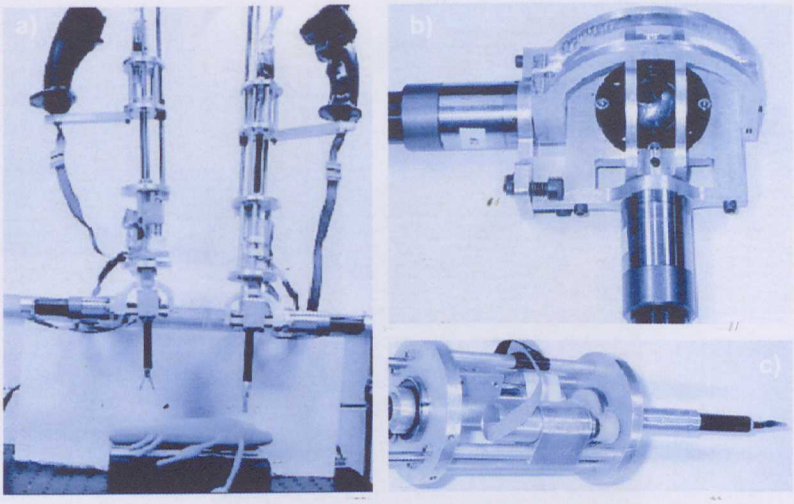


Figure 2.14: Docking station with two EndoBot manipulators (a), with a close-up of the arch joint (b), and the assembly for the roll and translational motion (c) [Kang and Wen, 2001].

a passive manipulator with powered joints, used to drive and hold an endoscopic probe at a predefined position and orientation. The motion can be activated by hand, voice control, or a foot-pedal. A comparative study between AESOP and EndoAssist has also been published [Ballester et al., 2001].

2.2.2.6 The Probot System

Probot is a special purpose robot developed at Imperial College London for transurethral resection of the prostate (TURP) [Harris et al., 1997a; Mei et al., 1996]. First developed in 1987, Probot was the first autonomous medical robotic system to actively remove tissue from a patient (April 1991), and remains one of the few systems for active resection of soft tissue to have successfully completed clinical trials. Even though TURP can be performed manually with good and repeatable results, the procedure is repetitive and tiring for the surgeon, and robotic assistance seemed a valuable alternative.

Probot, illustrated in Figure 2.16, utilises a gross positioner (passive) and a specially designed (active) four DOF spherical manipulator, with a conical working envelope to ensure safe and predictable behaviour. The tissue of the enlarged prostate is resected by performing a series of small circular cuts with a diathermy, which follow a pre-operative plan. Clinical trials proved the system could produce repeatable results that were comparable to those of an experienced surgeon.



Figure 2.15: The AESOP system [Miller, 1988].

2.3 CAS Systems in Orthopaedics

Section 1.1 described the main advantages of CAS systems over conventional techniques. This section provides a brief overview of some of the most successful image guided navigation systems for orthopaedics surgery.

As described in Section 2.2.1, the natural stiffness and hardness of the skeletal system provide a solid frame work for referencing and guidance in image guided surgery. As a result, many of the CAS systems commercially available on the market have focused on orthopaedic and brain surgery, by providing imaging and tracking facilities for knee surgery [PI Precision Ltd., 2002; Ellis et al., 1999; Aesculap, 2002], total hip arthroplasty (THA) [Levison et al., 2000; Aesculap, 2002], spine surgery [Brain Lab GmbH, 2002; Gumprecht et al., 1999; Jaafar et al., 1999], and conventional minimal access brain surgery [Brain Lab GmbH, 2002; Gumprecht et al., 1999; Jaafar et al., 1999]. While the actual training process may take longer for CAS procedures, the quality of outcome and overall success rate achieved by any trainee after proper training can be compared to those of an experienced surgeon. More surgeons can be trained to perform complex procedures successfully, resulting in shorter patient waiting lists, and smaller work load for the more experienced surgeon.

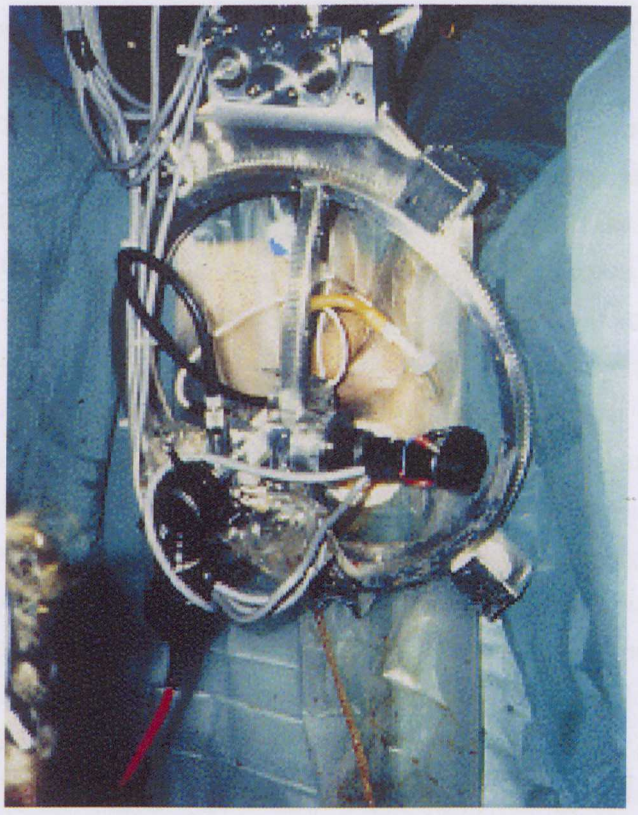


Figure 2.16: The Probot system [Mei et al., 1996].

Virtually all CAS systems in orthopaedic surgery utilise some form of tracking device, for initial registration and intra-operative real-time position update. Today, infrared (IR)-optical digitisers are state of the art. The pioneer, Northern Digital [Northern Digital, Waterloo, Ont., Canada] set precision standards with Optotrak™. The precision of these heavy and expensive digitisers has never been equalled by the more recent optical navigation devices. However, as such high accuracy is rarely required for intra-operative tracking purposes, Northern Digital replaced Optotrak™ with the smaller Polaris™. A very similar system, developed at S. Louis University, is now also commercially available under the label Flashpoint™. All these systems are equipped with line array CCD cameras, and active reflective localisers [Reinhardt et al., 1999].

While Polaris™ and Flashpoint™ tracking equipment lies at the core of many commercially available CAS systems, the software, registration techniques, and tracking algorithms are application and manufacturer specific. One of the most successful systems has been developed and marketed by BrainLab [BrainLab GmbH, Heimstetten, Germany]. The company has recently engineered an infrared-optical digitiser with two plain-image cameras and passive reflective localisers, under the label VectorVision™. As passive markers do not require cabling to connect to the

intra-operative console, this technology offers the advantage of a neater and less cumbersome system, but clinical experience will show whether it can achieve the high accuracy and reliability of existing IR-led-equipped digitisers. BrainLab offers computer guidance for brain, spine, hip, and, recently, total knee replacement surgery [Brain Lab GmbH, 2002; Gumprecht et al., 1999; Jaafar et al., 1999].

Another recently developed CAS system is being developed at the Center for Medical Robotics and Computer Assisted Surgery (MRCAS), Carneige Mellon University, USA [DiGioia et al., 1998]. The Hip Navigation, or HipNav, system has been developed to permit accurate placement of the acetabular component during total hip replacement (THR) surgery. The system consists of three components: a pre-operative planner, a range of motion simulator, and an intra-operative tracking and guidance system. The pre-operative planner allows the surgeon to specify the alignment of the acetabular component within the pelvis, based upon pre-operative CT images. A kinematic range of motion (ROM) simulator determines range of joint motion based upon the specific bone and implant geometry and alignment. Intra-operatively, a tracking system, and feedback display is used to guide the surgeon through the procedure, according to the pre-operative plan. HipNav has successfully undergone a number of clinical trials, with promising results [Levison et al., 2000].

Orthopilot, manufactured by Aesculap Ag & CO, Germany [Aesculap, 2002], is a CAS system for image guided total knee replacement surgery. While the tracking capabilities of the system are similar to those of other commercially available systems, Orthopilot does not require any pre-operative planning, and works without the need for CT data acquisition. The company has produced a novel intra-operative registration procedure able to reconstruct a three-dimensional model of the patient's limb by morphing standard bone anatomy using an interactive acquisition process. The surgeon is prompted to digitise a number of anatomical landmarks defining patient specific anatomical features required for the surgery. The leg is then driven by the surgeon through a range of motions in order to define the mechanical axis passing through the hip, knee, and ankle. Once this phase is completed, the surgeon is guided through the procedure by an intra-operative display. Custom built jigs and fixtures, which are modelled and integrated into the intra-operative software, have also been developed in order to facilitate the surgery. The system has undergone a number of clinical trials in several centres for orthopaedic surgery across Germany [Stulberg, 2001].

Finally, the Galileo Nav and Cas Galileo systems, manufactured by PI Precision Implants Ltd. [PI Precision Ltd., 2002], provide an intra-operative mini-robot that assists the surgeon during the computer assisted procedure. Galileo Nav and Cas Galileo, illustrated in Figure 2.17, do not require a pre-operative CT scan, as image-free registration techniques are used to define the cut positions intra-operatively.

While the CAS system provides intra-operative tracking and visual feedback, the mini-robot, which is actively driven to predefined positions around the knee joint, is used to define the conventional oscillating saw entry points required to produce both the tibial and femoral cuts. Even though the mini-robot acts as a glorified jig, its light and compact architecture have proved appealing to the surgeon. Galileo CAS has been tested in more than 200 operations with promising results.



Figure 2.17: The Galileo Nav and CAS Galileo system [PI Precision Ltd., 2002].

In recent years, CAS systems have become increasingly present in the operating theatre, but their benefit on procedure outcome compared to conventional techniques is still in doubt. As a number of published clinical studies have illustrated the existence of significant outliers in their performance in many orthopaedic applications, CAS is still in the process of gaining acceptance as the definitive solution for consistently accurate surgery.

2.4 Registration

Registration can be defined as the determination of a one-to-one mapping between the coordinates in one space with those in another, such that the points in the two spaces that correspond to the same anatomical point are matched to each other. Registration also means the determination of the mapping operation that can transform one object from its space into the space of the other, whether in two or three

dimensions. When the transformation has been determined, the images are said to be registered. These two images may then be compared or superimposed to give one co-registered image.

Registration is an unavoidable step in virtually any procedure where different data-sets, whether generated by the same technology at different times and circumstances, or by different technology altogether, need to be compared or contrasted. This process is necessary for a number of applications, spanning from diagnostics, and statistical studies, to intra-operative image guidance and robotic assisted surgery [Reinhardt et al., 1999].

2.4.1 Registration Methods

A broad review covering all aspects of registration, and its implementation across different fields is beyond the scope of this thesis. Therefore, a well know classification [Maintz and Viergever, 1998], comprising nine criteria, has been used in an attempt to highlight the area of interest associated with the implementation of a quick and efficient registration procedure suitable for both open and minimally invasive orthopaedic surgery. Where necessary, reference material for a criteria or method relevant to the study has been included. An extended repertory of reference material covering all aspects and available options for each criteria and sub-criteria can be found in the aforementioned paper.

The nine criteria formulated for the classification of all available registration methods are: dimensionality, nature of registration basis, nature of transformation, domain of transformation, interaction, optimisation procedure, modalities involved, subject, and object. A brief evaluation of each criteria in relation to the development of a suitable registration technique is presented in the following sections.

2.4.1.1 Dimensionality

This criterion defines what type of information needs to be registered. A two dimensional (2D) image may need to be registered with a three-dimensional (3D) model; two 2D images may have to be registered against a common co-ordinate system; finally, registration may occur between two 3D images. In the case of orthopaedic surgery, where two sets of bone surface models need to be registered, 3D-3D dimensionality is required, whether the 3D models are reconstructed from 2D slices (CT and ultrasound), or a 3D surface model is generated from a cluster of points in 3D space (point touching schemes).

2.4.1.2 Nature of Registration Basis

Registration methods may be *intrinsic* or *extrinsic*. Extrinsic methods, whether invasive (fiducial marker screws) or non-invasive (fiducial skin markers, molds, etc.), require foreign objects to be introduced into the imaged space. On the other hand, intrinsic methods, such as landmark based, segmentation based, and voxel based methods, are based on the information as generated by the patient.

In orthopaedic surgery in general, and knee surgery in particular, fiducial marker screw based registration has proved to be the golden standard for accuracy, neatness, and speed [Ellis et al., 1997; Ellis et al., 1996]. However, any form of invasive approach is now becoming obsolete, as patient discontentment for the additional operation required to insert the screws pre-operatively has changed perceptions of the advantages of this technique. Therefore, registration methods based on non-invasive approaches have become the only option. Among non-invasive extrinsic methods, several attempts have been made to produce custom built straps that can be repeatedly placed in the same location on the limb. However, the accuracy of such devices is still in doubt, as skin motion, temporary localised swelling, and user misuse may greatly affect the outcome.

Alternatively, landmark and geometrical based intrinsic models can be used to obtain reasonable accuracy while minimising any discomfort to the patient. The acquisition phase, described in Section 2.4.1.6, may vary depending on the technology used. However, the method relies on the surgeon (if an interactive process is used) or the algorithm (if an automatic process is used) to identify sets of corresponding features (e.g. femoral notch, medial and lateral condyles, etc.) or geometries on both images to be registered. The accuracy of the registration outcome usually relies on the accuracy of the acquisition phase, and the reliability of the optimisation technique used (Section 2.4.1.5). One of the most common and widely researched optimisation algorithms associated with rigid body landmark based registration (to which bone registration belongs to) is the Iterative Closest Point (ICP) algorithm [Besl and McKay, 1992].

2.4.1.3 Nature and Domain of Transformations

The "shape" of the registration outcome i.e. the form in which the result is presented and interpreted, depends on the method and application used. *Rigid*, *affine*, *projective*, and *curved* registration forms can be used, but their definition and possible applications are beyond the scope of this description. Virtually all rigid body registration methods require a *rigid* transformation, which is usually presented in the form of a homogeneous transformation matrix, as described in Section 2.6.

A transformation can also be *global* or *local*. If the image is registered as a whole,

such as in the case of knee surgery, the domain is global. In contrast, if subsections of the image each have their own transformation defined, the transformation is defined as local.

2.4.1.4 Interaction

The registration algorithm may require different levels of interaction, depending on the acquisition process and the nature of the application. A *fully automatic* system requires the user to input image data and some initialisation information, and the algorithm automatically reaches a solution after a number of automated computations. Automated registration is usually associated with extrinsic methods, since the marker objects are designed to be well visible and detectable in the images involved. These systems are usually preferred from the user point of view, but need to be extremely fast, and robust if no interaction is allowed.

Semi-automatic systems, while more cumbersome and time consuming, allow for increased robustness and flexibility. Such systems allow the user to adjust parameters, initialise the algorithm, and make corrections as they see fit, considerably reducing the risk of degeneracy. Intrinsic landmark based systems are usually semi-automatic, as the registered image is usually acquired intra-operatively, while supervised by the surgeon. For instance, the presence of osteophytes (outgrowths or excrescences of a bone), which may or may not appear in a poorly segmented CT model (Section 3.3.1), may require the surgeon to make contingent decisions during the data acquisition process, once the bone is actually exposed. The anatomical registration technique described in Section 3.3 belongs to this category.

There are very few examples of *fully interactive* registration procedures, where the user remains in charge of the process at all times, in the literature, and their description is beyond the scope of this study.

2.4.1.5 Optimisation Procedure

The parameters that make up the registration transformation can either be computed *directly*, i.e. determined in an explicit fashion from the available data, or *searched for*, i.e. determined by finding an optimum of some function defined on the parameter space. The latter method is the most commonly used, and is best suited for multi-modal approaches (Section 2.4.1.6), which are of interest to this description.

Many popular searching optimisation methods, for instance Powell's method, Levenberg - Marquardt optimisation, Newton - Raphson iteration, stochastic search methods, etc., have been extensively described in the literature [Hajnal et al., 2001a; Webb, 1988]. However, some registration methods employ non-standard optimisa-

tion algorithms that are designed specifically for the type of approach used. The ICP algorithm, created for rigid-model-based registration, belongs to this category.

Many variations on the ICP algorithm have been implemented over the years from the original paper [Besl and McKay, 1992] describing the concept. Some have optimised the algorithm for robustness [Ma et al., 1999], while others have implemented fast and efficient search engines, and tailored the method for a specific application [Faugeras and Hebert, 1986; Simon et al., 1994; Zhang, 1992; Fadda et al., 1998]. A general review of the various ICP implementations, updated to the year 2000, can be found in [Audette et al., 2000].

Because it can be implemented regardless of the nature of the image data and the application for which it is used, the ICP algorithm has become the preferred optimisation method for intra-operative anatomical registration. Its versatility, computational speed, and ease of implementation have all contributed to its success [Taylor et al., 1996; Hajnal et al., 2001b].

2.4.1.6 Modalities Involved

This criterion highlights the vast amount of techniques and methods that involve registration, ranging from diagnostic, and treatment, to surgical intervention. Four classes of registration tasks can be recognised based on the modalities involved: *mono-modal*, *multi-modal*, *modality to model*, and *patient to model*. In *mono-modal* applications, both images to be registered have been generated using the same technology, for example computer tomography (CT) or magnetic resonance imaging (MRI). Among these are a variety of diagnostic systems, where different images acquired at different intervals or circumstances with the same modality need to be compared and contrasted.

Multi-modal applications involve the registration of two images that have been generated utilising different modalities. An example of this category in medical imaging involves the registration process required to blend MR and CT images for complex procedures. This process is required to adequately visualise both the soft tissue from the former data set, and the hard tissue, which is more evident in the high density CT images.

Modality to model methods involve the registration of images acquired with one modality to be registered against an actual model. These methods can be applied in gathering statistics on tissue morphology, and segmentation tasks, where the acquired image dataset is mapped against models of standard anatomy.

Patient to modality involves the registration of patient specific anatomy with an image acquired using one of many modalities. It is usually associated with intra-operative registration, and radiotherapy, where the actual patient position needs

to be known with respect to a pre-operative or previously acquired image. Even though the acquisition of patient specific information may itself involve the use of a modality, the purpose of the process is to register the patient's position against the model. The two co-ordinate systems to be registered belong to the patient and the modality used to acquire the registration image, respectively. This differs from multi-modal applications, where the two co-ordinate systems belong to the two modalities, irrespective of the patient. As patient to modality methods are mainly used for intra-operative patient registration, this category includes all available options for a registration procedure suitable for robotic assisted orthopaedic surgery.

Given that Acrobot's pre-operative planning currently relies on CT-based images (Section 1.3), viable alternatives for a registration method suitable for the ACROBOT System include CMM-to-CT, Ultrasound-to-CT, Laser-to-CT, and X-Ray-to-CT. The modality used in the pre-operative stage is CT based, while a number of alternatives can be used intra-operatively. Surface data can be acquired in the operating theatre by means of a co-ordinate measuring machine (CMM). A CMM enables 3D points to be measured in a co-ordinate system which is tied to the patient, therefore allowing pre-operative and intra-operative datasets to be co-registered against a common reference frame. CMMs can take the form of mechanical digitisers, such as the FARO arm [FARO Technologies Inc., FL, USA], or the back-drivable end effector of the ACROBOT System (Section 1.3), or optical tracking devices, such as Polaris^{TM} (Section 2.3). Mechanical digitisers are generally more accurate than optical devices, however their restricted workspace can be a limiting factor when access is constrained, which is a key characteristic of MIS. Camera based systems have a large working envelope and are highly dexterous, however expensive and cumbersome sensors and camera systems introduce a significant increase in setup complexity and cost. Line of sight between the camera and markers, which needs to be maintained at all times for appropriate monitoring, represents another significant limitation of this technology.

Ultrasound (US) technology has, in the past few years, shown significant potential as a fast and effective modality for intra-operative data acquisition. Early research in the area of US-based registration appeared in the literature in 1995 [Ault and Siegel, 1995], and consists of an initial feasibility study of intra-operative US image registration of a distal femur against a pre-operative model constructed from CT image slices. US-based registration of bony anatomy has recently been successfully applied in Neurosurgery [Amstutz et al., 2003], and spine surgery [Brendel et al., 2003] with reported results that are comparable to those obtained with more conventional techniques. The developers of the HipNav system (Section 2.3) are also in the process of integrating US technology in their THA navigation software, with preliminary encouraging results [Amin et al., 2003]. US imaging is inexpen-

sive, and compact, and the effects of patient exposure to US radiation is negligible. Furthermore, transcutaneous location of the bone surface by using the beam of a navigated ultrasound probe permits completely noninvasive registration, which is an important requirement for MIS. However, a robust means to improve the poor image quality regarding bones, and to mitigate the high level of noise associated with this modality have yet to be fully identified.

Laser-based registration has been successfully implemented in both dentistry [Alcaniz et al., 1998; Hayashi et al., 2002], and computer assisted endoscopy [Hayashibe and Nakamura, 2001]. BrainLab [Brain Lab GmbH, 2002] has also recently marketed a new technology under the label Z-Touch^{TM}. The technique is based on surface acquisition of anatomical features with a laser beam. It offers considerable advantage over other techniques, including speed, versatility, and ease of use, but is still undergoing trials to assess its robustness and overall accuracy. Furthermore, the technology is applied in brain surgery, where the facial anatomy, which has many unique and extremely visible features, can be used to register the head position intra-operatively. The technology may not be suitable for knee surgery, where most of the anatomy is hidden, and the exposed surfaces are usually covered in soft tissue and debris, which are not present in the CT reconstructed model.

Registration of 3D CT or MR images to 2D X-ray images is particularly difficult, in part because automated contour extraction from 2D images is not yet well solved and in part because of the considerable computational expense in matching the contours to the 3D images. However, X-ray-to-CT registration of fiducial markers has been successfully performed, and has shown encouraging results [Tang et al., 2000]. Tang's work addresses the problem of fiducial registration from a single X-ray image. The algorithm was developed for fast and efficient registration of 3D fiducial locations to the lines cast from the X-ray source to the 2D projective image that is 60 times faster than the ICP algorithm. The algorithm has been tested on fluoroscopic images from portable C-arms [Webb, 1988] and on portal images from a radiotherapy device. This research, while promising, offers a solution for fiducial registration, which is an extrinsic and invasive procedure that no longer represents a long term viable option. At the time of writing, no anatomical registration technique based on intra-operative X-ray image acquisition was found.

2.4.1.7 Subject and Object

When all of the images involved belong to a single patient, such as in the case of intra-operative knee surgery, registration is defined as *intra-subject*. Alternatively, registration is referred to as *inter-subject*, where two images of different patients are registered against a common co-ordinate system, or where the image of a patient is

mapped against a standard anatomical model. The object of registration describes the part of the patient anatomy on which registration is performed, and includes the head, thorax, abdomen, pelvis and perineum, and limbs.

2.4.2 Summary

Criteria	First Subdivisions	Area of Interest
Dimensionality	2D-2D, 2D-3D, or 3D-3D	3D-3D
Nature of Registration Basis	Extrinsic or Intrinsic	Intrinsic and Landmark based (Landmarks if ICP)
Nature of Transformation	Rigid, affine projective, curved	Rigid (as bone reg. involves rigid objects)
Domain of Transformation	Local or global	Global
Interaction	Interactive, semi-automatic, and automatic	Semi-automatic with initialisation supplied
Optimisation Procedure	Parameters computed or parameters searched for	Parameters searched for (e.g. modified ICP)
Modalities Involved	Monomodal, multimodal, mixed, or patient to mod.	Patient to modality
Subject	Intrasubject or intersubject registration	Intrasubject registration
Object	Head, thorax, abdomen, pelvis and perineum, limbs	Limbs (knee surgery)

Table 2.2: Table illustrating the nine classification criteria and relative areas of interest.

Table 2.2 schematically illustrates the result of the survey, which establishes a well defined working envelope for the research. An intrinsic, rigid, patient-to-modality registration technique is required.

After considering the literature for available registration algorithms and technologies, an ICP based technique, using the back-drivable end effector of the ACROBOT System as an accurate CMM for data acquisition intra-operatively, was chosen. As the ACROBOT System can be appropriately calibrated (Section 2.5), extremely accurate readings on the bone surface (better than $0.2mm$ accuracy) can be obtained without the aid of additional equipment. Given the well established track record of the ICP algorithm and its variants across a variety of applications, a fast ICP based method, using a combination of published optimisation techniques, was implemented.

Chapter 3 describes the initial implementation of the ICP algorithm and its integration in the ACROBOT System's intra-operative software. Chapter 5 provides

an overview of the enhancements carried out on the original implementation, to address issues such as execution speed and global minima identification. Although the techniques used to accelerate and improve the performance of the algorithm are known, the development of a robust point touching protocol suitable for both open (Section 5.3.4) and minimally invasive (Section 6.3.1) orthopaedic surgery has never been published.

As described in Chapter 5 and Chapter 6, the registration technique presented has been exhaustively tested through simulations and plastic bone trials. Fiducial marker screws, as well as a novel *reference point-set-based* method (Section 5.4.3.2) have been used to corroborate the experimental results.

2.5 Robotic Calibration

One of the key problems encountered in the use of robots in the medical field is that robots are normally considered to have very good repeatability, frequently fractions of a millimetre, but their absolute position accuracy is considerably worse, sometimes reaching several millimetres [Hidalgo and Brunn, 1998]. As described in Section 3.3.4, a medical knee surgery robot must have very good absolute position accuracy, which *depends on the quality of the manufactured robot and the accuracy of the robot model used for motion control* [Schroeer et al., 1997]. Therefore, in order to maximise the absolute accuracy of a robot, it must be accurately manufactured and assembled and have the most accurate model possible. While the former requirement is manufacturer dependent, an accurate model can be established through a process known as *robotic calibration.*

Robotic calibration is a widely used procedure to compensate for inaccuracies in manufacturing and robotics. There are many different methods of calibration that can be used, as there are many different types of robots and many different applications in which these robots are used. It may not seem immediately intuitive that a robot should have inaccuracies but, no matter how accurately its components have been manufactured and assembled, there will always be some degree of inaccuracy in its function, particularly in robots with many joints and degrees of freedom. Calibration techniques have to overcome two main sources of errors: *geometrical errors* and *non-geometrical errors.* Examples of geometrical errors include: imprecise link lengths, angular offsets due to axis misalignment, and imperfections in the machine axes (i.e., the motions of prismatic and revolute joints are not exclusive from each other). Examples of non-geometric errors include: varying joint compliance due to differing payloads and configurations, backlash, gear transmission errors, base tilt, feedback quantisation errors, cross coupling of joint rotations, and temperature

variations [Young and Chen, 1999]. Clearly these errors are difficult to anticipate or measure.

There are two main types of calibration, *on-line* and *off-line*. During *on-line* calibration the robot is active during the calibration process, and an external calibration device mounted on the robot end effector is usually involved. On-line methods are usually used when local accuracy is required, and the working envelope is small and well defined, such as in the case of automated assembly lines. Many examples of on-line calibration methods have been published over the years, such as laser based [Nakamura et al., 1994] and camera based [Van Albada et al., 1994] on-line calibration, and have shown to be successful in tackling both geometrical and non-geometrical errors. However, there are extremely stringent accuracy requirements for invasive procedures such as knee surgery and, because of this, an on-line method of calibration is not suitable. It is not possible to accommodate for errors once the surgery has begun, since the robot must be very accurate from the first insertion at the beginning of the operation.

Off-line calibration is done while the robot is switched off, and is largely based on corrections to the kinematic equations due to manufacturing errors. This process has inaccuracies and many calibration processes exist to reconcile the differences between the kinematic model and the actual model. Kinematic calibration, however, only calibrates against geometrical errors by *identifying a more accurate geometrical relationship between the joint encoder readings and the actual position of the end-effector; then the robot positioning software is changed according to the relationship identified* [Renders et al., 1991]. A robot that has been well manufactured to tighter tolerances would suffer less from these errors.

Almost all of the kinematic methods begin with using the Denavit-Hartenberg (DH) parameters [Denavit and Hartenberg, 1955] to generate a kinematic model of the robot, and then branch off using a combination of existing methods and their own developments [Chen et al., 2001; Hayati et al., 1988; Hidalgo and Brunn, 1998; Paul and Zhang, 1986]. A co-ordinate measuring machine (CMM) is used to obtain a true reading of the end effector position, which is then compared to the position derived from the model in order for accommodations to be made. CMMs can take many forms, ranging from camera-based tracking systems, such as Optotrak™ (Section 2.3), to mechanised turn tables equipped with high resolution encoders.

The basic principle of any kinematic calibration method, however, remains the same. A kinematic model of the robot is derived, followed by an acquisition phase where pairs of 3D positions are recorded by deriving the position from encoder readings for each axis, and reading the output of the CMM. An off-line calibration process, based on a variety of minimisation algorithms, is then carried out in order for a more accurate set of kinematic parameters (i.e. DH parameters) to be generated.

Even though a variety of literature exists on the subject, including a versatile and comprehensive computer calibration program [Shroer, 1987], during the author's investigation of a new gross positioner for the ACROBOT System, a novel calibration procedure was developed. Based on a well known least-squares minimisation algorithm [Sciavicco and Siciliano, 1996], the procedure takes full advantage of the robot's back-drivability to generate accurate position readings at minimum cost. This off-line kinematic calibration procedure is described in detail in Section 3.2.3.

2.6 Robot Kinematics

Various approaches can be used to analyse a robotic manipulator in order to obtain means to calculate the position of its end effector at any given moment. The most widely spread technique, however, involves an in depth investigation of the kinematics of the mechanism. By definition, kinematics is *the study of the geometry and the time-independent motion of connected links, without consideration about the forces and/or moments that may have produced the motion* [Craig, 1989]. Here, forward and inverse kinematics of the manipulator will be developed to obtain an analytical solution for the end effectors position relative to the joint angles and the link lengths. The steps that must be taken to obtain this solution, with a brief explanation of the techniques used, are described in Chapter 3.

2.6.1 Forward Kinematics

In this stage, the most widespread method involves the use of the Denavit Hartenberg Transformation Matrix [Denavit and Hartenberg, 1955]. To develop this transformation matrix, one should start by considering any manipulator characterised by a series of movable links. These are physically connected at specific joints, with each link capable of either rotational (revolute) motion about or transitional (prismatic) motion along a single joint axis. The general link depicted in Figure 2.18 can be used to illustrate the procedure.

From successive steps involving the analysis of such a system with respect to its kinematics behaviour, the following matrix can be found:

$$T_{i-1}^{i} = \begin{bmatrix} cos\theta_i & -sin\theta_i & 0 & a_{i-1} \\ sin\theta_i cos\alpha_{i-1} & cos\theta_i cos\alpha_{i-1} & -sin\alpha_{i-1} & -sin\alpha_{i-1} d_i \\ sin\theta_i sin\alpha_{i-1} & cos\theta_i sin\alpha_{i-1} & cos\alpha_{i-1} & cos\alpha_{i-1} d_i \\ 0 & 0 & 0 & 1 \end{bmatrix} \quad (2.1)$$

where:

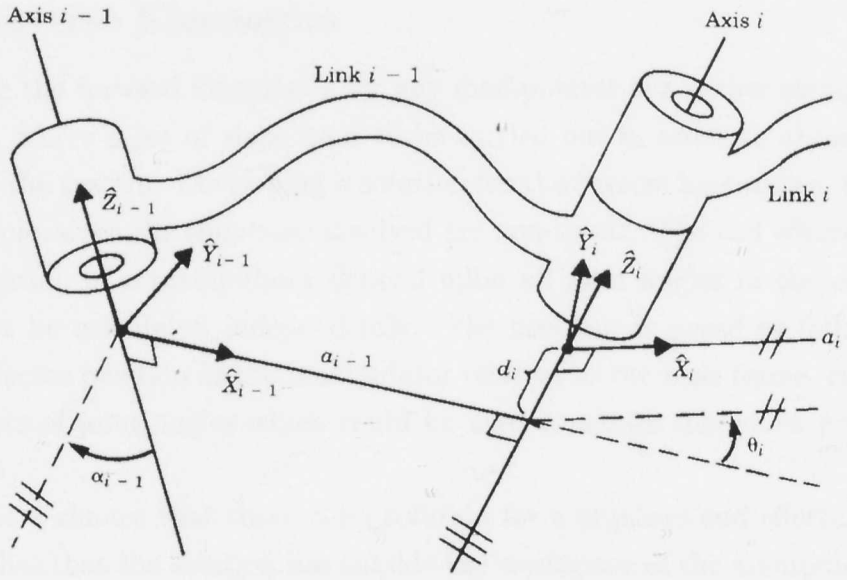


Figure 2.18: DH convention for affixing frames to links [Craig, 1989]

a_i is the distance from $\widehat{Z}_{i-1}$ to $\widehat{Z}_i$ measured along $\widehat{X}_i$.

α_i is the angle between $\widehat{Z}_{i-1}$ to $\widehat{Z}_i$ measured about $\widehat{X}_i$.

d_i is the distance from the origin of frame $\{i-1\}$ to $\widehat{X}_i$ measured along $\widehat{Z}_{i-1}$.

θ_i is the angle between $\widehat{X}_{i-1}$ to $\widehat{X}_i$ measured about $\widehat{Z}_{i-1}$.

This matrix is known as the D-H transformation matrix, and a, α, d and θ are the DH parameters. The matrix contains all the necessary information to fully define any link in relation to the following and succeeding ones. It can therefore be used to obtain an analytical solution for the forward kinematics of a mechanism. Once the link frames have been defined, D-H parameters will be found for every link in the open chain. The individual link transformation matrices can then be multiplied together to obtain the single transformation matrix which relates the first and last frames of the given mechanism. This operation can be schematised as follows:

$$T_1^n = T_1^2 \cdot T_2^3 \cdot \cdots \cdot T_{n-1}^n \tag{2.2}$$

Where n is the number of links in the open chain and T_k^j describes $\{j\}$ relative to $\{k\}$.

This matrix specifies how to compute the position and orientation of the last frame relative to the first (or fixed) frame of any robot. Further details can be found in [Craig, 1989; Paul and Zong, 1981; Sciavicco and Siciliano, 1996; Wolovich, 1987]

2.6.2 Inverse Kinematics

Developing the forward kinematics for any manipulator is a rather straightforward procedure, where a set of steps have to be carried out in order to obtain the D-H matrix for the system. Developing a solution for the inverse kinematics, however, is not as simple, since the equations involved are non-linear. The end effector position and orientation of a manipulator depend upon all joint angles in the open chain, and cannot be calculated independently. The problem is posed as follows: given the end effector position of the manipulator relative to the base frame, calculate all possible sets of joint angles which could be used to attain this given position and orientation.

There is a chance that there is no solution for a required end effector position, which implies that the solution lies outside the workspace of the manipulator. Also, the presence of singularities, which are special configurations where a manipulator loses one or more degrees of freedom, need to be dealt with. In such configurations there is some direction (or subspace) along which it is impossible to move the end effector, no matter which joint rates are selected.

Finally, the issue of multiple solutions needs particular attention, since there might be more than one set of orientation angles for each link that produce the required position of the end effector. A method for selecting the one solution that is required (e.g. the solution which minimises the distance travelled by the arm to reach the required position) needs to be established.

Two general approaches can be adopted when working on the inverse kinematics of a manipulator. One can either try to establish the relationship between the end effector position and the joint angles required to produce it via a *direct solution* or by means of a *computational solution.* In the former case, some general analytical formulae, which are required to define links orientations relative to the last frame position, will have to be developed using the D-H transformation matrix obtained for the forward kinematic model. With a computational solution, the high performance speed of computers is fully utilised by establishing an iterative procedure, which produces the required solution over a number of cycles. In such circumstances, a way to quantify the difference between the present solution and the required solution, and a fairly good initial estimate, have to be established.

2.7 Conclusion

This chapter has described some of the techniques and technologies associated with this research. The growing field of medical robotics has been broadly reviewed, and specific examples of robotic systems for orthopaedic surgery, and minimally invasive

surgery have been presented. The benefits of Computer Aided Surgical systems, supported by a number of examples of successful implementations, have also been described in an attempt to justify the need for visual feed-back and user interaction for complex surgical procedures. Finally, the critical aspects of registration and calibration have been reviewed as an aid for the research carried out on the ACROBOT System, which is presented in detail in the following chapters.

Chapter 3

ACROBOT - A Hands-On Robotic System for TKA

3.1 Introduction

By the time the author started researching into the field of active constraints in orthopaedic surgery, the ACROBOT System, in the embodiment illustrated in Figure 3.1, had successfully undergone preliminary plastic bone and cadaver trials [Davies et al., 1999b; Harris et al., 1999; Davies et al., 1999a].

However, two critical aspects of the system had to be addressed in order for a prototype suitable for clinical use to be implemented: gross positioning and registration. This chapter focuses on early research carried out on the original ACROBOT prototype, which led to the first clinical application of the system for seven robotic assisted total knee arthroplasty (TKA) procedures. More specifically, research described in the following sections includes an investigation of the critical aspects of gross positioning and registration, with the development of novel techniques aimed at improving accuracy and safety, in order to realise a system suitable for clinical use. Section 3.2 describes the integration, and subsequent calibration, of a new gross positioner with the ACROBOT System, while the development of an anatomical registration technique suitable for open surgery is presented in Section 3.3.

3.2 Gross Positioning System Integration

The greatest challenge for the design of a GPS is to balance the need for a highly stiff and accurate system, with the necessity for a light and mobile structure, which also has a minimal footprint and a sense of aesthetic appeal. In the original ACROBOT System prototype, the four DOF manipulator illustrated in Figure 3.1, with linear actuators for the three translational axis and an exceptionally stiff revolute joint to

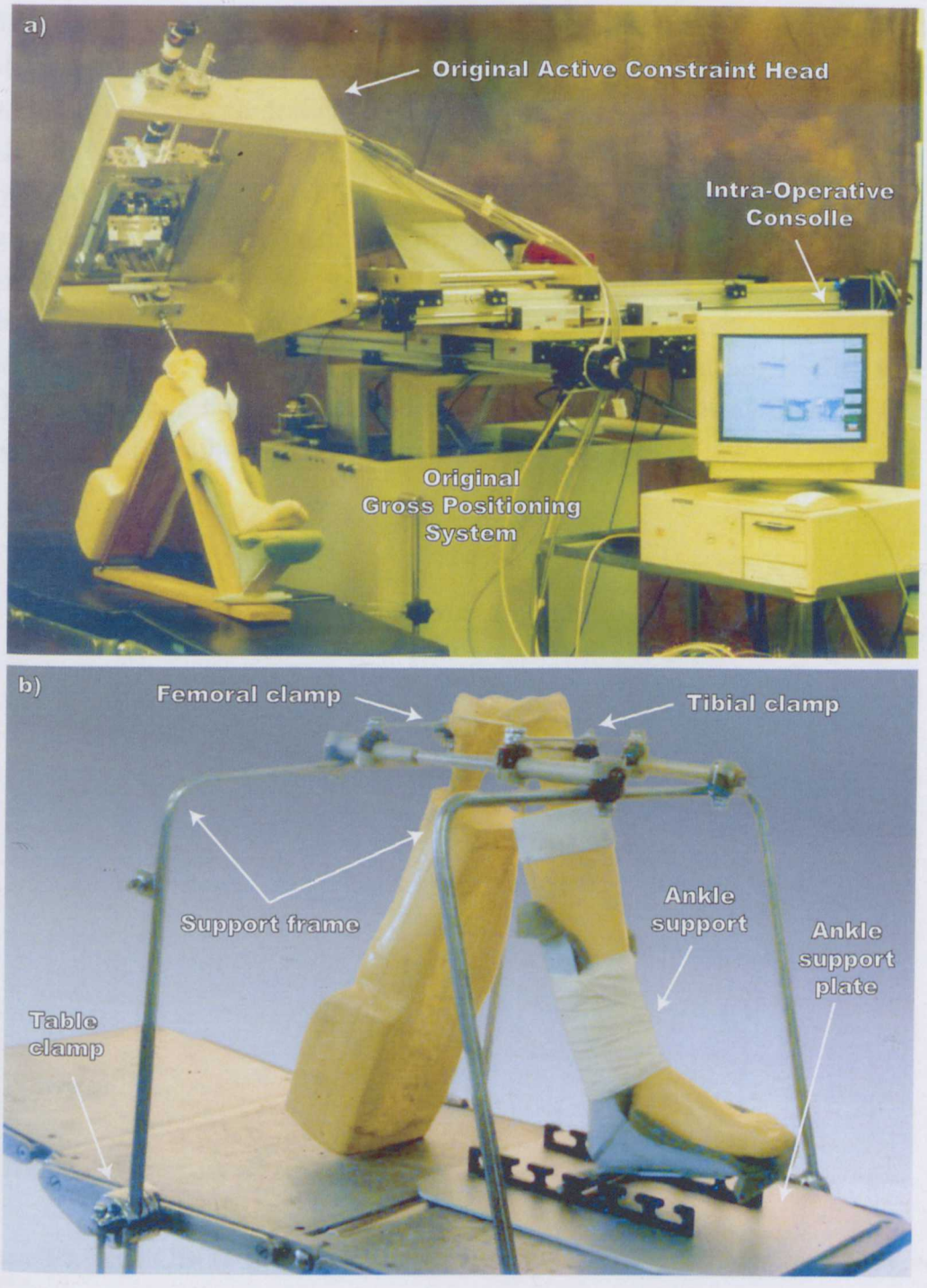


Figure 3.1: Preliminary ACROBOT System concept demonstrator (a), and original clamping system (b) used for early plastic bone and cadaver trials [Jakopec, 2001].

provide for the *roll* motion, was used. Although *The Tank*, named after its appearance, fulfilled all requirements for stiffness and accuracy, it could be argued that its appearance would not appeal to the surgeon, due to its extremely large footprint and intrusiveness. Furthermore, the tank was not designed and manufactured in conformity to the medical devices directive [EEC, 1993], which would prevent it from being used in a clinical environment.

In order to turn the concept demonstrator described in [Jakopec, 2001] into a system suitable for clinical use, a new gross positioner was integrated with the original active constraint head. The aim was to ensure the GPS would be safe for clinical use, and would provide sufficient positional accuracy for a hands-on robotic assisted procedure. The robot is an Armstrong VM,which is a six degrees of freedom serial manipulator, developed by Armstrong Healthcare [Armstrong Healthcare Ltd., UK] in accordance with the safety specifications required for a *"Class 1"* medical application [EEC, 1993].



Figure 3.2: ACROBOT System with the Armstrong VM gross positioner (in green)

The robot, illustrated in Figure 3.2 as an integral part of the ACROBOT System, was delivered with a fully enclosed control system and a communication protocol to be accessed via the serial port. However, the development of an entire library of functions that would interface the intra-operative workstation to the robot was required. This became the initial objective of the study.

In order to provide the user with the required functionality, and obtain the desired accuracy within the working envelope of the system, several steps had to be carried out by the author. The communication protocol needed to be designed and implemented, while also maintaining the existing programming style and modular architecture of the intra-operative software. The robot characteristics needed to be investigated, in order to produce an adequate kinematic model for the system. A workspace analysis had to be performed in order to assess the actual working envelope within which the knee could be placed for the TKA procedure to be carried out successfully. Finally, the entire mechanism, comprising the VM and AC Head, had to be accurately calibrated for the system to reach the required positional accuracy, which originally needed to be well within 0.5mm. A brief description of each one of these aspects can be found in the following sub-sections.

3.2.1 Modelling the VM Robot

After an initial assessment of the robot was carried out, it was decided that the implementation of the internal control software provided by Armstrong Health-care Ltd. was not suitable for complex Cartesian motion around the patient, due to the lack of adequate safety critical software features. Therefore, it was assumed that only smooth and reliable joint motion would be provided by the enclosed controller, which nonetheless would avoid the need for the implementation of a sophisticated dynamic model. Joint readings would be read-in via the serial port, then processed and converted, using the forward kinematics model, into Cartesian co-ordinates in the form of homogeneous transformation matrices. Conversely, required Cartesian motions would be converted, by means of the inverse kinematics model, into joint co-ordinates to be passed back to the robot.

The first stage of this study by the author was to develop the complete kinematic model for the ACROBOT System, which would then provide the grounds for both calibration and workspace analysis. Given that the Gross Positioning System was provided in a calibrated state, which guaranteed accuracy of the tip of its end-effector, it was decided to opt for a two stage approach, developing separate models for each of the two components. This would also enable each aspect to be replaced without affecting the other.

By correctly specifying all of the robot parameters and developing a complete and reliable model, it is always possible to bound the motion of the robot in Cartesian space in a predictable and repeatable way, which is an indispensable requirement in medical robotic applications. As described in Section 2.6, the DH convention for affixing frames to links was used to derive the kinematics of the ACROBOT System. Initially, only the six joints of the VM robot were considered, in order

to isolate gross positioner related functions into a self contained module. Then, however, a complete model of the system, including GPS and AC Head, had to be implemented for calibration purposes, as will be described in Section 3.2.3.

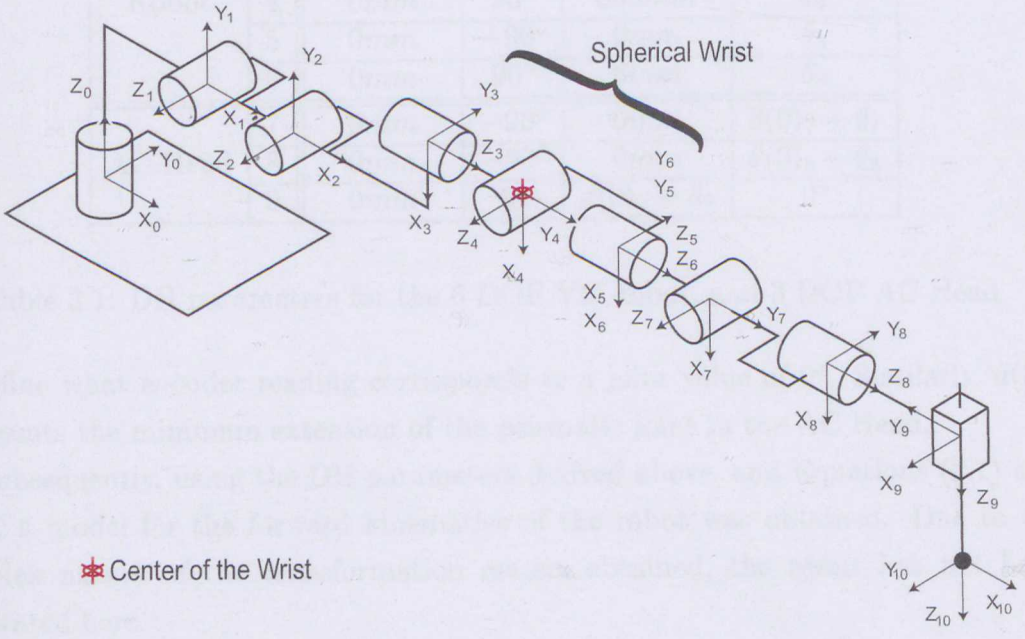


Figure 3.3: Kinematic model for the ACROBOT System, comprising both the VM robot and AC Head.

Figure 3.3 provides a schematic representation of the ACROBOT System, where the first six revolute joints belong to the VM robot, and the last three (Revolute-Revolute-Prismatic) to the AC Head. For the VM robot, theoretical values for each parameter were chosen by following the robot's specification sheet, and two main assumptions were made in order to proceed. First, all joints were assumed to be either parallel or perpendicular to each other, and secondly it was assumed that the axes passing through the last three joints intersected at a common point. Both of these assumptions had to be made in order to obtain a solution for the inverse kinematics of the robot, as will be illustrated in the following paragraphs. Furthermore, it was decided that the distance between the origin of the VM wrist and that of the AC Head should be regarded as one, rather than split at the mounting interface. In other words, the distance between the centre of the VM's wrist and the end effector (i.e. the end of joint six), namely d_6, was considered to be equal to the distance between the VM's wrist and the AC Head's centre. Section 3.2.3 provides further details.

Using the simple rules described in Section 2.6.1, the four DH parameters for each link, illustrated in Table 3.1, were obtained. $\theta(0)_i$ represents the home (or zero) position for joint angle i. This variable was used during calibration (Section 3.2.3)

	i	a	α	d	θ
VM Robot	1	$150mm$	90°	$475mm$	θ_1
	2	$350mm$	0°	$0mm$	θ_2
	3	$-135mm$	-90°	$0mm$	$-90^o + \theta_3$
	4	$0mm$	90°	$350mm$	θ_4
	5	$0mm$	-90°	$0mm$	θ_5
	6	$0mm$	90°	$6mm$	θ_6
AC Head	7	$0mm$	-90°	$0mm$	$\theta(0)_7 + \theta_7$
	8	$0mm$	-90°	$0mm$	$\theta(0)_8 + \theta_8$
	9	$0mm$	0°	$d(0)_9 + d_9$	0°

Table 3.1: DH parameters for the 6 DOF VM robot, and 3 DOF AC Head.

to define what encoder reading corresponds to a joint value of 0°. Similarly, $d(0)_9$ represents the minimum extension of the prismatic joint in the AC Head.

Subsequently, using the DH parameters derived above, and Equations (2.1) and (2.2), a model for the forward kinematics of the robot was obtained. Due to the complex nature of the transformation matrix obtained, the result has not been illustrated here.

As opposed to the forward kinematics, solving for the inverse kinematics of a robot is not a straightforward task. In the case of a six DOF robot, one would have to solve a system of highly coupled and non-linear equations containing a combination of the six joint variables θ_1 to θ_6 for the six parameters defining a position in three-dimensional space, namely X, Y, and Z for position and α, β, and γ for orientation. Mathematical techniques have been devised to simplify these equations, but realistically it would prove almost impossible to solve for the inverse kinematics of a completely *general* 6 DOF robot.

Therefore, many robots available on the market have adopted a configuration similar to the one originally developed for the Puma 560® [Craig, 1989; Wolovich, 1987]. Having six DOF, these types of robots have complete freedom of movement in their subspace, while maintaining a finite number of solutions for each Cartesian position required (i.e. *non-redundant*). However, these robots are designed in a way that allows the position and orientation of the end effector to be controlled independently of each other. The axis of the three orientational degrees of freedom, often referred to as the *yaw*, *pitch* an *roll*, meet at a common point called the *origin*, producing what is known as a spherical wrist. Such a configuration allows the inverse kinematic task to be separated in two steps:

- Finding joint angles for the last three links, namely the *roll, pitch* and *yaw*, which will produce the desired end effector orientation.

- Finding joint angles for the first three links, which will produce the

desired position of the centre of the wrist, directly related to the end effector position for a given orientation (i.e. using the result of the previous step).

In such a way, a direct solution for the inverse kinematics of a six DOF manipulator with a spherical wrist can be developed using highly simplified trigonometric relationships.

As can be seen in Figure 3.3, the VM robot belongs to this category of serial manipulators. Therefore, the aforementioned two-stage approach was used to derive the inverse kinematic model for the VM robot, and was optimised for speed by following a well known technique that minimises the number of computations required for each conversion [Paul and Zhang, 1986]. Once again, due to the complex nature of the generated equations, the outcome has not been included here.

3.2.2 Workspace Analysis

Any GPS will provide a unique working envelope for the placement of the centre of the AC Head. In turn, this will determine the envelope constraining the position of the knee with respect to the robot, once in the operating theatre. Therefore, an accurate estimate of the workspace of the GPS can make the difference between success and failure during surgery. If this knowledge is not acquired pre-operatively, there is a chance the robot will be placed outside the reach of one or more of the bone cutting positions.

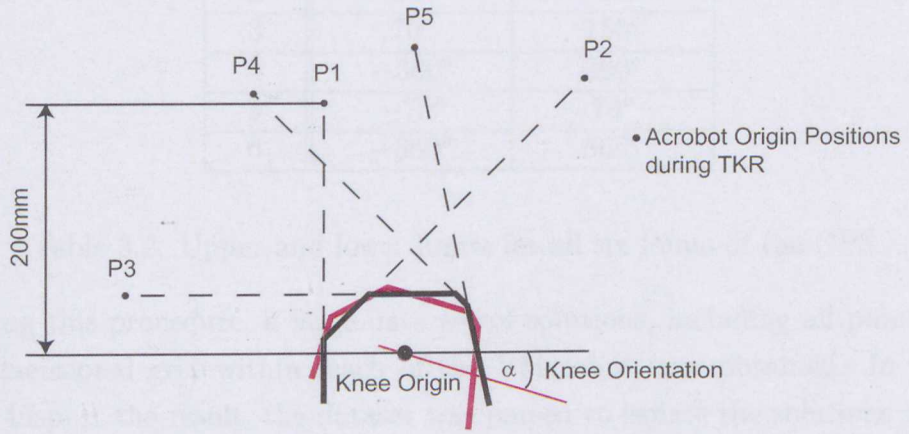


Figure 3.4: ACROBOT head origin positions for the five femoral cuts.

Figure 3.4 illustrates the five AC Head's origin positions required to complete all femoral cuts during TKA with the optimised cutting effort and surface finish. In this simplified model, the origin is placed on the plane of each cut, 200mm away from the centre of the knee. Therefore, working backward by following the diagram

in Figure 3.3, five corresponding positions for the centre of the VM wrist were obtained. An algorithm was then developed using *MatLab*^{TM}V. 6.0 [MathWorks Inc., 1998] mathematical test-bed to obtain a three-dimensional grid covering the entire workspace of the GPS. The X, Y, and Z parameters were linearly incremented, one at a time, in order for all possible combinations to be covered by the program. Furthermore, the grid was tested for different values of the angular variable α in Figure 3.4, which defines the orientation of the knee that was supposedly set during the clamping procedure. It was assumed that the variation of the other two angular components affecting the orientation of the knee could be discarded.

The Inverse Kinematics (IK) model derived in Section 3.2.1 was used to obtain corresponding joint angles for each point on the grid. Of the set of solutions recorded (i.e. those points for which a solution for the IK did exist), only those meeting the following constraints were chosen:

- Right-hand, upper-elbow solutions [Craig, 1989].
- Only solutions where all joint values lay within the upper and lower limits as illustrated in Table 3.2.

The joint limits were defined by Armstrong Health-care Ltd. as a result of the physical constraints imposed by the additional covers that were provided as an aid to sterility.

Joint	Lower Limit	Upper Limit
1	-150°	150°
2	20°	-130°
3	70°	150°
4	-360°	360°
5	-70°	70°
6	-360°	360°

Table 3.2: Upper and lower limits for all six joints of the GPS.

During this procedure, a large data set of solutions, including all points in the three-dimensional grid within reach of the VM robot, was obtained. In order to visually inspect the result, the dataset was parsed to isolate the solutions which lie on the boundaries of the working envelope. The co-ordinates of these solutions were then converted into polar co-ordinates for display purposes. Figure 3.5 illustrates the working envelope for the knee origin position at 0° and 15° angles.

A close investigation of these results allowed a protocol for the TKA procedure setup to be adequately defined. As a result, it became possible to ensure the GPS would always be fixed to the operating table in a position that would allow all cutting configurations to be reached successfully.

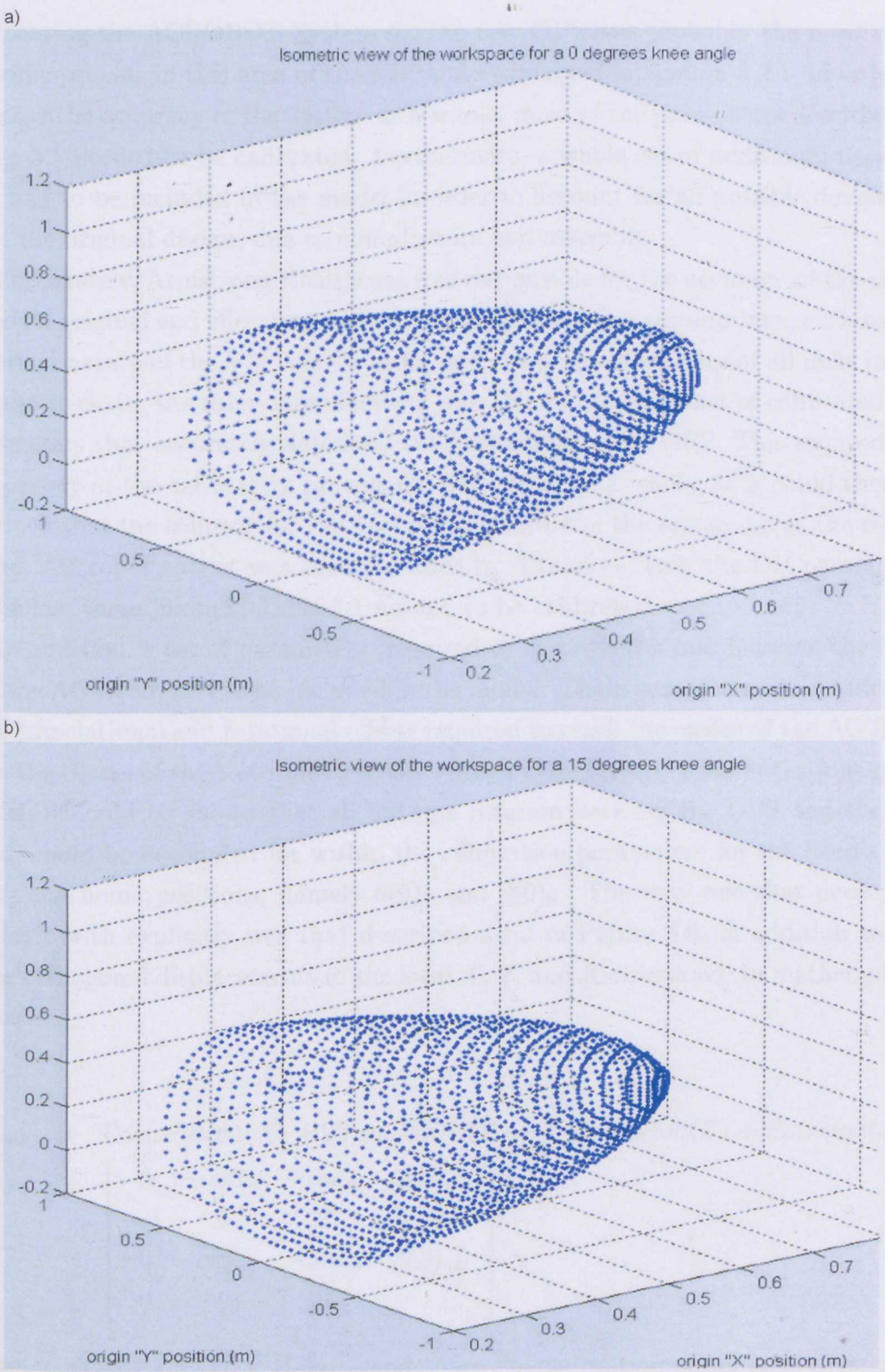


Figure 3.5: Placement constraints for the knee joint origin w.r.t. the VM robot base co-ordinate system for an orientation of 0° (a), and 15° (b) from the vertical axis.

3.2.3 Calibration

Calibrating the ACROBOT System for the new GPS was probably the most cumbersome process in this area of the study. As explained in Section 3.2.1, in order to increase the accuracy of the system as a whole, most of the parameters described in Table 3.1 needed to be calibrated. Furthermore, a whole set of additional parameters had to be included in the model in order to account for all possible deviations from the original design, due to manufacture and assembly.

Fortunately, Armstrong Healthcare was responsible for the accuracy of the robot up to its original end effector position. Having made a few assumptions, such as the spherical nature of the VM robot's wrist, and the perpendicularity of all links in the kinematic chain, the robot manufacturer was able to provide a list of calibrated DH parameters that accurately described the kinematics of the GPS. This reduced the complexity of the calibration process for the system as a whole, as it could then be assumed that the solution for the forward kinematics of the system up to the centre of the VM robot's wrist was accurate already. Therefore, only the DH parameters of the last three joints in Table 3.1 needed to be calibrated.

In addition, a set of parameters, required to describe the *link* between the GPS and the AC Head, had to be included in the model. These parameters would include both translational and rotational offsets required to reach the centre of the AC Head from the centre of the VM robot's wrist. After a close investigation of the kinematic model, it could be shown that all but one rotation between the GPS and the AC Head would be accounted for within the calibration parameters for the head's *yaw* and *pitch* home positions, namely $\theta(0)_7$ and $\theta(0)_8$. The only one that needed to be dealt with explicitly was that described as ω in Figure 3.6, in addition to the three orthogonal displacements in the local X, Y, and Z directions. In mathematical terms:

$$\begin{aligned} T_{Link} &= Translation(X) + Translation(Y) + Translation(Z) + Rotation(X) \\ &= \begin{bmatrix} 0 & -sin\omega & -cos\omega & X_{Offset} \\ -1 & 0 & 0 & Y_{Offset} \\ 0 & cos\omega & -sin\omega & Z_{Offset} \\ 0 & 0 & 0 & 1 \end{bmatrix} \end{aligned} \tag{3.1}$$

where X_{Offset}, Y_{Offset}, Z_{Offset}, and ω are the calibration parameters illustrated in Figure 3.6. Since local offsets were applied, the rotation due to ω revolves around the x axis. By comparing Figures 3.3 and 3.6, it is clear that the desired rotation affects the x axis of the co-ordinate system affixed to the sixth joint.

Considering the VM robot as the base co-ordinate system, and using the con-

vention defined in Section 2.6.1, a model of the entire kinematic chain can be summarised as follows:

$$P_{VM} = T_{VM} \times T_{Link} \times T_{ACH} \times P_{ACH} = T_{VM}^{ACH} \times P_{ACH} \tag{3.2}$$

where:

P_{VM} is the position of a point (x,y,z co-ordinates) in VM base co-ordinates.

T_{VM} defines the forward kinematics of the VM robot, having set the value for d_6 temporarily equal to zero (as illustrated in Figure3.6, this parameter coincides with the *calibration* parameter Z_{Offset}).

T_{Link} is the homogeneous matrix in Equation (3.1).

T_{ACH} defines the forward kinematics of the AC Head, derived in the same way as described in Section 3.3 for the GPS.

P_{ACH} is the position of a point in ACROBOT head space.

T_{VM}^{ACH} defines the AC Head end effector frame in relation to the VM robot base co-ordinate frame.

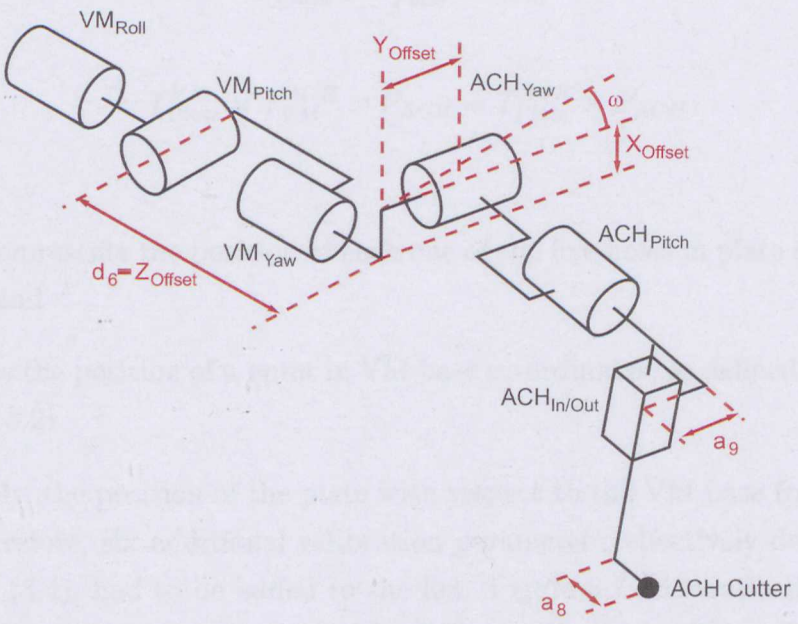


Figure 3.6: Calibration parameters for the ACROBOT System.

3.2.3.1 Method

For the calibration process, a well known least squares technique was used [Sciavicco and Siciliano, 1996]. However, changes had to be made to the usual calibration procedure, due to the lack of a suitable Co-ordinate Measuring Machine (CMM) on the premises. Conventionally, a CMM is used to precisely measure the effective motion of the robot, in order to acquire a set of corresponding points in both joint and Cartesian space. A "least-squares" solution is then applied to the data set in order to derive the best fit for the calibration parameters i.e. the calibration parameters that will produce the closest correspondence between the Cartesian points obtained by applying the Forward Kinematics (FK) model to the measured joint space data set, and the actual position readings from the CMM.

In order to overcome the lack of a CMM, an accurately machined plate was used (Figure 3.7). Firstly, five holes were drilled into the plate at known locations. The plate was then measured and modelled in order to obtain a set of five Cartesian positions for each hole in local co-ordinates i.e. the hole co-ordinates relative to the plate. Finally, the kinematic model in Equation (3.2) was modified in order to transform the plate co-ordinates into VM base co-ordinates, and vice versa. In mathematical form:

$$P_{Plate} = T^{VM}_{Plate} \times P_{VM} \tag{3.3}$$

$$= T^{VM}_{Plate} \times T^{ACH}_{VM} \times P_{ACH} = T^{ACH}_{Plate} \times P_{ACH} \tag{3.4}$$

where:

P_{Plate} represents the position of each one of the five holes in plate co-ordinates, and

P_{VM} is the position of a point in VM base co-ordinates, as defined in Equation (3.2).

Unfortunately, the position of the plate with respect to the VM base frame was not known. Therefore, six additional calibration parameters, effectively defining T^{VM}_{Plate} in Equation (3.4), had to be added to the list. Figure 3.7 schematically illustrates the six additional parameters required to fully specify the position of the plate in three-dimensional space. An initial estimate for each parameter was derived by inspection.

The objective function to be minimised was then:

$$\min(\Delta X) = \min\left(\left(T^{ACH}_{Plate} \times P_{ACH}\right) - P_{Plate}\right) \tag{3.5}$$

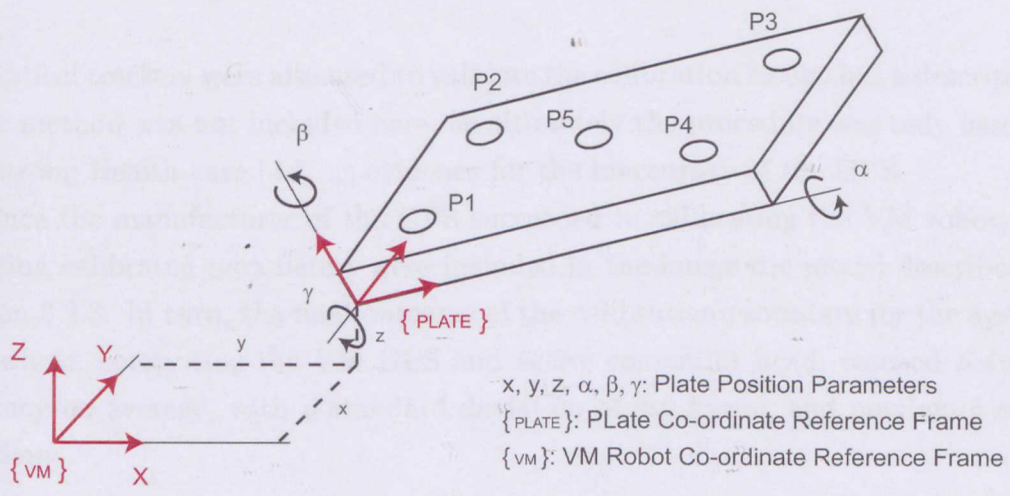


Figure 3.7: Calibration plate, and relative parameters.

Therefore, during the least squares minimisation algorithm, the transformation matrix T^{ACH}_{Plate} in Equation (3.5) was partially differentiated with respect to each one of the final set of calibration parameters schematically illustrated in Table 3.3 until convergence was reached.

Parameter Type	Parameter List	Initial Estimates
AC Head	a_8, a_9, α_2, $\theta(0)_7$, $\theta(0)_8$, $d(0)_9$	0, 0, -90°, 0, -90°, 70
Link	X_{Offset}, Y_{Offset}, Z_{Offset}, ω	0, 0, 260, 0°
Plate	x, y, z, α, β, γ	Derived by inspection

Table 3.3: Final set of calibration parameters for the ACROBOT System.

3.2.3.2 Results

The algorithm behind the method devised in Section 3.2.3 was fully implemented in Maple™ V. 6 [Waterloo Maple Inc., 2000], a problem solving environment that offers interactive mathematical visualisation.

The calibration process was repeated on several occasions, every time taking a minimum of 80 readings of the plate position (each of the five holes) for different GPS configurations. Unfortunately, sensible results were only obtained towards the end of the year, as considerable amount of time was "lost" due to the inaccuracy of the GPS itself. Even though it was initially assumed that the VM robot was accurate to the agreed specification, extensive testing revealed that the theoretical parameters specified by the manufacturer required additional calibration. The period of time spent trying to solve the GPS accuracy problems resulted in the development and implementation of the patented block registration procedure described in Section

3.3.4.

Optical trackers were also used to validate the calibration result, but a description of the method was not included here, as ultimately the procedure was only used by Armstrong Health-care Ltd. as evidence for the inaccuracy of the GPS.

Once the manufacturer of the GPS succeeded in calibrating the VM robot, the resulting calibrated parameters were included in the kinematic model described in Section 3.2.3. In turn, the final outcome of the calibration procedure for the system as a whole, comprising the VM GPS and active constraint head, reached *0.4mm*[1] accuracy on average, with a standard deviation of $\approx 0.25mm$, and maximum error of *1.5mm*.

3.3 Anatomical Registration for TKA

Once the integration process between the ACROBOT System and the VM gross positioner was successfully completed, work had to be carried out in order to improve upon a crucial element of any robotic assisted procedure, *Registration*. As outlined in Section 2.4, this well established technique can be described as the determination of a one-to-one mapping between the coordinates in one space with those in another, such that the points in the two spaces that correspond to the same anatomical point are matched to each other. In any robotic assisted application that involves planning, the relationship between the modelled space, where the procedure is planned, and the robot's workspace, where the procedure is executed, needs to be established. Identifiable features, such as fiducial marker screws or anatomical landmarks (Section 2.4.1.2), are first extracted from the model and then "sensed," or located, in the operating theatre. This process provides the system with enough positional information for the modelled space and robot's workspace to be *registered* against a common co-ordinate system. Assuming no unforeseen intra-operative anomalies, such as undetected bone motion or system malfunction, the surgery can then be accurately carried out according to the plan.

In the ACROBOT System, the three-dimensional model used during the planning stage to identify the position and size of the bone cuts, and the location of the 2.5D AC boundaries [Jakopec, 2001, Chapter 2.5] is defined in a unique reference co-ordinate system, namely $\{PLAN\}$. However, the robotic assisted procedure is carried out in a global co-ordinate system attached to the base of the gross positioner, namely $\{BASE\}$. Therefore, before surgery can commence, a relationship between

[1] Accuracy is defined as the average distance:

$$d = \sqrt{(P_x - Pa_x)^2 + (P_y - Pa_y)^2 + (P_z - Pa_z)^2}$$

where P is the calculated position and Pa is the actual position.

these two co-ordinate systems needs to be established, so that:

$$P_{BASE} = T_{Reg} \times P_{PLAN} \tag{3.6}$$

where:

P_{BASE} is a point in the robot base co-ordinate system.

P_{PLAN} is a point in the 3D model space generated from CT data.

T_{Reg} represents the relationship between the two co-ordinate systems, and can be rewritten as T_{VM}^{PLAN}.

The transformation matrix T_{Reg} in Equation (3.6) represents the outcome of the registration process, where the correctness of the stated relationship will directly affect the final accuracy of the robotic procedure.

Prior to the author's involvement in the project, a registration method using fiducial markers was used for early trials, performed on plastic phantoms and cadavers [Harris et al., 1999]. This involved placing 4 marker screws prior to taking a CT scan of the leg. The markers represent 4 corresponding non-colinear points in the pre-operative (the marker centre is detected in the CT images) and robot's co-ordinate systems (the marker is touched by the tip of the robot intra-operatively), from which the transformation T_{Reg} can be computed. As this method requires an additional surgery to implant the markers, it was regarded as unacceptable for clinical trials.

The following sections focus on the development of a non-invasive registration technique suitable for robotic assisted TKA, to be used for early clinical trials with the ACROBOT System. After a careful study of the various registration techniques described in Section 2.4, *anatomical registration*, based on anatomical similarities between the two surfaces to be co-registered, proved to be best suited for the proposed task. It is non-invasive, as it does not require fiducial markers, and can make full use of the "robotic advantage" described in Section 2.4.2.

3.3.1 Planning and Execution Issues for Registration

During the pre-operative planning stage, the size and fit of both the tibial and femoral components of a knee joint prosthesis are chosen for a specific bone model, which is obtained by digitising a patient's limb by means of a CT scanner [Webb, 1988]. However, the dataset obtained by scanning the leg first needs to be processed and "labelled" in order for the surgeon to be able to adequately plan for the procedure on screen. This technique is known as *segmentation*, and allows a single dataset

containing the information for the limb as a whole to be split into the various knee components, having isolated the bone from the surrounding soft tissue.

This procedure is computationally expensive and requires considerable human input, as it is often difficult to distinguish between bones for a heavily arthritic knee. In some instances, it can prove impossible to differentiate between osteophytes at the interface between the femur and tibia and actual bone.

Furthermore, the quality of the segmentation outcome may be compromised by the presence of *artefacts* in the dataset, which are often generated by the existence of metal in or around the patient. A previously implanted prosthesis on the other knee or a hip, for instance, may cause the rays generated by the CT scanner to bounce off the reflective surface of the components, creating "noise" in the surrounding image slices. As a result, the shape of the generated 3D model may differ slightly from the actual bone, which may affect accuracy during the registration procedure.

Once a TKA procedure has been adequately defined pre-operatively, the generated plan, containing information about the bone model and the constraint boundaries, is transferred to the intra-operative workstation. The intra-operative software has to process two supposedly similar "objects," the first loaded on screen and the other exposed on the operating bed. However, initially the relationship between the virtual and the actual surfaces is unknown. It is the objective of the registration process to provide this missing link, thus enabling the surgical procedure to be carried out according to the pre-operative plan.

During the initial phase of the surgery, the knee joint is exposed, and the tibia and femur are both firmly immobilised to the operating bed by means of custom designed clamps [Jakopec, 2001, Chapter 3.6]. As mentioned in Section 2.4.1.6, optical tracking technology allows for real-time update speeds that would enable motion of individual bones to be monitored continuously during surgery. However, optical trackers require the use of expensive and cumbersome sensors and camera systems, which would add to the overall system's complexity and cost unnecessarily. Therefore, a rigid link between the knee bones and the robot is established by means of the clamps, ensuring the knee joint *will not* move with respect to the ACROBOT base co-ordinate system. Following early clinical experience with the system, motion detection facilities have subsequently been integrated into the clamping system in order to ensure this assumption remains true throughout the procedure (Section 4.4.2).

Once exposed, the knee joint needs to be carefully prepared, removing any soft tissue, such as meniscus or cartilage, from the bone. This is necessary because the reconstructed 3D model does not contain any information about the soft tissue surrounding the bone. Care must be taken not to damage the posterior cruciate and collateral ligaments, as they should be preserved during TKA. Large osteophytic

deposits should also be preserved, as they might not have been removed from the model during the segmentation process.

However, even in optimal working conditions, some soft tissue that is scattered unevenly on the surface of the bone alongside osteophytic residues, will remain. This will directly affect the outcome of the procedure, since, during anatomical registration, the similarity between corresponding features is directly proportional to the resulting mapping accuracy.

All of the above represent critical aspects affecting registration accuracy in most orthopaedic surgical procedures, however their effect becomes more evident as the amount of surface available for registration decreases. Extensive experimental and clinical testing has proved that anatomical registration based on the ICP algorithm described below is suitable for open surgery, where the knee anatomy can be fully exposed. However, the challenges presented by minimally invasive registration, which became necessary once unicompartmental knee arthroplasty (Chapter 6) was investigated further, ultimately resulted in the design and implementation of the novel registration algorithm described in Chapter 7.

3.3.2 The Iterative Closest Point Algorithm

After a careful study of the registration techniques described in Section 2.4.1.5, it was decided an Iterative Closest Point (ICP) algorithm should be used [Besl and McKay, 1992; Faugeras and Hebert, 1986; Fitzpatrick et al., 1998; Ma et al., 1999; Simon et al., 1994]. In brief, ICP is a general purpose algorithm that can be used to register 3D shapes that are mapped in different co-ordinate systems. One of the advantages over other techniques is that it can be shown to always converge monotonically to the closest local minimum. Therefore, given an adequate set of initial conditions and a sufficiently accurate dataset, the algorithm will produce the desired solution, and should always converge.

From a computational point of view, registration does not differ from the calibration procedure described in Section 3.2.3 as, here too, a minimisation algorithm is used to find the closest correspondence between two data sets over a number of iterations. Given a set of points measured on an actual surface, the ICP algorithm allows the best fit to be found between these points and the model. The flow chart illustrated in Figure 3.8 summarises the main steps of the registration process based on the ICP algorithm, which was implemented as a self contained class in C^{++} and integrated into the intra-operative software.

As can be seen, the algorithm requires an initial transform, T_I, defining a rough estimate of the relationship between the two surfaces. T_I is computed by defining a set of initial registration points, or landmarks, on the 3D model of the knee joint

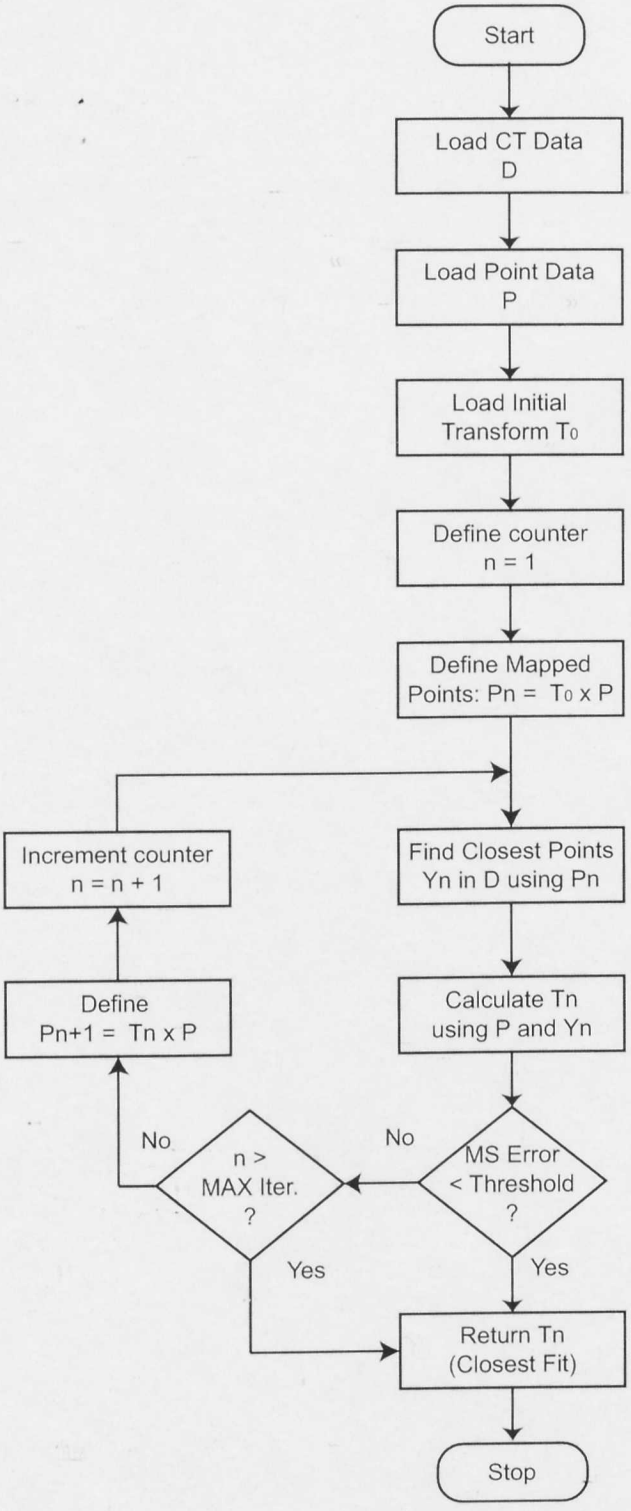


Figure 3.8: ICP Registration flow diagram.

during the pre-operative planning stage. In order to obtain an initial estimate, those same landmarks are identified on the actual knee during surgery, by moving the back-drivable AC Head's end effector to the desired position on the bone. This procedure provides the control software with a minimum of three sets of corresponding points, which are used to estimate a value for T_I. Unique anatomical features on the bones are generally chosen, as they are easier to recognise in the operating theatre.

P_I represents a set of points measured along the surface of the bone, and is assembled using the same procedure defined to acquire the landmarks. As the registration method implemented is based on anatomical correspondences, the characteristics of P_I are important. Defining the appropriate point distribution and point-set size for a specific task is not straightforward, as poor point collection may result in a drastic degeneration of accuracy, which is difficult to detect intra-operatively, as no absolute measure of performance is available. The definition and validation of a robust point acquisition protocol for two specific operations, namely TKA and UKA, are presented in Chapter 5 and Chapter 6 respectively.

Finally, D represents the bone model dataset generated from CT data during the pre-operative planning stage. It is stored in the form of a triangular mesh describing the surfaces of the femur and tibia, and represents the object surface points to which the intra-operatively defined points are registered. D contains all of the modelling inaccuracies, such as segmentation errors, described in the previous section.

The closest point search, which is described in greater detail in Section 5.3.1, is used to define a set of corresponding points for the current iteration, which, in turn, is used to find the next registration estimate. The set of closest points (P_C) on the modelled surface, and the set of probe points (P_I) are used to generate T_N by means of a well known minimisation algorithm [Horn, 1987; Horn, 1991], which was implemented as a self contained C^{++}class, and is also used to generate the initial registration estimate (T_I) from the paired points obtained through landmark identification.

The algorithm converges to a solution after a number of iterations, which can vary as a result of the reliability of the initial estimate and the quality of the CT image. As shown in Figure 3.8, the condition for success is defined by the mean square error of the sum of the distances between each mapped point and the CT surface. If the error does not change between successive iterations, a local minimum has been reached. However, the algorithm will also drop out after a maximum number of iterations, defined in software.

The basic ICP algorithm described above has shown to be adequate for the task through extensive simulations and experimental trials. A formal description of the validation process, including several algorithm and protocol enhancements which have resulted from early clinical experience with the ACROBOT System [Jakopec

et al., 2001; Jakopec et al., 2003c; Jakopec et al., 2003b], is included in Chapter 5.

3.3.3 Registration in the OR

The author's registration algorithm described above became an integral part of the intra-operative software for the ACROBOT System. With this arrangement, the existing display could be used as the foundation for the graphical user interface (GUI) guiding the surgeon throughout the registration procedure. The GUI is not the author's work, but has been included here for illustrative purposes.

In the initial stage of the registration procedure, the GUI displays the landmarks defined pre-operatively, one at a time, in order for the user to be able to recognise and touch the corresponding point on the actual bone. Once all landmarks have been obtained, an initial registration RMS error is calculated. As long as the value obtained is reasonable (i.e, less than 1.5cm), the user can proceed with the surface point acquisition phase.

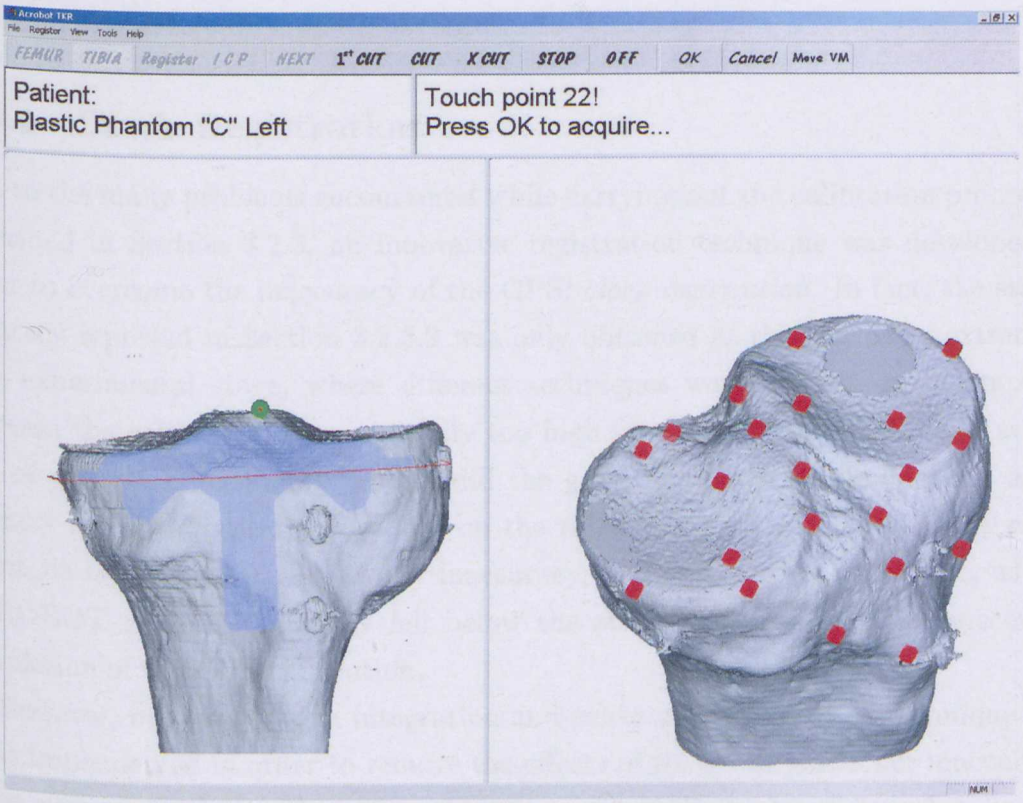


Figure 3.9: Snapshot of the intra-operative software display of the tibia during registration. The red circles represent the position of the points touched with respect to the 3D model, based on the current registration transform.

Figure 3.9 provides a snapshot of the intra-operative software display, as the surgeon is prompted to acquire points on the surface of the tibia. As can be seen, a

total of 21 points, evenly spaced across the surface of the bone, have already been stored by the user. This number of points and their distribution is usually enough to obtain a reasonable registration accuracy. However, the outcome of the procedure is strongly dependent on the quality of both the 3D model, and the actual bone preparation.

If the first run of the algorithm does not provide the desired accuracy, the result is set as the initial estimate for the next iteration, and the point touching procedure has to be carried out once again. Early experimental results, carried out before the algorithm enhancements presented in Chapter 5 were implemented, have shown that an average of two runs of the registration algorithm are required to achieve the desired accuracy, typically when both the 3D model and bone preparation are of an acceptable standard. The surgeon can also visually inspect the outcome by comparing the position of the AC Head registration tip with its virtual counterpart, an example of which is displayed in green in Figure 3.9. As described in Section 3.3.5, the final registration accuracy may differ between procedures, depending on the setup, model quality, and bone state.

3.3.4 Block Registration

Due to the many problems encountered while carrying out the calibration procedure described in Section 3.2.3, an innovative registration technique was developed in order to overcome the inaccuracy of the GPS: *block registration.* In fact, the stated accuracy reported in Section 3.2.3.2 was only obtained at the end of an extremely long experimental stage, where different techniques were used in an attempt to decrease the calibration error, initially too high for the task at hand. Only at the end of this time consuming process did the gross positioner's manufacturer agree to carry out a calibration procedure on the robot alone. It seemed the VM robot might be the cause for the system inaccuracy, and this proved to be true, as the ACROBOT System's accuracy fell below the stated requirement after successful completion of the GPS calibration.

However, between system integration and calibrating the GPS, a technique had to be implemented in order to remove the effects of the gross positioner inaccuracy. After a careful investigation of tracking systems available on the market, it was decided that the "tracking" approach could be used while replacing the conventional means of a tripod mounted infra-red camera with the *robotic advantage.* Despite the inaccuracy of the GPS, which directly affects the final accuracy of the system as a whole, the AC Head is individually calibrated to the desired level of accuracy. Therefore, shifting the position of the robot's base co-ordinate system from the base of the GPS to the base of the AC Head would remove the GPS from the accuracy

loop (see Figure 3.10).

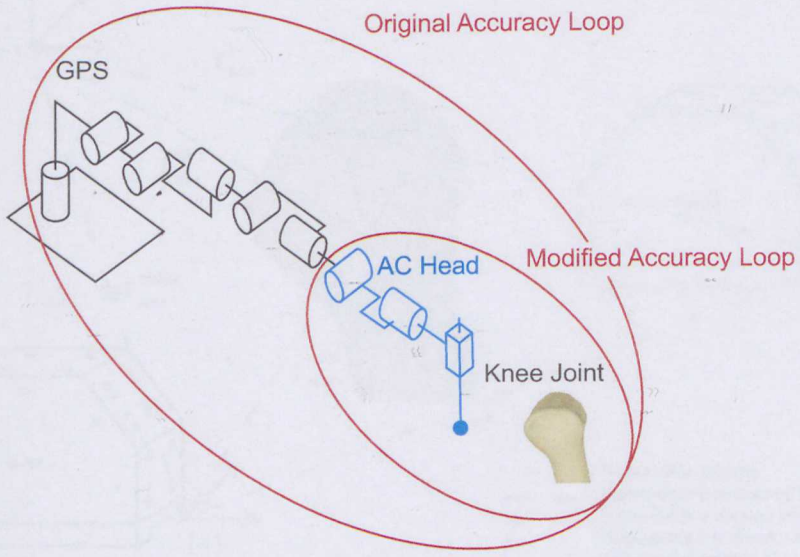


Figure 3.10: ACROBOT System accuracy loop.

When mentioning accuracy, it is worth distinguishing between *placement* accuracy and *positional* accuracy. In the case of the ACROBOT System, the former relates to the ability to place the AC Head in a desired location accurately. This requirement can be less stringent, since a small placement error (in the order of 1mm) can be accommodated for by the redundant joints in the AC Head. The latter, however, describes how accurately the position of the end effector can be read. This represents a much tighter requirement because, while the first type of inaccuracy can be quantified if the positional accuracy meets the requirements, the opposite does not apply. Accurate positional information allows any placement error to be quantified and compensated for. However, if the measured position is inaccurate, accurate placement becomes impossible, as a means to quantify the error is no longer available. Therefore, changing the location of the base/global co-ordinate frame, would allow most of the effects due to the inaccuracy of the GPS to be overcome, greatly improving the positional accuracy of the ACROBOT System as a whole.

Block registration only requires a point touching probe and a set of accurately machined holes on a surface/surfaces that will not move in relation to the object that needs to be registered. It can be applied in different ways, with different means, and different purposes. However, since a general technique has already been described in the relevant patent produced [The Acrobot Company Ltd., 2001], the following explanation refers to hardware and software modifications required to add *block registration* functionality to the ACROBOT System.

Two accurately machined blocks were used to host the holes required for this technique. The blocks were securely locked to the clamping device designed for

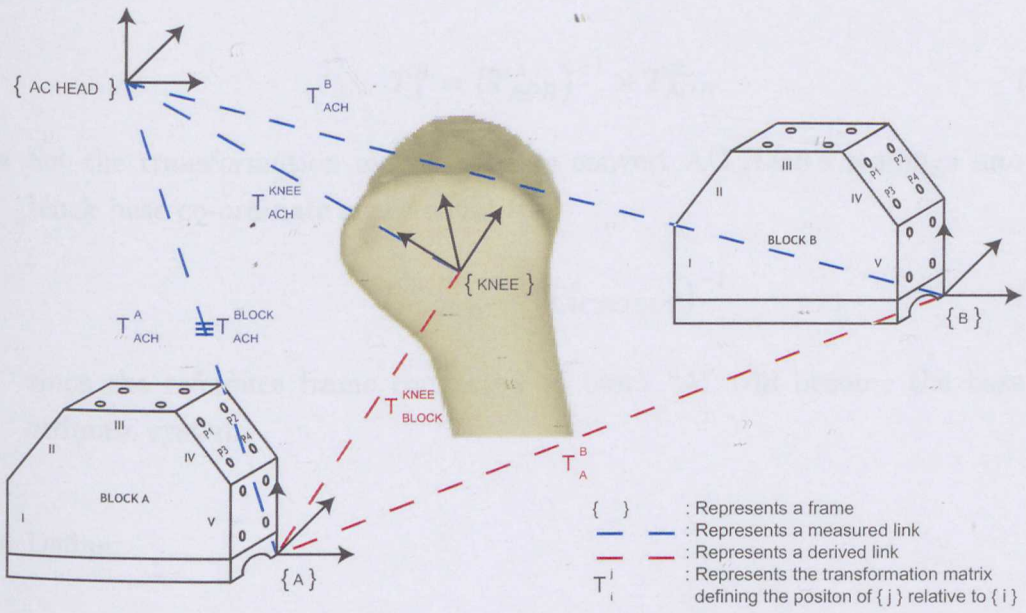


Figure 3.11: Block touching technique.

the ACROBOT System [Jakopec, 2001, Chapter 4.2], in a position that would be accessible by the AC Head at all times during surgery. The design included five surfaces at different inclinations, with four accurately machined holes on each one. This would ensure at least four holes would be accessible for any orientation of both the AC Head and the knee. Four holes provide three points, the minimum required to define a three-dimensional location, with a spare fourth point for error correction through redundancy. Figure 3.11 diagrammatically illustrates the blocks' position relative to the knee. The clamping system has not been included in the figure, as its design and appearance lies beyond the scope of this description.

The blocks were accurately measured and modelled in software, utilising a small Co-ordinate Measuring Machine (CMM) available on the premises. This ensured that the shape and location of all planes would be known once the location of a minimum of four conical locating holes was defined in the operating theatre. In other words, once four holes are located during registration, the position of the entire block is automatically known and can be used during surgery. Using Figure 3.11 as reference, the block registration technique can be summarised as follows:

- Define T_{ACH}^{KNEE} by using the registration technique described in Section 3.3.3. Since the GPS is assumed to be unreliable, all points on the bone surface have to be touched *without* moving the GPS.

- Define T_{ACH}^{A} and T_{ACH}^{B} by touching at least one plane on each block with the registration tip connected to the end effector of the AC Head.

- Define:

$$T_A^B = \left(T_{ACH}^A\right)^{-1} \times T_{ACH}^B \tag{3.7}$$

- Set the transformation matrix used to convert AC Head's readings into the block base co-ordinate space equal to:

$$T_{BLOCK}^{ACH} = \left(T_{ACROBOT}^A\right)^{-1} \tag{3.8}$$

since the reference frame connected to block "A" will become the base co-ordinate system.

- Define:

$$T_{BLOCK}^{KNEE} = T_{BLOCK}^{ACH} \times T_{ACH}^{KNEE} \tag{3.9}$$

- Every time the GPS is moved, T_{BLOCK}^{ACH} needs to be recomputed by touching a minimum of four points on either block. If a point on the "B" block is touched, it will simply be converted as follows:

$$P_{BLOCK} = T_A^B \times T_{BLOCK}^{ACH} P_{ACH} \tag{3.10}$$

since, once again:

$$T_{BLOCK}^{ACH} \equiv T_A^{ACH} \tag{3.11}$$

As a result, the entire procedure is carried out using the block base co-ordinate system as the reference frame for the cuts defined in the pre-operative plan, eliminating the GPS from the accuracy loop. As the position of the bone cuts is defined relative to the BLOCKS, the motion of the GPS is calculated backward, and is relative to the position of the knee. Therefore, even though the placement accuracy is affected by the gross positioner's inaccuracy, positional accuracy is maintained. Both the resolution of the calibrated AC Head, and the accuracy of the point-touching technique, which would affect positional accuracy, have been shown to be well within the requirements for this type of surgery, enabling the registration procedure and successive motions to be carried out successfully.

3.3.5 Results

Once the registration algorithm was implemented and integrated into the intra-operative software, a substantial number of tests was carried out in order to validate

the accuracy and reliability of the procedure. Initially, plastic bone trials were performed, followed by a set of clinical trials, in which the ACROBOT System was used to perform a number of TKA procedures.

A first set of tests made use of the point based registration technique described in Section 3.3.4. However, once the accuracy issues concerning the GPS were addressed, and the full potential of the *robotic advantage* described in Section 2.4.2 could finally be unleashed, block registration was replaced by the conventional technique i.e the complete kinematic chain was used to obtain accurate positional information about the knee and the AC Head's centre during the six cuts necessary for TKA.

Results obtained for registration with and without blocks, for both experimental and clinical tests, are comparable, which suggests block registration successfully addressed and overcame the inaccuracy of the GPS. Formal validation of the registration algorithm implemented for the ACROBOT System, through simulations and plastic bone trials, is presented in Chapter 5. This chapter also outlines the intra-operative protocol developed for the specific task of TKA. A description of the results obtained during the first clinical application of the system for seven TKA procedures can be found in [Rodriguez y Baena et al., 2002; Jakopec et al., 2001; Jakopec et al., 2003c; Jakopec et al., 2003b], which have been included in Appendix H.

3.4 Discussion

This chapter has described early research carried out in the areas of gross positioning and registration. Both the VM gross positioner and AC Head were successfully modelled and calibrated. A registration method based on the well known ICP algorithm was defined, implemented, and integrated into the intra-operative software. Block registration was implemented in order to overcome the inaccuracy of the GPS. The technique was successful, allowing the team to carry out a number of experimental tests, and ultimately clinical trials were conducted with satisfactory results. The cumbersome process described in Section 3.3.4 was carried out by the surgeon successfully, but was excessively time consuming. As a result of the GPS accuracy issues being solved, block registration as described above was eliminated from the surgical protocol. However, the technique is still used for re-registration of the knee joint and for motion detection, as described in Section 4.4.2.

3.5 Conclusion

This chapter has focused on very early research carried out alongside the R&D team of the Acrobot Company Ltd., which led to the first clinical application of the ACROBOT System for a number of TKA procedures. Published results on both accuracy and protocol [Jakopec et al., 2001], have demonstrated this first implementation was appropriate for the task.

However, the clinical performance of the ACROBOT System highlighted a number of issues, concerning both hardware and software, which needed to be addressed in order to improve the accuracy of the procedure as a whole. Resolution of these issues, which became the focus of the author's later research, led to the development of a new redesigned system, the ACROBOT II. The clinical experience obtained during the TKA trials also led to the development of a fast and robust registration technique based on the ICP algorithm, and ultimately to a novel registration algorithm, suitable for minimal access surgery. A description of the hardware redesign that resulted in the ACROBOT II System can be found in the next chapter. Chapter 5 describes enhancements to the original registration algorithm presented in Section 3.3.3, while Chapter 7 describes the design, development, and validation of novel registration algorithm, the Bounded ICP algorithm, suitable for minimal access surgery.

Chapter 4

Achieving Accuracy in the OR - The ACROBOT II

4.1 Introduction

The first clinical application of the ACROBOT System for seven total knee arthroplasty procedures succeeded in validating the concept of a hands-on robot for orthopaedic surgery. However, these early results also highlighted the current limitations of the system, which, in turn, showed that the current implementation had yet to provide a viable alternative to the conventional technique.

While the clinical performance of the system demonstrated that both the pre-operative and intra-operative stages of the procedure could be carried out to completion as planned, the clinical results, both in terms of accuracy of the clinical outcome, and length of the procedure, showed a large margin for improvement. More specifically, a number of aspects relating to the current implementation proved to be inadequate for the task, and required re-engineering.

Limitations of the ACROBOT System can be broadly divided into performance related and safety related issues. Performance issues include lack of stiffness of the gross positioner, backlash in both the GPS and AC Head, excessive bone motion due to the clamping system design, and poor correlation between the co-registered surfaces. Safety issues arise from the natural limitations of a dexterous gross positioning system with an excessive working envelope but a small reach, and also from excessive length of procedure mainly due to registration time, clamping time and clinical protocol.

The need to tackle the above issues in order to prove that the ACROBOT System can improve upon the conventional technique resulted in the following objectives list:

1. To improve accuracy, by redesigning both GPS and active constraint head for a stiffer and backlash free system, with measurements taken directly at

the motion output, by designing a suitable calibration technique, by modifying the registration algorithm for better global minima identification, and by developing a suitable registration protocol.

2. To decrease the amount of bone motion, by redesigning the clamps, by improving the clamping protocol, and by checking and accounting for any bone motion occurring during the robotic assisted part of the surgery.

3. To decrease procedure time, by speeding up the registration algorithm, by refining the clinical protocol, and by decreasing setup time.

Work carried out to achieve these objectives is described in the following sections, in terms of robot redesign (4.2), calibration (4.3), and clamping system redesign (4.4), while registration algorithm optimisation is discussed in Chapter 5.

4.2 Robot Redesign

Having analysed the clinical results of the prototype ACROBOT System, it became apparent that, in order to achieve accuracy in the operating theatre, redesign of both the gross positioner and active constraint head was necessary. This led to the development of a final prototype system capable of submillimetric positional accuracy, and enough stiffness to resist both static and dynamic loads applied during surgery, namely the ACROBOT II. The following sections provide a brief outline of the concept design for both the new GPS and new AC Head, with a final overview of the system as a whole.

4.2.1 Gross Positioning System

Having assessed the performance of a modified industrial robot for robotic assisted surgery, it transpired that only the design and development of a custom gross positioner could ensure the degree of placement and positional accuracy necessary for a hands-on robotic procedure. As described in Section 3.2, while the main requirement of the GPS is to place the active constraint head in proximity of the exposed limb, any inaccuracies in its kinematic chain or any bending under load affect the final accuracy of the system as a whole.

The three fundamental prerequisites affecting the accuracy of a GPS within the context of the ACROBOT System are: placement accuracy, positional accuracy and stiffness. Therefore, the GPS redesign process described in the following paragraphs centres upon how these requirements have been tackled, while the extensive work involved in defining a specification document has been omitted for simplicity. To

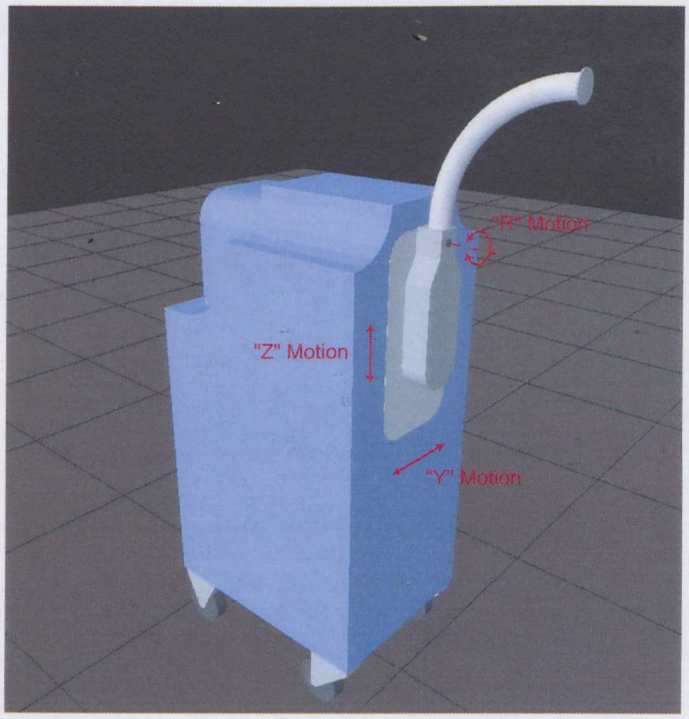


Figure 4.1: Kinematic configuration of the new gross positioning system.

guarantee submillimetric accuracy of the system as a whole during use, the following requirements were placed on the GPS design:

- Positional accuracy $\approx 0.2mm$.
- Placement accuracy $< 5mm$.
- Deflection $\approx 0.2mm$ under $10Kg$ static load $+2Kg$ dynamic load applied at the end of the third axis.

The goal of the design process was then to meet these specifications, while upholding to all requirements imposed by the medical devices directive [EEC, 1993].

One of the major contributors to the overall stiffness of a robotic system is the number of links in the kinematic chain. The more joints between the base of the robot and the end effector, the more likely it is for the system to bend under load. Therefore, it was imperative for the design of the new GPS to include the least amount of links possible, while meeting the access requirements for TKA described in Section 3.2.2. After an in depth analysis of the possible joint combinations that would result in the desired working envelope for the system, the three-links kinematic configuration illustrated in Figure 4.1 was obtained.

The design consists of a three DOF "P-P-R" manipulator, with two prismatic joints in a Cartesian configuration, followed by a revolute joint which links to the base of the AC Head.

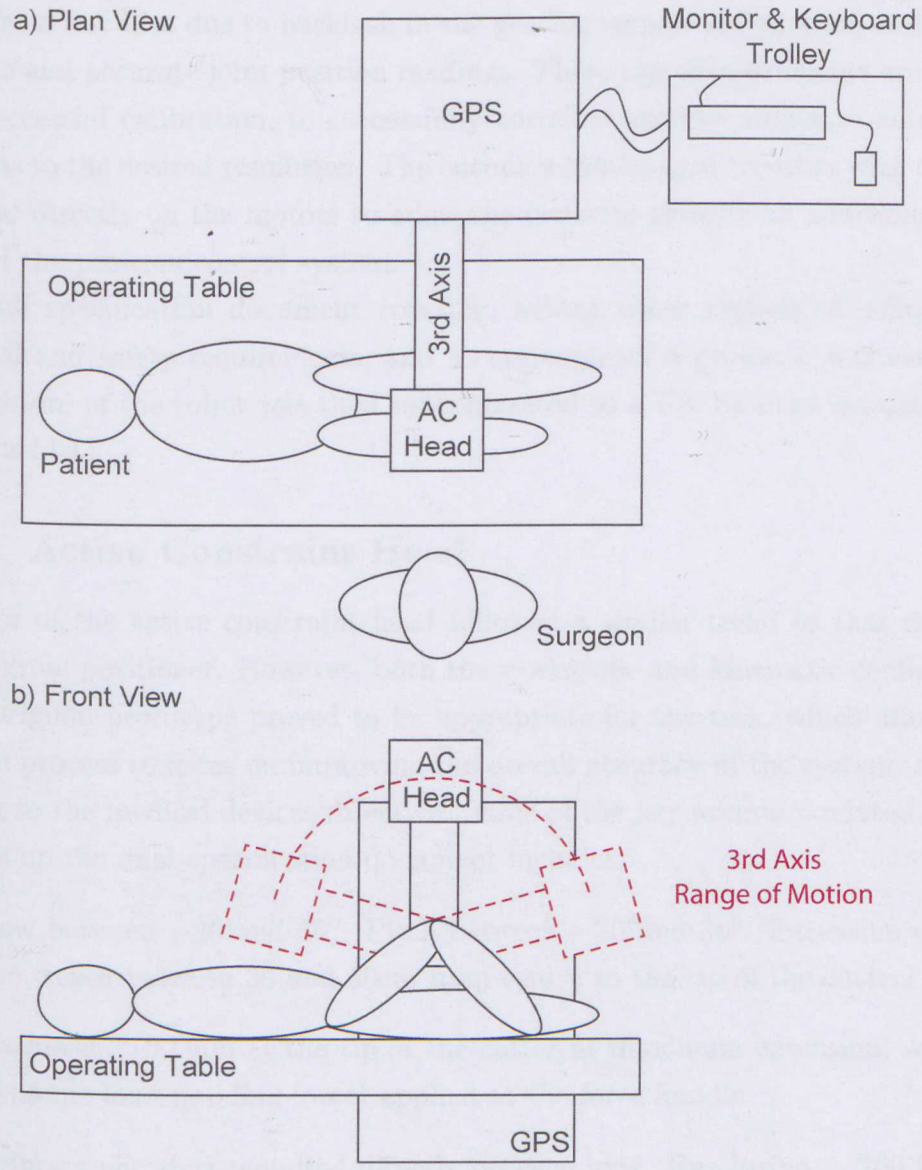


Figure 4.2: Gross positioning system placement with respect to the patient.

As illustrated in Figure 4.2, the circular motion of the third axis, or GPS Roll (R), alone fulfils the access requirements for TKA by providing remote-centre motion of the AC Head once the knee joint has been aligned with the third joint axis, and the end effector is pointing straight down onto the femoral notch. The first two prismatic links are used for initial placement of the AC Head, but can subsequently be locked off for the entire duration of the procedure.

As described in Section 3.3.4, while *placement* accuracy in the order of millimetres is adequate for approximate placement of the AC Head within reach of the cuts, submillimetric *positional* accuracy is needed. In order to ensure appropriate positional accuracy, it was decided to mount high resolution absolute encoders on each axis of the GPS. These axes mounted encoders ensure a positional reading that

is free from any bias due to backlash in the gearing system and motors, and provide absolute and accurate joint position readings. These raw measurements are needed, after successful calibration, to successfully correlate encoder values to actual joint positions to the desired resolution. The encoders can be used together with encoders mounted directly on the motors to allow the latter to provide an additional safety check of the position control system.

A full specification document covering, among other aspects, sterility issues, electrical and safety requirements, and a communication protocol, was assembled. Manufacture of the robot was then subcontracted to a UK robotics company [RTS Robotics Ltd.].

4.2.2 Active Constraint Head

Redesign of the active constraint head followed a similar trend to that described for the gross positioner. However, both the workspace and kinematic configuration of the original prototype proved to be appropriate for the task, which allowed the redesign process to focus on improving the overall accuracy of the system, and conforming to the medical devices directive. Some of the key accuracy related features to make up the final specification document include:

- Yaw between $-30^o$and 30°. Pitch between $-30^o$and 30°. Extension of 20cm, (i.e. reach between 30 and 50cm from centre to the tip of the cutter).
- Backlash $<$ 0.1mm at the tip of the cutter at maximum extension, with 2Kg dynamic load (guiding force) applied at the force handle.
- Primary encoders mounted directly on each axis. Resolution $>$ 200 Encoder Edges/mm at the tip of the cutter at maximum extension.
- A spherical configuration, with the three joint axes intersecting at a single point, the centre of the AC Head, within 0.1mm, which allows for substantial simplifications in the kinematic model of the system.

The redesign process resulted in the prototype design illustrated in Figure 4.3, which was contracted out for manufacture.

As shown in Figure 4.3, the new head has a more ergonomic design, its size and weight have been reduced, whilst the back-drivability has been improved. In addition, as for the GPS, each axis now has double encoders, improving the accuracy and safety of the device. The primary encoders are placed on the axis output, which eliminates any error in position reading due to backlash in the system, while motors are equipped with secondary encoders. The tip of the robot consists of a detachable high-speed milling tool and a force sensor handle [Jakopec et al., 2003a].

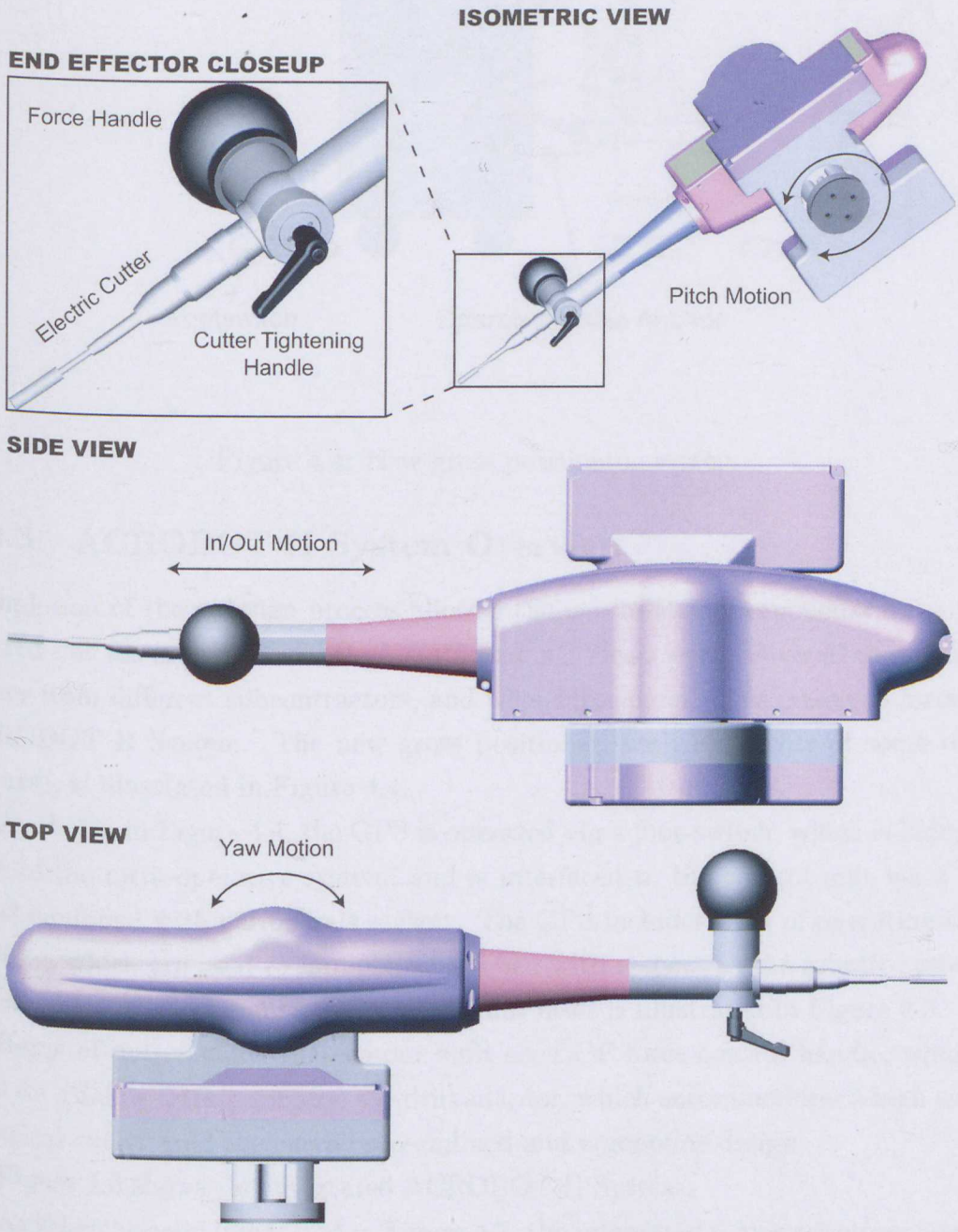


Figure 4.3: The Active Constraint Head II.

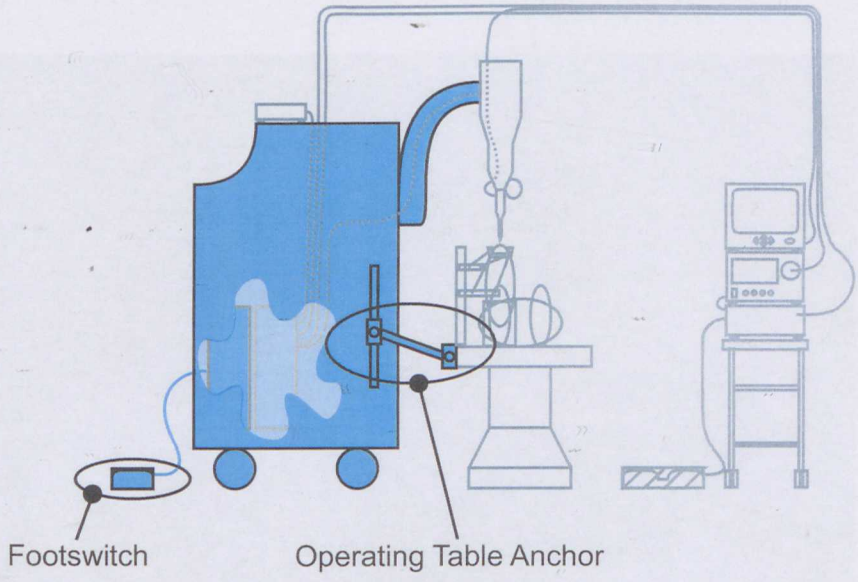


Figure 4.4: New gross positioning system.

4.2.3 ACROBOT II System Overview

Completion of the redesign process allowed the two robotic components to be contracted out for manufacture. Both GPS and AC Head were delivered to our laboratory from different subcontractors, and were subsequently integrated to form the ACROBOT II System. The new gross positioner, with highlights of some of its features, is illustrated in Figure 4.4.

As shown in Figure 4.4, the GPS is operated via a foot-switch, which is independent of the intra-operative system, and is interfaced to the control unit via a side panel equipped with peripherals sockets. The GPS includes a set of operating table anchors, which are used to immobilise the bed with respect to the robotic system.

Similarly, the redesigned active constraint head is illustrated in Figure 4.5.

Items of note include the custom built six DOF force control handle, which is used for guiding during surgery, the drill adaptor, which accommodates a high speed electrical cutter, and the overall streamlined and ergonomic design.

Figure 4.6 shows the integrated ACROBOT II System.

As schematically illustrated in Figure 4.7, the integrated 6-axis robotic system is mounted onto a wheeled trolley, together with its control hardware. As in the original prototype ACROBOT System, the trolley is clamped (4) to the operating table (18) during the surgery, with its wheels locked. The surgeon operates the system with a foot-switch panel (9) and an intuitive graphical user interface displayed on a computer monitor (7). The surgeon guides the AC Head by pushing on the force control handle (6), while the control software constrains the motion of the head to

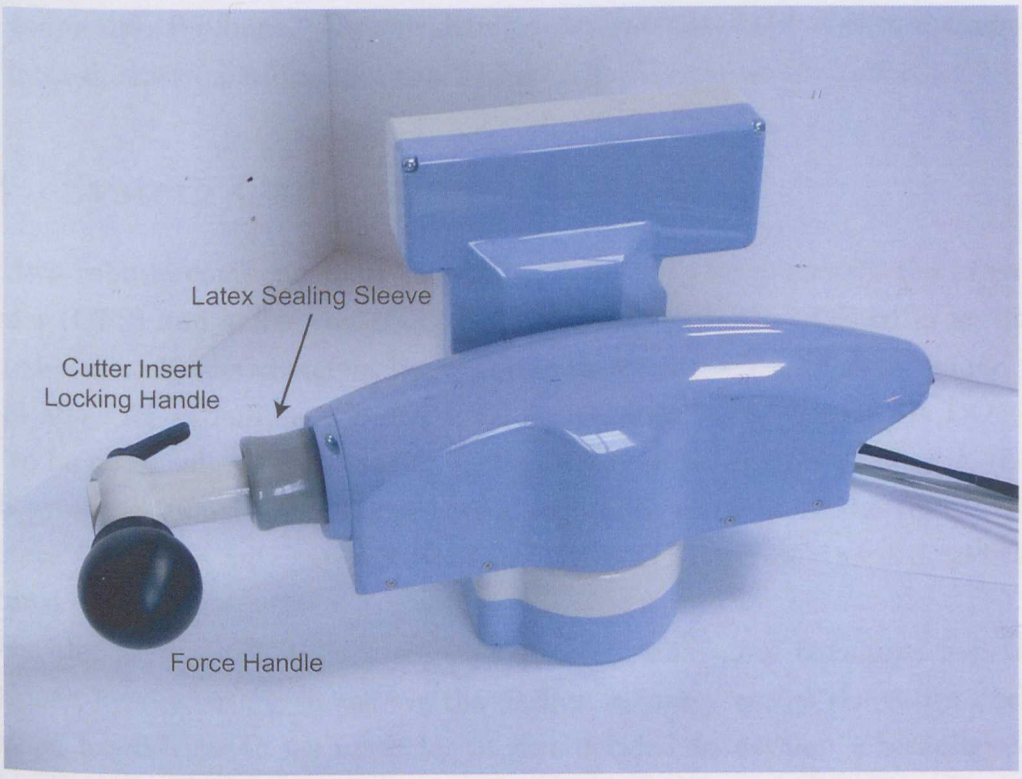


Figure 4.5: New active constraint head.

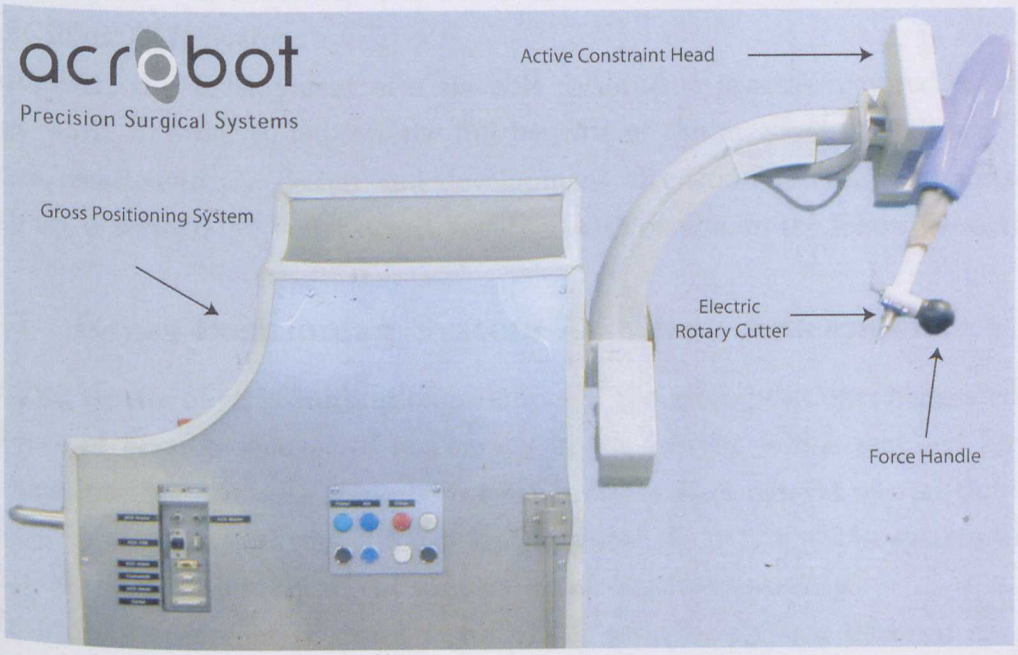


Figure 4.6: The ACROBOT II System, gross positioner and active constraint head.

the pre-defined safe region. In this way, the surgeon can safely machine an accurate 3-D shape into the bone. A more detailed description of the system components and intra-operative performance can be found in [Jakopec et al., 2003b].

4.3 System Calibration

The two robotic components of the ACROBOT II System, namely the gross positioner (GPS) and active constraint head (AC Head), were delivered in an uncalibrated state. It was therefore necessary to develop a calibration technique that would allow for submillimetric positional accuracy of the integrated six DOF system to be obtained. As described in Section 3.2.3, in the original prototype, the six DOF gross positioner was delivered with positional accuracy at the tip of its end effector. Therefore only the AC Head and GPS-AC Head link needed additional calibration.

For the ACROBOT II, a more sophisticated calibration technique had to be developed by the author to achieve the desired accuracy across the entire working envelope for the system as a whole. It was decided to develop a technique centred upon a high accuracy mechanical digitiser [FARO Technologies Inc., FL, USA] available on the premises. This mechanical back-drivable arm, illustrated in Figure 4.8, provides positional accuracy better than 0.05mm at the probe end with a repeatability of 0.01mm, which are both more than adequate for the calibration process objective of submillimetric worst-case accuracy at the end effector end of the ACROBOT II System.

However, the development of a suitable calibration process required extensive design work, in order to harvest the full benefits of the mechanical digitiser. This process resulted in the design and development of custom tooling, and software, which are described in greater detail, together with results, in the following sections.

4.3.1 Gross Positioning System Accuracy Assessment

Worrying results of early calibration attempts of the gross positioner suggested the existence of possible sources of inaccuracy in the system, which required further investigation. As a result, a number of experiments were carried out on the GPS in order to validate both the stiffness and dynamic distortion of the system under load, and the raw accuracy of the axes-mounted absolute encoders.

In order to pinpoint the root cause of the poor correlation between encoder readings and effective joint positions, a separate set of tests was carried out for the third axis (R), and the two prismatic joints (Z and Y). Firstly, the extent of dynamic distortion across the entire working envelope of the first two axes was assessed by

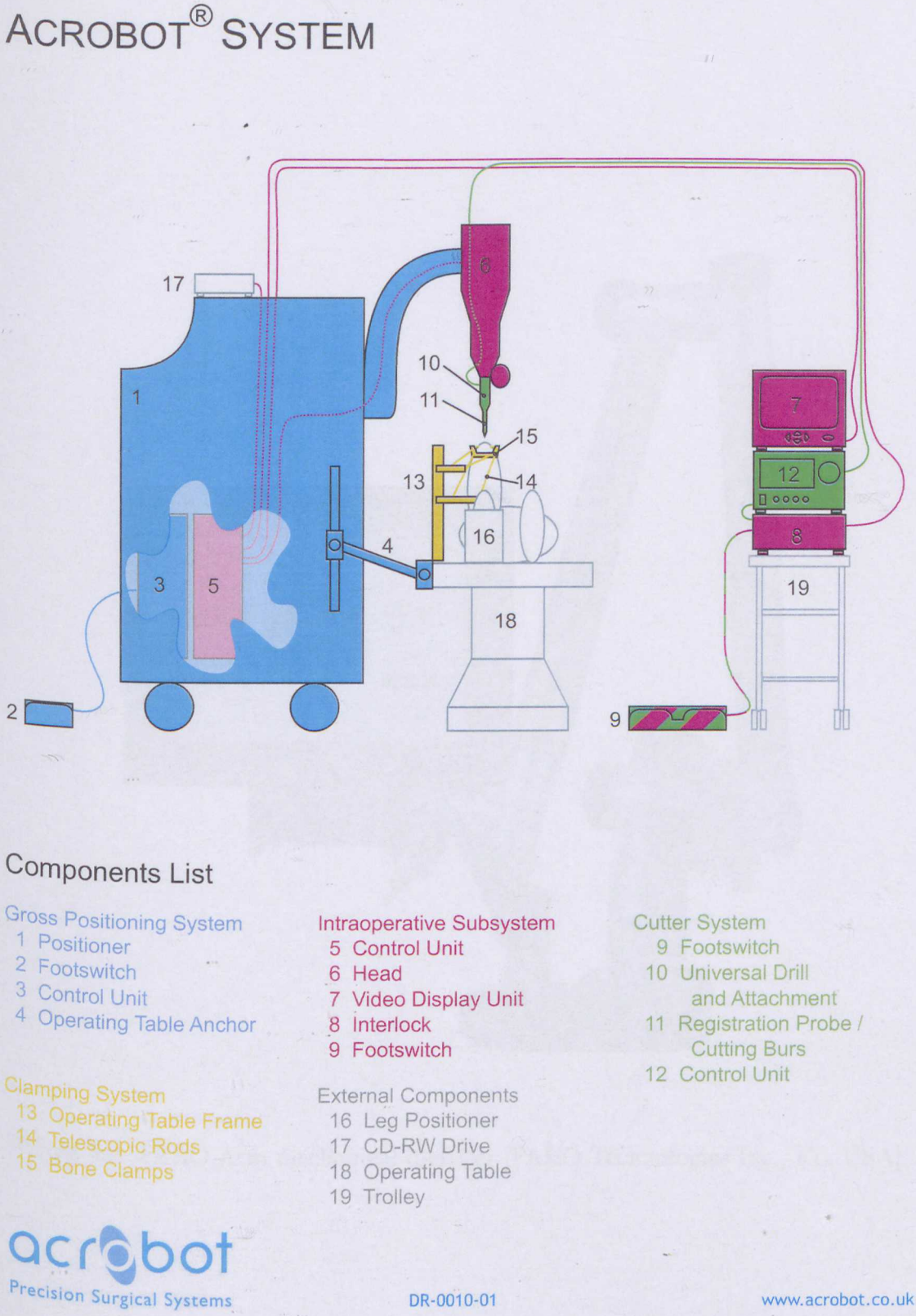


Figure 4.7: ACROBOT II System schematic overview.



Figure 4.8: FARO Arm mechanical digitiser [FARO Technologies Inc., FL, USA].

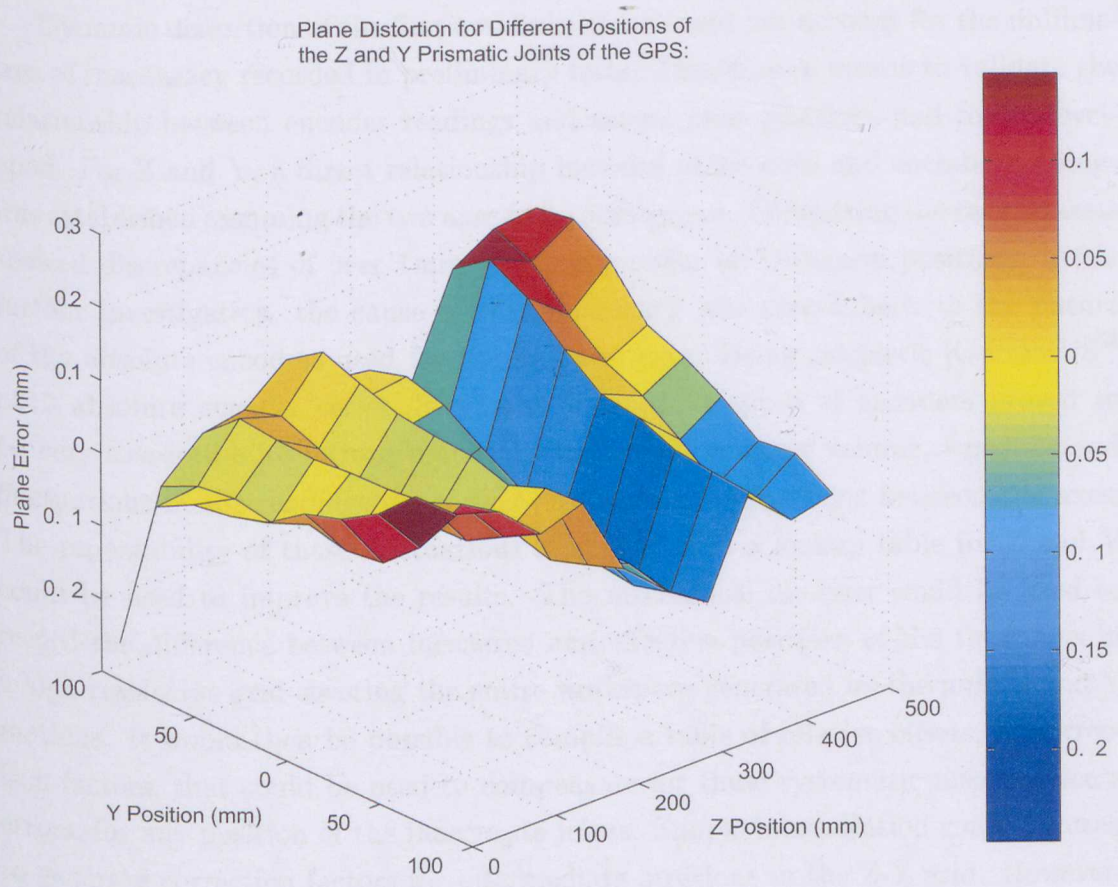


Figure 4.9: Least square fit of 3D data obtained from the mechanical digitiser as Z and Y are moved in a grid across their entire range of motion.

using the mechanical digitiser to record instantaneous positions of the full range of motion for each joint. The values recorded for each position of the mechanical digitiser were then fitted on a plane, using a well known least squares fit [Smith, 2003]. Results are illustrated in Figure 4.9.

As can be seen, these results already highlight one source of inaccuracy, which is due to the bending and twisting of the first two joints as they move between end stops. The colour-coded display in Figure 4.9 illustrates positional deflection of up to $\pm 0.2mm$, which already renders positional accuracy within 0.2mm for the system as a whole impossible to achieve.

In order to measure the amount of distortion affecting R, positional readings at ten degrees intervals, with no motion of Z and Y, were recorded using the mechanical digitiser, and the resulting data set was fitted on a circle using a least squares approximation. Results showed that the accuracy of the rotational motion is within the accuracy of the mechanical digitiser (50 microns), which proves the absence of any detectable dynamic distortion of the GPS third axis as it is moved in an arc between $\pm 90^o$.

Dynamic distortion of the first two links alone could not account for the millimetres of inaccuracy recorded in preliminary tests. Therefore, a means to validate the relationship between encoder readings and actual joint positions had to be developed. For Z and Y, a direct relationship between plane data and encoder readings was established assuming the two axes to be orthogonal. Comparing the two datasets showed discrepancies of over 1mm between encoder and effective positions. After further investigation, the cause of this inaccuracy was traced back to the nature of the absolute encoders used for the first two axes. Being magnetic [C-POMUS® p510 absolute encoder series, Stegmann Inc.], these types of encoders proved to be very susceptible to ferrous material within their working volume, which caused fluctuations in the readings depending on the relative positions between the axes. The repeatability of these fluctuations suggested that a lookup table for Z and Y could be used to improve the results. The mechanical digitiser could be used to record the difference between measured and effective positions of the third axis in a high resolution grid covering the entire workspace generated by the joint Z and Y motions. It would then be possible to compile a table of relative offsets, or correction factors, that could be used to compensate for these systematic measurements errors, for any position of the inaccurate joints. Simple interpolation could be used to generate correction factors for intermediate positions in the Z-Y grid. However, given the proven dynamic distortion of the first two links (Figure 4.9), the decision of using Z and Y with millimetric accuracy, and excluding them from the accuracy chain, was made. The Z and Y joints would be used for initial placement of the AC Head in close proximity to the patient, and would be subsequently locked off for the remainder of the procedure.

For R, the equation of the least squares circle [Smith, 2003] was used to generate corresponding joint values for each step in the grid, and results were compared to the encoders' readout. Results are illustrated in Table 4.1.

These results highlighted discrepancies of up to 7° between derived and measured joint angles, which suggested inaccurate encoder readings or undetected backlash in the system.

In order to assess whether the error in the third axis could be traced back to undetected backlash in the axis configuration (e.g. compliance in the pinned interface between the large bearing located at the end of the secondary brake on the axis, and the substantially smaller rod passing through the absolute encoder), the following experiment was carried out. With the system at rest an accurate reading of the third axis end position was taken. A load of approximately 5N was then applied in opposite directions from the original position (i.e. load applied CWS and CCWS) and the position recorded again. The result was repeated twice, having swapped the order of the loads applied (TEST 1 and TEST 2). Then, instead of applying a load,

Angle between subsequent pts measured by encoder (rad)	Angle between subsequent pts measured by CMM (rad)	Relative error between readings types (rad)	Relative error between readings types (deg)	Effect of Error at 400mm Extension (mm)
0.1557	0.1551	0.0006	0.0347	0.242
0.3298	0.3291	0.0008	0.0432	0.3016
0.5024	0.5014	0.001	0.0588	0.4107
0.6765	0.6754	0.0011	0.0611	0.4264
0.8491	0.8476	0.0015	0.0874	0.6103
1.022	1.0201	0.0019	0.1086	0.7584
1.1919	1.1893	0.0026	0.1498	1.0461
1.3614	1.3582	0.0032	0.1831	1.2784
1.5064	1.5029	0.0035	0.2003	1.3986
1.6582	1.6541	0.0041	0.2363	1.6495
1.8201	1.8153	0.0048	0.2745	1.916
1.9827	1.977	0.0056	0.3218	2.2469
2.1499	2.1434	0.0064	0.3684	2.5719
2.3232	2.3161	0.0071	0.4046	2.8245
2.4947	2.4868	0.0079	0.4503	3.1434
2.6661	2.6571	0.009	0.5153	3.5975
2.8394	2.8293	0.0101	0.5782	4.0363
2.997	2.9844	0.0126	0.7229	5.047
2.8398	2.8282	0.0116	0.666	4.6493
2.6665	2.6555	0.011	0.6305	4.4017
2.4935	2.483	0.0105	0.6026	4.2071
2.3205	2.3106	0.0099	0.5698	3.978
2.1487	2.1394	0.0093	0.5341	3.7286
1.9869	1.9787	0.0082	0.4712	3.2895
1.8174	1.8091	0.0083	0.4732	3.3033
1.6747	1.6672	0.0076	0.4335	3.0262
1.5056	1.4983	0.0073	0.4179	2.9172
1.3349	1.3281	0.0069	0.3936	2.7481
1.1658	1.16	0.0058	0.334	2.3315
1.0236	1.022	0.0016	0.0889	0.6205
0.8513	0.8504	0.0009	0.0528	0.3686
0.6803	0.68	0.0003	0.0185	0.1291
0.5066	0.5066	0	-0.0017	-0.0117
0.3348	0.3353	-0.0005	-0.028	-0.1953
0.1614	0.162	-0.0006	-0.0327	-0.2286
0.0015	0.0018	-0.0003	-0.0174	-0.1213

Table 4.1: Difference between derived (from the circle equation) and measured (encoder) joint angles for R.

	Encoder	FARO X	FARO Y	FARO Z		Encoder Dif (rad)	X Dif	Y Dif	Z Dif	FARO Dif (mm)
TEST 1	0.48	157.94	408.31	470.18	Dif (Mid Point - Top Point)	0.01	3.43	-2.40	-0.71	4.25
	0.49	161.37	405.91	469.47	Dif (Mid Point - Bottom Point)	0.00	-0.63	0.49	0.26	0.84
	0.49	162.00	405.42	469.21						
						Encoder Dif (mm)				
						(at 360mm Ext)				
						2.64				
						-0.25				

	Encoder	FARO X	FARO Y	FARO Z		Encoder Dif (rad)	X Dif	Y Dif	Z Dif	FARO Dif (mm)
TEST 2	0.49	160.83	406.28	469.68	Dif (Mid Point - Top Point)	0.00	0.84	-0.59	-0.24	1.05
	0.49	161.67	405.69	469.44	Dif (Mid Point - Bottom Point)	-0.01	-4.07	2.68	0.56	4.90
	0.50	165.74	403.02	468.88						
						Encoder Dif (mm)				
						(at 360mm Ext)				
						0.50				
						-4.03				

	Encoder	FARO X	FARO Y	FARO Z		Encoder Dif (rad)	X Dif	Y Dif	Z Dif	FARO Dif (mm)
TEST 3	0.49	162.18	405.35	469.36	Dif (Mid Point - Top Point)	0.02	5.03	-3.83	-0.82	6.38
	0.51	167.21	401.52	468.54	Dif (Mid Point - Bottom Point)	0.04	10.42	-7.74	-1.69	13.09
	0.47	156.79	409.26	470.23						
						Encoder Dif (mm)				
						(at 360mm Ext)				
						6.42				
						13.09				

Table 4.2: Third axis backlash test.

the third axis was moved by 1° in each direction and relative positions recorded (TEST 3). Results for this experiment are illustrated in Table 4.2.

These results illustrate that loads applied at the end of the third axis caused errors in the order of millimetres, which are not detected by the absolute encoders. This proved the existence of backlash in the system between the absolute encoder position and the end of the third axis, not including the absolute encoder shaft. Furthermore, TEST 3 illustrates how, under constant load (i.e. same static load at the three positions of TEST 3, which are only 2° apart) the encoder records a position well within the stated accuracy. From this experiment the following conclusions could be made:

1. The encoder itself relays accurate information concerning the position of the shaft that it monitors. For small envelopes, the change in angle recorded by the encoder agrees with that provided by the measurements taken with the mechanical digitiser.

2. It is apparent that the third axis suffers from backlash, which is not detected by the encoder.

3. This backlash has to be mainly in the plane generated by the arm, as a best fit circle estimate for the points recorded by the mechanical digitiser is convincingly accurate.

After some consideration, it was decided to mount an additional high resolution optical encoder [RGH25 linear encoder series, Renishaw Plc.] on the base of the third

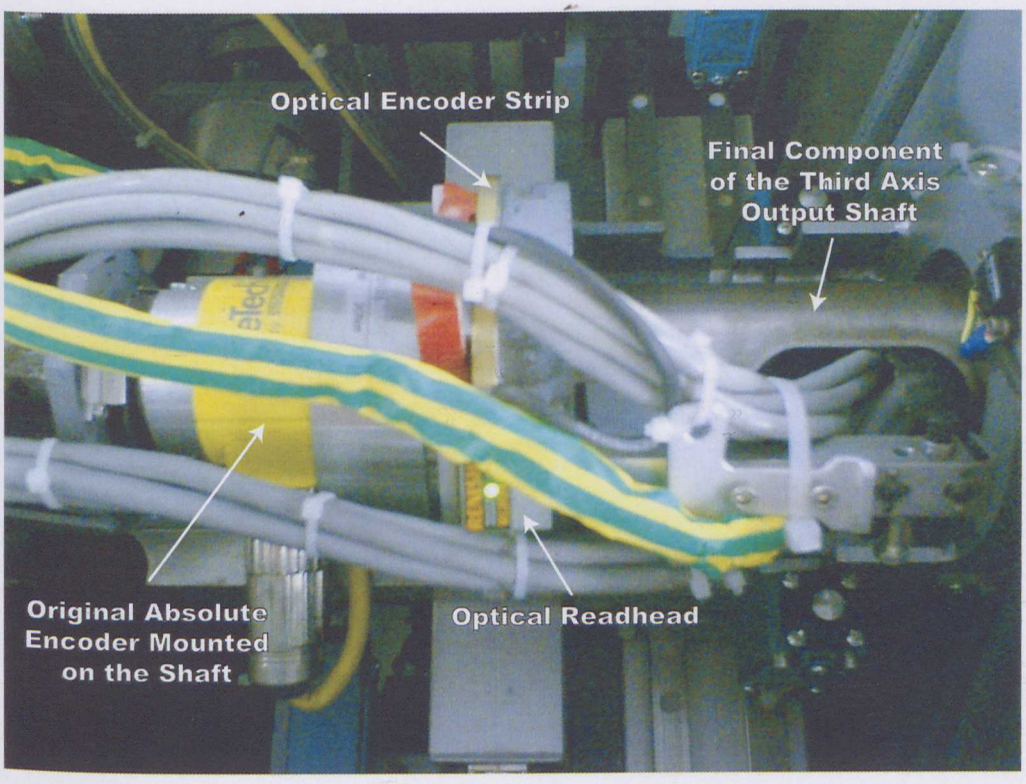


Figure 4.10: Additional optical encoder mounted at the base of R.

axis, in order to guarantee backlash free readings. This configuration is illustrated in Figure 4.10.

As described in the following sections, this addition allowed the final four axes of the ACROBOT II System to be successfully calibrated. It was decided that Z and Y would only be used for initial placement of the AC Head, therefore did not require submillimetric positional accuracy.

4.3.2 System Kinematics

As for the original ACROBOT prototype, a full kinematic model of the integrated six DOF robot had to be derived for calibration purposes. Since neither the GPS or AC Head were individually calibrated, the combined GPS-AC Head system was treated as a whole to simplify the modelling process. The result is schematically illustrated in Figure 4.11.

The Denavit Hartenberg (DH) parameters [Craig, 1989] were then directly derived from the model, and are summarised in Table 4.3.

$\theta(0)_3$, $\theta(0)_4$, and $\theta(0)_5$ represent the three revolute joints "zero angles," which, once calibrated (Section 4.3.3), are needed to accurately specify the positions of each link where the value of the angle is equal to zero. $d(0)_6$ represents the active constraint head In/Out joint position at minimum extension, and coincides with

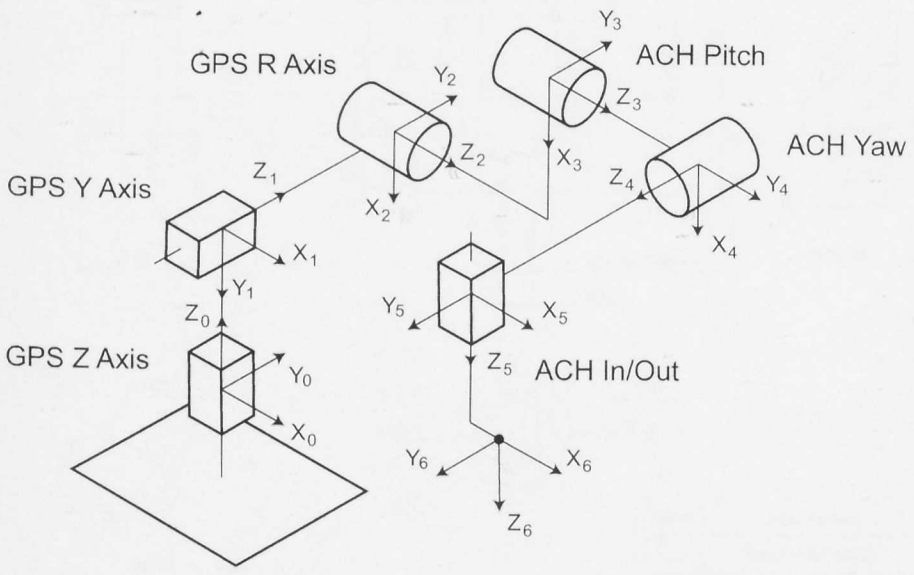


Figure 4.11: Schematic kinematic model of the six DOF integrated ACROBOT II System.

	i	*Joint*	a	α	d	θ
GP	1	Z	$0mm$	-90°		0°
	2	Y	$0mm$	90°	d_2	90°
	3	R	$-400mm$	0°	$0mm$	$\theta(0)_3 + \theta_3$
AC Head	4	Roll	$0mm$	90°	$0mm$	$\theta(0)_4 + \theta_4$
	5	Pitch	$0mm$	90°	$d_5 = T0_y$	$\theta(0)_5 + \theta_5$
	6	In/Out	$a_6 = T0_x$	0°	$d_6 + d(0)_6$	0°

Table 4.3: DH parameters for the six DOF integrated ACROBOT II System.

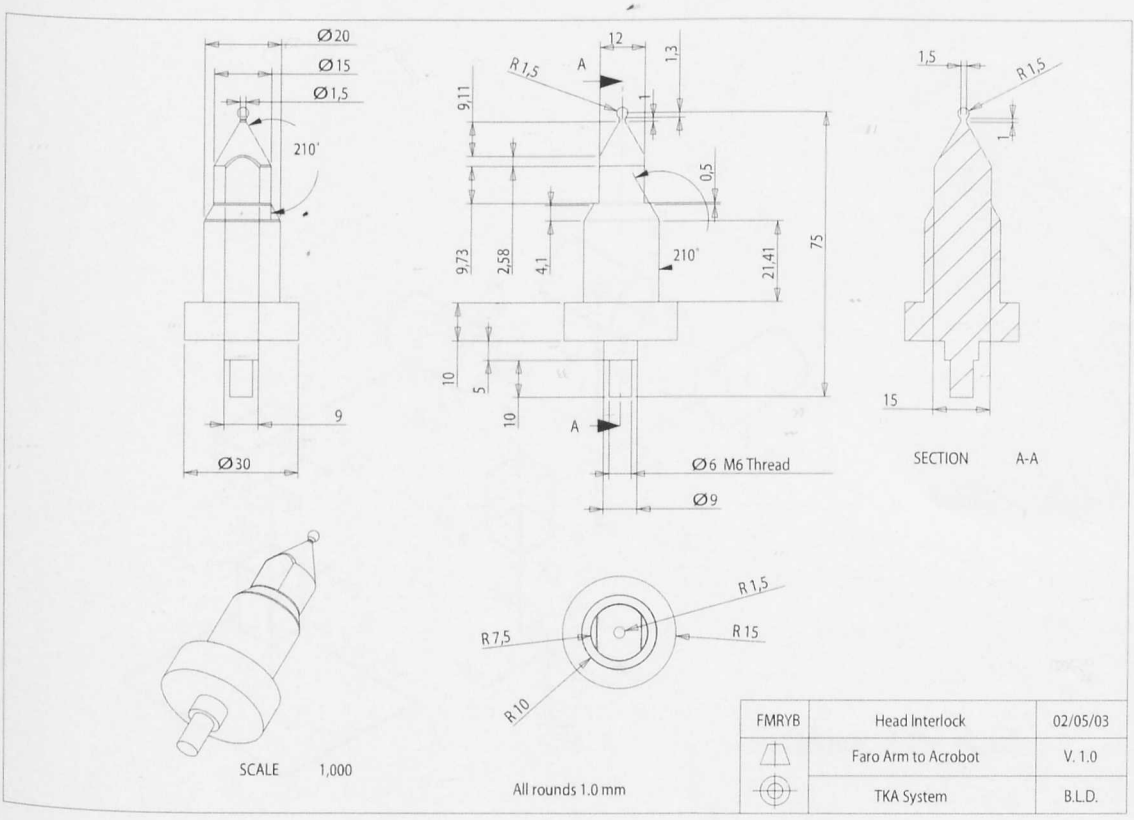


Figure 4.12: Mechanical digitiser-cutter socket interlock.

$T0_z$, the tool offset in the "Z" direction of the sixth frame. $T0_x$, $T0_y$, and $T0_z$ represent the three offsets of the tool attached to the end effector, which are needed to derive an accurate Cartesian of the robot position at the tip.

4.3.3 Enhanced Calibration Method

As mentioned earlier, it was decided to use a mechanical digitiser (FARO Titanium Arm, Model N. 4) to acquire the set of corresponding points needed for the calibration algorithm described in Section 3.2.3. A custom probe for the mechanical digitiser was designed and manufactured for this purpose.

This custom probe, illustrated in Figure 4.12, has a 3mm spherical tip, needed to carry out the digitiser's own calibration procedure, and a cylindrical extension, which locks in the AC Head cutter socket. This allows very accurate points to be measured about the centre of the probe's spherical tip, which is fixed with respect to the system at an offset to the centre of the AC Head along the In/Out joint axis. This configuration enabled points covering the entire workspace of the system to be collected in one session.

Further investigation of the DH parameters summarised in Table 4.3 produced the sublist of parameters requiring calibration, reported in Table 4.4.

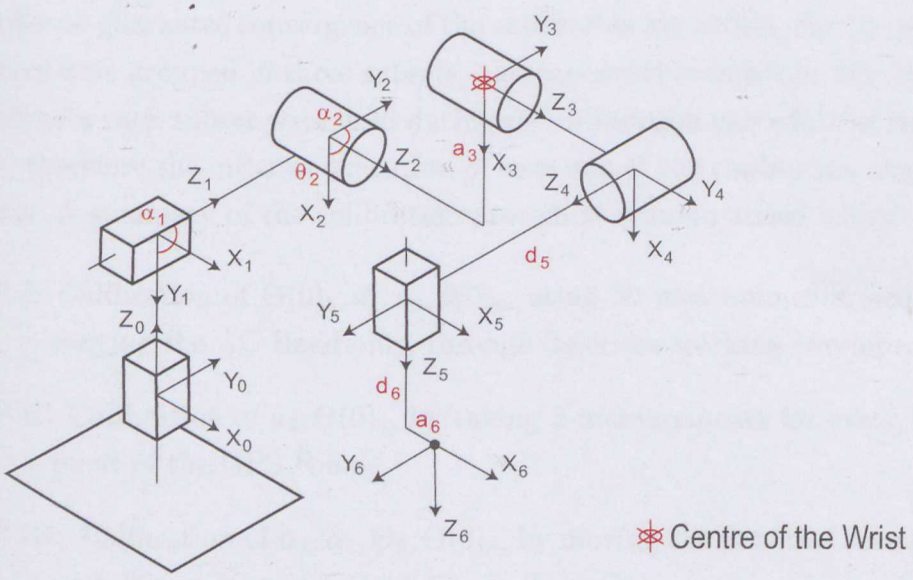


Figure 4.13: Schematic illustration of the calibration parameters for the ACROBOT II System.

Parameter Type	Parameter List	Initial Estimates
GPS	α_1, α_2, θ_2, a_3	-90°, 90°, 90°, $-400mm$
(zero angles)	$\theta(0)_3$	0°
AC Head	d_5, a_6	$0mm$, $0mm$
(zero angles)	$\theta(0)_4$, $\theta(0)_5$, $d(0)_6$	0°, 90°, $0mm$
FARO	x, y, z, α, β, γ	Derived by pair point matching

Table 4.4: Calibration parameters for the ACROBOT II System.

Since the custom probe was manufactured using a turning process, it could be assumed that the axis of the interlock would be aligned with that of the cutter, which allows all but $T0_z = d(0)_6$ to be calibrated with points gathered with the mechanical digitiser.

In order to guarantee convergence of the calibration algorithm, the 16 calibration parameters were grouped in three subsets, and processed separately. The calibrated parameters for each subset were used during the calibration procedure of the following ones, therefore the order of execution of each run of the calibration algorithm is important. A summary of the calibration procedure is summarised below:

GROUP I: Calibration of $\Theta(0)_5, d_5, a_6, d(0)_6$, using 80 measurements, acquired by moving the AC Head only, through its entire working envelope.

GROUP II: Calibration of $a_3, \Theta(0)_4$, by taking 3 measurements for every 5° increment of the GPS R axis.

GROUP III: Calibration of $\alpha_1, \alpha_2, \Theta_2, \Theta(0)_3$, by moving the first two axes in a grid with 20mm Y spacing, and 50mm Z spacing.

All six parameters defining the relative position and orientation of the FARO arm with respect to the robot (Table 4.4) have to be included in each of the three groups. To guarantee the absence of any unaccounted relative motion between the base of the gross positioner and the mechanical digitiser, the ACROBOT II System was lifted off its wheels and supported on wooden blocks, and the digitiser was securely fastened to a table with a set of "G" clamps. The calibration layout is illustrated in Figure 4.14.

4.3.4 Cutter Probe Calibration

As mentioned in the previous section, all parameters but the tool offset in the direction of the AC Head In/Out motion ($T0_z$) could be calibrated using the mechanical digitiser. However, in order to retain the calibration accuracy obtained with the enhanced calibration method, a technique to accurately estimate a value for the extension had to be developed. For this last parameter, it was decided to revert back to the original calibration method described in Section 3.2.3. However the accurately machined plate was replaced by a custom designed and manufactured calibration block, which is illustrated in Figure 4.15.

The shape of the block ensures that, for one position of the AC Head, a large percentage of the working envelope of the head could be covered. The position of each hole on the block was accurately measured with the mechanical digitiser. The

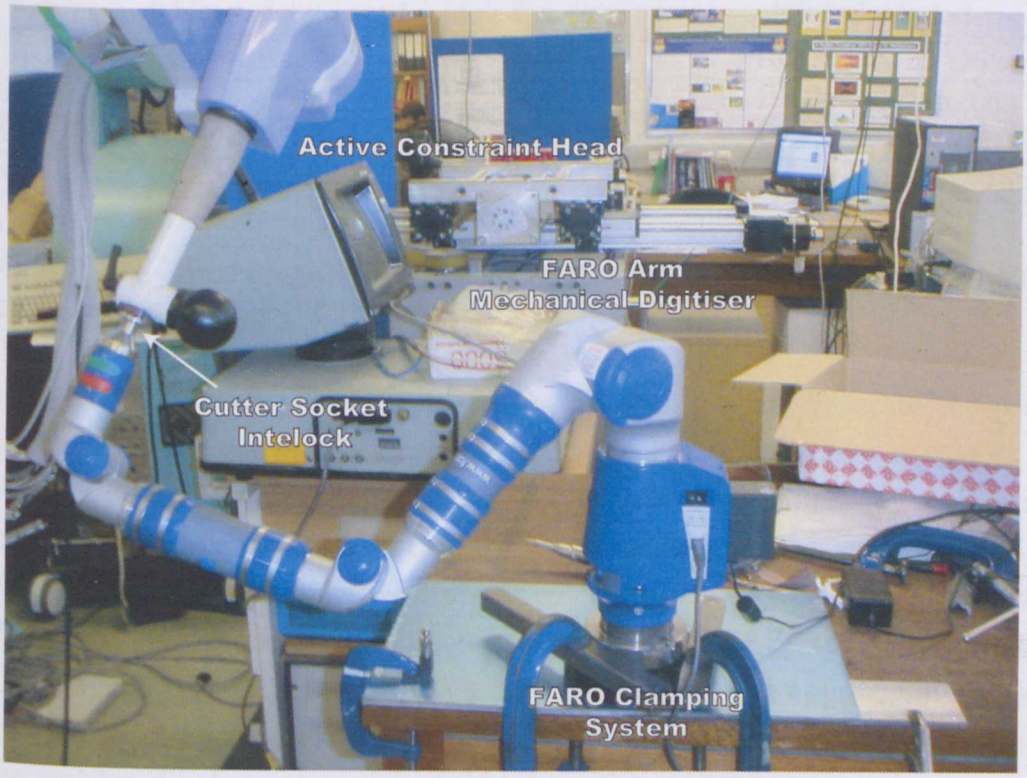


Figure 4.14: ACROBOT II calibration setup.

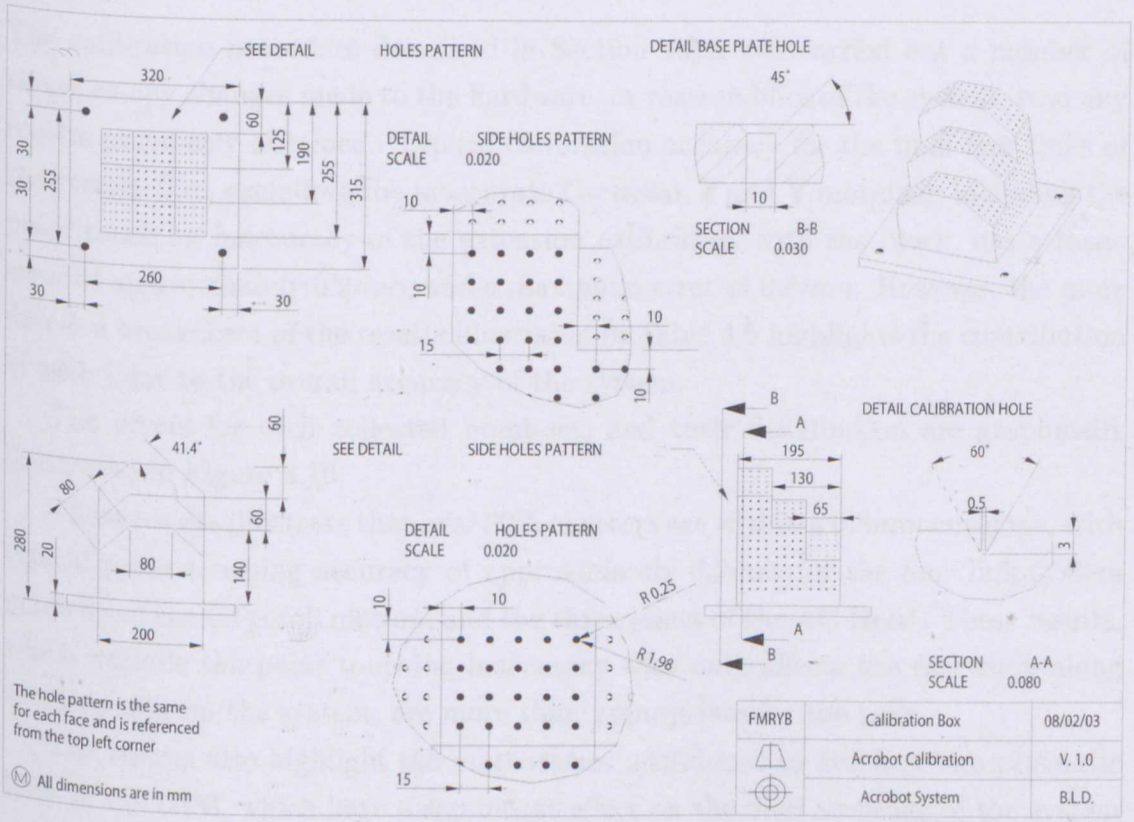


Figure 4.15: Calibration block used to calibrate the axial offset of the tool.

Subset	Mean Accy (mm)	Max Err (mm)	Joints Included
GROUP I	0.2	0.42	Pitch, Yaw, In/Out
GROUP II	0.23	0.81	R, Pitch, Yaw, In/Out
GROUP III	0.33	0.89	Z, Y, R, Pitch, Yaw, In/Out
Probe ($T0_z$)	0.24	0.47	Pitch, Yaw, In/Out, Tool

Table 4.5: Individual contribution of each calibration parameter subset to the final accuracy of the ACROBOT II System.

resulting datafile of effective hole locations was then used to generate the paired points list that was used to calibrate the extension.

A three millimetre diameter spherical insert for the electrical cutter was used to touch approximately 120 holes on the block. To speedup the acquisition process, the kinematic model of the partially calibrated system was used to register the position of the block with respect to the base of the ACROBOT II System, which allowed the holes touched to be identified automatically. Each hole is approximately 10mm away from any other hole, which ensures that a closest point search (Section 5.3.2) of the registered hole location list would return the correct one.

4.3.5 Results

The calibration procedure described in Section 4.3.3 was carried out a number of times, as any changes made to the hardware, or reassemblies of the system, void any results previously obtained. Typical calibration accuracy for the final four links of the system (i.e., excluding the inaccurate Cartesian Z and Y motions), including the point touching inaccuracy of the extension calibration with the block, has a mean error of approximately $0.2mm$, and a maximum error of $0.8mm$. However, the more detailed breakdown of the results illustrated in Table 4.5 highlights the contribution of each joint to the overall accuracy of the system.

The errors for each collected point-set, and their distribution are graphically illustrated in Figure 4.16.

These results illustrate that over 90% of errors are within a $0.8mm$ envelope, with typical point touching accuracy of approximately $0.2mm$ for the four link system made up of the GPS roll motion, and the three joints of the AC Head. These results, which exclude the point touching inaccuracy that only affects the extension along the final axis on the system, are more than appropriate for the task.

The results also highlight the inaccuracies introduced by the first two prismatic links of the GPS, which have a significant effect on the final accuracy of the system as a whole. Given the marginal contribution of these two additional degrees of freedom to the functionality of the system, it was decided to omit both joints from

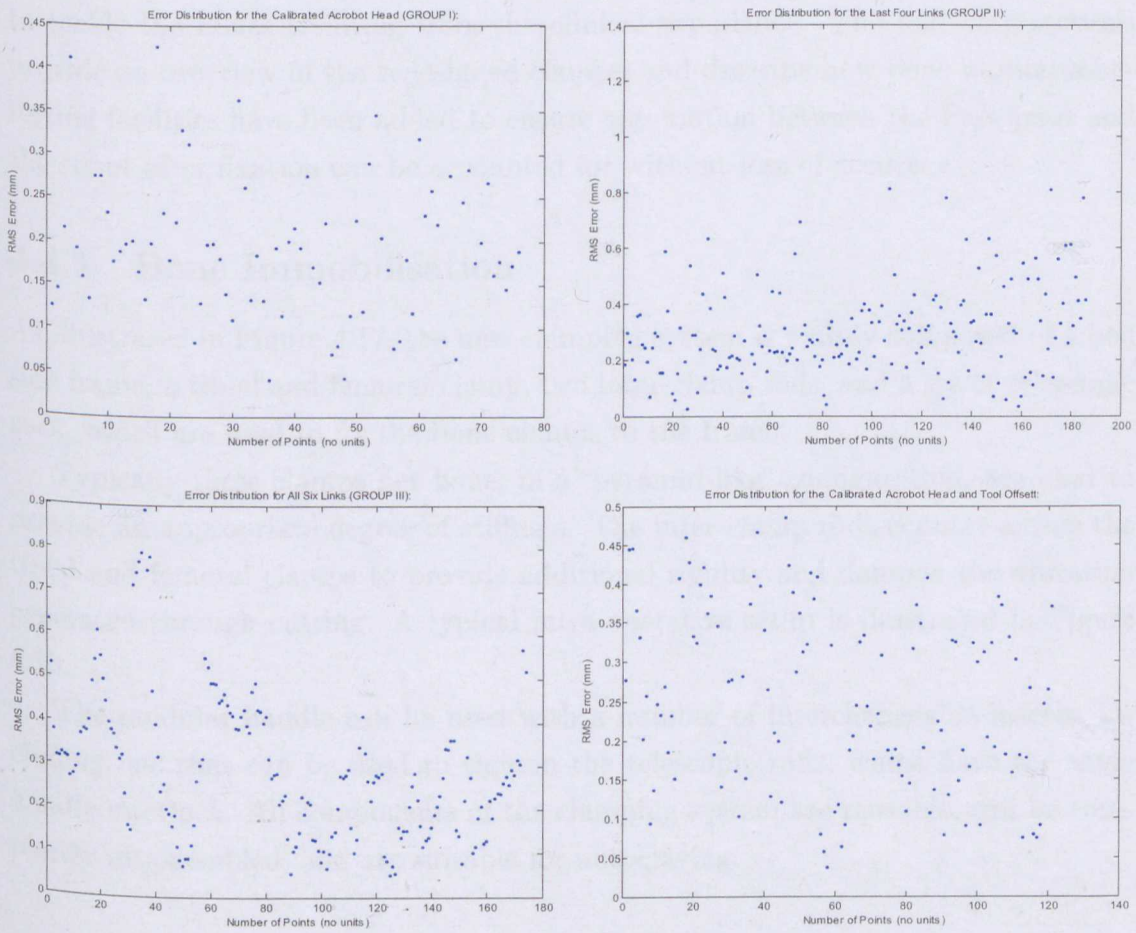


Figure 4.16: Error distribution for the four calibration parameter subsets after successful calibration.

the accuracy chain, in order to retain the degree of accuracy required for a robotic assisted procedure.

4.4 Clamping System Redesign

The original clamping system used for the early TKA trials (Figure 3.1) proved not to be suitable for the task due to excessive bone motion, setup difficulties, and sterilisation issues. Therefore, a new clamping system was designed and manufactured to tackle the issues resulting from the clinical experience. The following sections provide an overview of the redesigned clamps, and describe how bone motion monitoring facilities have been added to ensure any motion between the knee joint and the robot after fixation can be accounted for without loss of accuracy.

4.4.1 Bone Immobilisation

As illustrated in Figure 4.17, the new clamping system is mainly composed of a bed side frame, a tibial and femoral clamp, two inter-clamp rods, and a set of telescopic rods, which are used to fix the bone clamps to the frame.

Typically three clamps per bone, in a "pyramid-like" configuration, are used to provide an appropriate degree of stiffness. The inter-clamp rods connect across the tibial and femoral clamps to provide additional rigidity and dampen the vibration generated through cutting. A typical intra-operative setup is illustrated in Figure 4.18.

The modular handle can be used with a number of interchangeable inserts, including one that can be used to tighten the telescopic rods, which have the same handle interlock. All components of the clamping system are reusable, can be completely disassembled, and are suitable for autoclaving.

4.4.2 Bone Motion Monitoring

The added advantages of the block registration procedure described in Section 3.3.4 became apparent once "block-like" functionality was added to the clamps themselves. As the original clamping system was redesigned to improve ease of use and stiffness, accurately machined conical holes were included, avoiding the need for separate blocks to be added during surgery. As illustrated in Figure 4.19, the holes are drilled on all surfaces of both the tibial and femoral clamps, which always remain in close proximity to the knee joint. This ensures that at least four holes are always accessible during surgery.

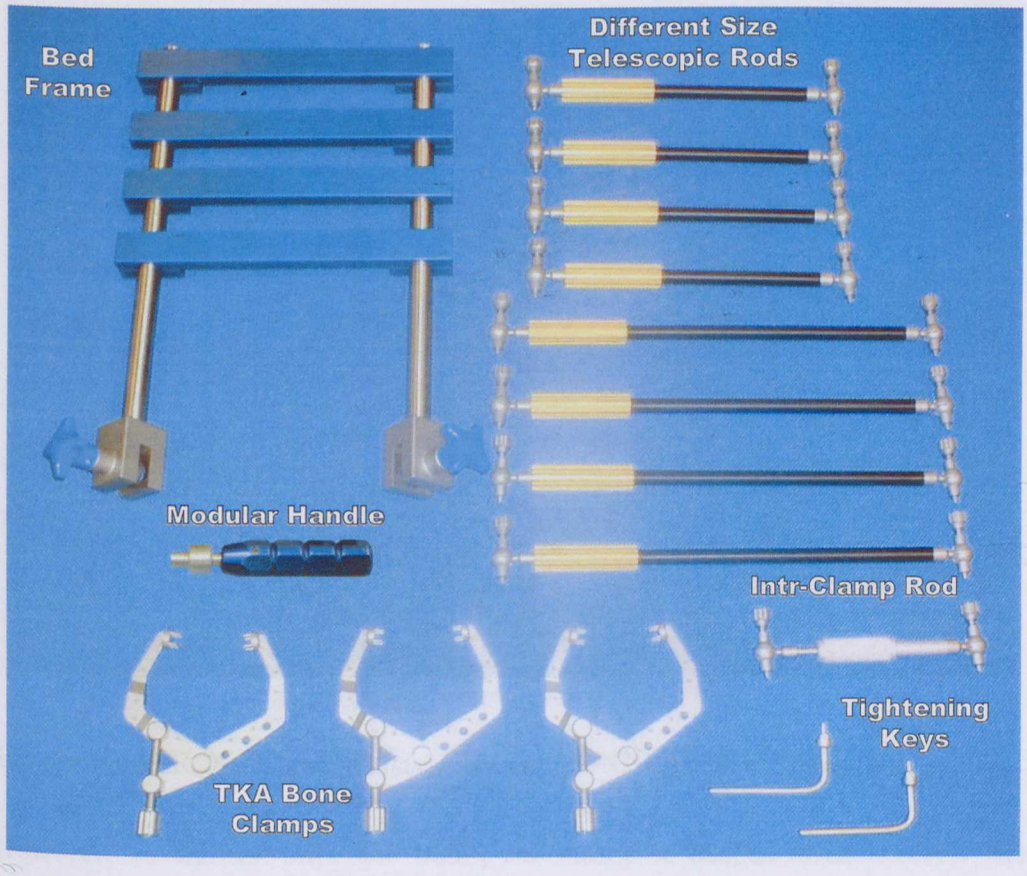


Figure 4.17: New TKA clamping system.

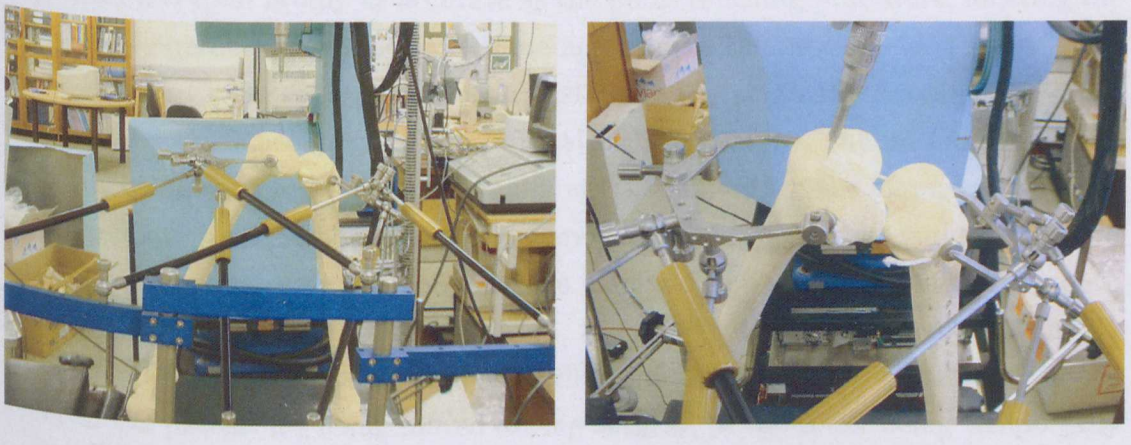


Figure 4.18: Typical clamping system intra-operative setup.

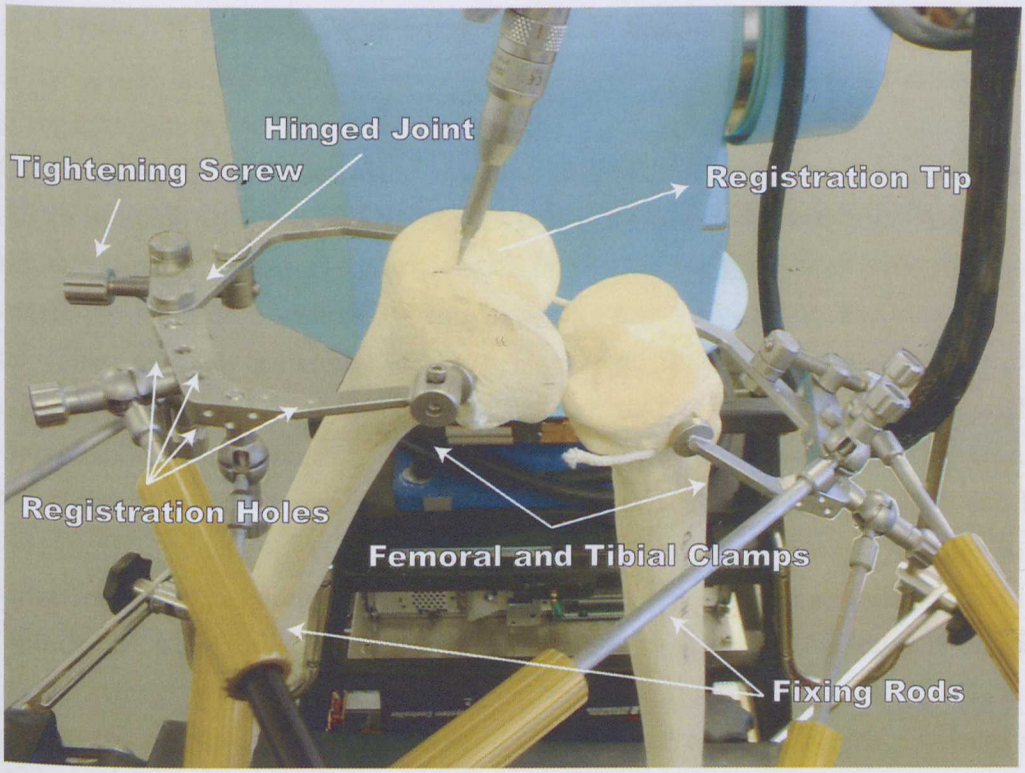


Figure 4.19: Point based registration using ACROBOT II clamping system.

However, to tighten onto the bone, the clamp is hinged with a screw, which causes relative motion in the clamp itself. As a result, groups of holes on each of the two clamp components move in relation to each other, defeating the purpose behind modelling them in software. Before registration can be carried out, the actual position of as many points on the clamps as possible needs to be stored in memory, as untouched holes cannot be used during the procedure. Since the block registration system is only as accurate as the point touching procedure, locating the holes intra-operatively will not affect the accuracy of the process.

Even though the concept of block registration was originally developed in order to overcome the inaccuracy of the original GPS prototype, this technique proved to be more advantageous than originally envisioned. Since the clamps should not move in relation to the bones to which they are hinged, it can be assumed the rigid transformation connecting the bone to the clamps will remain constant throughout the procedure. Therefore, once registered, the knee joint and clamping system can be treated as one, dramatically reducing the time needed for re-registration. In the event of the patient leg being moved during surgery, or the robot being temporarily removed from the OR due to an emergency, touching three holes on the clamps will be all that is needed to re-confirm the robot's position in relation to the knee. This improves the robustness of the procedure, and increases flexibility from a user's

point of view. If necessary, the surgeon may loosen the fixing rods, and test the mobility of the joint, without having to carry out the relatively time consuming bone registration procedure once again.

Clamp-based block registration can also be used to ensure the knee joint has not moved in relation to the ACROBOT II System during the procedure. At any time during the surgery, the stored positional information for the femur and tibia can be compared to the one obtained by touching any three points on the clamps. As a result, either an error is flagged to alert the surgeon that the knee has moved (if the difference is substantial), or the information can be automatically updated without the need for full re-registration. For this technique to work however, the assumption that the clamp does not move relative to the bone is made. Independent checking of bone motion relative to the clamping system is therefore recommended for future work. Alternatively, small holes drilled in the bone, or fiducial screws, can be used to replace the holes built in the clamps. As the location of the holes is collected intra-operatively, it is sufficient that a set of reproducible locations (fixed to the rigid body to be monitored) is passed to the re-registration algorithm. Occasional checking of the holes machined on the bone, for instance, would ensure that the bone monitoring process would be free from any bias due to undetected movement between the bone and clamping system.

To accelerate the clamp re-registration process, a novel hole-finding algorithm was developed, which automatically generates the paired points list once a unique set of holes has been touched. As soon as the user touches upon a set of holes that generates a unique pattern on the clamps, the algorithm automatically finds the corresponding stored hole locations. Therefore, assuming the holes fit a unique configuration, a minimum of three holes can be touched in random order at any time for the algorithm to instantaneously generate an updated transformation matrix defining the difference between the original and current clamp locations. The algorithm works on the principle of a distance map defining the relative position of each hole to every other hole. The candidate list is then pruned using an iterative procedure to remove impossible hole combinations as successive holes are touched. As shown in Figure 4.20, which illustrates a snapshot of the intra-operative software, once only one hole combination remains, an estimate is returned, but more points can be collected to improve the re-registration accuracy. A full mathematical derivation of the hole locating algorithm can be found in Appendix A.

Even though this bone motion monitoring facility does not provide real-time bone motion detection, the robustness and speed of the re-registration algorithm developed ensures that periodic checks can be carried out intra-operatively without significant contributions to the operating time.

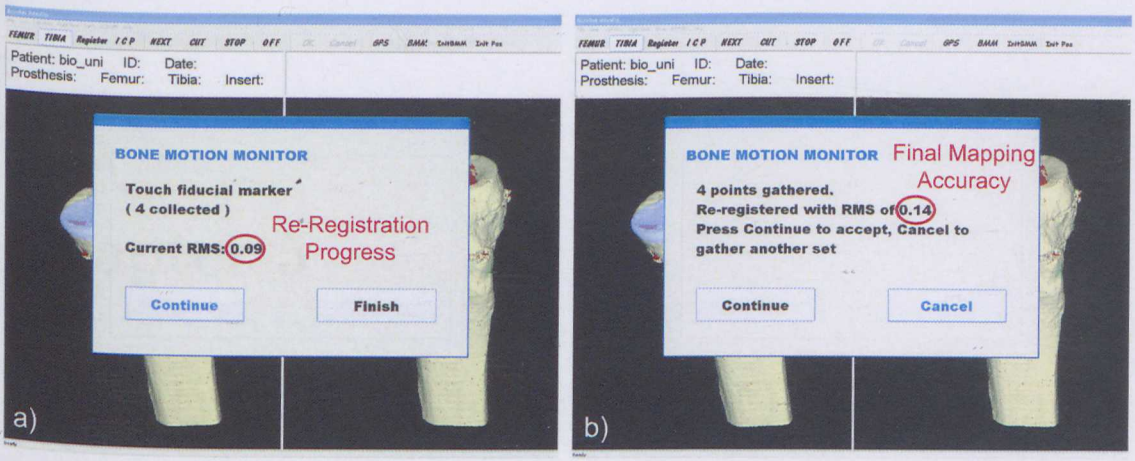


Figure 4.20: Intra-operative screen snapshot of the clamp re-registration procedure during point collection (a), and after the final computation (b).

4.5 Conclusion

This chapter has described aspects of the ACROBOT System redesign, which led to the successful implementation of the ACROBOT II System, illustrated in Figure 4.6. The redesign process described, which became necessary after its first clinical application for a number of TKA trials, has focused on the accuracy and safety of the system, although a complex set of specifications had to be assembled for manufacture. Both elements of the robot, the GPS and AC Head, were successfully redesigned and manufactured. The integrated 6 DOF system was then calibrated with submillimetric accuracy at the tip using a novel calibration technique, developed using the advantages of a back-drivable robot and an accurate mechanical digitiser.

The clamping system was also successfully redesigned, and block registration functionality (Section 3.3.4) was integrated into the bone clamps to allow fast and accurate re-registration and bone motion monitoring. Although this technique does not offer real time motion tracking, it enables the surgeon to periodically check the current setup for any relative motion of the immobilised leg with respect to the robotic system. Further enhancements to the bone monitoring technique described in this chapter have been addressed as areas for future work in Section 8.3.

Chapter 5

Registration Algorithm Optimisation

5.1 Introduction

The original anatomical registration procedure described in Chapter 3 was largely based on the standard Iterative Closest Point algorithm, which proved to be a viable alternative to pre-operative fiducial markers. However, early clinical experience in Total Knee Arthroplasty (TKA) surgery with the prototype ACROBOT System highlighted a number of areas for improvement, which, if successfully addressed, could substantially improve the outcome of the procedure.

Firstly, one run of the original algorithm required up to two minutes to converge, which proved to be an unacceptable delay for the surgeon. This was mainly due to the exhaustive search of the surface dataset carried out for every intra-operatively acquired point to find its corresponding closest point. Any speed enhancement in the closest point search would have a direct impact on the overall execution speed of the algorithm.

The original implementation was also highly susceptible to the quality of the initial estimate generated from paired point matching of anatomical landmarks. As described in Section 3.3, the ICP algorithm converges monotonically to the closest local minimum. Therefore, it is reasonable to assume that a solution to any intra-operative setup can always be found, given an appropriate selection of initial landmarks and surface points. However, distinguishing between any local minimum and the global minimum, which describes the true mapping of the intra-operatively acquired set of points to the corresponding modelled surface, represents one of the greatest registration challenges.

In the original implementation, the first run of the algorithm would return the local minimum that was closest to the initial estimate. Therefore, a poor initial estimate would often result in a very distant minimum being found, which in turn required further time consuming runs to be carried out in order to obtain better

estimates. A means to address local minima suppression was therefore required.

Furthermore, through extensive testing of the algorithm carried out during early experimentation, it was noticed that convergence to a local minimum would not always be monotonic. In other words, it was found that sometimes successive iterations of the algorithm would oscillate about a minimum without converging fully. A reason and a solution for this problem had to be found.

Finally, clinical experience strengthened the belief that a robust point touching protocol is essential for successful registration. Therefore, a simulation platform was developed to isolate both the algorithm and the procedure from the robotic implementation and intra-operative environment. A number of different tests was carried out in order to validate the performance of the registration technique for different simulated conditions. The conditions include different bone models, noise in the intra-operatively acquired dataset, and point touching schemes, which were then corroborated through plastic bone testing. This exhaustive validation process resulted in the development of a robust point acquisition protocol, suitable for robotic assisted TKA.

This chapter describes the work that was carried out on the original registration algorithm described in Chapter 3 to address the above issues and achieve the ultimate goal of a fast, robust, and accurate system for registration suitable for robotic assisted orthopaedic surgery.

5.2 Objectives

The objectives of this study can be summarised as follows:

- To address the issue of monotonic convergence.
- To speed up the registration method by implementing a fast search algorithm based on 3D data structures.
- To develop a means for local minima suppression.
- To define a robust point touching protocol.
- To empirically validate the results through simulation and on plastic phantom bones.

A detailed discussion of each of these issues can be found in the following sections.

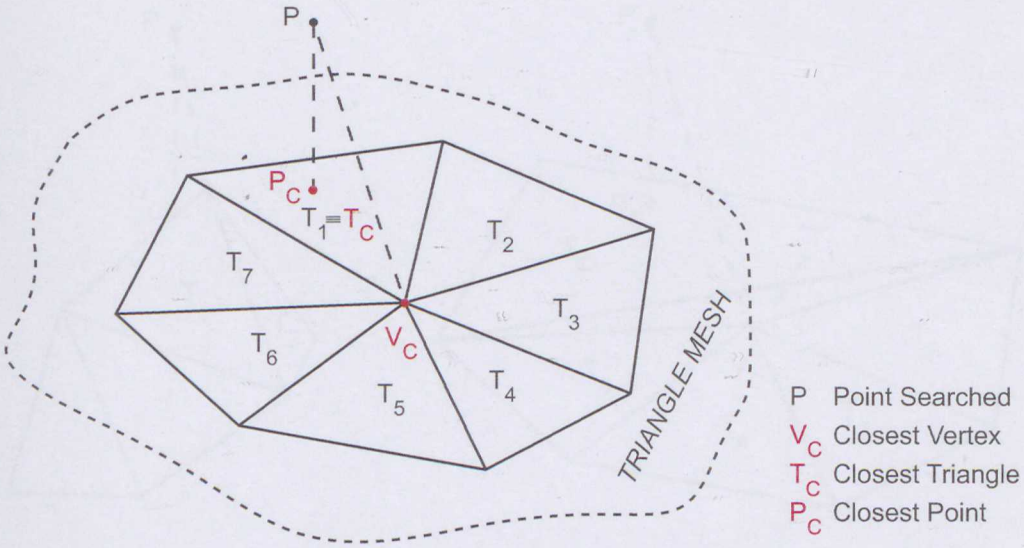


Figure 5.1: Closest point estimation for a triangular mesh.

5.3 Algorithm Optimisation

This section describes the methods, algorithm enhancements, and techniques developed to improve the performance of the original registration algorithm implementation described in Section 3.3. These changes have resulted in a definite performance improvement, which, as described in Section 5.4, has been assessed through extensive simulation and plastic bone testing.

5.3.1 Closest Point Estimation and Monotonic Convergence

As outlined in Section 5.1, the original implementation of the algorithm would some times not monotonically converge, but would fluctuate about a minimum. Even though of negligible magnitude, these fluctuations made it harder to identify a local minimum as the simple assumption of monotonically decreasing error values could not be made.

After some investigation, the source of this inaccuracy was traced back to the way the closest points were calculated. As described in Chapter 3, the registration surface is described in the form of a triangular mesh corresponding to the bone to be registered. As described in Figure 5.1, the closest point estimation was originally carried out in two stages. First, the closest vertex (V_C) is found, then the closest point (P_C) is calculated by projecting the normal of the original point (P) on the plane of one of the triangles (T_{1-7}) surrounding V_C.

The assumption that, for any point in 3D space, the closest point on the surface would lie on one of the triangles sharing the closest vertex, was made. As can be seen in Figure 5.1, in many cases the correct closest point can be found in this way.

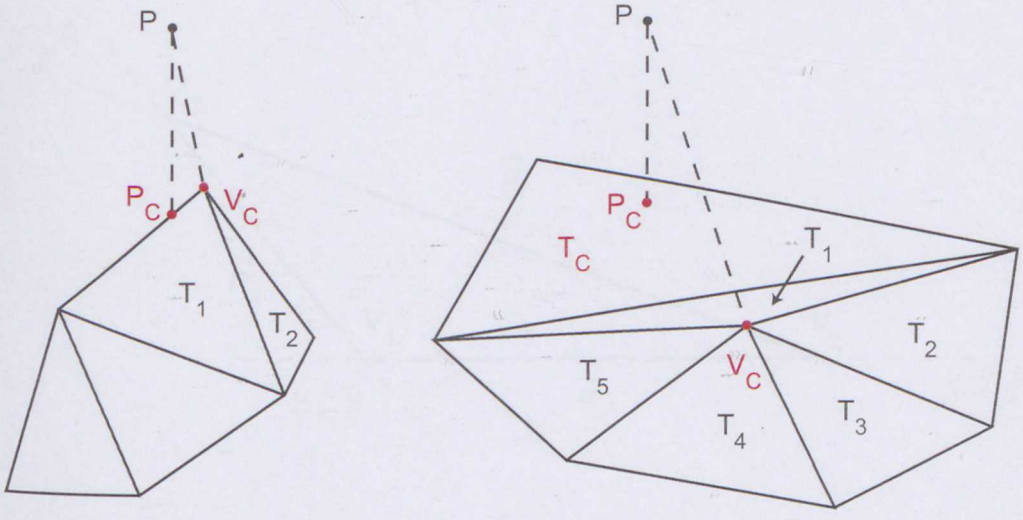


Figure 5.2: Special mesh configurations complicating the closest point search.

However, as described in Figure 5.2, there are special mesh configurations where this assumption no longer holds.

As can be seen, the assumption is no longer valid if the closest point does not coincide with the normal projection of P on T_C (the closest point actually lies on an edge of the mesh), or if the closest triangle (T_C) does not share the closest vertex.

To solve the former problem, a means to accurately define the closest point to a triangle, and a method to generate a list of candidates to be searched for every vertex in the surface mesh had to be developed. The triangle search mechanism should ensure the closest point search always returns the correct result, while minimising the search time overheads introduced by unnecessary checking of distant triangles. A *u-v* decomposition, based on the optimised algorithm presented in [Möller and Trumbore, 1997] was used to find the closest point on a triangle. As described in Figure 5.3, for any point in 3D space u-v coordinates can be used to define the position of the projection of P_C on the plane of the triangle.

Let:

$$\vec{a} = \overrightarrow{V_1V_2},\ \vec{b} = \overrightarrow{V_1V_3},\ and\ \vec{c} = \overrightarrow{V_2V_3}$$

Also:

$$\tilde{a} = \frac{\vec{P} \cdot \vec{a}}{|\vec{a}|},\ \tilde{b} = \frac{\vec{P} \cdot \vec{b}}{\left|\vec{b}\right|},\ and\ \tilde{c} = \frac{\vec{P} \cdot \vec{c}}{|\vec{c}|}$$

Then, if the projection (P_J) of P on the plane of the triangle falls within the triangle:

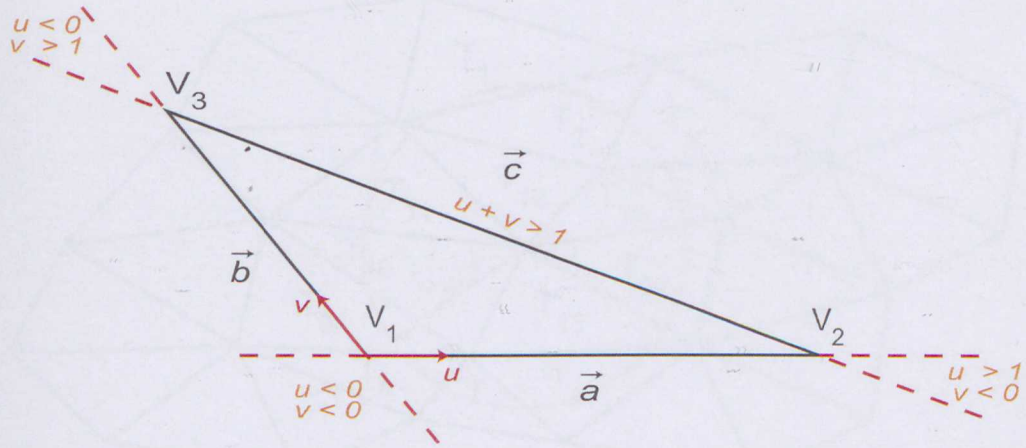


Figure 5.3: u-v co-ordinates used to describe a triangle in 3D space.

Cond	$\tilde{a}$	$\tilde{b}$	$\tilde{c}$	u	v	Closest Point
I	< 0 or > 1	< 0 or > 1	-	-	-	V_1
II	< 0 or > 1	-	< 0 or > 1	-	-	V_2
III	-	< 0 or > 1	< 0 or > 1	-	-	V_3
IV	< 0 or > 1	-	-	-	< 0	$V_1 + \tilde{a} * \vec{a}$
V	-	-	-	< 0	-	$V_1 + \tilde{b} * \vec{b}$
VI	-	-	-	-	-	$V_2 + \tilde{c} * \vec{c}$

Table 5.1: Table used to define the closest point on a triangle for any point in 3D space.

$$\begin{aligned} &0 < u < 1, \\ &0 < v < 1, \quad \textit{and} \\ &u + v < 1. \end{aligned}$$

Then, P_C can be defined as:

$$P_C = V_1 + u * \vec{a} + v * \vec{b} \tag{5.1}$$

If the normal falls outside the triangle, then the closest point is calculated by checking the conditions summarised in Table 5.1 in order, from I to VI. As soon as a set of conditions is met, the closest point can be calculated without checking further ones. For instance, if conditions I-III do not apply, but $\tilde{a} > 0$, then $P_C = V_1 + \tilde{a} * \vec{a}$.

In order to ensure that the triangle containing the closest point is always checked, a triangle list is precomputed and stored into a file to be used during registration. The triangle list provides a list of indexes identifying triangles to be checked for every vertex in the mesh. Therefore, once a closest vertex (V_C) is found, every triangle in the list for that vertex is checked for a closer point, as described in Table 5.1.

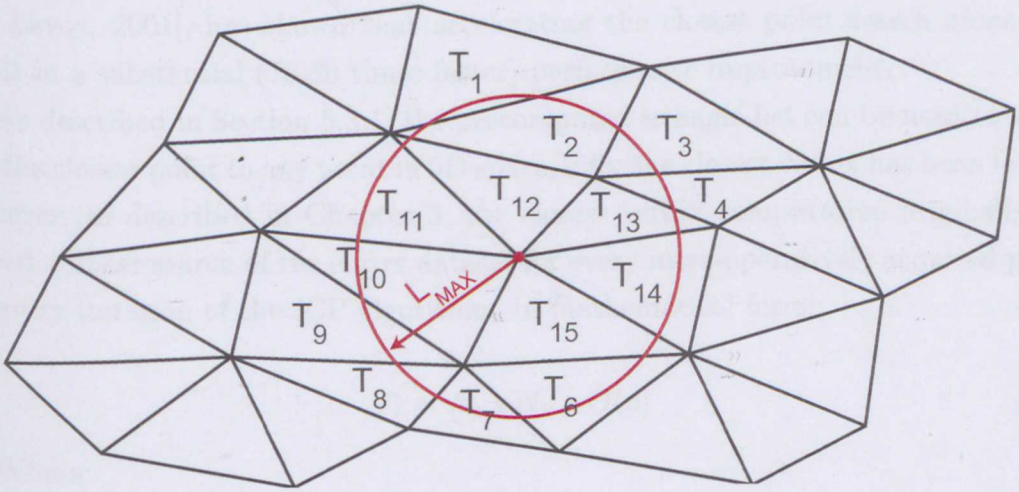


Figure 5.4: Generating the triangle list describing all triangles to be checked for any given vertex.

For any given mesh, the list of triangles to be checked is generated by comparing the distance between each triangle and each vertex against the computed maximum length of a side of a triangle. As illustrated in Figure 5.4, L_{MAX} is used to generate a candidate list which guarantees the closest point will be found once the closest vertex to any given point has been identified. The triangle list pre-computation is relatively time consuming, as $N_V \times N_T$(representing total number of vertices and triangles in a mesh) "closest point to triangle" calculations have to be performed. However, the list can be computed offline, therefore does not affect registration speed. An alternative method has been presented in [Ma et al., 1999], which uses an advanced search based on triangle centroids.

5.3.2 Accelerated Search

A large number of techniques to accelerate and optimise the execution of specific ICP algorithm implementations have been published in the literature [Chetverikov et al., 2002; Faugeras and Hebert, 1986; Jost and Hugli, 2002; Ma et al., 1999; Simon et al., 1994; Zhang, 1992]. Results have shown that a combination of these techniques can be used to improve the performance of the algorithm, which can be executed in interactive time. The iterative process can be accelerated by keeping track of the solutions at each iteration. If there is good alignment between the solutions (to within some tolerance), then both a parabola and straight line are fitted through the solutions, and the registration estimate is updated using one or the other of these estimates [Besl and McKay, 1992]. This has shown to accelerate execution speed by a factor of 3 or 4. However, a comparative review, detailing the characteristics and performance of a number of efficient ICP variants [Rusinkiewicz

and Levoy, 2001], has shown that accelerating the closest point search alone can result in a substantial (70-80 times faster) performance improvement.

As described in Section 5.3.1, the precomputed triangle list can be used to identify the closest point to any point in 3D space, once the closest vertex has been found. However, as described in Chapter 3, the closest vertex computation originally involved a linear search of the entire dataset for every intra-operatively acquired point for every iteration of the ICP algorithm. In mathematical form:

$$T_I = N_p * N_V * O(p) \tag{5.2}$$

Where:

T_I Total time per iteration of the ICP algorithm.

N_P Number of probe points (points acquired intra-operatively on the surface to be registered).

N_V Number of vertices in the triangular mesh representing the surface of the bone ($\approx 300,000$).

$O(p)$ Euclidean distance computation time for two points in 3D space i.e.
$\overline{P_1P_2} = \left|\overrightarrow{P_1} - \overrightarrow{P_2}\right|$
$= \sqrt{(P_1(x) - P_2(x))^2 + (P_1(y) - P_2(y))^2 + (P_1(z) - P_2(z))^2}$

Therefore a decrease in the number of Euclidean distance computations to be performed for every iteration of the algorithm would greatly improve execution speed. The solution was to develop a method to organise and structure the data contained in the surface file in order to speed up the closest vertex search.

After a careful investigation of available 3D data structures, an exhaustive review of which is reported in [Samet, 1990], it was decided to opt for a three dimensional k-d tree (k = 3). More specifically, the algorithm published in 1977 by Friedeman, Bently, and Finkel [Friedman et al., 1977], which describes an optimised k-d tree, was used. Unlike the standard k-d tree, an optimised k-d tree ensures near constant search time for any point in the dataset, regardless of the dataset distribution in 3D space. Therefore this implementation could produce comparable performance enhancements for any shape used for registration, such as distal and proximal femurs, tibias, etc. This was a prerequisite to ensure that the shape of the surface to be registered did not impose an unnecessary constraint on performance.

In the optimised k-d tree implementation, all data is stored at terminal nodes, or leaves, while non-terminal nodes just store a key or discriminator, "x," "y," or "z," in this case, and a separator or partition, defining what is found in the left and right

child branches. During tree generation, at every level, the discriminator is chosen as the key which has the greatest spread for the current set, while the partition is defined as the median value of the dataset. Tree generation for a sample 2D dataset is graphically illustrated in Figure 5.5.

The main aims of the implementation to be used for registration were fast execution speed, as any enhancement in performance would have a direct impact on registration speed, and minimum space requirements, as two full trees containing vertex information for large object files would be required simultaneously during registration of the femur and tibia.

Therefore, rather than rearranging 3D vectors of decimal numbers (representing mesh vertices in 3D space) into the different branches of the tree, integer indexes pointing to a large array of vectors stored separately were used to organise the data. In order for the pointers to the two "children" nodes to be available to every node without the need to store two additional values for every node in the tree, a full binary tree, large enough to contain all data describing the surface, is used. The number of levels and nodes is calculated as follows:

$$\begin{aligned} N_{Levels} &= ceil(log_2(N_P)) + 1, \; and \\ N_{Nodes} &= 2^{N_{Levels}} - 1 \end{aligned} \tag{5.3}$$

where:

N_{Levels} represents the number of levels in the binary search tree

N_{Nodes} represents the number of nodes required to completely fill an N_{Levels} binary search tree

$ceil()$ rounds the value within brackets up to the closest integer value

N_P is the number of points (in the form of indexes to 2D points (in the dataset)

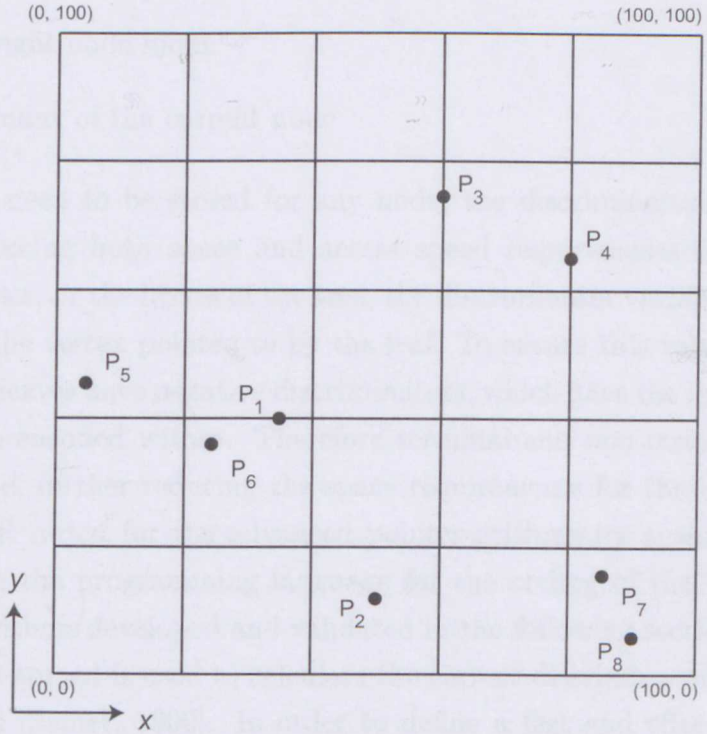
If a complete binary tree is used, then, for every node in the tree, the position of the two offsprings can easily be calculated by knowing the current node's position with respect to the base of the tree. If all nodes are numbered in ascending order from left to right, top to bottom, with "0" representing the root of the tree, then:

$$N_L = (N_C * 2) + 1 \tag{5.4}$$

and

a) 2D Point-Set Co-ordinates and Layout:

2D Point	x	y
P_1	35	40
P_2	50	10
P_3	60	75
P_4	80	65
P_5	5	45
P_6	25	35
P_7	85	15
P_8	90	5



b) Corresponding Optimised k-d Tree (k = 2) for the Dataset:

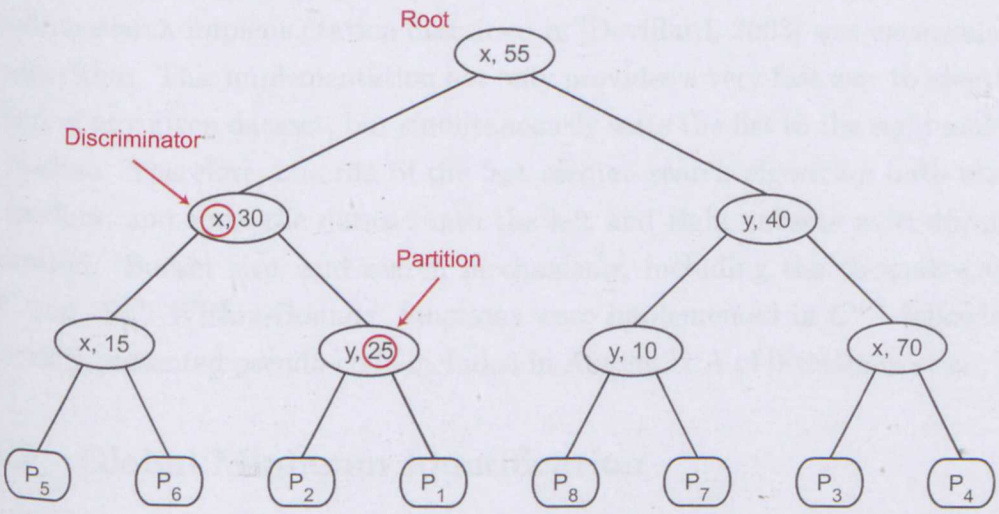


Figure 5.5: Optimised k-d tree example based on [Friedman et al., 1977].

$$N_R = (N_C * 2) + 2 \tag{5.5}$$

where:

N_L represents the left node index

N_R represents the right node index

N_c represents the index of the current node

This way, only two values need to be stored for any node, the discriminator and partition, considerably reducing both space and access speed requirements for a large tree. For terminal nodes, or the leaves of the tree, the discriminator variable is used to store the index of the vertex pointed to by the leaf. To ensure this value is not confused with a key, all leaves have negative discriminators, which have the index of the vertex they point to encoded within. Therefore terminal and non-terminal nodes can be treated as one, further reducing the space requirements for the tree. This implementation is well suited for the advanced pointer arithmetics available in C^{++}, which was used as the programming language for the coding of the tree generation and search algorithms developed and validated in the following sections.

The key with the largest spread is used to calculate the correct discriminator for every node, as described in [Samet, 1990]. In order to define a fast and effective partitioning method to structure the data in the tree, the well known fast ANSI C median search implementation described in [Devillard, 2003] was encapsulated in the algorithm. This implementation not only provides a very fast way to identify the median of any given dataset, but simultaneously sorts the list to the right and left of the median. Therefore, one run of the fast median search algorithm both identifies the median, and sorts the dataset into the left and right subsets used during tree generation. Bucket size, and search mechanisms, including the "Bounds-Overlap-Ball" and "Ball-Within-Bounds" functions were implemented in C^{++} following the accurately presented pseudo-code included in Appendix A of [Friedman et al., 1977].

5.3.3 Global Minimum Identification

As stated in a number of occasions already, the ICP algorithm, which provides the basis for the registration algorithm described in the previous chapter and which is optimised in this chapter, monotonically converges to a local minimum. However, in any complex multi-dimensional search problem it is possible to get trapped in local minima of the search space, which do not coincide with the global minimum which should be the result of successful registration. During registration, two possible types

of local minima can be found: those close to the global minimum, and those distant from it. For the work described in this thesis, it is assumed that the latter condition will not arise since sufficiently good initial pose estimates are available via anatomical landmark correspondences. When distant local minima are problematic, techniques which attempt to guide the search towards the global minimum can be helpful at avoiding them [Grimson et al., 1995; Besl and McKay, 1992]. A particularly promising approach to this problem based on geometric hashing is described in [Johnson and Hebert, 1997]. However, in order to deal with the former type of local minima (i.e., those near the global minimum) several researchers have suggested repeating the registration process several times, each time randomly perturbing the solution about the current optimum [Cuchet et al., 1995; Grimson et al., 1995]. A similar approach has been implemented in this work and is explained in the following sections.

Several researchers have demonstrated the existence of local minima very close to the global minimum [Cuchet et al., 1995; Grimson et al., 1995]. Getting trapped in one of these local minima can lead to sub-optimal registration accuracy. Using the notation described in [Besl and McKay, 1992], let the right "class" of minima be identified by successfully carrying out landmark-based initial registration. Then, the object of the minima suppression scheme described is to correctly identify the global minimum corresponding to the class of local minima identified during initial registration.

An approach similar to that presented in [Grimson et al., 1995] has been implemented in this work and is outlined below.

- The ICP algorithm is run, and the resulting pose transformation is recorded. If the RMS error of the distance of the intra-operatively acquired points to the mapped surface resulting from this trial of ICP is smaller than errors from all previous trials of ICP, set the best transformation to the current transformation.

- A new initial pose is generated by randomly perturbing about the current best transformation. The random perturbations are uniformly distributed, with maximum translation magnitude and rotation angle (from angle-axis representation) empirically defined from simulation results described in Section 5.4.2.5.

- Steps 1 and 2 are iterated until a predefined number of runs of the ICP algorithm has been performed with no additional improvement in the resulting "least-square" error.

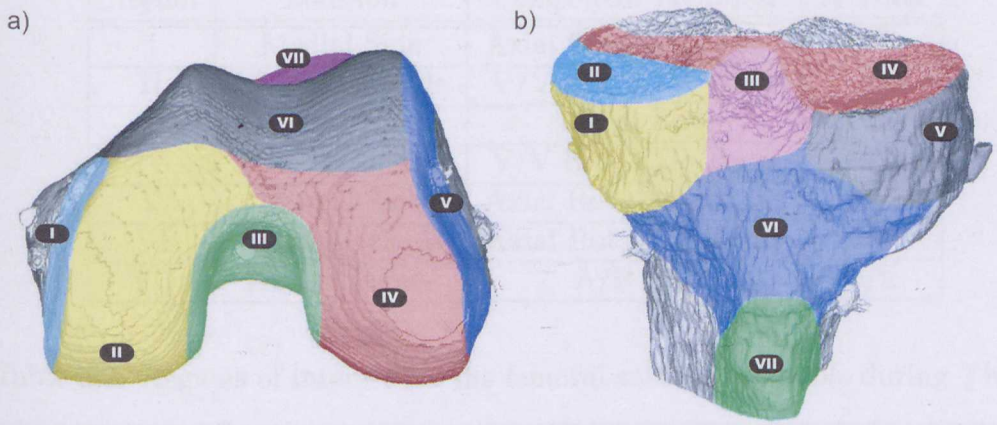


Figure 5.6: Registration regions for the femur (a) and tibia (b) suitable for TKA.

The effect of such a suppression scheme is to perform an exhaustive search of current class of minima in order to identify the solution which provides the smallest RMS error for the current point-set. As explained in [Besl and McKay, 1992], all rotations are carried out about the centroid of the point-set and no random translational perturbations are applied.

5.3.4 Defining a Robust Point Acquisition Protocol

Extensive experimentation with the simulator described in Section 5.4.2 allowed a number of prototype point-sets to be analysed, which enabled key areas of interest on the registration surface to be identified. These regions include significant features that are characteristic for the shape to be registered, and allow important components of the registration matrix to be robustly bound. The regions of interest identified, alongside their impact on registration outcome are graphically illustrated in Figure 5.6 and summarised in Table 5.2 and Table 5.3 for the tibia and femur respectively. The bounding effect of each region on registration outcome, listed under "Component Identified" in Table 5.2 and Table 5.3, is presented in the $\{BONE\}$ frame of reference defined in Section 5.4.1. The tabular representation of the surfaces includes the percentage of points to be collected in each region out of the total set size, which guarantees an even distribution of the points on the surface available for registration.

Simulation and plastic bone trials have shown that, by hand picking points in a number of key locations on each identified region of the surface, robust point-sets can be consistently obtained. The number of points required to accurately represent the surface to be registered depends on the location, spread, and accuracy of the points. If prominent features are precisely located, and all regions graphically identified in

Region	*Location*	*Component Identified*	% Total
I	Medial Side	Axial Rot, M/L Trans	10%
II	Medial Condyle	V/V Rot, P/D Trans	20%
III	Femoral Notch	Axial Rot	10%
IV	Lateral Condyle	V/V Rot, P/D Trans	20%
V	Lateral Side	Axial Rot, M/L Trans	10%
VI	Medial Groove	Axial Rot, A/P Trans	20%
VII	Frontal Femur	A/P Rot	10%

Table 5.2: Regions of interest for the femoral surface accessible during TKA.

Region	*Location*	*Component Identified*	% Total
I	Medial Side	Axial Rot, M/L Trans	10%
II	Medial Condyle	V/V Rot, P/D Trans	20%
III	Anterior Intercondylar Fossa	Axial Rot	10%
IV	Lateral Condyle	V/V Rot, P/D Trans	20%
V	Lateral Side	Axial Rot, M/L Trans	10%
VI	Frontal Tibia	A/P Rot, A/P Trans	20%
VII	Tibial Tuberosity	A/P & Axial Rot	10%

Table 5.3: Regions of interest for the tibial surface accessible during TKA.

Figure 5.6 are included, a relatively small number of points (20-30) is sufficient to robustly identify the surface. Examples of manually chosen 20 points point-sets for the femur and tibia, which have shown robust performance characteristics, are illustrated in Figure 5.7. As can be seen, the two sets are made up of 20 points each in key locations, which make up a robust representation of the surface.

The aim of any registration method is to accurately establish the position of one co-ordinate system with respect to another. However, a robust registration method is one where this relationship can be derived with a high degree of confidence, irrespective of the current environmental conditions. For a registration algorithm which uses a set of points measured in one co-ordinate system and a surface measured in another co-ordinate system, such as the one described, the quality of both the point-set and the surface has a direct effect on registration outcome.

As described in Section 3.3.1, the quality of the surface used for registration is affected by a number of factors, including, for instance, the quality of the bone and the accuracy of the CT scanner and scanning process. These factors are difficult to isolate, and their effect on registration outcome, which would involve a study that goes beyond the scope of this thesis, is hard to quantify. Therefore, in order to describe a robust point-touching protocol, the relationship between point-set quality and registration outcome needs to be defined.

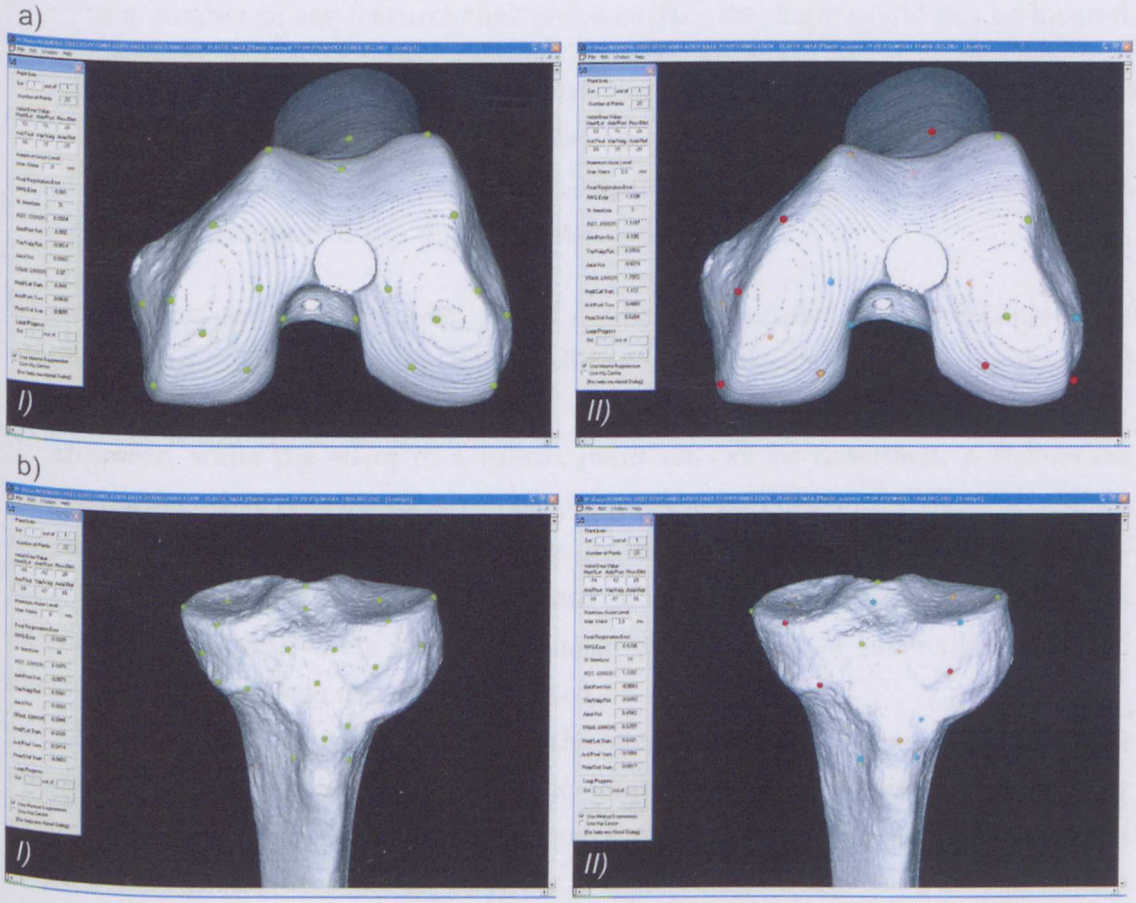


Figure 5.7: Registration accuracy for typical hand-picked robust point-sets for the femur (a), and tibia (b), with no noise (I), and 2mm random noise added (II).

The quality of a point-set is defined in terms of three factors:

1. *Number of points in the point-set:* As point collection is time consuming, the number of points required for registration is important and should be minimised.

2. *Distribution of the points on the surface available for registration:* Point distribution provides a direct measure of how accurately a set of points identifies a surface. Poor distribution would result in a poor representation of the surface, as a number of key features that give a surface its shape would not be located.

3. *Accuracy of the points:* Point accuracy is a representation of the extent to which the point-set fits the surfaces, and is affected by a number of factors, which, as described in Section 5.4.2.3, include point collection inaccuracies, and the accuracy of the digitising method.

Therefore, the optimum point-set would consistently produce an acceptable registration outcome in a minimum time, with the least amount of points possible, and a high degree of noise applied.

However, while the effect of a robust point-set can be described, a theoretical derivation for what constitutes a robust point-set is harder to provide. The regions described in Tables 5.2 and 5.3 and the general distribution of the robust point-sets illustrated in Figure 5.7 are the result of extensive experimentation with the simulation platform, where the performance of a number of manually assembled characteristic point-sets could be evaluated.

The robustness of a point-set such as the one illustrated in Figure 5.7, however, is compromised by the accuracy to which the points represent the surface. For the very reason that points in key locations are important to bound important components of the registration transform, large errors is these points would have a large impact on the final registration accuracy. Therefore the robustness of a point-set cannot be guaranteed unless the accuracy of the point collection process is known.

A robust *distribution of the points on the surface available for registration* is guaranteed by the point acquisition protocol based on regions, as described above. The *number of points* required to obtain an appropriate registration outcome is inversely proportional to the *accuracy of the points*. A very noisy point-set, which would represent poor point accuracy, has a larger probability to affect points describing key features, which would result in a degeneration of the registration outcome. Collecting a larger number of points in key features has the effect of mitigating the effect of noise on registration outcome for a representative point-set.

Therefore, a robust point acquisition protocol can be obtained as follows:

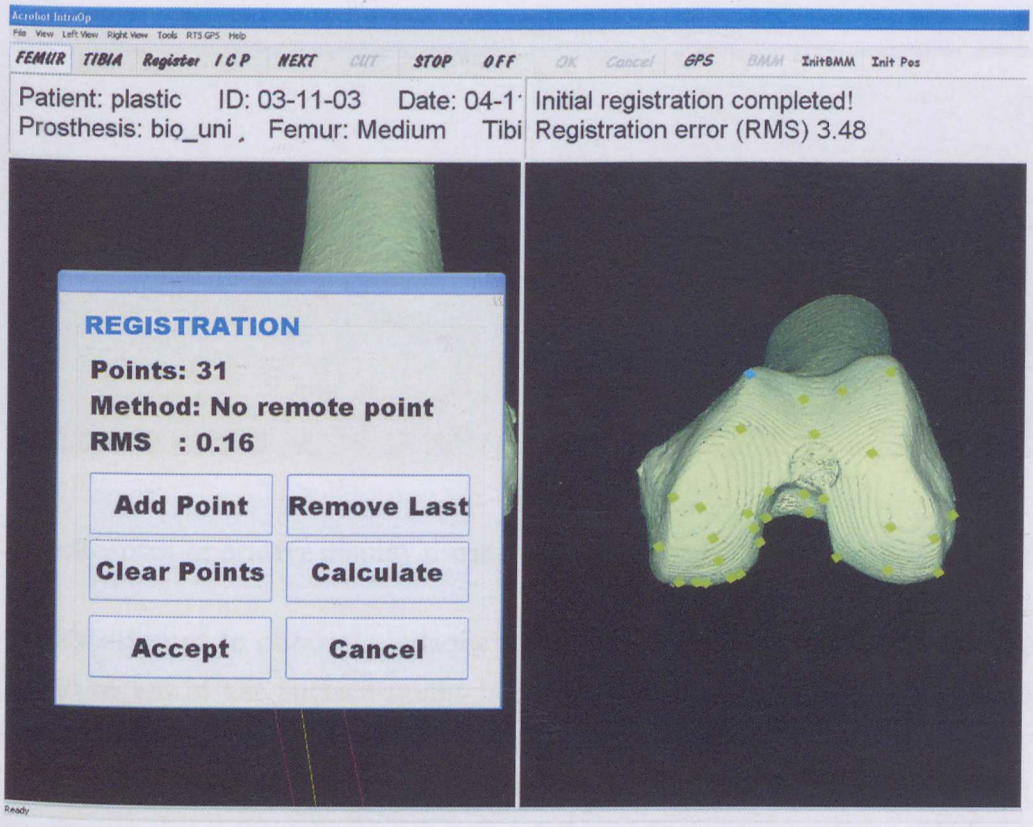


Figure 5.8: Improved GUI for the ACROBOT II System.

1. Define the point-set size required to ensure robust registration based on an estimation of achievable point accuracy. Representative figures based on simulation are presented in Section 5.4.2.5.4.

2. Use the region-based acquisition process, with a proportion of the total point-set size in each region, as described in Tables 5.2 and 5.3.

This point touching protocol is enforced intra-operatively by visually guiding the surgeon during the point acquisition process, as described in the following section.

5.3.5 Intra-Operative Guidance

In order to aid the surgeon through the point acquisition process, the intra-operative user interface described in Section 3.3.3 was modified to address a number of issues that were raised during early experimentation. A snapshot of the improved user interface is illustrated in Figure 5.8.

The user can now selectively add and remove points during registration, which allows different point combinations to be tested with ease, without the need to start over if a new set is required. Although a robust point acquisition process has been developed and validated (Section 5.3.4), the added flexibility of the GUI ensures

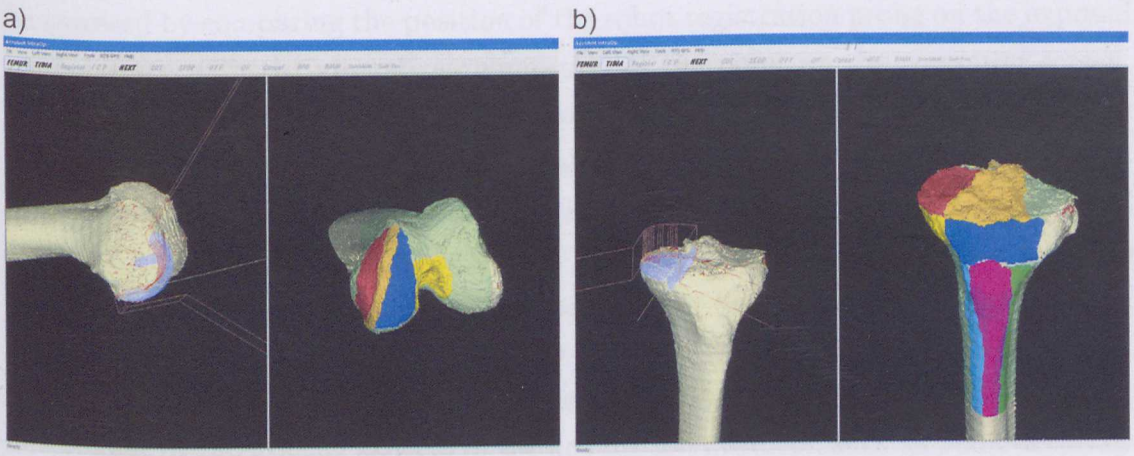


Figure 5.9: Intra-operative display during the region based point acquisition process.

that every attempt to obtain an adequate point-set can be made although access to a specific region of the surface might be restricted by a particular intra-operative setup.

To ensure the robust point acquisition protocol described in Section 5.3.4 is enforced, during the point collection process different regions are colour coded against the surface available for registration on the intra-operative GUI (Figure 5.9). The surgeon is directed to collect a number of points in each region, but can decide to ignore the on-screen guidance, if a particular surface is not available for registration due to the current intra-operative setup. The number and position of the surface regions, and the number of points required during intra-operative guidance have been empirically derived through exhaustive testing of a number of femoral and tibial CT generated surfaces. An explanation of the testing method and the results obtained for a typical set of plastic phantom bones [Sawbones Europe AB, part number: 1145] is included in Section 5.4.2.5.3. An equivalent set of results obtained from patient-generated surfaces is included in Appendix B.

As a result of the speed enhancements introduced by the k-d tree based vertex search, and by the triangle list pre-computation (Section 5.3.2), single runs of the enhanced ICP algorithm (i.e. a run of the registration algorithm without minima suppression) are performed in interactive-time after every additional point is collected intra-operatively. Once at least six points have been collected, the algorithm is executed, which results in a temporary registration RMS error and a colour-coded display of the collected points on the mapped surface appears on screen. This visual enhancement serves two main purposes, which both require visual inspection of the intra-operative display during the point collection process: global minimum identification, and qualitative assessment of the robustness of the current point-set. As the display is updated after every point collected, the contribution of each addition can

be assessed by comparing the position of the robot registration probe on the exposed bone surface with the virtual representation of the point on the computer screen. For instance, a large number of red points would suggest that the current solution is trapped in a local minimum, which could be overcome by the addition of a point in another region of the surface. Also, large positional changes between registration solutions obtained for consecutive points, which would show as large motions of the point-set represented on screen with respect to the virtual surface, is the result of a weak point-set, which in turn identifies the need for more points to be collected. The interactive point collection process described above could be, to a large extent, automated by integrating aspects of the acquisition protocol, such as point accuracy estimation, into the registration protocol. This additional intra-operative guidance enhancement has been addressed in Section 8.3 as an area for future work.

Although the enhanced guidance illustrated above only provides qualitative feedback during the point acquisition process, step by step instructions and an intuitive visual interface have resulted in a robust acquisition protocol, which has proved successful with surgeons.

5.3.6 Assessing Registration Accuracy in the OR

The Root Mean Square (RMS) of the distance of each collected point to the mapped surface is the only quantitative piece of information available intra-operatively to assess registration quality. This value provides a numerical representation of the quality of the fit between the intra-operatively acquired point-set and the surface to be registered. This value is complemented by a colour-coded display of the points on the mapped surface, which, as described in Section 5.3.5, allows the user to visualise the distribution of the error on the surface, and to recognise any exceptionally poor points that may have resulted from surgeon error or poor contact between the surface and registration probe. Furthermore, the user can check the quality of the fit by sweeping the bone surface with the registration probe and verifying that the visual feedback on the computer screen is correct. However, the RMS error, the colour coded display, and the virtual representation of the registration probe only provide the user with relative information about the registration outcome, as no absolute measure of performance is available intra-operatively.

Therefore, registration accuracy cannot be adequately assessed in the operating theatre, unless a robust point acquisition protocol is defined and rigidly enforced. As described in Section 5.4.2.5.5, the RMS error and colour coded display are only representative of the accuracy of the point collection process if an adequate point-set has been assembled. A robust point-set, which is one that robustly describes the surface to be registered, ensures that the global minimum of the points on the

mapped surface coincides with the actual position of the points on the surface. If the region-based acquisition protocol is used to assemble the point-set, careful inspection of the qualitative information provided by the visual display can then be used to assess the quality of registration. Having chosen an appropriate point-set size based on the predicted point accuracy (Section 5.4.2.5.3), an even distribution of colours, and a relatively low RMS error become robust indicators for good registration. In contrast, a very low RMS error and a perfect fit between the points and the surface may not be representative of actual registration accuracy unless the point-set used is appropriately assembled. This can be highly misleading to the untrained eye.

A relative indication of point-set robustness has also been empirically derived from the simulation results carried out for the validation of the point acquisition protocol described earlier. An overview of this novel intra-operative validation procedure, which allows a statistically significant set of figures (e.g. worst case error magnitude, based on 2 standard deviations from the mean, for each component of the registration matrix) for the degree of robustness of a particular point-set to be identified, is described in Section 5.3.6.1. Preliminary validation of the technique (Section 5.4.2.5.6) has shown promising results, although the computation time requirements, illustrated in Table 5.10, are still too high for use in a clinical environment. This limitation of the current implementation, which was used as a concept demonstrator, has been addressed in Section 8.3 as an area for future work.

5.3.6.1 Defining Point-set Robustness Indicators

If the protocol described in the previous paragraphs is followed, a ballpark figure for the overall point accuracy achieved for a specific intra-operative scenario can be estimated by visually inspecting the colour-coded display of the points on the mapped surface. As the colour-coding is a function of the residual error for each registered point, an evenly distributed set of colours for a representative point-set, an example of which can be seen in Figure 5.10, coupled with the RMS error value (Section 5.4.2.5.5) can provide an approximate figure for the point touching accuracy. Mostly green and blue points, for instance, would indicate probable point accuracy of under 0.5mm.

From here forth, let the assumption that the point-set in question is assembled with points of predictable accuracy be made, and let the predicted maximum inaccuracy, which represents an estimate of how inaccurately each point can been acquired, be defined as ε. Then, each registered point can be interpreted as a surface point within a ε envelope of the actual surface, assuming the global minimum for the set has been identified (Section 5.4.2.5.2). Then, a robust point-set would be one that still accurately identifies the shape of the surface to be registered, irrespective of the

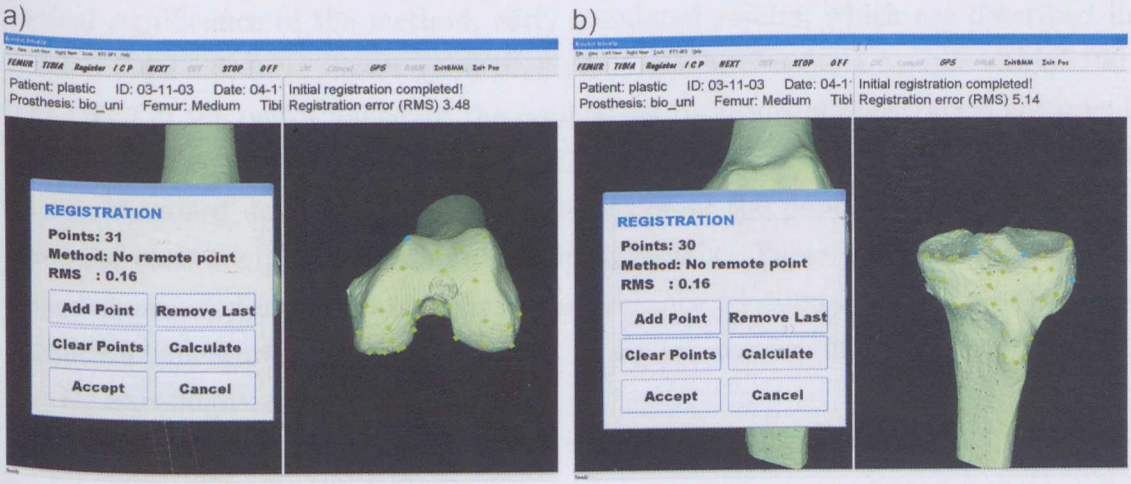


Figure 5.10: Colour-coded display of a representative point-set showing probable point-touching accuracy of under 0.5mm for the femur (a) and tibia (b).

inaccuracy introduced by ε.

For every point-set there is a set of errors within the envelope defined by ε that has the maximum impact on the robustness of the set. This worst case point-set is hard to derive, and could only be accurately identified by examining an infinite number of equivalent point-sets where each point is shifted by a random value between $\pm\varepsilon$ in a random direction. However, a reasonable estimate of robustness can be obtained by analysing the performance of a significant number of equivalent point-sets derived from the point-set to be assessed.

Appropriately deriving the point-sets that make up the population to be analysed is important for the results to be significant. Assuming the original point-set (PS_O) has been assembled with points that are inaccurate, a representation of what PS_O should look like if it was accurate can be derived by assembling a point-set made up of the closest points of each point of PS_O on the registered surface. Although this derived point-set (PS_D) is made up of actual surface points, calculated using the procedure described in Section 5.1, it preserves the shape of the original point-set, and is free from any bias introduced by the point touching inaccuracy of PS_O. PS_D can then be used to generate a number of equivalent point-sets calculated by perturbing each point by a random amount within ε, where ε is used as the maximum perturbation magnitude, $Rand_{MAX}$, as described in Section 5.4.2.3. Since PS_D is an "accurate equivalent" of PS_O, the mean, maximum, and minimum errors generated by analysing the population are centred about zero i.e they can be used to provide a meaningful representation of the robustness of the point-set with respect to the surface.

Although a large population size generated from PS_D would improve the sta-

tistical significance of the method, early simulated results, which are described in Section 5.4.2.5.6, have shown good prediction capabilities for a sample size of 100. The trend of the performance for the population (in terms of registration accuracy) has been shown to follow a normal distribution, therefore confidence figures based on two standard deviations from the mean (95% of the population) can be calculated for each component of the registration matrix. These values, interpreted in a co-ordinate system which has clinical significance (Section 5.4.1), can be used as "confidence measures" for the robustness of a point-set for different components of the leg axis alignment.

5.4 Empirical Validation

The following sections describe the work carried out to evaluate the performance of the enhanced ICP based registration algorithm described in this and the previous chapters for different surface models and environmental conditions. Although the performance of the general purpose ICP algorithm used is well documented, the effectiveness and robustness of the enhanced implementation described in this thesis had to be assessed through extensive simulations and plastic bone trials. This validation process, described in detail in the following sections, also provided a means to verify the effectiveness of the robust intra-operative point touching protocol described in Section 5.3.4, which has proved to be appropriate for clinical use with the ACROBOT II System.

The study focuses on CT generated models of a number of distal femurs and proximal tibias, as the registration procedure described was aimed at robotic-assisted TKA. However, this enhanced ICP algorithm implementation is a general purpose means for point-based surface registration, and would be suitable for a number of other orthopaedic procedures and data acquisition methods, some of which have been outlined in Section 8.3 as future work.

5.4.1 Error Representation

As described in Section 3.3, the outcome of registration is presented in the form of a transformation matrix describing the relative position and orientation of the frames of reference attached to the two co-registered surfaces. The position of the two frames of reference in space is not important, as the registration process will produce the correct transformation to map one onto the other. Using the notation of Equation (3.6), let:

$$T_{Reg} = T_{BASE}^{PLAN} \tag{5.6}$$

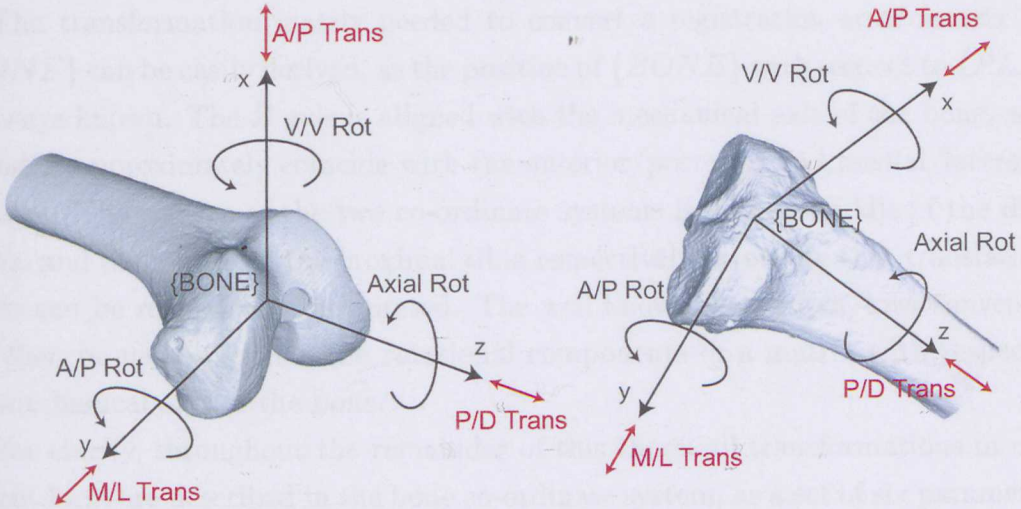


Figure 5.11: Co-ordinate systems attached to both the femur and tibia, used to provide a clinical interpretation of the registration error.

be the transformation matrix describing the position of the co-ordinate system of the plan, namely $\{PLAN\}$, with respect to the co-ordinate system of the intra-operative environment, namely $\{BASE\}$. The reliability of the relationship described by T_{Reg} is directly affected by the quality of the registration process. In prefect conditions, that could be only obtained through simulation, T_{Reg} would describe the true position of $\{PLAN\}$ with respect to $\{BASE\}$. However, the inevitable inaccuracies associated with registration will produce a residual error, proportional to the actual registration accuracy, which needs to be quantified in order for any registration method to be robustly assessed. Let T_{Reg} be rewritten as T^{Reg}_{BASE}, which describes the fact that the registration transform is in the $\{BASE\}$ frame of reference, and let T^{Ref}_{BASE} describe the true mapping between the two co-ordinate systems in $\{BASE\}$. Then:

$$T^{Reg}_{Ref} = \left(T^{Ref}_{BASE}\right)^{-1} * T^{Reg}_{BASE} = T_{Err} \tag{5.7}$$

T_{Err} describes the difference between the registration transform and reference transform in matrix form, which can be decomposed into six components that describe three rotations and three translations about the main axes of the co-ordinate system. However, the error matrix needs to be "attached" to a meaningful co-ordinate system in order for registration errors to be correctly interpreted, and their effect on clinical outcome accurately assessed. Therefore, in both simulation and plastic bone trials, registration error matrices are presented in component form about a co-ordinate system, namely $\{BONE\}$, which is aligned with the anatomical axes of the bone, as described in Figure 5.11 for both femur and tibia.

The transformation matrix needed to convert a registration error matrix into $\{BONE\}$ can be easily derived, as the position of $\{BONE\}$ with respect to $\{PLAN\}$ is always known. The Z axis is aligned with the mechanical axis of the bone, while Y and Z approximately coincide with the anterior/posterior and medial/lateral directions. The centres of the two co-ordinate systems lie in the middle of the distal femur, and the middle of the proximal tibia respectively, to ensure that translational errors can be realistically interpreted. The well known Roll/Pitch/Yaw convention can then be used to define the rotational components of a matrix with respect to the mechanical axis of the bone.

For clarity, throughout the remainder of this thesis all transformations in component form are described in the bone co-ordinate system, as a set of six parameters, coinciding with translations and rotations about X, Y, and Z, using the following notation:

A/P Trans Anterior/Posterior translation.

M/L Trans Medial/Lateral translation.

P/D Trans Proximal/Distal translation.

A/P Rot Anterior/Posterior rotation.

V/V Rot Varus/Valgus rotation.

Axial Rot Axial rotation.

When the translational error is not required in component form, it is referred to as:

$$Trans\,Err = \sqrt{(A/P\,Trans)^2 + (M/L\,Trans)^2 + (P/D\,Trans)^2} \tag{5.8}$$

which represents the overall magnitude of the translational error vector. Similarly, the axis/angle notation, which describes the compound sum of the three rotations about the principal axes in terms of a single rotation, *Rot Err*, about an arbitrary axis (θ in Figure 5.14), is used to describe the overall magnitude of the rotational error.

5.4.2 Simulation

The single most important advantage of simulation over *in vitro* experimentation is the ability to test a large number of test cases for a large number of different scenarios, which would take an unrealistic amount of time to be completed under real experimental conditions. Simulation can then provide an invaluable means

to build a statistically significant result set, which can then be corroborated with focused and controlled in vitro experiments.

Therefore a computer program was developed to simulate the point-touching procedure (normally performed intra-operatively) using the mouse interactively to generate a point dataset. Since under simulated conditions the position of both surfaces to be co-registered is known, simulation allows the relationship between the actual rotational and translational errors in the registered surface and the RMS error to be identified, and the performance of the algorithm in different scenarios to be explored. Simulation was used to validate the robust point acquisition protocol described in Section 5.3.4, and to show the effect of the algorithm optimisation process described on execution speed and global minimum identification.

Setting the correct framework for the simulation, establishing the correct parameters, and identifying the experiments to be carried out is key for meaningful simulation results. A description of the method used for simulation, including representation of noise, and point-set generation, can be found in the following sections, while the experiments carried out, and results obtained can be found in Section 5.4.2.5.

5.4.2.1 Simulation Software

The simulation platform was developed to isolate the algorithm and procedure from the robotic implementation and intra-operative environment. The program developed for the simulation was compiled in C^{++} using Microsoft Foundation Classes® (MFC), and OpenGL®. The aim was to define a test-bed to analyse the performance of a large number of different point sets for different scenarios and initial conditions.

The program is interactive, but can also run automatically, with a number of different configurations being loaded from file at startup. A screen-shot of the program is illustrated in Figure 5.12.

As illustrated in Figure 5.12, the user can interactively select a number of parameters including the error in the initial estimate, and the maximum noise to be used during the simulated point collection procedure. The program can then be used to run the enhanced ICP algorithm, which can be executed with or without minima suppression, for the dataset. After completion, the simulator displays the computed RMS error, alongside the magnitude of the effective rotational and translational errors in the registered surface, and the six components of the error matrix in the $\{BONE\}$ reference frame. These results are complemented by the number of iterations required for the algorithm to converge, and a colour coded display of the points on the mapped surface. The difference between the position of the registered surface (in yellow) and the actual surface (in grey) provides a visual representation

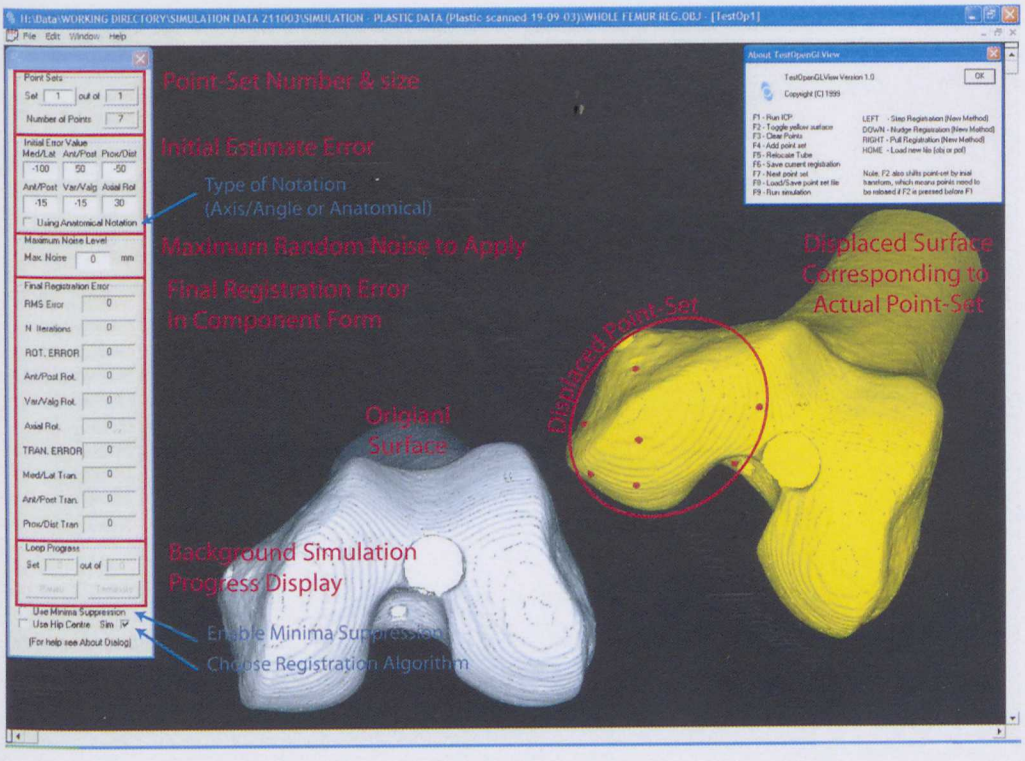


Figure 5.12: Simulation program screen-shot.

of the registration error for the current point-set. Formatted text files including a number of different point-sets and configurations can be loaded into the program, and computed in the background, while retaining normal program functionality.

5.4.2.2 Modelling Initial Registration Inaccuracy

The error in the initial estimate (usually generated during landmark collection intra-operatively) is simulated by systematically translating and rotating a copy of the bone surface about each of the axes attached to the centre of the bone (see Figure 5.13).

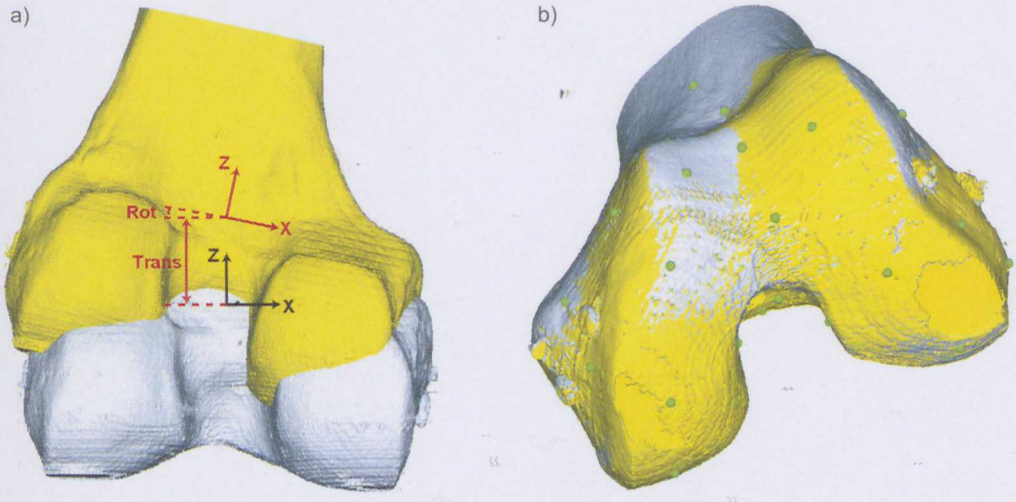


Figure 5.13: The shifted surface (a) is represented in grey against the original surface (yellow). The corresponding registered surface (b) for a predefined point set is also shown. All green points lie within 0.1mm of the mapped surface.

Therefore, a "perfect" initial registration would be simulated by an overlap of the two surfaces (represented in grey and yellow in Figure 5.13) before running the algorithm, while poor initial registration would include large translations and rotation about all three axes.

The simulator provides control over the initial error by allowing the user to select the six parameters of the initial transformation matrix using the notation described in Section 5.4.1, which allows the user to have complete freedom in three dimensions using an intuitive framework. Alternatively, the axis/angle notation, graphically represented in Figure 5.14, can be used to define the rotational component of the initial error as a single rotation of defined magnitude about an axis, which is specified by two angles.

5.4.2.3 Adding Random Noise

In a perfect system, every three-dimensional point measured on the surface of the bone corresponds to a unique point on the modelled surface to be registered. However, a number of variables affects both the point touching procedure and registration algorithm performance. Sources of error include any inaccuracies in the kinematic chain linking the base of the gross positioning system to the tip of the active constraint head, and any differences between the virtual and actual bone surfaces that need to be co-registered. In addition, the point touching process introduces further inaccuracies, which, for instance, may result from variations in the force used to touch the bone with the registration probe.

As these sources of error and their effect on registration outcome are difficult to

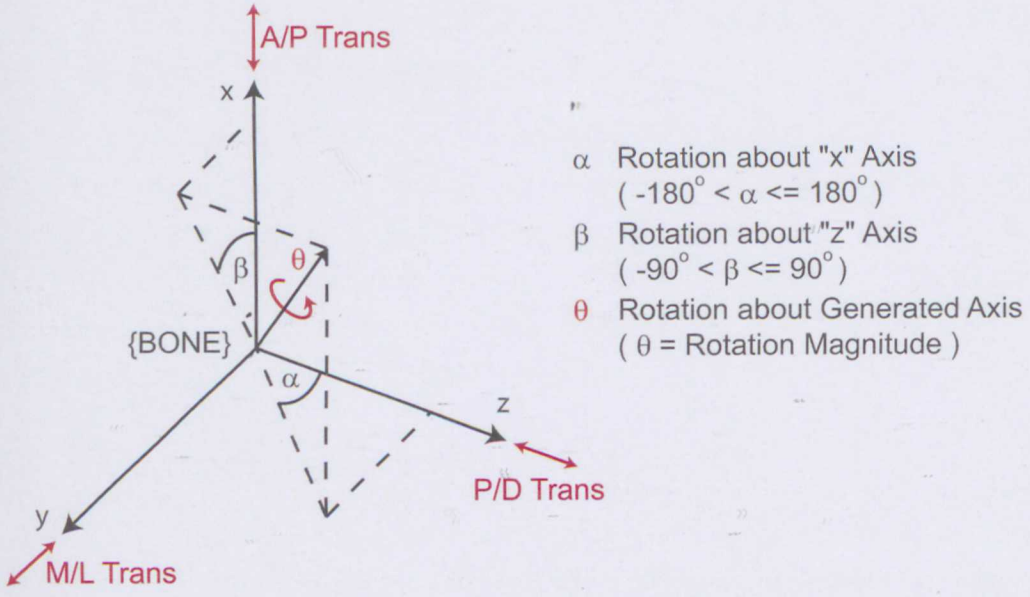


Figure 5.14: Axis/angle notation described in terms of three angles, α, β, and θ.

isolate and to quantify, it was decided to integrate noise in the simulated point-set as a single value that would result in a realistic error distribution, which could mimic the quality of an actual point-set collected intra-operatively. Random perturbations in a direction normal to the surface would mimic errors resulting from discrepancies between the modelled and actual surfaces (e.g. due to scaling), and differences in the impact force used during point collection, which would result in different levels of penetration of the registration probe into the bone surface. Errors in the tangent direction would account for poor contact during point collection (e.g. due to slippage of the probe on the surface), and inaccuracies in the kinematic chain of the robotic system, introducing error offsets in random directions depending on the current robotic configuration.

Therefore random noise is added to each point in a random direction with a random magnitude, as follows:

$$P_{mod} = P \times P_{rand} \tag{5.9}$$

where:

P is the original point in 3D space

P_{rand} is a random 3D vector defined as $(rand(), rand(), rand())$, whose maximum effect is defined as $|P_{Rand}| = \sqrt{3 * Rand_{MAX}^2}$

$rand()$ is a random number between $-Rand_{MAX}$ and $Rand_{MAX}$.

$Rand_{MAX}$ varies between "0" (a perfect system) and a maximum value defined by investigation of the system.

Therefore, all points in the dataset can be shifted by a random amount in a random direction by as much as $\sqrt{3 * Rand^2_{MAX}}$, resulting in some points floating above, and others being embedded, in the surface to be registered.

The "Max. Noise" parameter, shown in Figure 5.12, was integrated into the program to allow the user to define a value for $Rand_{MAX}$, which can be used to add random noise to any point-set loaded from file.

5.4.2.4 Generating Random Point-Sets

As described in Section 5.3.4, a large number of manually assembled point-sets was used for the early stages of validation with the simulator. This interactive process, which involved an in-depth analysis of each manually specified point-set for different simulated conditions, resulted in the definition of the regions-based point acquisition protocol described in Section 5.3.4. However, a structured validation method was required to show that the defined point-touching protocol was suitable for clinical use.

For this type of validation process to have statistical significance, a large number of point-sets needed to be analysed for a number of different conditions. Therefore, it became necessary to develop a means to generate a large number of viable point-sets, which, although automatically generated, would still mimic manually created ones. For this purpose, a set of surface files describing individual regions of the surface available for registration was assembled for every model analysed. The regions identified by the surface files resemble those graphically illustrated in Figure 5.6 for the tibia and femur. Subdividing the available registration surface into different files allowed point-sets to be generated by assembling random points collected on each one of the regions, in the proportions specified in Tables 5.2 and 5.3, for the femur and tibia respectively. For instance, to automatically generate a 10 points point-set for a femur, the software would randomly select 1 point on the medial side, 2 points on the medial condyle, 1 point on the femoral notch, etc.

This procedure, which was implemented as a self-contained C^{++} class, enabled a large number of viable point-sets of different sizes and spread to be automatically generated. These large datasets, stored as formatted text files, were used for a number of experiments, as described in Section 5.4.2.5.

5.4.2.5 Tests and Results

The main aim of the simulation was to show that the region-based acquisition protocol, which was developed through manual experimentation on the simulator, pro-

vides a *reliable means* for robust point-set generation. This objective can be achieved by addressing the problem in two stages. It is first necessary to provide evidence, by means of a structured experiment, to show that by carefully selecting a number of points in each region, which is the essence of the region-based protocol, robust point-sets can be consistently generated. Then, the impact of the inherent variability associated with point-collection within regions on registration accuracy needs to be quantified. Attainment of the first aim would show that the concept of a "region-based" registration procedure is viable, while the second stage would show that robust registration can be achieved by implementing the protocol described in Section 5.3.4.

Experiments described in the following sections also allowed different aspects of the registration software, such as global minimum identification, execution speed, and the relationship between RMS error and registration accuracy, to be tested in isolation. The objectives of the tests carried out were:

1. To evaluate the execution speed of the optimised algorithm described in this chapter.

2. To assess the effectiveness of the local minima suppression procedure described in Section 5.3.3.

3. To provide evidence that the region-based point touching protocol represents a viable means to assemble robust point-sets.

4. To evaluate the performance of the region-based protocol coupled with the enhanced ICP algorithm described in this chapter.

5. To investigate the relationship between RMS error and actual registration accuracy.

6. To provide preliminary results about the efficacy of the intra-operative point-set robustness assessment method described in Section 5.3.6.

Typical femoral and tibial surfaces generated from a CT scanned plastic phantom have been used for descriptive purposes, although, where necessary, each test has been carried out on models generated from real patients' anatomies. A complete set of results for patient generated surfaces can be found in Appendix B.

5.4.2.5.1 Execution Speed Triangle list pre-computation, and the k-d tree based closest vertex search, have improved the execution speed of the original algorithm described in Section 3.3.3 by approximately a factor of one hundred. One

	Distal Femur		Proximal Tibia		Reduced Femur		Reduced Tibia	
Vertices	130711		92368		60243		55304	
Triangles	260841		184311		119243		109554	
File Size (KB)	10,151		6,983		4,551		4,140	
Execution	*No MS*	*MS*	*No MS*	*MS*	*No MS*	*MS*	*No MS*	*MS*
Time (ms)	72.34	1832.65	56.56	1881.09	68.13	1620.95	55.95	1654.53

Table 5.4: Execution speed for the enhanced ICP algorithm implementation with and without minima suppression (MS) for different size surface models.

hundred ICP computations can be carried out in the same time that the original algorithm took to execute once, which means that the minima suppression procedure described in Section 5.3.3 can be executed without an increase in registration time. This radical speed enhancement allows one run of the algorithm to be completed in interactive time, which is more than appropriate for this type of application, and renders additional speed improvements unnecessary.

Since only a portion of the surface model generated from CT data is available for registration, the object file used for registration is reduced by manually removing inaccessible regions from the bone model. Typical computation speeds for the algorithm with and without minima suppression (MS) are summarised in Table 5.4 for both the original and reduced surface models representing a typical femur and tibia generated from CT data.

The results described in Table 5.4 were obtained for a typical point-set size of 35, on a PC workstation running Windows® XP Professional, with a 2.0GHz Intel Pentium® 4 processor.

5.4.2.5.2 Minima Suppression For the minima suppression technique adopted in this implementation, which is based on the RMS error of the distance of each point to the mapped surface, the global minimum for any point-set is identified by the position of the set with respect to the surface which produces the lowest RMS value. In theory, the global minimum identified should coincide with the best description of the surface that can be achieved for a particular point-set. The accuracy to which the global minimum describes the true position of the point-set on the surface is a function of the quality of the set, which, as described in Section 5.3.4, is affected by point distribution and point accuracy.

For the purpose of this experiment let the quality of the point-set, which affects the quality of the global minimum identified, be neglected, as the efficacy of a local minima suppression mechanism can be tested independently of the quality of the registration transform obtained. For a perfect minima suppression method, the position of the set which produces the smallest RMS error should always be

identified, regardless of the original (prior to registration) position of the set with respect to the surface. However, landmark-based initial registration (Section 3.3.3) can be used to provide a rough estimate of the position of the set, which avoids the need for the suppression mechanism to deal with distant minima. Therefore, in order to assess the efficacy of the minima suppression mechanism described in Section 5.3.3, a set of typical point-sets of different sizes were selected and tested for a large number of initial errors of different magnitude. The axis/angle notation illustrated in Figure 5.14 was used to generate random initial errors, centred about the object centre, in random directions but of known magnitude. Larger magnitudes (described by the angle θ in Figure 5.14) would result in larger rotational displacements of the point-set away from the surface. For the translational component, offsets of known magnitude but random direction were used to translate the points away from the surface. For simplicity, random initial errors of known magnitude have been generated with the same magnitude for both the rotational and translational components.

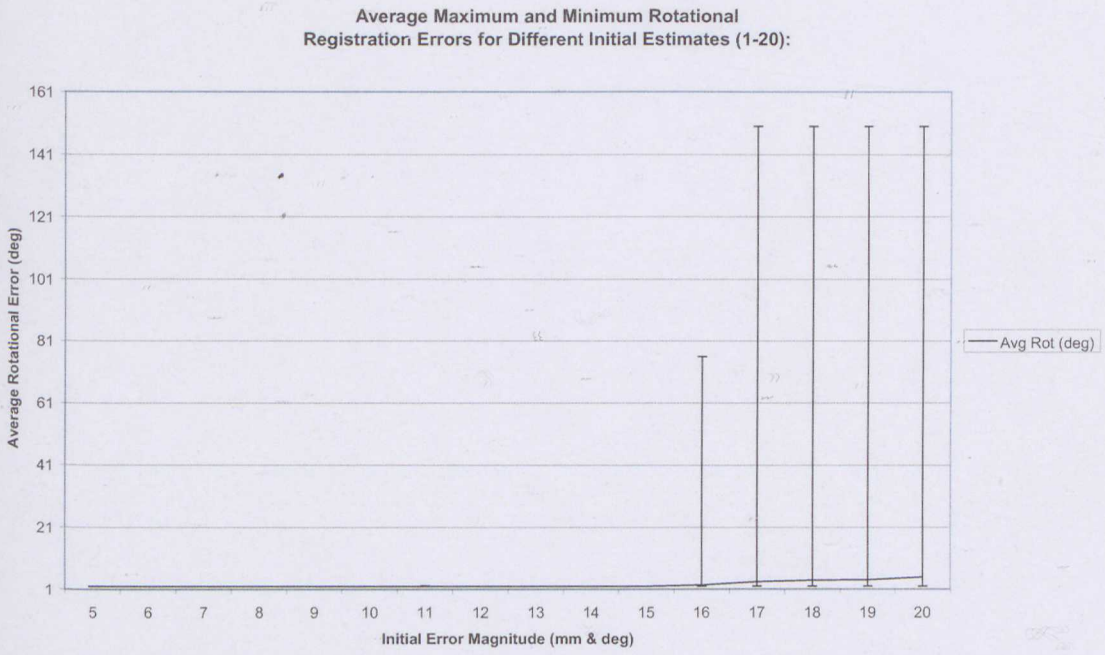
Each point-set was tested for a number of different initial estimate errors, and the resulting registration outcomes compared. 200 random rotational error matrices for every one unit increment in magnitude between 5 and 20 (degrees and millimetres) were used to shift the point-set away from the modelled surface. This resulted in 16 sets of 200 initial transformation states, which were set as the starting point for the enhanced ICP algorithm, which was executed with minima suppression. Results for a typical 35 points point-set, with 1.5mm maximum noise, are illustrated in Figure 5.15.

As can be seen, for perturbations of up to 15 units in magnitude, the minima suppression mechanism has produced the same registration result, irrespective of the initial perturbation. This result, which has been obtained for a set of equivalent point-sets of the same size, shows that for a typical point-set size of 35, the global minimum for the set can be robustly identified if it can be assumed that the initial estimate provided is accurate within $15mm$ and 15°.

However, for smaller set sizes, the number of local minima around the global minimum that needs to be identified grows, as can be intuitively expected. The fewer the number of points in a point set, the more ways there are to obtain a fit for the points on the same surface. Therefore, the adopted suppression mechanism has shown to be weaker for smaller point-set sizes, as illustrated by the results presented in Figure 5.16 for a typical 15 points point-set with 1.5mm maximum noise.

As the suppression mechanism utilised performs a focused high resolution sweep of the solution space surrounding the current "best minimum" (within approximately a 2 degrees envelope), the smaller the point-set size, the more likely it is that a solution remains trapped in a distant local minimum. Distant minima lie outside

a)

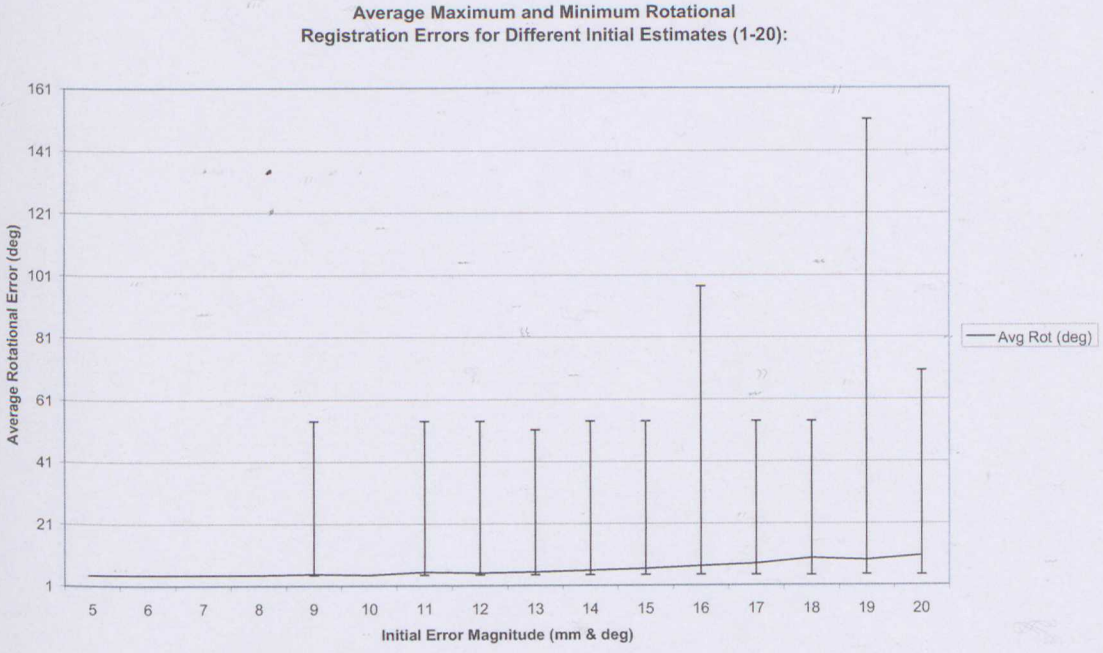


b)



Figure 5.15: Registration outcome for a 35 points point-set, expressed in terms of final rotational error for the entire range (a), and rotation and translation for the range where the global minimum has been consistently identified (b).

a)



b)

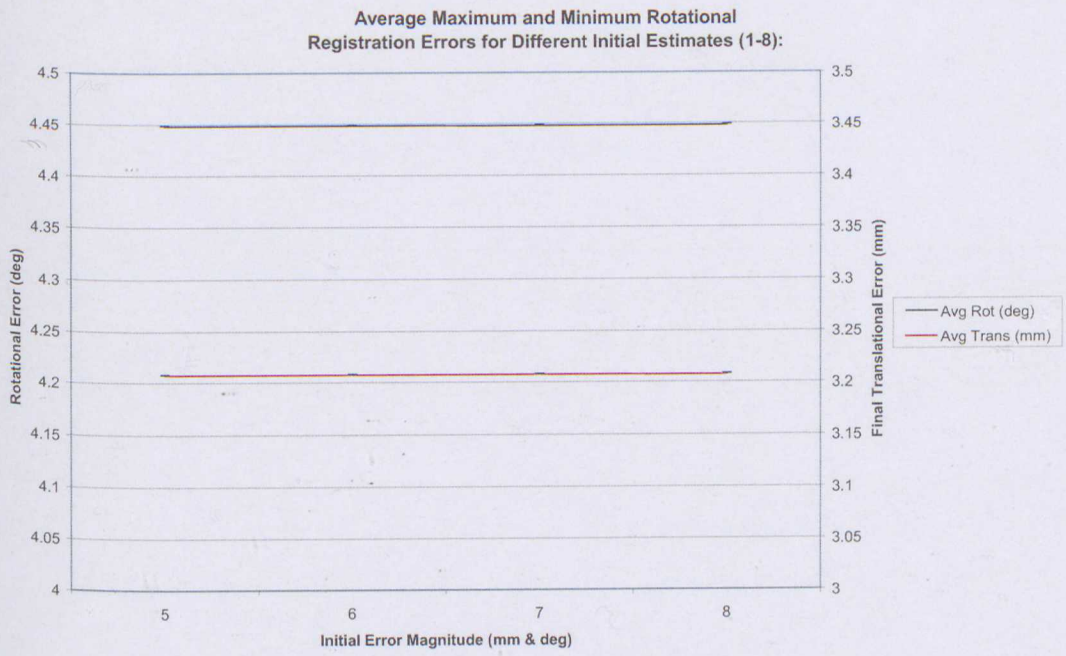


Figure 5.16: Registration outcome for a 15 points point-set, expressed in terms of final rotational error for the entire range (a), and rotational and translational error for the range where the global minimum has been consistently identified (b).

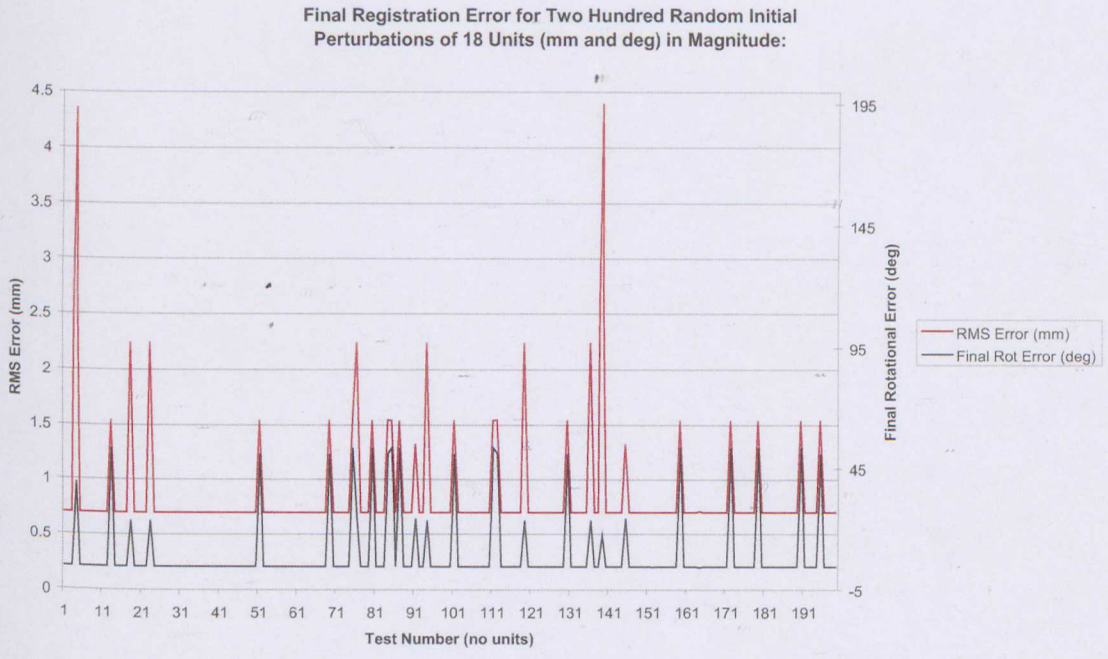


Figure 5.17: Relationship between RMS error and final rotational alignment for different local minima.

the region of interest searched during minima suppression, which means the global minimum will not be correctly identified.

However, closer inspection of the results shows that failed results, where the correct minimum has not been identified, have a significantly higher RMS error than the one obtained for the global minimum. As illustrated in Figure 5.17, where the algorithm has not converged to the correct solution, the average RMS and that obtained for the failed registration, generally differ by two or three orders of magnitude.

These results suggest that, when the global minimum has not been correctly identified, the initial estimate had placed the point-set outside of the correct class of minima. As the aim of the suppression algorithm implemented is to identify the global minimum out of surrounding local minima, these results show that, if the correct class of minima is correctly identified, the global minimum can be reliably found. If, however, the initial estimate is poor, results have shown that the RMS error can be used as a robust indicator for failed convergence to the correct global minimum.

5.4.2.5.3 Point-Set Size and Registration Accuracy For this experiment, a number of manually chosen point-sets of different sizes were assembled using the point acquisition protocol described in Section 5.3.4. These point-sets, that were generated using the simulator to interactively choose representative points in each

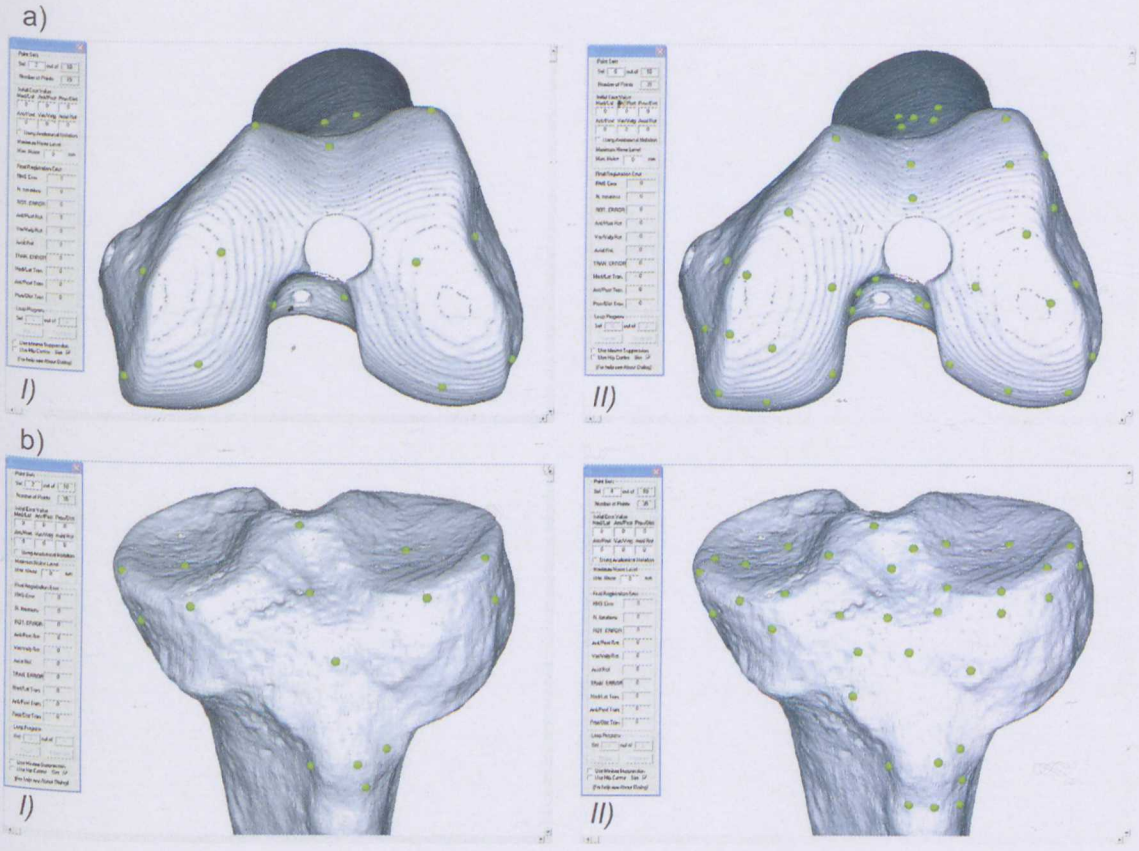


Figure 5.18: Ideal point distribution for both femur (a) and tibia (b), for 15 (I) and 35 (II) points per set.

region, are characterised by robust point distribution, for a specific point-set size, on the available surface. Examples of 15 and 35 points point-sets for the femur and tibia are illustrated in Figure 5.18. The layout of the points in each set is based on experience obtained on the simulator, and exemplifies a "best-case-scenario," founded on the region-based protocol, for a particular surface.

A guideline for the expected performance of the acquisition protocol for different degrees of point accuracy can then be derived by evaluating the robustness of these manually assembled point-sets. As each point-set represents a "desirable outcome" for the region-based procedure for a specific surface and point-set size, results obtained for these sets would provide a clear indication of achievable registration accuracy. In turn, a set of statistically significant values providing a degree of confidence for the robustness of a particular set size can be obtained.

As described in Section 5.3.4, for any point-set there is a set of random offsets, introduced by the addition of noise (Section 5.4.2.3), that will maximise the effect of the resulting error on registration accuracy. Therefore, by randomly perturbing a characteristic point-set a large number of times, an estimate of the greatest impact for a particular maximum noise value can be obtained. The extent of deviation about

the mean can be used to predict the robustness of a point-set for different degrees of random noise. For a representative population size, the maximum registration error obtained for a specific point-set would correspond to the set of random perturbations that produce the largest degradation of the result. A large population size would add statistical strength to the results, however reliable results have been obtained for 100 samples.

To ensure that 100 random perturbations of a point-set would be sufficient to reasonably represent the potential effect of noise on a point-set, the Matlab® "*normplot()*" function [MathWorks Inc., 1998] was used to check whether the trend followed a normal distribution. A typical plot illustrating the quality of the fit for the rotational error resulting from 100 random perturbations of a 15 points point-set (a) and a 50 points point-set (b) for 2mm maximum noise is illustrated in Figure 5.19.

For a true normal distribution, all results (plotted as blue crosses in Figure 5.19) would lie on the red line. As can be seen, the majority of points show a normal trend, with few degenerate solutions at either end of the probability scale. As the fit shows a tendency to improve with set size, poor solutions could represent results where the global minimum for the point-set has not been found. As a larger population size would have resulted in an unreasonable increase in computation time, it was decided that 100 perturbations would be enough to reasonably describe the effect of error on a point-set.

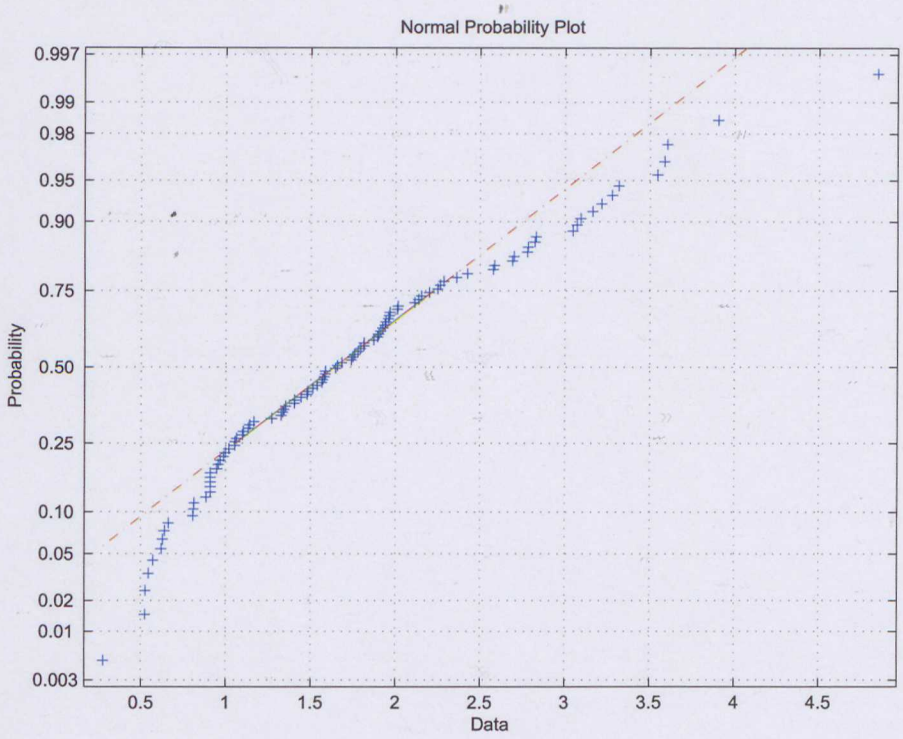
For each point-set examined, random initial estimate errors of 5° and $5mm$ in magnitude in random directions were chosen. Based on the results presented in Figure 5.16, these values were chosen to ensure that, while mimicking the error introduced during landmark-based initial registration, the right class of minima could, in the majority of cases, be adequately defined. In order for the experiment to produce meaningful results, the global minimum for every point-set should, if possible, be always identified.

100 perturbations for 10 robust point-sets of different set sizes were carried out, and average, maximum, and minimum registration errors for the resulting modified point-sets recorded. These values are reported in Table 5.5 and Table 5.6 for the femur and tibia respectively.

The registration error is expressed in component form, in terms of overall rotational (in axis/angle notation) and translational (Equation 5.8) errors. The results, expressed in tabular form, illustrate the probability that the point-set will fall within a maximum error value, which is defined in terms of 1 standard deviation (75%) and 2 standard deviations (95%) from the mean.

These results show what registration accuracy can be expected for a robust point-set as the point accuracy decreases. A clear relationship between point-set size and noise can be identified by inspecting the values in each table. As the magnitude of

a)



b)

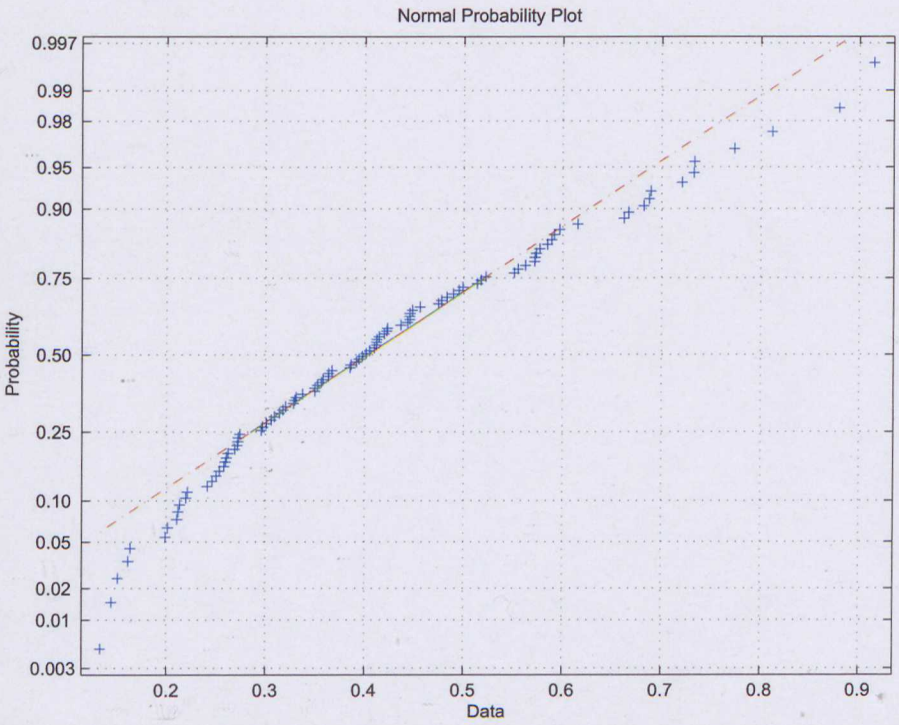


Figure 5.19: Normal distribution plot for a 15 (a) and 50 (b) points point-set with 1mm random noise.

	Performance of Robust Point-Sets of Different Sizes for 0.5mm Maximum Noise						
	Point-Set Size	**Average Err**	**Max Error**	**Min Error**	**STD**	**95% of Pop**	**75% of Pop**
Rotational Error (deg)	*10*	0.93	2.23	0.15	0.41	1.76	1.34
	15	0.71	1.48	0.12	0.28	1.27	0.99
	20	0.61	1.55	0.15	0.28	1.17	0.89
	25	0.43	1.03	0.08	0.19	0.82	0.63
	30	0.42	0.96	0.07	0.18	0.78	0.60
	35	0.38	0.89	0.08	0.16	0.70	0.54
	40	0.36	0.97	0.08	0.17	0.71	0.53
	50	0.30	0.78	0.04	0.14	0.59	0.45
	75	0.25	0.57	0.08	0.10	0.46	0.36
	100	0.20	0.38	0.02	0.08	0.36	0.28
Translational Error (mm)	*10*	0.77	1.93	0.13	0.39	1.54	1.16
	15	0.50	1.20	0.07	0.24	0.99	0.75
	20	0.43	1.22	0.05	0.21	0.86	0.65
	25	0.34	0.78	0.07	0.16	0.67	0.50
	30	0.34	0.87	0.08	0.15	0.64	0.49
	35	0.30	0.64	0.05	0.14	0.58	0.44
	40	0.29	0.72	0.03	0.16	0.60	0.45
	50	0.25	0.68	0.05	0.12	0.50	0.38
	75	0.22	0.52	0.05	0.10	0.42	0.32
	100	0.17	0.37	0.02	0.08	0.34	0.26

	Performance of Robust Point-Sets of Different Sizes for 1.0mm Maximum Noise						
	Point-Set Size	**Average Err**	**Max Error**	**Min Error**	**STD**	**95% of Pop**	**75% of Pop**
Rotational Error (deg)	*10*	1.77	4.85	0.28	0.88	3.53	2.65
	15	1.27	2.87	0.23	0.58	2.43	1.85
	20	1.16	2.78	0.25	0.56	2.28	1.72
	25	0.88	2.43	0.21	0.40	1.69	1.28
	30	0.87	2.05	0.23	0.34	1.55	1.21
	35	0.74	1.43	0.07	0.28	1.31	1.03
	40	0.77	1.84	0.12	0.37	1.51	1.14
	50	0.63	1.57	0.15	0.30	1.24	0.94
	75	0.53	1.40	0.14	0.24	1.01	0.77
	100	0.42	0.91	0.13	0.17	0.76	0.59
Translational Error (mm)	*10*	1.40	3.94	0.14	0.66	2.71	2.06
	15	0.96	2.21	0.18	0.47	1.90	1.43
	20	0.84	2.11	0.16	0.41	1.66	1.25
	25	0.73	2.09	0.15	0.34	1.42	1.07
	30	0.67	1.64	0.12	0.31	1.29	0.98
	35	0.53	1.24	0.03	0.23	0.99	0.76
	40	0.60	1.44	0.09	0.28	1.15	0.87
	50	0.51	1.09	0.06	0.24	0.99	0.75
	75	0.41	1.02	0.05	0.22	0.85	0.63
	100	0.35	0.81	0.07	0.15	0.65	0.50

Table 5.5: Relationship between point-set size and registration robustness, expressed in terms of overall rotational and translational accuracy, for a set of robust point-sets describing a distal femur.

	Performance of Robust Point-Sets of Different Sizes for 1.5mm Maximum Noise					
	Point-Set Size	**Average Err**	**Max Error**	**Min Error**	**STD**	**95% of Pop**	**75% of Pop**
Rotational Error (deg)	*10*	2.35	6.33	0.66	1.22	4.79	3.57
	15	1.89	4.29	0.19	0.89	3.66	2.77
	20	1.82	4.40	0.47	0.90	3.61	2.72
	25	1.41	3.41	0.30	0.64	2.69	2.05
	30	1.28	3.50	0.43	0.53	2.35	1.81
	35	1.10	2.57	0.29	0.45	2.00	1.55
	40	1.10	2.42	0.17	0.48	2.05	1.58
	50	0.90	2.34	0.26	0.44	1.78	1.34
	75	0.83	1.87	0.14	0.37	1.58	1.21
	100	0.69	1.40	0.06	0.30	1.28	0.99
Translational Error (mm)	*10*	1.94	5.64	0.12	0.99	3.92	2.93
	15	1.36	3.28	0.27	0.63	2.63	2.00
	20	1.33	3.93	0.11	0.69	2.70	2.01
	25	1.14	2.71	0.11	0.57	2.28	1.71
	30	0.95	2.30	0.06	0.43	1.82	1.38
	35	0.85	1.90	0.13	0.37	1.58	1.22
	40	0.83	1.82	0.15	0.35	1.54	1.19
	50	0.68	1.60	0.09	0.36	1.40	1.04
	75	0.66	1.71	0.04	0.35	1.35	1.01
	100	0.53	1.60	0.06	0.26	1.04	0.79

	Performance of Robust Point-Sets of Different Sizes for 2.0mm Maximum Noise					
	Point-Set Size	**Average Err**	**Max Error**	**Min Error**	**STD**	**95% of Pop**	**75% of Pop**
Rotational Error (deg)	*10*	3.46	9.01	0.67	1.61	6.67	5.06
	15	2.72	7.84	0.60	1.18	5.08	3.90
	20	2.43	5.60	0.50	1.18	4.79	3.61
	25	1.82	3.60	0.31	0.78	3.38	2.60
	30	1.88	3.94	0.34	0.82	3.52	2.70
	35	1.34	3.36	0.09	0.70	2.75	2.05
	40	1.42	3.05	0.18	0.63	2.69	2.05
	50	1.29	2.66	0.09	0.55	2.40	1.85
	75	1.09	2.68	0.21	0.48	2.05	1.57
	100	0.94	1.77	0.25	0.33	1.61	1.27
Translational Error (mm)	*10*	2.60	5.84	0.59	1.12	4.84	3.72
	15	2.04	6.44	0.28	0.96	3.96	3.00
	20	1.81	4.89	0.38	0.82	3.45	2.63
	25	1.50	3.37	0.33	0.67	2.85	2.18
	30	1.38	3.48	0.27	0.64	2.66	2.02
	35	1.19	2.44	0.29	0.52	2.23	1.71
	40	1.09	2.87	0.19	0.51	2.11	1.60
	50	1.04	2.80	0.11	0.54	2.13	1.59
	75	0.81	2.47	0.11	0.44	1.68	1.25
	100	0.75	1.74	0.11	0.36	1.48	1.12

Table 5.5: (cont'd) Relationship between point-set size and registration robustness, expressed in terms of overall rotational and translational accuracy, for a set of robust point-sets describing a distal femur.

	Performance of Robust Point-Sets of Different Sizes for 0.5mm Maximum Noise						
	Point-Set Size	**Average Err**	**Max Error**	**Min Error**	**STD**	**95% of Pop**	**75% of Pop**
Rotational Error (deg)	*10*	1.36	6.16	0.28	1.15	3.66	2.51
	15	0.84	2.61	0.14	0.50	1.85	1.35
	20	0.63	1.44	0.12	0.26	1.15	0.89
	25	0.59	1.66	0.12	0.29	1.16	0.88
	30	0.51	1.30	0.03	0.24	0.99	0.75
	35	0.45	1.16	0.09	0.22	0.90	0.68
	40	0.45	1.18	0.07	0.18	0.81	0.63
	50	0.37	0.91	0.06	0.17	0.72	0.54
	75	0.29	0.68	0.06	0.13	0.55	0.42
	100	0.26	0.61	0.03	0.11	0.49	0.37
Translational Error (mm)	*10*	0.90	3.85	0.08	0.71	2.32	1.61
	15	0.50	1.61	0.07	0.31	1.12	0.81
	20	0.37	0.86	0.05	0.18	0.74	0.56
	25	0.39	0.88	0.04	0.17	0.73	0.56
	30	0.31	0.72	0.05	0.16	0.62	0.47
	35	0.27	0.72	0.04	0.13	0.53	0.40
	40	0.29	0.63	0.06	0.12	0.54	0.41
	50	0.25	0.70	0.03	0.13	0.50	0.37
	75	0.20	0.53	0.02	0.09	0.39	0.30
	100	0.17	0.39	0.02	0.08	0.33	0.25

	Performance of Robust Point-Sets of Different Sizes for 1.0mm Maximum Noise						
	Point-Set Size	**Average Err**	**Max Error**	**Min Error**	**STD**	**95% of Pop**	**75% of Pop**
Rotational Error (deg)	*10*	3.23	11.62	0.32	2.47	8.16	5.69
	15	1.84	8.17	0.17	1.32	4.48	3.16
	20	1.41	3.86	0.22	0.71	2.83	2.12
	25	1.12	3.30	0.17	0.61	2.34	1.73
	30	0.89	2.21	0.06	0.44	1.77	1.33
	35	0.92	2.23	0.15	0.42	1.75	1.33
	40	0.90	2.15	0.15	0.43	1.75	1.32
	50	0.72	1.95	0.11	0.35	1.41	1.06
	75	0.63	1.65	0.08	0.29	1.21	0.92
	100	0.50	1.05	0.08	0.21	0.92	0.71
Translational Error (mm)	*10*	2.06	7.20	0.22	1.64	5.35	3.71
	15	1.00	5.25	0.16	0.77	2.53	1.77
	20	0.81	2.38	0.13	0.45	1.71	1.26
	25	0.74	1.98	0.17	0.40	1.53	1.14
	30	0.52	1.47	0.03	0.27	1.06	0.79
	35	0.51	1.22	0.07	0.25	1.01	0.76
	40	0.58	1.44	0.09	0.28	1.14	0.86
	50	0.47	1.26	0.10	0.23	0.94	0.71
	75	0.42	1.18	0.11	0.20	0.83	0.62
	100	0.30	0.71	0.02	0.15	0.59	0.44

Table 5.6: Relationship between point-set size and registration robustness, expressed in terms of overall rotational and translational accuracy, for a set of robust point-sets describing a proximal tibia.

	Performance of Robust Point-Sets of Different Sizes for 1.5mm Maximum Noise					
	Point-Set Size	**Average Err**	**Max Error**	**Min Error**	**STD**	**95% of Pop**	**75% of Pop**
Rotational Error (deg)	*10*	5.16	14.73	0.71	3.05	11.26	8.21
	15	2.94	7.66	0.65	1.56	6.06	4.50
	20	2.27	5.32	0.54	0.94	4.15	3.21
	25	1.87	4.59	0.23	0.89	3.65	2.76
	30	1.43	4.11	0.31	0.65	2.74	2.09
	35	1.41	3.37	0.38	0.65	2.72	2.06
	40	1.40	3.14	0.32	0.68	2.76	2.08
	50	1.20	2.47	0.21	0.61	2.41	1.80
	75	0.99	2.02	0.20	0.40	1.80	1.39
	100	0.77	1.94	0.18	0.40	1.57	1.17
Translational Error (mm)	*10*	3.29	8.91	0.38	2.11	7.51	5.40
	15	1.67	6.23	0.23	1.04	3.74	2.70
	20	1.28	3.94	0.12	0.69	2.65	1.96
	25	1.17	3.42	0.06	0.60	2.36	1.77
	30	0.85	2.32	0.12	0.42	1.68	1.27
	35	0.84	1.90	0.08	0.42	1.68	1.26
	40	0.86	1.78	0.09	0.39	1.63	1.25
	50	0.75	1.99	0.21	0.40	1.55	1.15
	75	0.62	1.32	0.14	0.28	1.17	0.89
	100	0.52	1.13	0.04	0.25	1.02	0.77

	Performance of Robust Point-Sets of Different Sizes for 2.0mm Maximum Noise					
	Point-Set Size	**Average Err**	**Max Error**	**Min Error**	**STD**	**95% of Pop**	**75% of Pop**
Rotational Error (deg)	*10*	6.10	16.12	1.33	3.25	12.59	9.35
	15	3.89	11.15	0.95	2.11	8.11	6.00
	20	2.93	6.52	0.46	1.31	5.55	4.24
	25	2.64	5.69	0.44	1.19	5.02	3.83
	30	1.99	5.76	0.08	1.13	4.25	3.12
	35	2.14	8.99	0.25	1.27	4.68	3.41
	40	1.81	6.37	0.30	0.91	3.63	2.72
	50	1.70	4.87	0.18	0.85	3.40	2.55
	75	1.26	2.78	0.18	0.58	2.42	1.84
	100	1.15	2.57	0.24	0.49	2.13	1.64
Translational Error (mm)	*10*	3.86	10.42	0.80	2.36	8.59	6.22
	15	2.14	5.95	0.39	1.26	4.66	3.40
	20	1.66	4.56	0.25	0.87	3.41	2.53
	25	1.72	3.41	0.38	0.74	3.19	2.46
	30	1.30	3.95	0.12	0.74	2.79	2.04
	35	1.22	5.33	0.19	0.75	2.73	1.97
	40	1.11	3.96	0.25	0.62	2.36	1.74
	50	1.10	3.74	0.21	0.60	2.30	1.70
	75	0.81	2.39	0.11	0.39	1.59	1.20
	100	0.69	1.97	0.05	0.36	1.41	1.05

Table 5.6: (cont'd) Relationship between point-set size and registration robustness, expressed in terms of overall rotational and translational accuracy, for a set of robust point-sets describing a proximal tibia.

noise increases, more points are required to robustly describe a surface. For instance, results in Table 5.5 show that at least 25 carefully chosen points are necessary to ensure rotational alignment of the registration transform within 2° of the actual position, if the noise during the acquisition process can be expected to fall within 1mm (i.e. for at least 1mm point accuracy as described in Section 5.3.4). Similarly, the performance of a robust point-set of a specific size will deteriorate as the noise increases. Therefore, from Table 5.6, rotational accuracy of under 2° for 15 carefully chosen points on a distal tibia can only be reasonably expected for point-touching accuracy better than $0.5mm$.

5.4.2.5.4 Performance Evaluation Values presented in Table 5.5 and Table 5.6 have described the expected performance of good quality point-sets assembled using the region-based acquisition protocol described in Section 5.3.4. Manual selection of the points in each region ensured an evenly distributed spread, and an emphasis on significant features of the surface to be registered. However, in order to evaluate the effectiveness of the protocol as a means for robust registration, an experiment that could be used to explore the effect of the variability introduced by collecting points in each region on registration outcome had to be defined.

The procedure described in Section 5.4.2.4 was used to assemble a large number of point-sets of different sizes, which, although viable in terms of the region-based protocol, had points randomly chosen in each of the predefined regions. This tailored randomisation process was used to produce a number of point-sets that were used to mimic the effect of unstructured point collection within the regions defined by the protocol.

A population size of 100 sets was chosen to represent each point-set size, for 5 different levels of maximum random noise between $0mm$ and $2mm$. As described in Section 5.4.2.5.3, random initial estimate errors of 5^0 and $5mm$ in magnitude, in random directions, were chosen for each set. Figure 5.20 and Figure 5.21 illustrate results for the average rotational error, in terms of leg alignment components (Section 5.4.1), and overall translational error for different point-set sizes and maximum noise values.

As the point-sets, as well as the noise values, were randomly selected, the mean can be used as an indicator for the average performance of the point acquisition protocol for a reasonable point-set and a reasonable error distribution. As expected, results in Figure 5.21 show a clear relationship between point-set size and maximum noise, and the effect of noise on the error matrix is comparable for both rotational and translational components.

The spread of the results for each point-set size, which was shown to have a normal distribution (as described in Section 5.4.2.5.3), was used to derive a set of

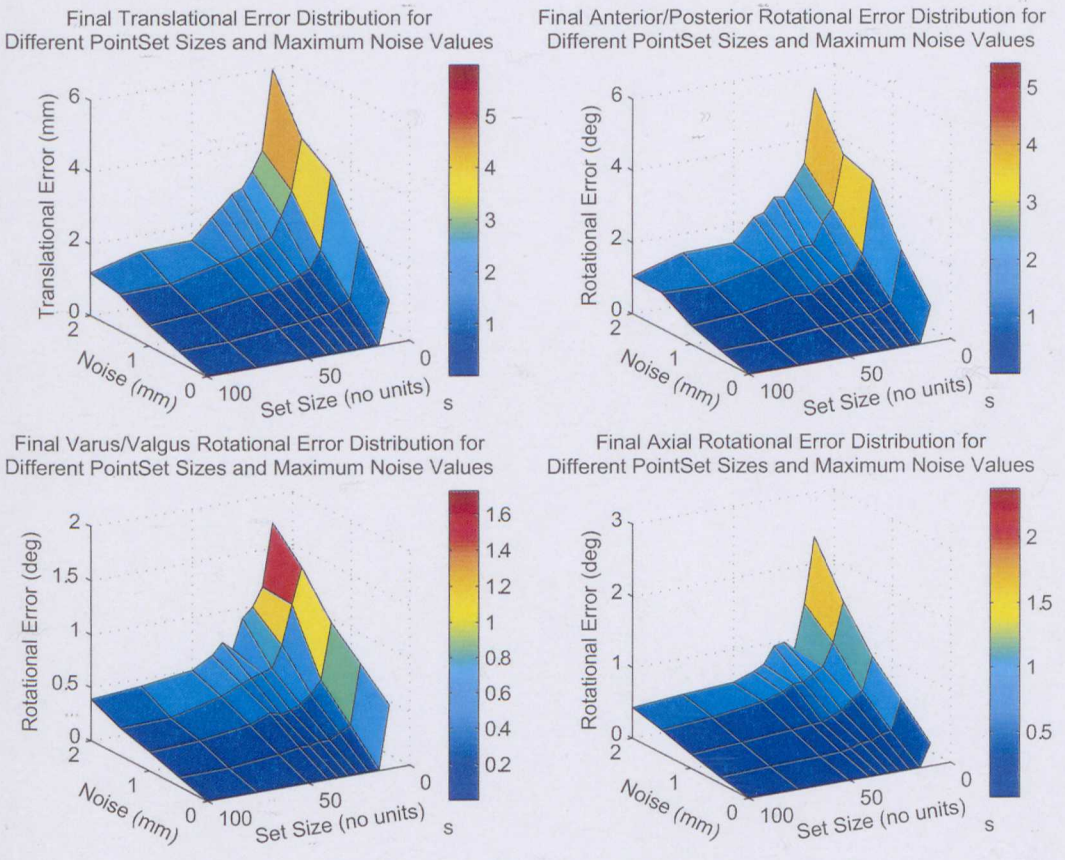


Figure 5.20: Registration accuracy for the enhanced ICP algorithm in terms of varus/valgus, anterior/posterior, axial, and translational components for different point-set sizes (10, 15, 20, 25, 30, 35, 40, 50, 75, 100) and maximum noise values (0, 0.5, 1, 1.5, 2), for the femur.

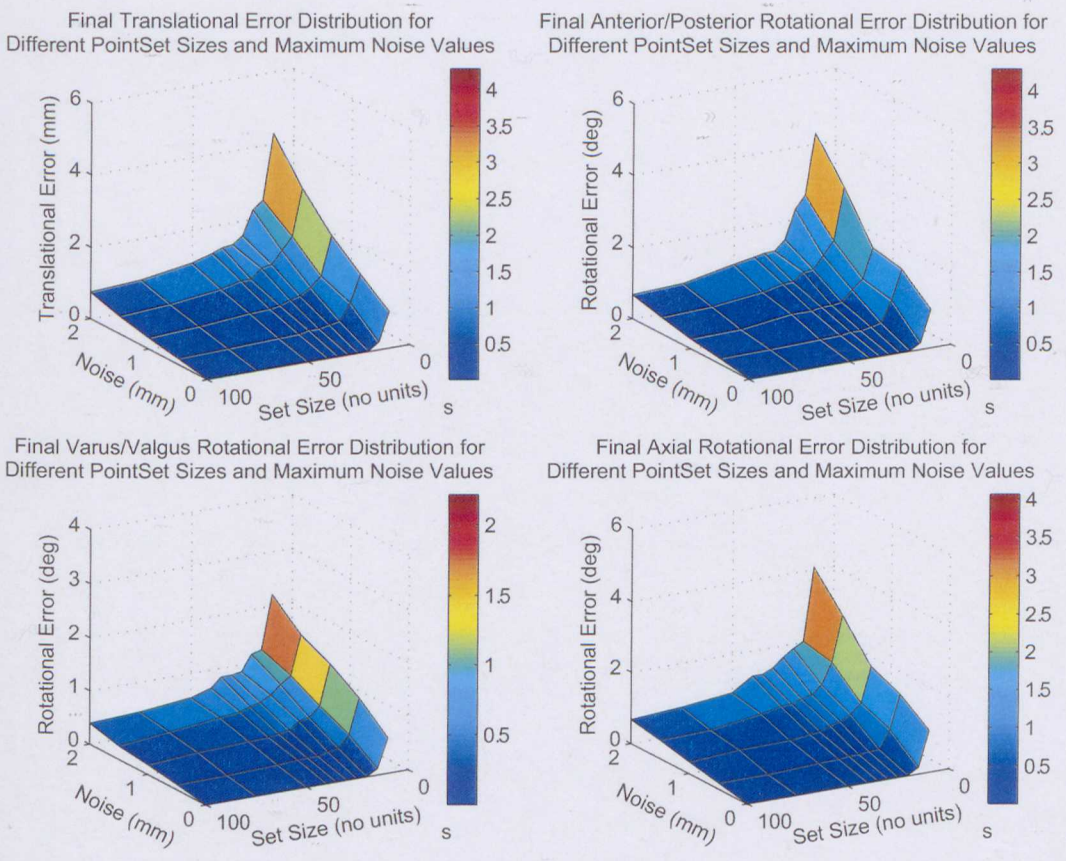


Figure 5.21: Registration accuracy for the enhanced ICP algorithm in terms of varus/valgus, anterior/posterior, axial, and translational components for different point-set sizes (10, 15, 20, 25, 30, 35, 40, 50, 75, 100) and maximum noise values (0, 0.5, 1, 1.5, 2), for the tibia.

statistical values that could be used to asses the extent of the error that could be introduced during the guided point-collection process. By nature of the randomisation process, the dataset for each point-set size would include a number of week point-sets, as well as very representative ones. Average, maximum, and minimum registration errors obtained for each point-set size, sorted by maximum random noise applied, are reported in Table 5.7 and Table 5.8 for the femur and tibia respectively.

As can be seen these, results show very similar characteristics to the ones presented in Table 5.5 and Table 5.6, although, generally, more points are required to achieve similar registration accuracy for the same maximum noise value. The results in Table 5.7 and Table 5.8 can be interpreted in the same way as those described in the previous section, and can be used to derive a set of guidelines that would increase the probability of obtaining robust registration for a particular intra-operative setup.

In order to explore the difference in performance between registration accuracy obtained with and without minima suppression, the same dataset used for the experiment described above was processed using a single run of the algorithm. Results are presented in Figure 5.22 and Figure 5.23.

Results for small point-set sizes have a higher probability of converging to a non global minimum. However, as point-size increases, results illustrated in Figure 5.21 and Figure 5.23 become comparable in terms of registration accuracy for all components. Therefore, although local minima suppression can be used to improve the robustness of the convergence process, if the point-set size is large enough, acceptable results can be obtained for a single run of the enhanced algorithm.

5.4.2.5.5 RMS Error and Registration Quality As described on a number of occasions, the RMS error of the distance of each point to the mapped surface can be used as an indicator for the registration outcome of a particular point-set acquired intra-operatively. Results presented in the previous experiments have shown a strong relationship between point distribution, point-set size, and actual registration quality. This experiment was carried out to explore the effective relationship between RMS error and the accuracy of registration.

Average, minimum, and maximum RMS error values obtained for the set of results described in Section 5.4.2.5.3, with 100 perturbations of robust point-sets of different sizes, were recorded. Results for the *average* RMS error obtained for the femur for different point-set sizes and maximum noise levels are graphically illustrated in Figure 5.24.

As can be seen, the trend of the RMS error value for each level of noise analysed shows a substantially different trend to that shown in Figure 5.21 for the femur. Figure 5.24 suggests that, for a specific maximum noise level, the RMS error increases

	Performance of Random Point-Sets of Different Sizes for 0.5mm Maximum Noise					
	Point-Set Size	**Average Err**	**Max Error**	**Min Error**	**STD**	**95% of Pop**	**75% of Pop**
Rotational Error (deg)	*10*	0.91	2.16	0.14	0.42	1.74	1.33
	15	0.62	2.52	0.13	0.36	1.35	0.98
	20	0.59	1.60	0.11	0.31	1.20	0.90
	25	0.47	1.15	0.10	0.22	0.90	0.69
	30	0.47	1.18	0.06	0.23	0.93	0.70
	35	0.41	0.97	0.05	0.19	0.79	0.60
	40	0.42	0.93	0.07	0.19	0.79	0.60
	50	0.34	0.86	0.08	0.15	0.65	0.49
	75	0.27	0.78	0.06	0.14	0.54	0.41
	100	0.22	0.53	0.05	0.10	0.41	0.31
Translational Error (mm)	*10*	0.75	1.92	0.19	0.36	1.48	1.12
	15	0.53	2.03	0.06	0.29	1.11	0.82
	20	0.48	1.32	0.06	0.28	1.05	0.76
	25	0.38	1.08	0.15	0.21	0.80	0.59
	30	0.37	1.05	0.08	0.19	0.74	0.55
	35	0.33	0.80	0.05	0.17	0.67	0.50
	40	0.36	1.00	0.05	0.19	0.74	0.55
	50	0.28	0.77	0.05	0.14	0.57	0.43
	75	0.22	0.57	0.03	0.12	0.45	0.34
	100	0.19	0.42	0.02	0.09	0.36	0.28

	Performance of Random Point-Sets of Different Sizes for 1.0mm Maximum Noise					
	Point-Set Size	**Average Err**	**Max Error**	**Min Error**	**STD**	**95% of Pop**	**75% of Pop**
Rotational Error (deg)	*10*	2.27	11.09	0.44	1.71	5.70	3.99
	15	1.33	3.87	0.21	0.69	2.70	2.01
	20	1.15	2.82	0.08	0.49	2.13	1.64
	25	0.94	2.50	0.20	0.43	1.79	1.37
	30	0.91	2.27	0.27	0.40	1.72	1.31
	35	0.78	1.71	0.19	0.37	1.53	1.16
	40	0.77	2.31	0.10	0.42	1.62	1.19
	50	0.69	1.28	0.16	0.28	1.25	0.97
	75	0.51	1.08	0.05	0.22	0.96	0.74
	100	0.48	1.44	0.08	0.23	0.95	0.72
Translational Error (mm)	*10*	1.78	8.30	0.51	1.16	4.10	2.94
	15	1.08	2.95	0.19	0.60	2.28	1.68
	20	1.01	2.39	0.22	0.47	1.95	1.48
	25	0.74	1.79	0.05	0.37	1.47	1.10
	30	0.71	1.98	0.10	0.36	1.43	1.07
	35	0.65	1.44	0.12	0.32	1.29	0.97
	40	0.64	1.94	0.15	0.35	1.33	0.98
	50	0.57	1.12	0.07	0.25	1.07	0.82
	75	0.45	1.04	0.07	0.22	0.88	0.66
	100	0.41	1.21	0.03	0.22	0.86	0.64

Table 5.7: Relationship between point-set size and registration robustness, expressed in terms of overall rotational and translational accuracy, for a set of robust point-sets describing a distal femur.

	Performance of Random Point-Sets of Different Sizes for 1.5mm Maximum Noise					
	Point-Set Size	**Average Err**	**Max Error**	**Min Error**	**STD**	**95% of Pop**	**75% of Pop**
Rotational Error (deg)	*10*	3.02	10.09	0.57	1.61	6.25	4.64
	15	2.28	5.95	0.24	1.00	4.28	3.28
	20	1.81	4.16	0.46	0.87	3.55	2.68
	25	1.45	3.54	0.41	0.67	2.79	2.12
	30	1.36	2.96	0.28	0.66	2.67	2.01
	35	1.18	2.77	0.27	0.57	2.33	1.76
	40	1.24	2.59	0.24	0.58	2.40	1.82
	50	1.06	2.71	0.17	0.48	2.02	1.54
	75	0.81	1.83	0.06	0.39	1.59	1.20
	100	0.74	1.92	0.13	0.36	1.45	1.09
Translational Error (mm)	*10*	2.40	8.86	0.53	1.29	4.97	3.68
	15	1.79	4.97	0.26	0.88	3.55	2.67
	20	1.51	4.01	0.27	0.73	2.98	2.24
	25	1.23	3.13	0.19	0.63	2.49	1.86
	30	1.15	2.97	0.21	0.52	2.19	1.67
	35	0.93	2.27	0.10	0.48	1.88	1.41
	40	1.01	2.45	0.20	0.51	2.03	1.52
	50	0.91	2.58	0.17	0.42	1.76	1.34
	75	0.70	1.65	0.13	0.37	1.43	1.06
	100	0.58	1.69	0.08	0.33	1.23	0.91

	Performance of Random Point-Sets of Different Sizes for 2.0mm Maximum Noise					
	Point-Set Size	**Average Err**	**Max Error**	**Min Error**	**STD**	**95% of Pop**	**75% of Pop**
Rotational Error (deg)	*10*	5.47	22.76	0.62	4.57	14.61	10.04
	15	3.16	12.29	0.54	1.88	6.93	5.04
	20	2.59	14.41	0.22	1.99	6.57	4.58
	25	2.03	7.39	0.44	1.21	4.44	3.23
	30	1.83	4.58	0.40	0.86	3.56	2.69
	35	1.67	4.97	0.16	0.88	3.43	2.55
	40	1.62	4.41	0.10	0.83	3.28	2.45
	50	1.39	3.44	0.29	0.59	2.57	1.98
	75	1.14	2.35	0.34	0.41	1.96	1.55
	100	1.02	2.53	0.19	0.49	2.00	1.51
Translational Error (mm)	*10*	4.44	16.75	0.44	3.60	11.64	8.04
	15	2.58	9.83	0.16	1.63	5.84	4.21
	20	2.26	14.50	0.35	1.85	5.96	4.11
	25	1.64	5.84	0.09	0.99	3.61	2.62
	30	1.54	3.33	0.32	0.66	2.86	2.20
	35	1.46	4.62	0.43	0.77	3.01	2.24
	40	1.41	3.52	0.25	0.65	2.72	2.06
	50	1.19	2.48	0.32	0.49	2.16	1.68
	75	0.99	2.15	0.23	0.42	1.84	1.42
	100	0.85	2.19	0.23	0.40	1.65	1.25

Table 5.7: (cont'd) Relationship between point-set size and registration robustness, expressed in terms of overall rotational and translational accuracy, for a set of robust point-sets describing a distal femur.

	Performance of Random Point-Sets of Different Sizes for 0.5mm Maximum Noise					
	Point-Set Size	**Average Err**	**Max Error**	**Min Error**	**STD**	**95% of Pop**	**75% of Pop**
Rotational Error (deg)	*10*	2.49	14.51	0.22	3.17	8.83	5.66
	15	1.16	16.43	0.11	1.87	4.90	3.03
	20	0.67	1.57	0.12	0.32	1.31	0.99
	25	0.56	1.46	0.11	0.24	1.04	0.80
	30	0.48	1.38	0.04	0.23	0.95	0.72
	35	0.51	1.29	0.08	0.24	0.99	0.75
	40	0.44	1.18	0.05	0.24	0.92	0.68
	50	0.40	0.92	0.09	0.17	0.74	0.57
	75	0.30	0.80	0.05	0.14	0.58	0.44
	100	0.27	0.74	0.05	0.12	0.52	0.40
Translational Error (mm)	*10*	1.34	8.16	0.16	1.70	4.74	3.04
	15	0.71	10.69	0.06	1.19	3.09	1.90
	20	0.43	1.30	0.12	0.24	0.91	0.67
	25	0.39	1.04	0.08	0.19	0.77	0.58
	30	0.32	0.87	0.04	0.15	0.62	0.47
	35	0.33	0.90	0.09	0.16	0.65	0.49
	40	0.27	0.82	0.03	0.15	0.57	0.42
	50	0.25	0.77	0.03	0.12	0.50	0.37
	75	0.20	0.61	0.05	0.10	0.40	0.30
	100	0.16	0.36	0.03	0.08	0.33	0.24

	Performance of Random Point-Sets of Different Sizes for 1.0mm Maximum Noise					
	Point-Set Size	**Average Err**	**Max Error**	**Min Error**	**STD**	**95% of Pop**	**75% of Pop**
Rotational Error (deg)	*10*	3.29	21.23	0.22	3.27	9.83	6.56
	15	1.80	10.17	0.09	1.20	4.20	3.00
	20	1.53	3.70	0.06	0.67	2.87	2.20
	25	1.23	2.94	0.30	0.53	2.29	1.76
	30	1.09	2.50	0.24	0.48	2.04	1.56
	35	0.97	3.29	0.19	0.51	1.99	1.48
	40	0.89	2.15	0.18	0.45	1.80	1.34
	50	0.84	1.72	0.29	0.32	1.48	1.16
	75	0.67	1.42	0.11	0.31	1.30	0.98
	100	0.55	1.46	0.09	0.28	1.10	0.82
Translational Error (mm)	*10*	1.99	13.22	0.15	2.05	6.09	4.04
	15	1.09	7.06	0.14	0.83	2.76	1.92
	20	0.96	2.60	0.20	0.49	1.95	1.46
	25	0.77	2.26	0.04	0.41	1.59	1.18
	30	0.71	1.74	0.08	0.33	1.37	1.04
	35	0.60	1.75	0.08	0.32	1.23	0.91
	40	0.56	1.27	0.11	0.30	1.15	0.85
	50	0.53	1.30	0.11	0.26	1.06	0.80
	75	0.40	0.97	0.10	0.20	0.79	0.59
	100	0.32	0.81	0.10	0.14	0.59	0.45

Table 5.8: Relationship between point-set size and registration robustness, expressed in terms of overall rotational and translational accuracy, for a set of robust point-sets describing a proximal tibia.

	Performance of Random Point-Sets of Different Sizes for 1.5mm Maximum Noise					
Point-Set Size	**Average Err**	**Max Error**	**Min Error**	**STD**	**95% of Pop**	**75% of Pop**
Rotational Error (deg)						
10	4.86	17.50	0.93	3.49	11.85	8.35
15	2.77	17.73	0.35	2.09	6.94	4.85
20	2.43	7.06	0.47	1.25	4.93	3.68
25	1.94	4.83	0.44	0.86	3.67	2.81
30	1.79	4.54	0.21	0.85	3.48	2.63
35	1.56	4.60	0.36	0.75	3.07	2.32
40	1.48	4.11	0.34	0.67	2.81	2.14
50	1.27	2.72	0.13	0.53	2.33	1.80
75	0.96	2.51	0.16	0.46	1.89	1.42
100	0.85	2.05	0.18	0.41	1.67	1.26
Translational Error (mm)						
10	2.84	8.79	0.20	1.61	6.07	4.45
15	1.76	11.87	0.23	1.43	4.62	3.19
20	1.56	3.91	0.28	0.77	3.09	2.33
25	1.22	3.03	0.14	0.59	2.40	1.81
30	1.16	3.55	0.15	0.64	2.44	1.80
35	0.90	3.12	0.19	0.48	1.86	1.38
40	0.91	2.07	0.22	0.39	1.69	1.30
50	0.78	1.80	0.15	0.40	1.57	1.17
75	0.61	1.52	0.07	0.30	1.20	0.90
100	0.50	1.24	0.05	0.25	1.00	0.75

	Performance of Random Point-Sets of Different Sizes for 2.0mm Maximum Noise					
Point-Set Size	**Average Err**	**Max Error**	**Min Error**	**STD**	**95% of Pop**	**75% of Pop**
Rotational Error (deg)						
10	7.23	22.21	0.67	4.97	17.17	12.20
15	4.01	17.63	0.91	2.52	9.04	6.52
20	3.57	17.74	0.40	2.37	8.31	5.94
25	2.71	17.07	0.34	1.85	6.40	4.56
30	2.35	6.04	0.47	1.27	4.88	3.62
35	2.25	6.82	0.71	1.15	4.54	3.40
40	2.10	6.00	0.36	1.02	4.15	3.13
50	1.71	4.17	0.05	0.80	3.30	2.51
75	1.36	2.99	0.22	0.61	2.57	1.97
100	1.19	3.76	0.11	0.61	2.42	1.80
Translational Error (mm)						
10	4.29	14.50	0.83	2.73	9.75	7.02
15	2.47	12.15	0.23	1.69	5.86	4.17
20	2.26	10.77	0.52	1.47	5.20	3.73
25	1.60	4.50	0.29	0.71	3.02	2.31
30	1.40	4.00	0.32	0.78	2.95	2.18
35	1.35	3.43	0.30	0.66	2.68	2.02
40	1.25	3.15	0.18	0.59	2.43	1.84
50	1.07	2.98	0.20	0.61	2.28	1.68
75	0.85	2.69	0.14	0.44	1.74	1.29
100	0.76	2.25	0.09	0.41	1.58	1.17

Table 5.8: (cont'd) Relationship between point-set size and registration robustness, expressed in terms of overall rotational and translational accuracy, for a set of robust point-sets describing a proximal tibia.

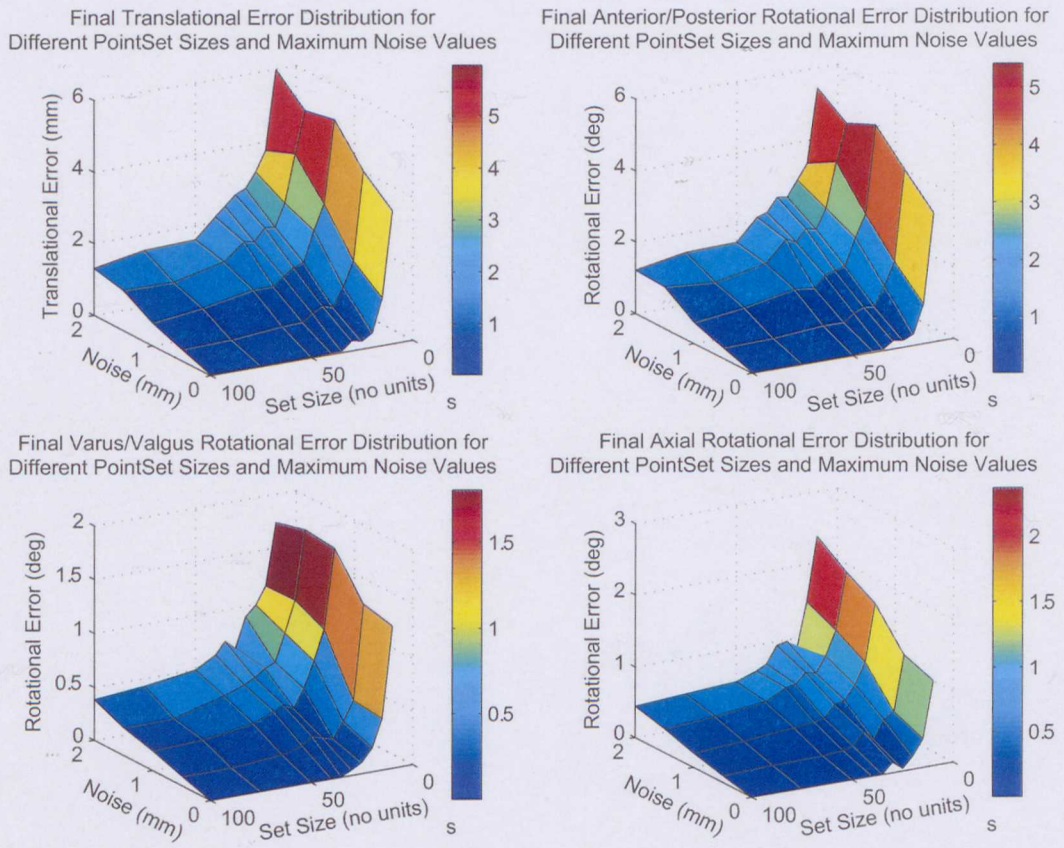


Figure 5.22: Registration accuracy for the enhanced ICP algorithm, in terms of varus/valgus, anterior/posterior, axial, and translational components, executed without minima suppression for different point-set sizes and maximum noise values, for the femur.

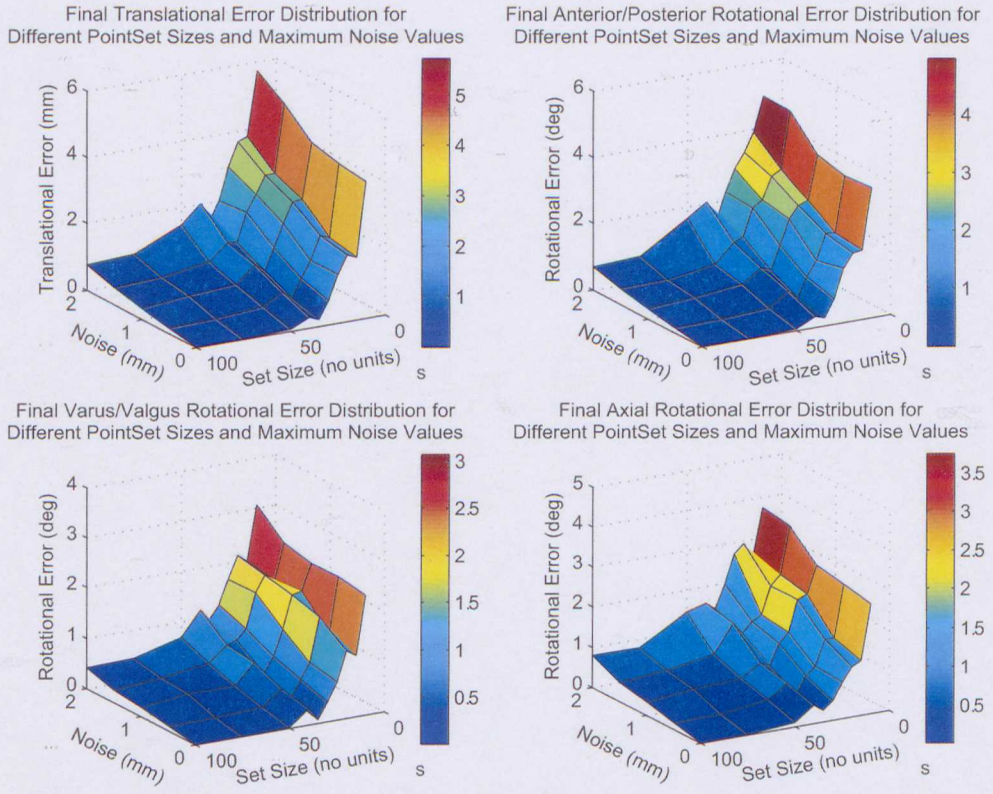


Figure 5.23: Registration accuracy for the enhanced ICP algorithm, in terms of varus/valgus, anterior/posterior, axial, and translational components, executed without minima suppression for different point-set sizes and maximum noise values, for the tibia.

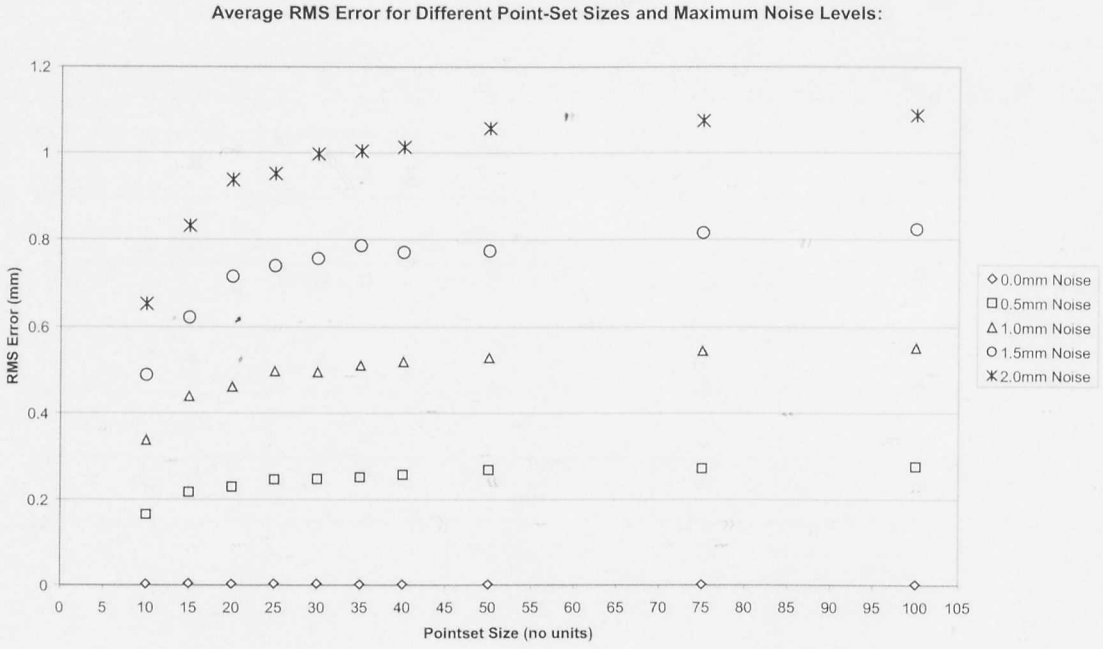


Figure 5.24: Average RMS error values obtained for different point-set sizes and maximum noise values for the femur.

with point-set size, rather than decreasing, as would be expected if this value was proportional to registration quality. However, the RMS error is a quantitative piece of information that provides a measure of the residual error (Section 3.3.3) for a particular point-set, which may not be indicative of registration quality. For instance, a few points gathered in a small region of the surface to be registered would probably generate a very low RMS error, but registration accuracy could be very poor. Therefore, as expected, for larger point-set sizes, the RMS value becomes more representative, and will be higher for a higher degree of noise.

Further evidence for the weakness of the link between RMS error and registration quality can be obtained by plotting the *maximum* RMS error values recorded for each point-set size for different levels of maximum noise. A graphical representation of the results can be seen in Figure 5.25. Figure 5.25 shows that the RMS error for each point-set analysed never exceeded $1.2mm$ for $1.5mm$ maximum noise, although results in Table 5.5 for the same dataset show that at least 50 points are required to ensure registration accuracy within $\pm 2^o$ and $\pm 2mm$.

Therefore, the RMS error alone cannot be used as an indication of registration accuracy. Results presented in Figure 5.24, which are virtually identical to those obtained for the tibia, can be used as bench-mark values to predict what RMS error value can be expected for a specific number of points and known point accuracy. The RMS error, coupled with the robust point touching protocol described in Section

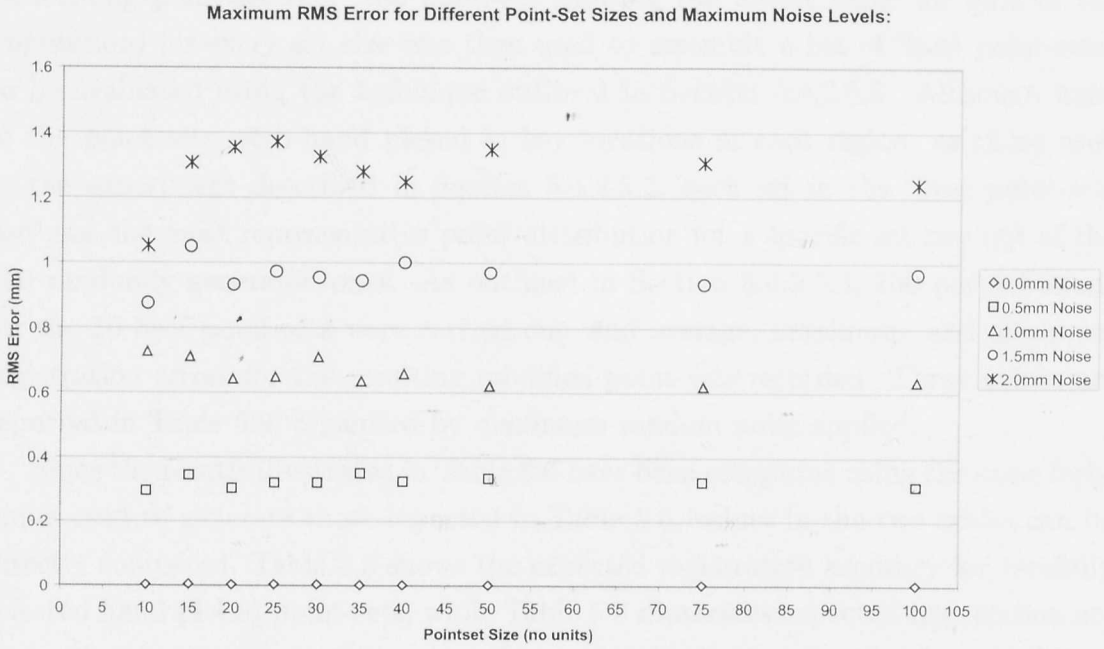


Figure 5.25: Maximum RMS error values obtained for different point-set sizes and maximum noise values for the femur.

5.3.4, can also be used to predict achievable point accuracy intra-operatively (Section 5.3.6), and to identify solutions where the global minimum for a point-set has not been correctly identified (Section 5.4.2.5.2).

5.4.2.5.6 Robustness Indicator Validation In order to evaluate the effectiveness of the robustness assessment method outlined in Section 5.3.6 as a means to evaluate the quality of a point-set intra-operatively, the following experiment was carried out. Each point-set in the dataset of random point-sets generated for the tibia with $0.5mm$ maximum noise (Section 5.4.2.5.4) was evaluated using the robustness evaluation method. The maximum point inaccuracy, ε, was set to $0.5mm$, indicating predicted point accuracy better than $0.5mm$. Although ε is set to the correct value, as all point-sets and perturbations are simulated (therefore known), this experiment would show how effective the indicators for the robustness of a specific point-set can be, if achievable point accuracy can be adequately predicted intra-operatively using the RMS error and colour-coded display (Section 5.3.6).

As described in Section 5.4.2.5.4, the dataset assembled for the tibia is made up of 1000 random point-sets with 100 points for every set size, in the following steps: 10, 15, 20, 25, 30, 35, 40, 50, 75, and 100 points. Each set was then evaluated using the robustness indicator algorithm, and results sorted by rotational robustness, expressed in terms of 95% of the population (2 STDs from the mean). The best

performing point-set (i.e. the point-set showing the lowest value for 95% of the population) for every set size was then used to assemble a list of "best point-sets" to be evaluated using the technique outlined in Section 5.4.2.5.3. Although none of the point-sets were hand picked in key locations in each region, as those used in the experiment described in Section 5.4.2.5.3, each set in the "best point-sets list" has the most representative point distribution for a specific set size out of the 100 randomly generated ones. As outlined in Section 5.4.2.5.3, 100 perturbations for the 10 best point-sets were carried out, and average, maximum, and minimum registration errors for the resulting modified point-sets recorded. These values are reported in Table 5.9, organised by maximum random noise applied.

Since the results illustrated in Table 5.9 have been computed using the same technique used to generate those reported in Table 5.6, values in the two tables can be directly compared. Table 5.6 shows the expected registration accuracy for carefully selected hand picked point-sets, while Table 5.9 illustrates expected registration accuracy for the best randomly generated sets, identified using the robustness indicator algorithm. The best random point-sets have consistently outperformed those hand picked in key locations using the simulator. For every set size, the best point-set out of the randomly generated ones has shown to be a more robust representation of the registration surface than the equivalent manually assembled one. A similar result would be expected for the femur, although time constraints imposed by lengthy computation time (Table 5.10) have not allowed the experiment to be replicated for the femoral surface.

As illustrated in Table 5.10, deriving robustness indicators for a specific point-set is currently excessively time consuming to be used intra-operatively. As can be expected, the computation time requirements are proportional to the set size, but for a typical 35 points point-set, 10 additional minutes of operating time would be required for every intra-operatively acquired set that needs to be evaluated. Results for this experiment, however, have shown that the method outlined in Section 5.3.6 can become an effective means for registration quality assessment, if computation time is reduced.

5.4.3 Registration With a Plastic Phantom

A set of plastic bone trials was carried out in order to corroborate the simulated results, and to evaluate the performance of the algorithm and point acquisition protocol integrated in the ACROBOT II System. This section provides an outline of the experimental setup and results obtained for tests carried out on 10 plastic tibias and 10 plastic femurs. Each plastic bone was CT scanned and planned using Acrobot's proprietary planning software, in order to generate the surface models needed for

	Performance of the Best Point-Sets of Different Sizes for 0.5mm Maximum Noise						
	Point-Set Size	**Average Err**	**Max Error**	**Min Error**	**STD**	**95% of Pop**	**75% of Pop**
Rotational Error (deg)	*10*	5.92	34.99	0.24	8.16	22.25	14.08
	15	0.67	1.47	0.11	0.30	1.27	0.97
	20	0.55	1.12	0.14	0.22	0.99	0.77
	25	0.46	0.94	0.07	0.20	0.87	0.67
	30	0.47	1.29	0.15	0.20	0.87	0.67
	35	0.42	0.97	0.07	0.19	0.79	0.61
	40	0.37	1.29	0.05	0.19	0.75	0.56
	50	0.31	0.81	0.09	0.15	0.60	0.46
	75	0.30	0.74	0.06	0.13	0.55	0.43
	100	0.26	0.61	0.01	0.12	0.49	0.37
Translational Error (mm)	*10*	2.80	18.74	0.17	3.78	10.35	6.58
	15	0.44	0.94	0.08	0.21	0.86	0.65
	20	0.39	0.89	0.06	0.19	0.77	0.58
	25	0.30	0.62	0.06	0.13	0.56	0.43
	30	0.30	0.76	0.05	0.15	0.61	0.46
	35	0.28	0.86	0.06	0.16	0.59	0.43
	40	0.25	0.76	0.06	0.14	0.53	0.39
	50	0.22	0.75	0.03	0.12	0.47	0.34
	75	0.19	0.51	0.02	0.09	0.37	0.28
	100	0.16	0.38	0.03	0.07	0.31	0.24

	Performance of the Best Point-Sets of Different Sizes for 1.0mm Maximum Noise						
	Point-Set Size	**Average Err**	**Max Error**	**Min Error**	**STD**	**95% of Pop**	**75% of Pop**
Rotational Error (deg)	*10*	6.75	44.78	0.13	9.74	26.22	16.49
	15	1.42	2.86	0.29	0.59	2.60	2.01
	20	1.10	2.30	0.24	0.48	2.05	1.58
	25	1.06	2.54	0.34	0.45	1.96	1.51
	30	0.98	1.96	0.17	0.44	1.87	1.42
	35	0.91	2.01	0.18	0.39	1.69	1.30
	40	0.79	2.22	0.09	0.38	1.56	1.17
	50	0.70	1.50	0.15	0.31	1.33	1.02
	75	0.60	1.55	0.08	0.28	1.17	0.89
	100	0.56	1.46	0.09	0.25	1.07	0.82
Translational Error (mm)	*10*	3.42	29.66	0.23	5.16	13.74	8.58
	15	0.92	1.99	0.13	0.40	1.72	1.32
	20	0.75	1.53	0.13	0.32	1.39	1.07
	25	0.62	1.56	0.05	0.34	1.29	0.95
	30	0.64	1.99	0.11	0.33	1.30	0.97
	35	0.57	1.17	0.04	0.25	1.08	0.83
	40	0.55	1.75	0.04	0.29	1.13	0.84
	50	0.46	1.15	0.07	0.22	0.90	0.68
	75	0.37	1.13	0.07	0.19	0.76	0.56
	100	0.33	0.92	0.07	0.16	0.66	0.49

Table 5.9: Relationship between point-set size and registration robustness, expressed in terms of overall rotational and translational accuracy, for the set of best randomly generated point-sets describing a proximal tibia.

	Performance of the Best Point-Sets of Different Sizes for 1.5mm Maximum Noise					
Point-Set Size	**Average Err**	**Max Error**	**Min Error**	**STD**	**95% of Pop**	**75% of Pop**
Rotational Error (deg)						
10	7.71	35.65	0.62	7.98	23.68	15.70
15	2.16	4.78	0.47	1.00	4.15	3.16
20	1.67	3.73	0.48	0.73	3.13	2.40
25	1.35	3.06	0.28	0.60	2.56	1.95
30	1.43	3.14	0.18	0.59	2.61	2.02
35	1.29	3.11	0.26	0.59	2.47	1.88
40	1.25	2.72	0.31	0.56	2.38	1.82
50	1.05	2.35	0.10	0.53	2.11	1.58
75	0.96	2.52	0.20	0.41	1.78	1.37
100	0.84	1.58	0.19	0.31	1.46	1.15
Translational Error (mm)						
10	3.74	22.76	0.22	3.89	11.53	7.63
15	1.26	2.62	0.27	0.55	2.36	1.81
20	1.23	2.87	0.31	0.57	2.37	1.80
25	0.81	2.16	0.15	0.40	1.60	1.21
30	0.86	2.29	0.12	0.43	1.73	1.29
35	0.83	2.32	0.10	0.42	1.67	1.25
40	0.80	2.39	0.14	0.41	1.63	1.21
50	0.72	1.77	0.06	0.38	1.47	1.10
75	0.64	1.93	0.11	0.34	1.31	0.98
100	0.52	1.19	0.11	0.24	1.00	0.76

	Performance of the Best Point-Sets of Different Sizes for 2.0mm Maximum Noise					
Point-Set Size	**Average Err**	**Max Error**	**Min Error**	**STD**	**95% of Pop**	**75% of Pop**
Rotational Error (deg)						
10	7.32	37.35	0.80	7.11	21.54	14.43
15	3.18	8.73	0.43	1.73	6.65	4.92
20	2.63	7.35	0.21	1.25	5.12	3.87
25	2.08	9.87	0.27	1.28	4.64	3.36
30	2.16	4.94	0.43	0.86	3.89	3.02
35	1.94	4.42	0.16	0.90	3.74	2.84
40	1.86	5.47	0.43	0.91	3.67	2.77
50	1.51	3.50	0.21	0.73	2.97	2.24
75	1.33	3.14	0.22	0.57	2.48	1.91
100	1.08	2.79	0.30	0.51	2.10	1.59
Translational Error (mm)						
10	3.97	22.09	0.69	3.76	11.49	7.73
15	1.88	6.05	0.36	1.02	3.93	2.91
20	1.73	4.54	0.35	0.89	3.51	2.62
25	1.34	5.29	0.27	0.76	2.86	2.10
30	1.34	3.07	0.26	0.63	2.60	1.97
35	1.30	2.73	0.27	0.63	2.56	1.93
40	1.17	4.37	0.15	0.59	2.36	1.76
50	1.00	3.06	0.10	0.59	2.18	1.59
75	0.75	1.72	0.10	0.34	1.43	1.09
100	0.68	1.70	0.16	0.29	1.27	0.97

Table 5.9: (cont'd) Relationship between point-set size and registration robustness, expressed in terms of overall rotational and translational accuracy, for the set of best randomly generated point-sets describing a proximal tibia.

Point-Set Size	Avg Time (HH:MM:SS)	Max Time (HH:MM:SS)	Min Time (HH:MM:SS)
10	00:06:12	00:10:47	00:04:40
15	00:10:16	00:13:16	00:08:27
20	00:12:04	00:15:06	00:09:55
25	00:15:38	00:19:39	00:12:49
30	00:17:29	00:23:48	00:12:57
35	00:20:55	00:25:24	00:17:05
40	00:22:38	00:31:00	00:18:40
50	00:27:15	00:39:42	00:23:47
75	01:11:56	02:04:11	00:33:34
100	01:30:05	02:43:51	00:54:31

Table 5.10: Typical computation time requirements for point-set robustness assessment, obtained on a PC workstation running Windows® XP Professional, with a 1.8GHz Intel Pentium® 4 processor.

registration. All hardware components described in Chapter 4, including the robotic system, and the custom manufactured bone clamps, were used for the experiments, which were carried out following the intra-operative acquisition protocol described in Section 5.3.5.

5.4.3.1 Experimental Setup

Following the intra-operative protocol, the gross positioner was fixed to the operating table, and each pair of plastic phantoms was immobilised by using the bone clamps described in Section 4.17. A typical experimental setup is illustrated in Figure 5.26.

The back-drivable end effector was used to collect points on both the distal tibia and proximal femur using the on-screen guidance provided by the intra-operative display (Section 5.3.5).

5.4.3.2 Defining a Reference Registration Transform

In order to evaluate the accuracy of the registration technique described for a specific intra-operative setup, a means to measure the actual position of each bone with respect to the robotic system had to be defined. Fiducial marker screws currently are the "gold standard" to validate non-invasive registration techniques based on anatomical features [Ellis et al., 1997; Ellis et al., 1996; Pennec and Thirion, 1995; Simon et al., 1995]. However, the screws, which have to be implanted in sets of 3 or 4 on both tibia and femur pre-operatively, have to be individually segmented and their position accurately defined in the pre-operative planning phase. This procedure is time consuming, and can result in undesirable inaccuracies, introduced by poor segmentation and inadequately locating the screws intra-operatively. These issues, however, can be quantified, and are independent of the current intra-operative

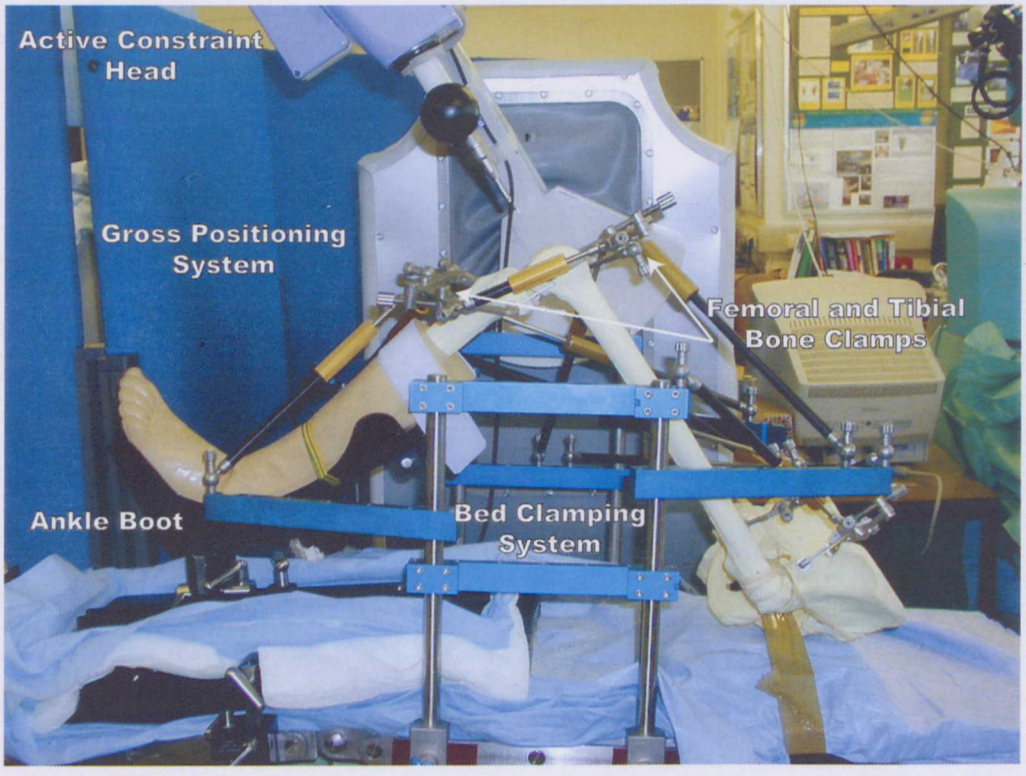


Figure 5.26: Experimental setup adopted for plastic bone trials with the ACROBOT II System for robotic assisted TKA.

setup. In an operating theatre environment, for instance, fiducial marker screws would provide a solid reference to assess the quality of registration for a method based on anatomical correspondences.

Under *in vitro* conditions, however, all aspects of the registration procedure affecting accuracy can be appropriately addressed, and their effect on registration outcome can be minimised. As described in Section 4.3, the ACROBOT II System can perform as a mechanical digitiser with accuracy at the tip of 0.2mm on average. The CT scan is performed with 0.5mm slices for the knee portion of the leg anatomy, which can potentially provide surface accuracy of the segmented model well within 0.5mm, since values between slices can be accurately interpolated. Furthermore, the scan of a plastic phantom generally allows quick and accurate segmentation of each bone, since it has homogeneous consistency, and is free from any soft tissue. Therefore expected point accuracy for the point acquisition process under experimental conditions would be well within 0.5mm on average.

By using the values in Table 5.7 and Table 5.8 as guidelines for robust registration, a point-set with more than 75 points (assembled on surgically accessible surfaces) for point accuracy better than 0.5mm has a very high probability (95%) of producing registration accuracy of under 0.4^o and $0.4mm$, with average values of

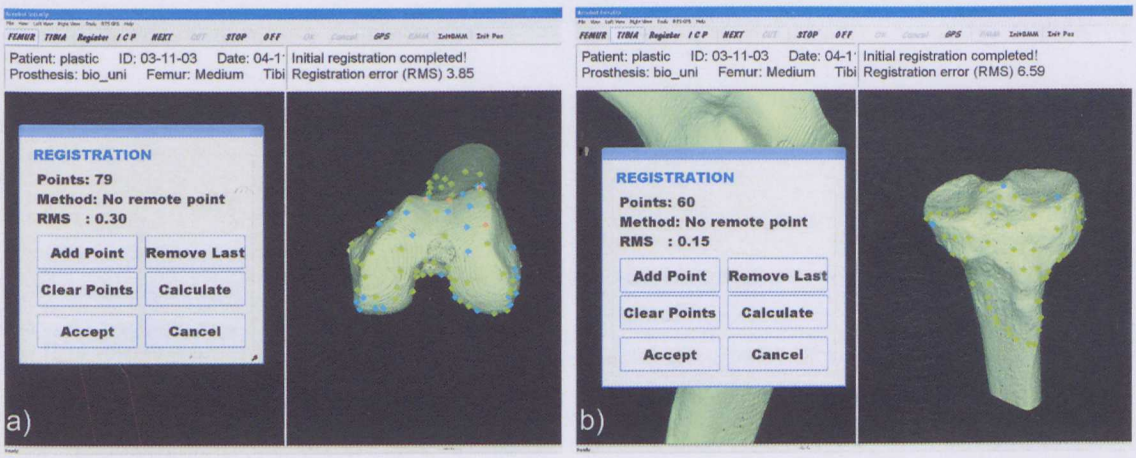


Figure 5.27: Examples of reference point-sets for the femur (a) and tibia (b) with typical colour-code distributions and RMS error values.

approximately 0.2^o and $0.2mm$. This degree of accuracy falls within the accuracy of the ACROBOT II System itself, therefore is more than appropriate for the task.

A robust registration matrix, to be used as a reference to assess accuracy, can be obtained by assembling a large point-set of over 75 points on all of the available surface (not only surgically accessible surfaces) for every bone prior to registration with the intra-operative protocol. This procedure results in a reference transform (T^{Ref}_{BASE} in Equation 5.7) that can be used to evaluate the performance of the algorithm using the protocol described in Section 5.3.4. Results of a focused experiment carried out to compare registration matrixes obtained using both fiducial screws and a reference point-set are included in Appendix C.

To verify the result obtained by registering the reference point-set, an example of which is illustrated in Figure 5.27, the procedure is always carried out twice and results compared. The difference between the registration matrices generated by the two reference point-sets has never exceeded 0.1^o and $0.1mm$ in all of the ten trials described in the following section.

5.4.3.3 Tests and Results

10 consecutive full registration procedures using the enhanced ICP algorithm described, including minima suppression, were carried out, and results compared to the ground truth defined by the reference transformation matrix defined above. Table 5.28 illustrates the results, in terms of rotational and translational alignment of the registered bone in the $\{BONE\}$ frame of reference (Section 5.4.1) for both the femur and tibia.

Table 5.28 illustrates the registration outcome obtained for point-sets of different sizes, between 25 and 40 points, assembled on surgically accessible surfaces using

a)

Test #	Point-Set Size	RMS Error (mm)	Error Matrix Components				
			V/V Error (deg)	*Axial Error (deg)*	*A/P Error (deg)*	*Rot Error (deg)*	*Trans Error (mm)*
1	38	0.19	-0.09	-0.05	0.15	0.18	0.19
2	40	0.2	-0.13	0.04	0.11	0.17	0.22
3	40	0.21	-0.11	-0.07	0.39	0.41	0.26
4	30	0.21	0.08	0.25	-0.72	0.77	0.24
5	35	0.19	-0.21	0.02	-0.60	0.64	0.15
6	35	0.17	-0.15	0.10	-0.42	0.46	0.27
7	30	0.17	0.12	-0.14	0.26	0.32	0.19
8	26	0.14	0.21	-0.27	0.31	0.46	0.10
9	25	0.13	0.35	-0.19	-0.61	0.73	0.08
10	31	0.16	0.01	-0.11	0.58	0.59	0.18
Maximum Error			0.35	0.25	0.58	**0.77**	**0.27**
Minimum Error			-0.21	-0.27	-0.72	**0.17**	**0.08**
Average Error			//	//	//	**0.47**	**0.19**

b)

Test #	Point-Set Size	RMS Error (mm)	Error Matrix Components				
			V/V Error (deg)	*Axial Error (deg)*	*A/P Error (deg)*	*Rot Error (deg)*	*Trans Error (mm)*
1	35	0.17	-0.04	0.13	0.32	0.35	0.23
2	35	0.14	-0.38	-0.02	0.03	0.39	0.55
3	35	0.19	-0.11	-0.33	-0.44	0.56	0.37
4	30	0.18	-0.33	0.30	0.31	0.54	0.43
5	30	0.14	-0.12	0.19	-0.02	0.22	0.27
6	28	0.16	-0.22	0.57	0.35	0.71	0.35
7	25	0.15	-0.01	0.03	-0.13	0.14	0.32
8	25	0.19	-0.20	-0.26	-0.19	0.38	0.41
9	25	0.15	-0.06	-0.22	0.10	0.25	0.57
10	30	0.16	-0.33	0.57	0.04	0.65	0.52
Maximum Error			-0.01	0.57	0.35	**0.71**	**0.57**
Minimum Error			-0.38	-0.33	-0.44	**0.14**	**0.23**
Average Error			//	//	//	**0.42**	**0.40**

Figure 5.28: Accuracy of registration outcome for 10 registration procedures using the enhanced ICP algorithm for both the femur (a) and tibia (b).

the point acquisition protocol described in Section 5.3.4. Results for both femur and tibia are all well within the range of accuracy defined in Table 5.5 and Table 5.6 for a specific point-set size for point accuracy better than 0.5mm. The minimum and maximum values, representing the envelope of the accuracy for each error matrix component, are all within the value for 95% of the population for a specific set size and point accuracy. Furthermore, the average accuracy is much higher, with differences of approximately 0.2mm and 0.2^o, which is to be expected looking at the average registration accuracy for the corresponding point-set size in Table 5.5 and Table 5.6.

5.5 Discussion

Speed enhancements to the algorithm, introduced by the k-d tree based vertex search (Section 5.3.2) and by pre-computing the triangle list (Section 5.3.1), have resulted in one run of the algorithm being executed in interactive time. As illustrated in Table 5.4, this speed enhancement has allowed minima suppression, which has shown to be an effective means to identify the global minimum for a specific point-set (Section 5.4.2.5.2), to be carried out without an increase in registration time from the original implementation (Chapter 3).

Although the RMS error value has been shown to have little relevance if used to represent the quality of registration, it can be used alongside the colour-coded display of the points mapped on the registration surface to predict achievable point accuracy for a specific intra-operative setup. For a representative point-set, the RMS error can also become a meaningful indicator for global minimum identification, as failure of the minima suppression mechanism generally results in a significantly higher value for the RMS error (Figure 5.17). Results presented in Figure 5.24 can be used as guidelines to predict what the RMS error should be for a specific point-set size and maximum noise value if the global minimum has been identified.

It has also been shown that a representative point-set can be assembled by following the intra-operative acquisition process described in Section 5.3.4, which involves collecting a proportion of the point-set size in each region identified in the protocol for the tibia and femur (Figure 5.6). An appropriate set size is defined by predicting the expected point accuracy for a specific intra-operative setup using the RMS value and intra-operative display, as described above.

Achievable registration accuracy, in terms of rotational and translational errors, for the region-based point acquisition protocol used in conjunction with the enhanced ICP algorithm described has been documented. Representative figures for the accuracy that can be expected by carefully following the acquisition protocol

have been presented (Table 5.5 and Table 5.6). "Worst-case" performance figures for intra-operative registration have also been derived through simulation, by exploring results obtained for a large number of randomly assembled point-sets of different sizes for a number of different maximum noise levels. If the acquisition protocol is rigidly enforced, representative results obtained for this process (Table 5.7 and Table 5.8) can be used as robust guidelines to predict the maximum inaccuracy for a specific point-set size and known point accuracy.

A powerful indicator for the robustness of a point-set has also been derived (Section 5.3.5), and preliminary results (Section 5.4.2.5.6) have shown significant potential for its implementation as an intra-operative assessment tool for registration quality evaluation. Speed limitations of the current implementation do not allow the indicator of point-set robustness to be used as an additional intra-operative tool during registration. It can however be used to post-operatively assess point-sets collected in the operating theatre, to derive a value for the maximum error, introduced during registration, on the outcome of the procedure.

A set of focused plastic bone trials have demonstrated that the algorithm and protocol have been successfully integrated in the ACROBOT II System. Results (Table 5.28) have shown that quick and robust registration can be achieved for both the tibia and femur using only surgically accessible surfaces for TKA. Plastic bone results closely corroborate those derived through simulation for the point-set size and point accuracy obtained during *in vitro* experimentation.

5.6 Conclusion

Anatomical registration, which avoids the need for fiducial markers, has been studied and used for over a decade. Implementations are mostly derived from the Iterative Closest Point (ICP) algorithm as described in [Besl and McKay, 1992]. The registration software described herein uses a variation of the well known ICP to map a set of points acquired intra-operatively to the 3D surface model of the bone obtained from the CT-scan. This implementation has been optimised for speed and robustness, and a point acquisition protocol has been devised for use during surgery, to provide a good and robust dataset. The algorithm and its accuracy have been validated with extensive simulations, and plastic bone trials, which have led to an Ethics-approved clinical evaluation, with preliminary results reported in [Rodriguez y Baena et al., 2003; Cobb et al., 2003; Henckel et al., 2003].

Whilst the ACROBOT II System does not make use of transosseous fiducial markers, it allows for intra-operative checks by using a patented bone clamp with registration markers. Furthermore, once the registration process has been completed

in the operating room, the surgeon checks its correctness by the root mean square error, inspecting the colour coded display of the points on the mapped surface, and by sweeping the bone surface with the registration probe to verify that the visual feedback on the computer screen is correct. The registration process can be repeated until satisfactory results are obtained.

Although no absolute measures of performance are available intra-operatively, tests described suggest that, by carefully selecting points in key locations on the surface, the size of the point-set can be minimised, without compromising the success rate. In turn, the results also highlight how an unstructured point collection procedure may compromise the outcome of registration, with significant implications to the rest of the surgery. However, intra-operative guidance, alongside a robust point acquisition protocol, can provide the required degree of confidence on the outcome of registration, which is required for this type of application. Preliminary validation of a novel indicator of robustness has shown that intra-operative guidance can be further improved by providing the surgeon with quantitative information for the robustness of a specific point-set. In turn, this can be used to achieve consistently appropriate registration. Further validation, and a fast implementation of the robustness indicator algorithm have been addressed in Section 8.3 as areas for future work.

Chapter 6

Active Constraints and Minimally Invasive Surgery

6.1 Introduction

As described in Section 6.2, the concept of active constraints is well suited for robotic assisted minimally invasive surgery (MIS), as the tactile feed-back provided by a back-drivable system would replace the loss of "feel" conventionally associated with MIS. A relatively smaller surgical procedure, such as Unicompartmental Knee Arthroplasty (UKA, Section 1.2.2), has significantly lower power and access requirements compared to a more invasive procedure, such as Total Knee Arthroplasty (TKA, Section 1.2.1). Less bone needs to be machined away in order to fit the two prosthesis components (Figure 1.5) on the femur and tibia, which can be inserted through a smaller skin incision. Therefore, the design of a robotic system suitable for MIS could be tailored for a minimal working envelope, small footprint, and low power requirements. The early concept design of a robotic system for UKA, comprising a passive gross positioner, a small back-drivable active constraint head, and optical sensors for positional information, is illustrated in Figure 6.1.

However, in order to validate the concept of an active-constraint robot for MIS, it was decided to adapt the ACROBOT II System, described in Chapter 4, for robotic-assisted UKA. Although the system, which was designed for TKA, is over-specified for this type of surgery, small changes to both hardware and software would enable the ACROBOT II System to be used as a concept demonstrator to prove the efficacy of active constraints as a means for quick and accurate completion of minimally invasive procedures. Successful results with this early prototype, would then set the foundations for the design and development of a dedicated system for robotic assisted UKA.

The following sections describe some of the changes carried out to the hardware

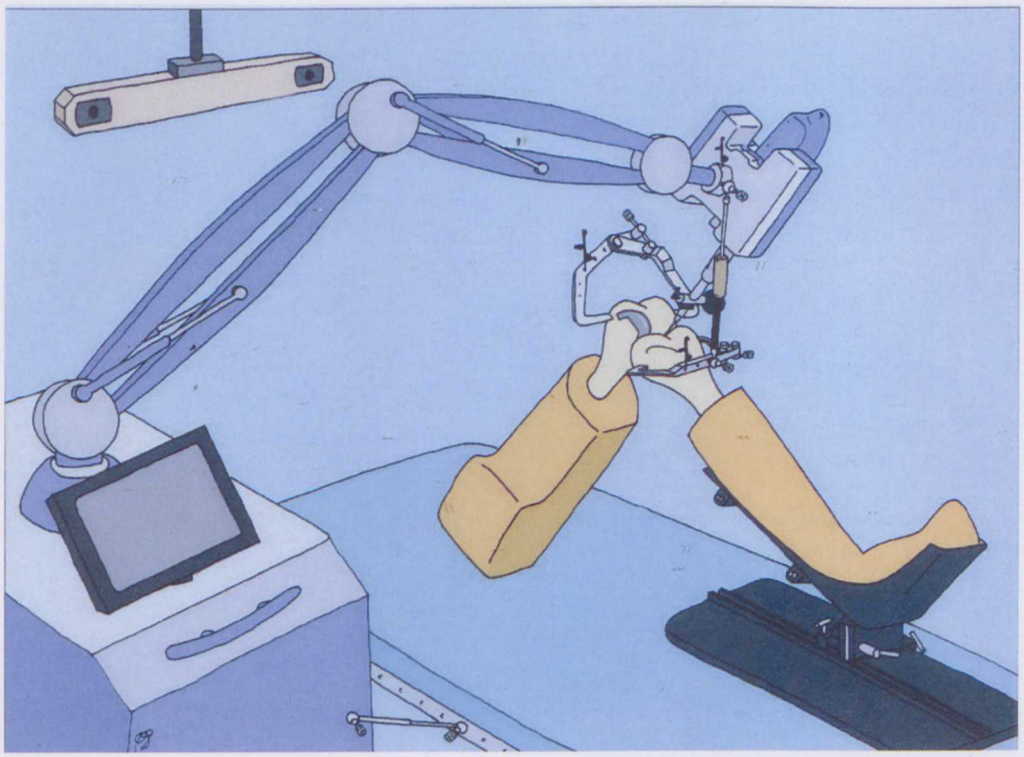


Figure 6.1: Early concept design of an active-constraint robotic system for Unicompartmental Knee Arthroplasty.

(Section 6.2), software (Section 6.3), and intra-operative protocol (Section 6.2.3) carried out on the original ACROBOT II System, including the validation of a point acquisition protocol for registration suitable for minimal access UKA (Section 6.3.3). This chapter focuses on the author's contribution to the adaptation process. It therefore does not include a detailed description of changes to the pre-operative and intra-operative software that were carried out to plan and execute a UKA procedure with the system described in Section 1.3. Published work on some of these aspects, which are not covered, can be found in [Jakopec et al., 2002b; Jakopec et al., 2003a].

6.2 Adapting the ACROBOT II System for MIS

This section presents changes to the robotic system (Section 4.2) and bone clamp design (Section 4.4) which were originally tailored for TKA. As a result of the smaller incision of a UKA procedure (Figure1.4), access to the exposed bone surfaces is significantly reduced. Therefore the bone clamps had to be redesigned to accommodate for the space restrictions imposed by the new procedure. A means to manage the soft tissue surrounding the skin incision to optimise access to the surfaces for both registration and cutting also had to be developed. This process also involved the definition of an intra-operative protocol that would allow the UKA procedure to be

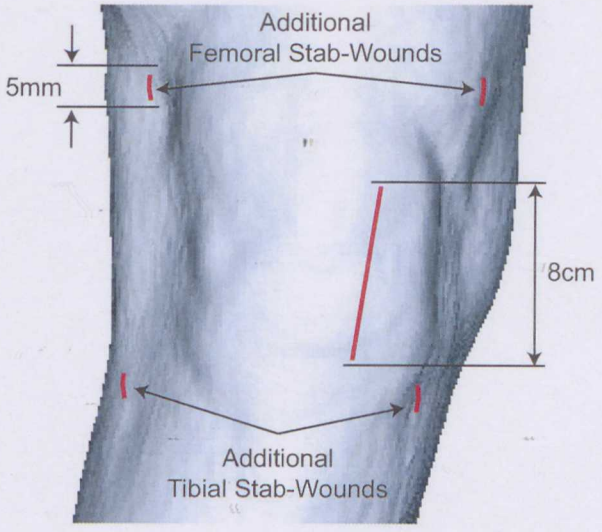


Figure 6.2: Layout of the main UKA skin incision and additional stab-wounds, required for the clamping system, over the knee joint.

completed, using the system's kinematic configuration and workspace limitations. A brief description of these changes can be found in the following sections.

6.2.1 Clamp Redesign

The clamps developed for TKA are tightened onto the bone through the main incision, which, as illustrated in Figure 1.4, exposes a large percentage of both the distal femur and proximal tibia. Because of reduced access, the UKA clamps were redesigned to be used with a set of additional small stab-wounds, two on the medial side and two on the lateral side, which, as illustrated in Figure 6.2, would complement the main incision over the frontal knee joint.

The prototype design, illustrated in Figure 6.3 in red over the TKA clamp outline, was developed to accommodate the thickness of the soft tissue between the bone and skin incision. The range of motion and mechanism are identical to those developed for the TKA clamps, but the insertion pins and thickness of the arms had to be modified to allow easy insertion through the skin.

A number of insertion pin configurations was studied in order to identify the design that would produce the maximum grip, needed to ensure stiffness, and minimum footprint. Some of the early concept designs are illustrated in Figure 6.4.

After considering a number of technical issues, such as manufacturing costs and force limitations, and clinical issues, such as the material properties of the bone and access, it was decided to opt for the design illustrated in Figure 6.5. As can be seen, the insertion pins dimensions, which have been shown to provide an appropriate degree of stiffness through experimental testing on different surfaces, allow the clamps

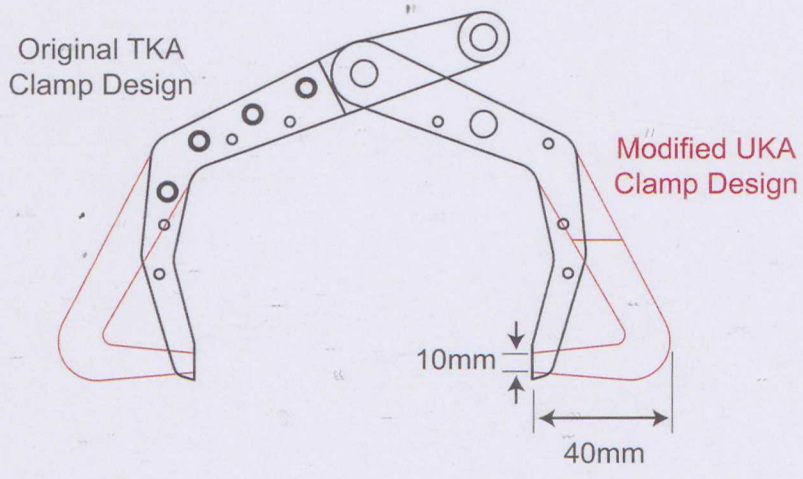


Figure 6.3: Prototype clamp design.

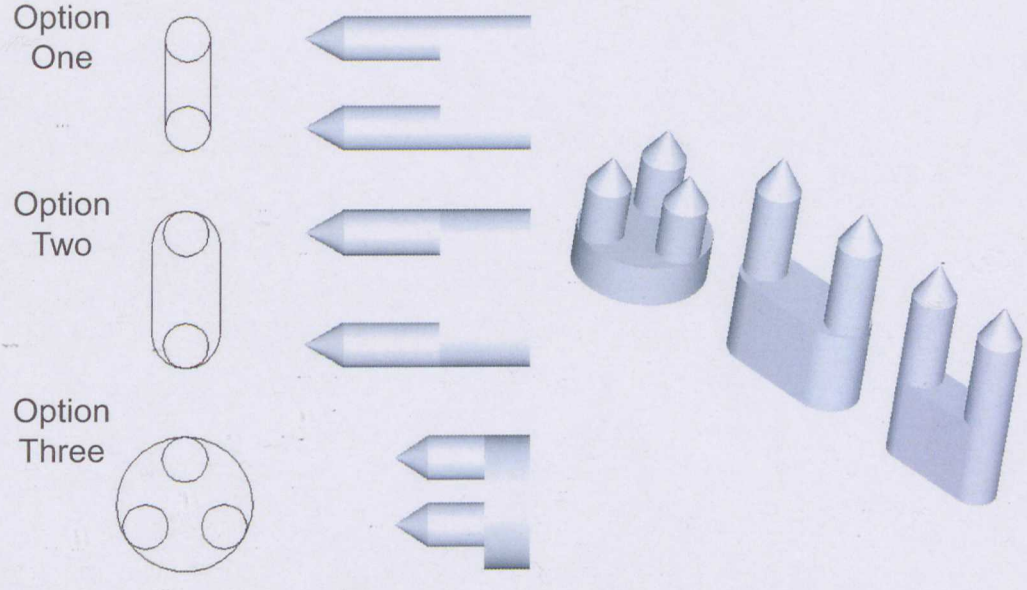


Figure 6.4: Early concept designs for the UKA clamps insertion pins.

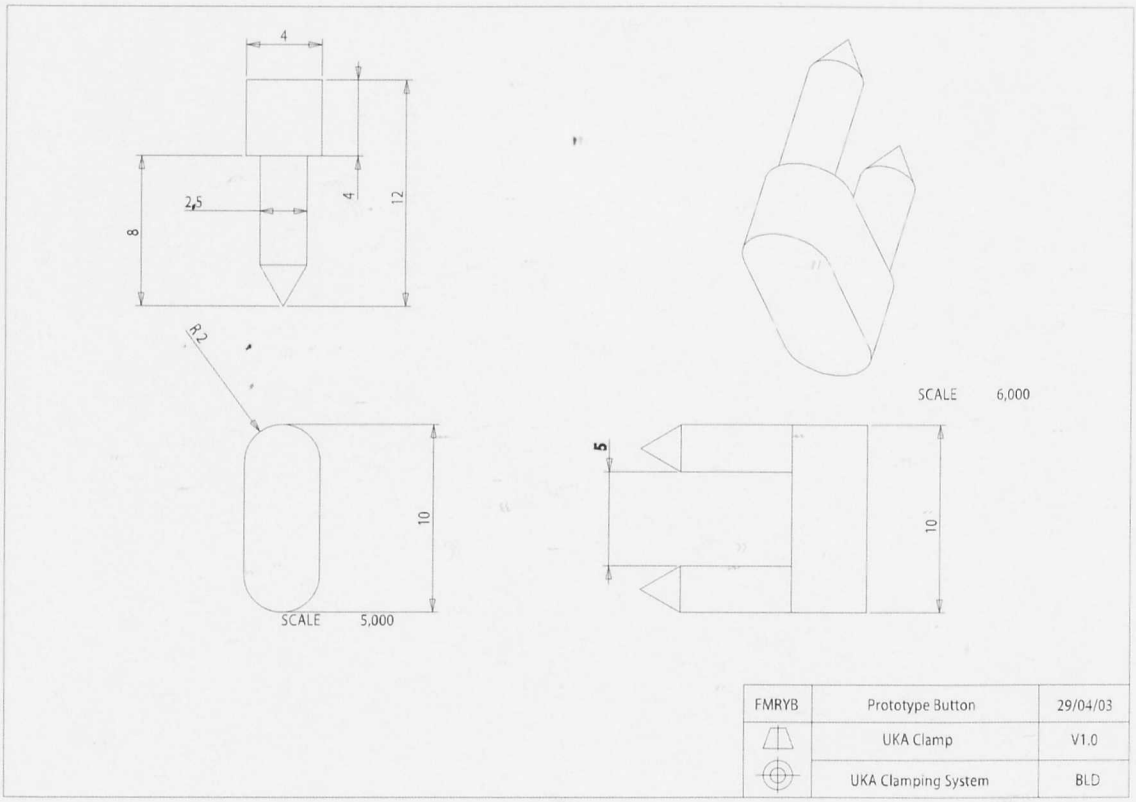


Figure 6.5: Technical drawing for the insertion pins of the UKA clamping system.

to be tightened onto the bone through two $5mm$ incisions on either condyle. These additional stab-wounds generally do not require stitching.

The outcome of the redesign process, which was subcontracted out for manufacture, is illustrated in Figure 6.6. Both the femoral and tibial clamps can be used interchangeably, therefore only one has been shown. All other components of the clamping system, including the telescopic rods, and bed mounted frame, are the same as those illustrated in Figure 4.17 for the TKA clamping system. The clamps developed for UKA include a number of accurately machined holes that can be used intra-operatively to monitor bone motion at different stages of the procedure (Section 4.4.2). A brief outline of the robotic UKA procedure with the ACROBOT II System, including clamping and bone motion monitoring with the minimally invasive clamps described, can be found in Section 6.2.3.

6.2.2 Soft Tissue Management

In order to optimise access to the bone surface through the conventional UKA incision, a novel tissue retaining tube, to be used in conjunction with the ACROBOT II System, was designed, and an early prototype manufactured and tested. This additional tool enables the surgeon or assistant to drag the soft tissue surrounding

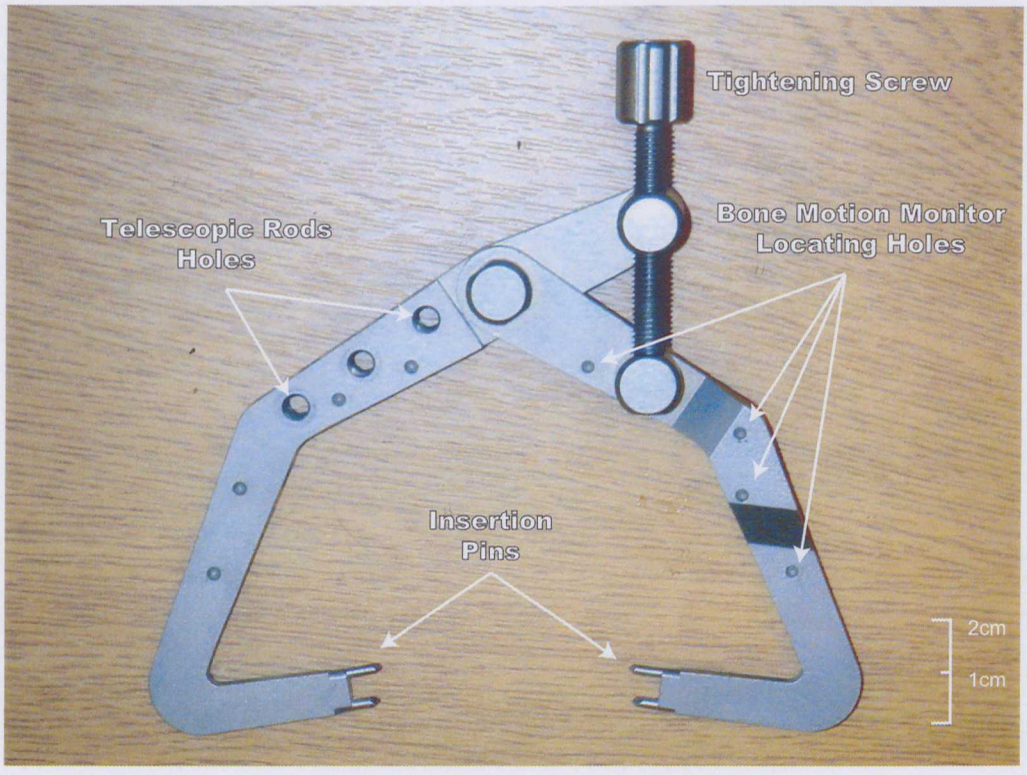


Figure 6.6: UKA bone clamp.

the main incision around, which in turn improves access to both the tibial and femoral surfaces during registration and cutting (Section 6.2.3). After the soft tissue preparation that follows the main skin incision, the tissue retaining tube is sutured into position to avoid unwanted slippage. An early concept design, illustrating the tube, handle attachment, and two options for the suturing posts is illustrated in Figure 6.7.

The tube attachment slots into the matching hole of the modular handle described in Section 4.4, which is used to grip the tube during surgery. The final design, used to manufacture the first prototype, is illustrated in Figure 6.8, and includes four suturing posts as those described in Figure 6.7 as "Option 1".

The tissue retaining tube was designed to have a large enough internal diameter to guarantee an appropriate degree of access for registration and cutting, and to allow the implants to be correctly inserted. As illustrated in Figure 6.9, the prototype tube, which was manufactured for preliminary testing, is large enough to fit each component. However, the largest side is $3.5cm$ in length, which is significantly smaller than the $8cm$ incision used in conventional UKA. Therefore the tissue retaining tube can potentially be used to decrease the size of the incision further, from $8cm$ to approximately $3.5cm$.

Early experimentation with the tube during conventional procedures (Figure

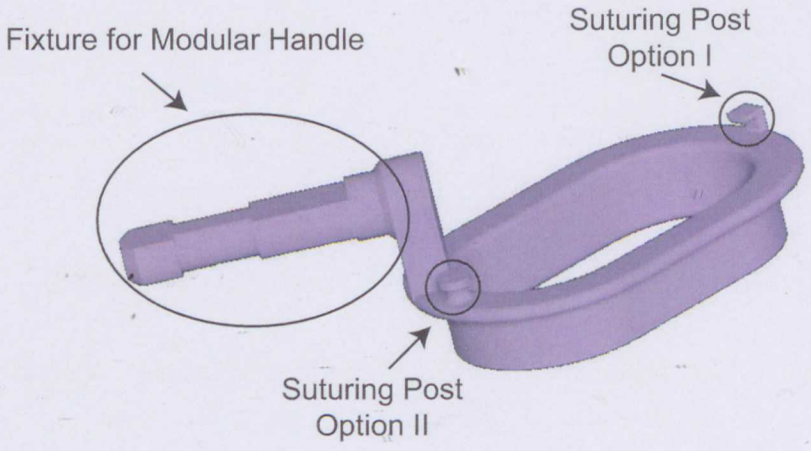


Figure 6.7: Tissue retaining tube: concept design.

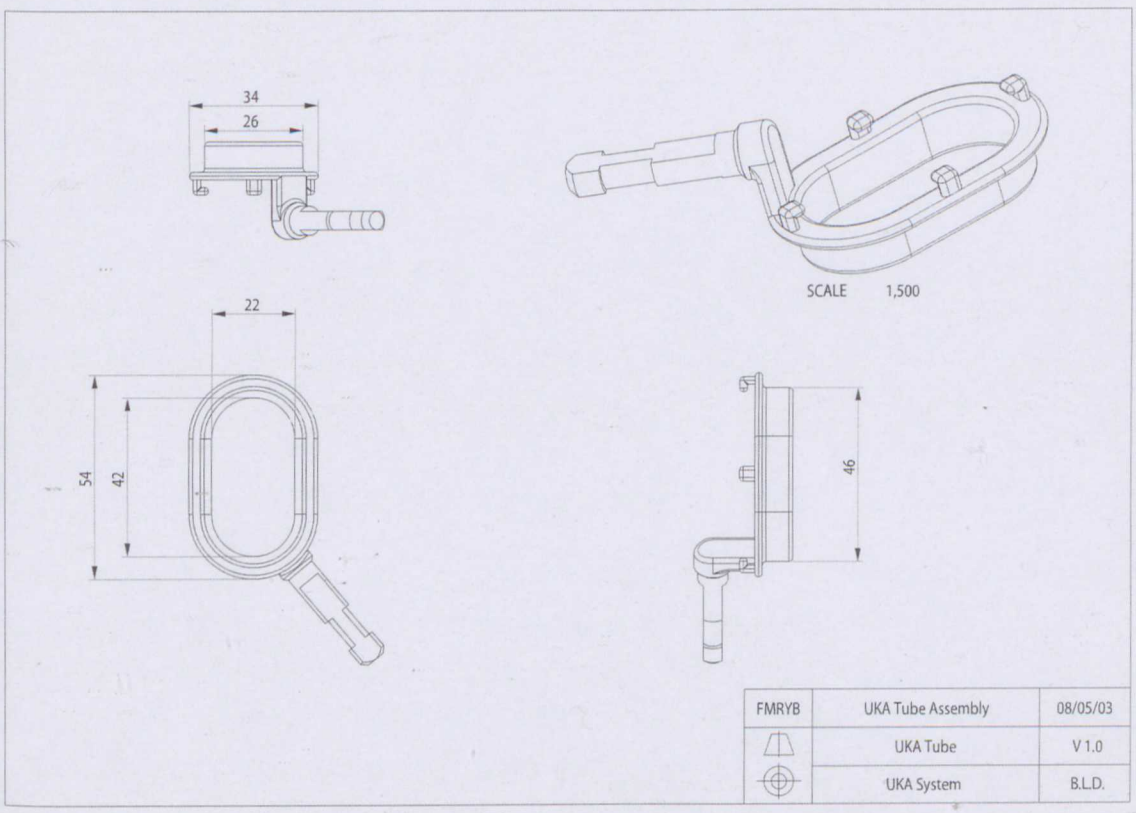


Figure 6.8: Tissue retaining tube: final design.

Component	Cut	Cutter Insert
Femoral	Main cylindrical cut	8mm Ball Cutter
	Locating hole	Auxiliary Cutter
Tibial	Main flat cut	8mm Ball Cutter
	Tibial groove	Auxiliary Cutter

Table 6.1: UKA cuts, and relative cutter inserts.

6.13), however, has highlighted a number of shortcomings in the current design, which do not allow the procedure to be successfully carried out through a smaller incision. The deficiencies of the early prototype include:

1. The shape of the edge that comes into contact with the bone does not sit neatly onto the surface, causing unwanted slippage during use.

2. The suturing posts, which seemed appropriate during the design phase, proved to be inadequate for the task. An alternative design, with holes instead of posts, is currently being developed.

3. The depth of the tube is too shallow to account for the soft tissue thickness surrounding the main incision.

4. The size of the internal hole is marginally too small, causing excessive difficulties during insertion of the trial implants.

The concept of a tissue retaining tube has shown significant potential, if complemented by a robot and visual feedback, and may, in future, allow UKA to be completed through a $3.5cm$ incision. The shortcomings of the current tube design have been addressed in Section 8.3 as an area for future work.

6.2.3 Intra-Operative Protocol for Minimal Access UKA

Unicompartmental knee arthroplasty generally requires a smaller number of cuts to place the tibial and femoral components compared to a total knee replacement. For this early concept demonstrator, it was decided to focus on the replacement of the medial condyle only, using the Oxford unicompartmental knee implant [Biomet Inc., 2002]. The bone cuts, to be performed with the back-drivable end effector, have been graphically illustrated in Figure 6.10, and summarised in Table 6.1, for both the femur and tibia.

As illustrated in Table 6.1, only two different cutter inserts are needed to machine the bones. One is used for large surfaces (the $8mm$ ball cutter), and the other

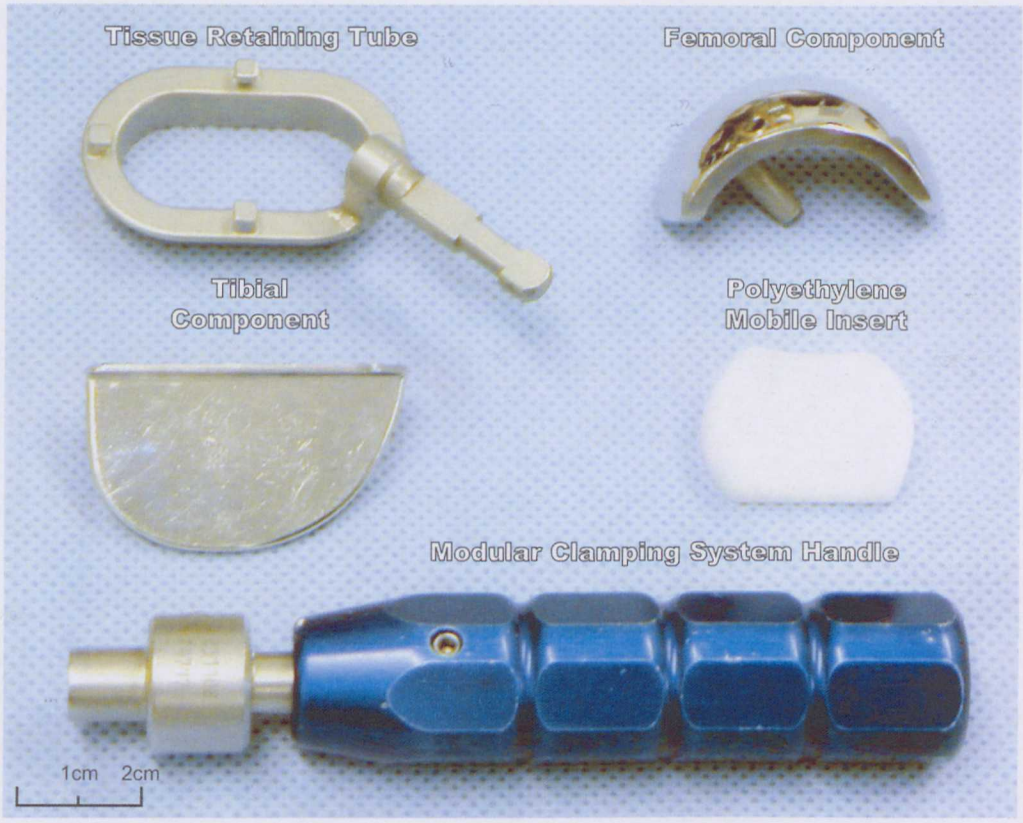


Figure 6.9: Retaining tube, interchangeable handle, and unicompartmental knee prosthesis.

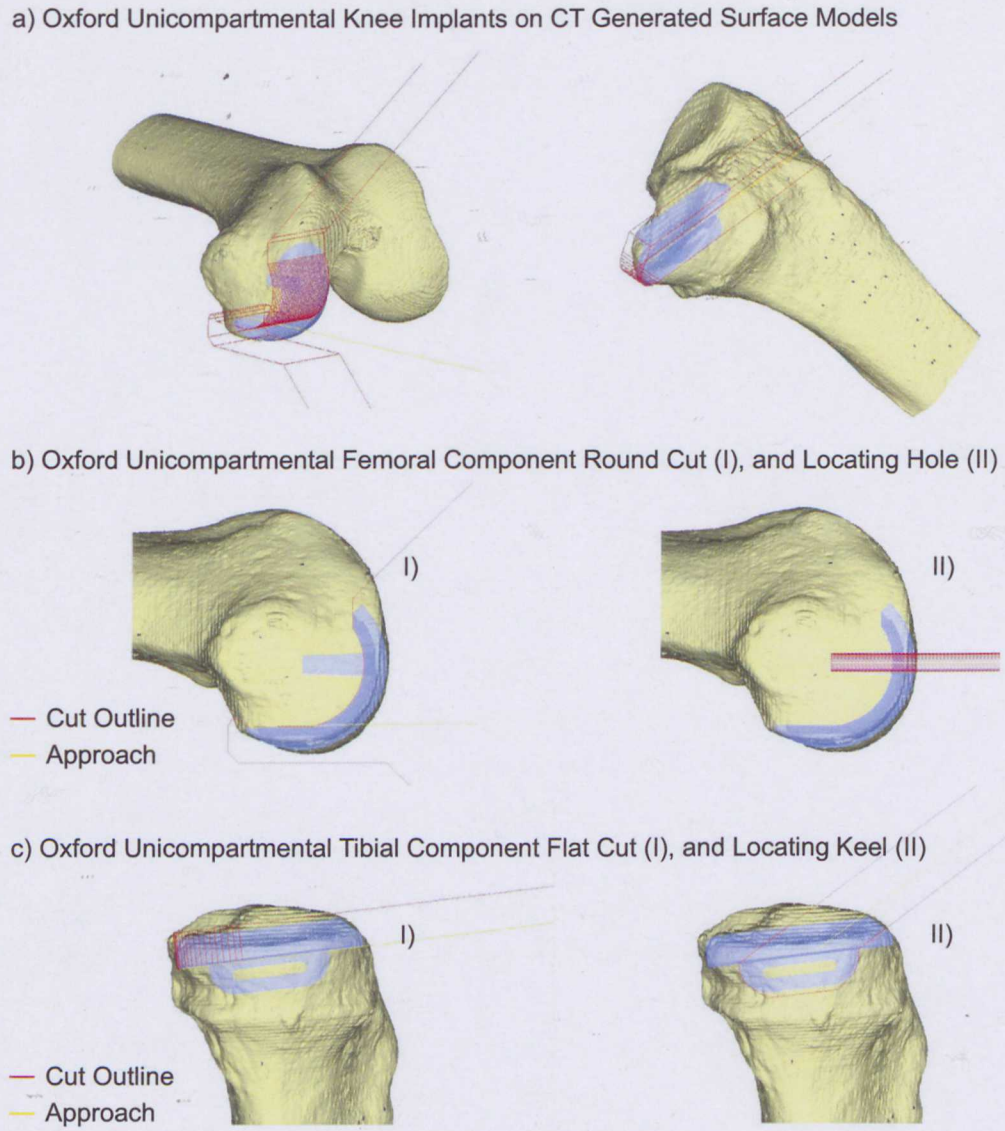


Figure 6.10: Graphical illustration of the cuts required to place both tibial and femoral components of the Oxford unicompartmental knee implant [Biomet Inc., 2002].

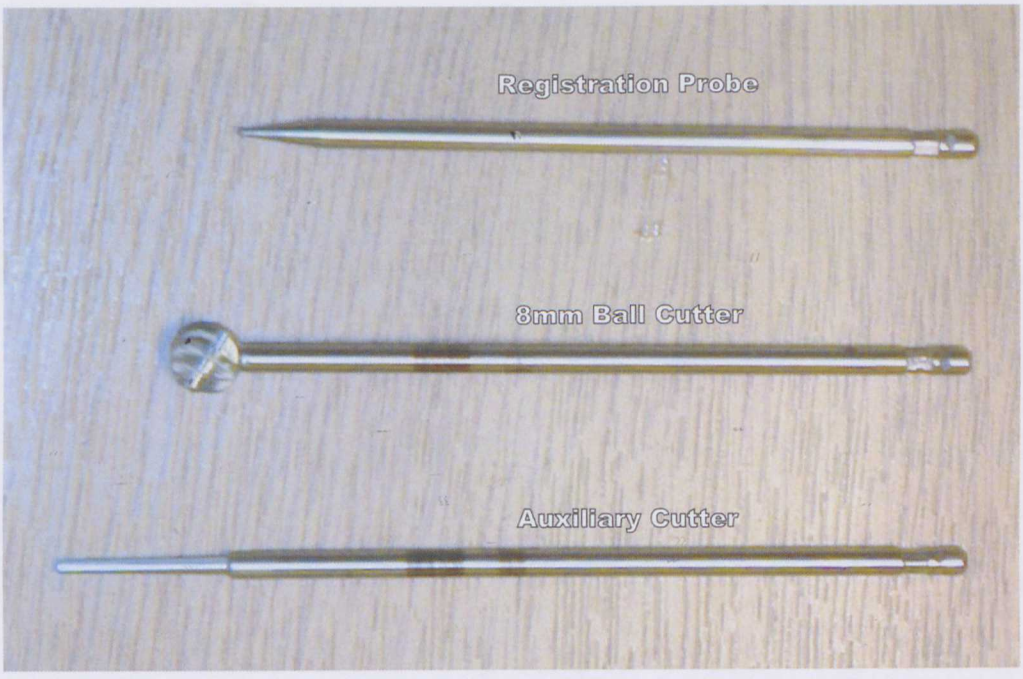


Figure 6.11: Cutter inserts, used during UKA with the ACROBOT II System, shapes and dimensions.

to accurately machine the locating hole and the tibial groove, for the femur and tibia respectively. As for the TKA procedure with the ACROBOT II System, an additional probe is used during registration to collect points on the bone surfaces. The three inserts needed for the procedure are illustrated in Figure 6.11.

Unicompartmental knee arthroplasty is a substantially smaller procedure compared to total knee arthroplasty. In many respects, the workspace requirements for a robotic system suitable for UKA would be significantly less, resulting in a lighter and smaller system. Therefore it would be expected that a system developed for TKA would have a large enough working envelope to be used for UKA. Unfortunately, during the early stages of the gross positioning system redesign, the decision to opt for a three degrees of freedom (DOF) mechanism was made, to ensure an appropriate degree of stiffness (Section 4.2). This kinematic configuration, although appropriate for TKA, misses an important DOF in the horizontal direction perpendicular to the long axis of the operating table, which does not allow the active constraint head (AC Head) to be accurately placed (i.e. motorised motion as opposed to manual placement of the system over the bed) when machining the locating hole and tibial groove. Therefore, alternative means to obtain the desired range of motion have been included in the UKA procedure outlined in the following sections. The procedure outline that follows assumes a $3.5cm$ skin incision, although the larger access obtained through a conventional $8cm$ cut would only simplify the placement requirements for the system, with no other effect on the protocol.

The procedure outline for UKA of the medial condyle using the ACROBOT II System and the Oxford unicompartmental knee implant now follows:

1. The patient is wheeled into the Operating Room (OR) and prepared for surgery.

2. The knee joint is exposed and both the tibial and femoral bones are prepared. The cut was originally chosen to have a "Mercedes" Type shape, with 3 radial cuts at 120°, which would facilitate the insertion of the tissue retaining tube (see point (4)). However, several clinical drawbacks of this type of incision, have led to a straight cut being used. In order to guarantee adequate access during both registration and cutting, the incision should be approximately $3.5cm$ long.

3. The leg is fixed into position by means of two retaining clamps tightened onto the tibia and femur through small slits in the skin over the medial and lateral epicondyles. This step of the procedure is currently rather complex, as an experienced surgeon is needed to ensure the stab-wounds for the tibial and femoral clamps are appropriately positioned without causing damage to the nerves. As illustrated in Figure 6.12, two small rods are used to stiffen the structure, by providing a link between the tibial and femoral clamps.

4. As illustrated in Figure 6.13, the tissue retaining tube is inserted into the $3.5cm$ incision and sutured into position. The picture, which has been included here for descriptive purposes, has been taken during a UKA procedure that was then carried out using the conventional method. Therefore the skin incision, which could be as small as $3.5cm$ in length for a robotic procedure, is actually about $8cm$ long.

5. In the mean time, the ACROBOT II System is wheeled into the OR and prepared for surgery. This implies:

   (a) Connecting all peripherals, and power cables.

   (b) Powering on the system.

   (c) Self testing the system.

   (d) Sterile draping of the system.

   (e) Inserting the sterile cutter and registration probe.

   (f) Assembling and preparing the operating table anchors.

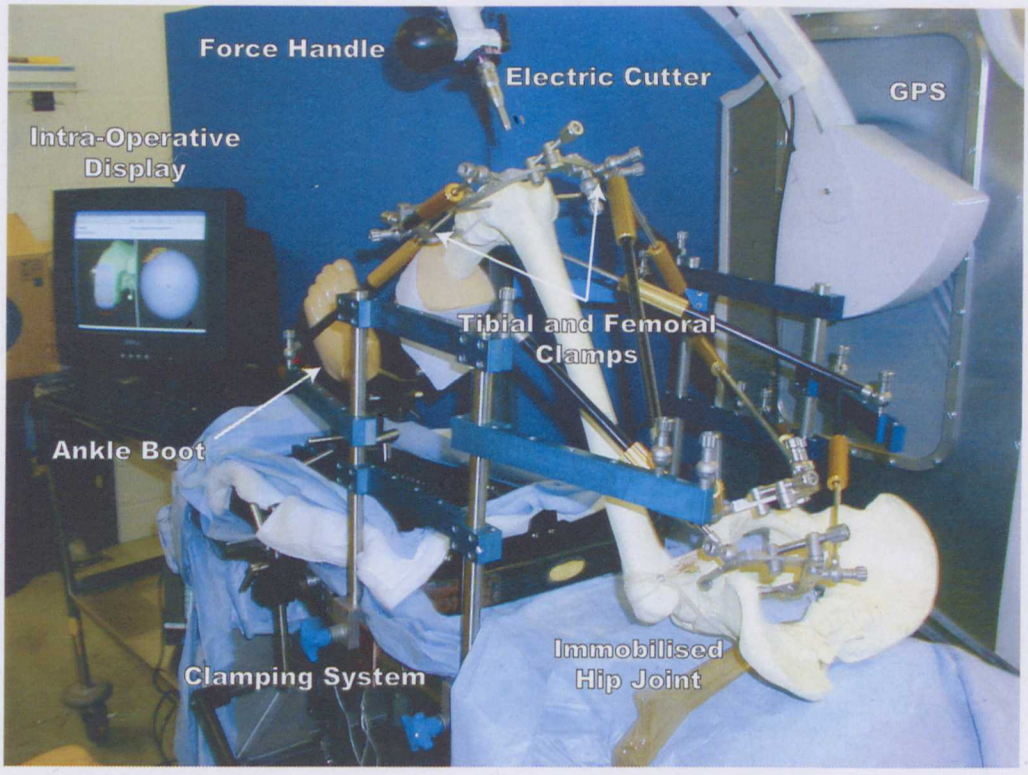


Figure 6.12: UKA with the ACROBOT II System intra-operative clamping setup.

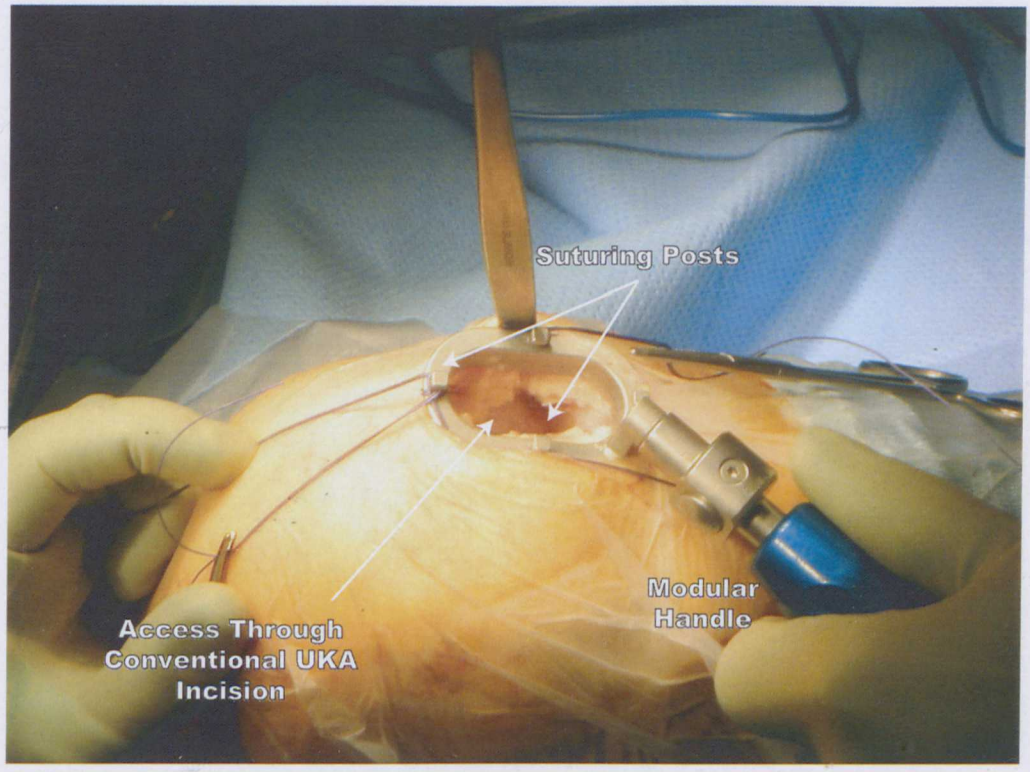


Figure 6.13: Intra-operative setup of the tissue retaining tube, during early testing on a conventional UKA procedure.

6. The robot GPS is wheeled close to the bed and securely fastened to the side rail by means of the operating table anchors. This procedure requires care as sterile and non-sterile surfaces may accidentally come into contact with one another. Accurate placement of the ACROBOT II System with respect to the immobilised leg represents the most critical aspect of this step of the procedure. Very careful placement is required to guarantee enough access to machine the groove on the tibia and the locating hole on the femur successfully, as the system lacks the degree of freedom associated with motion towards and away from the bed. Because the AC Head has a spherical configuration, its centre has to lie as close to the axis of the hole as possible in order for it to be machined to the required depth (Figure 6.14). A solution that would simplify this process would be to clamp the ACROBOT II System at an angle with respect to the side of the bed, which would allow the missing movement to be generated through a combination of motions of both the GPS (Y axis) and AC Head (Pitch, Yaw, and In/Out) joints (Figure 6.16). Placement and locking of the system with respect to the bed could be further simplified by wheeling the GPS close the bed whilst the AC Head joints are locked with a specific orientation of the end effector. This would enable clamping the GPS into the correct position, i.e. that where the tip of the cutter is pointing in the direction of the exposed knee. In turn, this would ensure that the working envelope of the system fully encloses all motions associated with the procedure. This option, however, requires the AC Head motors to be powered-on during placement.

7. The tibia is registered. It has to be registered at this point, since the tibial cut has to be completed before the femur can be machined to allow adequate access to the femur. As described in greater detail in Section 6.3.1, robust registration can be obtained by collecting a number of points on the exposed surface of the bone by means of the back-drivable end effector, which is equipped with a registration probe. Given the tube size, and some elasticity of the skin, the amount of access for registration was assumed to have a 35mm x 50mm envelope. This results in the typical registration scenario illustrated in Figure 6.15, and should be achieved with a single motion of the GPS. Some of the tibial plateau will not be available for registration as it is obstructed by the femoral condyle. As described in Section 6.3.1, a number of points is collected on the distal part of the tibia through an additional $8mm$ stab-wound, placed in proximity to the tibial tuberosity with the aid of visual feedback (Section 6.3.2).

8. As many of the holes machined on the tibial clamp as possible are touched with

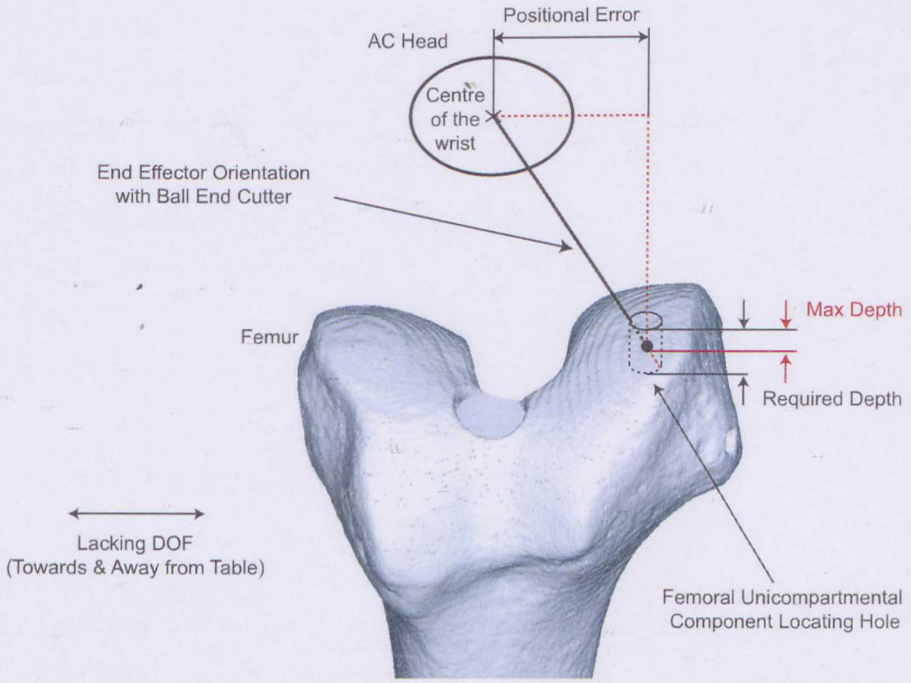


Figure 6.14: Relationship between hole depth and placement accuracy.

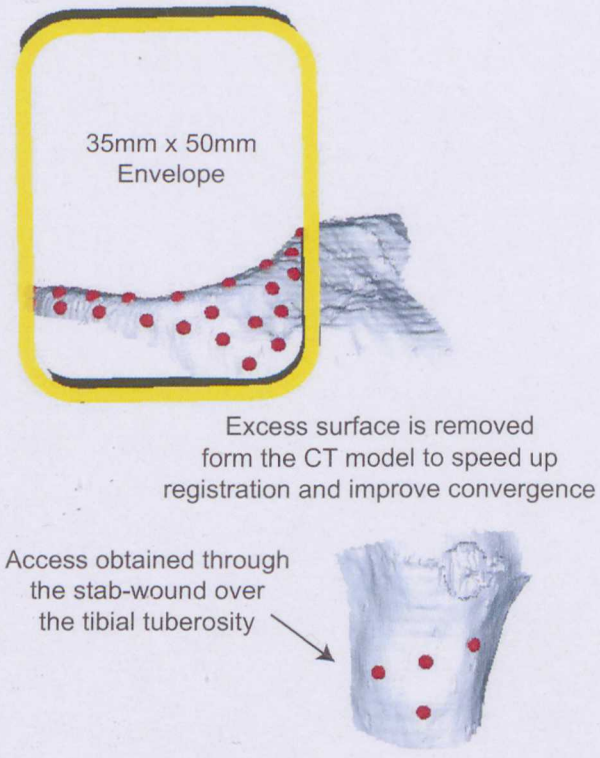


Figure 6.15: Typical registration scenario for UKA of the medial condyle.

the robot end effector using the registration probe and the foot pedal (Figure 4.6). The hole locations, which are logged by the intra-operative software, can be used at any time during the procedure to reconfirm the tibial position with respect to the robot. From this point forth, the position of the tibia derived through registration (point(7)) is referenced to the tibial clamp, which can be placed in the robotic system's workspace by touching at least four holes with the back-drivable end effector. Although the holes can be touched in any order, only those identified at this point will be available during the surgery (Section 4.4.2).

9. The tibia is machined using a ball end cutter. During this process the assistant or registrar has to hold the tube in position, following the cutter tip movements to clear the area of any soft tissue. This step of the procedure should require a single motion of the GPS, which places the centre of the AC Head both on the plane of the cut, and in line with the groove that needs to be machined after the flat cut is completed. If the GPS is clamped at an angle, correct placement can be achieved using a combination of joint motions, as illustrated in Figure 6.16. Alternatively, the operating table can be moved, and the bone motion monitor (Section 4.4.2) can be used to reconfirm the position of the knee with respect to the robot. As for the TKA procedure, the intra-operative user interface displays the cutting progress using a colour-coded plan view of the cut, which, as illustrated in Figure 6.17, shows the current cutting depth, updated in real-time during the machining process. The graphical user interface is not the author's work, but has been included here for illustrative purposes.

10. The tibial groove is machined, without any additional motions of the GPS, using an $8mm$ spherical cutter.

11. The femur is registered in much the same way as the tibia, which results in the typical registration scenario illustrated in Figure 6.18. As described in the intra-operative point acquisition protocol presented in Section 6.3.1, the small slit above the frontal side of the knee joint, required for the drainage tube used during post-operative recovery, is used to collect a small number of additional points on the bone to improve registration. Therefore, the GPS needs to be moved twice during this phase of the procedure, once to collect all points on the condyle and femoral notch, and once to collect the points through the drainage tube slit.

12. All available holes on the femoral clamp are accurately located using the registration probe. The bone motion monitor can then be used to reconfirm

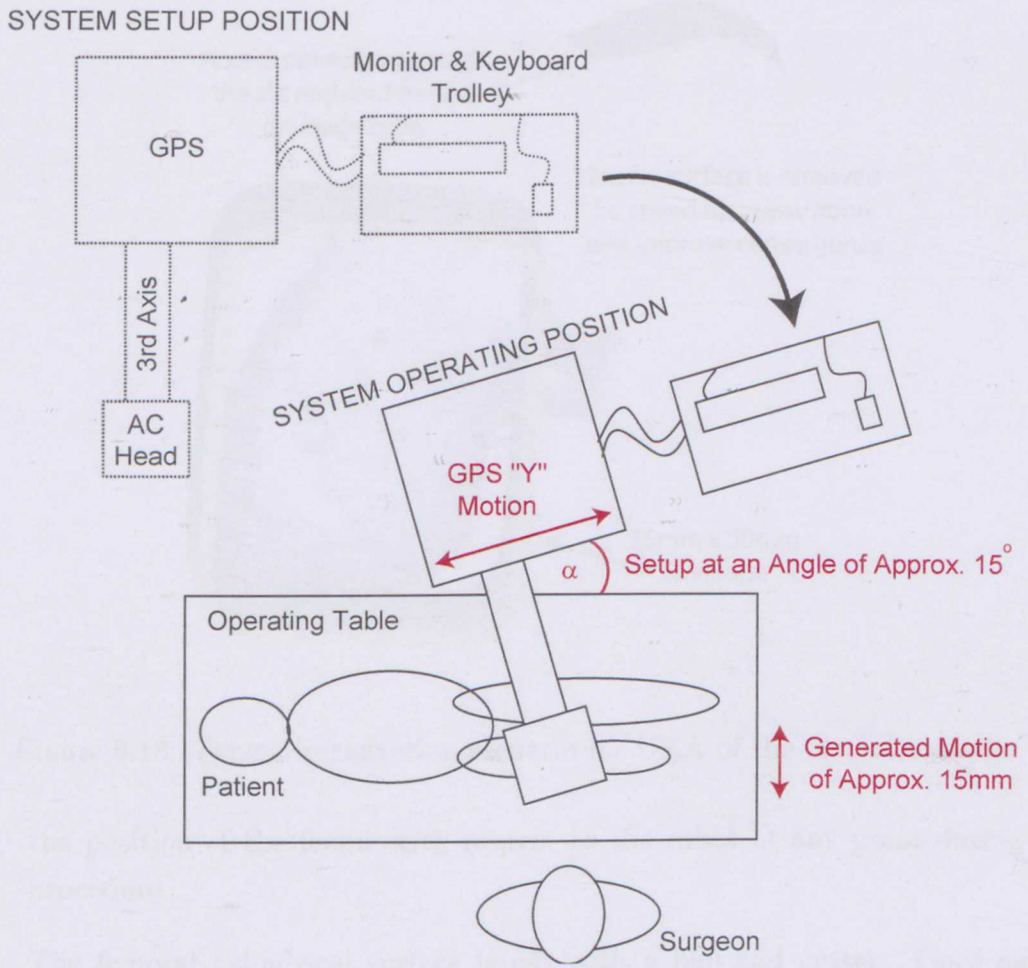


Figure 6.16: Using the GPS at an angle to gain a range of motion in the missing degree of freedom, towards and away from the table.

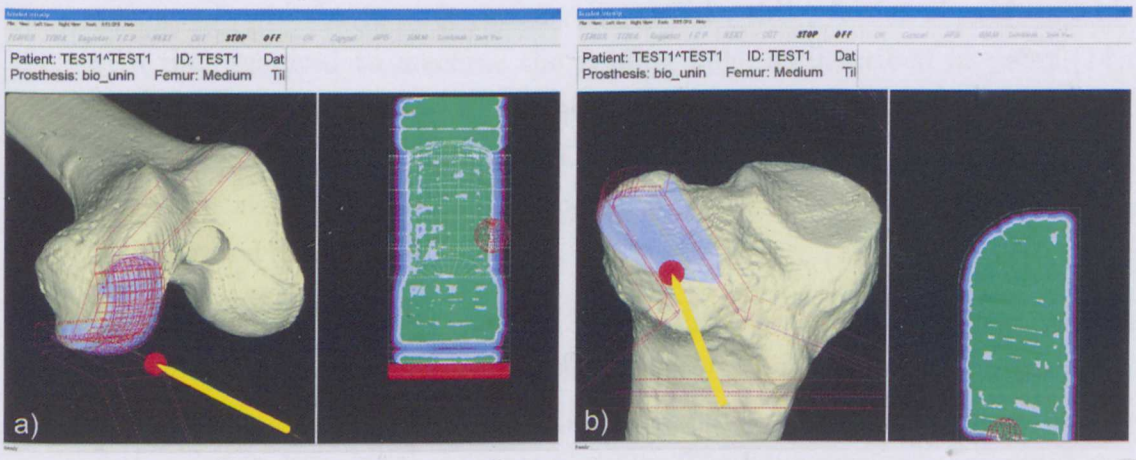


Figure 6.17: ACROBOT II System intra-operative visual feedback during cutting of the femur (a) and tibia (b).

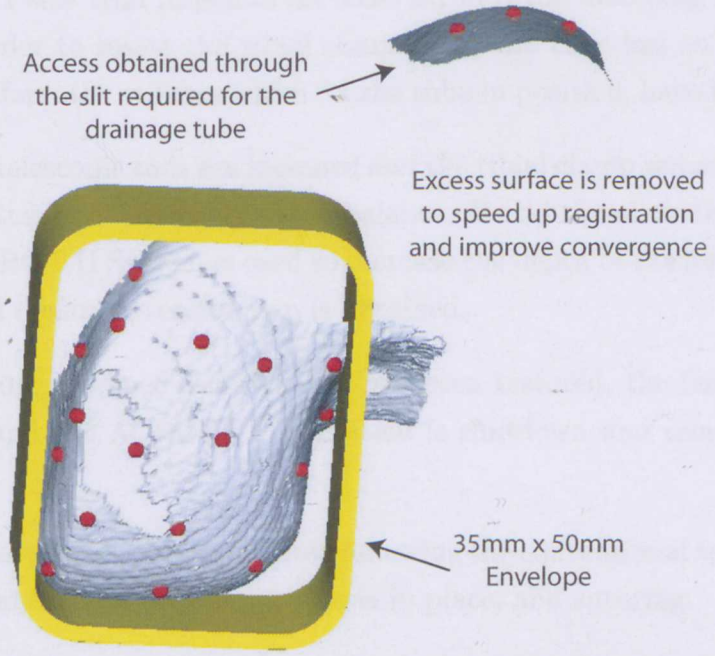


Figure 6.18: Typical registration scenario for UKA of the medial condyle.

the position of the femur with respect to the robot at any point during the procedure.

13. The femoral cylindrical surface is cut with a ball end cutter. Once again, during this process the assistant or registrar has to hold the tube in position, following the cutter tip movements to clear the area of any soft tissue. This operation should require a single motion of the GPS, which is carried out before cutting takes place in order to optimally position the AC Head centre with respect to the cutting surface. If possible, this position should coincide with that required to machine the guiding hole, as described in point (14). Correct placement would be obtained by moving a combination of GPS and AC Head joints so that the centre of the head lays on the axis of the hole. Any placement error would reduce the depth to which the hole can be machined, as illustrated in Figure 6.14.

14. The locating hole for the femur is machined. The depth of the cut will be affected by the position of the AC Head with respect to the knee, as described above. If the hole cannot be machined to the required depth, the knee can be unclamped and moved to a better position. The bone motion monitor (8) can be used to re-register the patient position with respect to the robot, once the clamps are tightened once again.

15. The correct size trial implants are inserted into the matching cavities. Note that, in order to insert the tibial component, the tube has to be rotated by 90°. Therefore, the stitches which fix the tube in position, have to be removed.

16. The tibial telescopic rods are loosened and the tibial clamp removed, to test the reconstructed knee joint soft tissue balance. If additional cutting is required, the ACROBOT II System is used to increase the depth of the femoral cut until the desired flexion-extension gap is obtained.

17. Once appropriate knee functionality has been restored, the femoral clamp is removed, and the ACROBOT II System is shutdown and removed from the theatre.

18. The surgical procedure is completed following the conventional technique. This includes cementing the final prosthesis in place, and suturing.

This protocol has been executed, and significantly fine tuned, on a large number of plastic bones, and has successfully been implemented, using a conventional $8cm$ incision due to the shortcomings of the tissue retaining tube (Section 6.2.2), on seven Ethics Committee approved clinical trials. Preliminary results on both protocol and accuracy have recently been presented in [Rodriguez y Baena et al., 2003; Henckel et al., 2003].

6.3 Anatomical Registration and MIS

Section 6.2 described the hardware and protocol changes carried out on the ACROBOT II System that were required to enable the robot to be used as a concept demonstrator for robotic assisted unicompartmental knee arthroplasty. This section provides an outline of the software and protocol modifications carried out on the registration procedure described in Chapter 5 to enable the algorithm to be used for minimal access knee surgery. As UKA, described in Section 1.2.2, results in a considerably smaller incision compared to TKA, access to the bone surface needed for registration is greatly reduced. A number of important anatomical features required to robustly identify the femoral and tibial surfaces are no longer available, which imposes tighter requirements on both the acquisition protocol and *point accuracy* (Section 5.3.4) for successful registration.

Changes to both software and protocol were carried out on the registration procedure developed for TKA, and results were validated through simulation and *in vitro* experimentation. The development of a new acquisition protocol (Section 6.3.1), and small enhancements to the intra-operative guidance (Section 6.3.2) are

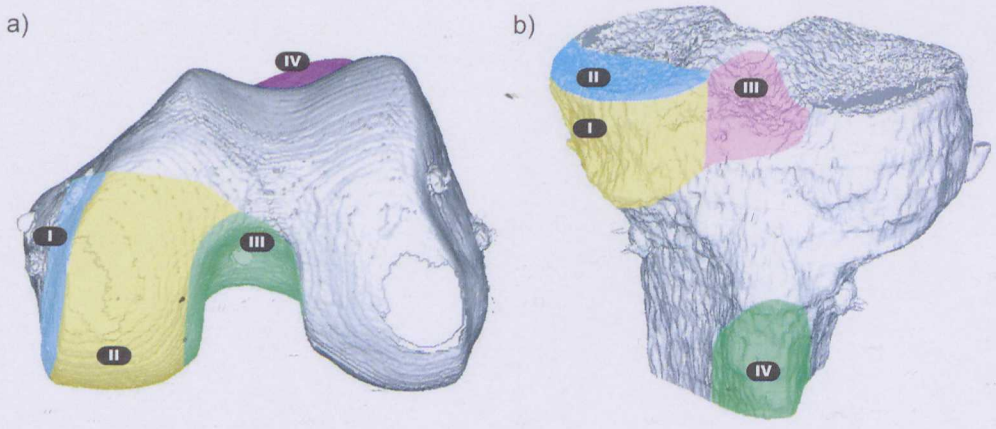


Figure 6.19: Registration regions for the femur (a) and tibia (b) suitable for UKA.

presented in the following sections, while results of the validation process, through simulation and plastic bone trials, are included in Section 6.3.3.

6.3.1 A Point Acquisition Protocol for UKA

During UKA, only small portions of both the distal femur and proximal tibia are accessible for registration through the conventional incision, which is approximately $8cm$ long (Figure 1.4). Early experimentation with the simulator (Section 5.4.2), which has been outlined in Section 6.3.3.1.2, showed that the extent of access on both surfaces provided by the conventional incision was not enough to bound all components of the registration matrix. For instance, simulation results for the femur highlighted that Anterior/Posterior (A/P) rotational alignment could not be adequately bound if the point-set did not include the frontal femur. Similarly, both A/P and axial rotational alignment cannot be robustly derived if the tibial tuberosity is not included in the tibial point-set. Intuitively, these results are to be expected, since, for instance, the tibial surface available for registration through the standard incision can be approximated to that of a "partial cylinder," therefore has no features which are useful for axial alignment.

As for the development of a protocol suitable for TKA, extensive experimentation with the simulator allowed a number of prototype point-sets to be analysed, which enabled key areas of interest on the registration surface to be identified. The regions of the knee joint anatomy needed for registration are graphically illustrated in Figure 6.19.

The first three regions (I-III) are accessible through the conventional incision, while the fourth one (region IV) can only be accessed through two stab wounds, one for the femur and one for the tibia. These additional incisions, which are graphically

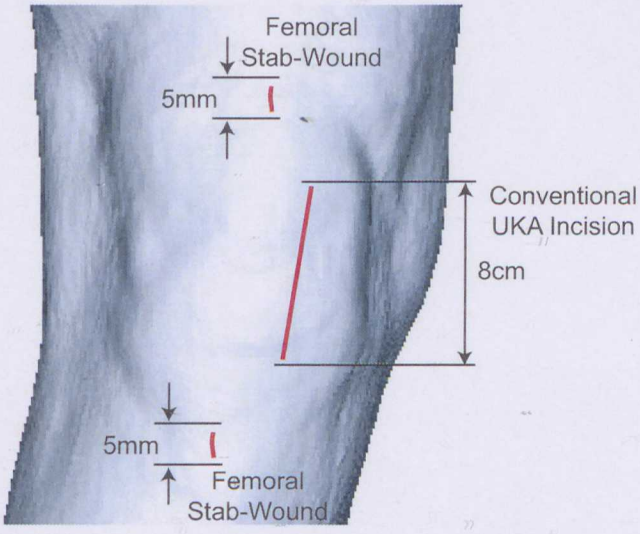


Figure 6.20: Approximate size and location of the two additional femoral and tibial stab-wounds, needed for registration.

Region	*Location*	*Component Identified*	% Total
I	Medial Side	Axial Rot, M/L Trans	20%
II	Medial Condyle	V/V Rot, P/D Trans	40%
III	Femoral Notch	Axial Rot	20%
(IV)	Frontal Femur	A/P Rot	20%

Table 6.2: Regions of interest for the femoral surface accessible during UKA.

illustrated in Figure 6.20, are approximately $5mm$ in length, and generally do not require suturing.

The regions illustrated in Figure 6.19 include significant features that are characteristic for the shape to be registered, and allow important components of the registration matrix to be robustly bounded. The regions of interest identified, alongside their impact on registration outcome, are summarised in Table 6.2 and Table 6.3 for the femur and tibia respectively. The tabular representation of the surfaces include the percentage of points to be collected in each region out of the total set size, which guarantees an even distribution of the points on the surface available for registration. Region IV is described in parenthesis to emphasise that it is only accessible through an additional skin incision.

As can be seen, A/P rotational alignment for the femur is only bounded by the inclusion of points through the stab-wound, since no other representative features of the surface are available through the conventional incision. Similarly, although some axial alignment can be obtained by harvesting points in the anterior intercondylar fossa, points collected on the tibial tuberosity are required for robust rotational alignment of the registered surface. As described in Section 6.3.2, accurately locating

Region	*Location*	*Component Identified*	% Total
I	Medial Side	Axial Rot, M/L Trans	20%
II	Medial Condyle	V/V Rot, P/D Trans	30%
III	Anterior Intercondylar Fossa	Axial Rot	30%
(IV)	Tibial Tuberosity	A/P & Axial Rot	20%

Table 6.3: Regions of interest for the tibial surface accessible during UKA.

the tibial tuberosity is an important element of the point acquisition process, and needs to be completed with care to ensure robust registration.

The size of the point-set needed to robustly identify the surface is proportional to the achievable point accuracy, and representative figures have been derived through simulation, as for the TKA registration process. The figures were obtained by analysing a large number of point-sets, assembled manually and automatically, for different environmental conditions. These results, presented in Table 5.7 and Table 5.8, can be used as guidelines to define the minimum number of points required to robustly identify a surface for a known degree of point accuracy. As described in Section 5.3.6, point accuracy can be predicted with some confidence during point collection by inspecting the RMS error and colour-coded display for a representative point-set.

The point acquisition protocol described above, which has been derived through simulation, and validated through plastic bone trials (Section 6.3.3.2), can be used to increase the probability of obtaining good registration. However, results described in Section 6.3.3 suggest that, because of the limited access resulting from a smaller incision, good point accuracy (i.e., better than $1mm$) is necessary for registration accuracy better than 2° and $2mm$. This degree of point accuracy can be expected for a good surface model and an appropriate intra-operative setup, but poses an important constraint on the requirements for a system suitable for robotic assisted UKA, if a registration method based on anatomical features is to be used.

6.3.2 Intra-Operative Guidance

Small enhancements to the visual feedback described in Section 5.3.5 were introduced in the intra-operative software, originally developed for TKA with the ACROBOT II System, to aid point collection using the protocol described in Section 6.3.1. To ensure an appropriate point-set is obtained, points have to be accurately assembled from all regions represented in Figure 6.19, including those that need to be collected through the stab-wounds on both tibia and femur. Therefore, during registration, points are gathered in regions I-III first, which allows the approximate position of the robot with respect to the knee joint to be established. The robot end effector

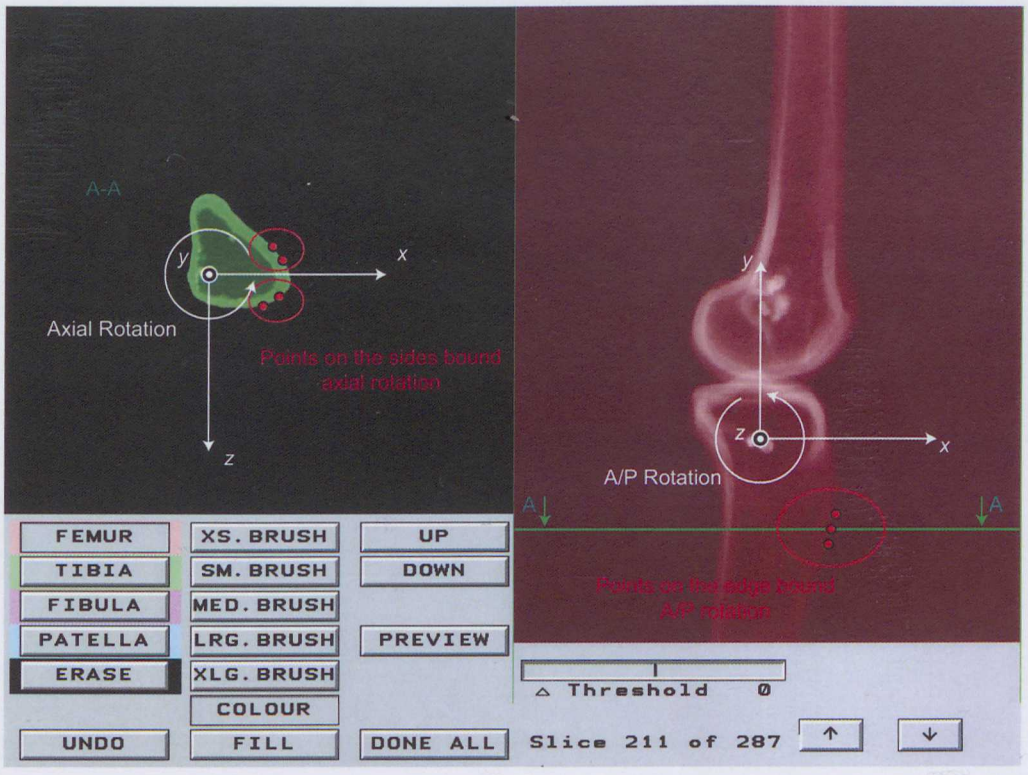


Figure 6.21: Relationship between the shape of the tibial tuberosity and rotational alignment, described using a snapshot of Acrobot's proprietary planning software.

can then be used as a pointer to locate the position of the stab-wounds. Once the virtual representation of the registration probe is positioned over the relevant region (i.e. region IV in Figure 6.19) on screen, an approximate location for the incision has been found. The robot can then be used to collect points on the frontal femur and tibial tuberosity.

Accurately locating the tibial tuberosity is the key to successful registration, as it is the single most characteristic feature of the tibial surface that is available for registration. As described in Section 6.3.1, without an appropriate representation of the tibial tuberosity, robust axial and A/P alignment cannot be derived. Although the number of points to be collected in region IV is proportional to the estimated point accuracy (Section 6.3.3.1.1), the position of the points on this specific feature is of particular importance. The shape of the tuberosity can be approximated to that of a prism, with a triangular cross-section in axial view. As described in Figure 6.21, points need to be collected on each one of the two "exposed" surfaces to ensure good axial alignment, while accurately locating the frontal edge is required for appropriate A/P rotational alignment.

To ensure this procedure is accurately followed during the point acquisition process, region IV in Figure 6.19 is split into three sub-regions, which are overlaid in

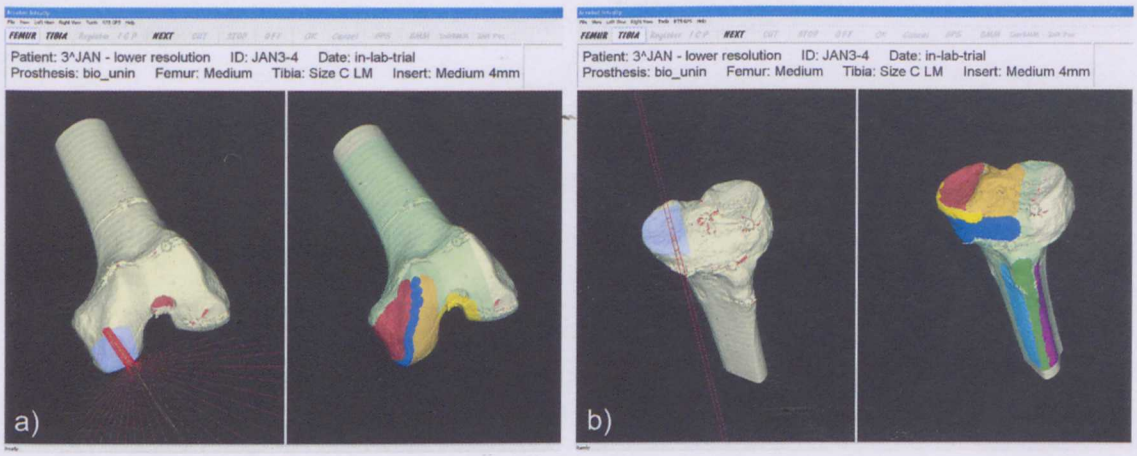


Figure 6.22: Colour-coded display of the tibia and femur, used to ensure appropriate point collection through the main incision, as well as the tibial and femoral stab-wounds.

different colours on the registration surface to ensure points are collected on either side of the "prism" as well as the edge. As illustrated in Figure 6.22, the three sub-regions cover the tibial tuberosity, as well as a large percentage of the distal tibia. In fact, if access to the tuberosity is restricted, the stab-wound can be performed more distally, without affecting the quality of the point-set. As the "quasi-triangular" cross section is maintained throughout the majority of the distal tibia, and is a characteristic feature of general human anatomy, the bounding effect of points harvested through the tibial stab-wound (Figure 6.21) is maintained regardless of the proximal/distal placement of the cut. Similarly, the optimal proximal/distal position of the stab-wound on the anterior femur can be chosen intra-operatively, as a function of the current setup, and can be made to coincide with the small incision used to place the drainage tube generally needed for post-operative treatment. The medial edge of the femoral condyle is highlighted in a different colour to ensure points are collected on either side as well as on the edge itself.

6.3.3 Protocol Validation

Validation of the enhanced ICP algorithm implementation, including speed of execution and suppression mechanisms, is the same for TKA and UKA, and has been described in Section 5.4.2.5. However, in order to ensure the protocol defined in Section 6.3.1 for robotic assisted UKA with the ACROBOT II System is an appropriate means for robust registration, the same validation process carried out on the protocol defined for TKA (Section 5.4.2.5) has been replicated for the new technique. Experiments aimed at ascertaining the link between point-set size and distribution, and point accuracy have been carried out to derive a set of guidelines describing

expected registration accuracy for a specific intra-operative scenario.

6.3.3.1 Simulation Tests and Results

As for validation of the TKA intra-operative protocol, the simulator was used to assess the performance of manually chosen characteristic point-sets of different sizes (Section 6.3.3.1.1) as well as a large number of random point-sets (Section 6.3.3.1.2), assembled automatically in the regions defined in Figure 6.19, using the procedure outlined in Section 5.4.2.4. Simulated results have been corroborated with a set of plastic bone trials, which are presented in Section 6.3.3.2. To aid interpretation of the data, all results are presented in the $\{BONE\}$ frame of reference, as illustrated in Figure 5.11, for both the tibia and the femur.

Typical femoral and tibial surfaces generated from a CT scanned plastic phantom have been used for descriptive purposes. A complete set of results for patient generated surfaces, which were tested using the same method described in the following sections, can be found in Appendix D.

6.3.3.1.1 Point-Set Size and Registration Accuracy This experiment was carried out using the same technique described in Section 5.4.2.5.3 for the validation of the TKA registration procedure, but following the protocol described in Section 6.3.1 for UKA. Examples of manually assembled 15 and 35 points point-sets for the femur and tibia are illustrated in Figure 6.23. The layout of the points in each set is based on experience obtained on the simulator, and exemplifies a "best-case-scenario," founded on the region-based protocol, for a particular surface.

Once again, a guideline for the expected performance of the acquisition protocol for different amounts of point-accuracy can be derived by evaluating the robustness of these manually assembled point-sets, as each point-set represents a "desirable outcome" for the region-based procedure for a specific surface and point-set size. 100 perturbations for 10 robust point-sets for each different set size were carried out, and average, maximum, and minimum registration errors for the resulting modified point-sets were recorded. These values are reported in Table 6.4 and Table 6.5 for the femur and tibia respectively.

The registration error is expressed in component form, in terms of overall rotational (in axis/angle notation) and translational (Equation 5.8) errors. The results, expressed in tabular form, illustrate the probability that the point-set will fall within a maximum error value, which is defined in terms of 1 standard deviation (75%) and 2 standard deviations (95%) from the mean.

As can be seen, these results differ quite considerably from those obtained for the TKA protocol, as, for instance, at least 75 points per set are required to have a 95%

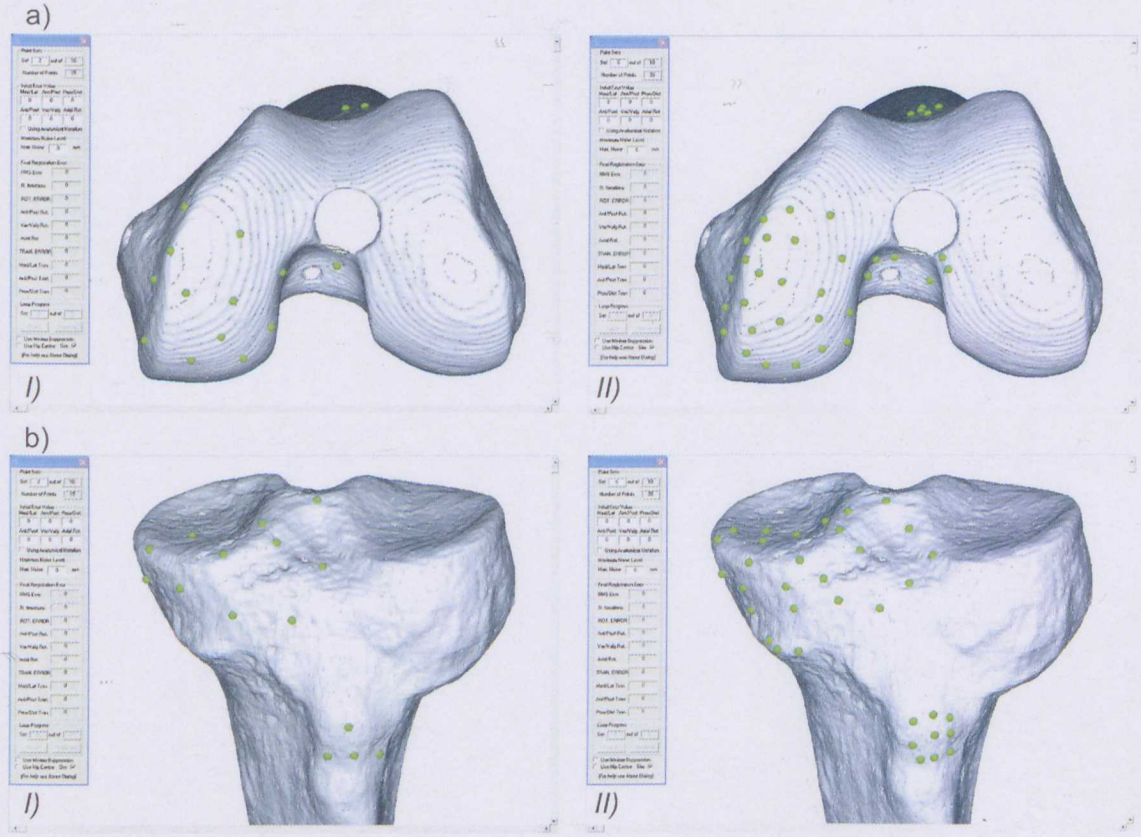


Figure 6.23: Ideal point distribution for both femur (a) and tibia (b), for 15 (I) and 35 (II) points per set.

	Performance of Robust Point-Sets of Different Sizes for 0.5mm Maximum Noise						
	Point-Set Size	**Average Err**	**Max Error**	**Min Error**	**STD**	**95% of Pop**	**75% of Pop**
Rotational Error (deg)	*10*	2.00	6.34	0.12	1.17	4.33	3.16
	15	0.96	2.21	0.16	0.44	1.84	1.40
	20	0.85	1.96	0.05	0.40	1.66	1.25
	25	0.67	1.52	0.15	0.32	1.30	0.98
	30	0.63	1.81	0.03	0.33	1.29	0.96
	35	0.58	1.43	0.14	0.27	1.11	0.84
	40	0.56	1.87	0.07	0.31	1.17	0.87
	50	0.47	1.15	0.11	0.23	0.92	0.70
	75	0.43	0.97	0.08	0.22	0.87	0.65
	100	0.41	0.95	0.06	0.19	0.78	0.60
Translational Error (mm)	*10*	1.06	3.55	0.08	0.66	2.37	1.72
	15	0.53	1.35	0.10	0.27	1.07	0.80
	20	0.46	1.29	0.06	0.26	0.99	0.73
	25	0.34	0.98	0.08	0.18	0.70	0.52
	30	0.29	0.82	0.07	0.15	0.59	0.44
	35	0.31	0.86	0.07	0.17	0.65	0.48
	40	0.26	0.91	0.02	0.16	0.58	0.42
	50	0.25	0.62	0.03	0.14	0.52	0.39
	75	0.21	0.51	0.03	0.13	0.46	0.33
	100	0.22	0.49	0.01	0.11	0.43	0.33

	Performance of Robust Point-Sets of Different Sizes for 1.0mm Maximum Noise						
	Point-Set Size	**Average Err**	**Max Error**	**Min Error**	**STD**	**95% of Pop**	**75% of Pop**
Rotational Error (deg)	*10*	3.81	18.70	0.45	2.55	8.92	6.37
	15	2.24	7.08	0.28	1.16	4.57	3.40
	20	1.89	4.55	0.46	0.91	3.70	2.80
	25	1.42	3.79	0.34	0.75	2.91	2.16
	30	1.24	2.80	0.10	0.55	2.34	1.79
	35	1.18	2.63	0.29	0.58	2.33	1.76
	40	1.34	3.58	0.19	0.65	2.64	1.99
	50	1.06	2.48	0.12	0.52	2.10	1.58
	75	0.94	2.11	0.18	0.41	1.75	1.35
	100	0.85	2.22	0.20	0.40	1.64	1.24
Translational Error (mm)	*10*	2.04	11.16	0.22	1.58	5.21	3.62
	15	1.12	3.88	0.07	0.75	2.63	1.88
	20	0.97	2.51	0.17	0.50	1.97	1.47
	25	0.63	1.63	0.12	0.30	1.23	0.93
	30	0.59	1.62	0.07	0.30	1.19	0.89
	35	0.60	1.58	0.18	0.31	1.22	0.91
	40	0.53	1.42	0.12	0.30	1.12	0.83
	50	0.48	1.35	0.08	0.25	0.99	0.73
	75	0.43	1.27	0.04	0.22	0.87	0.65
	100	0.38	1.18	0.06	0.22	0.82	0.60

Table 6.4: Relationship between point-set size and registration robustness, expressed in terms of overall rotational and translational accuracy, for a set of robust point-sets describing a distal femur.

	Performance of Robust Point-Sets of Different Sizes for 1.5mm Maximum Noise					
Point-Set Size	**Average Err**	**Max Error**	**Min Error**	**STD**	**95% of Pop**	**75% of Pop**
Rotational Error (deg)						
10	5.46	23.80	0.37	3.97	13.40	9.43
15	3.31	7.85	0.85	1.49	6.30	4.81
20	2.74	8.34	0.33	1.52	5.78	4.26
25	2.13	4.44	0.20	0.93	3.98	3.05
30	1.92	5.71	0.47	0.98	3.87	2.90
35	1.82	4.07	0.42	0.86	3.55	2.68
40	1.87	4.91	0.56	0.96	3.79	2.83
50	1.62	4.80	0.23	0.83	3.27	2.45
75	1.43	3.44	0.30	0.70	2.83	2.13
100	1.27	3.02	0.20	0.59	2.45	1.86
Translational Error (mm)						
10	2.94	13.94	0.39	2.28	7.49	5.21
15	1.61	5.16	0.21	0.95	3.51	2.56
20	1.39	4.42	0.21	0.87	3.13	2.26
25	1.03	2.52	0.18	0.53	2.10	1.57
30	0.87	1.85	0.13	0.40	1.67	1.27
35	0.89	1.93	0.19	0.43	1.74	1.32
40	0.81	2.09	0.19	0.42	1.65	1.23
50	0.74	2.33	0.07	0.44	1.61	1.18
75	0.68	1.79	0.06	0.39	1.45	1.06
100	0.58	1.52	0.12	0.31	1.19	0.88

	Performance of Robust Point-Sets of Different Sizes for 2.0mm Maximum Noise					
Point-Set Size	**Average Err**	**Max Error**	**Min Error**	**STD**	**95% of Pop**	**75% of Pop**
Rotational Error (deg)						
10	7.76	22.88	0.78	5.00	17.76	12.76
15	4.74	14.75	1.52	2.51	9.76	7.25
20	4.21	14.01	0.73	2.33	8.87	6.54
25	2.80	7.12	0.36	1.44	5.68	4.24
30	2.73	7.64	0.37	1.50	5.73	4.23
35	2.47	6.67	0.52	1.33	5.12	3.80
40	2.55	12.47	0.12	1.72	5.98	4.26
50	2.29	7.72	0.36	1.37	5.03	3.66
75	1.87	4.82	0.29	0.90	3.66	2.76
100	1.79	4.83	0.30	0.89	3.57	2.68
Translational Error (mm)						
10	4.28	12.55	0.44	2.79	9.85	7.06
15	2.19	6.52	0.53	1.39	4.97	3.58
20	2.17	7.64	0.24	1.21	4.60	3.39
25	1.38	4.75	0.12	0.85	3.07	2.22
30	1.22	3.95	0.22	0.64	2.50	1.86
35	1.24	4.55	0.28	0.69	2.63	1.93
40	1.15	5.00	0.04	0.83	2.80	1.97
50	1.10	4.40	0.24	0.64	2.38	1.74
75	0.90	2.32	0.10	0.49	1.88	1.39
100	0.83	2.48	0.06	0.47	1.77	1.30

Table 6.4: (cont'd) Relationship between point-set size and registration robustness, expressed in terms of overall rotational and translational accuracy, for a set of robust point-sets describing a distal femur.

	Performance of Robust Point-Sets of Different Sizes for 0.5mm Maximum Noise						
	Point-Set Size	**Average Err**	**Max Error**	**Min Error**	**STD**	**95% of Pop**	**75% of Pop**
Rotational Error (deg)	*10*	2.09	26.46	0.48	2.73	7.55	4.82
	15	1.11	3.33	0.11	0.56	2.22	1.67
	20	1.15	7.70	0.07	1.23	3.62	2.39
	25	0.76	1.95	0.13	0.37	1.49	1.12
	30	0.91	25.07	0.12	2.46	5.83	3.37
	35	0.59	1.81	0.05	0.29	1.18	0.88
	40	0.57	1.45	0.09	0.30	1.17	0.87
	50	0.53	1.15	0.07	0.24	1.00	0.76
	75	0.40	1.29	0.06	0.20	0.80	0.60
	100	0.36	0.79	0.03	0.17	0.69	0.52
Translational Error (mm)	*10*	0.50	6.26	0.09	0.67	1.84	1.17
	15	0.35	0.84	0.06	0.16	0.67	0.51
	20	0.34	1.76	0.03	0.27	0.88	0.61
	25	0.27	0.62	0.06	0.12	0.51	0.39
	30	0.30	7.19	0.03	0.70	1.71	1.01
	35	0.20	0.53	0.04	0.09	0.39	0.29
	40	0.20	0.56	0.03	0.11	0.42	0.31
	50	0.17	0.31	0.05	0.06	0.29	0.23
	75	0.16	0.37	0.01	0.08	0.32	0.24
	100	0.15	0.34	0.03	0.07	0.29	0.22

	Performance of Robust Point-Sets of Different Sizes for 1.0mm Maximum Noise						
	Point-Set Size	**Average Err**	**Max Error**	**Min Error**	**STD**	**95% of Pop**	**75% of Pop**
Rotational Error (deg)	*10*	4.06	39.04	0.54	4.02	12.11	8.09
	15	2.92	45.53	0.24	4.49	11.90	7.41
	20	1.82	7.18	0.39	1.07	3.97	2.90
	25	1.59	4.68	0.43	0.81	3.21	2.40
	30	1.37	3.57	0.08	0.60	2.57	1.97
	35	1.33	3.18	0.26	0.59	2.52	1.93
	40	1.30	2.99	0.29	0.65	2.61	1.96
	50	1.04	2.35	0.15	0.50	2.04	1.54
	75	0.90	1.99	0.29	0.34	1.59	1.24
	100	0.72	1.57	0.06	0.32	1.35	1.04
Translational Error (mm)	*10*	1.02	8.97	0.15	0.96	2.93	1.97
	15	0.81	9.32	0.20	0.93	2.66	1.73
	20	0.58	1.86	0.10	0.28	1.14	0.86
	25	0.53	1.36	0.13	0.26	1.05	0.79
	30	0.41	0.91	0.09	0.18	0.77	0.59
	35	0.46	1.05	0.06	0.22	0.89	0.68
	40	0.46	1.30	0.06	0.25	0.96	0.71
	50	0.37	0.81	0.05	0.17	0.72	0.55
	75	0.32	0.73	0.05	0.14	0.60	0.46
	100	0.26	0.61	0.07	0.10	0.46	0.36

Table 6.5: Relationship between point-set size and registration robustness, expressed in terms of overall rotational and translational accuracy, for a set of robust point-sets describing a proximal tibia.

	Performance of Robust Point-Sets of Different Sizes for 1.5mm Maximum Noise						
	Point-Set Size	**Average Err**	**Max Error**	**Min Error**	**STD**	**95% of Pop**	**75% of Pop**
Rotational Error (deg)	*10*	4.73	38.53	0.66	4.03	12.78	8.76
	15	4.48	22.26	0.48	3.34	11.16	7.82
	20	3.32	9.36	0.24	1.70	6.72	5.02
	25	2.45	6.68	0.22	1.27	4.98	3.72
	30	2.41	18.81	0.23	1.95	6.31	4.36
	35	1.88	5.55	0.29	0.98	3.84	2.86
	40	1.92	4.69	0.47	0.97	3.87	2.90
	50	1.87	4.87	0.08	0.95	3.76	2.82
	75	1.32	3.42	0.35	0.57	2.47	1.90
	100	1.14	3.07	0.19	0.52	2.19	1.66
Translational Error (mm)	*10*	1.30	8.93	0.31	0.95	3.19	2.24
	15	1.31	5.19	0.11	0.82	2.95	2.13
	20	0.90	2.30	0.17	0.44	1.77	1.33
	25	0.78	2.08	0.21	0.36	1.49	1.14
	30	0.78	5.73	0.02	0.58	1.95	1.36
	35	0.63	1.96	0.08	0.31	1.25	0.94
	40	0.66	1.69	0.13	0.35	1.36	1.01
	50	0.58	1.74	0.09	0.29	1.16	0.87
	75	0.47	0.99	0.13	0.20	0.87	0.67
	100	0.39	0.91	0.09	0.18	0.76	0.58

	Performance of Robust Point-Sets of Different Sizes for 2.0mm Maximum Noise						
	Point-Set Size	**Average Err**	**Max Error**	**Min Error**	**STD**	**95% of Pop**	**75% of Pop**
Rotational Error (deg)	*10*	7.45	37.72	0.87	4.75	16.94	12.19
	15	6.26	40.97	1.40	5.52	17.29	11.78
	20	4.22	12.34	0.40	2.32	8.86	6.54
	25	3.38	11.97	0.97	1.85	7.07	5.23
	30	3.18	12.45	0.73	1.81	6.79	4.98
	35	2.79	7.53	0.36	1.47	5.74	4.26
	40	2.86	8.63	0.31	1.66	6.17	4.52
	50	2.56	6.06	0.48	1.32	5.19	3.87
	75	1.99	4.27	0.44	0.83	3.65	2.82
	100	1.42	3.56	0.30	0.69	2.79	2.10
Translational Error (mm)	*10*	1.97	8.32	0.07	1.19	4.35	3.16
	15	1.73	10.61	0.21	1.33	4.39	3.06
	20	1.31	2.87	0.32	0.55	2.41	1.86
	25	1.21	3.32	0.28	0.56	2.32	1.76
	30	1.02	2.30	0.11	0.51	2.04	1.53
	35	0.89	2.39	0.15	0.46	1.80	1.34
	40	0.93	2.85	0.12	0.51	1.95	1.44
	50	0.85	2.24	0.18	0.45	1.74	1.30
	75	0.69	1.37	0.18	0.28	1.24	0.97
	100	0.53	1.23	0.10	0.24	1.02	0.78

Table 6.5: (cont'd) Relationship between point-set size and registration robustness, expressed in terms of overall rotational and translational accuracy, for a set of robust point-sets describing a proximal tibia.

chance that the registration error falls within the required $\pm 2^o$ and $\pm 2mm$ threshold for point accuracy of $1mm$. For $1.5mm$ maximum error, at least 100 points would be required to have a 75% chance to obtain rotational alignment within $\pm 2^o$ for the femur. For point accuracy worse than $1mm$, it is no longer possible to robustly (95% probability) register the tibia or the femur using the available surface.

These results are to be expected, as only a small portion of the surface available during TKA is accessible through the conventional UKA incision. Key features, such as the femoral notch and tibial tuberosity, need to be accurately located in order for a point-set to provide a robust representation of the surface. Furthermore, the registration surfaces of both the femur and tibia are no longer symmetric, as only the medial condyle are accessible. Therefore, any inaccuracies during point-collection cannot be "mitigated" by points touched on the opposite side.

6.3.3.1.2 Performance Evaluation Once again, the same procedure described in Section 5.4.2.5.4 for the validation of the TKA protocol was replicated using randomly generated sets assembled using the UKA point acquisition protocol described in Section 6.3.1. Figure 6.24 and Figure 6.25 illustrate results for the average rotational error, in terms of leg alignment components (Section 5.4.1), and overall translational error for different point-set sizes and maximum noise values.

As the point-sets, as well as the noise values, were randomly selected, the mean can be used as an indicator for the average performance of the point acquisition protocol for a reasonable point-set and a reasonable error distribution. The average registration accuracy obtained for the femur and the tibia shows that appropriate registration is possible for all degrees of point accuracy considered. The three rotational components of the error matrix, as well as the translational error have shown to be within 2° and $2mm$ on average for point set sizes greater than 50. For smaller set sizes, however, the charts in Figure 6.24 and Figure 6.25 show a clear degradation of the solution, which could also be attributed to point-sets where the global minimum has not been correctly identified.

The spread of the results for each point-set size, which was shown to have a normal distribution (as described in Section 5.4.2.5.3), was used to derive a set of statistical values that can be used to assess the extent of the error that can be tolerated during the guided point-collection process. Average, maximum, and minimum registration errors obtained for each point-set size, sorted by maximum random noise applied, are reported in Table 6.6 and Table 6.7 for the femur and tibia respectively.

As can be seen, these results show very similar characteristics to the ones presented in Table 6.4 and Table 6.5, although, generally, more points are required to achieve similar registration accuracy for the same maximum noise value. Once

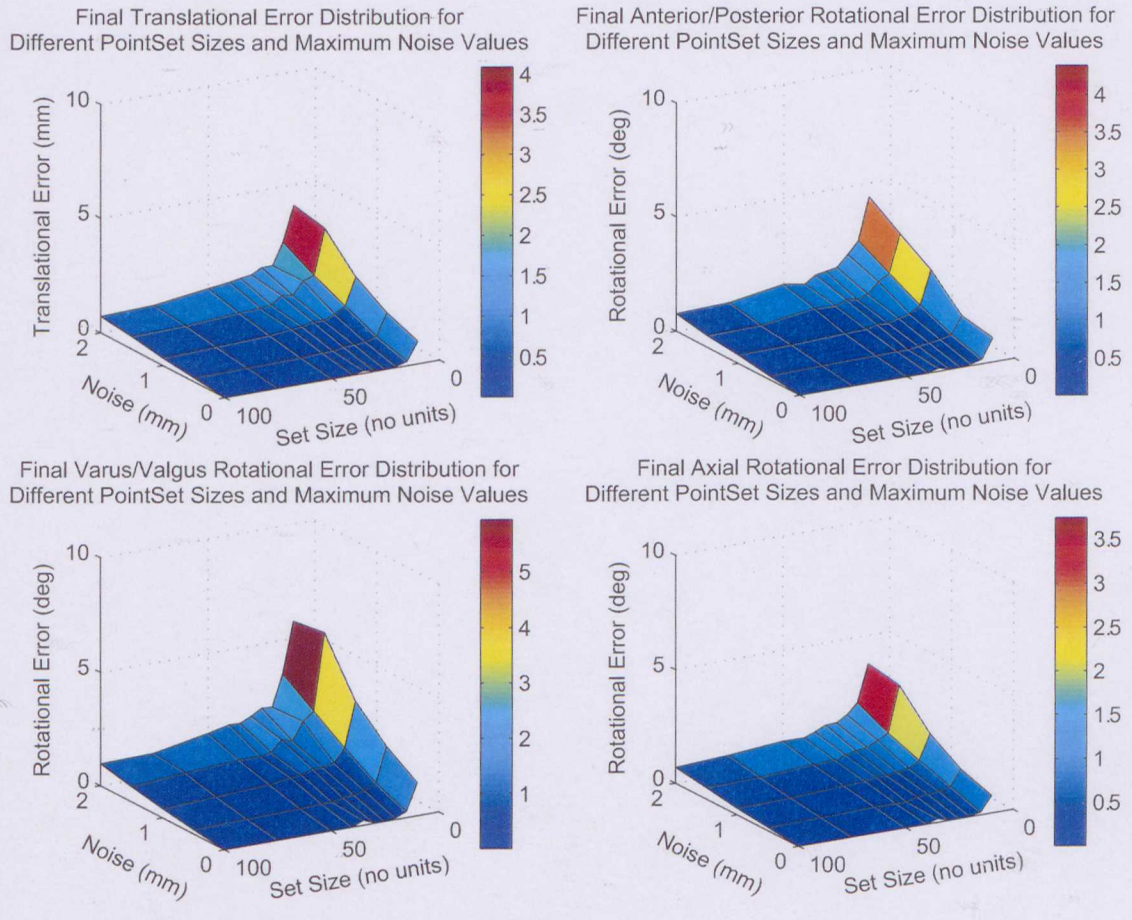


Figure 6.24: Registration accuracy for the enhanced ICP algorithm in terms of varus/valgus, anterior/posterior, axial, and translational components for different point-set sizes and maximum noise values, for the femur.

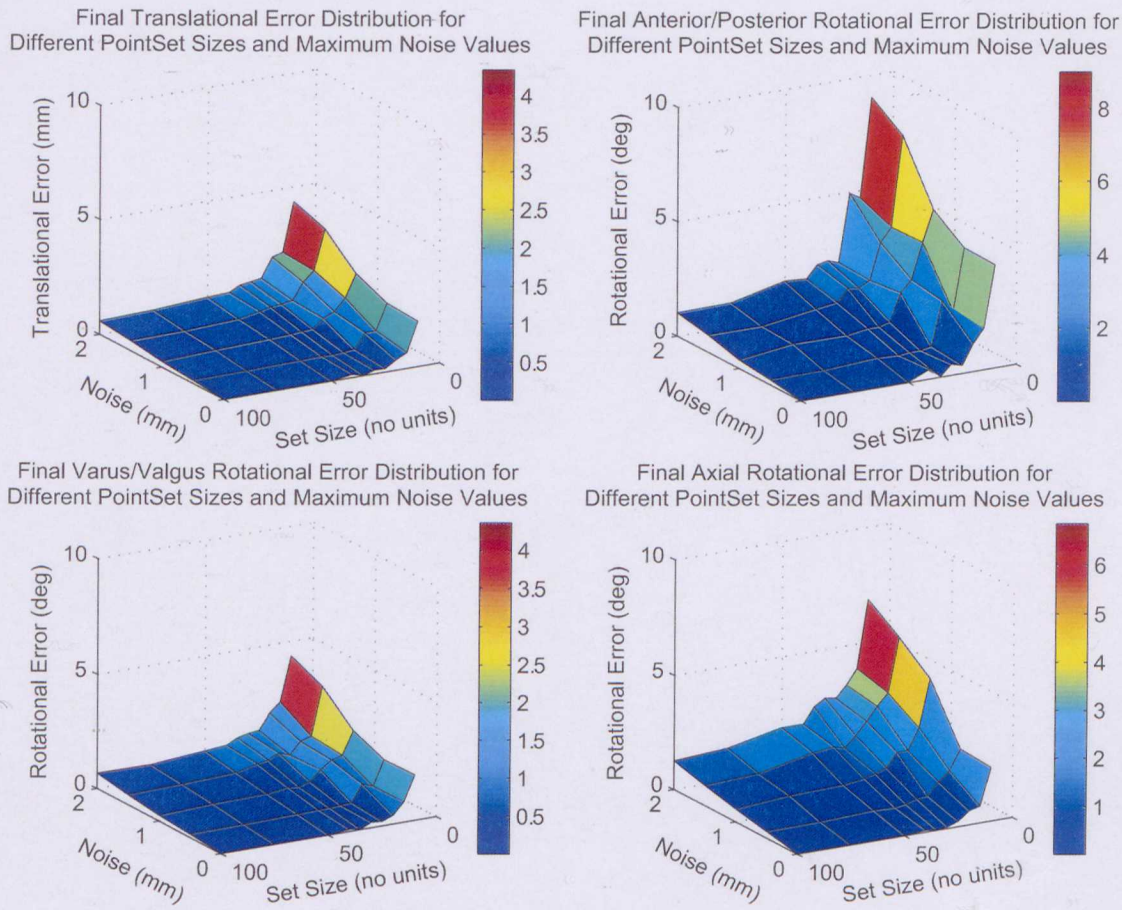


Figure 6.25: Registration accuracy for the enhanced ICP algorithm in terms of varus/valgus, anterior/posterior, axial, and translational components for different point-set sizes and maximum noise values, for the tibia.

	Performance of Random Point-Sets of Different Sizes for 0.5mm Maximum Noise					
	Point-Set Size	**Average Err**	**Max Error**	**Min Error**	**STD**	**95% of Pop**	**75% of Pop**
Rotational Error (deg)	*10*	2.16	13.98	0.38	2.14	6.44	4.30
	15	1.11	5.71	0.15	0.72	2.55	1.83
	20	0.95	7.28	0.11	0.81	2.58	1.77
	25	0.83	1.93	0.21	0.38	1.58	1.21
	30	0.73	1.98	0.11	0.38	1.48	1.11
	35	0.52	1.17	0.06	0.25	1.03	0.78
	40	0.54	1.65	0.11	0.29	1.11	0.82
	50	0.48	1.27	0.06	0.25	0.98	0.73
	75	0.42	1.09	0.04	0.22	0.85	0.63
	100	0.32	0.96	0.02	0.17	0.66	0.49
Translational Error (mm)	*10*	1.05	4.98	0.02	1.03	3.12	2.08
	15	0.50	2.08	0.06	0.37	1.24	0.87
	20	0.42	2.95	0.07	0.36	1.15	0.79
	25	0.38	1.47	0.06	0.25	0.88	0.63
	30	0.36	1.23	0.01	0.22	0.81	0.58
	35	0.28	0.79	0.06	0.15	0.58	0.43
	40	0.28	0.94	0.07	0.15	0.58	0.43
	50	0.23	0.62	0.03	0.14	0.50	0.36
	75	0.20	0.64	0.03	0.12	0.44	0.32
	100	0.16	0.43	0.03	0.09	0.34	0.25

	Performance of Random Point-Sets of Different Sizes for 1.0mm Maximum Noise					
	Point-Set Size	**Average Err**	**Max Error**	**Min Error**	**STD**	**95% of Pop**	**75% of Pop**
Rotational Error (deg)	*10*	3.50	14.22	0.41	2.41	8.33	5.92
	15	2.19	8.10	0.48	1.33	4.85	3.52
	20	1.77	5.05	0.29	0.86	3.48	2.63
	25	1.55	3.74	0.27	0.76	3.08	2.31
	30	1.49	4.12	0.15	0.83	3.14	2.31
	35	1.34	4.67	0.35	0.72	2.78	2.06
	40	1.20	2.78	0.31	0.54	2.28	1.74
	50	1.05	2.50	0.05	0.48	2.01	1.53
	75	0.84	2.12	0.13	0.40	1.65	1.25
	100	0.72	1.47	0.22	0.30	1.32	1.02
Translational Error (mm)	*10*	1.70	6.69	0.32	1.25	4.19	2.95
	15	1.09	3.61	0.11	0.77	2.64	1.87
	20	0.93	3.41	0.15	0.55	2.03	1.48
	25	0.74	1.86	0.04	0.42	1.58	1.16
	30	0.75	3.10	0.11	0.59	1.94	1.35
	35	0.63	2.22	0.04	0.38	1.40	1.02
	40	0.60	1.92	0.03	0.36	1.32	0.96
	50	0.49	1.52	0.05	0.27	1.03	0.76
	75	0.41	1.24	0.03	0.25	0.90	0.66
	100	0.33	0.84	0.04	0.16	0.65	0.49

Table 6.6: Relationship between point-set size and registration robustness, expressed in terms of overall rotational and translational accuracy, for a set of robust point-sets describing a distal femur.

	Performance of Random Point-Sets of Different Sizes for 1.5mm Maximum Noise						
	Point-Set Size	**Average Err**	**Max Error**	**Min Error**	**STD**	**95% of Pop**	**75% of Pop**
Rotational Error (deg)	*10*	6.04	19.04	0.49	3.99	14.01	10.03
	15	3.51	16.41	0.31	2.07	7.65	5.58
	20	3.18	8.98	0.51	1.92	7.03	5.11
	25	2.35	6.01	0.50	1.12	4.58	3.46
	30	2.34	6.70	0.34	1.20	4.75	3.55
	35	1.95	4.97	0.38	0.83	3.60	2.77
	40	1.69	4.88	0.40	0.80	3.29	2.49
	50	1.71	3.98	0.27	0.83	3.37	2.54
	75	1.28	2.97	0.08	0.64	2.56	1.92
	100	1.12	2.94	0.19	0.54	2.21	1.66
Translational Error (mm)	*10*	3.06	13.00	0.33	2.40	7.86	5.46
	15	1.68	9.25	0.27	1.18	4.04	2.86
	20	1.61	6.00	0.24	1.08	3.77	2.69
	25	1.11	4.18	0.06	0.63	2.37	1.74
	30	1.19	3.86	0.18	0.74	2.66	1.93
	35	0.87	2.55	0.13	0.50	1.87	1.37
	40	0.80	2.69	0.12	0.52	1.84	1.32
	50	0.76	2.79	0.09	0.46	1.69	1.22
	75	0.62	1.46	0.04	0.32	1.27	0.94
	100	0.55	1.63	0.16	0.30	1.15	0.85

	Performance of Random Point-Sets of Different Sizes for 2.0mm Maximum Noise						
	Point-Set Size	**Average Err**	**Max Error**	**Min Error**	**STD**	**95% of Pop**	**75% of Pop**
Rotational Error (deg)	*10*	7.46	18.80	1.00	4.05	15.55	11.51
	15	5.43	16.85	0.82	3.15	11.74	8.58
	20	3.82	16.25	0.65	2.23	8.28	6.05
	25	3.38	10.64	0.61	1.71	6.80	5.09
	30	3.03	8.47	0.68	1.41	5.85	4.44
	35	2.76	8.48	0.36	1.43	5.62	4.19
	40	2.51	5.70	0.44	1.17	4.85	3.68
	50	2.43	5.09	0.69	0.96	4.34	3.39
	75	1.74	4.00	0.37	0.89	3.51	2.62
	100	1.61	4.86	0.15	0.85	3.31	2.46
Translational Error (mm)	*10*	3.46	10.73	0.38	2.25	7.97	5.71
	15	2.58	9.75	0.10	1.76	6.10	4.34
	20	1.64	7.13	0.31	1.14	3.92	2.78
	25	1.64	4.99	0.16	1.00	3.64	2.64
	30	1.40	4.14	0.16	0.81	3.01	2.21
	35	1.33	4.95	0.31	0.81	2.94	2.14
	40	1.24	3.40	0.20	0.77	2.78	2.01
	50	1.12	2.63	0.20	0.58	2.28	1.70
	75	0.81	2.43	0.12	0.49	1.80	1.30
	100	0.73	2.49	0.07	0.46	1.65	1.19

Table 6.6: (cont'd) Relationship between point-set size and registration robustness, expressed in terms of overall rotational and translational accuracy, for a set of robust point-sets describing a distal femur.

	Performance of Random Point-Sets of Different Sizes for 0.5mm Maximum Noise					
	Point-Set Size	**Average Err**	**Max Error**	**Min Error**	**STD**	**95% of Pop**	**75% of Pop**
Rotational Error (deg)	*10*	2.68	18.23	0.19	3.00	8.68	5.68
	15	1.39	5.81	0.37	1.01	3.41	2.40
	20	1.14	3.34	0.14	0.55	2.24	1.69
	25	0.94	2.26	0.14	0.47	1.87	1.41
	30	0.85	2.33	0.17	0.42	1.70	1.27
	35	0.73	1.67	0.16	0.35	1.43	1.08
	40	0.63	1.56	0.11	0.30	1.23	0.93
	50	0.67	2.17	0.12	0.36	1.38	1.02
	75	0.48	0.99	0.05	0.21	0.89	0.68
	100	0.43	1.26	0.04	0.22	0.86	0.64
Translational Error (mm)	*10*	0.82	4.64	0.02	0.88	2.58	1.70
	15	0.44	1.65	0.08	0.29	1.01	0.72
	20	0.36	1.07	0.04	0.19	0.73	0.55
	25	0.28	0.77	0.01	0.15	0.59	0.43
	30	0.24	0.62	0.06	0.10	0.45	0.35
	35	0.21	0.54	0.03	0.10	0.41	0.31
	40	0.22	0.55	0.04	0.10	0.42	0.32
	50	0.20	0.43	0.03	0.09	0.39	0.30
	75	0.15	0.39	0.02	0.07	0.28	0.22
	100	0.14	0.31	0.02	0.07	0.27	0.20

	Performance of Random Point-Sets of Different Sizes for 1.0mm Maximum Noise					
	Point-Set Size	**Average Err**	**Max Error**	**Min Error**	**STD**	**95% of Pop**	**75% of Pop**
Rotational Error (deg)	*10*	7.34	40.07	0.19	7.30	21.94	14.64
	15	2.77	20.15	0.19	2.90	8.56	5.66
	20	2.13	6.92	0.19	1.43	4.99	3.56
	25	1.97	6.03	0.19	1.12	4.21	3.09
	30	1.84	9.20	0.20	1.36	4.55	3.19
	35	1.58	4.52	0.34	0.82	3.23	2.41
	40	1.50	4.34	0.17	0.79	3.07	2.29
	50	1.26	4.01	0.19	0.69	2.64	1.95
	75	1.18	2.55	0.24	0.52	2.21	1.69
	100	0.79	2.61	0.11	0.41	1.60	1.19
Translational Error (mm)	*10*	2.10	12.61	0.18	2.44	6.97	4.53
	15	0.81	3.85	0.10	0.55	1.91	1.36
	20	0.64	1.73	0.21	0.31	1.27	0.95
	25	0.55	1.58	0.08	0.29	1.14	0.85
	30	0.54	2.06	0.08	0.36	1.26	0.90
	35	0.52	1.34	0.09	0.24	1.00	0.76
	40	0.47	1.39	0.05	0.23	0.94	0.70
	50	0.42	0.91	0.13	0.18	0.77	0.60
	75	0.35	0.93	0.12	0.16	0.67	0.51
	100	0.25	0.58	0.02	0.11	0.47	0.36

Table 6.7: Relationship between point-set size and registration robustness, expressed in terms of overall rotational and translational accuracy, for a set of robust point-sets describing a proximal tibia.

	Performance of Random Point-Sets of Different Sizes for 1.5mm Maximum Noise						
	Point-Set Size	**Average Err**	**Max Error**	**Min Error**	**STD**	**95% of Pop**	**75% of Pop**
Rotational Error (deg)	*10*	11.46	60.41	0.99	10.91	33.28	22.37
	15	5.18	30.87	0.43	4.40	13.98	9.58
	20	4.64	36.28	0.99	4.58	13.80	9.22
	25	3.64	20.91	0.48	2.89	9.41	6.52
	30	2.84	9.71	0.47	1.62	6.08	4.46
	35	2.34	5.21	0.27	1.13	4.60	3.47
	40	2.45	7.26	0.41	1.42	5.29	3.87
	50	2.16	6.29	0.57	1.17	4.51	3.33
	75	1.52	3.44	0.38	0.73	2.98	2.25
	100	1.43	3.43	0.18	0.68	2.79	2.11
Translational Error (mm)	*10*	3.56	20.02	0.40	3.72	10.99	7.28
	15	1.67	10.46	0.41	1.45	4.57	3.12
	20	1.39	12.37	0.21	1.40	4.20	2.79
	25	1.01	3.29	0.19	0.61	2.22	1.62
	30	0.78	2.28	0.14	0.38	1.54	1.16
	35	0.72	1.62	0.08	0.32	1.36	1.04
	40	0.77	2.28	0.03	0.42	1.62	1.19
	50	0.59	1.85	0.11	0.31	1.21	0.90
	75	0.48	1.20	0.08	0.24	0.96	0.72
	100	0.43	1.09	0.08	0.19	0.81	0.62

	Performance of Random Point-Sets of Different Sizes for 2.0mm Maximum Noise						
	Point-Set Size	**Average Err**	**Max Error**	**Min Error**	**STD**	**95% of Pop**	**75% of Pop**
Rotational Error (deg)	*10*	12.21	57.32	2.21	9.82	31.85	22.03
	15	6.50	44.67	1.07	5.77	18.05	12.28
	20	5.74	34.66	0.43	4.77	15.27	10.51
	25	4.10	15.24	0.42	2.54	9.18	6.64
	30	4.20	16.78	0.43	2.97	10.14	7.17
	35	3.47	9.55	0.24	1.93	7.34	5.41
	40	2.93	7.40	0.34	1.59	6.10	4.51
	50	2.95	8.19	0.61	1.48	5.90	4.43
	75	2.06	6.00	0.20	1.15	4.37	3.21
	100	1.95	7.61	0.23	1.15	4.24	3.10
Translational Error (mm)	*10*	3.94	15.91	0.62	3.18	10.30	7.12
	15	1.95	12.93	0.18	1.59	5.13	3.54
	20	1.67	13.63	0.16	1.57	4.82	3.25
	25	1.26	3.33	0.15	0.64	2.55	1.91
	30	1.19	3.99	0.20	0.74	2.68	1.93
	35	0.99	1.95	0.20	0.45	1.89	1.44
	40	0.89	1.75	0.10	0.41	1.71	1.30
	50	0.84	2.67	0.07	0.41	1.66	1.25
	75	0.67	1.46	0.12	0.27	1.22	0.94
	100	0.60	1.75	0.05	0.30	1.20	0.90

Table 6.7: (cont'd) Relationship between point-set size and registration robustness, expressed in terms of overall rotational and translational accuracy, for a set of robust point-sets describing a proximal tibia.

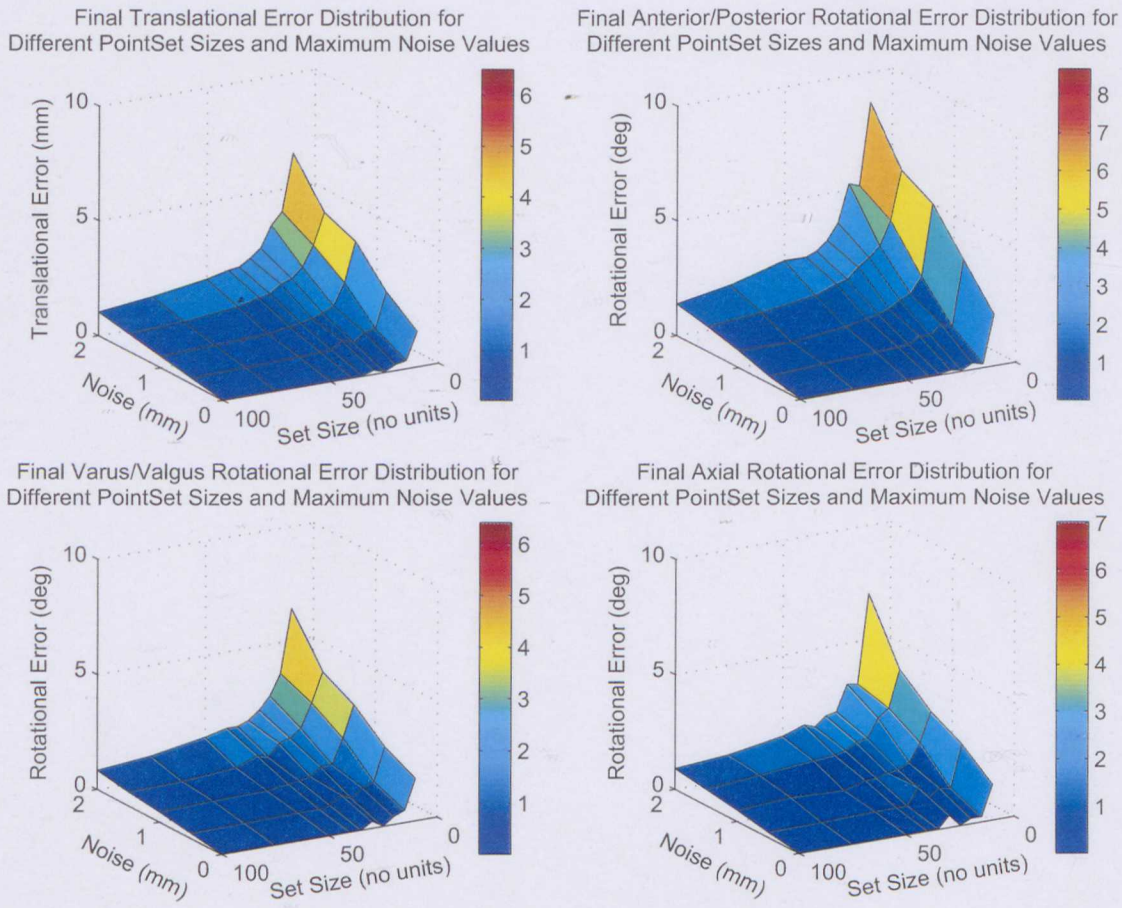


Figure 6.26: Registration accuracy for the enhanced ICP algorithm, in terms of varus/valgus, anterior/posterior, axial, and translational components, executed for different point-set sizes and maximum noise values, without points assembled through the stab-wound, for the femur.

again, robust registration has shown to be only possible for point accuracy better than $1mm$, where at least 75 points, which is an impractical number of points to be collected intra-operatively, is required for rotational alignment within $\pm 2^o$.

To provide evidence for the need to collect points through the stab-wound, which, as explained in Section 6.3.2, are required to appropriately bound all elements of the registration matrix, the same experiment described above was carried out with random point-sets assembled using points in regions I-III only. The percentage of points (20%) out of the total set sizes to be collected in region IV (Table 6.2 and Table 6.3) was evenly redistributed in the first three regions for both the femur and tibia. Results are presented in Figure 6.26 and Figure 6.27.

For the femur, the effect of the missing region on registration outcome can be derived by comparing results presented in Figure 6.26 and Figure 6.24. The two charts show similar characteristics, in terms of registration accuracy for the different components of the error matrix in the $\{BONE\}$ reference frame, with the

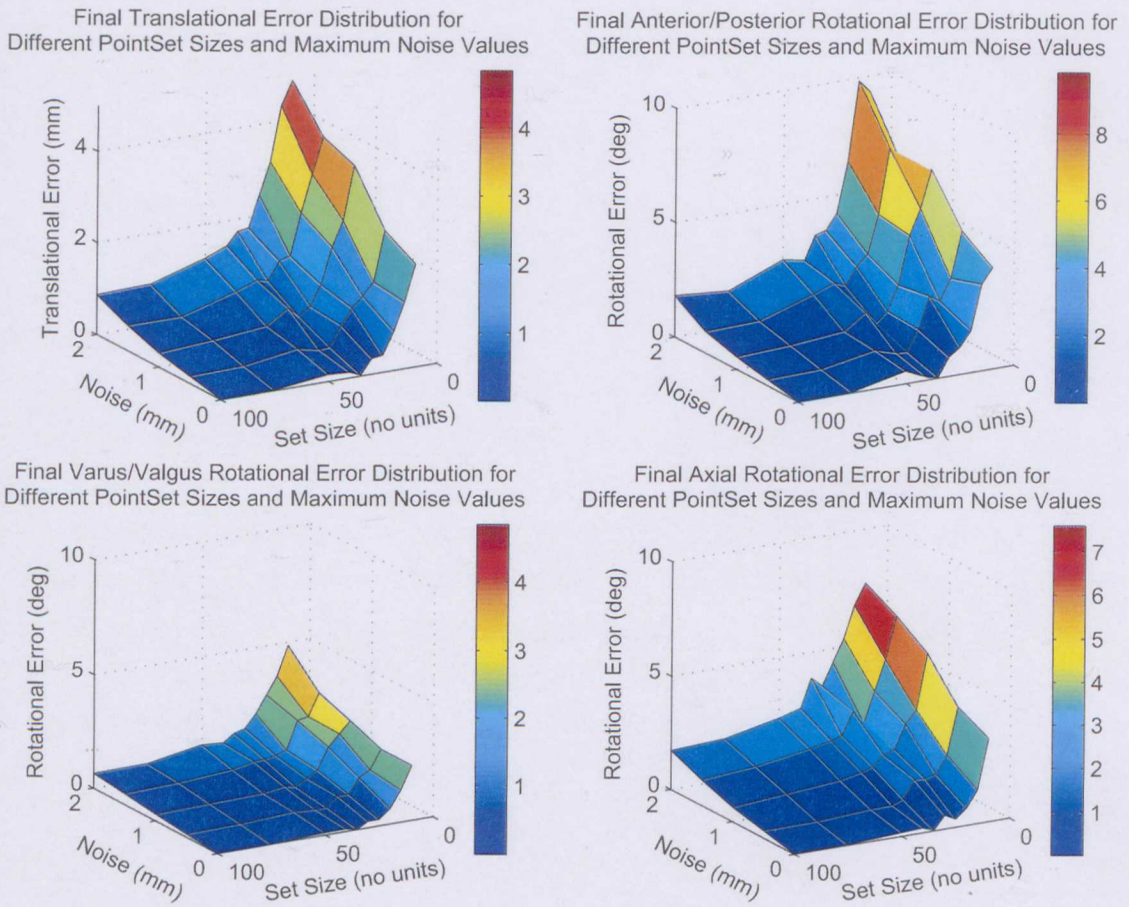


Figure 6.27: Registration accuracy for the enhanced ICP algorithm, in terms of varus/valgus, anterior/posterior, axial, and translational components, executed for different point-set sizes and maximum noise values, without points assembled through the stab-wound, for the tibia.

exception of A/P alignment. This component in Figure 6.26 has a significantly higher average value for all point-set sizes and maximum noise values considered, if compared to the corresponding figure presented in the chart illustrated in Figure 6.24. Similarly, if Figure 6.27 and Figure 6.25 for the tibia are considered, A/P and axial rotational alignment are clearly less accurate if points through the tibial stab-wound over the tuberosity are not included in the point-set. Therefore, unless additional stab-wounds are used to harvest a number of points on the frontal femur and tibial tuberosity, representative point-sets that robustly bound all elements of the registration matrix cannot be assembled.

6.3.3.2 Plastic Phantom Tests and Results

A set of plastic bone trials, similar to the one described in Section 5.4.3 to validate the TKA registration protocol, was carried out in order to corroborate the simulated results, and to evaluate the performance of the algorithm and point acquisition protocol integrated in the ACROBOT II System. A set of plastic bones was CT scanned, and a set of plans, defining UKA of the medial condyle with an Oxford unicompartmental knee implant, was generated using Acrobot's proprietary planning software. 10 consecutive full registration procedures using the enhanced ICP algorithm described, including minima suppression, were carried out, and results compared to the ground truth defined by the reference transformation matrix, which, as for the TKA plastic trials, was assembled for each tested point-set using the method outlined in Section 5.27. Table 6.28 illustrates the results, in terms of rotational and translational alignment of the registered bone in the $\{BONE\}$ frame of reference (Section 5.4.1) for both the femur and tibia.

Table 6.28 illustrates the registration outcome obtained for point-sets of different sizes, between 18 and 25 points, assembled on surgically accessible surfaces using the point acquisition protocol described in Section 6.3.1. As can be seen, results for both femur and tibia are all well within the range of accuracy defined in Table 6.4 and Table 6.5 for a specific point-set size for point accuracy better than $0.5mm$. The minimum and maximum values, representing the envelope of the accuracy for each error matrix component, are all within the value for 95% of the population for a specific set size and point accuracy. Furthermore, the average accuracy is much higher, with differences of approximately $0.5mm$ and 0.5^o, which is to be expected looking at the average registration accuracy for the corresponding point-set size in Table 6.4 and Table 6.5.

a)

Test #	Point-Set Size	RMS Error (mm)	Error Matrix Components				
			V/V Error (deg)	*Axial Error (deg)*	*A/P Error (deg)*	*Rot Error (deg)*	*Trans Error (mm)*
1	23	0.19	-0.01	1.54	-1.09	1.89	0.27
2	23	0.2	0.33	1.18	-0.51	1.33	0.37
3	23	0.19	1.02	1.00	-1.06	1.77	0.57
4	18	0.14	0.24	1.09	-0.35	1.17	0.53
5	18	0.2	0.07	0.18	0.38	0.43	0.43
6	23	0.17	0.29	0.88	-0.85	1.26	0.32
7	18	0.12	-0.60	0.10	0.29	0.67	0.18
8	18	0.15	1.02	0.67	-0.63	1.38	0.34
9	18	0.11	0.37	0.64	-0.14	0.75	0.16
10	20	0.17	1.06	1.35	-1.00	1.99	0.13
Maximum Error			1.06	1.54	0.38	**1.99**	**0.57**
Minimum Error			-0.60	0.10	-1.09	**0.43**	**0.16**
Average Error			//	//	//	**1.26**	**0.33**

b)

Test #	Point-Set Size	RMS Error (mm)	Error Matrix Components				
			V/V Error (deg)	*Axial Error (deg)*	*A/P Error (deg)*	*Rot Error (deg)*	*Trans Error (mm)*
1	20	0.12	-0.18	-0.60	-0.44	0.77	0.58
2	20	0.14	-0.54	-0.08	0.01	0.54	0.55
3	25	0.13	-0.28	-0.37	-0.42	0.63	0.58
4	20	0.19	-0.33	0.30	0.31	0.54	0.43
5	20	0.12	-0.39	-0.05	-0.26	0.47	0.58
6	16	0.11	-0.04	-0.06	-0.12	0.14	0.50
7	15	0.13	-0.19	-0.30	-0.68	0.77	0.71
8	16	0.15	-0.42	-0.30	-0.64	0.82	0.83
9	15	0.09	-0.26	-0.77	-0.27	0.86	0.78
10	20	0.11	-0.29	-0.30	-0.44	0.60	0.65
Maximum Error			-0.04	0.30	0.31	**0.86**	**0.83**
Minimum Error			-0.54	-0.77	-0.68	**0.14**	**0.43**
Average Error			//	//	//	**0.61**	**0.62**

Figure 6.28: Accuracy of registration outcome for 10 registration procedures using the enhanced ICP algorithm for both the femur (a) and tibia (b).

6.4 Discussion

This chapter has focused on some of the hardware and software changes carried out on the ACROBOT II System. They were carried out in order to prove the concept of an active-constraint system for unicompartmental knee arthroplasty of the medial condyle. The clamping system, originally developed for TKA, was successfully redesigned, and both plastic bone and a preliminary set of clinical trials, have shown the new design is an appropriate means to rigidly immobilise the knee joint during UKA with the ACROBOT II System. The current design requires two sets of stab-wounds for placement during surgery. These additional incisions, although currently accepted by the clinical community, represent a drawback for the procedure, and have been addressed in Section 8.3 as an area for future work.

Although the tissue retaining tube described in Section 6.2.2 has shown some potential through experimental testing during conventional UKA procedures, significant changes to the preliminary prototype illustrated in Figure 6.9 need to be made. In order to successfully complete a robotic assisted UKA procedure with the ACROBOT II System through a $3.5cm$ incision, which seems possible examining preliminary results, the concept of a tissue retaining tube needs to be investigated further. The design of a suitable tissue retaining tube for minimally invasive UKA has been addressed in Section 8.3 as an area for future work.

The intra-operative protocol described in Section 6.3.2, developed to carry out a UKA procedure with the ACROBOT II System, has shown to be appropriate for the task through extensive plastic bone trials, and a small set of Ethics Committee approved clinical trials. Early results, presented in [Rodriguez y Baena et al., 2003; Henckel et al., 2003; Cobb et al., 2003], have shown that both the system and minimally invasive registration protocol described in Section 6.3.1 have successfully been implemented in a clinical environment, but further work, described in Section 8.3, will need to be completed to improve the performance of both system and registration software.

The registration algorithm described in Chapter 5 has been successfully adapted for minimally invasive UKA with the ACROBOT II System. The point acquisition protocol described in Section 6.3.1 has been validated through simulation and a set of plastic bone trials. Results have shown that robust registration can be successfully performed through the conventional UKA incision and two additional stab-wounds. Given an adequate CT scan and intra-operative setup, if the region-based protocol is adopted and the point-set size is chosen as a function of expected point accuracy, the registration technique described can be used to robustly identify the position of both the femur and tibia with respect to the robotic system. However, the results presented in Table 6.6 and Table 6.7 clearly highlight the need for the expected *point*

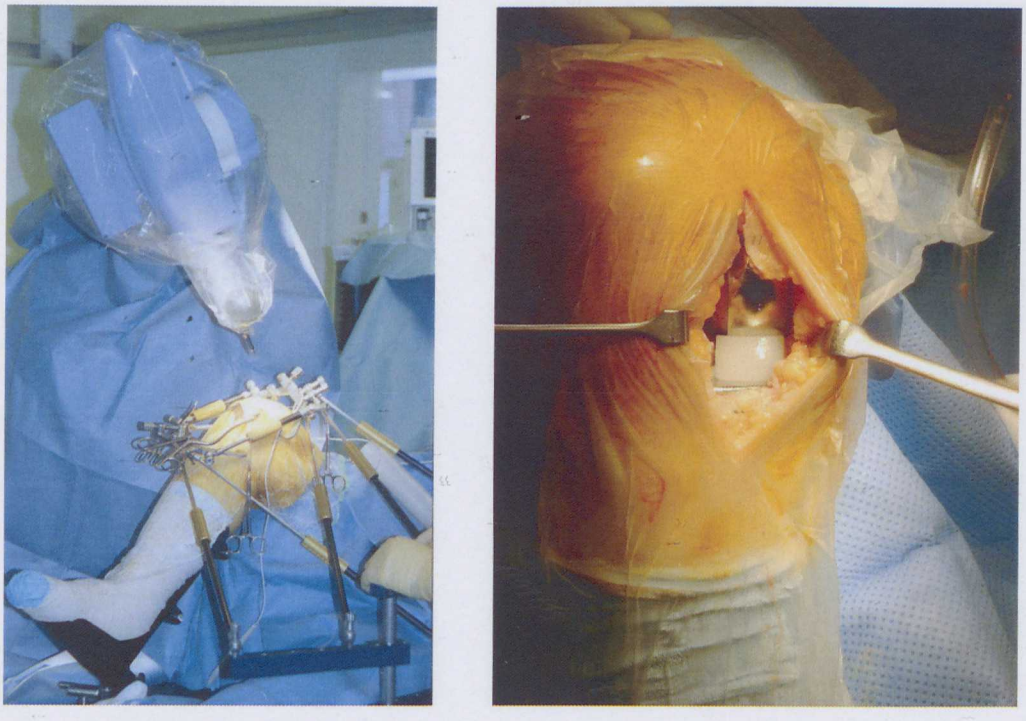


Figure 6.29: Early clinical trials of robotic assisted UKA with the ACROBOT II System.

accuracy to be better than $1mm$. This limitation, which can be expected given the restricted access available in the UKA procedure, imposes an important constraint on the requirements for a system suitable for this type of procedure, if a registration method based on anatomical features is to be used. Although a preliminary study of the clinical results has shown that sub-millimetric point accuracy is possible, an alternative means of registration has been developed which improves the robustness of the procedure. This novel registration algorithm is the focus of the next chapter.

6.5 Conclusion

Changes to both the hardware and software of the ACROBOT II System have allowed the concept of an active constraint system for minimally invasive surgery to be demonstrated. The adapted system was successfully used to implant a large number of unicompartmental knee implants on plastic phantom bones. Encouraging results of an extensive plastic bone study, which will shortly be published, has led to a set of Ethics Committee approved clinical trials, to be planned and executed with the ACROBOT II System.

The adapted registration algorithm and protocol have shown to be appropriate for the task if good correspondence between the intra-operatively collected points and CT generated surface can be expected. Plastic bone results (Section 6.3.3.2)

have shown that this amount of accuracy is achievable for the current system under experimental conditions. Sub-millimetre and sub-degree accuracy has consistently been obtained on phantom bones in a controlled environment, which is to be expected, as both the CT scanner and mechanical digitiser are well within the range of accuracy required for point accuracy better than $1mm$. However, a clinical environment presents a number of additional variables affecting point accuracy, such as the quality of segmentation, and bone motion generated by an improper intra-operative setup. The effect of these variables on the system's performance is hard to quantify, and complex to plan for. Therefore, the "worst case scenario" for a registration method based on anatomical correspondences is hard to derive, which represents a significant weakness of the enhanced registration algorithm and acquisition protocol, if used through a minimally invasive approach. The shortcomings of the anatomical registration method described in this chapter have led to the development of a novel algorithm suitable for minimally invasive registration, the Bounded ICP algorithm. This algorithm, which is currently being patented, and validation process are presented in Chapter 7 for the femur, while a possible implementation suitable for robust registration of the tibia is included in Section 8.3 as an area for future work.

Chapter 7

Anatomical Registration for Minimal Access Surgery

7.1 Introduction

Simulation and plastic bone trials of the adapted ICP algorithm described in Section 6.3 have shown that the registration protocol defined in Section 6.3.1 for unicompartmental knee arthroplasty can be used to accurately register both the tibia and femur using a minimally invasive approach. However, as described in Section 6.3, well spread and accurate points are required over a large percentage of the exposed femoral and tibial surfaces, as well as through the stab-wounds, in order to ensure registration accuracy for the femur and tibia below the stated requirement of $\pm 2^o$ and $\pm 2mm$. Unfortunately, early clinical experience with the ACROBOT II System for two UKA procedures illustrated that good points through the femoral stab-wound, as well as accurate medial side and notch points could not be guaranteed at all times. Alongside lack of vision through the stab-wound, the intra-operative setup could impair adequate point collection as incorrect placement of the femoral clamp obstructs the path between the robot end effector and the stab-wound. Osteophytic bone on the edge of the lateral condyle, as well as the patella, also has the potential to get in the way during point collection in regions II and III in Figure 7.1.

Although the requirement of an additional incision during the procedure proved to be a viable temporary solution to obtain adequate registration accuracy, a more definite solution was required. With the ultimate goal of a robotic assisted procedure being carried out minimally invasively, the need for a new algorithm that would shift the accuracy requirements away from the quality of the femoral point-set became apparent. After an investigation of the anatomical features available for registration, it became clear that estimating the functional centre of the hip joint could provide the degree of rotational accuracy required for this type of surgery. As will

be described in the following sections, the hip centre, which can easily be identified during the pre-operative planning stage as well as intra-operatively, provides very remote paired points which have the potential to constrain the registration outcome to a much higher degree than any points collected on the distal femoral surface.

Both translational displacement and axial rotational error can be partially compensated for by the polyethylene insert between the femoral and tibial components. As the insert provides a mobile bearing for the two components to pivot against, a few degrees of axial rotation, which can be represented as a rotation about the femoral implant post, have a marginal effect on the reconstructed joint functionality. Similarly, a small translational error in the direction of the post can be mitigated by different insert thicknesses, therefore does not have a significant impact on the leg axis alignment.

As a result, the primary objective for the development of a new algorithm suitable for minimally invasive knee surgery was to be able to bound important rotational components of the registration error matrix, namely varus/valgus and anterior/posterior angles, by using positional information obtained from the functional centre of the hip. The algorithm, based on pre-operatively acquired data, should ideally enable accurate registration of the femur through a small wound, and should be less susceptible to poor point collection on the distal femoral surface. It should also provide reliable and robust varus/valgus and anterior/posterior alignment, well within $\pm 2^o$.

The following sections describe the design, development, and validation process of a novel algorithm, the Bounded ICP algorithm, that has been successfully tested in simulation, phantom studies, and clinical trials. This registration algorithm has proved to be exceptionally resistant to noise during point collection, has minimal access and point-set size requirements, and robustly produces accurate varus/valgus and anterior/posterior alignment for an adequate hip centre estimate. The Bounded ICP algorithm, designed and developed for minimal access registration of the femur, has the potential to be adapted for robust tibial registration, using the ankle centre to obtain a distant set paired points. This algorithm enhancement, which would enable minimal access tibial registration, has been described in Section 8.3 as an area for future work. Note that, in the following sections, the optimised registration algorithm described in Chapter 5 is sometimes referred to as "the original algorithm."

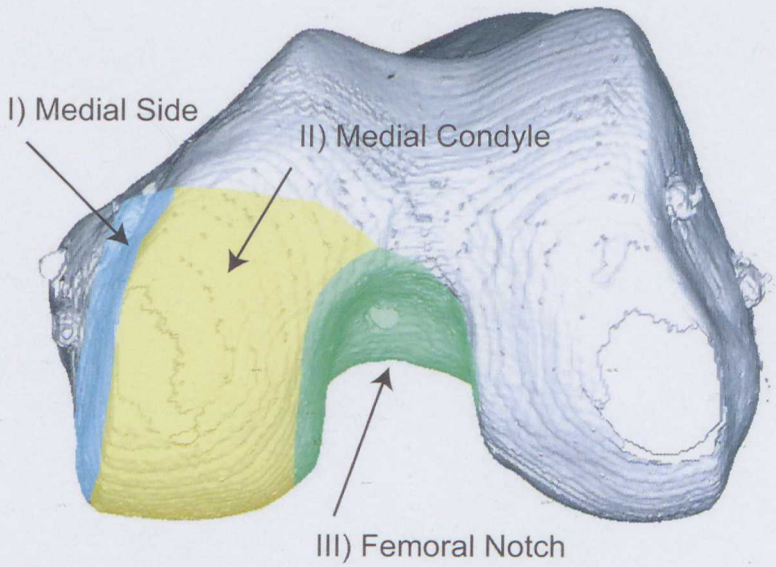


Figure 7.1: Accessible surfaces on the femur during conventional UKA.

7.2 Minimal Access Femoral Registration

7.2.1 Assumptions

As described in Section 6.3.1, during conventional unicompartmental knee arthroplasty, regions I-III in Figure 7.1 are accessible for registration, without the need for additional stab-wounds. However, as highlighted by the results in Section 6.3.3.1.2, a poor quality of point-set, both in terms of point touching accuracy and point spread, can cause the registration result to quickly degenerate, resulting in large rotational errors, which are unacceptable for robotic assisted UKA.

As illustrated in Figure 7.2, let correct varus/valgus and anterior/posterior alignment be specified by defining the position of the knee, which can be approximated by a single point situated somewhere on the distal femur, and the centre of the femoral head. Then, once the hip centre has been accurately located, the knee centre can be correctly aligned by minimising the distance error of the points measured on the exposed surface of the distal femur.

Accurately estimating the centre of the femoral head then enables a three dimensional point that is very far from the distal femur, where the points for anatomical registration are collected, to be obtained. As illustrated in Figure 7.3, a lateral displacement error of $1cm$ in the hip centre estimate will result in less than 1.3^o of varus/valgus misalignment, assuming a $40cm$ average length of femur and correct distal alignment. Therefore, correctly locating the position of the functional centre of the hip has the potential to guarantee correct anterior/posterior and varus/valgus

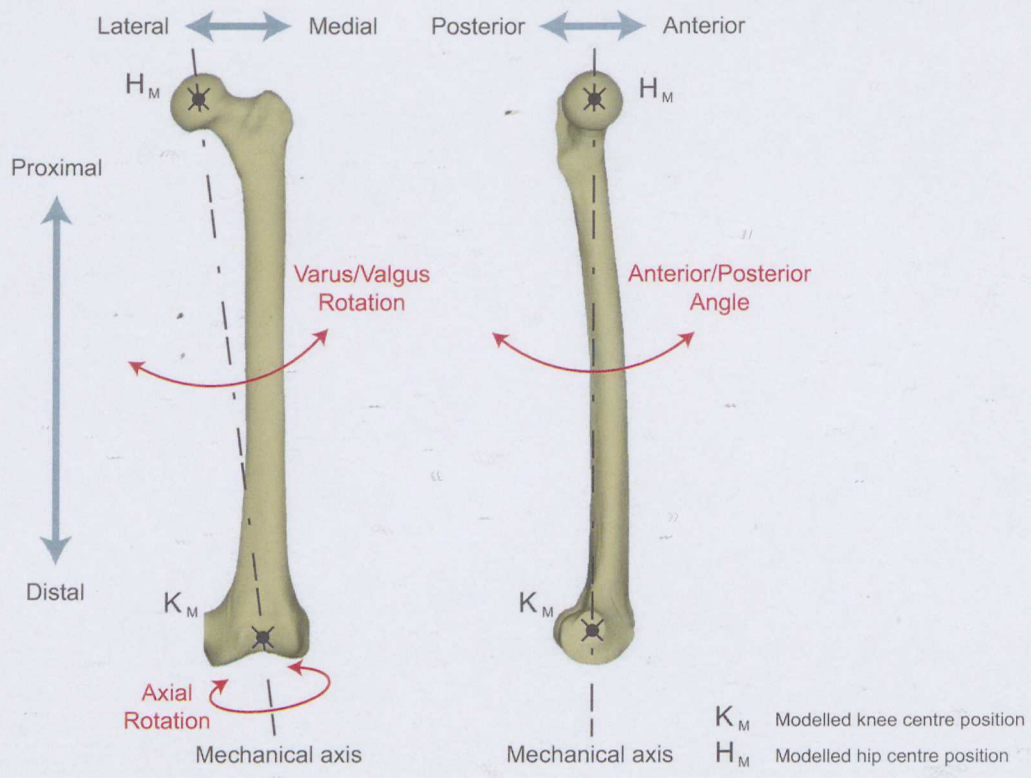


Figure 7.2: Leg alignment in terms of knee and hip centres.

alignment of the leg.

However, the same does not apply to translational error, as a $1cm$ error during hip estimation will result in a $1cm$ translational error of all points collected on the distal surfaces. Assuming a rigid relationship between distal points and the hip centre, a perfect hip centre estimate would be required in order for correct translational registration to be possible. This poses an unrealistic constraint on the algorithm, nullifying the advantage of adding the hip centre to improve registration outcome.

Therefore, an algorithm capable of harvesting the full potential from the hip centre, without impairing correct registration of the other degrees of freedom had to be developed. The overall characteristics of the algorithm can be summarised as follows. The new method should:

- Bound the axis defining varus/valgus and anterior/posterior alignment of the leg by estimating the functional centre of the hip (proximal side) and the anatomical points measured on the exposed surfaces of the distal femur (distal side).
- Use anatomical points on the distal femur only, for correct translational alignment and axial rotation.

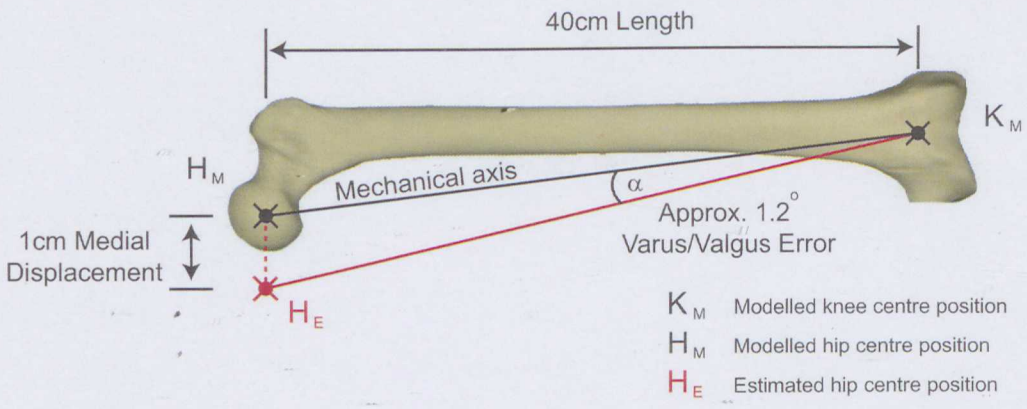


Figure 7.3: Effect of hip centre estimate error on the overall alignment of the leg.

7.2.2 Locating the Hip Centre

Estimation of the functional centre of the hip has been well documented over the years in a number of applications, for instance in biomechanics [Kang et al., 2002; Kang et al., 2003] and, more recently, in CT free registration of the knee joint [Fleute and Lavallee, 1998; Rajamani et al., 2004]. As the hip joint can be approximated to a "ball and socket" joint, its functional centre can be obtained by fitting a sphere on points measured about a fixed distal location on the femur, as the leg is moved in a grid while pivoting about the hip with the pelvis immobilised. A well known least squares Gauss-Newton method was used for this purpose, although a number of alternative methods could be used to improve estimation accuracy. Details of the algorithm are not discussed, as they are not the author's work.

In the following sections it will be assumed that both modelled and estimated hip centres can be accurately defined. Section 7.3.3 provides a brief overview of both the pre-operative and intra-operative steps that need to be carried out to define modelled and estimated hip centre positions for the current implementation of the ACROBOT II System.

7.2.3 The Bounded ICP Algorithm

As mentioned in Section 7.1, an algorithm capable of harvesting the full potential from the hip centre position, without compromising correct alignment of all degrees of freedom between robot and model spaces, had to be developed. During early experimentation, the hip centre was added as a set of paired points in the data which was loaded in the accelerated ICP algorithm described in Chapter 5. The modelled hip centre was inserted as an additional vertex in the surface model of the femur, while the hip centre estimate, measured in the robot's co-ordinate system, was added as an additional probe point in the point-set. However, an analysis of

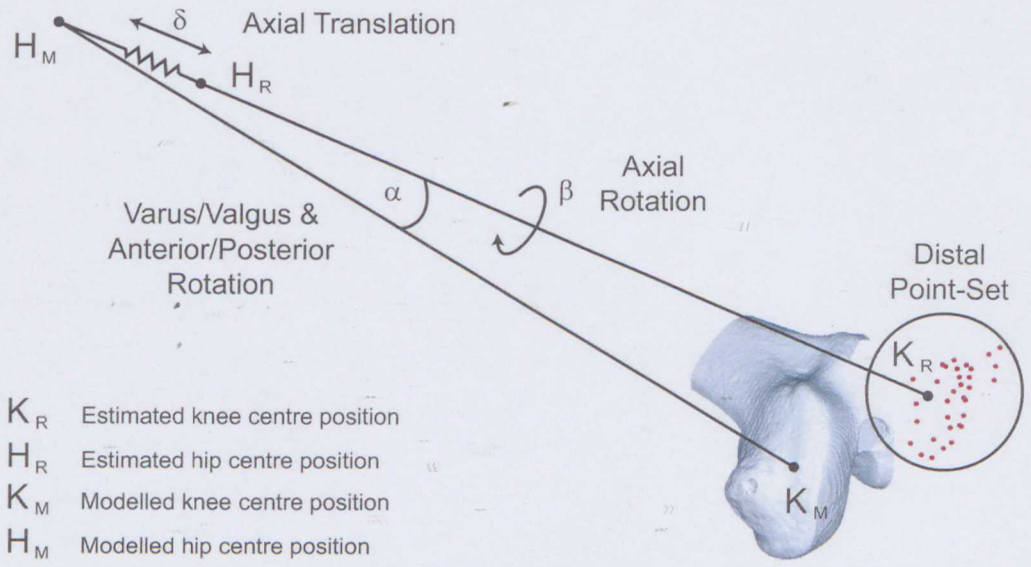


Figure 7.4: "Physical model" for the Bounded ICP convergence theorem.

the results showed that the addition of this pair of points had a negligible effect on the registration outcome. Although the set of closest points is correctly identified by the algorithm, its impact on registration alignment is significantly dampened by the contribution of the distal points harvested on the bone surface. The next experiment was then to add the hip centre estimate as a weighted point, in order to guarantee an effect on the overall registration outcome. However, no combination of points and weights could be found that would maximise the effect of the hip centre on rotational accuracy, without compromising global minimum identification with respect to translation and axial rotation.

Hip centre estimation provides an invaluable constraint on varus/valgus and medial lateral alignment, but has a detrimental effect on translation if considered as a set of co-ordinates in three-dimensional space. Furthermore, the hip centre does not provide any additional information when trying to bound axial rotation. To aid the generation of a suitable algorithm it was decided to design a "physical" model for the convergence process. In the following paragraphs, "robot space" describes a set of co-ordinates measured in the robot co-ordinate system, while "model space" describes a point in the co-ordinate system of the surface model of the femur to be registered. The aim of registration is to define the rigid transformation that accurately maps model space into robot space. Figure 7.4 schematically illustrates this model.

To start with, the modelled and estimated hip centre positions (which are in model and robot space respectively) coincide. All probe points measured on the distal femur are regarded as a whole, by referring to them in terms of their centroid

– the "knee centre estimate." Finally, the knee centre estimate is connected to the modelled hip centre with a spring, able to stretch and compress, but not bend. Each probe point has a corresponding representation on the modelled surface, which needs to be correctly identified for the best solution to be found. Pairs of points and respective closest points provide the "potential" to be minimised, which is expressed in terms of the Root Mean Square (RMS) of their relative distance, and is used in the minimisation process until the error falls below a specified threshold. The distal point-set is allowed to oscillate about the modelled hip centre (α), to move away or toward the modelled hip centre (δ) and to rotate about the axis defined by the knee centre estimate and modelled hip centre (β). A possible solution, or local minimum, is obtained for the position of the probe points on the modelled surface where the error distance between points and closest points is minimum.

As in the original ICP algorithm [Besl and McKay, 1992] and all its variants, convergence is achieved by iterating upon closest points. Therefore this new algorithm, described in mathematical form in the following sections, can be categorised as a "type" of Iterative Closest Point algorithm. However, instead of using the minimum distance algorithm based on quaternions [Horn, 1987] described in Chapter 3, the transformation matrix used to map the points onto the surface at every iteration (namely T_n in Figure 3.8) is calculated by applying rotations about and translations along the axis generated by the hip centre and centroid of the probe point set. Successive transformations applied to the original point-set are therefore bound at one end while free to move at the other, giving the Bounded ICP algorithm its name.

The following paragraphs provide a mathematical description of the algorithm. The subscript "R" is used to define a vector in the robot co-ordinate system, while "M" refers to a position in model space, which corresponds to the coordinate system of the pre-operative plan. Before the algorithm is applied, H_M and H_R are aligned in space, where:

H_M represents the 3D vector describing the position of the modelled hip in the coordinate system of the plan. This position is estimated during the pre-operative planning stage by inspecting successive CT slices (Section 7.3.1).

H_R represents the hip centre, estimated intra-operatively by a least squares sphere fit, as outlined in Section 7.3.3.

The leg axis, $\overrightarrow{l}$, is calculated in the direction of the vector defined by the knee centre estimate, K_R, and H_M. K_R is calculated by estimating the centroid of the points collected on the distal femoral surface in the robot co-ordinate system:

$$K_R = \frac{1}{N_P} \sum_{i=1}^{N_P} (\overrightarrow{p}_i) \tag{7.1}$$

where:

K_R is the knee centre estimate in robot coordinates.

N_P is the size of the probe point-set.

$\overrightarrow{p}_i$ is probe point i, measured in the robot co-ordinate system.

At every iteration, a new estimate for the registration transform T_{n+1} is calculated in two steps. For each step, a new estimate is produced by pre-multiplying the current estimate by a transformation matrix, defined by the error vectors generated by the difference between each probe point and respective closest point. In the first step, the translational component of the registration matrix is minimised, while the second step is used to solve for axial rotation. The remaining two rotational components of the registration matrix, namely varus/valgus and anterior/posterior rotation, are bound by the hip centre position. Let the two phases of the estimation process be referred to as Phase I and Phase II.

In Phase I, let:

$$\Delta S_n = \frac{1}{N_P} \sum_{i=1}^{N_P} (\overrightarrow{y}_{i,n} - \overrightarrow{p}_{i,n}) \tag{7.2}$$

where:

N_P Number of probe points.

$p_{i,n}$ is point $p_{i,0}$ transformed by T_n.

$y_{i,n}$ is $p_{i,n}$ corresponding closest point on the surface.

ΔS_n represents the average translational error for the current set of points and closest points.

If ΔS_n was to be added to each probe point as a translational offset, it can be shown that this process would minimise the current translational error for the same set of points and closest points (see Appendix E). At every iteration, ΔS_n is minimised, which minimises the average error (RMS) of the probe points as well. Therefore, the same *convergence theorem* described in [Besl and McKay, 1992] can be used to

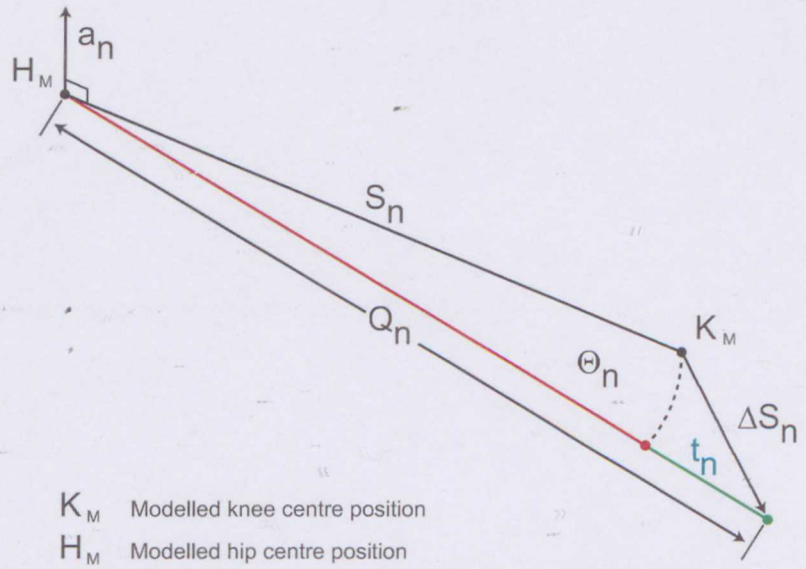


Figure 7.5: Phase I of convergence.

prove that this algorithm will converge monotonically to the closest local minimum. However, at this point an approximation is made. Instead of translating all points by ΔS_n, all points are first rotated about an axis which is orthogonal to the leg axis and passes through H_M, and then translated by a vector in the direction of the new leg axis, as illustrated in Figure 7.5.

In mathematical form, let:

$$S_n = K_M - H_M \tag{7.3}$$

where:

$$K_M = T_n * K_R \tag{7.4}$$

As in the original implementation described in Section 3.3, T_n represents the registration estimate for iteration "n".

Also, let:

$$Q_n = S_n + \Delta S_n \tag{7.5}$$

Then, the axis of the first rotation is defined by:

$$a_n = S_n \times Q_n \tag{7.6}$$

Note that a_n is normal to the leg axis, which means a rotation about it will only have varus/valgus and anterior/posterior components.

The angle of rotation about a_n is defined as:

$$\Theta_n = cos^{-1}\left(\frac{(S_n * Q_n)}{|S_n| * |Q_n|}\right) \tag{7.7}$$

Finally the translation along Q_n is defined as:

$$t_n = Q_n * (|Q_n| - |S_n|) \tag{7.8}$$

then Phase I results in the transformation R_1:

$$R_1 = R(a_n, \Theta_n) + T(t_n) \tag{7.9}$$

Now for:

$$(K_R - H_R) >> (K_R - p_i), \; for\, any\, i \in [1, N_p] \tag{7.10}$$

$$R_1 \approx T(\Delta S_n) \tag{7.11}$$

Therefore:

$$T_n^{'} = T(H_M) * R_1 * T(-H_M) * T_n \tag{7.12}$$

Because the rotation of Θ_n about an axis passing through a very remote point adds a negligible rotational error to the shifted points, compared to the benefit provided by the translational component, the algorithm has been empirically proven to converge monotonically to a minimum (Section 7.4).

In Phase II, graphically illustrated in Figure 7.6, let :

$$S_n^{'} = K_M - H_M \tag{7.13}$$

where:

$$K_M = T_n^{'} * K_R \tag{7.14}$$

Now, for every probe point p_i:

$$\delta s_{i,n} = \overrightarrow{y}_{i,n} - \overrightarrow{p}_{i,n} \tag{7.15}$$

and let,

$$j_{i,n} = \overrightarrow{y}_{i,n} - H_M \tag{7.16}$$

$$k_{i,n} = j_{i,n} + \delta s_{i,n} \tag{7.17}$$

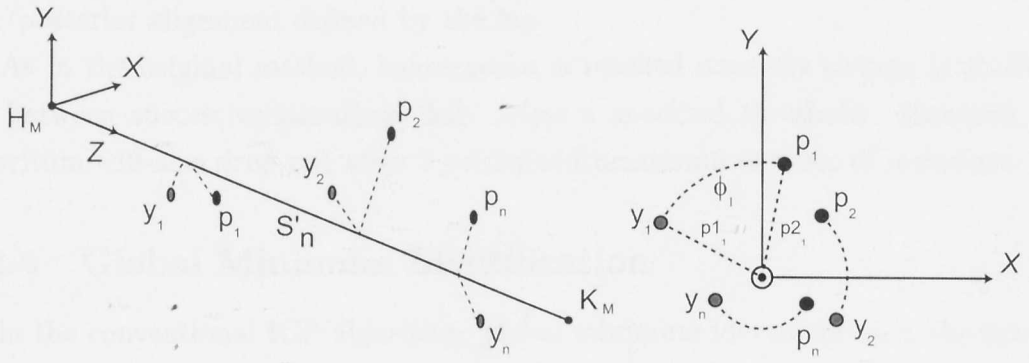


Figure 7.6: Phase II of convergence.

Then, the components of $j_{i,n}$ and $k_{i,n}$ which are orthogonal to the leg axis $S_n^{'}$ are calculated as:

$$p1_{i,n} = \frac{j_{i,n} * K_M}{|j_{i,n}|} \tag{7.18}$$

and:

$$p2_{i,n} = \frac{k_{i,n} * K_M}{|k_{i,n}|} \tag{7.19}$$

As this is a simple 1 degree of freedom case, from $p1$ and $p2$ for every probe point, the average axial rotational angle that will minimise the axial rotational error can be defined as:

$$\Phi_n = \frac{1}{N_P} \sum_{i=1}^{N_P} \left(sign\left((p1_{i,n} \times p2_{i,n}) * S_n^{'} \right) cos^{-1} \left(\frac{(p1_{i,n} * p2_{i,n})}{|p1_{i,n}| * |p2_{i,n}|} \right) \right) = \frac{1}{N_P} \sum_{i=1}^{N_P} \phi_i \tag{7.20}$$

So:

$$R_2 = R(S_n^{'}, \Phi_n) \tag{7.21}$$

which can be used to find the transformation estimate for the following iteration:

$$T_{n+1} = T(H_M) * R_2 * T(-H_M) * T_n^{'} \tag{7.22}$$

As can be seen, all transformations made to T_n are about axes which pass through the modelled hip centre H_M, which forces the estimated hip position, H_R, to lie on $\overrightarrow{l}$. Therefore, as for the conventional ICP algorithm, the Bounded ICP algorithm will monotonically converge to a minimum, but will retain varus/valgus and ante-

rior/posterior alignment defined by the hip.

As in the original method, convergence is reached once the change in RMS error between successive iterations falls below a specified threshold. However, the algorithm will also drop out after a predefined maximum number of iterations.

7.2.4 Global Minimum Identification

As in the conventional ICP algorithm, global minimum identification is the process that allows the global minimum, describing the true mapping of the intra-operatively acquired set of points on the surface model to be registered, to be correctly identified among the surrounding local minima. As the reasoning behind the local minima suppression process used for the Bounded ICP algorithm follows along the line of that described in Section 5.3.3 for conventional ICP, only details of the perturbations applied to the estimate will be described below.

In order to locally perturb the current registration estimate, random rotations and translations about the leg axis are applied. The simulator described in Section 7.4.1 was used to explore the effect of perturbations on global minimum identification, which resulted in the development of a technique, based on a two-stage strategy, that has shown to be a reliable means for global minimum identification. In the first stage, the right "class" of minima is identified, while, in stage two, a high resolution sweep of the solution set is performed to find the global minimum for a given class.

As for other minimisation processes, it is important to distinguish between local minima which are far away from the true global minimum, and those that lie within close proximity of it. Because the Bounded ICP algorithm is constrained at the hip centre end during the minimisation process, it has shown to be considerably more susceptible to local minima which are distant from the global minimum than the conventional technique (Figure 7.7).

Therefore, in order to guarantee that the right "class" of local minima (which is the class of minima containing the global minimum) is found, a number of quick runs of the algorithm are carried out. During these runs, which make up the first stage of the suppression mechanism, all computations relating to axial rotation (described as Phase II in Section 7.2.3) are omitted. As shown in Section 7.4.1.2.1, this technique considerably speeds up the convergence process. After successful convergence, the current registration estimate is perturbed with a random rotation about a random axis. This axis is perpendicular to the leg axis, and passes through the modelled hip centre converted into robot co-ordinates. This ensures that the perturbation keeps the estimated hip centre on the axis defined by the knee centre estimate and the modelled hip centre. This rotation is followed by a defined (usually 20mm)

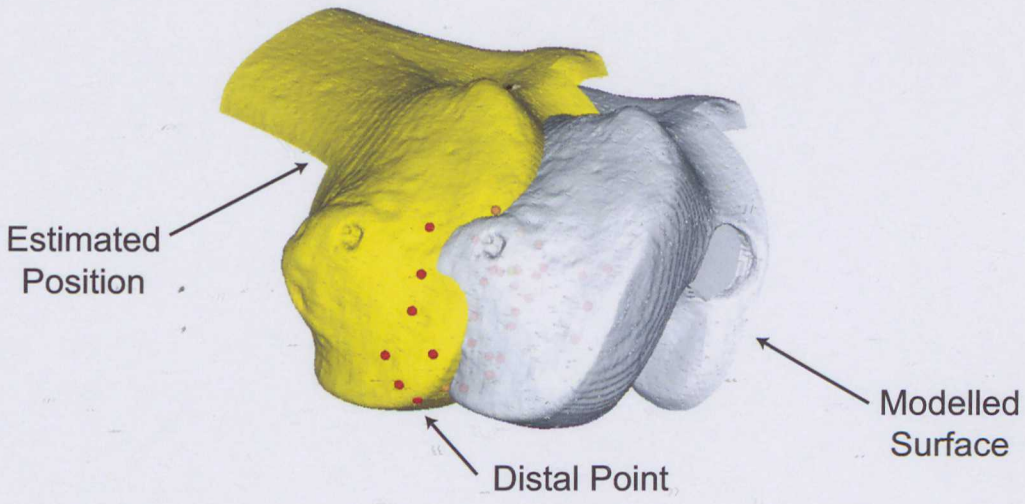


Figure 7.7: Distant local minimum affecting the Bounded ICP algorithm.

translation in the direction of the leg axis, and away from the hip centre. It has been shown through experimental testing that, because of the concave nature of the femoral surface, the algorithm has problems in converging if the set of probe points is heavily embedded in the surface. Initially translating all the points, so that most of them lie over the surface to be registered, has proved to subtract a considerable number of iterations from the convergence process.

The correct class of local minima is currently identified by inspecting the magnitude of the best RMS error found during the first stage of the minima suppression process. Local minima, such as the one described in Figure 7.7, have consistently shown substantially higher RMS values compared to local minima around the global minimum. Therefore, a thresholding technique, which has been empirically set at less than $3mm$ RMS, is used to identify the transition from the first to the second stage. It is important to note that the minima suppression process carried out in the first stage will only succeed if the axial alignment provided by initial registration (Section 7.3.4) is within a maximum allowable envelope, which has been empirically set at $\pm 20^o$. This is because, for initial axial errors greater than 20°, the RMS error will fail to fall below the threshold that will initiate the second stage of the minima suppression process. Currently the first stage is carried out until the RMS value falls below the threshold, or until a predefined maximum number of runs is carried out. If the first stage exceeds the maximum number of runs, the minimisation process is terminated early.

In stage two, it is assumed that the correct class of minima has been identified, therefore, the algorithm is allowed to converge fully, with both Phase I and Phase II of the convergence process (Section 7.2.3) being executed. After each run, the

current registration estimate is perturbed by rotating it by a random angle about the leg axis. This process is currently carried out 20 times, but more sophisticated techniques are outlined under future work (Section 8.3). The global minimum is identified by the registration transform that produces the lowest RMS error.

7.3 Implementation

While the Bounded ICP algorithm was exhaustively tested in simulation, changes were made to the ACROBOT II System in order to integrate the new registration method with the UKA procedure. A brief outline of the main changes made to the pre-operative and intra-operative phases of the procedure can be found in the rest of Section 7.3. Aspects of the robotic assisted UKA procedure that have not changed from the original registration implementation (described in Chapter 6) have not been described in this thesis.

7.3.1 Pre-Operative Planning

During the pre-operative planning phase, the functional centre of the hip joint has to be identified by inspecting the three-dimensional reconstruction of the femoral head generated from computer tomographic (CT) data. As illustrated in Figure 7.8, frontal and anterior/posterior (AP) views are used to find the outer edges of the femoral head, which are then used to overlay a spherical shape on the screen. The schematically depicted sphere, shown as two circles in the frontal and AP views, is placed on the reconstructed leg anatomy so that its centre coincides with the functional centre of the femoral head. The three-dimensional co-ordinates of the sphere centre are then stored as the co-ordinates of the modelled hip centre.

More robust techniques are being developed which will allow the hip centre to be estimated automatically through pattern recognition in successive CT slices. However the current implementation has been shown experimentally to provide an estimate of the modelled hip centre within a few millimetres of its actual position, which provides an adequate degree of accuracy for this type of application.

7.3.2 Pelvis Fixation

In order to generate an estimate for the hip centre position intra-operatively, the pelvis of the patient has to be immobilised. In a first attempt, the patient's pelvis was strapped to the operating table by means of surgical tape. However, this setup proved to be insufficient to provide the degree of fixation which is necessary for accurate hip centre estimation. Therefore, it was decided to use a set of auxiliary

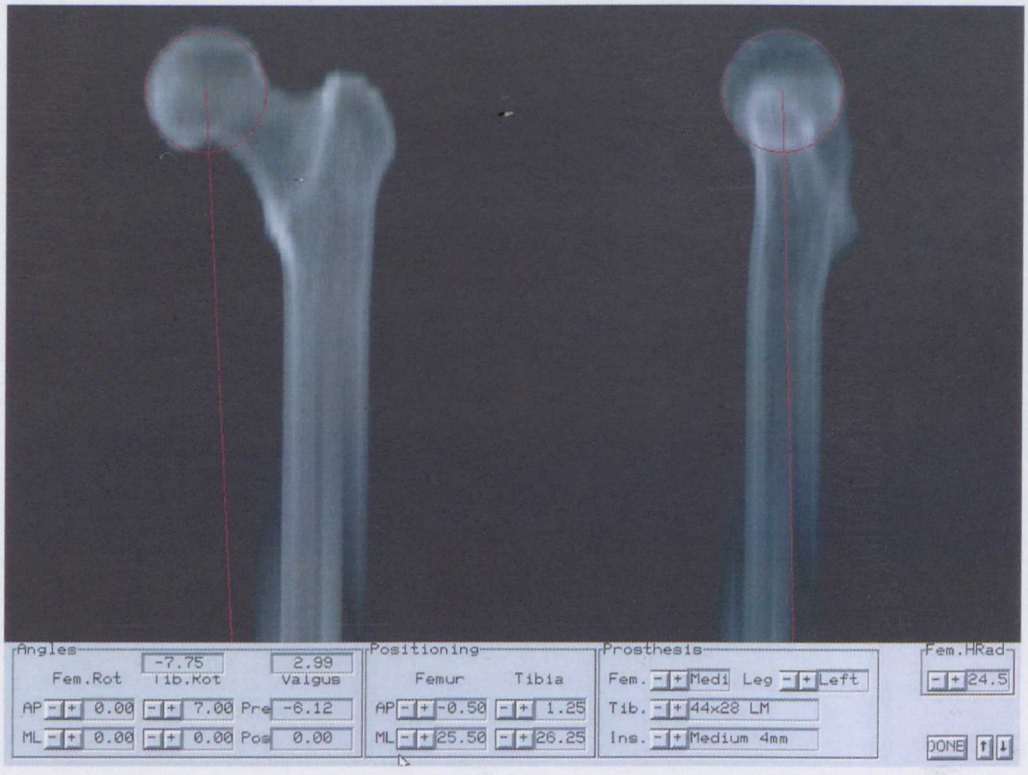


Figure 7.8: Pre-operative hip centre estimation.

bed clamps, which are tightened to the side rails and pushed against the patient's iliac crests, effectively pinning the pelvis down onto the operating table.

This setup, shown in Figure 7.9, allows the femur to be moved without any significant motion of the pelvis, which minimises a potentially large source of error.

7.3.3 Hip Centre Estimation

Intra-operatively, the hip centre estimation process is aided by a graphical user interface (GUI), which directs the surgeon through the acquisition process, and provides visual and quantitative feedback on the convergence process. Although this aspect of the procedure is not the author's work, it has been included here for the purposes of a complete description.

As described in Section 7.2.2, the functional centre of the hip can be obtained by fitting a sphere on points measured about a fixed distal location on the femur as the leg is moved in a grid while pivoting about the hip with the pelvis immobilised. In order to identify a unique point on the distal femur, a custom cutter insert was devised, which enables the femur to be moved while connected to the robot's end effector. The insert, illustrated in Figure 7.10, has a spherical ball-joint which, allowing complete freedom in three dimensions, enables the surgeon to move the leg through an adequate range of its working envelope.

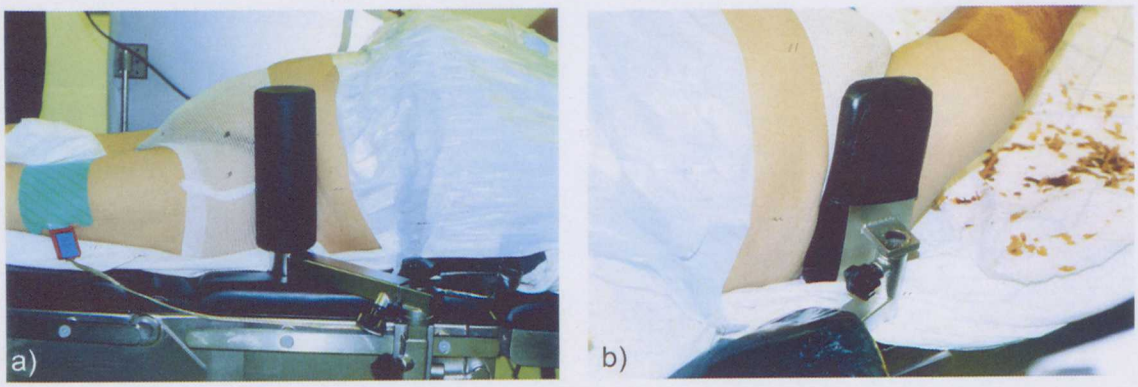


Figure 7.9: Intra-operative pelvis fixation by means of auxiliary bed clamps, tightened against the patient's left (a) and right (b) sides.

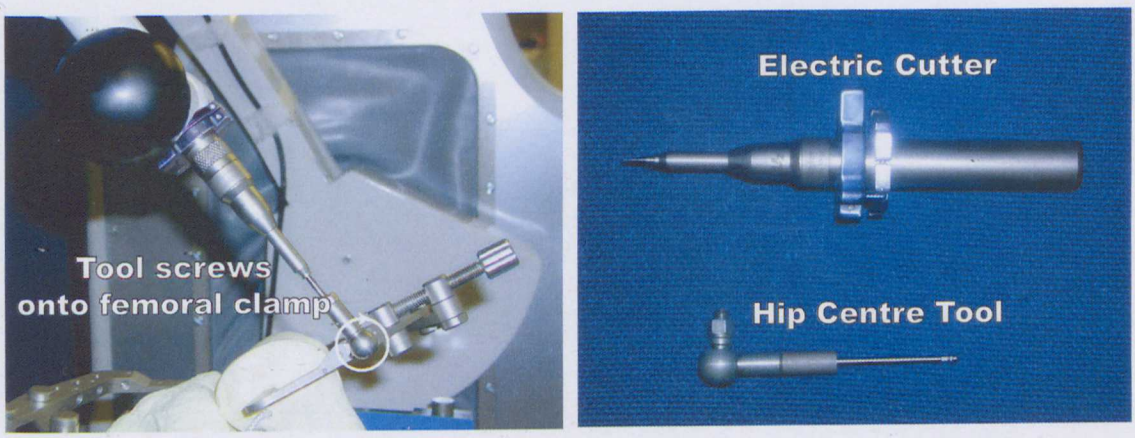


Figure 7.10: Cutter insert used to generate a set of measurements for the distal femur location during hip centre estimation.

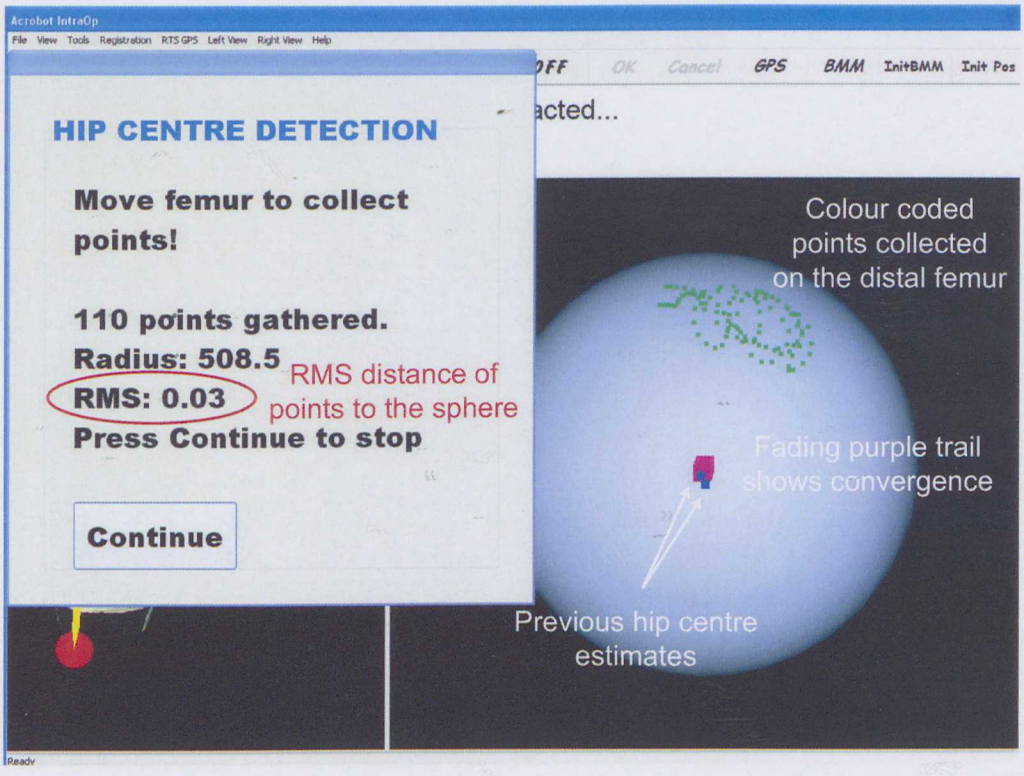


Figure 7.11: Intra-operative GUI for the hip centre estimation process.

For accurate hip centre estimation, it is important that a large percentage of the surface of the sphere which centres on the hip joint is covered. For this purpose, the intra-operative GUI graphically illustrates the acquisition process by plotting the points harvested on the distal femur against a $1cm$ radius circle centred about the last successful estimate. The display, illustrated in Figure 7.11, enables the surgeon to visually inspect the current progress to ensure coverage of all areas in the legs available workspace.

Points are collected by the software automatically at regular intervals, as the surgeon slowly moves the leg in a grid through as much of the available space as possible (Figure 7.12), while making sure the hip joint is not over stretched.

As more points are collected, the latest estimated centre of the sphere is plotted on screen in a clear purple colour. However, previous estimates are kept on screen in fading purple colours, illustrating a "trail" for the convergence process (Figure 7.11). When the trail generated by the fading centres disappears, which graphically illustrates that additional points do not shift the current hip centre estimate, convergence is reached.

The points are also colour coded proportionally to the error distance between each point and the sphere surface. The colour coded display, alongside the final RMS error of the distance of the generated point-set to the mapped surface, enables



Figure 7.12: Surgeon carefully moving the leg in a grid during *in vitro* testing.

the surgeon to qualitatively assess the convergence process.

In order to gauge the robustness of the current estimate, hip centres of all successful runs are plotted against each other on the same GUI. Visual inspection of the position and spread of different hip centre estimates can provide the surgeon with a confidence factor for the quality of the result. As illustrated in Figure 7.11, distances between successive runs can be approximated by evaluating their relative position against the grey circle, which has a $1cm$ radius, and is centred about the last acquired hip centre. At any point during the procedure, the display can be rotated in three-dimensional space in order to assess the quality of the acquired points and of successive hip centre estimates from different points of view.

7.3.4 Clamping and Initial Registration

After a valid hip centre estimate is obtained, the femur and tibia are fixed into position by means of the custom designed clamps described in Section 6.2.1. During the clamping process it is imperative that the patient's pelvis, which should be securely fixed to the operating table, is not moved with respect to the robot. In the current implementation, the hip centre will only be referenced to the clamping system (bone motion monitoring Section 4.4.2) after both bones have been immobilised. At this point, as many of the available conical holes on both femoral and tibial clamps as

possible are located by touching them with the robot end effector. As described in Section 4.4.2, these locations will provide the basis for the reference co-ordinate system.

Initial registration is carried out in the same way as in the original implementation, however the hip centre estimate, and respective modelled hip centre (defined at the pre-operative stage), are added as a set of paired points for the matching algorithm. Even though the addition of this set of points might result in a higher RMS error for the initial registration estimate, it ensures adequate initial alignment of the modelled and estimated hip centres. In turn, this process guarantees a good starting point for the Bounded ICP algorithm, after the initial translation to align modelled and estimated hip centres is carried out.

7.3.5 Distal Femur Point Collection

Point collection on the distal femoral surface is carried out through the conventional UKA incision. For the Bounded ICP algorithm the additional frontal stab-wound is not necessary. However, experimental results (Section 7.4) show that, for correct axial alignment, care must be taken to ensure a small number of points is collected in each one of the following three regions:

1. The front of femur.
2. The femoral notch.
3. The medial side of the medial femoral condyle.

A typical point-set covering the three main regions of interest is illustrated in Figure 7.13. As illustrated in Figure 7.13, with the new method, 15 to 20 points are sufficient for successful and robust registration of the femur.

7.3.6 Assessing Registration Accuracy in the OR

In the original registration algorithm, the final RMS of the distance of the mapped points onto the femoral surface was used to qualitatively assess registration accuracy. However, experimental testing has shown that the quality of the hip centre estimate is a much more robust indicator of performance for the Bounded ICP algorithm. Since points collected on the distal femur are only used to bound the distal end of the femur, a poor RMS value may describe poor correlation between the points and the surface, but may not reflect the registration quality for the two important varus/valgus and anterior/posterior components. For instance, a 1cm lateral translation of the hip centre will result in approximately 1.2^o of varus/valgus

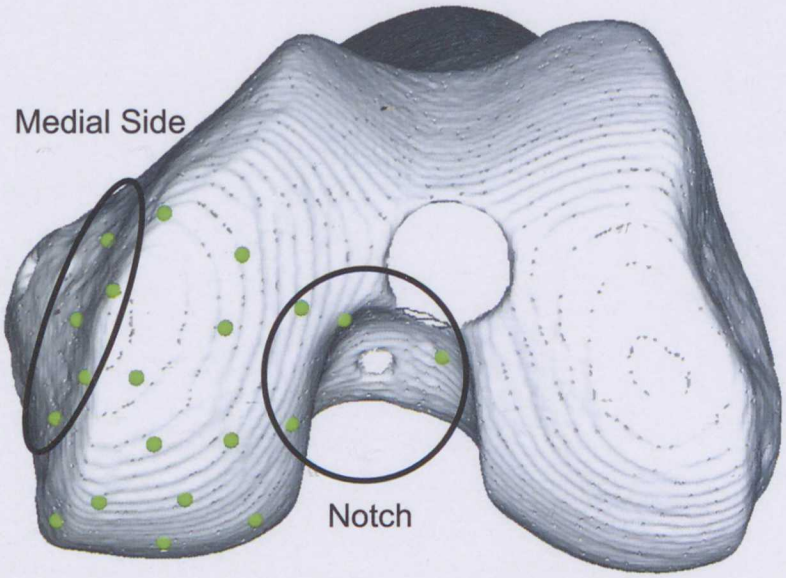


Figure 7.13: Typical femoral point-set for the Bounded ICP algorithm.

misalignment. Consequently, points on the distant femur will settle in the minimum position allowed by the fixed hip centre, which may have a significantly higher RMS value than that obtained if the same points were used with the original algorithm. Similarly, for a perfect hip centre, varus/valgus and anterior/posterior angles are very likely to have near zero misalignment, even though the RMS value may be relatively high because of poor correlation between the probe points and the surface. However, as will be shown in the next section, a large RMS error may be an indication of poor axial rotational alignment.

Therefore, to ensure accurate registration, a careful analysis of the quantitative and qualitative feedback produced by the GUI during hip centre estimation is important. The process should be repeated a number of times to show that the least squares spherical fit systematically converges to the same minimum.

7.4 Empirical Validation

The Bounded ICP algorithm was subjected to rigorous testing in order to ensure better results than those for the original algorithm could be consistently obtained. For this purpose the simulation platform described in Section 5.4.2 was modified in order to investigate the effect of initial error and hip centre estimation error on the algorithm's performance. This study was followed by a set of plastic bone trials aimed at ascertaining the viability of the new method for clinical use. Both simulation and plastic bone results are described in the following sections.

7.4.1 Simulation

The simulator was used to provide empirical validation for registration robustness, monotonic convergence, initial error sensitiveness and global minimum identification, under different noise levels, for different bone models and hip centre estimates. After considering the literature, available algorithms and the hardware limitations of the current robotic system, the hip centre estimate could be assumed to be within $1cm$ of the actual hip centre.

7.4.1.1 Simulation Software

In order to test the Bounded ICP algorithm, additional functionality for the simulation software described in Section 5.4.2.2 was required. Firstly, a means to test the effect of hip centre estimation error on registration outcome was required. For this purpose, a translational offset in the three principal directions can be manually added to the actual hip centre position by typing values (in mm) in the main screen. To simulate an initial estimation error, the same procedure, as described in Section 5.4.2.2, was used. However, only rotations are considered, since the modelled and estimated hip centres need to be initially aligned for the algorithm to converge correctly. In addition, all rotations are applied about the hip centre, in order to ensure a realistic representation of the error generated during initial registration. As the estimated hip centre is added to the pre-existing set of paired points used for landmark based initial registration, it is reasonable to assume that modelled and estimated hip centres will always be relatively close to each other at the start of the registration process. If rotations were made about the knee centre, as in the version of the simulator used to test the original algorithm, initial alignment of modelled and estimated hip centres would generate unrealistic initial errors. Noise can be added to the points collected on the distal femur as described in Section 5.4.2.3.

The updated simulation software, described in Figure 7.14, allows every aspect of the new algorithm to be manually tested. The red line connects the estimated knee centre, corresponding to the centroid of the distal points, to the estimated hip centre. The purple line connects the corresponding knee centre in model space to the modelled hip centre. The green line, connecting modelled and estimated hip centres, graphically illustrates the Bounded ICP algorithm's allowed translation along the axis of the leg. As the relationship between modelled and estimated co-ordinates is known during simulation, for perfect convergence the red and purple lines should coincide, and, for a perfect hip centre estimate, the length of the green segment should shrink to zero.

As illustrated in Figure 7.15, the algorithm can be manually stepped through, while the current solution can be nudged, pulled away from the hip centre, and ax-

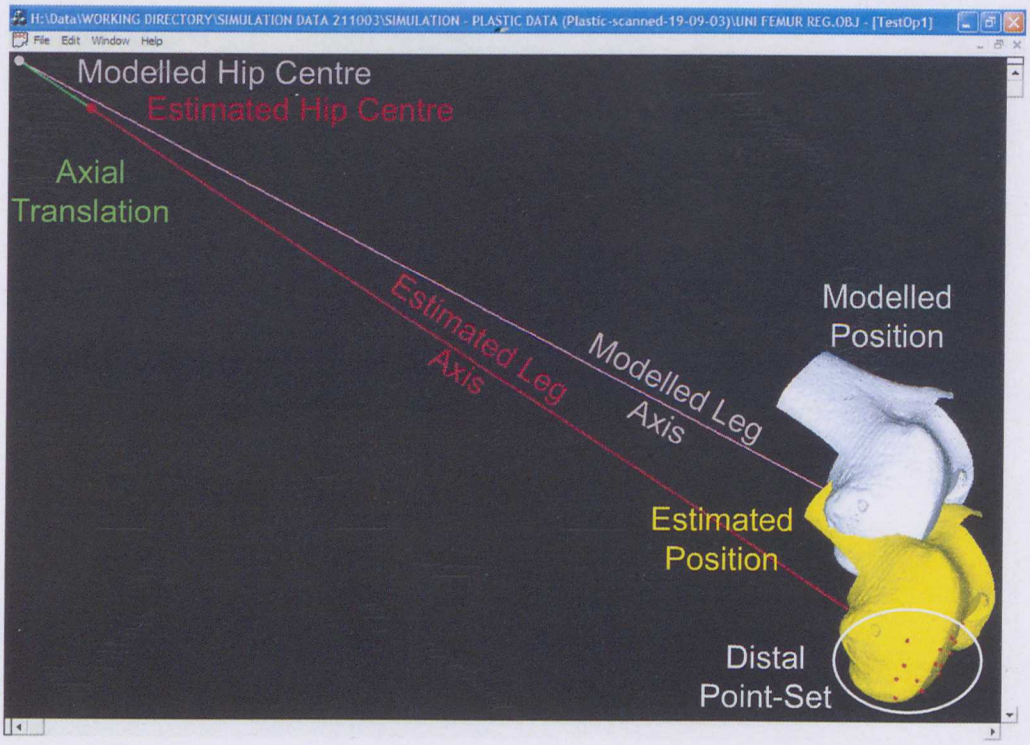


Figure 7.14: Updated simulation software screen-shot.

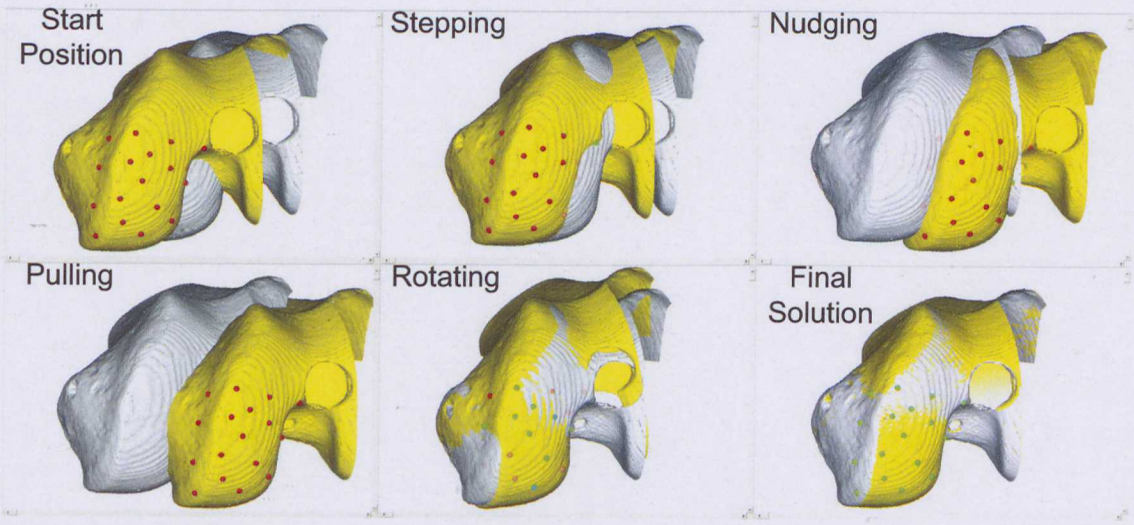


Figure 7.15: Examples of stepping, nudging, pulling, and axially rotating of the current registration estimate.

ially rotated (about the estimated leg axis). The ability to dissect the performance of the algorithm through simulation has allowed precise tuning of the algorithm's parameters, such as thresholds, maximum number of iterations and maximum perturbation values, for optimum performance.

7.4.1.2 Tests and Results

In order to develop a robust framework for the validation of the new algorithm, several experiments were carried out that enabled individual aspects, contributing to the registration outcome, to be tested individually. Furthermore, tests carried out on the original algorithm used for UKA (Section 6.3) were replicated for the Bounded ICP algorithm, in order for comparisons between the two techniques to be possible. The tests carried out were:

1. To provide empirical validation for monotonic convergence to the closest local minimum.
2. To assess the effect of hip error on accuracy of registration.
3. To evaluate the ability to predict registration outcome from prior knowledge of hip centre estimation accuracy.
4. To evaluate the effectiveness of local minima suppression, as described in Section 7.2.4.
5. To evaluate the performance of the algorithm for different surface models, point-set sizes, and maximum noise values.

Test results for a typical set of plastic bone scans have been included for descriptive purposes in the following sections. An equivalent analysis of patient CT generated surface models is included in Appendix F.

7.4.1.2.1 Monotonic Convergence Appendix E provides theoretical proof of monotonic convergence for the Bounded ICP algorithm, which is derived from the "Convergence Theorem" presented in [Besl and McKay, 1992]. However, Figure 7.16 graphically illustrates the convergence process for the implementation, written in C^{++}, that was subsequently used for simulation and plastic bone trials.

As illustrated by the trend of the black line in Figure 7.16, the Bounded ICP algorithm monotonically converges to a minimum after a number of iterations. Although the interaction between the two phases of the algorithm causes the convergence process to slow down and pick up speed, with a significant impact on execution time, the

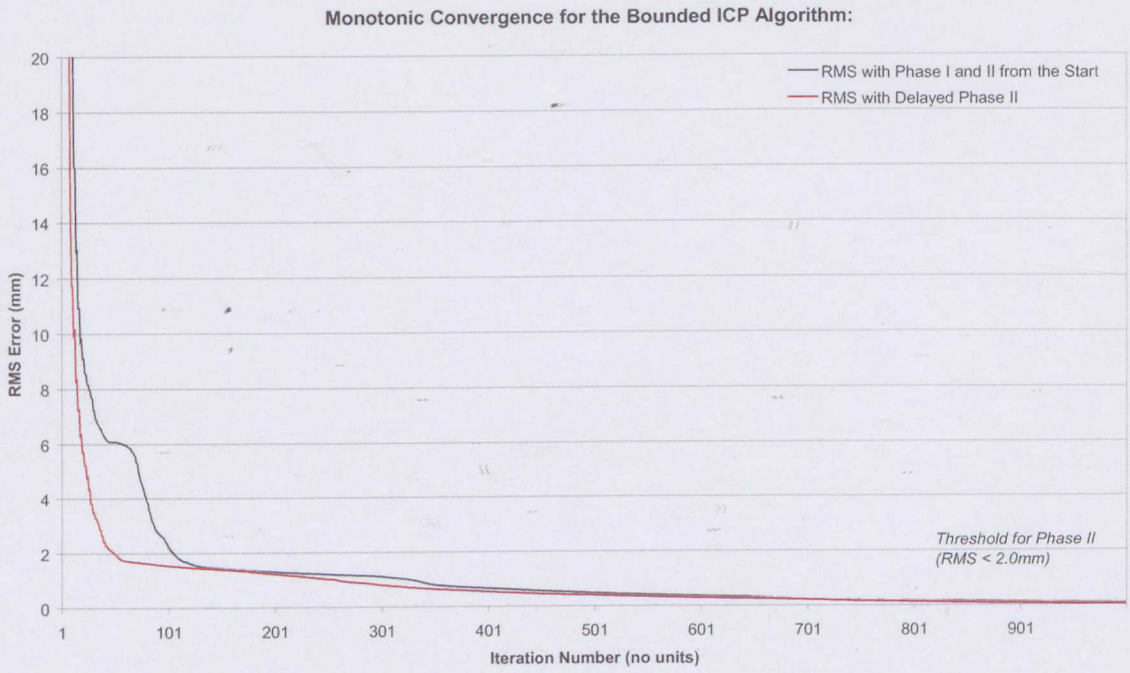


Figure 7.16: Monotonic convergence for the Bounded ICP algorithm.

RMS error of the current iteration never becomes greater than the error of the previous one. The algorithm currently requires a large number of iterations (1000-1500) to fully converge, as bounding one end of the leg axis used for convergence substantially decreases the momentum generated by the distance error between points and closest points, when applied to Phase II. Section 7.4.1.2.4 describes this issue in more detail.

Figure 7.16 also illustrates the significant benefits of delaying the execution of the second phase of the algorithm, as described in Section 7.2.4, until the RMS value falls below a predefined threshold. This is shown by the red line, which shows a much smoother trend compared to the black line and requires fewer iterations to reach a local minimum. More substantial enhancements to the algorithm can be implemented to decrease the number of iterations required for convergence, and are described as future work in Section 8.3.

7.4.1.2.2 Hip Error and Registration Accuracy In order to investigate the effect of hip centre estimation error on the accuracy of the Bounded ICP algorithm, the following experiment was carried out. The simulator was used to add known translational offsets to the simulated hip centre estimate, in known directions with respect to the leg axis. The maximum allowed translational error of 1cm was used to generate a set of 3D vectors in a spherical grid, resulting in error offsets of equal magnitude, but in different directions.

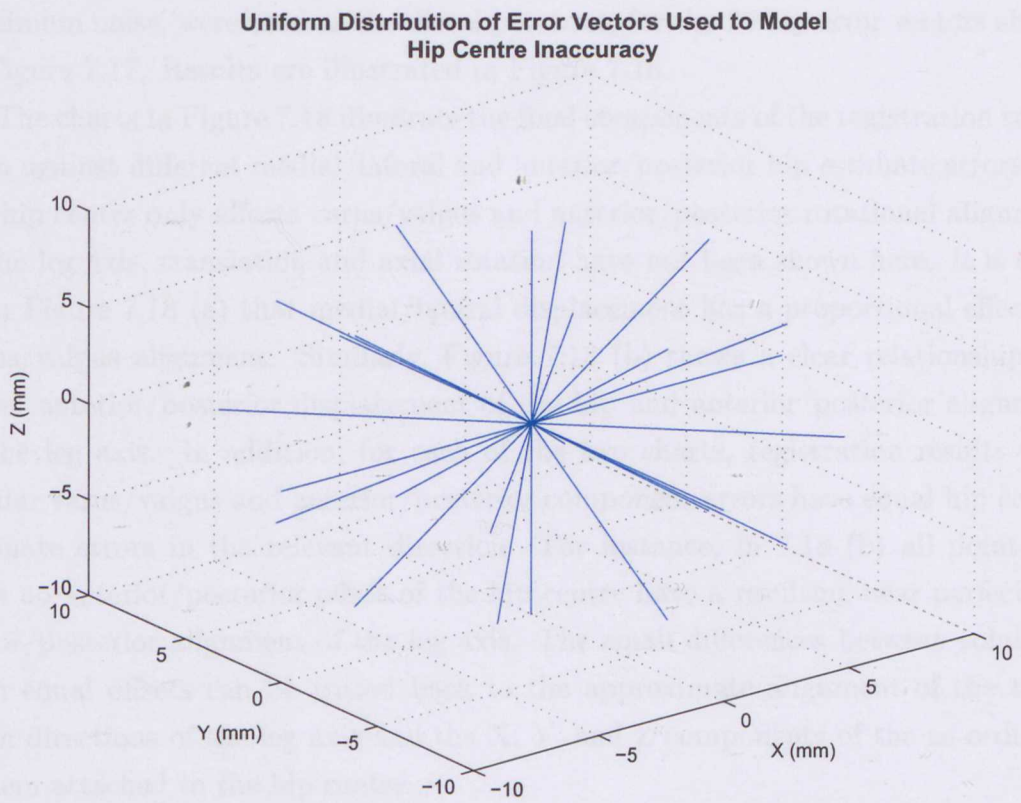


Figure 7.17: Set of 3D vectors describing possible hip centre estimate errors.

As illustrated in Figure 7.17, all error vectors (even though of equal magnitude) contribute in different proportions to the three principal directions X, Y, and Z, which, for clarity, have been approximately aligned with those describing the leg anatomy. Therefore:

- $\pm X$ Offset = Offset in the Medial/Lateral direction.
- $\pm Y$ Offset = Offset in the Anterior/Posterior direction.
- $\pm Z$ Offset = Offset in the Proximal/Distal direction.

The aim of the experiment was to prove that each component of the offset would have a direct effect on the relevant degree of freedom of the registration transform. An offset in the medial/lateral direction would introduce an error in the resulting registration transform for varus/valgus alignment. Similarly, anterior/posterior displacement of the hip estimate would produce corresponding anterior/posterior misalignment of the leg axis. Proximal/distal displacement of the hip estimate should have virtually no effect on registration outcome, as it can be compensated for by translation along the leg axis as the algorithm is executed.

A worst case scenario was used to evaluate the performance of the algorithm for different hip centre estimate errors. 25 points, collected in regions I-III, with 1.5mm

maximum noise, were used as the distal point-set, for the 26 hip error vectors shown in Figure 7.17. Results are illustrated in Figure 7.18.

The charts in Figure 7.18 illustrate the final components of the registration transform against different medial/lateral and anterior/posterior hip estimate errors. As the hip centre only affects varus/valgus and anterior/posterior rotational alignment of the leg axis, translation and axial rotation have not been shown here. It is clear from Figure 7.18 (a) that medial/lateral displacement has a proportional effect on varus/valgus alignment. Similarly, Figure 7.18 (b) shows a clear relationship between anterior/posterior displacement of the hip and anterior/posterior alignment of the leg axis. In addition, for each of the two charts, registration results with similar varus/valgus and anterior/posterior component errors have equal hip centre estimate errors in the relevant direction. For instance, in 7.18 (b) all point-sets with no anterior/posterior offset of the hip centre have a resulting near perfect anterior/posterior alignment of the leg axis. The small differences between solutions with equal offsets can be traced back to the approximate alignment of the three main directions of the leg axis and the X, Y, and Z components of the co-ordinate system attached to the hip centre.

This experiment was carried out for a number of other point-sets and bone models, with virtually identical error distributions. These results show a distinct correlation between the direction of the error of the hip centre estimate and final varus/valgus and anterior/posterior alignment of the leg axis, demonstrating the Bounded ICP algorithm's ability to shift the requirements for an accurate registration away from the quality of the distal point-set. Experiments described in the following section provide further backing for this statement.

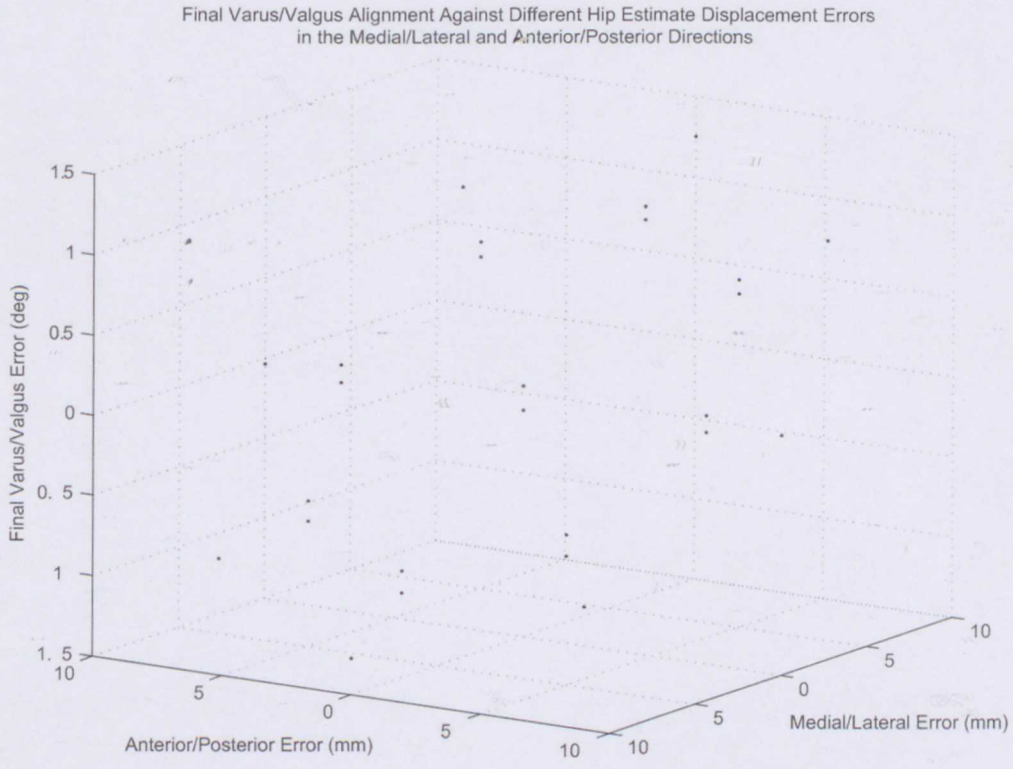
7.4.1.2.3 Predicting Registration Outcome Results described in the previous section provided the grounds for an experiment aimed at ascertaining whether varus/valgus and anterior/posterior components of the registration transform could be accurately predicted from prior knowledge of the quality of the hip centre estimate. Even though such knowledge could only be available under simulated conditions, probable registration outcome could be predicted intra-operatively by a careful analysis of the qualitative information generated during the hip centre estimation procedure (Section 7.3.6).

Let $\overrightarrow{l}$ define the vector linking the modelled hip centre, H_M, and the centroid of the distal point-set in model space, K_M, as illustrated in Figure 7.3. Then:

$$\overrightarrow{l} = K_M - H_M \tag{7.23}$$

Now, let the hip estimate error in model space be described as a vector $\overrightarrow{t}$ with

(a)



(b)

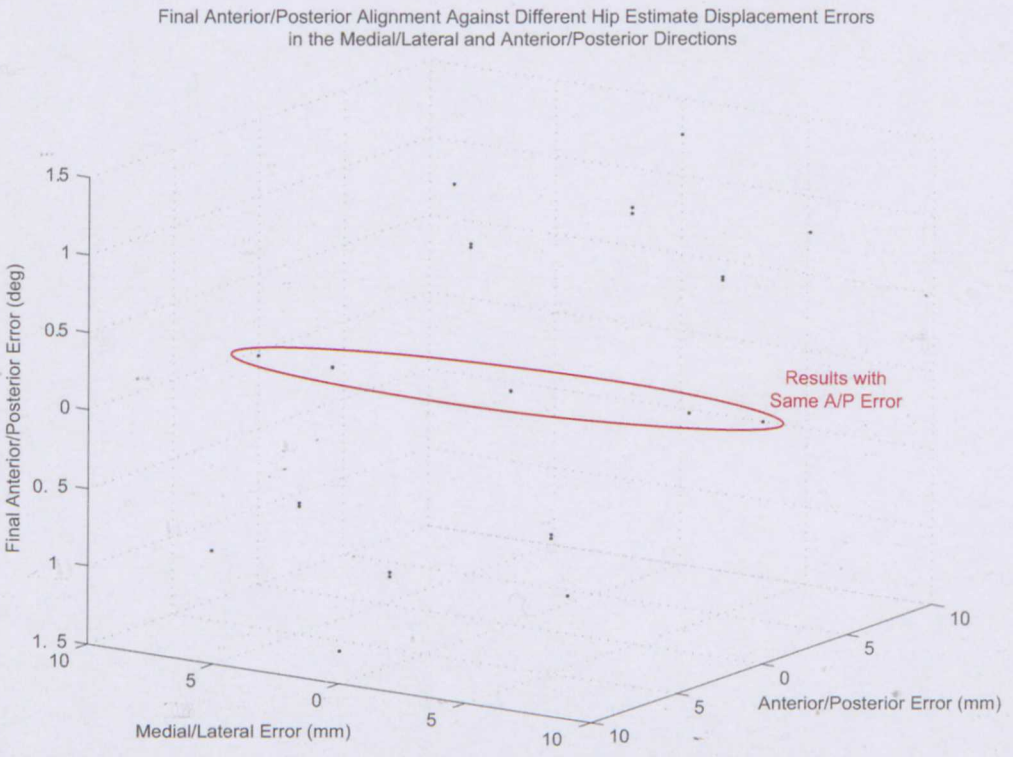


Figure 7.18: Final error distribution for the Varus/Valgus (a), and Anterior/Posterior (b), components of the registration transform for different hip centre estimate errors.

components in the three principal directions. Then:

$$\overrightarrow{dl} = \overrightarrow{l} - \overrightarrow{t} \tag{7.24}$$

represents the leg axis displaced by the hip error. The resulting rotational error, generated by fixing the estimated hip centre in the offset position, can be approximated by a rotation of an angle, Θ, about an axis, $\overrightarrow{a}$, perpendicular to both $\overrightarrow{l}$ and $\overrightarrow{dl}$:

$$\Theta = acos\left(\frac{\overrightarrow{l} * \overrightarrow{dl}}{\left|\overrightarrow{l}\right|\left|\overrightarrow{dl}\right|}\right) \tag{7.25}$$

$$\overrightarrow{a} = \overrightarrow{l} \times \overrightarrow{dl} \tag{7.26}$$

Splitting the transformation matrix $R = Rot(\Theta, \overrightarrow{a})$ into the three principal direction of the leg axis, namely varus/valgus, anterior/posterior and axial, will result in two angles and a zero value, since R does not have an axial component. These two angles describe approximate values for varus/valgus and anterior/posterior alignment of the leg axis after registration, assuming perfect alignment of the distal point-set. These values only relate to $\overrightarrow{t}$, the hip centre error, and the distance between the hip centre and the centroid of the distal points.

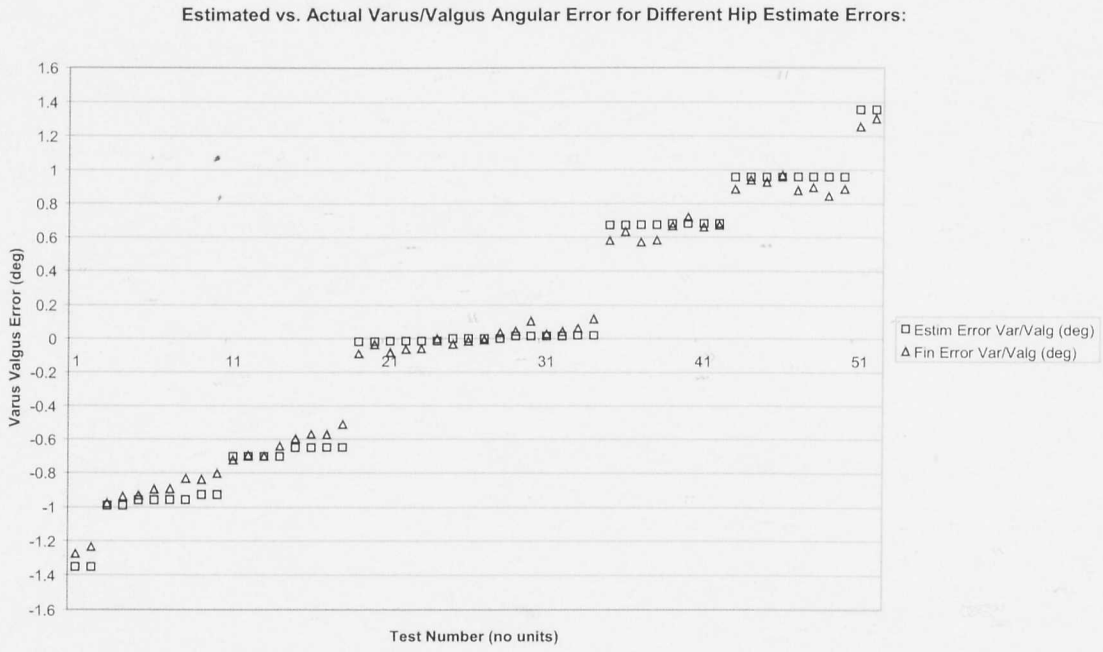
The experiment described in the previous section was repeated using two random point-sets with 15 and 25 points per point-set respectively, and 1.5mm maximum random noise. The Bounded ICP algorithm was then executed 26 times for each point-set, with each of the hip error offsets illustrated in Figure 7.17. Results are shown in Figure 7.19.

For convenience, both datasets have been sorted in ascending order, although neighbouring tests bear no relevance with each other. The results presented in these charts illustrate that in all test scenarios, estimated and actual values for both varus/valgus and anterior/posterior components lie within 0.2mm of each other, providing further backing for the robustness of the Bounded ICP algorithm in predicting and bounding registration outcome.

7.4.1.2.4 Minima Suppression In order to validate the global minimum identification procedure described in Section 7.2.4, the same experiment described in Section 5.4.2.5.2 for the optimised ICP algorithm was carried out. The aim of the experiment was to prove that the global minimum for any given point-set could be reliably identified, regardless of the quality of the initial estimate.

A typical point-set with 1.5mm maximum random noise was used to describe the distal femur, alongside a random hip centre estimate within a 1cm radius sphere

a)



b)

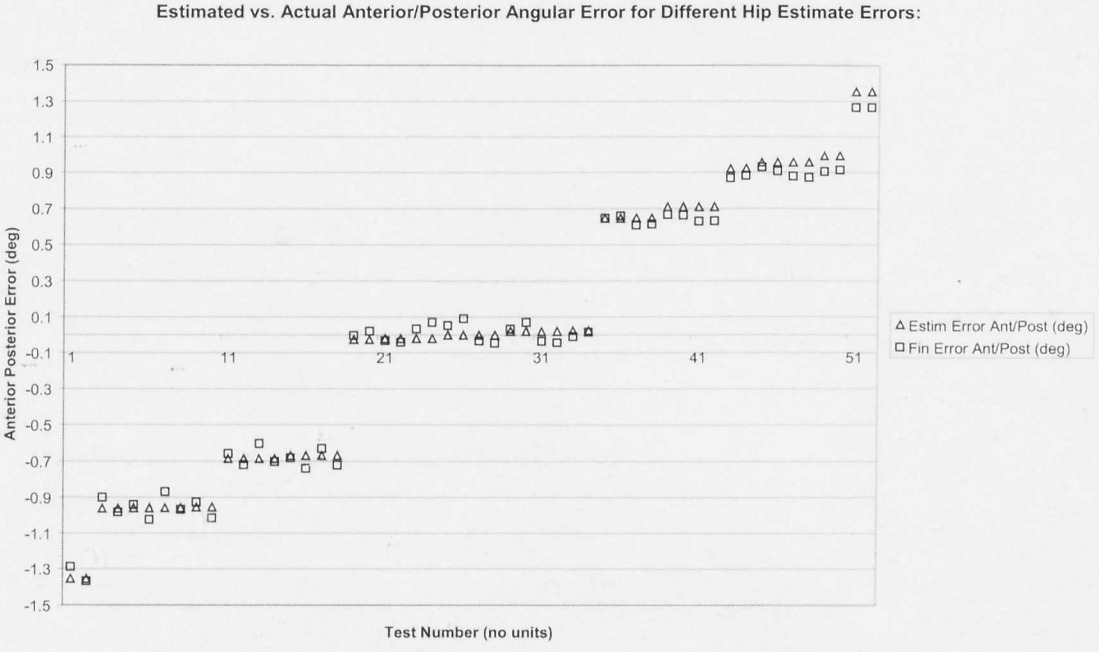


Figure 7.19: Estimated versus actual registration accuracy, in terms of Varus/Valgus (a), and anterior/Posterior (b) components.

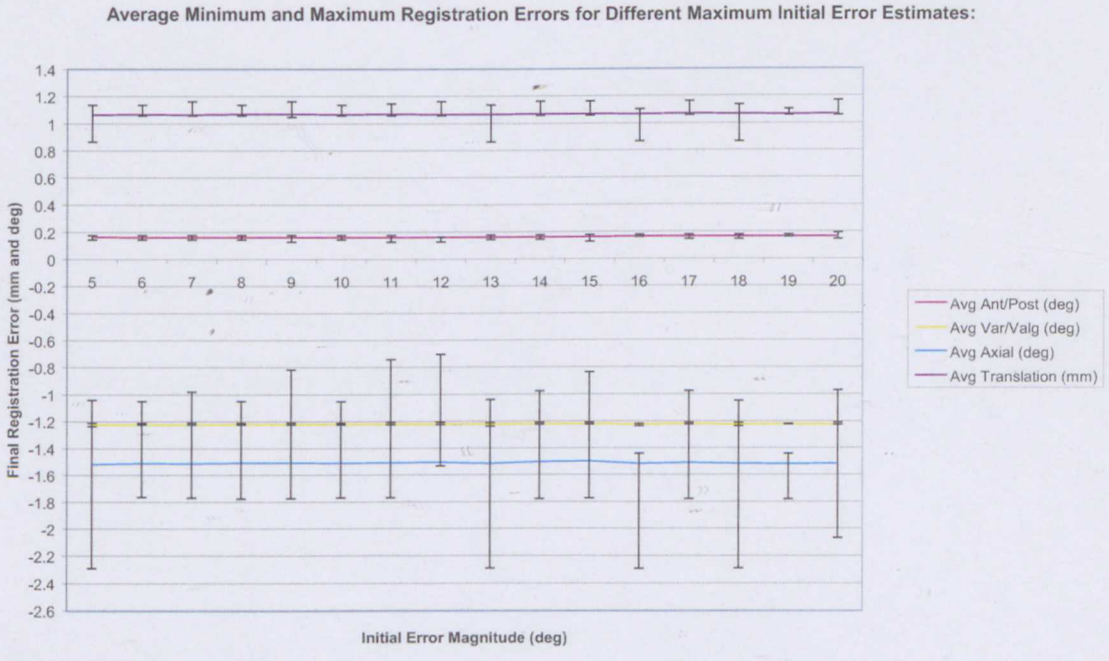


Figure 7.20: Error distribution in terms of anterior/posterior, varus/valgus, axial, and translational alignment for different initial error states and $1.5mm$ maximum noise.

of its modelled counterpart. The generated dataset was then tested for a number of different initial estimate errors, and the resulting registration outcomes compared. 200 random rotational error matrices for every unit increment between 5 and 20 degrees were used to shift the point-set away from the modelled surface, as described in Section 5.4.2.2. This resulted in 16 sets of 200 initial transformation states, which were set as the starting point for the Bounded ICP algorithm. Results are illustrated in Figure 7.20.

By examining the chart in Figure 7.20, it is clear that the characteristics of the suppression mechanism, used for the new algorithm, present significant differences from the original implementation described in Chapter 5.4.2.5.2 (Figure 5.15). Each of the 3200 initial error states produces virtually the same value for the varus/valgus and anterior/posterior alignment, which closely match the predicted values of 1.3^o and 0° respectively for the chosen hip centre estimate error. Therefore, even for unrealistic initial estimates, the algorithm systematically identifies correct alignment of the leg axis, which, as described in the previous section, is directly related to the quality of the hip centre estimate.

Correct identification of the varus/valgus and anterior/posterior components of the registration transform suggests that the correct global minimum is always identified. However, Figure 7.20 shows large maximum and minimum deviations from the

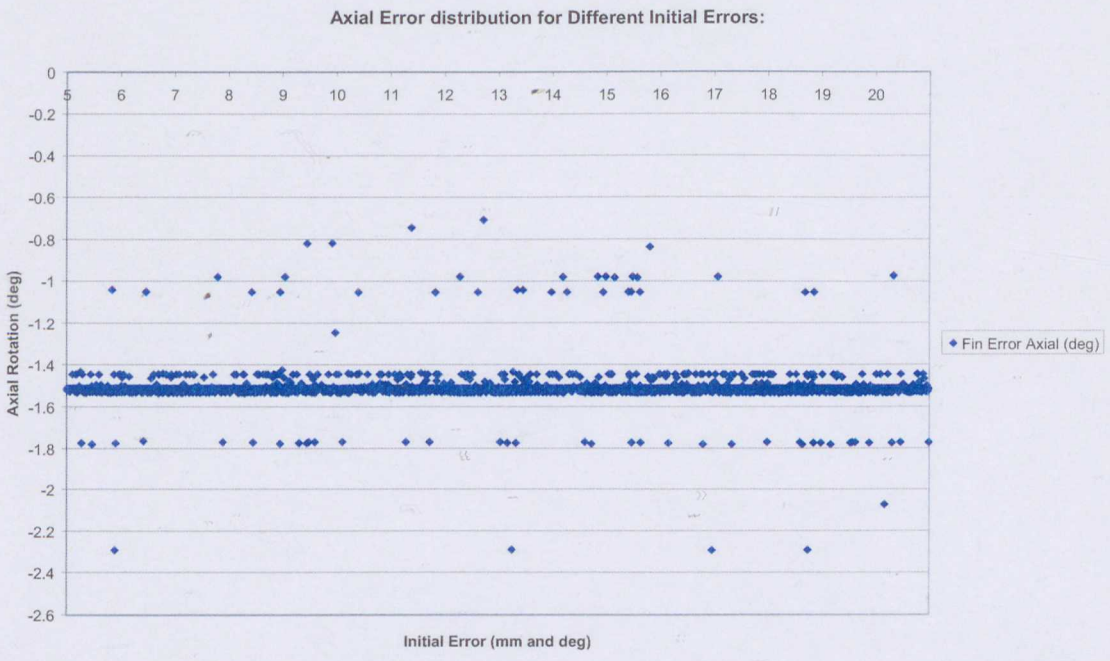


Figure 7.21: Distribution of the axial rotational errors for different initial states.

mean on the two plots describing axial rotation and translation. Figure 7.21 illustrates how the minima for axial rotation lie within a 1° envelope around the mean i.e. the value with the greatest probability of occurrence. Over 90% of the test results lie within 0.2^o of the mean, which suggest that for a significant proportion of the test cases virtually the same solution is found.

However, these spikes illustrate local minima around the global minimum, which do not seem to have any effect on the two components of the leg axis alignment. Plotting these spikes against their corresponding RMS error (Figure 7.22) helps to identify the reason behind the failure of the minima suppression mechanism to distinguish between solutions that apparently lie within the same class of minima. All local minima identified by the spikes on the axial rotational error plot have virtually the same RMS error.

It is apparent from these results that the Bounded ICP algorithm suffers from a weakness, the nature of which may be conceptually traced back to the very structure of the convergence process. A poor quality point-set, such as the one used for this experiment, will provide a poor representation of the surface it describes. As illustrated by the experiments carried out on the original algorithm (Section 5.4.2.5), if the convergence process was completely unbounded, there would be a unique registration transform that would generate a clear minimum, based on the RMS error of the distance of each probe point and the mapped surface. However, restricting the motion of one end of the leg axis forces the algorithm to converge to a solution

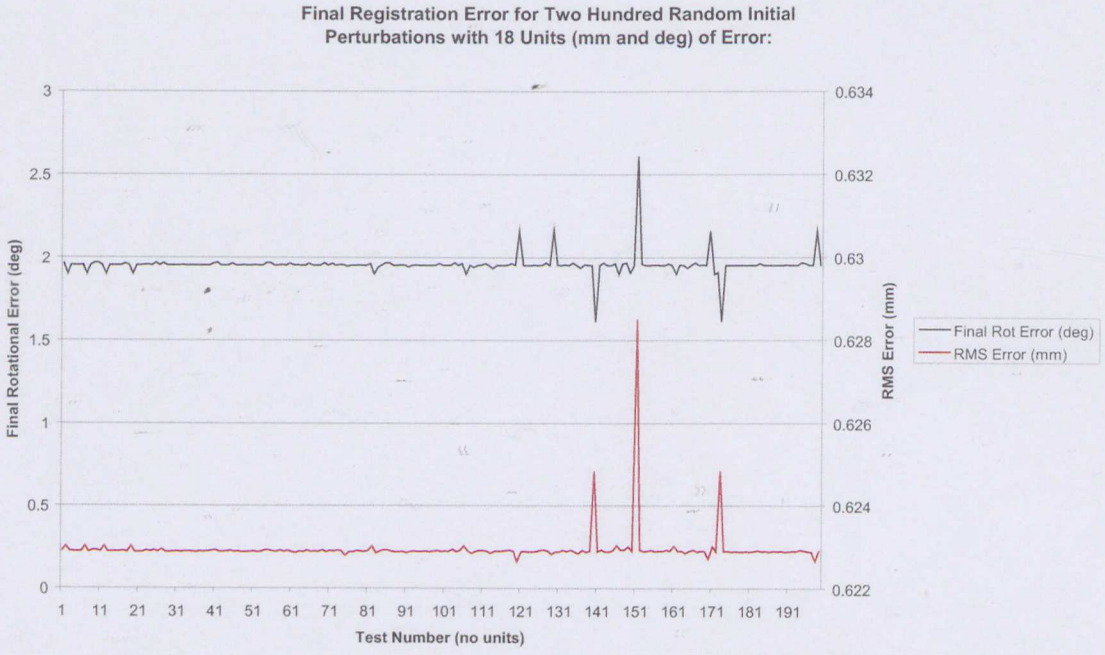


Figure 7.22: Relationship between RMS error and final rotational alignment for different local minima.

which, while providing a low RMS error value, is partially governed by the constraints defined by the estimated hip centre position. For a poor quality point-set, where on average all points will be either embedded in or floating over the surface, effectively fixing varus/valgus and anterior/posterior angles has the unavoidable effect of generating a large number of "equivalent" minima, with near identical leg axis alignment, but different translational and axial values. Translation and axial rotation effectively complement each other, producing a whole class of "equivalent global minima" based on the RMS error. Therefore, in order to identify the best solution for axial rotational alignment, a more sophisticated selection technique is required, which will be an important area for future work.

In order to provide some backing for this explanation, the experiment described above was repeated with an identical point-set with 0.8mm random noise. Since both hip error and point distribution are identical, a decrease in random noise should result in a range of global minima with tighter upper and lower thresholds. Results are shown in Figure 7.23.

Comparing Figure 7.20 and Figure 7.23 it is apparent that a better quality point-set results in a tighter range of equivalent minima, generated by the interaction of the axial rotational component and the translational component. These results show that better correspondence between the point-set and the surface improves axial rotational alignment, but has virtually no effect on the other rotational components

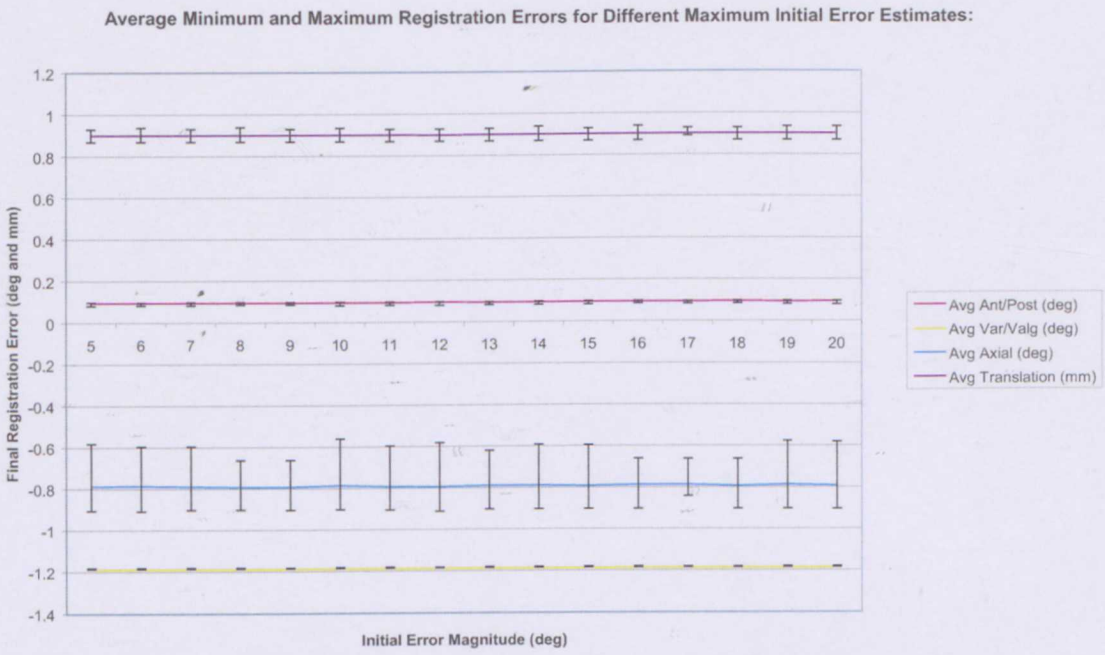


Figure 7.23: Error distribution in terms of anterior/posterior, varus/valgus, axial, and translational alignment for different initial error states and $0.8mm$ maximum noise.

of the registration transform. The following section provides further evidence on the impact of point-set quality on axial alignment.

7.4.1.2.5 Performance Evaluation In order to create a robust infrastructure for comparisons between the original ICP algorithm and the Bounded ICP algorithm to be made, the experiment described in Section 6.3.3.1.2 was replicated using the new method to generate the results. The same set of point-sets used in Section 6.3.3.1.2 (without stab-wound access, Figure 6.26) was used to describe the distal femur, while the hip centre error was chosen in a random direction with 1cm magnitude, as described in Section 7.4.1.2.2. The resulting set of point-sets is therefore identical to that used in Section 6.3.3.1.2, with the addition of a realistic hip centre estimate needed for the Bounded ICP algorithm. In practice, this experiment illustrates the difference in registration accuracy between the two methods for the same point-set and a worst case scenario hip centre estimate. Results for this experiment are graphically illustrated in Figure 7.24.

By comparing the data presented in Figure 7.24 with the results illustrated in Figure 6.26 for the original algorithm, a number of observations can be made. Clearly, the Bounded ICP algorithm's performance in term of varus/valgus and anterior/posterior alignment drastically differs from that described by the equivalent

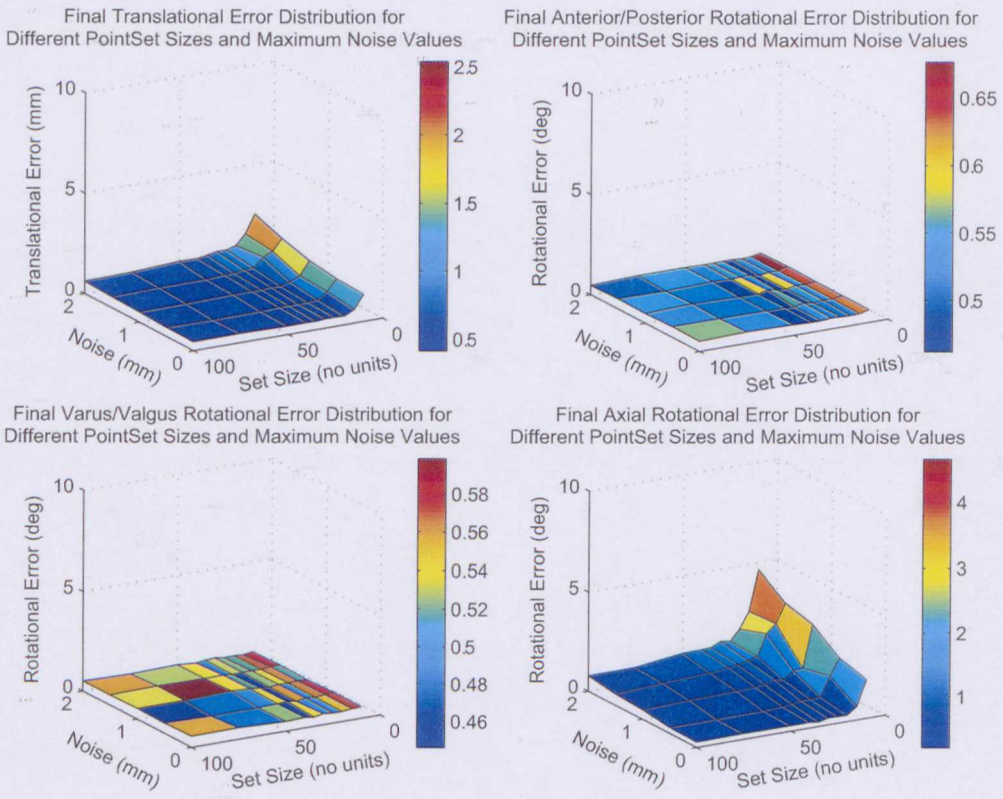


Figure 7.24: Registration accuracy for the Bounded ICP algorithm in terms of varus/valgus, anterior/posterior, axial, and translational components for different point-set sizes and maximum noise values.

charts in Figure 6.24. Regardless of point-set size and maximum noise value, charts for these two components of the error matrix can be approximated to a plane. More specifically, the two planes lie at approximately 0.6^o rotational error, which coincides with the average rotational error generated by a $1cm$ translational offset of the hip centre estimate, if the random direction for the offset follows a normal distribution. Intuitively, if all randomly generated offsets lie on a 1cm radius sphere, on average each component will be affected by approximately half the magnitude of the error vector. For a $1cm$ error magnitude, the average varus/valgus error will be that corresponding to $5mm$ medial/lateral displacement for the length of femur used for the experiment i.e. approximately 0.6^o. Similarly, a media/lateral offset of $\pm 5mm$ would result in the same varus/valgus error of 0.6^o.

The translational and axial components of the registration error matrix show a similar trend to that described in Section 6.3.3.1.2 for the original algorithm. Both translational and axial alignment deteriorate as a function of the quality of the distal point-set. A few, noisy points are clearly not enough to accurately describe a surface, therefore a reasonable point set is required to guarantee good axial alignment. Furthermore, a comparison of the axial rotational errors in Figure 7.24 and Figure 6.24 provides further evidence for the weakness of the Bounded ICP algorithm described in the previous section. Since the new algorithm restricts the movement of one end of the leg axis, noise in the point-set results in large number of equivalent minima, with near identical RMS error values, but different axial rotation - translation pairs. Although these minima lie within an envelope, the range of which is defined by the extent of noise in the point-set, this peculiar characteristic of the Bounded ICP algorithm results in a "bumpier" chart for axial rotational alignment compared to the original algorithm.

7.4.2 Registration with a Plastic Phantom

In order to corroborate the simulated results described in the previous section, a set of tests was carried out on plastic-phantoms, which were CT scanned and planned for using the pre-operative planning software of the ACROBOT II System. The two main aims of this study were:

1. To assess the quality of the hip centre estimate obtained with the intra-operative setup described in Section 7.3.

2. To prove that the results obtained in simulation could be reliably reproduced on plastic bones.

The following sections provide a brief description of the experimental setup, the method used and the results obtained for these experiments.

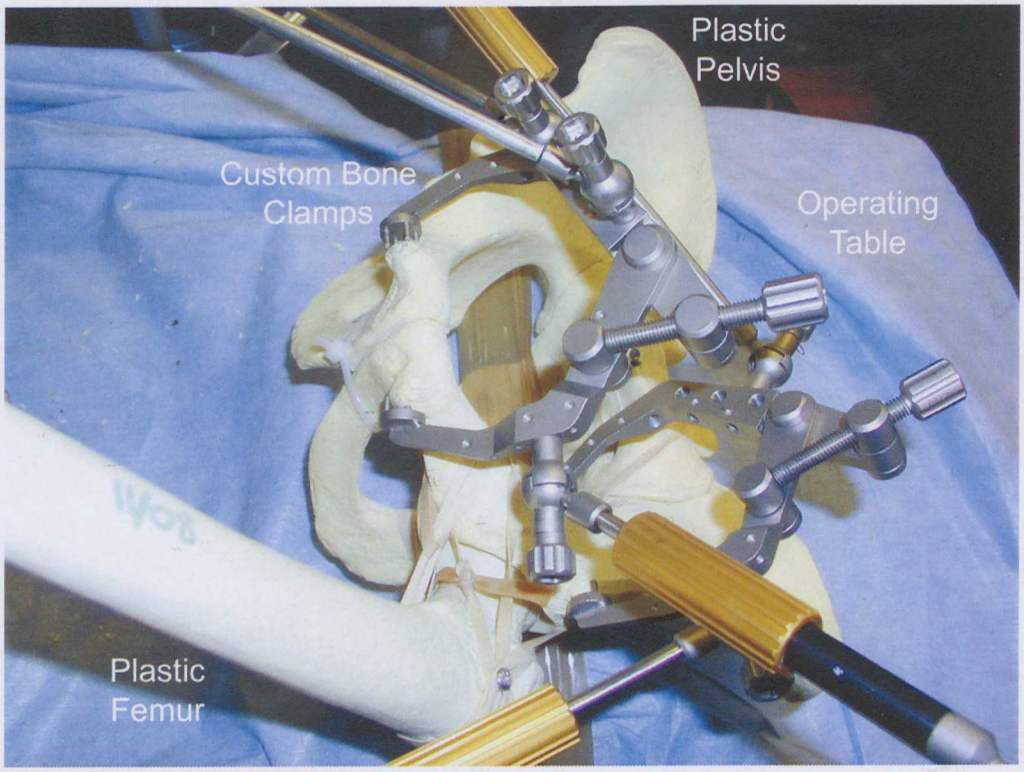


Figure 7.25: Plastic pelvis securely fixed to the operating table by means of custom designed bone clamps.

7.4.2.1 Experimental Setup

In order to reproduce the motion of a hip joint under experimental conditions, a plastic pelvis was fixed to the operating table, as described in Figure 7.25.

Although the immobilised pelvis provided rough placement for the socket of the hip joint, a hip replacement cup was implanted in the plastic bone in order to guarantee smooth motion of the femoral head during the point collection process. To improve the spherical motion of the "ball-and-socket" setup described above, restraining rubber bands were placed around the neck of the femur attached by a piece of string, as described in Figure 7.26.

Although rather primitive, this setup provides nearly uniform distribution of the forces generated by the rubber bands on the hip cup, resulting in smooth motion of the femur, with little unwanted translational displacement of the functional centre of the rotation. The clamping system described in Section 6.2.1 was used to fix the femur in place after completion of the hip centre estimation procedure, to allow precise point collection of the distal femoral dataset. All data generated during the experiments was logged to file, to enable post-processing of the results.

Figure 7.27 shows the experimental layout for the hip centre estimation process (a), and distal point collection process (b). The intra-operative graphical user in-

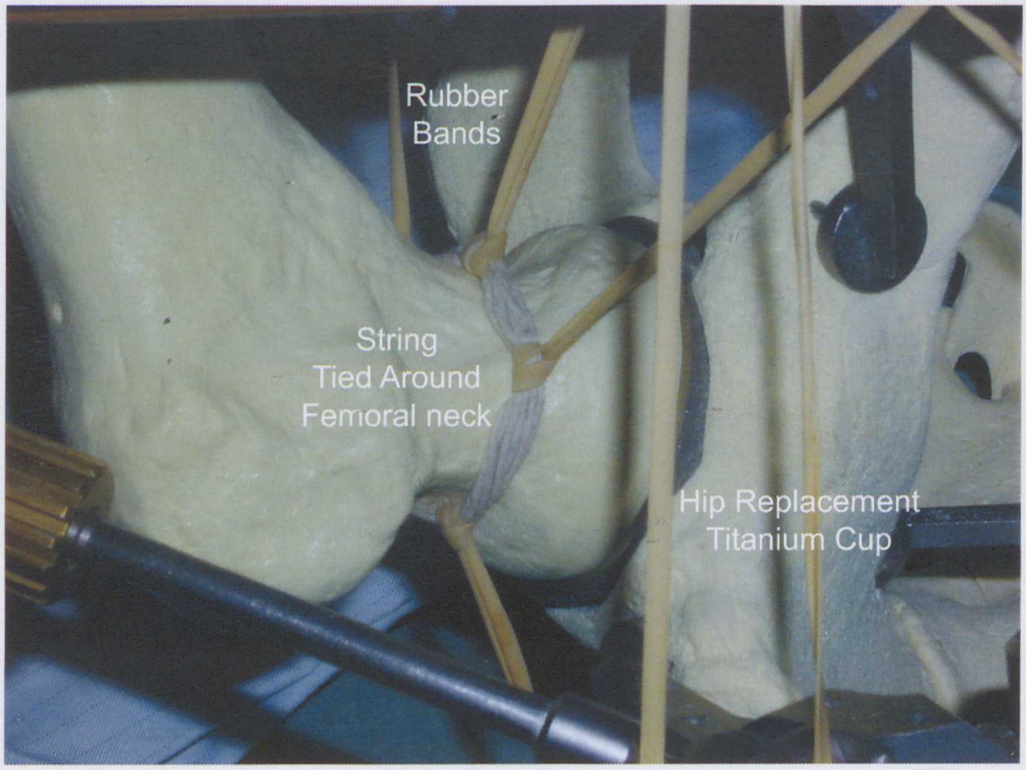


Figure 7.26: "Ball-and-socket" setup of the pelvis and femoral head.

terface was used to guide both steps of the acquisition process, which included an average of 400 points for hip centre generation, and 20 surgically accessible points for the distal dataset.

7.4.2.2 Tests and Results

In order to assess the quality of the hip centre estimate generated with the ACROBOT II System, both the precision and accuracy of the estimation procedure had to be evaluated. For this purpose, 10 consecutive hip centre estimates were taken for the same experimental setup, which produced 10 different approximations of the same hip centre position. The spread of these estimates would provide a measure for the precision of the estimation process, while the deviation of their mean from the true hip position would define its accuracy.

In order to obtain a value for the actual hip centre position, a reference registration transformation matrix was used to transform the hip centre estimate in model space. The reference transform was generated by subsequently fixing the femur in position and carrying out a robust registration procedure, using all of the available surface, as described in Section 5.4.3.2. This registration transform accurately describes the relationship between model and robot space, and can be used to transform each hip estimate, measured in robot space, so that it can be com-

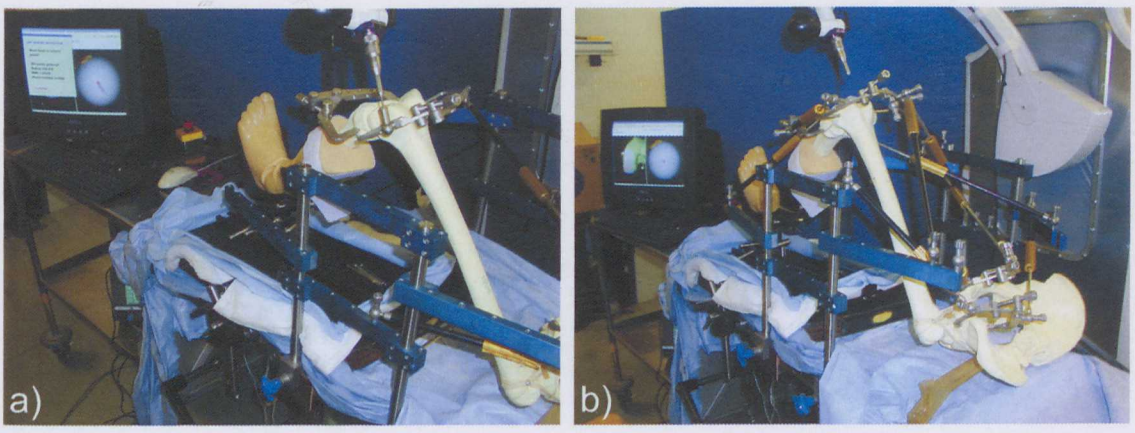


Figure 7.27: Experimental layout for the hip centre estimation (a) and point collection process (b) during plastic bone testing of the Bounded ICP algorithm.

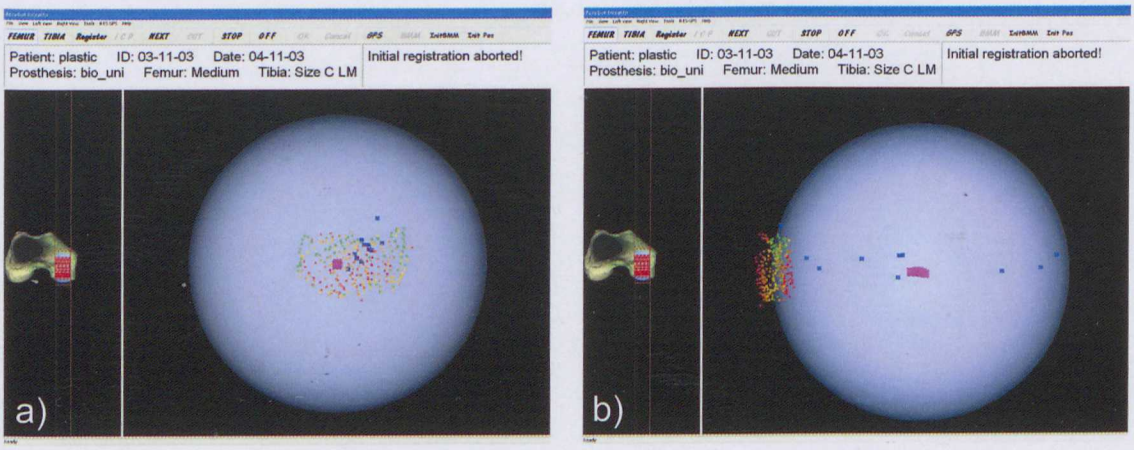


Figure 7.28: Screen-shot of the intra-operative GUI illustrating the distribution of 10 consecutive hip centre estimates. The picture shows both axial (a) and lateral (b) views.

Hip Centre Estimates (mm)			Real Error Distribution (Estimate - Real)		
M/L	*A/P*	*P/D*	*Hx - Rx*	*Hy - Ry*	*Hz - Rz*
103.16	105.18	592.79	1.17	3.18	-8.12
103.39	108.13	600.68	1.39	6.13	-0.23
104.20	107.40	598.15	2.21	5.40	-2.75
104.70	109.56	600.22	2.71	7.56	-0.69
105.25	107.58	595.27	3.26	5.58	-5.63
103.15	110.13	607.04	1.15	8.13	6.14
102.44	110.64	609.51	0.44	8.64	8.60
103.51	107.79	600.54	1.52	5.79	-0.36
101.51	110.12	610.57	-0.49	8.12	9.66
103.64	106.97	600.89	1.65	4.97	-0.01
Mean Hip Centre			***Minimum and Maximum***		
103.48	108.50	601.64	-0.49	3.18	-8.12
Real Hip Centre in M Space			3.26	8.64	9.66
102.00	102.00	600.90	***Worst Case Error (mm)***		
Mean Hip Error (mm)			**3.26**	**8.64**	**9.66**
-5.31	**-5.03**	**11.11**	***Estimated Effect (deg)***		
Standard Deviation			*Varus/Valgus*	*Anterior/Post*	*Axial*
1.07	**1.73**	**5.84**	**0.38**	**1.00**	//

Table 7.1: Accuracy and precision of the hip estimation procedure developed for the ACROBOT II System for ten consecutive hip centre estimates.

pared to the actual hip position defined during the pre-operative planning process. As the model co-ordinate system is purposely aligned with the anatomical axis of the femur, the effect of the measured errors in the three principal directions can be readily evaluated. Table 7.1 shows the results.

All 10 hip centre estimates have been transformed into model space using the reference registration transform described above. From these results a number of observations can be made about the accuracy and precision of the estimation process. Firstly, it is important to note that any error offset of the hip centre estimate in the proximal/distal direction has virtually no effect on registration outcome, as it is almost completely compensated for by translation along the leg axis during the algorithm's convergence process. Therefore the proximal/distal component of the error vector has been omitted from the following considerations. The standard deviation for the components of the error vector show that, in over 95% of cases, the estimate falls within a 1cm radius sphere of the mean. The difference between the mean and real hip centre (obtained from CT data), which provides a measure for the accuracy of the estimation process, shows approximately 5mm of medial/lateral and anterior/posterior displacement of the hip centre. However, this difference includes the error generated during the pre-operative definition of the functional centre of the hip from CT data, which should ideally be removed from the results in order to isolate the accuracy of the estimation procedure.

		Test #									
		1	*2*	*3*	*4*	*5*	*6*	*7*	*8*	*9*	*10*
Hip Error Comp (mm)	*M/L*	-1.169	-1.646	-1.391	-2.206	-2.705	-3.257	-1.153	-0.443	-1.517	0.487
	A/P	-3.176	-4.971	-6.127	-5.401	-7.562	-5.582	-8.129	-8.642	-5.787	-8.117
	P/D	8.117	0.014	0.227	2.755	0.688	5.631	-6.14	-8.603	0.362	-9.663
Estimated Error (deg)	*V/V*	0.15	0.211	0.178	0.283	0.347	0.417	0.148	0.057	0.194	0.062
	A/P	-0.407	-0.637	-0.785	-0.692	-0.969	-0.715	-1.042	-1.107	-0.742	-1.04
Error Comp (mm & deg)	*V/V*	0.137	0.206	0.216	0.268	0.379	0.42	0.184	0.087	0.205	0.007
	A/P	-0.529	-0.663	-0.796	-0.696	-0.953	-0.739	-1.078	-1.105	-0.763	-1.004
	Axial	1.813	0.75	0.987	0.61	0.716	0.836	0.658	0.356	-0.065	0.306
	Trans	0.238	0.157	0.384	0.336	0.487	0.328	0.346	0.199	0.312	0.159
Prediction Error (deg)	*V/V*	**0.013**	**0.005**	**-0.038**	**0.015**	**-0.032**	**-0.003**	**-0.036**	**-0.03**	**-0.011**	**0.055**
	A/P	**0.122**	**0.026**	**0.011**	**0.004**	**-0.016**	**0.024**	**0.036**	**-0.002**	**0.021**	**-0.036**

Table 7.2: Accuracy of registration outcome for 10 registration procedures using the Bounded ICP algorithm.

The worst case estimate is identified as the error vector formed by the largest components of the 10 hip centre estimates. As described by the estimated values in Table 7.1, in all ten cases the generated hip error lies well with a 1cm radius sphere, which can guarantee a registration outcome well within the 2° accuracy requirement for this type of procedure.

In order to corroborate the results, obtained during simulation, described in Section 7.4.1.2.5, 10 consecutive full registration procedures using the Bounded ICP algorithm were carried out, and results compared to the ground truth defined by the reference transformation matrix defined above. Table 7.2 illustrates the results, in terms of rotational and translational alignment of the registered femur against measured hip centre errors, identified using the procedure described above.

It is evident from these results that registration outcome for the Bounded ICP algorithm is directly proportional to the quality of the hip centre estimate, with a clear correlation between estimated and actual varus/valgus and anterior/posterior alignment. Appendix G provides a complete set of results for each of the 10 tests, including actual and reference registration transforms, and clear evidence for lack of effect of the proximal/distal component of the hip error vector.

7.5 Discussion

The Bounded ICP algorithm has shown to be a very robust means for femoral registration performed through a conventional UKA incision. The algorithm is suitable for minimal access surgery, as a few inaccurate distal points are enough to bound the registration outcome for a reasonable hip centre estimate. It has been shown that varus/valgus and anterior/posterior components of the registration error matrix can be accurately predicted from prior knowledge of the accuracy of the hip

centre estimate. Therefore, by ensuring that the hip centre estimation procedure produces a reliable result, within a 1cm radius sphere of its modelled counterpart, it is possible to bound the outcome of the femoral registration process. Worst case scenarios can also be robustly predicted by analysing the error contribution of each step of the registration process.

The Bounded ICP algorithm has proved to be susceptible to a poor quality distal point-set in terms of axial rotational alignment. As the algorithm restricts the motion of one end of the leg axis, poor correlation between the points and respective surface generates a number of equivalent minima within an envelope which is proportional to the extent of the inaccuracy. Therefore, a reasonable quality point-set is required for the Bounded ICP algorithm to produce good rotational alignment, although accurate varus/valgus, and anterior/posterior alignment can be guaranteed for a 10 points point-set even when 2mm of maximum random noise is added to the set.

The local minima suppression mechanism described in Section 7.2.4 has also shown to be a robust means for global minimum identification. The current implementation converged to the same solution for all considered initial error states, proving the algorithm is impervious to a poor quality initial estimate.

Plastic bone trials corroborated the simulated results, showing very good correlation between predicted and actual leg axis alignment. Plastic bone trials have also shown that the current hip centre estimation procedure is an appropriate means for accurate hip centre generation, as all hip estimates fell within the required $1cm$ radius sphere. A comparison between the performance of the Bounded ICP algorithm and the optimised ICP algorithm described in Chapter 5 highlights a substantial improvement in terms of leg axis alignment for identical point-sets. Currently, short people require a better hip centre estimate for equivalent accuracy of registration, as the effect of the hip error on registration outcome has been shown to be a function of the length of the femur.

7.6 Early Clinical Results

The Bounded ICP algorithm has recently been used in a clinical environment to carry out a robotic assisted UKA procedure with the ACROBOT II System. Post-operative assessment of leg axis alignment has been carried out with Acrobot's proprietary software. Figure 7.29 shows the post-operative femoral alignment of the prosthesis compared with its planned position.

Figure 7.29 shows the CT based post-operative alignment error in terms of anterior/posterior, varus/valgus, axial, and translational alignment of the achieved

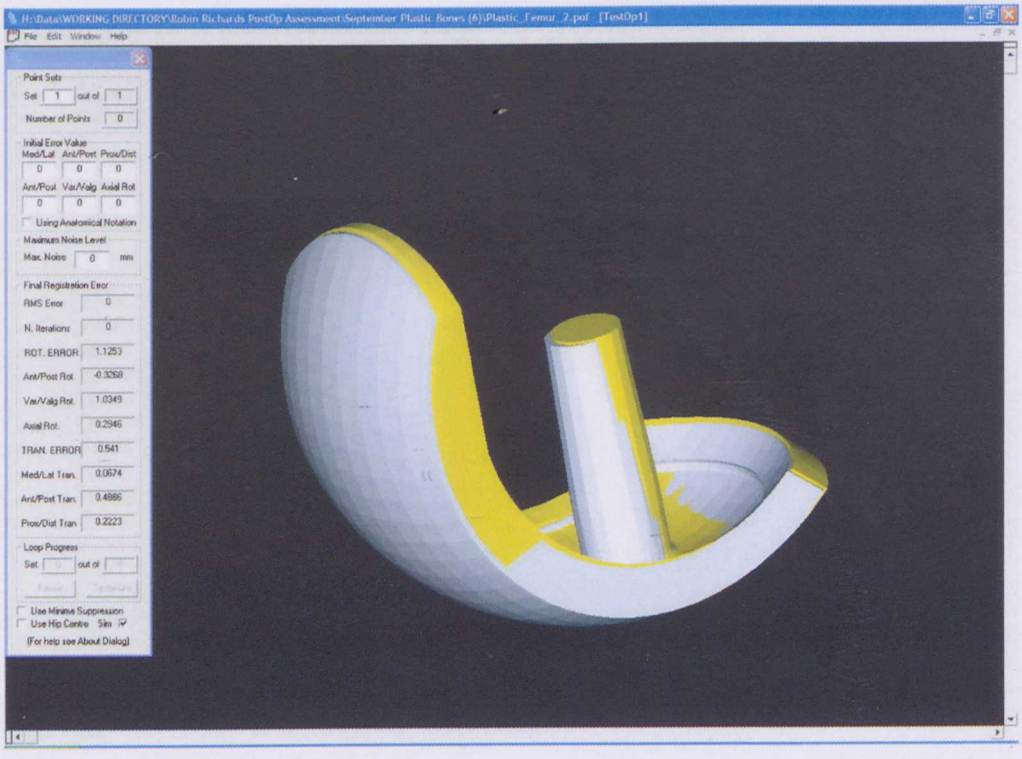


Figure 7.29: Post-operative femoral implant alignment for UKA clinical trial carried out with the ACROBOT II System.

versus planned position, which are all well within the required 2°, $2mm$ threshold. The positive outcome of these early clinical trials has laid the foundations for an Medicines and Healthcare products Regulatory Agency (MHRA) approved 30-patient randomised controlled double-blind clinical trial, which has just started.

7.7 Conclusion

This chapter has focused on the design, development and validation of a novel registration algorithm suitable for image-based minimal access femoral registration, the Bounded ICP algorithm. This novel registration method has clearly outperformed the original ICP algorithm, allowing for consistently better registration, in terms of varus/valgus and anterior/posterior alignment.

Results of both simulation and plastic bone trials have provided solid backing for the robustness and efficacy of the algorithm, which has been shown to be impervious to both the quality of the distal point-set and of the initial estimate. Even for exceptionally poor correlation between the points collected on the distal femur and the corresponding modelled surface, the Bounded ICP algorithm has produced consistently accurate results given a reasonable hip centre estimate. Therefore, by carefully estimating the position of the functional centre of the hip joint intra-

operatively, it is possible to bound registration outcome. Worst-case scenarios can also be readily estimated by pre-operatively evaluating the contribution of each phase of the algorithm, from pre-operating planning, to the intra-operative point collection method.

The current implementation, however, suffers from the existence of equivalent minima in the solution set, which may produce sub-optimal axial rotational alignment for a poor-quality distal point-set, and also has yet to be optimised for speed. The performance characteristics of the algorithm described in this chapter could also be extended to produce a generalised multi-purpose algorithm for accurate image-based surface registration. These and other enhancements have been outlined as suggestions for future work in Section 8.3.

Chapter 8

Conclusion

8.1 Overview

The aim of this study was to improve the accuracy of robotic surgery, and specifically of the ACROBOT System, as demonstrated by two orthopaedic operations, namely Total Knee Arthroplasty (TKA) and Unicompartmental Knee Arthroplasty (UKA). The research presented has successfully addressed a number of accuracy related issues, some of which have a broad spectrum of applicability, while others are specific to the ACROBOT System.

Chapter 2 described some of the techniques and technologies associated with this research. The growing field of medical robotics was broadly reviewed, and specific examples of robotic systems for orthopaedic surgery, and minimally invasive surgery, were presented. The benefits of Computer Aided Surgical systems, supported by a number of examples of successful implementations, were described in an attempt to justify the need for visual feed-back and user interaction for complex surgical procedures. Finally, the critical aspects of registration and calibration were reviewed to see how they could aid the research carried out on the ACROBOT System, which was presented in detail in the subsequent chapters.

Chapter 3 focused on very early research carried out alongside the R&D team of the Acrobot Company Ltd., which led to the first clinical application of the ACROBOT System for a number of Total Knee Arthroplasty (TKA) procedures. Published results on both accuracy and protocol [Jakopec et al., 2001], have demonstrated that this first implementation was appropriate for the task. However, the clinical performance of the ACROBOT System highlighted a number of issues, concerning both hardware and software, which needed to be addressed in order to improve the accuracy of the procedure as a whole. Resolution of these issues, which became the focus of the author's later research, led to the development of a redesigned system, called the ACROBOT II.

Chapter 4 described aspects of the ACROBOT System redesign, which has led to the successful implementation of the ACROBOT II System. Both elements of the robot, the GPS and AC Head, were successfully redesigned and manufactured. The integrated 6 DOF system was then calibrated with submillimetric accuracy at the tip to exploit a novel calibration technique, developed using the advantages of a back-drivable robot and an accurate mechanical digitiser. The clamping system was also successfully redesigned and block registration functionality was integrated into the bone clamps to allow fast and accurate re-registration and bone motion monitoring. Although this patented technique does not offer real time motion tracking, it enables the surgeon to periodically check (and to compensate for) the current setup for any relative motion of the immobilised leg with respect to the robotic system.

Chapter 5 described the enhancements carried out on the original registration algorithm presented in Chapter 3 in order to improve the efficacy of both the algorithm and of the registration method, validated for TKA. The implementation was optimised for speed and robustness and a point acquisition protocol was then devised for use during surgery, to provide an optimised dataset. The algorithm and its accuracy were explored with extensive simulations and plastic bone trials, which have led to an Ethics Committee approved clinical evaluation, with preliminary results reported in [Rodriguez y Baena et al., 2002; Cobb et al., 2002; Jakopec et al., 2001]. Intra-operative guidance, alongside a robust point acquisition protocol, can provide the required degree of confidence on the outcome of registration, which is required for this type of application. Chapter 5 also presented a novel indicator of robustness, which can be used as an aid for the assessment of registration outcome. This technique has the potential to be used to provide the surgeon with quantitative information for the robustness of a specific point-set, which in turn can be used to achieve consistently appropriate registration.

Chapter 6 provided an overview of the hardware and software changes, which became necessary in order to use the ACROBOT II System as a concept demonstrator for hands-on robotic assisted minimally invasive UKA. Hardware changes include the redesign of the clamping system developed for TKA and the design and development of a novel tissue retaining tube. Software changes include enhanced intra-operative guidance and the development and validation of a robust point acquisition protocol suitable for minimally invasive UKA. The adapted registration algorithm and protocol have shown to be appropriate for the task for those cases where good correspondence between the intra-operatively collected points and the CT generated surface can be expected. However, a clinical environment presents a number of additional variables affecting point accuracy, which are hard to quantify and complex to plan for. The "worst case scenario" for a registration method based on anatomical correspondences is hard to derive, which represents a significant

weakness of the enhanced registration algorithm and acquisition protocol, particularly if used together with a minimally invasive approach. These shortcomings have led to the development of a novel registration algorithm, known as the Bounded ICP Algorithm, which has been shown to consistently outperform the ICP-based method.

Chapter 7 described the design, development and validation of the Bounded ICP algorithm. This novel registration algorithm, suitable for model-based minimal access femoral registration, has been shown to perform better than the original ICP algorithm, leading to consistently robust registration. Results of both simulation and plastic bone trials have provided solid backing for the robustness and efficacy of the algorithm, which has been shown to be impervious to both the quality of the distal point-set and of the initial estimate. Research has shown that, by carefully estimating the position of the functional centre of the hip joint intra-operatively, it is possible to bound registration outcome. For the ICP based method, point-set size is chosen as a function of estimated point accuracy, which can degenerate as a result of poor correspondence to the surface to be registered. For the Bounded ICP algorithm, results have clearly shown that a minimal point-set size (≈ 15) for the dataset assembled through the main incision is sufficient to ensure robust leg axis alignment of the femur.

The novel calibration methods described in this thesis, although originally developed to improve the accuracy of the ACROBOT System, can also be applied for a number of similar applications. The optimised ICP-based registration method and its implementation, can be used for any procedure where points collected in one co-ordinate system need to be mapped against a surface described in another co-ordinate system. The modalities used to assemble the point-set and the registration surface are irrelevant to the registration method implemented, although the efficacy and speed of execution of the algorithm may vary in relation to the dataset size. The robust region-based point acquisition protocol, validated for the two specific tasks of TKA and UKA, can be adapted for use in other surgical procedures. Although the regions layout and point-set makeup are application specific, the method derived can be reinterpreted for a number of equivalent applications. The patented bone motion monitoring technique has a broad spectrum of applicability, as both the method and algorithm described are implementation independent. The Bounded ICP algorithm concept and derivation are universal and are therefore not tied to a particular application. Although this novel algorithm has been validated for the femur, alternative applications have been outlined in Section 8.3 as areas for future work.

Changes to both the hardware and software of the ACROBOT II System have allowed the concept of an active constraint system for minimally invasive surgery to

be demonstrated both *in vitro* and *in vivo*. The adapted system was successfully used to implant a large number of unicompartmental knee prostheses on plastic phantom bones. Encouraging results of an extensive plastic bone study, which will shortly be published, have led to a set of Ethics Committee approved clinical trials, which have been planned and executed using the ACROBOT II System. The ACROBOT II System, together with the robust registration protocol, is currently undergoing a Medicines and Healthcare products Regulatory Agency (MHRA) approved 30 patient double-blind randomised controlled trial to assess the clinical performance of the system for robotic-assisted UKA.

8.2 Summary

This research has resulted in the following specific contributions:

- The redesign of the ACROBOT System, which can now be used for both TKA and UKA.
- The development of novel calibration solutions, which have been successfully used to obtain sub-millimetric *positional* accuracy of the ACROBOT System as a whole.
- The development of a novel bone-motion monitoring technique, which has been patented.
- The development of a fast and efficient anatomical registration method suitable for both open and minimal access registration of the knee.
- The implementation and validation of robust point-touching strategies, which enable reliable registration of both the femur and tibia (to within $\pm 2^o$ and $\pm 2mm$) during both TKA and UKA.
- The development of a novel indicator of robustness, which can be used to post-operatively assess the quality of an intra-operatively assembled point-set.
- The design, derivation and validation of a novel registration algorithm, known as the Bounded ICP algorithm, suitable for accurate and robust registration of the femur.

8.3 Future Work

The research presented in this thesis has covered a broad range of topics, spanning from robotic design and calibration, through to model based anatomical registration.

For clarity, areas for future work have been categorised in three main sections: improvements to hardware, improvements to the enhanced registration algorithm presented in Chapter 5 and improvements to the Bounded ICP algorithm described in Chapter 7. A brief outline for future work on each topic now follows.

8.3.1 Improvements to Hardware

The following suggestions for future work are specific to the ACROBOT System and were highlighted as limitations of the current implementation. Although the bone motion monitoring method was successfully integrated into the clamping system, the locating holes are machined into the clamps themselves. Therefore any relative motion between the clamps and the bones they are fixed to, cannot be detected. An appropriate clamp design would minimise the risk of this motion occurring, however a better technique may be necessary to ensure accuracy is maintained at all times. An alternative would be to insert, at the intra-operative stage, a minimum of three special screws on each bone to be monitored. By touching the heads of each screw, which would have a conical hole, it would then be possible to apply the monitoring method to the bones themselves, without the bias introduced by the clamps. Alternatively, three small conical holes could be drilled precisely into the surface of each bone to be monitored.

The clamps developed for minimally invasive UKA have shown to be adequate for the task, although two small stab-wounds are needed for insertion through the skin. These additional incisions are currently accepted by the clinical community, however a less invasive method may be preferred. A number of alternative designs have been briefly considered, but a viable alternative has not been found yet.

Chapter 6 described the design and preliminary testing of a novel tissue-retaining tube, which allows access to the bone surfaces during both registration and cutting to be optimised. However, the current implementation has proved to be inadequate for clinical use and needs to be re-engineered. Further testing of the current implementation may be necessary before a new prototype is manufactured.

8.3.2 Improvements to the Enhanced ICP Algorithm

The enhanced ICP implementation presented in Chapter 5 has shown to be a fast and robust means for registration using anatomical correspondences. The techniques developed to accelerate convergence are well known and have been successfully applied to enhance the performance of the algorithm. The current implementation was found to be appropriate for the tasks of TKA and UKA, but further speed improvements may be necessary if the algorithm is to be used in other contexts. Well

known techniques can be readily integrated into the current implementation for this purpose.

Currently, expected point accuracy for a specific point-set is estimated by inspecting the RMS error and colour-coded display of the points on the mapped surface for a representative set. This technique relies on user interaction, which may not be ideal for relatively inexperienced users. Both steps of the expected point accuracy estimation process could be fully automated in the following way. A lookup-table detailing typical RMS values for a number of point-set sizes and maximum noise values (i.e. values presented in Figure 5.24) could be integrated into the intra-operative software. The spread of the residual error for all points on the surface (visually presented to the user by means of the colour-coded display), could be automatically computed, and used to evaluate global convergence. A small spread would suggest that all points have a similar residual error (e.g. all points are green/blue), which is to be expected if the global minimum has been found. The lookup table of RMS error values and the spread of the errors on the surface could then be used to automatically estimate the current expected point accuracy.

The point-set robustness indicator can be used to assess the quality of a specific point-set post-operatively, as the current computation time (Table 5.10) is excessive for use intra-operatively. A number of techniques could be used to increase execution speed drastically, which would allow any point-set to be quickly assessed. A statistically significant set of figures for the degree of robustness of a particular point-set layout could then be available to the user for every intra-operatively acquired point-set.

The enhanced ICP algorithm and robust region-based point acquisition protocol have been validated for the specific tasks of TKA and UKA. However the methodology outlined can be readily applied to a number of alternative applications, such as total hip replacement surgery and spine surgery.

8.3.3 Improvements to the Bounded ICP Algorithm

The Bounded ICP algorithm presents a novel approach to registration by outlining a method that bounds registration outcome if a set of correspondences, which is distant from the focus of registration, is available intra-operatively. Although the algorithm and implementation have been validated for the specific task of femoral registration with the ACROBOT II System, a similar approach could be used to adapt the Bounded ICP algorithm for a number of alternative applications. The performance characteristics of the algorithm could also be extended to produce a generalised multi-purpose algorithm for accurate model-based surface registration.

In particular, the Bounded ICP algorithm could be easily adapted for the task

of tibial registration, by using the ankle centre as a source for the distant paired points needed to bound the outcome. As a result, the additional tibial stab-wound, currently required for accurate registration through the conventional UKA incision (Figure 6.20), would no longer be necessary.

Results of the validation process have highlighted a weakness of the current implementation. By bounding convergence, the Bounded ICP algorithm generates a large number of "equivalent" minima, with near identical leg axis alignment, but different translational and axial rotational values. An area for future work would be to find a better means to distinguish between equivalent minima concerning axial rotational alignment.

Finally, both the enhanced ICP algorithm and Bounded ICP algorithm currently have a similar execution time. However, for the latter algorithm, a large number of iterations (> 1000) is necessary to reach a local minimum, as illustrated in Figure 7.16. Techniques could be developed to dramatically accelerate the convergence process, which would result in a substantial speed enhancement.

8.4 Conclusion

The research described in this thesis has resulted in improvements in hardware design and calibration. The ACROBOT System has been tested on plastic bones and on a number of patients for both TKA and UKA, and has shown a considerable improvement in accuracy and performance over the original system described in [Jakopec, 2001].

The robust point-touching strategies described for TKA and UKA have shown that achieving consistently accurate registration is possible, even if performed using a minimally invasive approach. However, as the ICP algorithm relies on anatomical correspondences, a good quality surface model and point-set are necessary to ensure a desirable outcome is obtained. This significant shortcoming, which is true for any intrinsic landmark based registration method, has been successfully addressed for the femur by developing the Bounded ICP algorithm. Results have shown that precise leg axis alignment can be robustly defined by ensuring that the functional centre of the hip is accurately estimated both pre-operatively and intra-operatively. Published research on this subject has already shown that accurate hip centre estimation is feasible, therefore appropriate femoral alignment can be guaranteed regardless of the quality of the distal point-set and of the surgical access.

The methods described in this thesis have considerable potential to benefit a wide range of clinical procedures, including orthopaedics, spine surgery and neurosurgery.

Bibliography

Aesculap (2002). Orthopilot system. world wide web page: http://www.aesculap.de.

Ahlberg, A. and Lunden, A. (1981). Secondary operations after knee joint replacement. *Clinical Orthopaedics*.

Alcaniz, M., Montserrat, C., Grau, V., Chinesta, F., Ramon, A., and Albalat, S. (1998). An advanced system for the simulation and planning of orthodontic treatment. *Medical Image Analysis*, 2(1):61–77(17).

Amin, D. V., Kanade, T., DiGioia, A. M., and Jaramaz, B. (2003). Ultrasound registration of the bone surface for surgical navigation. *Computer Aided Surgery*, 8(1):1–16.

Amstutz, C., Caversaccio, M., Kowal, J., Bachler, R., Nolte, L. P., Hausler, R., and Styner, M. (2003). A-mode ultrasound-based registration in computer-aided surgery of the skull. *Archives of Otolaryngology Head and Neck Surgery*, 129(12):1310–1316.

Armstrong Healthcare Ltd. (2002). World wide web page: http://www.armstrong-healthcare.com/.

Audette, M. A., Ferrie, F. P., and Peters, T. M. (2000). An algorithmic overview of surface registration techniques for medical imaging. *Medical Image Analysis*, 4(3):201–217.

Ault, T. and Siegel, M. (1995). Frameless patient registration using ultrasonic imaging: a preliminary study. *Image Guided Surgery*, 1(2):94–102.

Ballester, P., Jain, Y., Haylett, K. R., and McCloy, R. F. (2001). Comparison of task performance of robotic camera holders endoassist and aesop. In Lemke, H. U., editor, *Computer assisted radiology and surgery; CARS 2001*, pages 1071–1076, Berlin. Elsevier Science.

Besl, P. and McKay, N. (1992). A method for registration of 3-d shapes. *IEEE Transactions on Pattern Analysis and Machine Intelligence*, 14(2).

Biomet Inc. (2002). Oxford(r) unicompartmental knee. world wide web pages: http://www.oxfordknee.net/, http://www.biomet.com/.

Birke, A., Reichel, H., Hein, W., Schietsch, U., Hube, R., Bernstein, A., and Kruger, T. (2000). Robodoc - a way to the future in hip endoprosthesis or a unnecessary investment? *Zeitschrift Fur Orthopadie Und Ihre Grenzgebiete*, 138(5):395–401.

Boerner, M., Lahmer, A., Bauer, A., and Stier, U. (1998). Experiences with the robodoc system in more than 1000 cases. In Lemke, H. U., Vannier, M. W., Inamura, K., and Farman, A. G., editors, *Computer Assisted Radiology and Surgery*, volume 1165 of *International Congress Series -Amsterdam- Excerpta Medica Then Elsevier Science-*, pages 689–693.

Borelli, J., Bello, F., Rodriguez y Baena, F. M., and Davies, B. L. D. (2004). An active constraint environment for minimali invasive surgery: early experience of a cutting operation. In *MMVR, Medicine Meets Virtual Reality 12*, CA, USA. IOS Press, Oxford, UK.

Brain Lab GmbH (2002). World wide web page: http://www.brainlab.com.

Brandt, G., Zimolong, A., Carrat, L., Merloz, P., Staudte, H. W., Lavallee, S., Radermacher, K., and Rau, G. (1999). Crigos: A compact robot for image-guided orthopedic surgery. *Ieee Transactions on Information Technology in Biomedicine*, 3(4):252–260.

Brendel, B., Winter, S., Rick, A., Stockheim, M., and Ermert, H. (2003). Bone registration with 3d ct and ultrasound data sets. In Lemke, H. U., editor, *Computer assisted radiology and surgery; CARS 2003 computer assisted radiology and surgery*, pages 426–432, London. Elsevier Science.

Broeders, I. A. M. J. and Ruurda, J. (2001). Robotics revolutionizing surgery: the intuitive surgical "da vinci" system. *Industrial Robot*, 28(5):387–391.

Butner, S. E. and Ghodoussi, M. (2003). Transforming a surgical robot for human telesurgery. *Ieee Transactions on Robotics and Automation*, 19(5):818–824.

Cadeddu, J. A., Stoianovici, D., Roberts, W., Taylor, R. H., Whitcomb, L. L., Sharpe, W. N., and Kavoussi, L. R. (1997). Paky: An efficient device for percutaneous access of the kidney. *Journal of Endourology*, 11 Supp/1:V6–3.

Cepolina, F. and Michelini, R. C. (2003). A family of co-robotic surgical set-ups. *Industrial Robot*, 30(6):564–574.

Chauhan, S. (1999). *The Application of HIFU and Robotic Technology in Surgery.* Ph.d. thesis, Imperial College, University of London.

Chen, I. M., Yang, G., Tan, C. T., and Yeo, S. H. (2001). Local poe model for robot kinematic calibration. *Mechanism and Machine Theory*, 36(11-12):1215–1239.

Chetverikov, D., Svirko, D., Stepanov, D., and Krsek, P. (2002). The trimmed iterative closest point algorithm. In Kasturi, R., Laurendeau, D., and Suen, C., editors, *Pattern recognition*, pages 545–548, Quebec, Canada. IEEE Computer Society.

Chitwood, W. R., Nifong, L. W., Elbeery, J. E., Chapman, W. H., Albrecht, R., Kim, V., and Young, J. A. (2000). Robotic mitral valve repair: Trapezoidal resection and prosthetic annuloplasty with the da vinci surgical system. *Journal of Thoracic and Cardiovascular Surgery*, 120(6):1171–1172.

Chung, J. H., Ko, S. Y., Kwon, D. S., Lee, J. J., Yoon, Y. S., and Won, C. H. (2003). Robot-assisted femoral stem implantation using an intramedulla gauge. *Ieee Transactions on Robotics and Automation*, 19(5):885–892.

Cleary, K. and Nguyen, C. (2001). State of the art in surgical robotics: Clinical applications and technology challenges. *Computer Aided Surgery, John Wiley and Sons*, 6(6):312–328.

Cobb, J. P., Henckel, J., Harris, S. J., Jakopec, M., Rodriguez y Baena, F. M., Gomes, M. P. S. F., and Davies, B. L. (2003). An active constraint robot improves outcomes in total knee arthroplasty. In *Computer Assisted Orthopaedic Surgery*, pages pp. 64–65, Third Annual Meeting of CAOS International, Marbella, Spain.

Cobb, J. P., Henckel, J., Harris, S. J., Jakopec, M., Rodriguez y Baena, F. M., Gomes, M. P. S. F., and Davies, B. L. (2002). First clinical trials of a "hands-on" active constraint robot. In *Computer Assisted Orthopaedic Surgery*, pages pp. 46–47, Second Annual Meeting of CAOS International, Santa Fe, USA.

Cohan, S. (2001). Robodoc achieves pinless registration. *Industrial Robot*, 28(5):381–386.

Craig, J. J. (1989). *Introduction to robotics : mechanics and control.* Addison-Wesley series in electrical and computer engineering. Control engineering. Addison-Wesley, Reading, Mass., 2nd edition.

Cuchet, E., Knoplioch, J., Dormont, D., and Marsault, C. (1995). Registration in neurosurgery and neuroradiotherapy applications. In *Medical robotics and computer assisted surgery*, pages 31–38, Baltimore; MD. Wiley-Liss.

Dakin, G. F. and Gagner, M. (2003). Comparison of laparoscopic skills performance between standard instruments and two surgical robotic systems. *Surgical Endoscopy*, 17(4):574–579.

Dario, P., Hannaford, B., and Menciassi, A. (2003). Smart surgical tools and augmenting devices. *Ieee Transactions on Robotics and Automation*, 19(5):782–792.

Davies, B. (2000). A review of robotics in surgery. *Proceedings- Institution of Mechanical Engineers Part H Journal of Engineering in Medicine*, 214(1):129–140.

Davies, B., Fan, K. L., Hibberd, R. D., and Jakopec, M. (1997). A mechatronic based robotic system for knee surgery. In Adeli, H., editor, *Intelligent information systems*, pages 48–52. Los Alamitos CA.

Davies, B. L., Jakopec, M., Harris, S. J., and Cobb, J. (1999a). Computer-assisted surgery for tkr. In *International Conference on Knee Replacement Surgery, IMechE*, pages pp. 256–259, London, UK.

Davies, B. L., Jakopec, M., Harris, S. J., and Cobb, J. (1999b). A novel hands-on robot for knee replacement. In *Second EUREL (European Advanced Robotic Systems Development) Workshop on Medical Robotics*, pages pp. 98–102, Pisa, Italy.

Davies, B. L. D. (2003). Robotic devices in surgery. *Minimally Invasive Therapy and Allied Technologies*, 12(1-2):pp. 5–13.

Degoulange, E., Urbain, L., Caron, P., and Boudet, S. (1998). Hippocrate: an intrinsically safe robot for medical applications. In *Intelligent robots and systems*, pages 959–964, Victoria; Canada. Ieee.

Delp, S. L., Stulberg, S. D., Davies, B., and Picard, F. (1998). Computer assisted knee replacement. In DiGioia, A. M., editor, *Computer assisted orthopaedic surgery: medical robotics and image guided surgery*, pages 49–56. Lippincott-Raven Publishers.

Denavit, J. and Hartenberg, R. S. (1955). A kinematic notation for lower-pair mechanisms based on matrices . *ASME. Journal of Applied Mechanics*, 22(39):215–221.

Detter, C., Reichenspurner, H., Boehm, D. H., and Reichart, B. (2001). Robotic manipulators in cardiac surgery: the computer-assisted surgical system zeus. *Minimally Invasive Therapy and Allied Technologies*, 10(6):275–282.

Devillard, N. (2003). Fast median search: an ansi c implementation.

DiGioia, A. M., Jaramaz, B., Blackwell, M., Simon, D. A., Morgan, F., Moody, J. E., Nikou, C., Colgan, B. D., Aston, C. A., and Labarca, R. S. (1998). Image guided navigation system to measure intraoperatively acetabular implant alignment. In Brand, R. A., editor, *The Papers Presented at The Hip Society Meeting 1998*, volume Issue 355 of *Clinical Orthopaedics and Related Research*, pages 8–22. J B Lippincott Co.

Eadie, L. H., Seifalian, A. M., and Davidson, B. R. (2003). Telemedicine in surgery huge potential to alter surgical practice. *British Journal of Surgery*, 90(6):647–658.

EEC (1993). Council directive 93/42/eec of 14 june 1993 concerning medical devices. *Official Journal- European Communities Legislation L*, 36(169):1.

Ellis, R. E., Fleet, D. J., Bryant, J. T., Rudan, J., and Fenton, P. (1997). A method for evaluating ct-based surgical registration. In Troccaz, J., Grimson, E., and Moesges, R., editors, *CVRMed-MRCAS'97: First Joint Conference Computer Vision, Virtual Reality and Robotics in Medicine and Medical Robotics and Computer-Assisted Surgery*, volume Issue 1205 of *Lecture Notes in Computer Science*, pages 141–150. Springer Verlag Kg.

Ellis, R. E., Toksvig-Larsen, S., Marcacci, M., Caramella, D., and Fadda, M. (1996). Use of a biocompatible fiducial marker in evaluating the accuracy of computed tomography image registration. *Investigative Radiology*, 31(10):658–667.

Ellis, R. E., Tso, C. Y., Rudan, J. F., and Harrison, M. M. (1999). A surgical planning and guidance system for high tibial osteotomy. *Computer Aided Surgery*, 4(5):264–274.

Fadda, M., Marcacci, M., Martelli, S., and La Palombara, F. (1998). A computer-aided surgical system complying with novel e.u. regulations. In *MICCAI'98*.

Faugeras, O. and Hebert, M. (1986). The representation, recognition, and locating of 3-d objects. *Journal of Robotic Research*, 5(3).

Feikes, J. D., O Connor, J. J., Zavatsky, A. B., and Clark, D. J. (2000). Unicompartmental knee replacement and joint mobility. In Prendergast, P. J., Lee,

T. C., and Carr, A. J., editors, *European Society of Biomechanics; incorporating symposia on biofluid mechanics, microdamage in bone, implant biomaterials, musculoskeletal loading, mechanobiology, and walking motion*, page 195, Dublin. Dublin.

Fitzpatrick, J. M., West, J. B., and Maurer, C. R. (1998). Predicting error in rigid-body point-based registration. *Ieee Transactions on Medical Imaging Mi*, 17(5):694–702.

Fleute, M. and Lavallee, S. (1998). Building a complete surface model from sparse data using statistical shape models: Application to computer assisted knee surgery system. *Lecture Notes in Computer Science*, pages 879–887.

Flury, P., Glauser, D., Villotte, N., and Burckhardt, C. W. (1992). Minerva, a robot dedicated to neurosurgery operations. *Proceedings of the International Symposium on Industrial Robots*, 23:729.

Friedman, J., Bentley, J. H., and Finkel, R. A. (1977). An algorithm for finding best matches in logarithmic expexted time. *ACM Transactions on Mathematical Sofieare*, 3(3):pp. 209–226.

Glauser, D., Fankhauser, H., Epitaux, M., and Hefti, J. L. (1995). Neurosurgical robot minerva: First results and current developments. In *Medical robotics and computer assisted surgery*, pages 24–30, Baltimore; MD. Wiley-Liss.

Glauser, D., Flury, P., and Burckhardt, C. W. (1993). Mechanical concept of the neurosurgical robot 'minerva'. In Kassler, M., editor, *Robotics in Health Care*, volume 11; Number 6 of *Robotica -Cambridge-*, page 567. Cambridge Univ Press.

Goldenberg, V. and Figgie, H. (1998). Use of a total condylar knee prosthesis for treatment of osteoarthritis and rheumatiod arthritis. long term results. *Journal of Bone Joint Surgery.*

Gray, H. and Carter, H. (1992). *Gray's Anatomy.* The Promotional Reprint Company Limited.

Grimson, W. E. L., Ettinger, G. J., White, S. J., and Gleason, P. L. (1995). Evaluating and validating an automated registration system for enhanced reality visualization in surgery. In Ayache, N., editor, *Computer vision, virtual reality and robotics in medicine*, pages 3–12, Nice; France. Berlin.

Grueneis, C., Ritcher, R., and Hening, F. (1999). Clinical introduction of the caspar system. In *4th International Symposium on Computer Assisted Orthopaedic Surgery*, Davos, Switzerland.

Gumprecht, H. K., Widenka, D. C., and Lumenta, C. B. (1999). Brainlab vectorvision neuronavigation system: Technology and clinical experiences in 131 cases. *Neurosurgery*, 44(1):97–105.

Gutt, C. N., Markus, B., Kim, Z. G., Meininger, D., Brinkmann, L., and Heller, K. (2002). Early experiences of robotic surgery in children. *Surgical Endoscopy*, 16(7):1083–1086.

Hajnal, J., Hill, D., and Hawkes, D., editors (2001a). *Medical Image Registration.* The Biomedical Engineering Series. CRC Press LLC.

Hajnal, J. V., Hill, D. L. G., and Hawkes, D. J. (2001b). *Medical Image Registration. Eds.*

Harris, S. J., Arambula-Cosio, F., Mei, Q., Hibberd, R. D., Davies, B. L., Wickham, J. E. A., Nathan, M. S., and Kundu, B. (1997a). The probot - an active robot for prostate resection. *Proceedings- Institution of Mechanical Engineers Part H Journal of Engineering in Medicine*, 211(4):317–326.

Harris, S. J., Davies, B. L., Jakopec, M., and Cobb, J. (1999). Intra-operative application of a robotic knee surgery system. In *MICCAI'99, Lecture Notes in Computer Science*, pages pp. 1116–1124, Cambridge, UK.

Harris, S. J., Lin, W. J., Fan, K. L., Hibberd, R. D., Cobb, J., Middleton, R., and Davies, B. L. (1997b). Experiences with robotic systems for knee surgery. In Troccaz, J., Grimson, E., and Moesges, R., editors, *CVRMed-MRCAS'97: First Joint Conference Computer Vision, Virtual Reality and Robotics in Medicine and Medical Robotics and Computer-Assisted Surgery*, volume Issue 1205 of *Lecture Notes in Computer Science*, pages 757–766. Springer Verlag Kg.

Hayashi, K., Araki, Y., Uechi, J., Ohno, H., and Mizoguchi, I. (2002). A novel method for the three-dimensional (3-d) analysis of orthodontic tooth movement-calculation of rotation about and translation along the finite helical axis. *Journal of Biomechanics*, 35(1):45–51(7).

Hayashibe, M. and Nakamura, Y. (2001). Laser-pointing endoscope system for intra-operative 3d geometric registration. *Ieee International Conference on Robotics and Automation*, 2:1543–1548.

Hayati, S., Tso, K., and Roston, G. (1988). Robot geometry calibration. In *Proceedings - 1988 IEEE International Conference on Robotics and Automation.*

Henckel, J., Richards, R., Cobb, J. P., Harris, S. J., Jakopec, M., Rodriguez y Baena, F. M., Gomes, M. P. S. F., and Davies, B. L. (2003). The use of x-ray

computerized tomography to measure the accuracy of total knee arthroplasty. In *Computer Assisted Orthopaedic Surgery*, pages pp. 142–143, Third Annual Meeting of CAOS International, Marbella, Spain.

Hewitt, B. and Shakespeare, D. (2001). A straightforward method of assessing the accuracy of implantation of knee prostheses. *Knee*, 8(2):139–144.

Hidalgo, F. and Brunn, P. (1998). Robot metrology and calibration systems - a market review. *Industrial Robot*, 25(1):42–47.

Ho, S., Davies, B., Hibberd, R., and Cobb, J. (1994). Robot knee surgery - implicit force control strategy with active motion constraint. In *Euriscon'94*, pages 1235–1248, Malaga; Spain. Bristol.

Ho, S. C., Davies, B. L., Hibberd, R. D., and Cobb, J. C. (1995a). Active force control as a dynamic constraint in robotic knee surgery. In *Medimec '95: mechatronics in medicine and surgery*, pages 108–125, Bristol. Bristol.

Ho, S. C., Hibberd, R. D., Cobb, J., and Davies, B. L. (1995b). Force control for robotic surgery. In *Advanced robotics*, pages 21–32, Sant Feliu de Guixols; Spain. Upc.

Ho, S. C., Hibberd, R. D., and Davies, B. L. (1995c). Robot assisted knee surgery. In Davies, B., editor, *Robots in Surgery*, volume 14; Number 3 of *Ieee Engineering in Medicine and Biology Magazine*, page 292. Ieee Institute of Electrical and Electronics.

Horn, B. K. P. (1987). Closed-form solution of absolute orientation using unit quaternions. *Journal of the Optical Society of America. A, Optics and image science*, 4(4):629–642.

Horn, B. K. P. (1991). Relative orientation revisited. *Journal of the Optical Society of America. A, Optics and image science*, 8(10):pp. 1630–1638.

Howe, R. and Matsuoka, Y. (1999). Robotics for surgery. *Annual Review of Biomedical Engineering*, 1:211–240.

Intuitive Surgical Inc. (2002). The da vinci system. world wide web page: http://www.intuitivesurgical.com/.

Jaafar, W. S., Hugtenburg, R., Julyan, P., Beddoe, A., McMullen, J., and Cruickshank, G. (1999). Registration of spect onto ct images using a brainlab stereotactic radiosurgery planning system. In Kondziolka, D., editor, *International Stereotactic Radiosurgery Society*, pages 117–123, Sydney, Australia. Karger.

Jacobs, S., Holzhey, D., Kiaii, B. B., Onnasch, J. F., Walther, T., Mohr, F. W., and Falk, V. (2003). Limitations for manual and telemanipulator-assisted motion tracking-implications for endoscopic beating-heart surgery. *Annals of Thoracic Surgery*, 76(6):2029–2036.

Jakopec, M. (2001). *An Integrated Robotic System for Total Knee Replacement Surgery*. Ph.d. thesis, Imperial College, University of London.

Jakopec, M., Harris, S., Rodriguez y Baena, F. M., Gomes, P., Cobb, J., and Davies, B. (2001). The first clinical application of a "hands-on" robotic knee surgery system. *Computer Aided Surgery, John Wiley and Sons*, 6(6):329–339.

Jakopec, M., Harris, S. J., Rodriguez y Baena, F. M., Gomes, P., Cobb, J., and Davies, B. L. (2002a). Preliminary results of an early clinical experience with the acrobottm system for total knee replacement surgery. *Lecture Notes in Computer Science*, (2488):256–263.

Jakopec, M., Harris, S. J., Rodriguez y Baena, F. M., Gomes, P., and Davies, B. L. (2002b). Acrobot: a "hands-on" robot for total knee replacement surgery. In *Advanced motion control*, pages 116–120, Maribor, Slovenia. IEEE Service Center.

Jakopec, M., Rodriguez y Baena, F. M., Harris, S. J., Gomes, M. P. S. F., Cobb, J. P., and Davies, B. L. (2003a). Evolution of the next generation acrobot orthopaedic surgery robot. In *Computer Assisted Orthopaedic Surgery*, pages pp. 152–153, Third Annual Meeting of CAOS International, Marbella, Spain.

Jakopec, M., Rodriguez y Baena, F. M., Harris, S. J., Gomes, P., Cobb, J., and Davies, B. L. (2003c). The acrobotő system for total knee replacement. *Industrial Robot*, 30(1):pp.61–66.

Jakopec, M., Rodriguez y Baena, F. M., Harris, S. J., Gomes, P., Cobb, J., and Davies, B. L. (2003b). The hands-on orthopaedic robot "acrobot": Early clinical trials of total knee replacement surgery. *Ieee Transactions on Robotics and Automation*, 19(5):902–911.

Johnson, A. and Hebert, M. (1997). Recognizing objects by matching oriented points. In *Computer vision and pattern recognition*, pages 684–689, San Juan. IEEE Computer Society.

Joskowicz, L. and Taylor, R. H. (2001). Computers in imaging and guided surgery. *Computing in Science and Engineering*, 3(5):65–72.

Jost, T. and Hugli, H. (2002). A multi-resolution scheme icp algorithm for fast shape registration. In *3D data processing visualization and transmission; First international symposium on 3D data processing visualization and transmission*, pages 540–543, Padova, Italy. Ieee.

Kang, H. and Wen, J. T. (2001). Robotic assistants aid surgeons during minimally invasive procedures. *Ieee Engineering in Medicine and Biology Magazine*, 20(1):94–104.

Kang, M., Sadri, H., Moccozet, L., and Magnenat-Thalmann, N. (2003). Hip joint modeling for the control of the joint center and the range of motions. In Science, E., editor, *IFAC symposium on modelling and control in biomedical systems.*

Kang, M., Sadri, H., Moccozet, L., Magnenat-Thalmann, N., and Hoffmeyer, P. (2002). Accurate simulation of hip joint range of motion. In *Computer animation; CA 2002*, pages 215–219, Geneva. Ieee.

Kim, V. B., Chapman, W. H. H., Albrecht, R. J., Bailey, B. M., Young, J. A., Nifong, L. W., and Chitwood, W. R. (2002). Early experience with telemanipulative robot-assisted laparoscopic cholecystectomy using da vinci. *Surgical Laparoscopy Endoscopy and Percutaneous Techniques*, 12(1):33–40.

Kumar, R., Berkelman, P., Gupta, P., Barnes, A., Jensen, P. S., Whitcomb, L. L., and Taylor, R. H. (2000). Preliminary experiments in cooperative human/robert force control for robot assisted microsurgical manipulation. In *Robotics and automation*, pages 610–617, San Francisco, CA. Ieee.

Kumar, R., Jensen, P., and Taylor, R. H. (1999). 11.40-12.00: Experiments with a steady hand robot in constrained compliant motion and path following. In *International workshop on robot and human interaction*, pages 92–97, Pisa, Italy. Ieee.

Kwon, D. S., Yoon, Y. S., Lee, J. J., Huh, K. H., Chung, J. H., Park, Y. B., Ko, S. Y., and Won, C. H. (2001). Arthrobot: A new surgical robot system for total hip arthroplasty. In *Intelligent robots and systems*, pages 1123–1128, Maui, HI. Ieee.

Laskin, R. (1990). Total condylar knee replacement in patients who have rheumatoid. a ten year followup study. arthritis. *Journal of Bone Joint Surgery.*

Lerner, A.G.Stoianovici, D. V. L. (1999). A passive positioning and supporting device for surgical robots and instrumentation. In *MiCCAI'99*, Cambridge, UK.

Levison, T. J., Moody, J. E., Jaramaz, B., Nikou, C., and DiGioia, A. (2000). Surgical navigation for thr: A report on clinical trial utilizing hipnav. In Delp, S. L., DiGioia, A. M., and Jaramāz, B., editors, *Medical Image Computing and Computer-Assisted Intervention - MICCAI 2000*, volume 1935 of *Lecture Notes in Computer Science*, pages 1185–1187. Springer-Verlag.

Ma, B., Ellis, R. E., and Fleet, D. J. (1999). Spotlights: A robust method for surface-based registration in orthopedic surgery. In Taylor, C. and Colchester, A., editors, *Medical Image Computing and Computer-Assisted Intervention - MICCAI '99*, volume Issue 1679 of *Lecture Notes in Computer Science*, pages 936–944. Springer Verlag Kg.

Maintz, J. and Viergever, M. (1998). A survey of medical image registration. *Medical Image Analysis*, 2(1):1–36.

Malvisi, A., Fadda, M., Valleggi, R., Bioli, G., and Martelli, S. (2001). A new robotic system for the operating theatre. *Computing and Control Engineering Journal*, 12(3):129–136.

Marescaux, J., Leroy, J., Rubino, F., Smith, M., Vix, M., Simone, M., and Mutter, D. (2002). Transcontinental robot-assisted remote telesurgery: Feasibility and potential applications. *Annals of Surgery*, 235(4):487–492.

MathWorks Inc. (1998). Matlab version 5.1.0.421 released may 25 1998. world wide web page: http://www.mathworks.com/.

Mei, Q., Harris, S. J., Arambula-Cosio, F., Nathan, M. S., Hibberd, R. D., Wickham, J. E. A., and Davies, B. L. (1996). Probot - a computer integrated prostatectomy system. In Hoehne, K. H. and Kikinis, R., editors, *Visualization in Biomedical Computing*, volume Issue 1131 of *Lecture Notes in Computer Science*, pages 581–590. Springer Verlag Kg.

Meister, D., Pokrandt, P., and Both, A. (1998). Milling accuracy in robot assisted orthopaedic surgery. *Iecon*, 4:2502–2505.

Melfi, F. M., Menconi, G. F., Mariani, A. M., and Angeletti, C. A. (2002). Early experience with robotic technology for thoracoscopic surgery. *European Journal of Cardiothoracic Surgery*, 21(5):864–868.

Menon, M. and Tewari, A. (2003). Robotic radical prostatectomy and the vattikuti urology institute technique: an interim analysis of results and technical points. *Urology*, 61(Supp/1):15–20.

Middelstadt, B. D., Cohan, S. M., and Schreiner, S. (1998). System and method for performing image directed robotic orthopedic procedures without a fiducial reference system.

Miller, C. E. (1988). Aesop 2000 with voice control. In Kruger, T., Gomel, V., and Van der Wat, J., editors, *International Society for Gynecologic Endoscopy*, pages 39–42, Sun City; South Africa. Bologna.

Möller, T. and Trumbore, B. (1997). Fast, minimum storage ray-triangle intersection. *Journal of graphics tools*, 2(1):21–28.

Moran, M. E. (2003). Reviews in endourology - robotic surgery: Urologic implications. *Journal of Endourology*, 17(9):pp. 695–708.

Nakamura, O., Goto, M., Toyoda, K., and Takai, N. (1994). A laser tracking robot-performance calibration system using ball-seated bearing mechanisms and a spherically cat's-eye retroreflector. *Review of Scientific Instruments*, 65(4//Pt1):1006.

Nakamura, Y. (2000). Robots for minimally invasive surgery. *Journal- Robotics Society of Japan*, 18(1):41–44.

Nio, D., Bemelman, W. A., Boer, K. T. d., Dunker, M. S., Gouma, D. J., and van Gulik, T. M. (2002). Efficiency of manual vs robotical (zeus) assisted laparoscopic surgery in the performance of standardized tasks. *Surgical Endoscopy*, 16(3):412–415.

Pather, P. (2001). *A Robotic System for HIFU Surgery Applied to Liver Tumours.* Ph.d. thesis, Imperial College, University of London.

Paul, R. and Zong, H. (1981). *Robot Manipulators: Mathemathics, Programming and Control.* MIT Press, Cambridge, Massachusetts.

Paul, R. P. and Zhang, H. (1986). Computationally efficient kinematics for manipulators with spherical wrists based on the homogeneous transformation representation. *International Journal of Robotics Research*, 5(2):32–44.

Pennec, X. and Thirion, J. P. (1995). Validation of 3-d registration methods based on points and frames. *Rapports De Recherche- Institut National De Recherche En Informatique Et En Automatique*, (2470):ALL.

Perrier, J. (2003). Computer and robotic acl replacement with caspar system, montpellier.

Petermann, J., Schierl, M., Pashimeh-Azah, A., Frohlich, J. J., Heeckt, P. F., and Gotzen, L. (2000). The caspar-system (computer assisted surgery planning and robotics) in the reconstruction of the acl - 1 year experiences. In Lemke, H. U., editor, *International Society for Computer Aided Surgery; Annual Conference; Computer assisted radiology and surgery*, pages 203–207, San Francisco, CA. Elsevier.

PI Precision Ltd. (2002). Galileo-nav galileo-cas systems. world wide web page: http://www.pi-ag.ch/pi-systems/galileo.html.

Pierrot, F., Dombre, E., Degoulange, E., Urbain, L., Caron, P., Boudet, S., Gariepy, J., and Megnien, J. (1999). Hippocrate: a safe robot arm for medical applications with force feedback. *Medical Image Analysis*, 3(3):285–300(16).

Pransky, J. (2001). An intelligent operating room of the future - an interview with the university of california, los angeles medical centre. *Industrial Robot*, 28(5):376–380.

Price, A. J., Webb, J., Topf, H., Dodd, C. A. F., Goodfellow, J. W., Murray, D. W., Oxford, H., and Knee, G. (2001). Rapid recovery after oxford unicompartmental arthroplasty through a short incision. *Journal of Arthroplasty*, 16(8):970–976.

Rajamani, K., Nolte, L.-P., and Styner, M. (2004). Bone morphing with statistical shape models for enhanced visualization. In *SPIE Medical Imaging*.

Reinhardt, H., Trippel, M., Westermann, B., and Gratzl, O. (1999). Computer aided surgery with special focus on neuronavigation. *Computerized Medical Imaging and Graphics*, 23(5):237–244.

Renders, J.-M., Rossignol, E., Becquet, M., and Hanus, R. (1991). Kinematic calibration and geometrical parameter identification for robots. *IEEE Transactions on Robotics and Automation*, 7(6):721–732.

Rockall, T. A. and Darzi, A. W. (2003). Tele-manipulator robots in surgery future promise, but expensive. *British Journal of Surgery*, 90(6):641–643.

Rodriguez y Baena, F. M., Harris, S. J., Jakopec, M., Gomes, M. P. S. F., Cobb, J. P., and Davies, B. L. (2002). Anatomical registration implementation and results for a "hands-on" robotic knee surgery system. In *Computer Assisted Orthopaedic Surgery*, pages pp. 101–102, Second Annual Meeting of CAOS International, Santa Fe, USA.

Rodriguez y Baena, F. M., Harris, S. J., Jakopec, M., Gomes, M. P. S. F., Cobb, J. P., and Davies, B. L. (2003). Fast and efficient registration for hands-on

robotic assisted knee surgery. In *Computer Assisted Orthopaedic Surgery*, pages pp. 74–75, Third Annual Meeting of CAOS International, Marbella, Spain.

Rusinkiewicz, S. and Levoy, M. (2001). Efficient variants of the icp algorithm. In *3-D digital imaging and modeling*, pages 145–152, Quebec City, Canada. Ieee.

Samet, H. (1990). Point data (chapter 2). In *The design and analysis of spatial data structures*, Addison-Wesley Series In Computer Science, pages pp. 47–81. Addison-Wesley Longman Publishing Co., Inc., Boston, MA, USA.

Schneider, O. and Troccaz, J. (2001). A six-degree-of-freedom passive arm with dynamic constraints (padyc) for cardiac surgery application: Preliminary experiments. *Computer Aided Surgery, John Wiley and Sons*, 6(6):340–351.

Schneider, O., Troccaz, J., Chavanon, O., and Blin, D. (2000). Padyc: A synergistic robot for cardiac puncturing. *Ieee International Conference on Robotics and Automation*, 3:2883–2888.

Schroeer, K., Albright, S. L., and Grethlein, M. (1997). Complete, minimal and model-continuous kinematic models for robot calibration. *Robotics and Computer Integrated Manufacturing*, 13(1):73–85.

Sciavicco, L. and Siciliano, B. (1996). *Modeling and Control of Robot Manipulators*. Electrical Engineering Series. McGrow-Hill, international editions edition.

Shoham, M., Burman, M., Zehavi, E., Joskowicz, L., Batkilin, E., and Kunicher, Y. (2003). Bone-mounted miniature robot for surgical procedures: Concept and clinical applications. *Ieee Transactions on Robotics and Automation*, 19(5):893–901.

Shroer, K. (1987). Robocal - robotic calibration software package. world wide web page: http://www.ar.ipk.fhg.de/projekteundprodukte/robocal-proj/robocal-index-e.html.

Siebert, W., Mai, S., Kober, R., and Heeckt, P. F. (2002). Technique and first clinical results of robot-assisted total knee replacement. *Knee*, 9(3):173–180.

Simon, D., Hebert, M., and Kanade, T. (1994). Techniques for fast and accurate intra-surgical registration. *MRCAS*.

Simon, D., O'Toole, R., Blackwell, M., Morgan, F., DiGioia, A., and Kanade, T. (1995). Accuracy validation in image-guided orthopaedic surgery. In *Proceedings of the Second International Symposium on Medical Robotics and Computer Assisted Surgery*, pages 185–192.

Smith, M. (2003). Lsge least-square sphere fitting.

Stoianovici, D., Cleary, K., Patriciu, A., Mazilu, D., Stanimir, A., Craciunoiu, N., Watson, V., and Kavoussi, L. (2003). Acubot: A robot for radiological interventions. *Ieee Transactions on Robotics and Automation*, 19(5):927–930.

Stryker Inc. (2002). Howmedica osteonics kinemax plus total knee system. world wide web page: http://www.osteonics.com.

Stulberg, S. D. (2001). Computer assisted total knee replacement surgery: An analysis of an initial experience with the orthopilottm system. In *Japanese Orthopaedic Association*, page S38, Chiba, Japan. Japanese Orthopaedic Association.

Sung, G. T. and Gill, I. S. (2001). Robotic laparoscopic surgery: a comparison of the da vinci and zeus systems. *Urology*, 58(6):893–898.

Tang, T. S. Y., Ellis, R. E., and Fichtinger, G. (2000). Fiducial registration from a single x-ray image: A new technique for fluoroscopic guidance and radiotherapy. In Delp, S. L., DiGioia, A. M., and Jaramaz, B., editors, *Medical Image Computing and Computer-Assisted Intervention - MICCAI 2000*, volume 1935 of *Lecture Notes in Computer Science*, pages 502–511. Springer-Verlag.

Taylor, R. H., Lavallee, S., Burdea, G. C., and Mosges, R. W., editors (1996). *Computer-integrated surgery: technology and clinical applications.* MIT Press, Cambridge (MA) USA.

Taylor, R. H., Mittelstadt, B. D., Paul, H. A., and Hanson, W. (1994). An image-directed robotic system for precise orthopaedic surgery. *Ieee Transactions on Robotics and Automation*, 10(3):261.

Taylor, R. H. and Stoianovici, D. (2003). Medical robotics in computer-integrated surgery. *Ieee Transactions on Robotics and Automation*, 19(5):765–781.

The Acrobot Company Ltd. (2001). Apparatus and method for registering the position of a surgical robot. date lodged: 19 nov 2001.

Troccaz, J., Lavallee, S., and Hellion, E. (1993). Padyc: A passive arm with dynamic constraints. In *Advanced Robotics*, pages 361–366, Tokyo. Japan Industrial Robot Association.

Uranus, S., Machler, H., Bergmann, P., Huber, S., Hobarth, G., Pfeifer, J., Rigler, B., Tscheliessnigg, K. H., and Mischinger, H. J. (2002). Early experience with

telemanipulative abdominal and cardiac surgery with the zeustm robotic system. *European Surgery*, 34:190–193.

Van Albada, G. D., Lagerberg, J. M., and Visser, A. (1994). Eye in hand robot calibration. *Industrial Robot*, 21(6):14.

Waterloo Maple Inc. (2000). Maple version 6 released january 31 2000. world wide web page: http://www.waterloomaple.com/flash/index.html.

Webb, E., editor (1988). *The Physics of Medical Imaging.* Medical Science Series. IOP.

Wolovich, W. A. (1987). *ROBOTICS: Basic Analysis and DESIGN 1st edition.* CBS College Publishing.

Young, K. Y. and Chen, J. J. (1999). Implementation of a variable d-h parameter model for robot calibration using an fcmac learning algorithm. *Journal of Intelligent and Robotic Systems*, 24(4):313–346.

Zamorano, L., Pandya, A., Li, Q. H., La Torre, R. P., Pittet, P., Badano, F., and Robert, V. (2000). The clinical use and accuracy of the neuromate robot for open neurosurgery. *International Congress Series*, 1214:185–192.

Zhang, Z. (1992). Iterative point matching for registration of free-form curves. Registration, INRIA Sophia-Antipolis.

Appendix A
Distance-Based Hole Locating Algorithm

Introduction

The hole locating algorithm is used to automatically detect the correct combination of holes touched with respect to the hole positions stored at the beginning of the procedure. Let the list of all available holes be referred to as *Available_ Hole_ Positions*, and let the list of holes (touched at a later stage) to be mapped be denominated as *Holes_ Touched*. Then, the aim of the algorithm is to find the right combination of entries in *Available_ Hole_ Positions* to match *Holes_ Touched*. The pseudo-code that follows describes a fast algorithm that uses the relative distance between successive holes to identify the correct hole combination. The algorithm has been implemented in C^{++}, and uses standard template library (STL) $< vector >$ functionality for dynamic editing and resizing of hole lists.

Pseudo-Code

```
Available_Hole_Positions = list of holes
                           located at start of
                           procedure.

Holes_Touched = list of holes touched for
                mapping.

Candidate_List = list of all possible
                 combinations of the entries in
                 Available_Hole_Positions.

LoadAvailableHoleList()
```

```
{
  Store the list of all available hole
  locations in Available_Hole_Positions.
}

GenerateCandidatesList(Candidate_List)
{
  if the Candidate_List is empty
  {
    Store a column vector of all entries in
    Available_Hole_Positions into
    Candidate_List
  }

  else
  {
    Replace each entry in Candidate_List with a
    list that includes all combinations(without
    repetitions) of the current entry and all
    holes in Available_Hole_Positions;
  }
}

// DifferenceMagnitude is the value to prune
// Candidate_List with
PruneByDistance(DifferenceMagnitude, Candidate_List)
{
  for all entries in Candidate_List:
  {
    Difference = last hole position - previous
                 hole position;

    // if the following condition is true this
    // hole combination is not the correct one
    if( ABS( MAGNITUDE(Difference) -
             DifferenceMagnitude ) >
             threshold )
    {
      eliminate entry from list;
```

```
    }
  }
}

// Find right combination of holes stored in
// Available_Hole_Positions to match
// Holes_Touched
DoMotionEstimate()
{
  // Make sure only one position per hole is in
  // the list
  PRUNEDUPLICATES(Holes_Touched);

  // Need at least three points
  if Holes_Touched has less than three entries
  {
    fail;
  }

  // Check if clamp holes have been loaded
  if Available_Hole_Positions is empty
  {
    fail;
  }

  // Make sure the candidate list of all
  // possible combinations is empty
  Candidate_List = {EMPTY};

  // Add first point to the list {this will be
  // a single column vector of all entries in
  // Available_Hole_Positions
  GenerateCandidatesList(Candidate_List);

  // First prune list of candidates by distance
  for all entries in Holes_Touched,
      excluding the first one:
  {
    // Add another point to the list
```

```
  GenerateCandidatesList(Candidate_List);

  // difference between two consecutive
  // points
  Difference = Current entry -
               previous entry;

  // Prune the candidate list to eliminate
  // all options where the difference between
  // the last two entries does not match
  // (within a specified threshold) the
  // magnitude of Difference
  PruneByDistance(MAGNITUDE(Difference),
                  Candidate_List);
}

// If the following condition is false, there
// might be two symmetric solutions, in which
// case use brute force to find correct one
if the Candidate_List does contain
   only one entry:
{
  return solution found;
}

else
{
  for each entry in the Candidate_List:
  {
    Use pair point matching and inspect
    residual error to find solution.
  }

  // if there is still more than one
  // combination of points in the list, not
  // enough points have been touched, which
  // means a solution cannot be found.
  if the Candidate_List contains
     only one entry:
```

```
    {
      return found solution;
    }

    else
    {
      fail;
    }
  } // End of pair point matching
} // End of function
```

Appendix B
ICP Patient Simulation Results - TKA

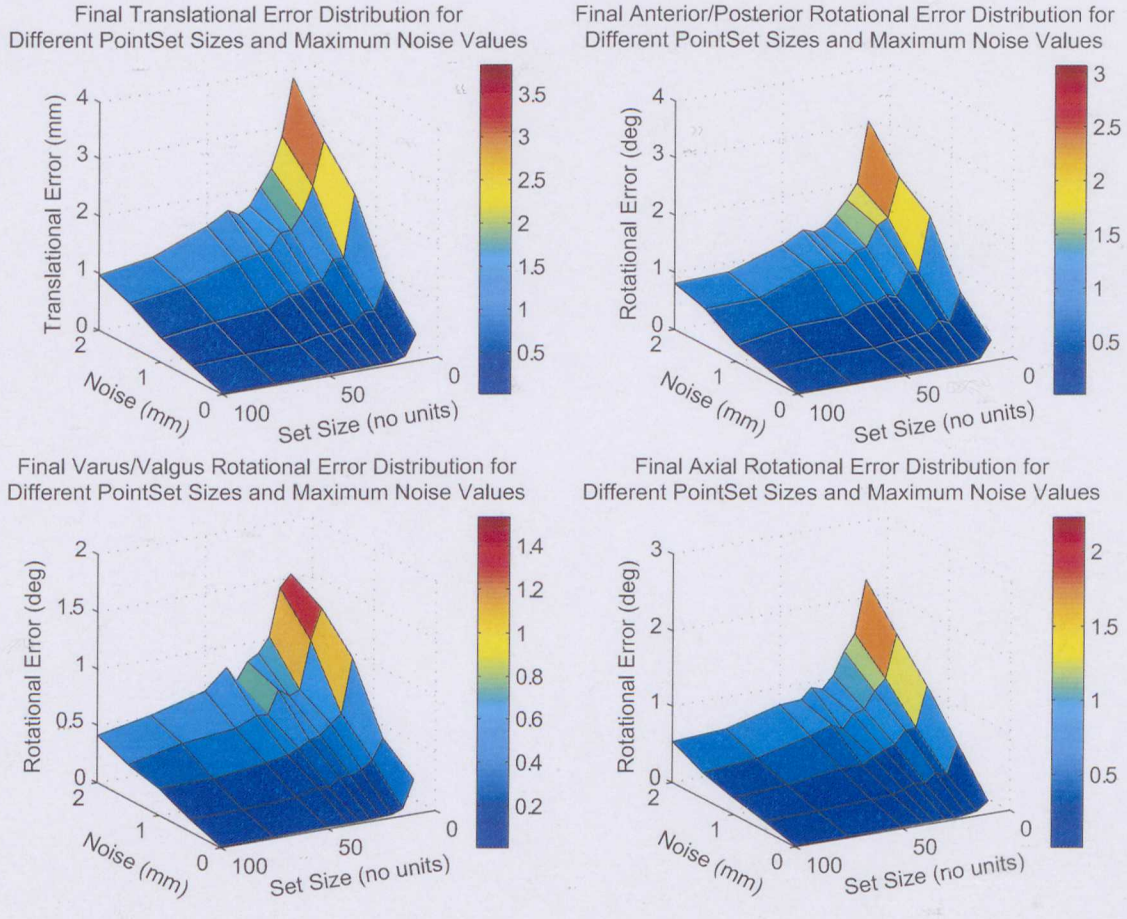


Figure B.1: Registration accuracy for the enhanced ICP algorithm in terms of varus/valgus, anterior/posterior, axial, and translational components for different point-set sizes and maximum noise values, for the femur.

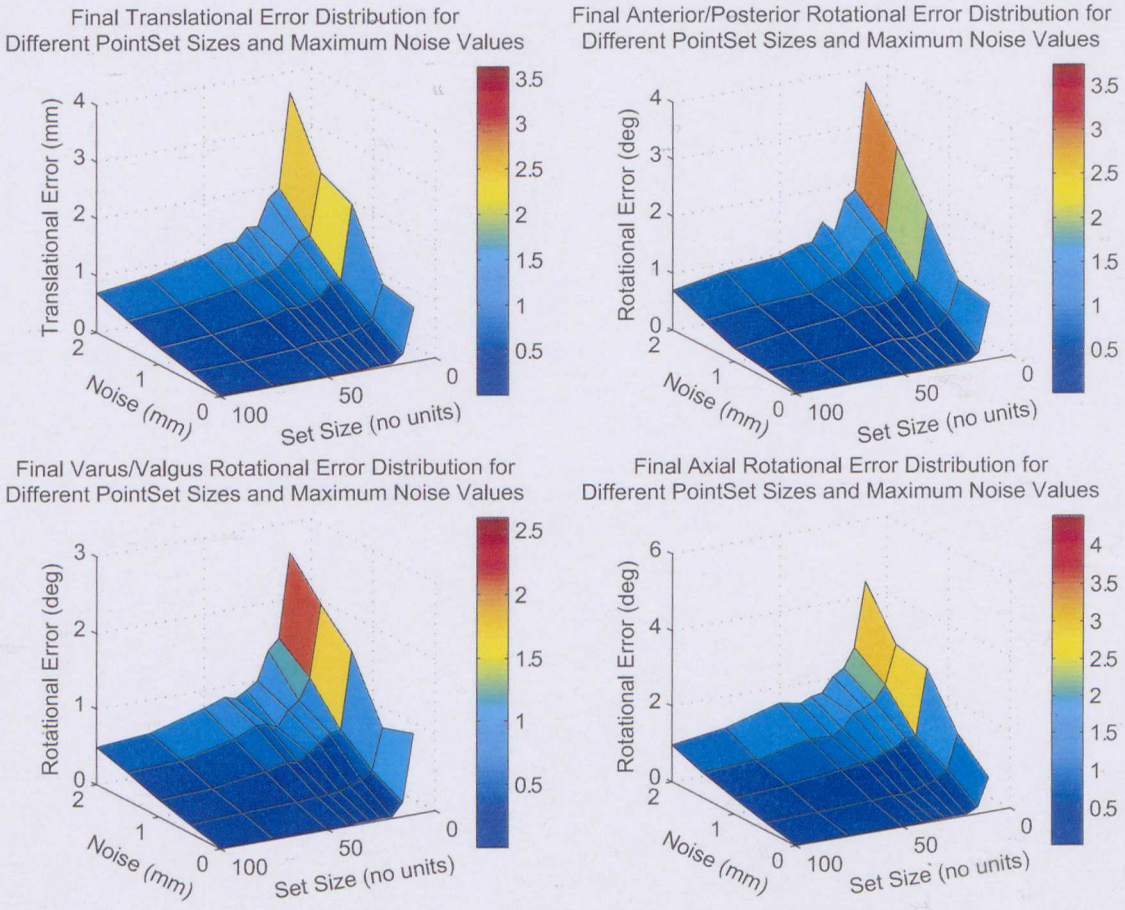


Figure B.2: Registration accuracy for the enhanced ICP algorithm in terms of varus/valgus, anterior/posterior, axial, and translational components for different point-set sizes and maximum noise values, for the tibia.

	Performance of Random Point-Sets of Different Sizes for 0.5mm Maximum Noise						
	Point-Set Size	Average Err	Max Error	Min Error	STD	95% of Pop	75% of Pop
Rotational Error (deg)	10	1.49	11.63	0.04	1.43	4.34	2.91
	15	0.83	1.96	0.14	0.58	1.89	1.11
	20	0.76	3.26	0.11	0.50	1.76	1.26
	25	0.56	1.60	0.16	0.25	1.06	0.81
	30	0.56	1.38	0.14	0.25	1.06	0.81
	35	0.45	1.58	0.06	0.25	0.96	0.70
	40	0.42	0.96	0.11	0.18	0.78	0.60
	50	0.34	0.80	0.12	0.15	0.65	0.50
	75	0.31	1.00	0.06	0.15	0.61	0.46
	100	0.26	0.79	0.03	0.12	0.49	0.38
Translational Error (mm)	10	1.14	3.70	0.04	0.82	2.79	1.96
	15	0.85	1.73	0.08	0.55	1.55	0.99
	20	0.65	2.63	0.05	0.40	1.45	1.05
	25	0.48	1.42	0.07	0.25	0.97	0.73
	30	0.45	1.35	0.03	0.25	0.95	0.70
	35	0.39	1.37	0.06	0.23	0.86	0.62
	40	0.38	1.06	0.01	0.18	0.75	0.56
	50	0.29	0.74	0.03	0.15	0.58	0.44
	75	0.27	0.85	0.01	0.15	0.57	0.42
	100	0.22	0.74	0.04	0.11	0.44	0.33

	Performance of Random Point-Sets of Different Sizes for 1.0mm Maximum Noise						
	Point-Set Size	Average Err	Max Error	Min Error	STD	95% of Pop	75% of Pop
Rotational Error (deg)	10	2.93	32.71	0.46	3.48	9.89	6.41
	15	1.57	3.82	0.29	0.74	3.06	2.31
	20	1.58	5.56	0.09	0.87	3.31	2.44
	25	1.10	3.03	0.12	0.55	2.20	1.65
	30	1.10	3.04	0.26	0.55	2.19	1.65
	35	0.97	2.60	0.13	0.48	1.92	1.45
	40	0.90	2.50	0.24	0.44	1.77	1.34
	50	0.75	1.96	0.16	0.37	1.50	1.13
	75	0.65	1.50	0.11	0.28	1.21	0.93
	100	0.50	1.43	0.04	0.27	1.05	0.77
Translational Error (mm)	10	2.37	31.22	0.30	3.14	8.66	5.51
	15	1.28	2.95	0.10	0.64	2.56	1.92
	20	1.29	4.37	0.07	0.71	2.72	2.01
	25	0.95	2.41	0.18	0.44	1.82	1.38
	30	0.93	2.82	0.20	0.49	1.90	1.41
	35	0.80	2.15	0.13	0.39	1.57	1.19
	40	0.79	2.32	0.16	0.40	1.59	1.19
	50	0.63	1.77	0.08	0.34	1.31	0.97
	75	0.55	1.40	0.03	0.25	1.06	0.81
	100	0.43	1.28	0.06	0.25	0.93	0.68

Table B.1: Relationship between point-set size and registration robustness, expressed in terms of overall rotational and translational accuracy, for a set of robust point-sets describing a distal femur.

	Performance of Random Point-Sets of Different Sizes for 1.5mm Maximum Noise					
Point-Set Size	**Average Err**	**Max Error**	**Min Error**	**STD**	**95% of Pop**	**75% of Pop**
Rotational Error (deg)						
10	3.68	12.40	0.56	2.35	8.38	6.03
15	2.66	14.35	0.69	1.78	6.21	4.44
20	2.27	6.98	0.25	1.34	4.96	3.61
25	1.84	4.88	0.32	1.02	3.87	2.86
30	1.82	5.92	0.44	0.90	3.63	2.73
35	1.46	4.00	0.39	0.68	2.82	2.14
40	1.51	4.09	0.21	0.70	2.91	2.21
50	1.41	3.40	0.37	0.66	2.74	2.08
75	1.01	2.37	0.25	0.43	1.88	1.44
100	0.88	1.77	0.19	0.40	1.68	1.28
Translational Error (mm)						
10	3.03	9.75	0.45	1.75	6.53	4.78
15	2.25	14.49	0.35	1.68	5.61	3.93
20	1.82	4.79	0.19	1.01	3.85	2.83
25	1.55	4.04	0.23	0.87	3.29	2.42
30	1.53	4.85	0.25	0.86	3.26	2.39
35	1.27	3.73	0.16	0.64	2.55	1.91
40	1.24	3.16	0.13	0.64	2.51	1.87
50	1.16	2.75	0.03	0.60	2.35	1.75
75	0.90	2.07	0.10	0.41	1.72	1.31
100	0.75	1.54	0.04	0.36	1.47	1.11

	Performance of Random Point-Sets of Different Sizes for 2.0mm Maximum Noise					
Point-Set Size	**Average Err**	**Max Error**	**Min Error**	**STD**	**95% of Pop**	**75% of Pop**
Rotational Error (deg)						
10	4.74	16.19	0.84	3.10	10.93	7.84
15	3.33	14.14	0.38	1.91	7.16	5.24
20	2.75	8.17	0.42	1.42	5.60	4.17
25	2.38	8.38	0.44	1.28	4.94	3.66
30	2.08	5.59	0.43	1.00	4.09	3.08
35	1.99	5.31	0.49	0.92	3.82	2.91
40	1.81	5.26	0.53	0.90	3.61	2.96
50	1.72	4.95	0.35	0.86	3.44	2.58
75	1.29	3.23	0.25	0.61	2.51	1.90
100	1.19	2.73	0.22	0.54	2.26	1.73
Translational Error (mm)						
10	3.84	12.26	0.73	2.35	8.54	6.19
15	2.84	8.59	0.42	1.58	6.00	4.42
20	2.31	6.76	0.65	1.18	4.67	3.49
25	2.02	7.33	0.38	1.17	4.35	3.19
30	1.72	4.41	0.48	0.89	3.50	2.61
35	1.61	4.19	0.30	0.81	3.23	2.42
40	1.58	4.92	0.17	0.78	3.14	2.63
50	1.50	3.90	0.22	0.71	2.92	2.21
75	1.12	3.53	0.13	0.56	2.24	1.68
100	0.97	2.49	0.18	0.45	1.86	1.41

Table B.1: (cont'd) Relationship between point-set size and registration robustness, expressed in terms of overall rotational and translational accuracy, for a set of robust point-sets describing a distal femur.

	Performance of Random Point-Sets of Different Sizes for 0.5mm Maximum Noise						
	Point-Set Size	**Average Err**	**Max Error**	**Min Error**	**STD**	**95% of Pop**	**75% of Pop**
Rotational Error (deg)	*10*	2.47	20.94	0.31	2.97	8.41	5.44
	15	1.11	11.91	0.17	1.50	4.10	2.60
	20	0.81	3.31	0.25	0.46	1.73	1.27
	25	0.66	1.99	0.12	0.35	1.36	1.01
	30	0.55	1.53	0.14	0.28	1.10	0.82
	35	0.50	1.41	0.06	0.27	1.04	0.77
	40	0.48	1.62	0.04	0.26	1.00	0.80
	50	0.44	1.74	0.06	0.25	0.95	0.70
	75	0.35	0.91	0.02	0.17	0.68	0.51
	100	0.30	0.73	0.05	0.15	0.61	0.46
Translational Error (mm)	*10*	1.09	6.08	0.13	1.09	3.27	2.18
	15	0.53	7.00	0.09	0.71	1.96	1.25
	20	0.42	1.60	0.09	0.25	0.91	0.66
	25	0.35	1.01	0.07	0.18	0.72	0.53
	30	0.31	1.06	0.06	0.17	0.65	0.48
	35	0.27	0.91	0.04	0.15	0.58	0.43
	40	0.26	0.95	0.07	0.14	0.54	0.44
	50	0.24	1.01	0.05	0.13	0.50	0.37
	75	0.18	0.41	0.01	0.08	0.33	0.26
	100	0.16	0.45	0.04	0.08	0.33	0.25

	Performance of Random Point-Sets of Different Sizes for 1.0mm Maximum Noise						
	Point-Set Size	**Average Err**	**Max Error**	**Min Error**	**STD**	**95% of Pop**	**75% of Pop**
Rotational Error (deg)	*10*	4.46	33.12	0.30	5.19	14.84	9.65
	15	1.80	7.26	0.36	1.12	4.04	2.92
	20	1.83	5.34	0.21	1.11	4.04	2.94
	25	1.48	3.89	0.20	0.83	3.14	2.31
	30	1.33	3.38	0.28	0.70	2.73	2.03
	35	1.15	3.17	0.12	0.63	2.42	1.79
	40	1.12	3.28	0.15	0.60	2.32	1.72
	50	1.00	2.61	0.13	0.48	1.96	1.48
	75	0.76	2.08	0.15	0.36	1.49	1.13
	100	0.60	1.64	0.10	0.31	1.21	0.91
Translational Error (mm)	*10*	2.21	19.95	0.27	2.62	7.44	4.82
	15	0.91	3.02	0.07	0.53	1.98	1.44
	20	0.89	2.98	0.25	0.49	1.87	1.38
	25	0.69	1.77	0.10	0.35	1.40	1.04
	30	0.63	2.00	0.15	0.34	1.30	0.96
	35	0.58	1.83	0.07	0.31	1.19	0.89
	40	0.53	1.52	0.19	0.29	1.11	0.82
	50	0.48	1.34	0.07	0.24	0.97	0.72
	75	0.37	0.94	0.08	0.19	0.76	0.57
	100	0.30	0.65	0.08	0.14	0.58	0.44

Table B.2: Relationship between point-set size and registration robustness, expressed in terms of overall rotational and translational accuracy, for a set of robust point-sets describing a proximal tibia.

	Performance of Random Point-Sets of Different Sizes for 1.5mm Maximum Noise					
Point-Set Size	**Average Err**	**Max Error**	**Min Error**	**STD**	**95% of Pop**	**75% of Pop**
Rotational Error (deg)						
10	5.51	24.76	0.52	4.20	13.91	9.71
15	3.22	10.67	0.55	1.97	7.16	5.19
20	2.70	9.41	0.30	1.76	6.22	4.46
25	2.43	5.46	0.45	1.08	4.60	3.52
30	2.12	7.41	0.38	1.21	4.53	3.33
35	1.74	5.35	0.29	1.04	3.81	2.78
40	1.61	4.64	0.20	0.79	3.19	2.40
50	1.48	3.49	0.33	0.71	2.90	2.19
75	1.15	3.21	0.17	0.58	2.30	1.73
100	0.99	2.47	0.19	0.52	2.03	1.51
Translational Error (mm)						
10	2.49	8.70	0.53	1.79	6.07	4.28
15	1.41	5.38	0.19	0.85	3.10	2.26
20	1.34	3.89	0.20	0.74	2.82	2.08
25	1.12	3.29	0.19	0.56	2.24	1.68
30	0.94	2.46	0.19	0.45	1.84	1.39
35	0.88	2.04	0.14	0.45	1.77	1.32
40	0.83	1.95	0.16	0.38	1.60	1.21
50	0.74	1.92	0.15	0.33	1.40	1.07
75	0.59	1.45	0.15	0.30	1.20	0.90
100	0.50	1.25	0.11	0.23	0.96	0.73

	Performance of Random Point-Sets of Different Sizes for 2.0mm Maximum Noise					
Point-Set Size	**Average Err**	**Max Error**	**Min Error**	**STD**	**95% of Pop**	**75% of Pop**
Rotational Error (deg)						
10	7.25	27.54	1.17	5.12	17.49	12.37
15	4.09	20.26	0.73	2.55	9.19	6.64
20	3.55	17.67	0.65	2.52	8.60	6.08
25	2.92	8.35	0.40	1.63	6.18	4.55
30	2.70	8.03	0.26	1.26	5.23	3.96
35	2.43	5.90	0.14	1.31	5.05	3.74
40	2.32	6.05	0.43	1.22	4.75	3.54
50	2.22	6.50	0.59	1.09	4.41	3.32
75	1.76	6.08	0.28	0.89	3.54	2.65
100	1.46	3.31	0.33	0.70	2.87	2.17
Translational Error (mm)						
10	3.63	16.15	0.54	2.91	9.45	6.54
15	1.96	12.86	0.25	1.39	4.75	3.36
20	1.81	7.12	0.28	1.19	4.19	3.00
25	1.37	3.45	0.04	0.73	2.83	2.10
30	1.38	4.67	0.18	0.73	2.85	2.11
35	1.15	2.77	0.14	0.61	2.38	1.77
40	1.10	2.78	0.26	0.57	2.24	1.67
50	1.04	3.31	0.10	0.51	2.07	1.55
75	0.82	2.36	0.15	0.42	1.66	1.24
100	0.69	1.75	0.11	0.37	1.44	1.07

Table B.2: (cont'd) Relationship between point-set size and registration robustness, expressed in terms of overall rotational and translational accuracy, for a set of robust point-sets describing a proximal tibia.

Appendix C
Fiducial Screws Vs. Reference Point-Set

Method

In order to validate the reference point-set method described in Section 5.4.3.2, a number of fiducial marker screws were inserted into the femur and tibia of a plastic phantom bone set prior to it being CT scanned. As illustrated in Figure C.1, fiducial titanium screws show up as bright elements in the CT data, and can be easily identified during segmentation. Pre-operatively, Acrobot's proprietary planning software (Figure C.2) was used to isolate and locate each screw in the CT dataset with respect to the corresponding surface model.

Intra-operatively, the position of each screw was established, using the spherical tip of the registration probe inserted in the back-drivable end effector of the ACROBOT II System. The screw positions in both the plan (generated pre-operatively) and the robot's co-ordinate systems were then used to calculate a reference matrix using a well known closed-form paired-point matching algorithm [Horn, 1987].

Results

Results, presented in Table C.1, show discrepancies between the reference matrices obtained using the two methods (reference point-set and fiducial markers) of approximately 1° and $2mm$. This amount of error is likely to be due to inaccuracies introduced during segmentation or while locating the screws intra-operatively.

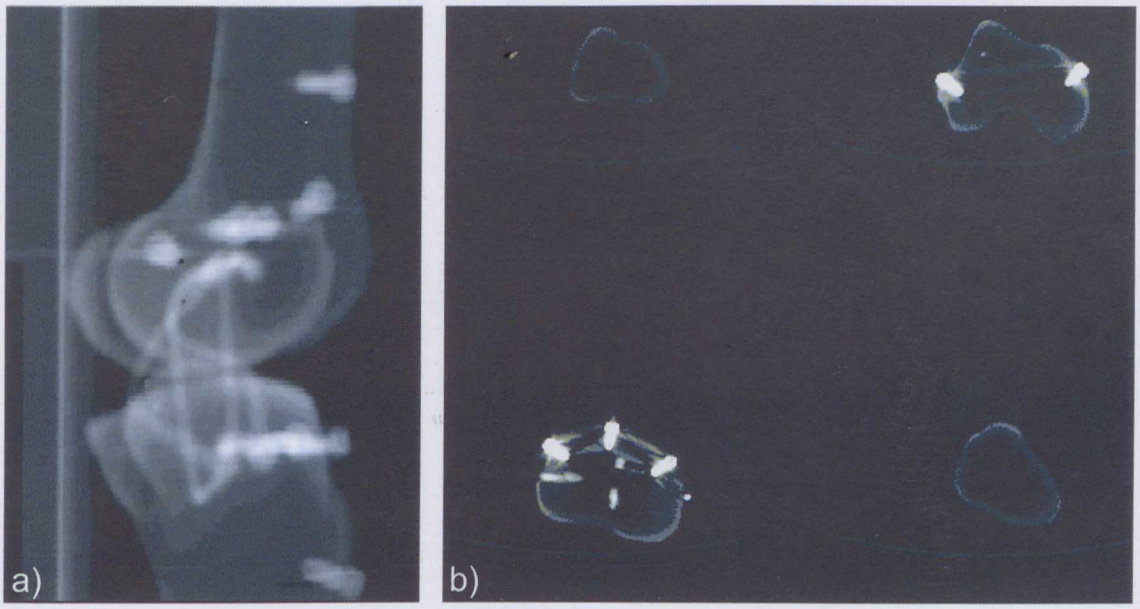


Figure C.1: Lateral (a) and sagittal (b) views of a plastic phantom bone with fiducial marker screws.

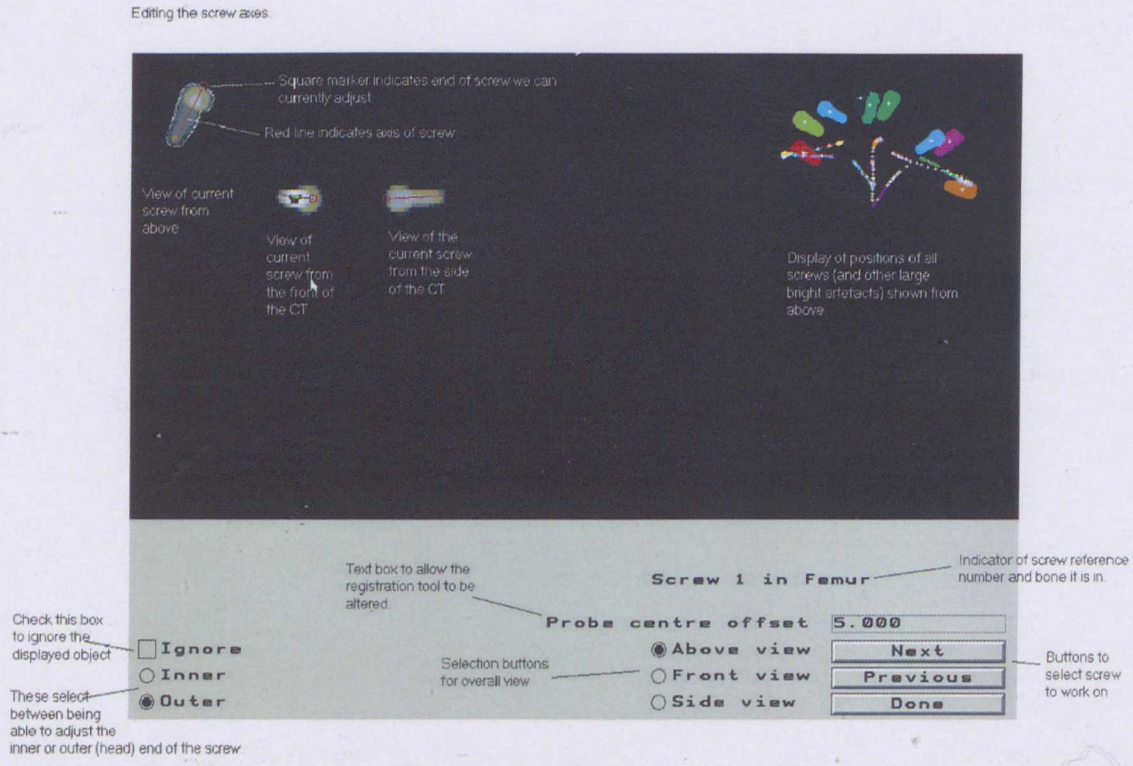


Figure C.2: Screen-shot of Acrobot's proprietary pre-operative software for fiducial screw identification.

a) PLASTIC FEMUR WITH FIDUCIALS

(from "tibia.cen")

Object Centre in M Space			
164.500	135.500	153.300	1.000

(from "EventLog.txt")

Reference Transformation Matrix (M to R)			
-0.995	-0.054	-0.090	156.095
-0.099	0.754	0.649	-253.679
0.033	0.655	-0.755	392.963
0.000	0.000	0.000	1.000

Fiducial Transformation Matrix (M to R)			
-0.996	-0.032	-0.089	152.742
-0.083	0.751	0.655	-256.836
0.046	0.659	-0.750	390.215
0.000	0.000	0.000	1.000

Reference Matrix Inverse (R to M)			
-0.995	-0.099	0.033	117.219
-0.054	0.754	0.655	-57.532
-0.090	0.649	-0.755	475.487
0.000	0.000	0.000	1.000

Fiducial Matrix Inverse (R to M)			
-0.996	-0.083	0.046	112.823
-0.032	0.751	0.659	-59.591
-0.089	0.655	-0.750	474.639
0.000	0.000	0.000	1.000

(Inverse of Ref x Actual)

Error Matrix in M Space			
1.000	-0.021	-0.001	3.557
0.021	1.000	0.008	-4.000
0.001	-0.008	1.000	0.327
0.000	0.000	0.000	1.000

Translational Error Relative To Knee Centre			
0.526	0.628	-0.613	0.000

Error Matrix Components				
V/V Error	*Axial Error*	*A/P Error*	*Rot Error*	*Trans Error*
-0.039	1.213	-0.442	1.291	1.023

b) PLASTIC TIBIA WITH FIDUCIALS

(from "tibia.cen")

Object Centre in M Space			
164.000	139.500	167.000	1.000

(from "EventLog.txt")

Reference Transformation Matrix (M to R)			
-0.985	0.142	0.099	96.801
-0.045	-0.760	0.649	-90.630
0.168	0.634	0.755	114.303
0.000	0.000	0.000	1.000

Fiducial Transformation Matrix (M to R)			
-0.980	0.171	0.102	92.263
-0.062	-0.748	0.661	-92.189
0.189	0.641	0.744	113.461
0.000	0.000	0.000	1.000

Reference Matrix Inverse (R to M)			
-0.985	-0.045	0.168	72.121
0.142	-0.760	0.634	-155.160
0.099	0.649	0.755	-37.057
0.000	0.000	0.000	1.000

Fiducial Matrix Inverse (R to M)			
-0.980	-0.062	0.189	63.277
0.171	-0.748	0.641	-157.483
0.102	0.661	0.744	-32.857
0.000	0.000	0.000	1.000

(Inverse of Ref x Actual)

Error Matrix in M Space			
1.000	-0.027	-0.005	4.398
0.027	1.000	-0.016	0.003
0.005	0.016	1.000	-2.095
0.000	0.000	0.000	1.000

Translational Error Relative To Knee Centre			
-0.321	1.775	0.955	0.000

Error Matrix Components				
V/V Error	*Axial Error*	*A/P Error*	*Rot Error*	*Trans Error*
-0.314	1.562	0.894	1.828	2.041

Values in these cells are pasted from the logs
Values in these cells illustrate actual registration accurcy split in the four error components

Table C.1: Error difference between a fiducial-based registration transform and one obtained with a reference point-set. Values are expressed in component form for both the femur (a), and tibia (b).

Appendix D
ICP Patient Simulation Results - UKA

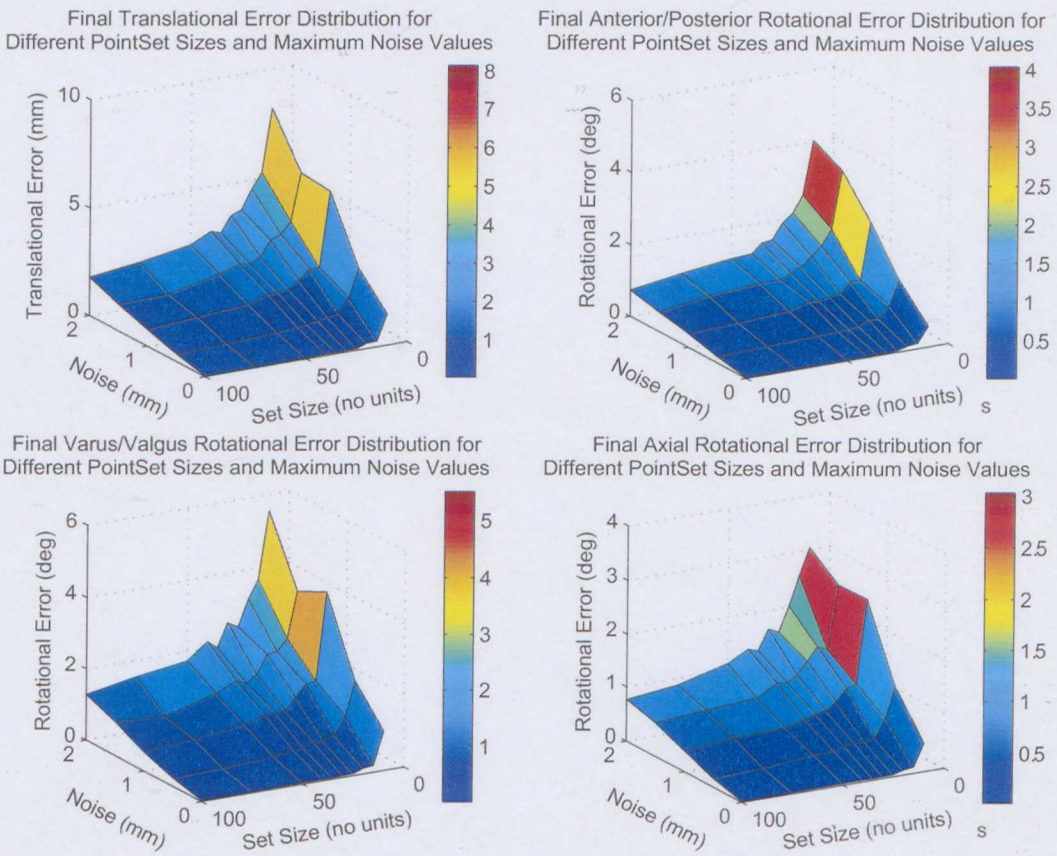


Figure D.1: Registration accuracy for the enhanced ICP algorithm in terms of varus/valgus, anterior/posterior, axial, and translational components for different point-set sizes and maximum noise values, for the femur.

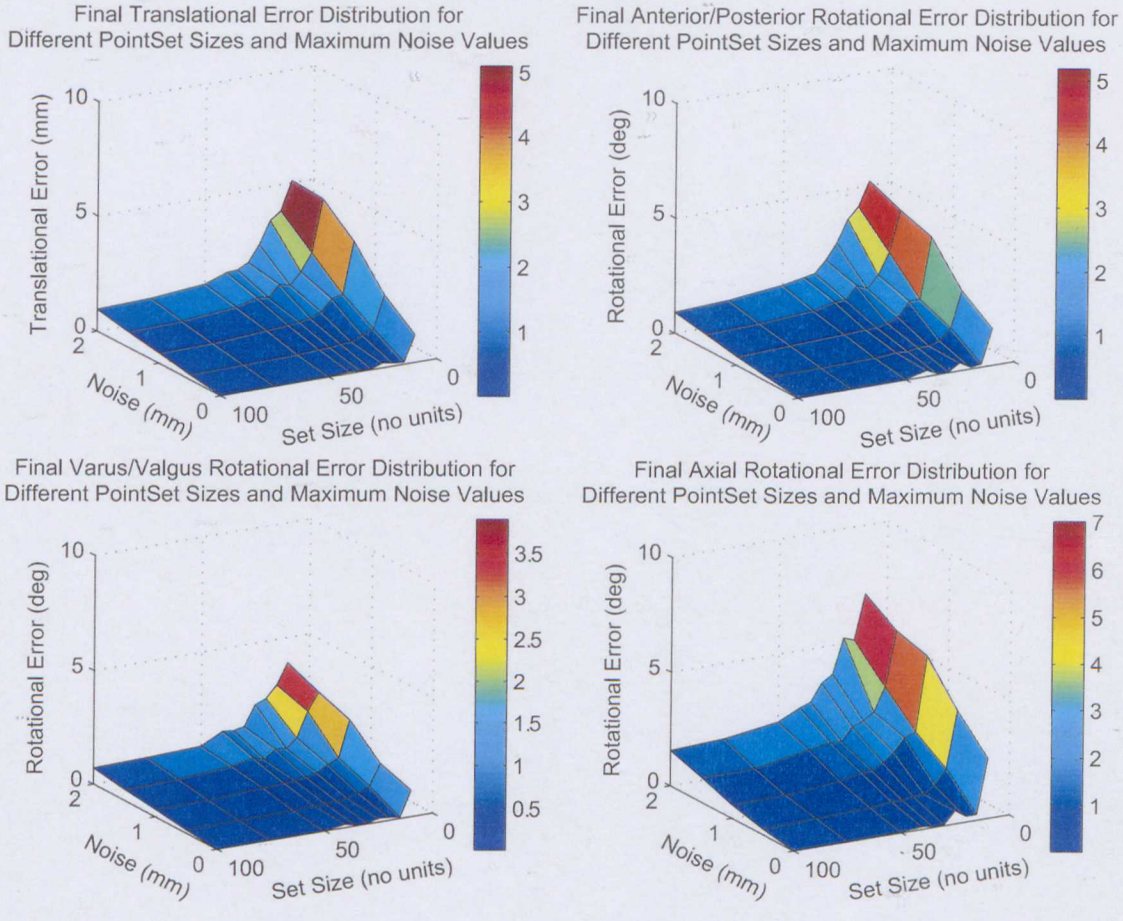


Figure D.2: Registration accuracy for the enhanced ICP algorithm in terms of varus/valgus, anterior/posterior, axial, and translational components for different point-set sizes and maximum noise values, for the tibia.

	Performance of Random Point-Sets of Different Sizes for 0.5mm Maximum Noise						
	Point-Set Size	**Average Err**	**Max Error**	**Min Error**	**STD**	**95% of Pop**	**75% of Pop**
Rotational Error (deg)	*10*	3.15	30.01	0.18	3.98	11.11	7.13
	15	1.72	19.39	0.31	2.10	5.92	3.82
	20	0.99	3.01	0.17	0.53	2.04	1.52
	25	0.89	2.78	0.15	0.48	1.84	1.37
	30	0.84	4.48	0.16	0.47	1.78	1.31
	35	0.73	2.64	0.13	0.45	1.63	1.18
	40	0.67	1.54	0.03	0.32	1.31	0.99
	50	0.59	2.43	0.10	0.30	1.19	0.89
	75	0.46	0.90	0.08	0.20	0.85	0.66
	100	0.37	0.97	0.08	0.16	0.70	0.54
Translational Error (mm)	*10*	2.88	22.49	0.12	3.37	9.61	6.24
	15	1.55	19.08	0.10	2.09	5.73	3.64
	20	0.92	3.59	0.14	0.59	2.10	1.51
	25	0.82	2.83	0.10	0.47	1.76	1.29
	30	0.77	5.25	0.08	0.45	1.67	1.22
	35	0.64	2.71	0.09	0.40	1.44	1.04
	40	0.62	1.47	0.08	0.34	1.29	0.96
	50	0.52	1.70	0.03	0.39	1.29	0.91
	75	0.41	0.90	0.02	0.21	0.83	0.62
	100	0.35	1.22	0.03	0.19	0.72	0.54

	Performance of Random Point-Sets of Different Sizes for 1.0mm Maximum Noise						
	Point-Set Size	**Average Err**	**Max Error**	**Min Error**	**STD**	**95% of Pop**	**75% of Pop**
Rotational Error (deg)	*10*	6.25	41.62	1.07	6.15	18.55	12.40
	15	2.48	8.31	0.49	1.43	5.33	3.91
	20	2.47	11.74	0.44	1.30	5.07	3.77
	25	1.95	7.04	0.32	1.27	4.48	3.22
	30	1.60	5.93	0.16	0.99	3.59	2.60
	35	1.53	4.61	0.11	0.84	3.22	2.38
	40	1.54	4.16	0.24	0.78	3.10	2.32
	50	1.22	4.15	0.21	0.69	2.60	1.91
	75	1.03	2.74	0.21	0.57	2.16	1.60
	100	0.86	3.18	0.17	0.47	1.81	1.33
Translational Error (mm)	*10*	5.71	36.30	0.17	6.05	17.82	11.76
	15	2.25	6.96	0.20	1.44	5.13	3.69
	20	2.28	9.24	0.13	1.40	5.08	3.68
	25	1.81	6.69	0.29	1.30	4.40	3.11
	30	1.50	6.87	0.16	1.13	3.76	2.63
	35	1.42	4.34	0.17	0.86	3.13	2.27
	40	1.43	5.11	0.16	0.80	3.03	2.23
	50	1.14	4.98	0.20	0.77	2.67	1.90
	75	0.94	3.42	0.16	0.60	2.13	1.53
	100	0.78	2.49	0.18	0.50	1.77	1.28

Table D.1: Relationship between point-set size and registration robustness, expressed in terms of overall rotational and translational accuracy, for a set of robust point-sets describing a distal femur.

	Performance of Random Point-Sets of Different Sizes for 1.5mm Maximum Noise					
	Point-Set Size	**Average Err**	**Max Error**	**Min Error**	**STD**	**95% of Pop**	**75% of Pop**
Rotational Error (deg)	*10*	6.62	21.51	1.07	4.36	15.34	10.98
	15	3.89	12.76	0.34	2.40	8.70	6.30
	20	3.45	12.46	0.84	1.82	7.08	5.27
	25	3.16	16.80	0.44	1.80	5.76	4.96
	30	2.50	6.80	0.25	1.26	5.02	3.76
	35	2.24	5.47	0.25	1.11	4.46	3.35
	40	2.23	7.14	0.16	1.17	4.56	3.40
	50	1.91	4.67	0.42	1.04	3.98	2.94
	75	1.52	3.79	0.36	0.77	3.05	2.28
	100	1.40	4.14	0.38	0.66	2.72	2.06
Translational Error (mm)	*10*	5.87	17.09	0.17	3.95	13.77	9.82
	15	3.70	10.31	0.52	2.37	8.44	6.07
	20	3.19	13.22	0.68	1.92	7.04	5.12
	25	2.98	19.11	0.38	1.81	6.60	4.79
	30	2.29	6.32	0.23	1.32	4.93	3.61
	35	2.05	6.26	0.16	1.27	4.59	3.32
	40	2.00	7.39	0.22	1.20	4.40	3.20
	50	1.81	4.76	0.42	1.11	4.03	2.92
	75	1.29	4.64	0.12	0.74	2.77	2.03
	100	1.26	4.52	0.26	0.76	2.78	2.02

	Performance of Random Point-Sets of Different Sizes for 2.0mm Maximum Noise					
	Point-Set Size	**Average Err**	**Max Error**	**Min Error**	**STD**	**95% of Pop**	**75% of Pop**
Rotational Error (deg)	*10*	8.50	25.70	1.01	5.09	18.68	13.59
	15	5.92	20.41	1.19	3.76	13.44	9.68
	20	4.83	27.07	0.61	3.36	11.56	8.20
	25	3.94	12.49	0.75	2.02	7.98	5.96
	30	3.84	9.75	0.45	1.84	7.53	5.68
	35	3.09	10.85	0.70	1.68	6.45	4.77
	40	3.01	9.63	0.54	1.41	5.83	4.42
	50	2.70	6.92	0.33	1.28	5.27	3.98
	75	2.26	4.80	0.21	0.98	4.21	3.23
	100	1.86	5.12	0.33	0.86	3.57	2.72
Translational Error (mm)	*10*	8.16	29.89	0.59	5.85	19.87	14.01
	15	5.27	15.38	0.71	3.45	12.16	8.71
	20	4.57	23.43	0.22	3.26	11.08	7.82
	25	3.69	15.81	0.25	2.18	8.04	5.87
	30	3.52	10.50	0.62	2.08	7.68	5.60
	35	2.79	13.11	0.42	1.83	6.46	4.62
	40	2.55	9.93	0.51	1.75	6.05	4.30
	50	2.47	6.27	0.31	1.47	5.41	3.94
	75	2.08	4.93	0.27	1.14	4.36	3.22
	100	1.79	3.96	0.30	0.90	3.60	2.69

Table D.1: (cont'd) Relationship between point-set size and registration robustness, expressed in terms of overall rotational and translational accuracy, for a set of robust point-sets describing a distal femur.

	Performance of Random Point-Sets of Different Sizes for 0.5mm Maximum Noise						
	Point-Set Size	**Average Err**	**Max Error**	**Min Error**	**STD**	**95% of Pop**	**75% of Pop**
Rotational Error (deg)	*10*	5.32	59.58	0.28	8.95	23.23	14.28
	15	2.12	30.61	0.23	3.80	9.71	5.91
	20	1.24	8.94	0.16	1.40	4.04	2.64
	25	0.86	3.14	0.04	0.50	1.86	1.36
	30	0.83	2.12	0.13	0.43	1.70	1.27
	35	0.69	2.58	0.15	0.41	1.51	1.10
	40	0.69	2.37	0.05	0.42	1.54	1.12
	50	0.56	1.31	0.10	0.28	1.12	0.84
	75	0.48	1.22	0.11	0.26	1.01	0.74
	100	0.38	1.10	0.07	0.20	0.79	0.58
Translational Error (mm)	*10*	2.24	39.72	0.24	4.44	11.12	6.68
	15	0.84	5.99	0.09	0.77	2.39	1.61
	20	0.66	3.48	0.08	0.55	1.76	1.21
	25	0.45	1.22	0.07	0.25	0.95	0.70
	30	0.43	1.11	0.06	0.22	0.87	0.65
	35	0.36	0.88	0.09	0.20	0.76	0.56
	40	0.35	1.18	0.05	0.21	0.76	0.56
	50	0.28	0.77	0.02	0.15	0.58	0.43
	75	0.25	0.68	0.06	0.11	0.47	0.36
	100	0.21	0.48	0.02	0.11	0.42	0.32

	Performance of Random Point-Sets of Different Sizes for 1.0mm Maximum Noise						
	Point-Set Size	**Average Err**	**Max Error**	**Min Error**	**STD**	**95% of Pop**	**75% of Pop**
Rotational Error (deg)	*10*	8.46	58.94	0.30	10.26	28.98	18.72
	15	3.40	24.43	0.62	3.09	9.57	6.48
	20	3.24	32.51	0.38	4.65	12.55	7.90
	25	2.23	6.99	0.41	1.30	4.84	3.53
	30	1.78	4.43	0.28	1.00	3.79	2.78
	35	1.49	4.49	0.31	0.92	3.32	2.41
	40	1.48	4.94	0.23	0.88	3.23	2.35
	50	1.26	3.12	0.26	0.62	2.50	1.88
	75	0.95	4.50	0.11	0.63	2.21	1.58
	100	0.84	2.75	0.13	0.50	1.84	1.34
Translational Error (mm)	*10*	3.87	29.88	0.45	4.95	13.78	8.82
	15	1.64	16.00	0.14	1.67	4.98	3.31
	20	1.52	17.42	0.19	1.92	5.36	3.44
	25	1.04	3.20	0.15	0.57	2.18	1.61
	30	0.85	2.53	0.08	0.53	1.90	1.38
	35	0.77	2.25	0.09	0.43	1.63	1.20
	40	0.72	2.28	0.15	0.42	1.55	1.14
	50	0.65	1.62	0.11	0.33	1.31	0.98
	75	0.49	1.62	0.14	0.28	1.05	0.77
	100	0.45	1.25	0.05	0.25	0.95	0.70

Table D.2: Relationship between point-set size and registration robustness, expressed in terms of overall rotational and translational accuracy, for a set of robust point-sets describing a proximal tibia.

	Performance of Random Point-Sets of Different Sizes for 1.5mm Maximum Noise						
	Point-Set Size	Average Err	Max Error	Min Error	STD	95% of Pop	75% of Pop
Rotational Error (deg)	10	9.22	65.40	1.66	8.50	26.23	17.73
	15	5.98	34.08	0.80	5.93	17.84	11.91
	20	4.04	37.78	0.50	4.29	12.62	8.33
	25	3.24	9.09	0.25	1.94	7.12	5.18
	30	3.14	13.75	0.61	1.88	7.52	5.02
	35	2.34	6.84	0.29	1.31	4.95	3.65
	40	2.30	7.62	0.47	1.30	4.90	3.79
	50	2.07	8.69	0.48	1.28	4.62	3.35
	75	1.52	5.49	0.25	0.90	3.31	2.41
	100	1.48	5.35	0.32	0.84	3.16	2.32
Translational Error (mm)	10	5.00	46.26	0.59	5.58	16.16	10.58
	15	2.76	15.95	0.25	2.40	7.56	5.16
	20	2.01	11.91	0.15	1.75	5.50	3.75
	25	1.48	4.57	0.17	0.82	3.12	2.30
	30	1.41	4.01	0.26	0.76	2.93	2.17
	35	1.11	3.16	0.10	0.63	2.36	1.73
	40	1.10	3.85	0.15	0.60	2.30	1.70
	50	0.95	2.73	0.11	0.53	2.01	1.48
	75	0.75	2.39	0.08	0.44	1.63	1.19
	100	0.68	1.89	0.12	0.37	1.42	1.05

	Performance of Random Point-Sets of Different Sizes for 2.0mm Maximum Noise						
	Point-Set Size	Average Err	Max Error	Min Error	STD	95% of Pop	75% of Pop
Rotational Error (deg)	10	10.78	39.90	1.56	7.91	26.61	18.69
	15	8.09	50.94	0.64	7.99	24.06	16.07
	20	7.42	45.38	1.14	6.87	21.16	14.29
	25	5.79	37.28	0.35	5.79	17.38	11.59
	30	4.61	28.25	0.44	3.40	11.41	8.01
	35	3.61	13.34	0.49	2.28	8.17	5.89
	40	3.41	9.89	0.52	1.82	7.04	5.23
	50	2.74	10.00	0.31	1.77	6.28	4.51
	75	2.29	5.97	0.33	1.28	4.85	3.57
	100	2.09	6.44	0.33	1.25	4.59	3.34
Translational Error (mm)	10	5.11	19.03	0.81	3.69	12.48	8.80
	15	3.86	18.58	0.22	3.55	10.97	7.42
	20	3.53	14.15	0.20	2.65	8.83	6.18
	25	2.55	15.44	0.37	2.37	7.30	4.93
	30	1.86	8.08	0.12	1.11	4.08	2.97
	35	1.63	5.43	0.25	0.97	3.57	2.60
	40	1.60	4.10	0.20	0.86	3.32	2.46
	50	1.26	3.76	0.24	0.77	2.80	2.03
	75	1.04	2.67	0.20	0.51	2.06	1.55
	100	0.95	2.88	0.07	0.52	1.98	1.47

Table D.2: (cont'd) Relationship between point-set size and registration robustness, expressed in terms of overall rotational and translational accuracy, for a set of robust point-sets describing a proximal tibia.

Appendix E
Bounded ICP Proof

Deriving the Minimum Translational Offset

Let there be n pairs of points, and let $\{p_i\}$ and $\{y_i\}$ denote the set of probe points and closest points respectively (where i ranges from 1 to n). Then, in order to map points $\{p_i\}$ into points $\{y_i\}$ using translation only, the following transformation is required:

$$y = p + t_0 \tag{E.1}$$

where:

p is a probe point.

y is p's corresponding closest point.

t_0 is the translational offset that moves p onto y.

Now, unless the data are perfect, finding a single translation such that the transformation in Equation E.1 is satisfied for each point will not be possible. Instead there will be a residual error:

$$e_i = y_i - p_i - t_0 \tag{E.2}$$

The sum of squares of these errors:

$$\sum_{i=1}^{n} \|e_i\|^2 \tag{E.3}$$

needs to be minimised.

In order to derive the value of t_0 that will minimise the residual error, it is useful to refer all measurements to the centroids defined by:

$$\bar{p} = \frac{1}{n} \sum_{i=1}^{n} (\overrightarrow{p}_i) \tag{E.4}$$

$$\bar{y} = \frac{1}{n} \sum_{i=1}^{n} (\overrightarrow{y}_i) \tag{E.5}$$

where:

$\bar{p}$ is the centroid of the probe points.

$\bar{y}$ is the centroid of the probes closest points.

Let the new co-ordinates be be denoted as:

$$p_i^{'} = p_i - \bar{p} \tag{E.6}$$

$$y_i^{'} = y_i - \bar{y} \tag{E.7}$$

Note that:

$$\sum_{i=1}^{n} p_i^{'} = 0, \; and \; \sum_{i=1}^{n} y_i^{'} = 0$$

Now the error term can be rewritten as:

$$e_i = y_i^{'} - p_i^{'} - t_0^{'} \tag{E.8}$$

where:

$$t_0^{'} = t_0 - \bar{y} + \bar{p} \tag{E.9}$$

The sum of errors becomes:

$$\sum_{i=1}^{n} \left\| y_i^{'} - p_i^{'} - t_0^{'} \right\|^2 \tag{E.10}$$

or:

$$\sum_{i=1}^{n} \left\| y_i^{'} - p_i^{'} \right\|^2 - 2t_0^{'} \cdot \sum_{i=1}^{n} \left[y_i^{'} - p_i^{'} \right] + n \left\| t_o^{'} \right\|^2 \tag{E.11}$$

The first two terms are zero, as the measurements are referred to the centroids. Therefore the total error is minimised with $t_0' = 0$, or:

$$t_0 = \bar{y} - \bar{p} \tag{E.12}$$

by substituting Equation E.9 into Equation E.12. Replacing the centroids with the expressions in Equation E.4 and Equation E.5:

$$t_0 = \frac{1}{n} \sum_{i=1}^{n} (\vec{y}_i - \vec{p}_i) \tag{E.13}$$

The expression in Equation E.13 is equivalent to that of Equation 7.2 for one iteration of the Bounded ICP algorithm.

Appendix F
Bounded ICP Patient Simulation Results - UKA

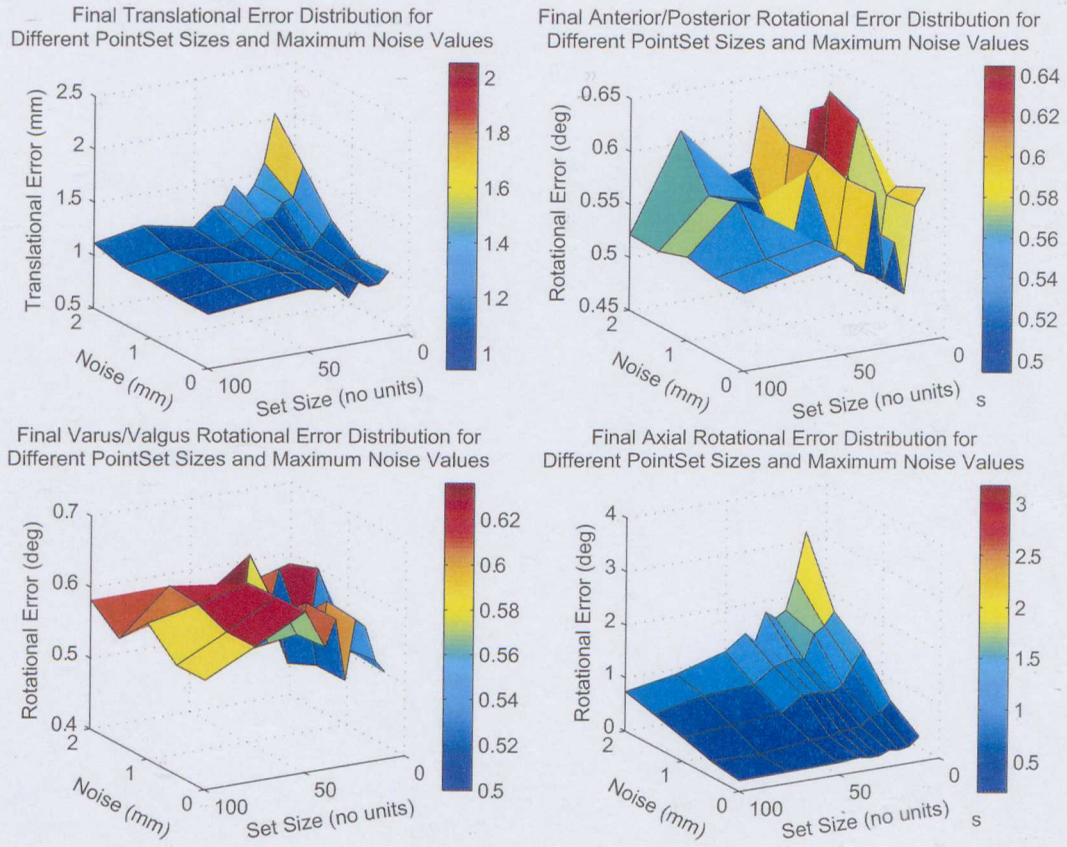


Figure F.1: Registration accuracy for the Bounded ICP algorithm in terms of varus/valgus, anterior/posterior, axial, and translational components for different point-set sizes and maximum noise values.

	Performance of Random Point-Sets of Different Sizes for 0.5mm Maximum Noise						
	Point-Set Size	**Average Err**	**Max Error**	**Min Error**	**STD**	**95% of Pop**	**75% of Pop**
Axial Error (deg)	*10*	0.02	2.98	-4.23	1.13	2.28	1.15
	15	0.02	1.97	-2.33	0.81	1.65	0.84
	20	0.07	2.39	-1.39	0.75	1.57	0.82
	25	-0.01	2.11	-2.43	0.65	1.30	0.65
	30	0.01	1.49	-1.69	0.53	1.08	0.55
	35	-0.14	1.11	-1.90	0.52	0.90	0.38
	40	0.05	1.69	-1.12	0.49	1.03	0.54
	50	-0.03	1.08	-1.64	0.48	0.92	0.44
	75	-0.02	0.66	-0.86	0.33	0.63	0.31
	100	0.01	1.39	-0.70	0.38	0.77	0.39
Ant/Post Error (deg)	*10*	-0.03	1.33	-1.34	0.71	1.39	0.68
	15	0.12	1.34	-1.28	0.70	1.51	0.81
	20	0.01	1.36	-1.30	0.64	1.29	0.65
	25	0.01	1.35	-1.32	0.68	1.36	0.69
	30	-0.04	1.36	-1.35	0.64	1.23	0.59
	35	-0.06	1.33	-1.32	0.71	1.36	0.65
	40	0.07	1.43	-1.33	0.67	1.40	0.74
	50	-0.04	1.31	-1.33	0.66	1.29	0.62
	75	0.00	1.29	-1.35	0.68	1.36	0.68
	100	0.07	1.31	-1.29	0.65	1.37	0.72
Var/Valg Error (deg)	*10*	-0.02	1.28	-1.34	0.66	1.31	0.65
	15	0.04	1.19	-1.38	0.65	1.34	0.69
	20	-0.03	1.32	-1.32	0.73	1.44	0.71
	25	0.03	1.36	-1.36	0.75	1.53	0.78
	30	0.08	1.36	-1.28	0.63	1.34	0.71
	35	-0.08	1.35	-1.33	0.73	1.38	0.65
	40	0.01	1.34	-1.35	0.70	1.41	0.71
	50	0.06	1.31	-1.33	0.75	1.56	0.81
	75	-0.01	1.36	-1.34	0.72	1.42	0.71
	100	0.05	1.31	-1.37	0.71	1.46	0.75
Translational Error (mm)	*10*	1.10	3.01	0.18	0.56	2.23	1.67
	15	1.11	1.96	0.09	0.45	2.02	1.56
	20	1.04	1.96	0.13	0.50	2.04	1.54
	25	1.08	2.08	0.08	0.50	2.07	1.58
	30	1.01	1.96	0.07	0.48	1.97	1.49
	35	1.13	1.85	0.08	0.48	2.09	1.61
	40	1.07	1.75	0.10	0.47	2.01	1.54
	50	1.12	1.93	0.07	0.47	2.06	1.59
	75	1.06	1.74	0.08	0.48	2.02	1.54
	100	1.01	1.78	0.07	0.52	2.06	1.53

Table F.1: Relationship between point-set size and registration robustness, expressed in component for using the $\{BONE\}$ co-ordinate system, for $0.5mm$ maximum random noise.

	Performance of Random Point-Sets of Different Sizes for 1.0mm Maximum Noise						
	Point-Set Size	**Average Err**	**Max Error**	**Min Error**	**STD**	**95% of Pop**	**75% of Pop**
Axial Error (deg)	*10*	-0.39	5.20	-10.39	2.14	3.88	1.75
	15	-0.30	3.41	-3.32	1.48	2.66	1.18
	20	-0.16	2.74	-3.36	1.22	2.28	1.06
	25	0.03	2.97	-2.70	1.05	2.14	1.09
	30	-0.13	3.42	-2.78	1.10	2.07	0.97
	35	-0.10	3.71	-2.78	1.10	2.10	1.00
	40	-0.01	2.47	-1.96	1.01	2.02	1.00
	50	-0.09	1.54	-2.30	0.75	1.40	0.65
	75	-0.04	1.70	-1.46	0.63	1.23	0.59
	100	-0.07	1.75	-2.11	0.58	1.08	0.50
Ant/Post Error (deg)	*10*	-0.01	1.43	-1.31	0.72	1.43	0.71
	15	-0.12	1.31	-1.41	0.75	1.38	0.63
	20	-0.02	1.37	-1.35	0.70	1.38	0.68
	25	-0.06	1.29	-1.37	0.66	1.26	0.60
	30	0.09	1.45	-1.35	0.71	1.52	0.80
	35	0.07	1.45	-1.28	0.73	1.53	0.80
	40	-0.02	1.36	-1.42	0.70	1.38	0.68
	50	-0.05	1.35	-1.21	0.62	1.20	0.58
	75	-0.04	1.38	-1.29	0.70	1.35	0.65
	100	0.01	1.38	-1.32	0.66	1.33	0.67
Var/Valg Error (deg)	*10*	-0.01	1.34	-1.37	0.66	1.31	0.65
	15	-0.01	1.30	-1.38	0.75	1.50	0.75
	20	-0.02	1.29	-1.31	0.64	1.26	0.62
	25	0.13	1.35	-1.29	0.69	1.50	0.82
	30	-0.03	1.26	-1.32	0.63	1.22	0.59
	35	-0.01	1.28	-1.28	0.71	1.40	0.70
	40	0.03	1.30	-1.30	0.66	1.35	0.69
	50	-0.02	1.28	-1.30	0.75	1.48	0.73
	75	-0.07	1.33	-1.33	0.74	1.40	0.66
	100	0.02	1.25	-1.33	0.71	1.44	0.73
Translational Error (mm)	*10*	1.32	4.76	0.19	0.71	2.74	2.03
	15	1.20	3.09	0.44	0.48	2.16	1.68
	20	1.08	2.41	0.19	0.52	2.12	1.60
	25	1.08	2.24	0.17	0.55	2.17	1.63
	30	1.12	2.69	0.19	0.51	2.13	1.62
	35	1.15	2.21	0.09	0.51	2.18	1.67
	40	1.06	2.05	0.15	0.51	2.08	1.57
	50	1.07	2.05	0.05	0.49	2.06	1.57
	75	1.12	2.00	0.26	0.45	2.02	1.57
	100	1.03	1.85	0.05	0.46	1.95	1.49

Table F.2: Relationship between point-set size and registration robustness, expressed in component for using the $\{BONE\}$ co-ordinate system, for $1.0mm$ maximum random noise.

	Performance of Random Point-Sets of Different Sizes for 1.5mm Maximum Noise						
	Point-Set Size	Average Err	Max Error	Min Error	STD	95% of Pop	75% of Pop
Axial Error (deg)	10	-0.05	13.67	-7.32	2.77	5.50	2.73
	15	0.03	5.13	-10.52	2.32	4.66	2.35
	20	-0.16	5.73	-8.02	2.09	4.01	1.92
	25	-0.17	3.46	-4.33	1.43	2.69	1.26
	30	0.20	4.49	-3.30	1.53	3.25	1.72
	35	-0.20	3.76	-3.16	1.43	2.66	1.23
	40	-0.25	5.87	-3.99	1.43	2.62	1.19
	50	-0.19	2.37	-2.64	1.07	1.96	0.89
	75	-0.04	2.45	-2.20	0.96	1.89	0.92
	100	-0.14	1.95	-2.56	0.78	1.42	0.64
Ant/Post Error (deg)	10	-0.07	1.65	-1.68	0.76	1.45	0.69
	15	-0.12	1.44	-1.59	0.77	1.41	0.65
	20	-0.01	1.40	-1.53	0.63	1.25	0.62
	25	0.00	1.30	-1.46	0.67	1.34	0.67
	30	-0.09	1.35	-1.48	0.72	1.35	0.63
	35	0.01	1.44	-1.38	0.73	1.48	0.74
	40	0.01	1.56	-1.37	0.66	1.33	0.67
	50	0.04	1.35	-1.38	0.69	1.42	0.73
	75	-0.04	1.23	-1.40	0.69	1.33	0.65
	100	0.11	1.38	-1.34	0.67	1.44	0.77
Var/Valg Error (deg)	10	-0.03	1.32	-1.29	0.65	1.28	0.63
	15	-0.01	1.39	-1.42	0.74	1.48	0.73
	20	0.01	1.37	-1.36	0.74	1.49	0.75
	25	-0.01	1.36	-1.33	0.67	1.33	0.66
	30	0.05	1.45	-1.25	0.71	1.46	0.76
	35	-0.20	1.33	-1.39	0.75	1.29	0.55
	40	-0.11	1.28	-1.24	0.63	1.14	0.51
	50	-0.08	1.30	-1.23	0.64	1.20	0.56
	75	-0.04	1.35	-1.31	0.73	1.43	0.69
	100	0.09	1.34	-1.31	0.67	1.42	0.75
Translational Error (mm)	10	1.70	10.54	0.36	1.11	3.91	2.80
	15	1.42	3.54	0.19	0.71	2.84	2.13
	20	1.38	2.88	0.27	0.51	2.40	1.89
	25	1.26	3.32	0.20	0.58	2.42	1.84
	30	1.26	2.62	0.13	0.51	2.27	1.76
	35	1.20	2.72	0.19	0.52	2.25	1.73
	40	1.12	2.21	0.14	0.51	2.14	1.63
	50	1.07	2.09	0.14	0.43	1.93	1.50
	75	1.11	1.88	0.18	0.45	2.00	1.55
	100	1.03	1.95	0.12	0.51	2.06	1.54

Table F.3: Relationship between point-set size and registration robustness, expressed in component for using the $\{BONE\}$ co-ordinate system, for $1.5mm$ maximum random noise.

	Performance of Random Point-Sets of Different Sizes for 2.0mm Maximum Noise						
	Point-Set Size	**Average Err**	**Max Error**	**Min Error**	**STD**	**95% of Pop**	**75% of Pop**
Axial Error (deg)	*10*	-0.27	12.55	-9.72	4.07	7.88	3.80
	15	-0.70	6.78	-7.87	2.94	5.18	2.24
	20	-0.13	4.49	-6.02	2.25	4.38	2.12
	25	-0.22	5.47	-4.65	2.04	3.87	1.83
	30	-0.37	6.12	-7.54	2.27	4.17	1.90
	35	-0.17	4.17	-5.34	1.73	3.28	1.55
	40	-0.48	4.79	-5.49	1.80	3.12	1.32
	50	-0.25	3.50	-4.02	1.44	2.63	1.19
	75	-0.11	3.22	-3.06	1.15	2.20	1.04
	100	-0.09	2.08	-2.81	0.92	1.75	0.83
Ant/Post Error (deg)	*10*	0.09	1.39	-1.36	0.72	1.54	0.81
	15	0.03	1.64	-1.50	0.65	1.33	0.68
	20	-0.09	1.45	-1.43	0.68	1.27	0.59
	25	0.11	1.55	-1.33	0.66	1.43	0.77
	30	0.10	1.46	-1.45	0.68	1.46	0.78
	35	-0.14	1.42	-1.43	0.73	1.32	0.59
	40	-0.14	1.33	-1.55	0.69	1.25	0.56
	50	0.00	1.54	-1.52	0.71	1.41	0.71
	75	0.07	1.47	-1.17	0.73	1.52	0.80
	100	-0.02	1.39	-1.25	0.64	1.27	0.63
Var/Valg Error (deg)	*10*	0.02	1.37	-1.46	0.70	1.42	0.72
	15	-0.04	1.43	-1.37	0.71	1.37	0.67
	20	-0.10	1.22	-1.28	0.68	1.25	0.58
	25	-0.13	1.34	-1.37	0.67	1.22	0.54
	30	-0.02	1.33	-1.37	0.69	1.37	0.68
	35	-0.06	1.39	-1.27	0.65	1.24	0.59
	40	0.03	1.37	-1.34	0.69	1.40	0.71
	50	0.01	1.41	-1.23	0.63	1.26	0.64
	75	0.03	1.31	-1.36	0.65	1.33	0.68
	100	0.01	1.33	-1.36	0.70	1.41	0.71
Translational Error (mm)	*10*	2.05	9.85	0.37	1.33	4.72	3.38
	15	1.60	3.41	0.39	0.66	2.93	2.26
	20	1.40	3.23	0.36	0.63	2.66	2.03
	25	1.28	2.81	0.25	0.56	2.40	1.84
	30	1.43	2.99	0.17	0.57	2.56	2.00
	35	1.26	3.46	0.08	0.62	2.49	1.87
	40	1.26	2.76	0.08	0.61	2.48	1.87
	50	1.11	2.36	0.13	0.56	2.22	1.66
	75	1.20	2.35	0.26	0.47	2.14	1.67
	100	1.11	2.27	0.18	0.49	2.10	1.60

Table F.4: Relationship between point-set size and registration robustness, expressed in component for using the $\{BONE\}$ co-ordinate system, for $2.0mm$ maximum random noise.

Appendix G
Bounded ICP Extended Experimental Results

PLASTIC FEMUR 1

(from "HipCentres.txt")

Hip Centre Estimate (in R Space)			
Hx	*Hy*	*Hz*	*Hom*
-70.585	359.401	40.081	1.000

(from "EventLog.txt")

Reference Transformation Matrix (M to R)			
-0.993	-0.078	-0.088	92.372
-0.116	0.781	0.614	-74.723
0.021	0.620	-0.784	437.677
0.000	0.000	0.000	1.000

Reference Matrix Inverse (R to M)			
-0.993	-0.116	0.021	73.934
-0.078	0.781	0.620	-205.784
-0.088	0.614	-0.784	397.321
0.000	0.000	0.000	1.000

Hip Estimate in M Space			
M/L	*A/P*	*P/D*	*Hom*
103.164	105.178	592.786	1.000

Real Hip - Hip Estimate (in M Space)			
M/L	*A/P*	*P/D*	*Magnitude*
-1.169	-3.176	8.117	8.795

(Inverse of Ref x Actual)

Error Matrix in M Space			
0.999	-0.032	0.002	2.820
0.032	0.999	0.009	-5.385
-0.002	-0.009	1.000	1.442
0.000	0.000	0.000	1.000

Error Matrix Components			
V/V Error	*Axial Error*	*A/P Error*	*Trans Error*
0.137	1.813	-0.529	0.238

(from "femur.txr")

Real Hip Centre in M Space		
101.995	102.002	600.904

(from "femur.cen")

Object Centre in M Space			
127.500	101.500	153.800	1.000

Actual Transformation Matrix (M to R) with Hip			
-0.995	-0.046	-0.091	89.866
-0.093	0.778	0.621	-78.368
0.042	0.626	-0.779	433.266
0.000	0.000	0.000	1.000

Reference Matrix Inverse (R to M)			
-0.995	-0.093	0.042	63.793
-0.046	0.778	0.626	-206.195
-0.091	0.621	-0.779	394.146
0.000	0.000	0.000	1.000

Hip Estimate in M Space			
M/L	*A/P*	*P/D*	*Hom*
102.379	101.868	592.556	1.000

Real Hip - Hip Estimate (in M Space)			
M/L	*A/P*	*P/D*	*Magnitude*
-0.384	0.134	8.348	8.358

Translational Error Relative To Knee Centre			
-0.135	0.024	0.194	0.000

(From bone length & hip error)

Estimated Error (deg)	
V/V Error	*A/P Error*
0.150	-0.407

PLASTIC FEMUR 2

(from "HipCentres.txt")

Hip Centre Estimate (in R Space)			
Hx	*Hy*	*Hz*	*Hom*
-71.732	366.524	35.727	1.000

(from "EventLog.txt")

Reference Transformation Matrix (M to R)			
-0.993	-0.078	-0.088	92.372
-0.116	0.781	0.614	-74.723
0.021	0.620	-0.784	437.677
0.000	0.000	0.000	1.000

Reference Matrix Inverse (R to M)			
-0.993	-0.116	0.021	73.934
-0.078	0.781	0.620	-205.784
-0.088	0.614	-0.784	397.321
0.000	0.000	0.000	1.000

Hip Estimate in M Space			
M/L	*A/P*	*P/D*	*Hom*
103.386	108.129	600.676	1.000

Real Hip - Hip Estimate (in M Space)			
M/L	*A/P*	*P/D*	*Magnitude*
-1.391	-6.127	0.227	6.287

(Inverse of Ref x Actual)

Error Matrix in M Space			
1.000	-0.017	0.004	1.033
0.017	1.000	0.014	-3.989
-0.004	-0.014	1.000	1.906
0.000	0.000	0.000	1.000

Error Matrix Components			
V/V Error	*Axial Error*	*A/P Error*	*Trans Error*
0.216	0.987	-0.796	0.384

(from "femur.txr")

Real Hip Centre in M Space		
101.995	102.002	600.904

(from "femur.cen")

Object Centre in M Space			
127.500	101.500	153.800	1.000

Actual Transformation Matrix (M to R) with Hip			
-0.994	-0.060	-0.093	91.490
-0.105	0.774	0.624	-76.787
0.034	0.630	-0.776	433.730
0.000	0.000	0.000	1.000

Reference Matrix Inverse (R to M)			
-0.994	-0.105	0.034	67.920
-0.060	0.774	0.630	-208.501
-0.093	0.624	-0.776	392.814
0.000	0.000	0.000	1.000

Hip Estimate in M Space			
M/L	*A/P*	*P/D*	*Hom*
102.007	101.999	600.635	1.000

Real Hip - Hip Estimate (in M Space)			
M/L	*A/P*	*P/D*	*Magnitude*
-0.012	0.003	0.268	0.269

Translational Error Relative To Knee Centre			
-0.197	0.330	-0.002	0.000

(From bone length & hip error)

Estimated Error (deg)	
V/V Error	*A/P Error*
0.178	-0.785

Values in these cells are pasted from the logs
Values in these cells should be similar as the proximal/distal hip error is compensated for by a translation along the leg axis
Values in these cells illustrate actual registration accuracy split in the four error components
Values in these cells illustrate predicted varus/valgus and anterior/posterior alignment based on bone length and hip error

Table G.1: Extended experiemental results for plastic femurs 1 and 2.

PLASTIC FEMUR 3

(from "HipCentres.txt")

Hip Centre Estimate (in R Space)			
Hx	*Hy*	*Hz*	*Hom*
-72.262	364.311	37.276	1.000

(from "EventLog.txt")

Reference Transformation Matrix (M to R)			
-0.993	-0.078	-0.088	92.372
-0.116	0.781	0.614	-74.723
0.021	0.620	-0.784	437.677
0.000	0.000	0.000	1.000

Reference Matrix Inverse (R to M)			
-0.993	-0.116	0.021	73.934
-0.078	0.781	0.620	-205.784
-0.088	0.614	-0.784	397.321
0.000	0.000	0.000	1.000

Hip Estimate in M Space			
M/L	*A/P*	*P/D*	*Hom*
104.202	107.403	598.149	1.000

Real Hip - Hip Estimate (in M Space)			
M/L	*A/P*	*P/D*	*Magnitude*
-2.206	-5.401	2.755	6.452

(Inverse of Ref x Actual)

Error Matrix in M Space			
1.000	-0.011	0.005	0.448
0.011	1.000	0.012	-2.907
-0.005	-0.012	1.000	1.956
0.000	0.000	0.000	1.000

Error Matrix Components			
V/V Error	*Axial Error*	*A/P Error*	*Trans Error*
0.268	0.610	-0.696	0.336

(from "femur.txr")

Real Hip Centre in M Space			
101.995	102.002	600.904	

(from "femur.cen")

Object Centre in M Space			
127.500	101.500	153.800	1.000

Actual Transformation Matrix (M to R) with Hip			
-0.993	-0.066	-0.094	91.982
-0.111	0.774	0.623	-75.844
0.031	0.629	-0.777	434.350
0.000	0.000	0.000	1.000

Reference Matrix Inverse (R to M)			
-0.993	-0.111	0.031	69.472
-0.066	0.774	0.629	-208.437
-0.094	0.623	-0.777	393.193
0.000	0.000	0.000	1.000

Hip Estimate in M Space			
M/L	*A/P*	*P/D*	*Hom*
102.132	101.946	597.960	1.000

Real Hip - Hip Estimate (in M Space)			
M/L	*A/P*	*P/D*	*Magnitude*
-0.137	0.056	2.944	2.948

Translational Error Relative To Knee Centre			
0.053	0.312	0.114	0.000

(From bone length & hip error)

Estimated Error (deg)	
V/V Error	*A/P Error*
0.283	-0.692

PLASTIC FEMUR 4

(from "HipCentres.txt")

Hip Centre Estimate (in R Space)			
Hx	*Hy*	*Hz*	*Hom*
-73.109	367.209	37.006	1.000

(from "EventLog.txt")

Reference Transformation Matrix (M to R)			
-0.993	-0.078	-0.088	92.372
-0.116	0.781	0.614	-74.723
0.021	0.620	-0.784	437.677
0.000	0.000	0.000	1.000

Reference Matrix Inverse (R to M)			
-0.993	-0.116	0.021	73.934
-0.078	0.781	0.620	-205.784
-0.088	0.614	-0.784	397.321
0.000	0.000	0.000	1.000

Hip Estimate in M Space			
M/L	*A/P*	*P/D*	*Hom*
104.701	109.564	600.216	1.000

Real Hip - Hip Estimate (in M Space)			
M/L	*A/P*	*P/D*	*Magnitude*
-2.705	-7.562	0.688	8.061

(Inverse of Ref x Actual)

Error Matrix in M Space			
1.000	-0.013	0.006	0.126
0.013	1.000	0.017	-3.705
-0.007	-0.017	1.000	2.675
0.000	0.000	0.000	1.000

Error Matrix Components			
V/V Error	*Axial Error*	*A/P Error*	*Trans Error*
0.379	0.716	-0.953	0.487

(from "femur.txr")

Real Hip Centre in M Space			
101.995	102.002	600.904	

(from "femur.cen")

Object Centre in M Space			
127.500	101.500	153.800	1.000

Actual Transformation Matrix (M to R) with Hip			
-0.993	-0.064	-0.096	92.300
-0.110	0.772	0.626	-75.988
0.034	0.633	-0.774	433.285
0.000	0.000	0.000	1.000

Reference Matrix Inverse (R to M)			
-0.993	-0.110	0.034	68.663
-0.064	0.772	0.633	-209.526
-0.096	0.626	-0.774	391.681
0.000	0.000	0.000	1.000

Hip Estimate in M Space			
M/L	*A/P*	*P/D*	*Hom*
102.026	101.991	600.008	1.000

Real Hip - Hip Estimate (in M Space)			
M/L	*A/P*	*P/D*	*Magnitude*
-0.031	0.011	0.896	0.896

Translational Error Relative To Knee Centre			
-0.181	0.437	0.119	0.000

(From bone length & hip error)

Estimated Error (deg)	
V/V Error	*A/P Error*
0.347	-0.969

Values in these cells are pasted from the logs
Values in these cells should be similar as the proximal/distal hip error is compensated for by a translstion along the leg axis
Values in these cells illustrate actual registration accurcy split in the four error components
Values in these cells illustrate predicted varus/valgus and anterior/posterior alignment based on bone length and hip error

Table G.2: Extended experiemental results for plastic femurs 3 and 4.

PLASTIC FEMUR 5

(from "HipCentres.txt")

Hip Centre Estimate (in R Space)			
Hx	*Hy*	*Hz*	*Hom*
-73.066	362.564	39.666	1.000

(from "femur.txr")

Real Hip Centre in M Space		
101.995	102.002	600.904

(from "femur.cen")

Object Centre in M Space			
127.500	101.500	153.800	1.000

(from "EventLog.txt")

Reference Transformation Matrix (M to R)			
-0.993	-0.078	-0.088	92.372
-0.116	0.781	0.614	-74.723
0.021	0.620	-0.784	437.677
0.000	0.000	0.000	1.000

Actual Transformation Matrix (M to R) with Hip			
-0.993	-0.062	-0.096	92.190
-0.109	0.774	0.623	-76.187
0.036	0.630	-0.776	433.766
0.000	0.000	0.000	1.000

Reference Matrix Inverse (R to M)			
-0.993	-0.116	0.021	73.934
-0.078	0.781	0.620	-205.784
-0.088	0.614	-0.784	397.321
0.000	0.000	0.000	1.000

Reference Matrix Inverse (R to M)			
-0.993	-0.109	0.036	67.806
-0.062	0.774	0.630	-208.366
-0.096	0.623	-0.776	392.991
0.000	0.000	0.000	1.000

Hip Estimate in M Space			
M/L	*A/P*	*P/D*	*Hom*
105.252	107.584	595.273	1.000

Hip Estimate in M Space			
M/L	*A/P*	*P/D*	*Hom*
102.241	101.930	595.217	1.000

Real Hip - Hip Estimate (in M Space)			
M/L	*A/P*	*P/D*	*Magnitude*
-3.257	-5.582	5.631	8.571

Real Hip - Hip Estimate (in M Space)			
M/L	*A/P*	*P/D*	*Magnitude*
-0.246	0.072	5.686	5.692

(Inverse of Ref x Actual)

Error Matrix in M Space			
1.000	-0.015	0.007	0.269
0.015	1.000	0.013	-3.554
-0.007	-0.013	1.000	2.185
0.000	0.000	0.000	1.000

Translational Error Relative To Knee Centre			
-0.140	0.286	-0.076	0.000

Error Matrix Components			
V/V Error	*Axial Error*	*A/P Error*	*Trans Error*
0.420	0.836	-0.739	0.328

(From bone length & hip error)

Estimated Error (deg)	
V/V Error	*A/P Error*
0.417	-0.715

PLASTIC FEMUR 6

(from "HipCentres.txt")

Hip Centre Estimate (in R Space)			
Hx	*Hy*	*Hz*	*Hom*
-72.215	372.025	31.969	1.000

(from "femur.txr")

Real Hip Centre in M Space		
101.995	102.002	600.904

(from "femur.cen")

Object Centre in M Space			
127.500	101.500	153.800	1.000

(from "EventLog.txt")

Reference Transformation Matrix (M to R)			
-0.993	-0.078	-0.088	92.372
-0.116	0.781	0.614	-74.723
0.021	0.620	-0.784	437.677
0.000	0.000	0.000	1.000

Actual Transformation Matrix (M to R) with Hip			
-0.994	-0.065	-0.093	91.735
-0.109	0.770	0.628	-76.707
0.030	0.634	-0.772	432.822
0.000	0.000	0.000	1.000

Reference Matrix Inverse (R to M)			
-0.993	-0.116	0.021	73.934
-0.078	0.781	0.620	-205.784
-0.088	0.614	-0.784	397.321
0.000	0.000	0.000	1.000

Reference Matrix Inverse (R to M)			
-0.994	-0.109	0.030	69.586
-0.065	0.770	0.634	-209.495
-0.093	0.628	-0.772	391.029
0.000	0.000	0.000	1.000

Hip Estimate in M Space			
M/L	*A/P*	*P/D*	*Hom*
103.149	110.132	607.044	1.000

Hip Estimate in M Space			
M/L	*A/P*	*P/D*	*Hom*
101.754	102.060	606.756	1.000

Real Hip - Hip Estimate (in M Space)			
M/L	*A/P*	*P/D*	*Magnitude*
-1.153	-8.129	-6.140	10.253

Real Hip - Hip Estimate (in M Space)			
M/L	*A/P*	*P/D*	*Magnitude*
0.241	-0.058	-5.852	5.858

(Inverse of Ref x Actual)

Error Matrix in M Space			
1.000	-0.012	0.003	0.761
0.011	1.000	0.019	-4.509
-0.003	-0.019	1.000	2.646
0.000	0.000	0.000	1.000

Translational Error Relative To Knee Centre			
0.041	-0.170	0.298	0.000

Error Matrix Components			
V/V Error	*Axial Error*	*A/P Error*	*Trans Error*
0.184	0.658	-1.078	0.346

(From bone length & hip error)

Estimated Error (deg)	
V/V Error	*A/P Error*
0.148	-1.042

Values in these cells are pasted from the logs
Values in these cells should be similar as the proximal/distal hip error is compensated for by a translstion along the leg axis
Values in these cells illustrate actual registration accurcy split in the four error components
Values in these cells illustrate predicted varus/valgus and anterior/posterior alignment based on bone length and hip error

Table G.3: Extended experiemental results for plastic femurs 5 and 6.

PLASTIC FEMUR 7

(from "HipCentres.txt")

Hip Centre Estimate (in R Space)			
Hx	*Hy*	*Hz*	*Hom*
-71.766	374.020	30.340	1.000

(from "femur.txr")

Real Hip Centre in M Space		
101.995	102.002	600.904

(from "femur.cen")

Object Centre in M Space			
127.500	101.500	153.800	1.000

(from "EventLog.txt")

Reference Transformation Matrix (M to R)			
-0.993	-0.078	-0.088	92.372
-0.116	0.781	0.614	-74.723
0.021	0.620	-0.784	437.677
0.000	0.000	0.000	1.000

Actual Transformation Matrix (M to R) with Hip			
-0.993	-0.070	-0.091	91.953
-0.112	0.769	0.629	-76.286
0.026	0.635	-0.772	433.498
0.000	0.000	0.000	1.000

Reference Matrix Inverse (R to M)			
-0.993	-0.116	0.021	73.934
-0.078	0.781	0.620	-205.784
-0.088	0.614	-0.784	397.321
0.000	0.000	0.000	1.000

Reference Matrix Inverse (R to M)			
-0.993	-0.112	0.026	71.569
-0.070	0.769	0.635	-210.042
-0.091	0.629	-0.772	391.096
0.000	0.000	0.000	1.000

Hip Estimate in M Space			
M/L	*A/P*	*P/D*	*Hom*
102.438	110.644	609.507	1.000

Hip Estimate in M Space			
M/L	*A/P*	*P/D*	*Hom*
101.716	102.049	609.390	1.000

Real Hip - Hip Estimate (in M Space)			
M/L	*A/P*	*P/D*	*Magnitude*
-0.443	-8.642	-8.603	12.203

Real Hip - Hip Estimate (in M Space)			
M/L	*A/P*	*P/D*	*Magnitude*
0.279	-0.047	-8.486	8.491

(Inverse of Ref x Actual)

Error Matrix in M Space			
1.000	-0.006	0.001	0.510
0.006	1.000	0.019	-3.779
-0.002	-0.019	1.000	2.355
0.000	0.000	0.000	1.000

Translational Error Relative To Knee Centre			
0.089	-0.039	0.174	0.000

Error Matrix Components			
V/V Error	*Axial Error*	*A/P Error*	*Trans Error*
0.087	0.356	-1.105	0.199

(From bone length & hip error)

Estimated Error (deg)	
V/V Error	*A/P Error*
0.057	-1.107

PLASTIC FEMUR 8

(from "HipCentres.txt")

Hip Centre Estimate (in R Space)			
Hx	*Hy*	*Hz*	*Hom*
-71.819	366.162	35.624	1.000

(from "femur.txr")

Real Hip Centre in M Space		
101.995	102.002	600.904

(from "femur.cen")

Object Centre in M Space			
127.500	101.500	153.800	1.000

(from "EventLog.txt")

Reference Transformation Matrix (M to R)			
-0.993	-0.078	-0.088	92.372
-0.116	0.781	0.614	-74.723
0.021	0.620	-0.784	437.677
0.000	0.000	0.000	1.000

Actual Transformation Matrix (M to R) with Hip			
-0.993	-0.078	-0.093	93.132
-0.119	0.772	0.624	-74.992
0.023	0.630	-0.776	434.768
0.000	0.000	0.000	1.000

Reference Matrix Inverse (R to M)			
-0.993	-0.116	0.021	73.934
-0.078	0.781	0.620	-205.784
-0.088	0.614	-0.784	397.321
0.000	0.000	0.000	1.000

Reference Matrix Inverse (R to M)			
-0.993	-0.119	0.023	73.530
-0.078	0.772	0.630	-208.876
-0.093	0.624	-0.776	392.791
0.000	0.000	0.000	1.000

Hip Estimate in M Space			
M/L	*A/P*	*P/D*	*Hom*
103.512	107.789	600.542	1.000

Hip Estimate in M Space			
M/L	*A/P*	*P/D*	*Hom*
102.025	101.995	600.275	1.000

Real Hip - Hip Estimate (in M Space)			
M/L	*A/P*	*P/D*	*Magnitude*
-1.517	-5.787	0.362	5.994

Real Hip - Hip Estimate (in M Space)			
M/L	*A/P*	*P/D*	*Magnitude*
-0.030	0.007	0.629	0.630

(Inverse of Ref x Actual)

Error Matrix in M Space			
1.000	0.001	0.004	-0.784
-0.001	1.000	0.013	-2.073
-0.004	-0.013	1.000	2.049
0.000	0.000	0.000	1.000

Translational Error Relative To Knee Centre			
-0.121	-0.179	0.225	0.000

Error Matrix Components			
V/V Error	*Axial Error*	*A/P Error*	*Trans Error*
0.205	-0.065	-0.763	0.312

(From bone length & hip error)

Estimated Error (deg)	
V/V Error	*A/P Error*
0.194	-0.742

Values in these cells are pasted from the logs
Values in these cells should be similar as the proximal/distal hip error is compensated for by a translation along the leg axis
Values in these cells illustrate actual registration accuracy split in the four error components
Values in these cells illustrate predicted varus/valgus and anterior/posterior alignment based on bone length and hip error

Table G.4: Extended experiemental results for plastic femurs 7 and 8.

PLASTIC FEMUR 9

(from "HipCentres.txt")

Hip Centre Estimate (in R Space)			
Hx	*Hy*	*Hz*	*Hom*
-70.895	374.368	29.164	1.000

(from "femur.txr")

Real Hip Centre in M Space		
101.995	102.002	600.904

(from "femur.cen")

Object Centre in M Space			
127.500	101.500	153.800	1.000

(from "EventLog.txt")

Reference Transformation Matrix (M to R)			
-0.993	-0.078	-0.088	92.372
-0.116	0.781	0.614	-74.723
0.021	0.620	-0.784	437.677
0.000	0.000	0.000	1.000

Actual Transformation Matrix (M to R) with Hip			
-0.993	-0.071	-0.090	92.039
-0.112	0.770	0.628	-76.173
0.024	0.633	-0.773	434.153
0.000	0.000	0.000	1.000

Reference Matrix Inverse (R to M)			
-0.993	-0.116	0.021	73.934
-0.078	0.781	0.620	-205.784
-0.088	0.614	-0.784	397.321
0.000	0.000	0.000	1.000

Reference Matrix Inverse (R to M)			
-0.993	-0.112	0.024	72.379
-0.071	0.770	0.633	-209.778
-0.090	0.628	-0.773	391.813
0.000	0.000	0.000	1.000

Hip Estimate in M Space			
M/L	*A/P*	*P/D*	*Hom*
101.508	110.119	610.566	1.000

Hip Estimate in M Space			
M/L	*A/P*	*P/D*	*Hom*
101.615	102.189	610.560	1.000

Real Hip - Hip Estimate (in M Space)			
M/L	*A/P*	*P/D*	*Magnitude*
0.487	-8.117	-9.663	12.629

Real Hip - Hip Estimate (in M Space)			
M/L	*A/P*	*P/D*	*Magnitude*
0.380	-0.187	-9.656	9.665

(Inverse of Ref x Actual)

Error Matrix in M Space			
1.000	-0.005	0.000	0.425
0.005	1.000	0.018	-3.291
0.000	-0.018	1.000	1.903
0.000	0.000	0.000	1.000

Translational Error Relative To Knee Centre			
-0.115	0.067	0.086	0.000

Error Matrix Components			
V/V Error	*Axial Error*	*A/P Error*	*Trans Error*
0.007	0.306	-1.004	0.159

(From bone length & hip error)

Estimated Error (deg)	
V/V Error	*A/P Error*
0.062	-1.040

PLASTIC FEMUR 10

(from "HipCentres.txt")

Hip Centre Estimate (in R Space)			
Hx	*Hy*	*Hz*	*Hom*
-71.914	365.723	34.848	1.000

(from "femur.txr")

Real Hip Centre in M Space		
101.995	102.002	600.904

(from "femur.cen")

Object Centre in M Space			
127.500	101.500	153.800	1.000

(from "EventLog.txt")

Reference Transformation Matrix (M to R)			
-0.993	-0.078	-0.088	92.372
-0.116	0.781	0.614	-74.723
0.021	0.620	-0.784	437.677
0.000	0.000	0.000	1.000

Actual Transformation Matrix (M to R) with Hip			
-0.994	-0.064	-0.093	91.570
-0.108	0.775	0.623	-76.399
0.032	0.629	-0.777	434.313
0.000	0.000	0.000	1.000

Reference Matrix Inverse (R to M)			
-0.993	-0.116	0.021	73.934
-0.078	0.781	0.620	-205.784
-0.088	0.614	-0.784	397.321
0.000	0.000	0.000	1.000

Reference Matrix Inverse (R to M)			
-0.994	-0.108	0.032	68.933
-0.064	0.775	0.629	-207.961
-0.093	0.623	-0.777	393.510
0.000	0.000	0.000	1.000

Hip Estimate in M Space			
M/L	*A/P*	*P/D*	*Hom*
103.642	106.973	600.890	1.000

Hip Estimate in M Space			
M/L	*A/P*	*P/D*	*Hom*
101.999	102.000	600.802	1.000

Real Hip - Hip Estimate (in M Space)			
M/L	*A/P*	*P/D*	*Magnitude*
-1.646	-4.971	0.014	5.236

Real Hip - Hip Estimate (in M Space)			
M/L	*A/P*	*P/D*	*Magnitude*
-0.004	0.002	0.102	0.102

(Inverse of Ref x Actual)

Error Matrix in M Space			
1.000	-0.013	0.003	0.920
0.013	1.000	0.012	-3.331
-0.004	-0.012	1.000	1.680
0.000	0.000	0.000	1.000

Translational Error Relative To Knee Centre			
0.106	0.110	0.035	0.000

Error Matrix Components			
V/V Error	*Axial Error*	*A/P Error*	*Trans Error*
0.206	0.750	-0.663	0.157

(From bone length & hip error)

Estimated Error (deg)	
V/V Error	*A/P Error*
0.211	-0.637

Values in these cells are pasted from the logs
Values in these cells should be similar as the proximal/distal hip error is compensated for by a translstion along the leg axis
Values in these cells illustrate actual registration accurcy split in the four error components
Values in these cells illustrate predicted varus/valgus and anterior/posterior alignment based on bone length and hip error

Table G.5: Extended experiemental results for plastic femurs 9 and 10.

Appendix H
Author's Reference Articles

Computer Aided Surgery 6:329–339 (2001)

Clinical Paper

The First Clinical Application of a "Hands-On" Robotic Knee Surgery System

M. Jakopec, Ph.D., S.J. Harris, Ph.D., F. Rodriguez y Baena, M.Eng., P. Gomes, Ph.D., J. Cobb, M.D., and B.L. Davies, Ph.D.

Department of Mechanical Engineering, Imperial College (M.J., S.J.H., F.R.y.B., P.G., B.L.D.), and Department of Orthopaedic Surgery, University College London Hospitals Trust (J.C.), London, United Kingdom

ABSTRACT The performance of a novel "hands-on" robotic system for total knee replacement (TKR) surgery is evaluated. An integrated robotic system for accurately machining the bone surfaces in TKR surgery is described. Details of the system, comprising an "active constraint" robot, called Acrobot, a "gross positioning" robot, and patient clamps, are provided. The intraoperative protocol and the preoperative, CT-based, planning system are also described. A number of anatomical registration and cutting trials, using plastic bones, are described, followed by results from two preliminary clinical trials, which demonstrate the accuracy achieved in the anatomical registration. Finally, the first clinical trial is described, in which the results of the anatomical registration and bone cutting are seen to be of high quality. The Acrobot system has been successfully used to accurately register and cut the knee bones in TKR surgery. This demonstrates the great potential of a "hands-on" robot for improving accuracy and increasing safety in surgery. Comp Aid Surg 6:329–339 (2001). ©2002 Wiley-Liss, Inc.

Key words: **robotic surgery, total knee replacement, TKR, active constraints, orthopedics, anatomical registration**

INTRODUCTION

Total knee replacement (TKR) surgery is a common orthopedic procedure to replace damaged surfaces of the knee bones with prosthetic implants. The purpose of the surgery is to relieve pain and to restore the normal functioning of the knee joint. Typically, a knee prosthesis consists of three components, one for each knee bone: femur, tibia, and patella. For a successful outcome of the procedure, the prosthetic components must be placed on the bones accurately, assuring proper alignment of the limb and good contact between the components, leading to smooth motion of the joint. In addition, the implant must have a long life. The latter requirement has become more important recently due to the increased numbers of young patients requiring implants as a result of sports injuries, in addition to older patients with degenerative bone disease. Improper alignment of the prosthesis components can lead to pain and reduced functionality of the joint, as well as accelerated wear and loosening of the components. In turn, this can lead to early failure of the joint and the need for difficult revision surgery.

Address correspondence/reprint requests to: Professor B.L. Davies, Mechatronics in Medicine Laboratory, Department of Mechanical Engineering, Imperial College of Science, Technology and Medicine, Exhibition Road, London SW7 2BX; Telephone: (+44) 020 7594 7054; Fax: (+44) 020 7584 7239; E-mail: b.davies@ic.ac.uk.

Published online in Wiley InterScience (www.interscience.wiley.com). DOI: 10.1002/igs.10023

©2002 Wiley-Liss, Inc.

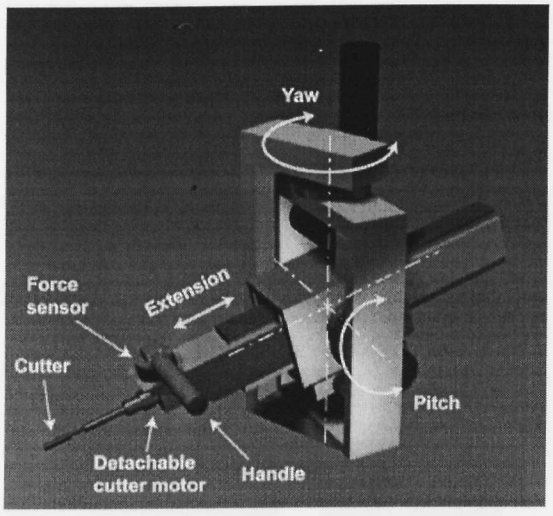


Fig. 1. The Acrobot—a special-purpose robot with two rotational axes (Yaw and Pitch) and a linear axis (Extension). The end-effector consists of a handle mounted on a 6DOF force sensor and a detachable cutter motor.

The bones have to be machined in a specific manner to mount the prosthesis. The manufacturer of the prosthesis supplies the cutting tools, as well as a range of special guiding and measuring fixtures that are used in conventional surgery in an attempt to accurately position the cuts. Usually, a series of flat cuts (typically one plane on the tibia and five planes on the femur) are made using an oscillating saw, and additional positional holes are made with a drill. It is very difficult to achieve a good fit and proper placement of the implant, even for a skilled surgeon using state-of-the-art cutting tools and fixtures. In a conventional TKR case study,[1] it was reported that the deviation from the ideal prosthesis alignment is over 9° in 7% of cases, and over 5° in 34% of cases. The reason for this is the sequential nature of positioning fixtures in the manual procedure, which can result in an accumulation of errors. In addition, the long, thin blade of the oscillating saw can flex, and tends to bounce off (or dig into) a hard part of the bone despite the guiding tools, which can result in a poor surface finish.

To overcome the problems of conventional surgery and improve the results of the procedure, a robotic surgery system is being developed at Imperial College[2–6] and is now undergoing clinical trials. In contrast to other robotic systems for orthopedic surgery, such as Robodoc[7–9] or Caspar,[10] which use modified industrial robots, a small, low-powered, special-purpose robot called Acrobot (active constraint robot) has been built for safe use in a crowded sterile operating theater environment. The robot is placed on a gross positioning manipulator, which is used to position a small active robot in the vicinity of the knee and is then locked in position with the power off. This enables the Acrobot to be a low-powered, small device, with motions and forces just sufficient for the task, rather than requiring large motors simply to position the tool over a large area. Other approaches to orthopedic surgery have been presented in refs. 11–15.

The research group at Imperial College has also presented a new type of robot control—active constraint control—where there is a synergy between the surgeon and the robot.[16–19] The surgeon guides the robot (using a handle with a force sensor attached to the robot tip), and thus uses his or her superior human senses and understanding of the overall situation to perform the surgery. The robot provides geometric accuracy and also increases safety by means of a predefined 3D motion constraint that prevents cutting outside the safe region. This "hands-on" approach is also very different from other robotic systems, in that the surgeon is kept in the control loop, rather than just being required to press a start button and then watch the robot with a finger hovering above the "emergency off" button. Other examples of a "hands-on" approach are PADyC[20] (a passive robot with controlled brakes to constrain the motion), and the "steady-hand" robot[21] (which aims to reduce the effects of tremor in microsurgery).

Tests on an early Acrobot prototype have shown that the robot can be guided under active

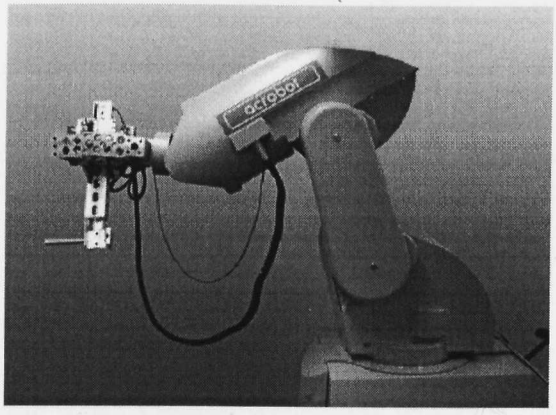
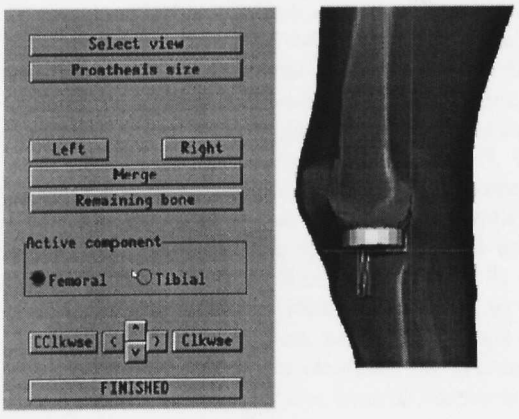


Fig. 2. The Acrobot mounted on a gross positioner and trolley.



(a)



(b)

Fig. 3. Planning software: (a) Bone axis set-up. (b) Prosthesis placement.

constraint control to produce the flat planes required for a TKR prosthesis. Further tests were performed on plastic phantom bones and cadaveric legs, using fiducial marker screws for registration.[22] The procedures were performed successfully, with a very good fit of the prosthesis onto the bones.

The system was subsequently further adapted to make it more suitable for the sterile operating theater environment, and an anatomical registration method was implemented to avoid the invasive fiducial marker-based registration. The Acrobot system is now ready to be used in clinical trials, and has been recently used in the first "hands-on" robotic TKR surgery. "Kinemax" TKR prostheses (Stryker Howmedica) were used in the clinical trials, although the Acrobot system can be used with any TKR prosthesis model.

MATERIALS AND METHODS

The Acrobot surgical procedure is divided into two phases: the preoperative planning and the intraoperative robotic procedure. The intraoperative robotic system consists of the Acrobot, a gross positioning manipulator, and leg fixtures.

Acrobot Robotic System

The Acrobot is a special-purpose robot with three orthogonal axes of motion (Yaw, Pitch, and Extension), which form a spherical manipulator (see Fig. 1). The Acrobot has a relatively small reach and range of angles, which ensures accurate operation with low-powered motors over a small region. Consequently, the robot is relatively safe, because potential damage is limited in terms of force and is constrained to a small region. The mechanical impedance of the Acrobot's axes is low and similar for all axes, allowing the robot to be moved by the surgeon with low force. A force-sensor handle is mounted at the tip of the Acrobot and measures the guiding force applied by the surgeon. The guiding force information is used in active constraint control. A high-speed orthopedic cutter system (Stryker Instruments) is used for machining the bones. To ensure the sterility of the system, a special mount is provided at the tip of the robot for mounting the cutter motor intraoperatively. At the beginning of the surgery, the cutter motor (autoclaved before surgery) is mounted on the Acrobot



Fig. 4. Intraoperative user interface during anatomical registration of the tibia. Two 3D views, which can be freely rotated, are displayed: The left view shows the preoperative plan (cutting constraints and prosthesis component); the right view shows colored registration points matched to the bone surface model.

Table 1. Anatomical Registration Sequence for Plastic Femur 1

	Number of points	RMS error (mm)	Standard deviation (mm)	Maximum error (mm)	Minimum error (mm)
Initial registration	4	7.09	—	—	—
ICP 1	34	0.41	0.230	0.86	0.00
ICP 2	19	0.45	0.259	1.07	0.09
ICP 3	20	0.24	0.152	0.51	0.00

through sterile drapes, which cover the robotic system throughout the whole procedure.

Due to its small working envelope, the Acrobot is placed on a gross positioning device (see Fig. 2), which moves the Acrobot to different optimal cutting locations around the knee. The device (manufactured by Armstrong Healthcare Ltd., High Wycombe, England) is built around a six-axis robot with motorized axes. The velocities of the axes are limited, and secondary encoders are fitted on each axis as a check for increased safety. In addition, all axes have brakes, which ensures that the robot stays in position when the motor power is cut off. The gross positioning robot is mounted on a wheeled trolley, which allows the system to be quickly placed near the operating table and moved away from it. The trolley wheels can be locked to fix the position of the robotic system with respect to the operating table. In addition, two table clamps are provided on the trolley for clamping the system to the operating table. All the control hardware is situated inside the trolley.

Leg Fixtures

During the surgery, the tibia and femur are immobilized with respect to the operating table, which, in turn, is rigidly linked to the base of the gross positioning device. This allows the bones to be treated as rigid objects to which the preoperative plan can be applied, leading to a much simpler control structure than allowing the leg to move and having to track its motion and adapt the control algorithm accordingly.

Two bone clamps are provided (manufactured by Finsbury Instruments Limited, Leatherhead, England), one for the tibia and one for the femur, which are rigidly clamped onto the exposed ends of the two bones in the knee area. Each of the two clamps is fixed to the operating table by means of three adjustable links, which are connected to a base block mounted on the side rails of the table (see Fig. 6). To ensure proper fixation, the proximal femur and distal tibia must be immobilized as well. However, external fixation at the hip and ankle is rigid enough, because the motion at these ends of the bones does not greatly affect the motion at the knee. For that reason, the foot is placed into a foot support, which is placed on the operating table and immobilizes the distal tibia. The weight of the patient has proven to be enough to immobilize the femur at the hip joint.

Robot Control

The Acrobot system incorporates a two-level control. A standard PC computer is used at the top level as a master controller, and a PCI controller board is used for low-level active constraint control of the Acrobot. In addition, the gross positioner has its own independent controller. The master controller communicates with the Acrobot and the gross positioner controllers to direct their respective actions. The master controller is also used for user interaction, for data storage, and for overall monitoring. Information about the system is displayed on the computer screen, which gives the surgeon enough information about the procedure. Currently, at this early stage, an assistant is required to control the actions of the system (according to the surgeon's demands), such as selecting the cutting plane or moving the gross positioning manipulator, by using the keyboard and mouse together with an on-screen graphical user interface. In future, the surgeon will be able to control the system directly

Table 2. Anatomical Registration Sequence for Plastic Femur 2

	Number of points	RMS error (mm)	Standard deviation (mm)	Maximum error (mm)	Minimum error (mm)
Initial registration	4	4.74	—	—	—
ICP 1	21	0.45	0.255	0.84	0.02
ICP 2	17	0.44	0.247	0.91	0.01

Table 3. Anatomical Registration Sequence for Plastic Femur 3

	Number of points	RMS error (mm)	Standard deviation (mm)	Maximum error (mm)	Minimum error (mm)
Initial registration	4	2.76	—	—	—
ICP 1	28	0.29	0.187	0.63	0.01

by using foot switches, a keypad, or a similar device.

Preoperative Planning

Interactive planning software that runs on a standard PC computer, and allows processing of the CT images of the patient's leg, has been developed. Three-dimensional models of the knee bones are built from the CT images, and the axes of the bones are determined (Fig. 3a). The surgeon then interactively decides prosthesis size and placement (Fig. 3b). The software provides a number of different 3D views of the leg and the implant to help the surgeon plan the procedure. Once the prosthesis model is in the correct position over the bone model, the planning software generates six constraint boundaries (five on the femur and one on the tibia) for each of the flat planes required to fit the femoral and tibial prosthesis components. Each of the boundaries is comprised of the cutting plane and a 2D outline where the cutting plane intersects the bone surface, thus forming a prismatic constraint. This ensures that the robot can only cut the bone, and prevents it from damaging the surrounding soft tissue. The software also generates bone surface models, which are used for anatomical registration during the surgery. The planning data is then transferred to the master controller of the intraoperative system.

Intraoperative Procedure

The surgery begins as for a manual TKR procedure: the surgical equipment is prepared, and the patient is anesthetized, placed on the operating table, and covered with sterile drapes. A pneumatic tourniquet is placed over the leg at the thigh, which stops the blood flow to the leg and ensures low blood loss during the procedure. The knee is exposed from the front by a straight longitudinal skin incision, through the quadriceps tendon. The patella is brought to one side and the anterior cruciate ligament is removed. The posterior cruciate ligament is preserved throughout the whole operation (in the case of a "Kinemax" prosthesis). The re-

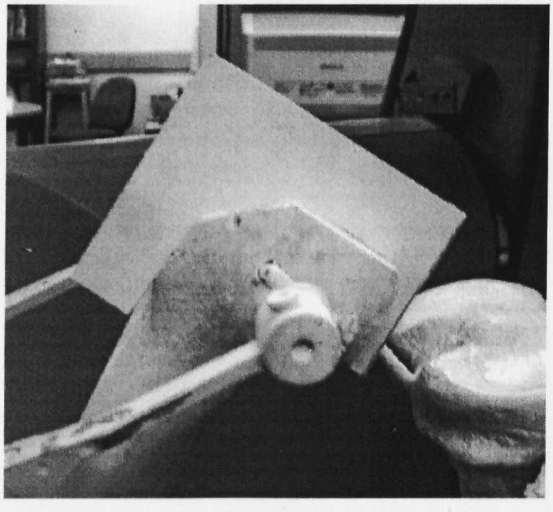


Fig. 5. Surfaces of a plastic femur after robotic procedure, with a custom-made trial in place showing a very good fit.

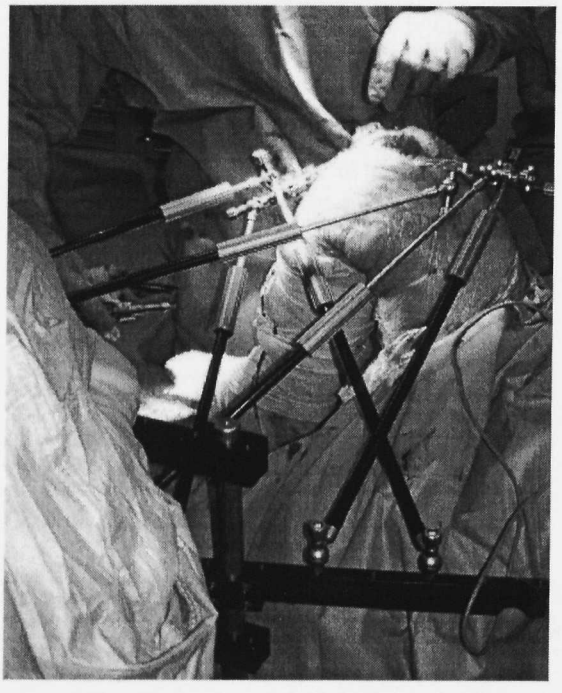


Fig. 6. Leg fixtures in place during the second preliminary clinical trial.

Table 4. Anatomical Registration Sequence for the Femur during Preliminary Clinical Trial 1

	Number of points	RMS error (mm)	Standard deviation (mm)	Maximum error (mm)	Minimum error (mm)
Initial registration	4	0.60	—	—	—
ICP 1	34	0.80	0.537	2.33	0.01
ICP 2	29	0.21	0.130	0.50	0.01

mains of the meniscus, and any debris, are removed.

The leg is then immobilized with sterile leg fixtures. The leg is flexed at an angle greater than 120°, and the foot is placed in a foot support. The surgeon places the two knee clamps onto the bones. The base block of the leg fixtures is clamped to the table's side rails through the sterile drapes. Each of the two knee clamps is then connected to the base block with three adjustable links. Once the surgeon is satisfied with the position of the knee, the links are tightened, forming a triangulated rigid structure.

In the meantime, the robot is prepared and covered with sterile drapes. The sterile cutter motor is mounted onto the tip of the Acrobot through the drapes. When the leg immobilization is completed, the robot trolley is wheeled next to the operating table and clamped to the side rails (below the sterile draping).

The robotic procedure can then begin. Each of the bones must be registered before it can be cut. Registration[23,24] is a process to determine the geometrical relationship between the intraoperative location of the bones and the preoperative CT models of the bones, so that the planned procedure can be executed. An anatomical registration method known as the iterative closest point (ICP) algorithm[25–27] is used. No fiducial marker screws are required to be mounted in the bone.

The procedure is as follows: first, the surgeon acquires four landmark points with a special ball probe (1 mm in diameter) mounted into the cutter motor. (The probe can be repeatedly mounted at a set location in the cutter motor, which has been calibrated.) These four points are then used to compute the initial registration estimate for the ICP algorithm. The surgeon then acquires a set of randomly selected points (typically 20–30) on the exposed bone surface. The ICP algorithm registers the bone location by matching the set of points to the preoperative surface model. The accuracy of the registration is verified by using the on-screen display of the point set matched onto the surface model (see Fig. 4). If the result is not accurate enough (indicated by a high RMS error and point mismatch), another set of points is acquired and the ICP registration is recomputed (with the result of the previous computation serving as an initial estimate).

Once the bone is registered, the registration probe is replaced with a drum cutter (7.8 mm in diameter) and the bone preparation can begin. For each of the cutting planes, the gross positioner moves the Acrobot to the optimal cutting position—the center of the Acrobot is placed onto the cutting plane, so that the plane can be prepared with the side-milling action to achieve a very smooth surface finish. The gross positioner is then locked off, and the surgeon uses the Acrobot in "active constraint" mode to cut the bone. The procedure is repeated for each of the cutting planes, which can be machined in any order.

The robot is also used to machine locating holes for accurate placement of the conventional punch guides, which are used as in manual surgery to punch the holes for the stems and other mounting features of the prosthesis components. This punch process normally compresses the bone tissue rather than removing it, and gives better stability to the prosthesis (especially in the case of soft underlying bone).

When all the surfaces on both the femur and the tibia are prepared, the robot is removed from

Table 5. Anatomical Registration Sequence for the Tibia during Preliminary Clinical Trial 1

	Number of points	RMS error (mm)	Standard deviation (mm)	Maximum error (mm)	Minimum error (mm)
Initial registration	4	9.99	—	—	—
ICP 1	29	0.61	0.361	1.71	0.04
ICP 2	40	0.59	0.366	1.59	0.01
ICP 3	36	0.38	0.240	0.85	0.01

Table 6. Anatomical Registration Sequence for the Femur during Preliminary Clinical Trial 2

	Number of points	RMS error (mm)	Standard deviation (mm)	Maximum error (mm)	Minimum error (mm)
Initial registration	4	2.56	—	—	—
ICP 1	22	0.96	0.615	2.95	0.09
ICP 2	19	0.52	0.264	1.13	0.12
ICP 3	12	0.17	0.116	0.35	0.00

the operating table. The patella is prepared manually, as its single flat plane can be cut using conventional guides with acceptable accuracy. The bone clamps are then removed and the procedure is finished as in conventional TKR surgery: the knee motion is tested with a trial prosthesis, the bones are thoroughly cleansed, the prosthesis is pressed into place (with a small cement mantle in the case of a cemented prosthesis), any soft-tissue balancing is carried out, and the incision is then closed.

RESULTS

Plastic Phantom Bone Trials

The Acrobot system, as described in this article, was first tested on plastic phantom bones to analyze the performance of the overall Acrobot system and the suitability of the devised surgical protocol, particularly the anatomical registration procedure, which had not been previously tested.

Three plastic bone phantoms were CT scanned with slices at 1-mm intervals and a pixel spacing of 0.391 mm. Preoperative planning was performed for these CT images, and the constraint boundaries were generated for the large-size prosthesis that was required. The constraints and the bone surface models were then passed to the intraoperative robotic system.

The intraoperative procedure was then performed as described above, with one modification: the proximal femur and the distal tibia were strapped to the operating table, due to the absence of the hip and the ankle. However, the rigidity of the clamped bones was comparable to the real case.

Tables 1–3 show the results of the registration procedures for the three femurs. It can be seen that the ICP algorithm was executed three times in the first trial and twice in the second, whereas only a single computation was required to produce a very close match of the points to the surface model. It was noted that an RMS error below 0.5 mm, and an evenly spread point set (covering most of the femoral head) are required to accurately register the bones.

Once successfully registered, the bone phantoms were cut. The flatness of the produced planes was very high, with no measurable waviness. Figure 5 shows the fit of the custom-made trial (whose internal dimensions were those of the prosthesis) onto the femur. The fit was extremely good, with no visible gap between the bone and the trial. The final surface was well within the prosthesis manufacturer's tolerances.

Preliminary Clinical Trials

Having obtained good results with plastic phantoms, the system was brought into the operating theater, and two preliminary clinical trials were performed to test the surgical protocol and anatomical registration, but without cutting the bone.

The procedure was similar in both cases: A CT scan of the patient's leg was taken a few days before the surgery. The CT slices were taken at 1-mm intervals in the region of the knee and every 5 mm for the rest of the leg. The resulting pixel spacing on CT slices was 0.742 mm in both cases. The procedure was planned using the planning software, and the intraoperative data was generated.

Intraoperatively, the knee was exposed and the leg fixtures were fitted (see Fig. 6), providing a firm support for the knee bones. When fitting the tibial knee clamp, it was thought that the clamp

Table 7. Anatomical Registration Sequence for the Tibia during Preliminary Clinical Trial 2

	Number of points	RMS error (mm)	Standard deviation (mm)	Maximum error (mm)	Minimum error (mm)
Initial registration	4	1.13	—	—	—
ICP 1	26	0.57	0.352	1.31	0.02
ICP 2	13	0.27	0.178	0.72	0.01

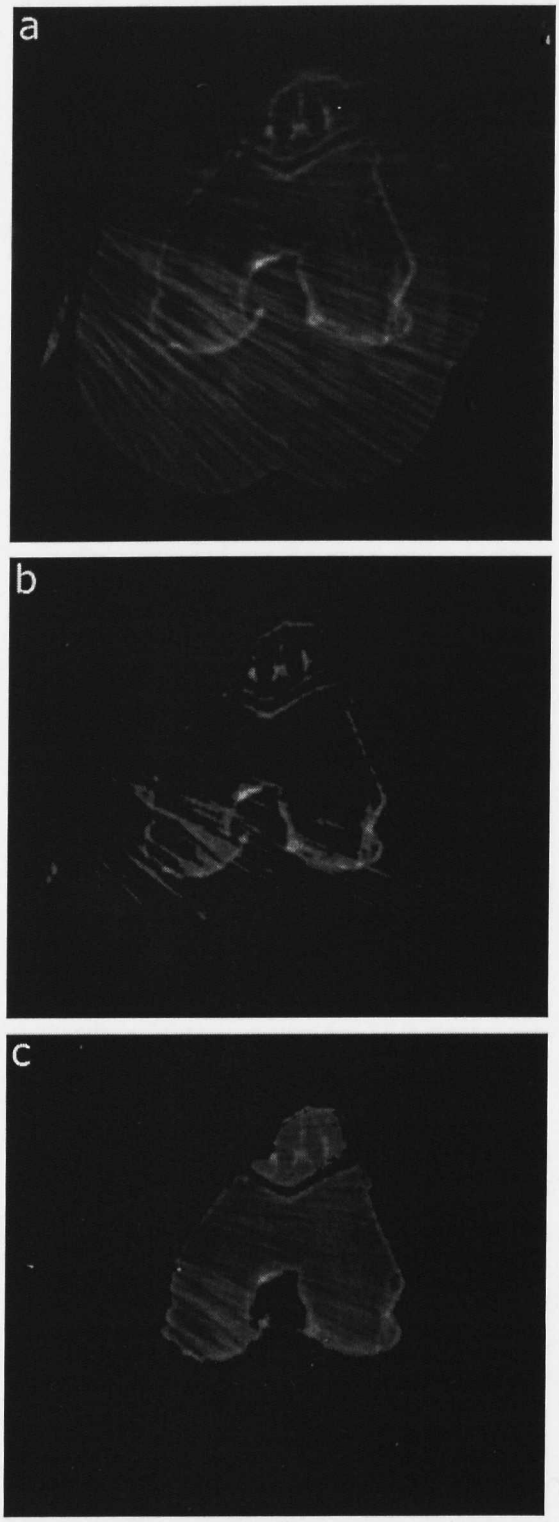


Fig. 7. Processing of CT images for the first clinical trial: (a) Original CT slice with interference from the implant in the other leg. (b) The bones separated from soft tissue using automatic segmentation. (c) The bones separated from soft tissue using interactive segmentation.

could be improved upon, and it was subsequently modified.

The robot was wheeled to the operating table, and the anatomical registration procedure was then performed for both the femur and the tibia. Tables 4–7 present the registration sequences for the femur and tibia in each of the two preliminary trials. In all instances, the low final RMS errors indicated that the bones were registered with high accuracy, which was confirmed on the intraoperative 3D display. Although the bones were successfully registered in both trials, the rest of the TKR procedure was completed manually, as it was intended to test only the protocols and the registration procedure.

First Clinical Trial

The good prosthesis fit achieved in cutting the plastic bone phantoms, and the encouraging results of the preliminary clinical trials, paved the way for the first full procedure to be performed.

Similarly to the preliminary trials, a CT scan of the patient's leg was taken a few days prior to the surgery (1-mm slice spacing in the knee area and 5 mm elsewhere, 0.836-mm pixel spacing). The patient had had a TKR and a major custom implant on the other leg, which gave rise to some artefacts in the CT images. While this made automatic segmentation difficult, interactive processing of the images using the surgeon's planning software allowed a good surface model of the bone to be produced (see Fig. 7).

Intraoperatively, the knee was exposed and the bones were immobilized using the leg fixtures. The modified tibial clamp substantially reduced the time required to fit the clamp onto the tibia. The robot was wheeled next to the operating table and clamped down.

Next, the femur was registered. Registration results are shown on Table 8. The accuracy of registration was verified by using the Acrobot to touch a number of landmarks on the surface of the femur and checking their location on the intraoperative display. As the displayed point location closely matched the real-world situation (indicating accurate registration), the registration was accepted and it was decided to proceed with the cutting sequence.

The five planes on the femur were success-

Table 8. Anatomical Registration Sequence for the Femur during the First Clinical Trial

	Number of points	RMS error (mm)	Standard deviation (mm)	Maximum error (mm)	Minimum error (mm)
Initial registration	4	5.71	—	—	—
ICP 1	26	0.85	0.620	3.19	0.11
ICP 2	24	0.44	0.280	1.16	0.04

fully cut. Figure 8 shows one of the planes being cut. Once all the planes were prepared, the femoral trial was placed onto the bone. It was observed that the fit of the trial onto the bone was very good, with no noticeable gap between the trial and the prosthesis (see Fig. 9). As planned, the top of the anterior femoral component was lying on the anterior surface of the bone and there was no femoral notching. The hole for the stem of the femoral prosthesis was then manually drilled through the femoral trial component.

The tibia and patella were prepared as in manual surgery. Note that the tibia could have been cut with the robot. However, due to the time spent checking and rechecking that the procedure was going according to plan, it was decided to prepare the tibia manually. The robot and the leg fixtures were then removed from the operating table.

Once the tibial trial was in place, the knee motion was tested. The two components were found to mate correctly, giving a good range of motion. The surface of the patella was then prepared manually, the three prosthesis components were cemented onto the bones, and the incision was closed.

DISCUSSION

A "hands-on" robotic system for TKR surgery was successfully used clinically. The preoperative planning system was found to be easy to use and was able to extract accurate quantitative data from the CT images. The planning procedure alone improved the surgery by giving the surgeon more information than is available in conventional surgery, helping him to decide the size of prosthesis preoperatively. The bone surface models, in con-

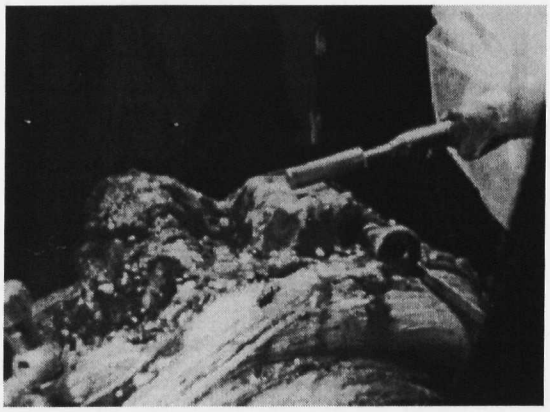
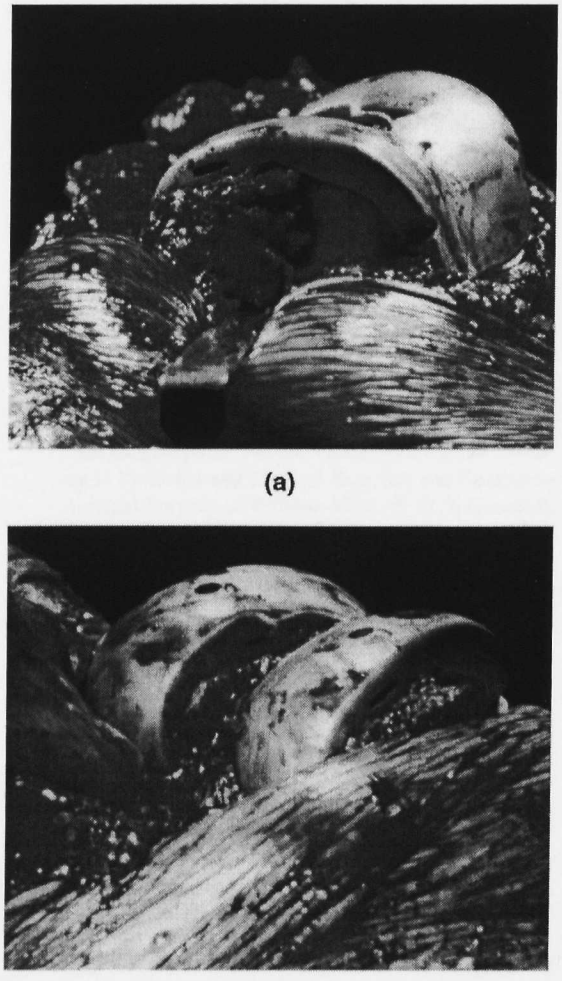


Fig. 8. First clinical trial: cutting a plane on the femur.



(a)

(b)

Fig. 9. First clinical trial: femoral trial component in place after the femur was successfully cut.

junction with the intraoperative display, proved to be a valuable source of information.

System trials on plastic bone phantoms showed that the robot is capable of accurately following the plan, resulting in a good component fit onto the bone and accurate placement of the components. The anatomical registration procedure using the robot as a point-acquisition tool produced good and repeatable results, confirming that the invasive fiducial-marker registration procedure used in previous trials could be replaced.

Two preliminary clinical trials were successfully performed to test the suitability of the surgical protocol and the performance of the anatomical registration procedure on a real bone. All parts of the robotic system performed very well, with only a minor modification being required to improve the tibial bone clamp. The registration results for both the femur and the tibia were encouraging in both clinical trials. However, the bones were not cut and the surgery was completed manually.

The system was then used to successfully cut the surfaces of the femur in the first "hands-on" robotic TKR surgery. The fit and placement of the femoral prosthesis was very good, with no noticeable gap between the component and the bone, and no femoral notching. However, the time required for the robotic procedure was longer than for conventional surgery, mainly due to time spent verifying the progress at each step of the procedure. The ease with which the bone could be accurately machined, as well as the constraint system, which prevented any damage or incorrect cuts, were welcome improvements over the conventional procedure.

Further clinical trials are planned to assess the accuracy of the procedure in more detail, and to compare its benefits and drawbacks with respect to conventional surgery. In addition, refining the surgical protocol will substantially reduce the duration of the surgery. However, it is felt that these early experiences demonstrate the considerable promise of a "hands-on" approach to robotic TKR surgery. The synergy between the surgeon's judgement and sensing capability and the robot's accuracy and ability to constrain the surgeon to safe regions has great potential for all future surgery.

ACKNOWLEDGMENT

The authors wish to acknowledge the Acrobot Company Limited for their support. The support of Stryker UK Limited, for supply of prostheses, of Armstrong Healthcare Limited, for supply of the gross positioning system, and of Finsbury (Instruments) Limited, for the supply of patient clamping systems, is also gratefully acknowledged.

REFERENCES

1. Tew M, Waugh W. Tibiofemoral alignment and the results of knee replacement. J Bone Joint Surg Br 1985;67:551–556.
2. Davies BL, Fan KL, Hibberd RD, Jakopec M, Harris SJ. A mechatronic based robotic system for knee surgery. International Conference on Intelligent Information Systems, Bahamas, 1997.
3. Davies BL, Harris SJ, Jakopec M, Cobb J. Computer-assisted surgery for TKR. In: Proceedings of International Conference on Knee Replacement 1974–2024, London, England, 1999.
4. Davies BL, Harris SJ, Jakopec M, Fan A, Cobb J. A special-purpose robotic system for knee surgery. In: Proceedings of the 4th International Conference on Computer-Assisted Orthopaedic Surgery, Davos, Switzerland, 1999.
5. Harris SJ, Jakopec M, Hibberd RD, Cobb J, Davies BL. Interactive pre-operative selection of cutting constraints, and interactive force controlled knee surgery by a surgical robot. In: Wells WM, Colchester A, Delp S, editors: Proceedings of the First International Conference on Medical Image Computing and Computer-Assisted Intervention (MICCAI'98), Cambridge, MA, October 1998. Lecture Notes in Computer Science 1496. Berlin: Springer, 1998. p 996–1006.
6. Harris SJ, Lin WJ, Fan KL, Hibberd RD, Cobb J, Middleton R, Davies BL. Experiences with robotic systems for knee surgery. In: Troccaz J, Grimson E, Mösges R, editors: Proceedings of First Joint Conference on Computer Vision, Virtual Reality and Robotics in Medicine and Medical Robotics and Computer-Assisted Surgery (CVRMed-MRCAS '97), Grenoble, France, March 1997. Lecture Notes in Computer Science 1205. Berlin: Springer, 1997. p 757–766.
7. Kazanzides P, Mittelstadt BD, Musits BL, Bargar WL, Zuhars JF, Williamson B, Cain PW, Carbone EJ. An integrated system for cementless hip replacement. IEEE Eng Med Biol 1995;14(3):307–313.
8. Mittelstadt BD, Kazanzides P, Zuhars JF, Williamson B, Cain P, Smith F, Bargar WL. The evolution of a surgical robot from prototype to human clinical use. In: Taylor RH, Lavallée S, Burdea GC, Mösges R, editors: Computer-Integrated Surgery: Technology and Clinical Applications. Cambridge, MA: The MIT Press, 1996. p 397–407.
9. Wiesel U, Lahmer A, Börner M, Skibbe H. ROBODOC at Berufsgenossenschaftliche Unfallklinik Frankfurt (BGU)—Experiences with the Pinless System. In: Third Annual North American Program on Computer Assisted Orthopaedic Surgery (CAOS USA '99) Pittsburgh, PA, June 1999. p 113–117.
10. Grueneis COR, Ritcher RH, Hening FF. Clinical introduction of the CASPAR system. In: Proceedings of

the 4th International Symposium on Computer Assisted Orthopaedic Surgery, Davos, Switzerland, 1999.

11. Brandt G, Zimolong A, Carrat L, Merloz P, Staudte HW, Lavallée S, Radermacher K, Rau G. CRIGOS: a compact robot for image-guided orthopedic surgery. IEEE Trans Information Tech Biomed 1999;3(4):252–259.
12. Fadda M, Wang T, Marcacci M, Martelli S, Dario P, Marcenaro G, Nanetti M, Paggetti C, Visani A, Zaffagnini S. Computer-assisted knee arthroplasty at Rizzoli Institutes. In: Proceedings of MRCAS '94, Pittsburgh, PA, 1994.
13. Kienzle III TC, Stulberg SD, Peshkin M, Quaid A, Lea J, Goswami A, Wu CH. Total knee replacement. IEEE Eng Med Biol, May 1995.
14. Kienzle III TC, Stulberg SD, Peshkin M, Quaid A, Lea J, Goswami A, Wu CH. A computer-assisted total knee replacement surgical system using a calibrated robot. In: Taylor RH, Lavallée S, Burdea GC, Mösges R, editors: Computer-Integrated Surgery: Technology and Clinical Applications. Cambridge, MA: The MIT Press, 1996. p 409–416.
15. Marcacci M, Dario P, Fadda M, Marcenaro G, Martelli S. Computer-assisted knee arthroplasty. In: Taylor RH, Lavallée S, Burdea GC, Mösges R, editors: Computer-Integrated Surgery: Technology and Clinical Applications. Cambridge, MA: The MIT Press, 1996. p 417–423.
16. Davies BL. Synergistic robots in surgery—surgeons and robots working co-operatively. ISER '97, Barcelona, Spain, 1997.
17. Davies BL, Fan KL, Hibberd RD, Jakopec M, Harris SJ. ACROBOT—using robots and surgeons synergistically in knee surgery. In: Proceedings of ICAR '97, Monterey, USA, 1997.
18. Cobb J, Harris SJ, Jakopec M, Davies BL. A robotic system for TKR surgery. In: Third Annual North American Program on Computer Assisted Orthopaedic Surgery (CAOS USA '99) Pittsburgh, PA, June 1999. p 71–74.
19. Ho SC, Hibberd RD, Davies BL. Robot assisted knee surgery. IEEE Eng Med Biol 1995;14(3):292–300.
20. Troccaz J, Delnondedieu Y. Semi-active guiding systems in surgery. A two-DOF prototype of the passive arm with dynamic constraints (PADyC). Mechatronics 1996;6(4):399–421.
21. Taylor R, Jensen P, Whitcomb L, Barnes A, Kumar R, Stoianovici D, Gupta P, Wang ZX, deJuan E, Kavoussi L. A steady-hand robotic system for microsurgical augmentation. In: Taylor C, Colchester A, editors: Proceedings of the Second International Conference on Medical Image Computing and Computer-Assisted Intervention (MICCAI'99), Cambridge, England, September 1999. Lecture Notes in Computer Science 1679. Berlin: Springer, 1999. p 1031–1041.
22. Harris SJ, Jakopec M, Cobb J, Davies BL. Intraoperative application of a robotic knee surgery system. In: Taylor C, Colchester A, editors: Proceedings of the Second International Conference on Medical Image Computing and Computer-Assisted Intervention (MICCAI'99), Cambridge, England, September 1999. Lecture Notes in Computer Science 1679. Berlin: Springer, 1999. p 1116–1124.
23. Faugeras OD, Hebert M. The representation, recognition, and locating of 3-D objects. Int J Robotic Res 1986;5(3):27–52.
24. Lavallée S. Registration for computer-integrated surgery: methodology, state of the art. In: Taylor RH, Lavallée S, Burdea GC, Mösges R, editors: Computer-Integrated Surgery: Technology and Clinical Applications. Cambridge, MA: The MIT Press, 1996. p 77–97.
25. Besl PJ, McKay ND. A method for registration of 3-D shapes. IEEE Trans Pattern Anal Machine Intell 1992; 14(2):239–256.
26. LaPalombara P, Fadda M, Martelli S, Marcacci M. Minimally invasive 3D data registration in computer and robot assisted total knee arthroplasty. Med Biol Eng Comput 1997;35(6):600–610.
27. Zhang Z. Iterative point matching for registration of free-form curves and surfaces. Int J Comp Vision 1994;13(2):119–152.

The Hands-On Orthopaedic Robot "Acrobot": Early Clinical Trials of Total Knee Replacement Surgery

Matjaz Jakopec, Ferdinando Rodriguez y Baena, Simon J. Harris, *Member, IEEE*, Paula Gomes, Justin Cobb, and Brian L. Davies

Abstract—**A "hands-on" robotic system for total knee replacement (TKR) surgery is presented. A computer tomography-based preoperative planning software is used to accurately plan the procedure. Intraoperatively, the surgeon guides a small special-purpose robot, called Acrobot, which is mounted on a gross positioning device. The Acrobot uses active constraint control, which constrains the motion to a predefined region, and thus allows the surgeon to safely cut the knee bones to fit a TKR prosthesis with high precision. A noninvasive anatomical registration method is described. The system has been successfully used in seven clinical trials with encouraging results.**

Index Terms—**Acrobot, active constraints, hands-on robotics, orthopaedic robotic surgery, total knee replacement (TKR).**

I. Introduction

TOTAL KNEE replacement (TKR) surgery is a common orthopaedic procedure to replace damaged surfaces of the knee bones with prosthetic implants. Typically, a TKR prosthesis consists of three components, one for each knee bone: tibia, femur, and patella (see Fig. 1). To fit the prosthesis, each of the knee bones is cut to a specific shape (usually a set of flat planes) which mates the mounting side of the corresponding prosthesis component. To ensure normal functionality of the knee, and a long-lasting, pain-free implant, all components must be placed onto the bones with high precision, both with regard to the bone axes, and with regard to the mating surfaces between the bone and prosthesis.

Conventionally, the surgeon cuts the bones using an oscillating saw, together with a complex set of jigs and fixtures, in an attempt to accurately prepare the surfaces of the bones. It is very difficult to achieve a good fit and proper placement of the prosthesis, even for a skilled surgeon using state-of-the-art cutting tools and fixtures. A conventional TKR study [1] reports a deviation from ideal prosthesis alignment greater than 9° in 7% of cases, and greater than 5° in 34% of cases. The reason for this is that the cutting tools and fixtures are made for an average human anatomy, and their placement largely depends on a surgeon's experience. Furthermore, the fixtures are used sequentially, which can result in an accumulation of errors. Another source of error lies in the oscillating saw, as its blade tends to bounce off a hard part of the bone despite the guiding tools, which can result in a poor surface finish.

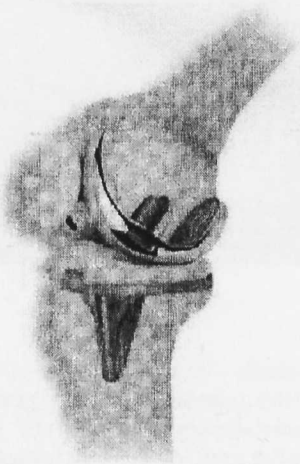


Fig. 1. Knee with TKR prosthesis.

To overcome the problems of the conventional TKR surgery and improve the results of the procedure, a robotic surgery system is being developed at Imperial College, London, U.K., and is currently undergoing clinical trials [2]. The system consists of a preoperative planning workstation and intraoperative robotic system.

II. Preoperative Planning

The planning stage of the Acrobot system is much more extensive than the planning for conventional TKR surgery (which involves placing prosthesis templates over X-ray images). First, a computer tomography (CT) scan of the patient's leg is taken. The interactive planning software (developed at Imperial College) is used to process CT images and plan the procedure. Three-dimensional (3-D) models of the knee bones are built and the bone axes are determined. The surgeon then interactively decides prosthesis size and placement (see Fig. 2). The software provides a number of different 3-D views of the leg and the implant to help the surgeon plan the procedure. Once the prosthesis model is in the correct position over the bone model, the planning software generates the constraint boundaries, which are then transferred to the intraoperative robotic system.

III. Acrobot Robotic System

Current work on robot-assisted knee replacement surgery has typically used industrial robots, adapted for the surgical

Manuscript received July 23, 2002; revised January 16, 2003. This paper was recommended for publication by Editor R. Taylor upon evaluation of the reviewers' comments. This work was supported by the Acrobot Company Ltd., London, U.K.

The authors are with the Mechatronics in Medicine Group, Department of Mechanical Engineering, Imperial College of Science, Technology and Medicine, London SW7 2AZ, U.K. (e-mail: b.davies@imperial.ac.uk).

Digital Object Identifier 10.1109/TRA.2003.817510

1042-296X/03$17.00 © 2003 IEEE

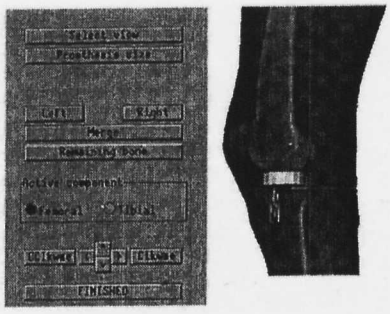


Fig. 2. User interface of the preoperative planning software.

task. Commercially available systems include Caspar (originally marketed by Orto-Maquet, and then URS, Germany, but recently discontinued) [3] and Robodoc (Integrated Surgical Systems, USA) [4]–[6], based on, respectively, an anthropomorphic PUMA style RX-90 "clean-room" robot (Staubli Automation, Switzerland) and a SCARA Sankyo Seiki modified industrial robot, under position control, to accurately machine the bone surface. While Caspar still uses fiducial markers, Robodoc recently started using an anatomical registration procedure [7] with fiducial pins screwed into the bone during the operation for motion checking. Both systems were initially aimed at hip replacement.

A system using a special-purpose parallel-link robot, a modified Stewart platform, is the Compact Robot for Image-Guided Orthopaedic Surgery (CRIGOS), which was developed at Helmholtz Institute, Germany [8], [9]. Two further research systems are based on an industrial PUMA robot. A group at the Instituti Ortopedici Rizzoli, Italy, [10]–[12] is researching an active robot system to resect the knee bones, under position control. Software has been developed for preoperative planning using a CT bone model. Registration is fiducial based, although the group has also investigated noninvasive anatomical registration [13].

All the above systems operate autonomously, i.e., they are set up by the surgeon and then proceed to carry out the task automatically without further surgeon intervention. A different approach has been undertaken by a research group at Northwestern University, Evanston, IL. In this approach, the PUMA robot has been used to position drill guides for drilling holes to locate a cutting block [14], [15]. Thus, the system can be classified as a passive system, since the motion of the robot purely positions the fixture and it is the surgeon who then undertakes the contact with the patient, and therefore, the system has lower safety requirements.

Another passive system is Galileo, commercialised by PI Precision Implants, Switzerland. A motorized device is directly clamped onto the bone and moved to position a cutting guide. The cuts are performed manually, using an oscillating saw, and may still result in inaccuracies in achieving the preoperative plan.

An alternative approach to robot-assisted surgery is the use of a navigation system, usually based on optically tracked surgical tools with a visual display of the bone models to aid in the positioning and alignment of tools. Numerous systems are available commercially, such as BrainLab's (BrainLab, Germany), Stryker Leibinger's (Leibinger, Germany), and Orthopilot (Aesculap, Germany). These systems, while helping to improve accuracy, do not prevent the surgeon from failing to follow the plan accurately. Several research systems have also been investigated, such as the computer-assisted spinal surgery system from Nolte *et al.*, 1994 [16] and that proposed by Lavallee *et al.*, 1994 [17].

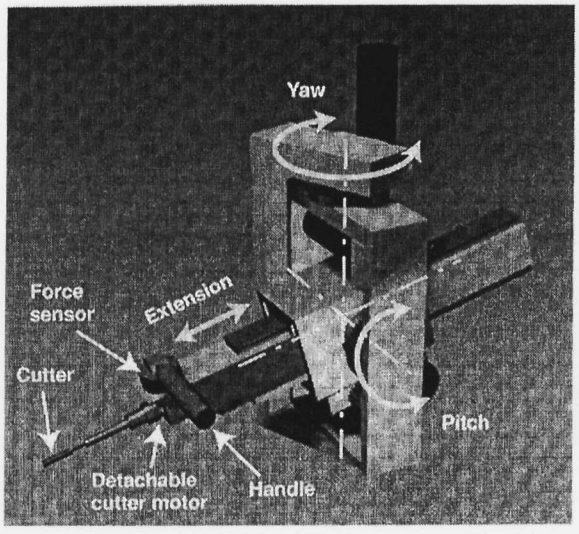


Fig. 3. Acrobot.

Comprehensive overviews of medical robotics can be found in [18]–[20]. The first robot-assisted surgery was performed in 1985 by Kwoh *et al.*, 1988 [21]. A PUMA robot was used to hold a fixture next to the patients head to locate a biopsy tool for neurosurgery. The robot was locked in position while the biopsy tools were inserted, through the fixture, into the skull by the surgeon. Thus, although a powered robot was used, it was locked off with power removed for safety, and can, therefore, be regarded as a robot system used passively. A research group at Imperial College London developed Probot, the world's first active robot-assisted surgery on a human patient, clinically tested in April 1991 to perform a prostatectomy [22]. At around the same time, the early Robodoc robotic system for total hip replacement surgery was being developed and used to prepare the surface of a femur on a human patient in 1992 [6].

In contrast to such robotic systems, which use modified industrial robots, a small, low-powered, special-purpose robot called Acrobot has been built for safe use in a crowded sterile operating theatre environment.

The Acrobot is a spherical manipulator with three orthogonal axes of motion: yaw, pitch, and extension (see Fig. 3). It has a relatively small reach (30–50 cm) and range of angles ($\pm$ 30°), which ensures accurate operation with low-powered motors. Consequently, the robot is relatively safe, because potential damage is limited in terms of force and is constrained to a small region. This kinematic structure was adopted so that the mechanical impedance of the axes is low and similar for all axes, allowing the robot to be moved by the surgeon with low force. This structure was chosen to ensure that forces encoun-

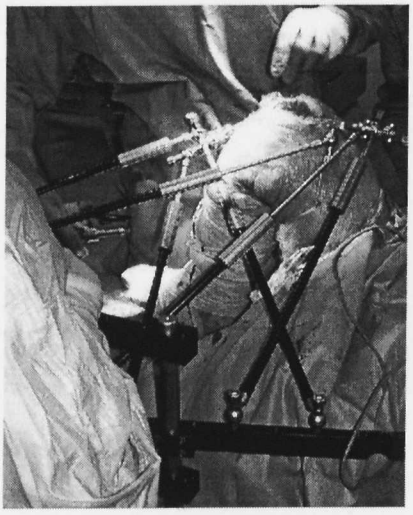


Fig. 4. Leg fixtures in place during a clinical trial.

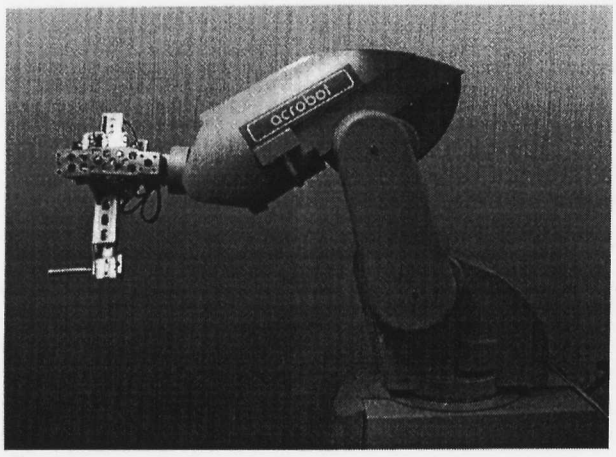


Fig. 5. Acrobot mounted on a gross positioning device.

tered when cutting hard bone could be detected without the need for force sensors in the robot cutter. The configuration is preferable to, say, a remote center of motion (RCM) about the skin entry point [23]. While an RCM system might be thought advantageous for minimally invasive surgery (MIS) to minimize the entry wounds, in practice, the range of motions required to suit both MIS and TKR surgery would be excessive.

The surgeon moves the robot by pushing the handle near the tip of the robot. The handle incorporates a six-axis force sensor, which measures the guiding forces and torques. This force/torque information is used in active constraint control of the robot (see Section IV). A high-speed orthopaedic cutter motor is mounted at the tip of the Acrobot. Different rotary cutters and tools can be repeatably mounted into the motor. For sterility reasons, the cutter motor is placed in a special mount, which allows the motor to be removed and autoclaved before the surgery, and placed onto the robot at the start of the surgery.

Sterilizable leg fixtures (see Figs. 4 and 9) are another important part of the robotic system, as they ensure that the bones do not move with respect to the robot base during the procedure. Two special bone clamps are rigidly clamped to the exposed parts of the tibia and femur. Both contact ends (medial and lateral) of each bone clamp include four small pins, which are inserted a few millimeters into the bone, and thus, prevent any rotation of the clamp. Each of the bone clamps is linked to a base frame (attached to the side rails of the table) with three telescopic arms. The ankle is placed into a special foot support mounted on the operating table, whereas the weight of the patient has proven to be enough to immobilize the femur at the hip joint.

Due to its small working envelope, the Acrobot is placed on a six-axis gross positioning device (see Fig. 5), which moves the Acrobot to different optimal cutting locations around the knee. The velocities of the axes are limited, and secondary encoders are fitted on each axis as a check for increased safety. Furthermore, the device is locked off when the bone is machined, and is only powered on for a short period between cutting two consecutive planes to move the Acrobot to the next optimal cutting position. The gross positioning robot is mounted on a wheeled trolley, to allow the system to be quickly placed near the operating table or removed from it. The trolley wheels can be locked, and the stiffness of the system is further increased by linking the trolley to the side rails of the operating table with two clamps, provided on the trolley. The Acrobot and the gross positioning device are covered with sterile drapes during the surgery, with the sterile cutter motor protruding through the drapes.

IV. Active Constraint Control

The Acrobot uses a novel type of robot control, active constraint control [24], [25]. The surgeon guides the robot by pushing on the force-controlled handle at the tip of the robot, and thus uses his/her superior human senses and understanding of the overall situation to perform the surgery. The robot provides geometric accuracy and also increases safety by means of a predefined 3-D motion constraint. This hands-on approach is very different from other surgical robots and is favored by the surgeons, as the surgeon is kept in the control loop. Related guided systems for computer-aided surgery (CAS) are PADyC [26] and Cobot [27].

The basic idea behind active constraint control is to gradually increase the stiffness of the robot as it approaches the predefined boundary. In other words, the robot is free to move inside the safe region (RI), due to the low mechanical impedance of the robot. At the boundary of the safe region, the robot becomes very stiff, thus preventing further motion over the boundary (RIII). In addition, the portion of the guiding force normal to the boundary is directly compensated, which substantially reduces the over-boundary error (this error is inevitable due to the limited motor power). To avoid instabilities at the boundary, the stiffness increases gradually over a small region (with width D_1) close to the boundary (RII). Furthermore, only the stiffness in a direction toward the boundary is adjusted, to allow motion along or away from the boundary with a very low guiding force (see Fig. 6).

This is achieved by a two-level control. The inner loop (2 ms) is a joint position/velocity control loop with friction, gravity,

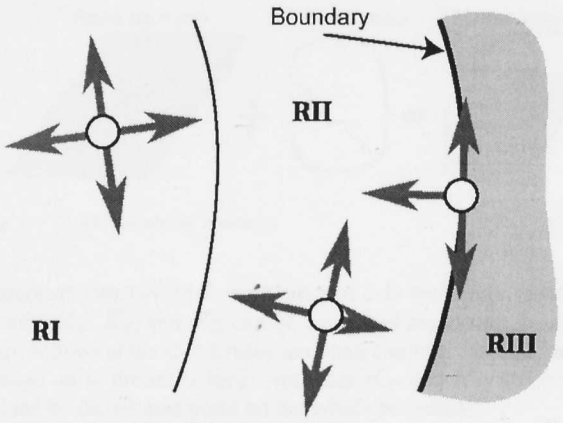


Fig. 6. Active constraint control principle.

and guiding force compensation, represented by the following control law:

$$\tau = K_P(\Theta_d - \Theta) + K_D(\dot{\Theta}_d - \dot{\Theta}) + \tau_C + f^*(\Theta, \dot{\Theta}) + g^*(\Theta). \tag{1}$$

τ is the torque output from the position controller to the robot motors. Position control gains K_P (proportional) and K_D (derivative) can be adjusted by the boundary controller (explained below) to achieve the desired stiffness and damping of the robot. Θ_d and $\dot{\Theta}_d$ are joint position and velocity demands, respectively, and are set by the boundary controller. Θ and $\dot{\Theta}$ are actual joint position and velocity, respectively (measured with encoders). τ_C is the guiding force compensation, which is also set by the boundary controller. f^* and g^* are friction and gravity compensation, respectively.

The outer, slower loop (approx. 10–15 ms, depending on complexity of the boundary) is the boundary controller, which is executed in Cartesian space and adjusts the control parameters: gains of the inner loop (K_P, K_D); position and velocity demands (X_d, $\dot{X}_d$); and the amount of force compensation (F_C). X_d, $\dot{X}_d$ and F_C are transformed into joint space before being passed to the inner loop

$$\Theta_d = K^{-1}(X_d) \tag{2}$$
$$\dot{\Theta}_d = J^{-1}\dot{X}_d \tag{3}$$
$$\tau_C = J^T F_C \tag{4}$$

where K^{-1} is the inverse kinematics computation, and J is the Jacobian matrix.

The control parameters are adjusted according to the robot's position X and the surgeon's guiding force F_G as follows. First, the nearest point X_{np} on the boundary is determined. The distance to this point is

$$d = \|X - X_{np}\| = (X - X_{np}) \cdot N_{np} \tag{5}$$

where N_{np} is the normal of the boundary at X_{np}, which is set to point inside the safe region. Inner loop control gains and demands depend on the d and are different in the three regions: RI, RII (inside the safe region), and RIII ("no-go" region).

A. Region RI ($d > D_1$)

In this region, the control gains are low to allow the surgeon to feel the cutting forces. Admittance A is the same in all directions. The demands are set as

$$X_d = X \tag{6}$$
$$\dot{X}_d = AF_G \tag{7}$$
$$F_C = 0 \tag{8}$$

where F_G is the surgeon's guiding force.

B. Region RII ($D_1 \geq d > 0$)

The control gains increase as the distance to the boundary decreases. The inner-loop position demand is the same as in Region RI . If the guiding force points away from the boundary ($F_G \cdot N_{np} \geq 0$) the velocity demand and force compensation are also the same. Otherwise, the guiding force is split into normal (F_{GN}) and tangential (F_{GT}) components

$$F_{GN} = (F_G \cdot N_{np})N_{np} \tag{9}$$
$$F_{GT} = F_G - F_{GN} \tag{10}$$

and $\dot{X}_d$ is comprised of two parts

$$\dot{X}_d = A_N F_{GN} + AF_{GT} \tag{11}$$

where A_N is the admittance in normal direction, which decreases with distance to the boundary

$$A_N = \frac{d}{D_1}A. \tag{12}$$

The amount of force compensation is increased over a smaller region D_2. Guiding force compensation $F_C = 0$ if $d > D_2$, and increases over the region $D_2 > d > 0$ to

$$F_C = -\frac{D_2 - d}{D_2}F_{GN}. \tag{13}$$

C. Region RIII ($d \leq 0$)

The control gains are high in this region. The inner-loop position demand is set to the nearest point

$$X_d = X_{np}. \tag{14}$$

If the guiding force points away from the boundary, the $\dot{X}_d$ and F_C are set as in Region RI. Otherwise, the force is again split into normal and tangential directions, and the demands are set as

$$\dot{X}_d = AF_{GT} \tag{15}$$
$$F_C = -F_{GN}. \tag{16}$$

Because of the nature of the prosthesis used, which requires a number of flat planes to be cut, the constraint boundary is defined as a "2.5-D" boundary, formed from a plane and a closed 2-D outline (see Fig. 7). The plane part allows a flat plane to be cut into the bone, whereas the 2-D outline part provides protection for the surrounding tissue. Since the two parts of the boundary are orthogonal, the boundary control problem can be

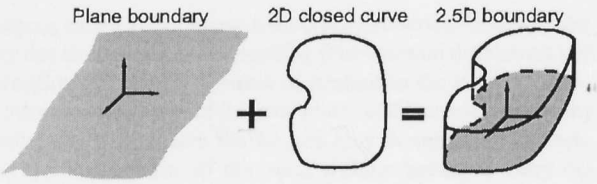


Fig. 7. "2.5-D" constraint boundary.

separated into two (1-D problem and 2-D problem). In other words, X_d, $\dot{X}_d$, and F_C can be computed separately for each part, following the above rules, and then combined before being passed on to the inner loop. Note that K_P and K_D are determined by the nearest point on the whole boundary.

V. Registration

Registration is a process to determine the geometrical relationship between different types of information about the patient and the surgical tools. In other words, the registration transformation R has to be determined from the coordinate system of the CT scanner (where preoperative planning data is defined) to the base coordinate system of the robot (relative to which the locations of the bones and the robot's tip are defined). The planning data is then transformed into the coordinate system of the robot.

At an early stage of the project, when trials were performed on plastic phantoms and cadavers [28], a registration method using fiducial markers was used. This involved placing four marker screws prior to taking a CT scan of the leg. The markers represent four corresponding noncollinear points in the preoperative plan (where the marker center is detected in the CT images) and the robot's coordinate system (where the marker is touched by the tip of the robot intraoperatively), from which the transformation R can be computed.

As this fiducial method required an additional surgery to implant the markers, it was regarded as unacceptable for clinical trials, and a noninvasive anatomical registration method has been implemented. The method is based on the iterative closest point (ICP) algorithm [29], [30], which determines the registration transformation by iteratively matching a set of surface points in one coordinate system to a corresponding surface in another coordinate system. The procedure is as follows. First, the surgeon acquires four landmark points, with a special 1-mm diameter ball probe mounted into the cutter motor. These four points are used to compute the initial registration estimate for the ICP algorithm. The surgeon then acquires a set of randomly selected points (typically 20–30) on the exposed bone surface. The ICP algorithm then registers the bone by matching this set of points to the preoperative bone surface model. The accuracy of the registration is then verified by using the on-screen color-coded display of the point set matched onto the surface model, and by touching various landmarks and checking their position on the real-time display (see Fig. 8). In the case of an unsatisfactory registration, the ICP procedure is repeated with a new set of points, with the initial estimate set to the last computed registration transformation.

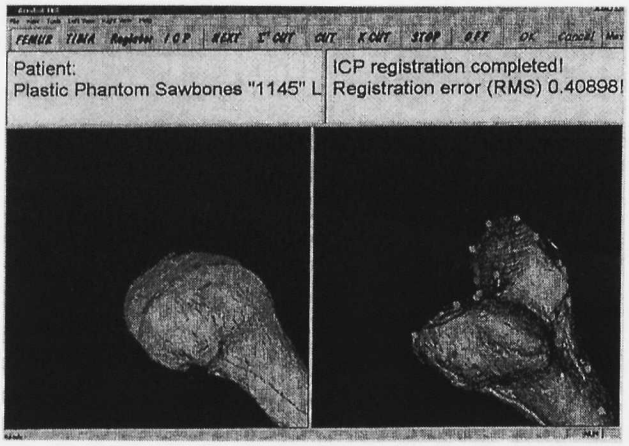


Fig. 8. Intraoperative user interface during registration.

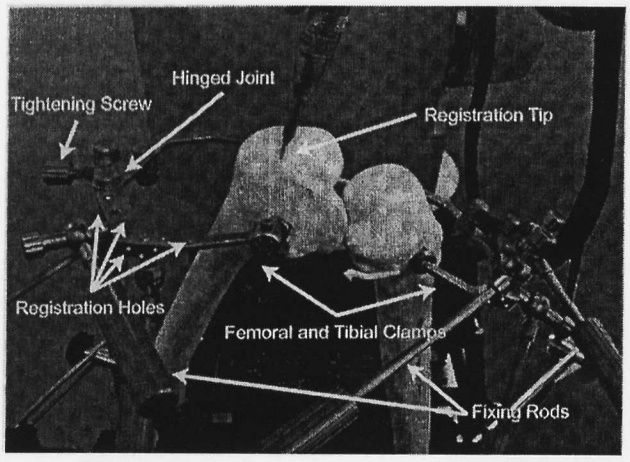


Fig. 9. Acrobot clamping system.

VI. Clamp Registration

The novel clamps designed for the Acrobot system include accurately machined conical holes, used to register the clamp position intra-operatively. As illustrated in Fig. 9, the holes are drilled on all surfaces of both the tibial and femoral clamps, which always remain in close proximity to the knee joint, and ensure that at least four holes are always accessible during surgery.

During registration, the position of both the knee (by means of anatomical registration) and clamping system (by locating at least four conical holes on each clamp) are stored in the computer's memory. The actual position of as many holes on the clamps as possible needs to be stored, as untouched holes will not be available during the procedure.

Since the clamps should not move in relation to each of the bones, it can be assumed the link connecting the bone to the clamps will remain constant throughout the procedure. Therefore, once registered, the knee joint and clamping system can be treated as one, dramatically reducing the time needed for reregistration. In the event of the patient leg being moved during

surgery, or the robot being temporarily removed from the theatre due to an emergency, touching four holes on the clamps will reconfirm the robot's position in relation to the knee. This improves the robustness of the procedure, and increases flexibility during use. If necessary, the surgeon may loosen the fixing rods, and test the mobility of the joint, without having to carry out the relatively time-consuming bone registration procedure once again.

Clamp registration is also used to ensure the knee joint has not moved in relation to the Acrobot system during the procedure. At any time during the surgery, the stored positional information for the femur and tibia can be compared to the one obtained by touching any four points on the clamps. As a result, either an error is flagged to alert the surgeon that the knee has moved (if the difference is substantial), or the information is automatically updated without the need for full reregistration. To ensure that the clamps do not move with respect to the bone, a separate bone-motion monitoring facility is being implemented.

VII. Registration Accuracy Assessment

A number of tests were carried out to investigate the performance of the registration procedure for different bone models, initial estimates, and point touching schemes. The root mean square (RMS) of the distance from each collected point to the mapped surface is the only quantitative piece of information available intraoperatively. This value is used to assess registration accuracy, and is complemented by a color-coded display of the points on the mapped surface. The color-coded display allows the user to visualise the distribution of the error on the surface, and to recognize any exceptionally poor points that may have resulted from surgeon error or poor contact between the surface and registration probe. A virtual representation of the registration probe can also be used to validate the registration result.

In order to evaluate the relationship between the actual rotational and translational errors in the registered surface and the RMS error, a computer program was developed to simulate the point-touching procedure (normally performed intraoperatively) using the mouse interactively to generate a point dataset. The error in the initial estimate (usually generated during landmark collection intraoperatively) was simulated by systematically translating and rotating a copy of the bone surface about each of the axes attached to the center of the model.

Different point sets were then tested for a combination, in the range of $\pm$ 10 mm translation and $\pm$ 2° rotation, of initial estimates. Even though larger initial errors were considered, the accuracy of the landmark-based initial registration appeared to lie within this range.

In early research, point-touching inaccuracies were not considered. As illustrated in Fig. 10, results have been more than satisfactory, with errors in the registered surface of 0.2° and 0.04 mm on average, which include the computational error resulting from limited depth buffer resolution, and floating point mathematics.

The results also demonstrate one of the key characteristics of the ICP algorithm: given an initial estimate, the solution will always converge to the closest local minimum. Therefore, it

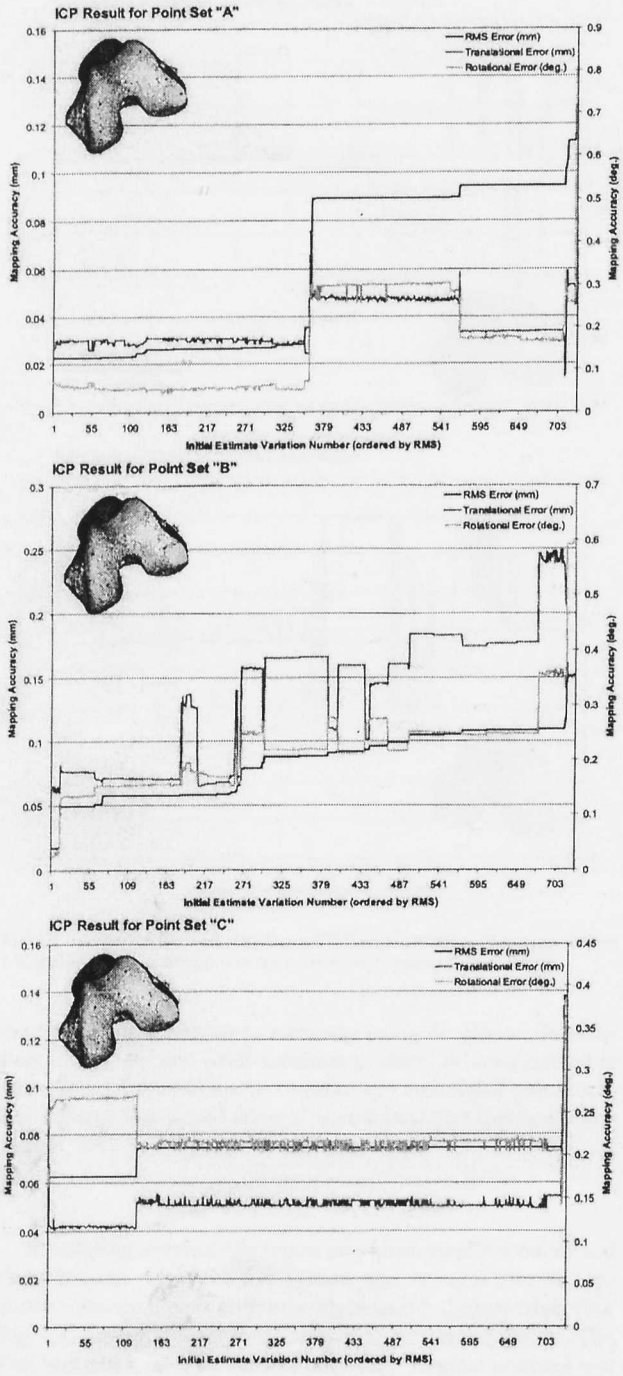


Fig. 10. Registration results for different point touching schemes: in scheme "A" most points lie around edges and features; in scheme"B" points lie on edges and features; in scheme"C" points are chosen as far away from edges and features as possible.

is reasonable to assume that a solution to any intraoperative setup can always be found, given an appropriate selection of initial landmarks and surface points. However, distinguishing between any local minimum and the global minimum, which describes the true mapping of the intraoperatively acquired set

of points to the corresponding modeled surface, represents the greatest registration challenge. It can be seen in Fig. 10 that a number of local minima exist for each point set. Furthermore, the point-touching scheme can greatly affect the location of the local minima. Scheme "C" in Fig. 10 has only three local minima, which are all close to the global minimum (i.e., low translational and rotational error). Therefore, the identification of an appropriate point-touching scheme will make the greatest impact on the registration outcome.

A golden standard during point collection has yet to be defined, however, progress is being made in trying to identify the characteristics of a point-touching scheme that need to be looked at for consistently successful registration. Notions such as "enough" (between 25 and 35) and "evenly spread out" set of points, covering as much of the available surface as possible, with particular focus on prominent landmarks such as the condyles and heliach crest, have been used during the first set of clinical trials. Appropriate convergence was obtained after one or two iterations of the registration process, without a predefined point set available to the surgeon.

Random noise was then added to the coordinates of the collected points in order to account for point-touching inaccuracy. This resulted in some points either being embedded in, or floating above, the surface. Results for different maximum noise values (see Fig. 11) illustrate how RMS error alone may not be representative of actual mapping accuracy. For instance, while RMS error values obtained for the entire grid at 1 mm maximum noise averaged at about 0.6 mm, actual rotational errors over 2° and translational error over 0.8 mm were observed.

Different point-set sizes and maximum noise values were then combined in order to quantify their effect on the algorithm's performance. 50 random point sets were generated for a range of point-set sizes varying between 10 and 100 points per set. Random noise, in 0.5 mm increments between 0 and 1.5 mm maximum error, was then added to each point set and the result was analyzed. Fig. 12 illustrates the outcome for a 0.5 mm noise. It can be noticed that for point-set sizes below 70, the ICP result starts to deteriorate. However, the minimum and maximum values highlight that, even for smaller set sizes, a good combination of points can produce a desirable outcome.

The current testing procedure, and results obtained, reinforce the belief that anatomical registration, based on surface matching between different frames of reference, is possible, and can provide an accurate means for registration with a reasonable degree of confidence. The algorithm has been found to be robust, consistently converging to the desired solution. Even when poor CT models were used, an evenly spread out set of points was found to generate enough information for the matching to take place successfully. The results, presented here, are based on the analysis of the femur. However, similar results were obtained for the tibia.

At present, the RMS error defining the distance of any registered point from the modeled surface is used to provide an estimate of the overall registration accuracy. However, this may not be representative of the quality of the actual fit between the two registered surfaces. Therefore, a more complete set of quantitative information to complement the RMS error and the intraoperative feedback display is currently being developed. In addition, the registration point-selection protocol is being refined to determine a minimum point-set size and associated point location scheme that would allow a more robust and accurate registration, even in the presence of noise.

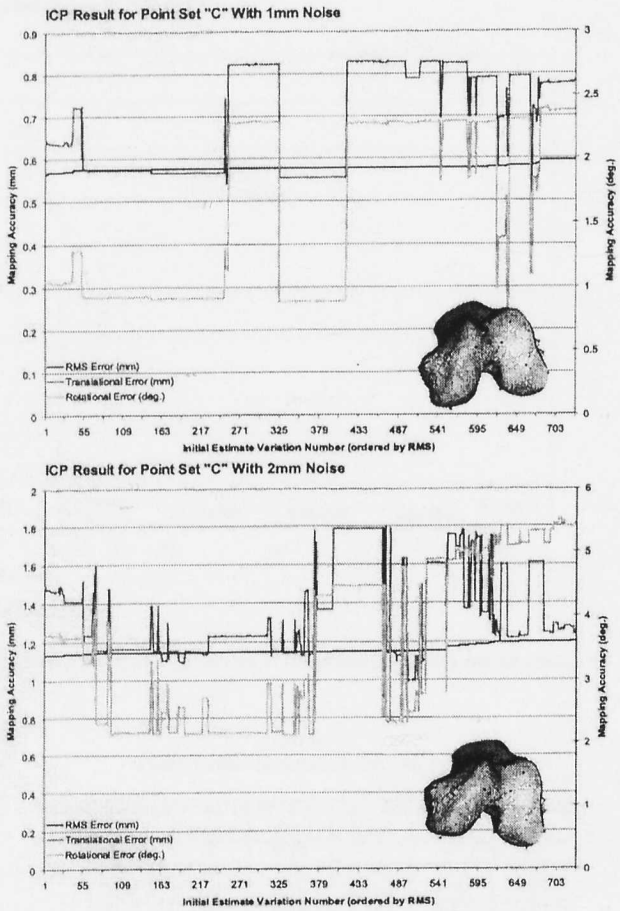


Fig. 11. Registration result for point set "C" for the entire grid, having applied 1 mm and 2 mm maximum random noise to each point in the dataset.

VIII. Clinical Application

After being successfully tested on plastic phantom bones and cadavers, the Acrobot TKR system was brought into the operating theater and is currently undergoing clinical trials (see Fig. 13). Seven clinical trials have been performed to date. The first two cases were performed to test the surgical protocol and anatomical registration, but without cutting the bone, whereas the rest of the cases also involved cutting the bone.

The procedure was as follows. A CT scan of the patient's leg was taken a few days before the surgery. The procedure was planned using the planning software and the data for the robotic system was generated. Intraoperatively, the knee was exposed and the bones were immobilized using the leg fixtures. In the meantime, the robot was set up and covered with sterile drapes. Once the leg was immobilized, the robot was wheeled next to the operating table and clamped to it. The femur and the tibia

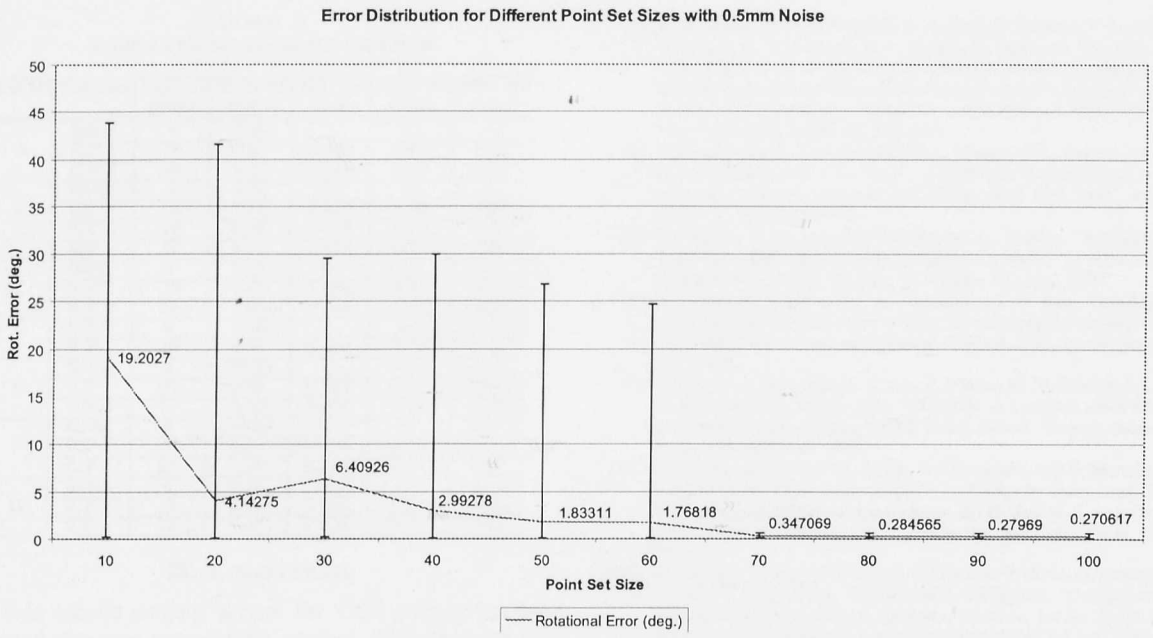


Fig. 12. This chart illustrates the performance of the ICP algorithm for different point-set sizes, from 10 points/set to 100 points/set (x axis), having added a 0.5 mm maximodel of themum error to each point in each data set.

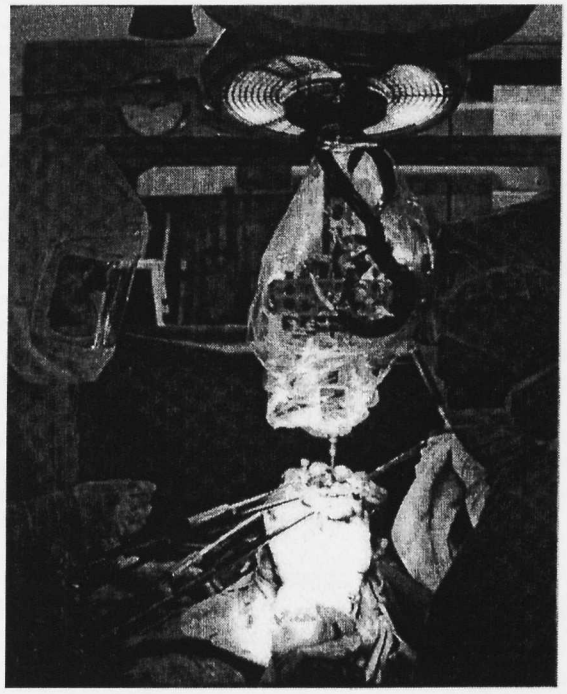


Fig. 13. Clinical application.

were then registered (with a 1-mm diameter ball probe) and cut (with a 7.8-mm diameter drum cutter). The patella was prepared manually, as the conventional procedure is regarded to be accurate enough, and the potential accuracy improvement does not justify the added complexity of the robotic-assisted procedure. The robotic system and leg fixtures were then removed from the operating table, and the procedure was finished as in conventional TKR surgery. The knee motion was tested with a trial prosthesis, the prosthesis components were fitted onto the bones, and the incision was closed.

TABLE I
REGISTRATION SEQUENCES FOR THE TIBIA

Patient	Sequence	Num. of points	RMS err. (mm)	Std. dev. (mm)	Max. err. (mm)	Min. err. (mm)
A	Initial	4	9.99	—	—	—
	ICP 1	29	0.61	0.361	1.71	0.04
	ICP 2	40	0.59	0.366	1.59	0.01
	ICP 3	36	0.38	0.240	0.85	0.01
B	Initial	4	1.13	—	—	—
	ICP 1	26	0.57	0.352	1.31	0.02
	ICP 2	13	0.27	0.178	0.72	0.01
D	Initial	4	18.58	—	—	—
	ICP 1	17	0.40	0.269	1.01	0.00
E	Initial	4	10.04	—	—	—
	ICP 1	18	1.69	1.255	5.37	0.07
	ICP 2	18	0.71	0.356	1.33	0.01
F	Initial	4	6.20	—	—	—
	ICP 1	17	0.67	0.369	1.20	0.00
	ICP 2	20	0.41	0.226	0.77	0.01
G	Initial	4	15.87	—	—	—
	ICP 1	14	0.36	0.218	0.96	0.02

In all cases, the surgeon was able to successfully register the bones, which was indicated by a low RMS error of the registration points, and confirmed by real-time display. The registration sequences and results for each patient are presented in Tables I and II (note that the tibia of the third patient (C) was not registered). In all cases involving cutting the bone with the aid of the robot, the fit of the prosthesis components onto the bone was very good. Furthermore, the components were found to mate correctly, giving proper bone alignment and a good range of motion. Early CT-based measurements of tibio–femoral alignment, comparing pre- and postoperative CTs, have shown a low deviation from plan within 2°.

TABLE II
REGISTRATION SEQUENCES FOR THE FEMUR

Patient	Sequence	Num. of points	RMS err. (mm)	Std. dev. (mm)	Max. err. (mm)	Min. err. (mm)
A	Initial	4	0.60	—	—	—
	ICP 1	34	0.80	0.537	2.33	0.01
	ICP 2	29	0.21	0.130	0.50	0.01
B	Initial	4	2.56	—	—	—
	ICP 1	22	0.96	0.615	2.95	0.09
	ICP 2	19	0.52	0.264	1.13	0.12
	ICP 3	12	0.17	0.116	0.35	0.00
C	Initial	4	5.71	—	—	—
	ICP 1	26	0.85	0.620	3.19	0.11
	ICP 2	24	0.44	0.280	1.16	0.04
D	Initial	4	5.46	—	—	—
	ICP 1	16	0.67	0.498	2.20	0.05
E	Initial	4	23.70	—	—	—
	ICP 1	20	0.86	0.534	2.09	0.06
	ICP 2	17	0.61	0.461	1.43	0.00
F	Initial	4	145.27	—	—	—
	ICP 1	18	0.74	0.462	1.76	0.01
	ICP 2	23	0.39	0.210	0.74	0.00
G	Initial	4	4.56	—	—	—
	ICP 1	18	0.99	0.640	1.97	0.03
	ICP 2	18	0.38	0.228	0.75	0.01

IX. CONCLUSIONS

A safe robotic surgery system for TKR surgery has been presented that was successfully applied clinically with very good results obtained. The planning software was found easy to use, and improved the surgery by giving the surgeon accurate qualitative information that is unavailable in conventional surgery, namely an accurate CT-based model of the patient's bones, which allows an informed choice of prosthesis. The intraoperative robotic system and its user interface has proven to be intuitive and easy to use, while providing the surgeon with valuable extra information about the procedure, such as an indication of areas for registration and visualization of the cutter position, cutting planes, and bone models. The ease with which the surgeon was able to guide the robot to accurately prepare the surfaces of the knee to fit the TKR prosthesis, and the increased safety due to the motion constraint, were welcome improvements over the conventional surgery. The system's "hands-on" approach makes it unique and currently more acceptable by the surgical community than purely active surgical robots, which take over the cutting process. Further clinical trials are planned to analyze the performance of the system in more detail, and to refine the surgical protocol. It is felt that these early clinical experiences demonstrate considerable promise of Acrobot's approach to robotic-assisted TKR surgery, as well as other robotic-assisted surgery.

REFERENCES

[1] M. Tew and W. Waugh, "Tibiofemoral alignment and the results of knee replacement," *J. Bone and Joint Surgery*, vol. 67-B, no. 4, pp. 551–556, 1985.

[2] M. Jakopec, S. J. Harris, F. R. Y. Baena, P. Gomes, J. Cobb, and B. L. Davies, "The first clinical application of a "hands-on" robotic knee surgery system," *Comput.-Aided Surgery*, vol. 6, no. 6, pp. 329–339, 2001.

[3] W. Siebert, S. Mai, R. Kober, and P. F. Heeckt, "Technique and first clinical results of robot-assisted total knee replacement," *Knee*, vol. 9, no. 3, pp. 173–180, 2002.

[4] B. D. Mittelstadt, P. Kazanzides, J. F. Zuhars, B. Williamson, P. Cain, F. Smith, and W. L. Bargar, "The evolution of a surgical robot from prototype to human clinical use," in *Computer-Integrated Surgery: Technology and Clinical Applications*, R. H. Taylor, S. Lavallee, G. C. Burdea, and R. Mösges, Eds. Cambridge, MA: MIT Press, 1996, pp. 397–407.

[5] R. H. Taylor, B. D. Mittelstadt, H. A. Paul, W. Hanson, P. Kazanzides, J. F. Zuhars, B. Williamson, B. L. Musits, E. Glassman, and W. L. Bargar, "An image-directed robotic system for precise orthopaedic surgery," in *Computer-Integrated Surgery: Technology and Clinical Applications*, R. H. Taylor, S. Lavallee, G. C. Burdea, and R. Mösges, Eds. Cambridge, MA: MIT Press, 1996, pp. 379–396.

[6] P. Kazanzides, B. D. Mittelstadt, B. L. Musits, W. L. Bargar, J. F. Zuhars, B. Williamson, P. W. Cain, and E. J. Carbone, "An integrated system for cementless hip replacement," *IEEE Eng. Med. Biol. Mag.*, vol. 14, pp. 307–313, May/June 1995.

[7] U. Wiesel, A. Lahmer, M. Borner, and H. Skibbe, "Robodoc at B.G. Frankfurt—Experiences with the pinless system," in *Proc. Computer Assisted Orthopaedic Surgery*, Pittsburgh, PA, June 1999.

[8] G. Brandt, K. Rademacher, A. Zimolong, and G. Rau, "Development of an integrated compact robot system for orthopaedic surgery," in *Proc. 29th ISR Conf. Advanced Robotics: Beyond 2000*, Birmingham, U.K., Apr. 1998.

[9] G. Brandt, A. Zimolong, L. Carrat, P. Merloz, H. W. Staudte, S. Lavallee, K. Radermacher, and G. Rau, "CRIGOS: A compact robot for image-guided orthopedic surgery," *IEEE Trans. Inform. Technol. Biomed.*, vol. 3, pp. 252–260, Apr. 1999.

[10] M. Marcacci, P. Dario, M. Fadda, G. Marcenaro, and S. Martelli, "Computer-assisted knee arthroplasty," in *Computer-Integrated Surgery: Technology and Clinical Applications*, R. H. Taylor, S. Lavallee, G. C. Burdea, and R. Mösges, Eds. Cambridge, MA: MIT Press, 1996, pp. 417–423.

[11] M. Fadda, T. Wang, M. Marcacci, S. Martelli, P. Dario, G. Marcenaro, M. Nanetti, C. Paggetti, A. Visani, and S. Zaffagnini, "Computer-assisted knee arthroplasty at Rizzoli Institutes," in *Proc. 1st Int. Symp. Medical Robotics and Computer-Assisted Surgery, MRCAS'94*, vol. 2, Pittsburgh, PA, 1994, pp. 26–30.

[12] A. Malvisi, M. Fadda, R. Vallegi, G. Bioli, and S. Martelli, "A new robotic system for the operating theater," *Comput. Contr. Eng. J.*, vol. 12, no. 3, pp. 129–136, 2001.

[13] P. LaPalombara, M. Fadda, S. Martelli, and M. Marcacci, "Minimally invasive 3-D data registration in computer and robot-assisted total knee arthroplasty," *Med. Biol. Eng. Comput.*, vol. 35, no. 6, pp. 600–610, Nov. 1997.

[14] T. C. Kienzle, III, S. D. Stulberg, M. Peshkin, A. Quaid, J. Lea, A. Goswami, and C. H. Wu, "Total knee replacement," *IEEE Eng. Med. Biol. Mag.*, vol. 14, pp. 301–306, May/June 1995.

[15] ——, "A computer-assisted total knee replacement surgical system using a calibrated robot," in *Computer-Integrated Surgery: Technology and Clinical Applications*, R. H. Taylor, S. Lavallee, G. C. Burdea, and R. Mösges, Eds. Cambridge, MA: MIT Press, 1996, pp. 409–416.

[16] L. P. Nolte, L. J. Zamorano, Z. Jiang, Q. Wang, F. Langlotz, E. Arm, and H. Visarius, "A novel approach to computer-assisted spine surgery," in *Proc. 1st Int. Symp. Medical Robotics and Computer Assisted Surgery, MRCAS'94*, vol. 2, Pittsburgh, PA, 1994, pp. 323–328.

[17] S. Lavallee, P. Sautot, J. Troccaz, P. Cinquin, and P. Merloz, "Computer-assisted spine surgery: A technique for accurate transpedicular screw fixation using CT data and a 3-D optical localizer," in *Proc. 1st Int. Symp. Medical Robotics and Computer Assisted Surgery, MRCAS'94*, vol. 2, Pittsburgh, PA, 1994, pp. 315–322.

[18] L. Joskowick and R. H. Taylor, "Computers in imaging and guided surgery," *Comput. Sci. Eng.*, vol. 3, no. 5, pp. 65–72, 2001.

[19] K. Cleary and C. Nguyen, "State of the art in surgical robotics: Clinical applications and technical challenges," *Comput.-Aided Surgery*, vol. 6, no. 6, pp. 312–328, 2001.

[20] B. L. Davies, "A review of robotics in surgery," *J. Eng. Med.*, vol. 214, no. 1, pp. 129–140, 2000.

[21] Y. S. Kwoh, J. Hou, E. A. Jonckeere, and S. Hayati, "A robot with improved absolute positioning accuracy for CT-guided stereotactic brain surgery," *IEEE Trans. Biomed. Eng.*, vol. 35, pp. 153–160, Feb. 1988.

[22] W. S. Ng, B. L. Davies, R. D. Hibberd, and A. G. Timoney, "A first-hand experience in transurethral resection of the prostate," in *Proc. IEEE EMBS*, vol. 12, Mar. 1993, pp. 120–125.

[23] D. Stoianovici, L. L. Whitcomb, J. H. Anderson, R. H. Taylor, and L. R. Kavoussi, "A modular surgical robotic system for image-guided percutaneous procedures," in *Proc. 1st Int. Conf. Medical Image Computing and Computer-Assisted Intervention (MICCAI'98)*, Cambridge, MA, Oct. 1998, pp. 404–410.

[24] S. C. Ho, R. D. Hibberd, and B. L. Davies, "Robot-assisted knee surgery," *IEEE Eng. Med. Biol. Mag.*, vol. 14, pp. 292–300, May/June 1995.

[25] S. J. Harris, M. Jakopec, I. Cobb, R. D. Hibberd, and B. L. Davies, "Interactive preoperative selection of cutting constraints, and interactive force-controlled knee surgery by a surgical robot," in *Proc. MICCAI'98*, Cambridge, MA, 1998, pp. 996–1006.

[26] J. Troccaz and Y. Delnondedieu, "Semi-active guiding systems in surgery A two-DOF prototype of the passive arm with dynamic constraints(PADyC)," *Mechatronics*, vol. 6, no. 4, pp. 399–421, 1996.
[27] ——, "Guiding systems for computer-assisted surgery: Introducing synergistic devices and discussing the different approaches," *Med. Image Anal.*, vol. 2, pp. 101–119, 1998.
[28] S. J. Harris, M. Jakopec, J. Cobb, and B. L. Davies, "Intraoperative application of a robotic knee surgery system," in *Proc. MICCAI'99*, Cambridge, U.K., 1999, pp. 1116–1124.
[29] P. J. Besl and N. D. McKay, "A method for registration of 3-D shapes," *IEEE Trans. Pattern Anal. Machine Intell.*, vol. 14, pp. 239–256, Feb. 1992.
[30] Z. Zhang, "Iterative point matching for registration of free-form curves and surfaces," *Int. J. Comput. Vis.*, vol. 13, no. 2, pp. 119–152, 1994.



Matjaz Jakopec received the B.Sc. degree in 1995 in electrical engineering from University of Ljubljana, Ljubljana, Slovenia, and the Ph.D. degree in 2001 from the Imperial College, University of London, London, U.K.

He joined the Mechatronics in Medicine Laboratory (MIMLab) at Imperial College, University of London, London, U.K. in 1996. Since 2000, he has worked as a Research Associate in medical robotics at the MIMLab. His research interests include control systems engineering, medical robotics, and human-machine interfaces.



Ferdinando Rodriguez y Baena received the M.Eng. degree in mechatronics and manufacturing systems from Kings College, University of London in 2000. He is currently working toward the Ph.D. degree in the Mechatronics in Medicine Laboratory, Imperial College, University of London, London, U.K.

He is currently working on the registration aspects of the Acrobot project, but his focus lies in the development of a minimally invasive robotic system for unicompartmental knee surgery.



Simon J. Harris (S'83–M'87) received the B.Sc. degree in electronic engineering from The Univerity of Hull, Hull, U.K., in 1986. He received the M.Sc. degree in medical electronics and physics from St. Bartholomews Hospital Medical School, London, U.K. in 1988, and received the Ph.D. degree in 1992 from the same institution.

Since 1991, he has worked at Imperial College, University of London, London, U.K. on vision-based adhesive dispensing, machine vision for civil engineering, robotic prostate surgery, and robotic knee surgery. He is currently working within the college as an Engineer for The Acrobot Company Ltd., London, U.K. His research interests include image processing, computer-based surgical planning, and robotic surgery.

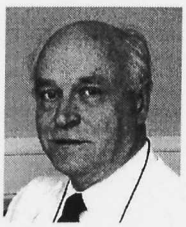


Paula Gomes received a first honors degree in computer science from the University of Minho, Minho, Portugal, and the Master's degree in industrial robotics and manufacturing automation, and a Ph.D. degree in automatic handling and inspection of composite materials, both from Imperial College, University of London, London, U.K.

She is a Research Associate with the Mechatronics in Medicine Laboratory (MIMLab) of Imperial College, University of London, London, U.K., and the R&D Manager for The Acrobot Company Ltd., London, U.K. Prior to joining MIMLab, in April 1998, she was a Research Fellow at Brunel University, London, U.K., with the Systems Engineering Department. She also still supervises research projects based at the University of Minho. She has done consultancy for academia and industry and worked in industry as a systems analyst and programmer. Her research interests comprise pattern recognition, image processing, visual inspection, manufacturing automation and, more recently, medical systems.



Justin Cobb is a consultant orthopaedic surgeon for University College London (UCL) NHS Trust, and Honorary Consultant at Great Ormond Street Hospital for Sick Children, both in London, U.K. He is an Honorary Senior Lecturer of UCL Medical School. His clinical practice is in lower limb reconstruction and musculoskeletal oncology. He has been collaborating with the Department of Mechatronics in Medicine since 1991, and first used the system in clinical trials in 2001. He was made Honorary Visiting Senior Lecturer to Imperial College, University of London, London, U.K. in 2003.



Brian L. Davies received the Ph.D. degree in medical robotics and was awarded a D.Sc. by the University of London, London, U.K. in 2001 for his international contribution to robotic and computer-aided surgery systems.

He has been Professor of Medical Robotics in the Department of Mechanical Engineering at Imperial College, University of London, London, U.K. since October 2000. He is Head of the Computer-Aided Systems Engineering Research section in the Mechanical Engineering Department. He started the Mechatronics in Medicine Group in 1988 which now has an international reputation for its work in robotic and computer-assisted surgery. He is an expert reviewer for a number of international computer-aided surgery projects.

Dr. Davies is a Fellow of the Institution of Mechanical Engineers and a Chartered Engineer.

BIBL. LONDIN. UNIV.